PILE FOUNDATION ANALYSIS AND DESIGN

SERIES IN GEOTECHNICAL ENGINEERING

Edited by

T. William Lambe
Robert V. Whitman
Professors of Civil Engineering
Massachusetts Institute of Technology

BOOKS IN SERIES:
Soil Testing for Engineers by T. William Lambe, 1951
Soil Mechanics by T. William Lambe and Robert V. Whitman, 1968
Soil Dynamics by Robert V. Whitman (*in progress*)
Fundamentals of Soil Behavior by James K. Mitchell, 1976
Elastic Solutions for Soil and Rock Mechanics by H. G. Poulos and E. H. Davis, 1974
Soil Mechanics, SI Version by T. William Lambe and Robert V. Whitman, 1978

The aim of this series is to present the modern concepts of soil engineering, which is the science and technology of soils and their application to problems in civil engineering. The word "soil" is interpreted broadly to include all earth materials whose properties and behavior influence civil engineering construction.

Soil engineering is founded upon many basic disciplines: mechanics and dynamics; physical geology and engineering geology; clay mineralogy and colloidal chemistry; and mechanics of granular systems and fluid mechanics. Principles from these basis disciplines are backed by experimental evidence from laboratory and field investigations and from observations on actual structures. Judgment derived from experience and engineering economics are central to soil engineering.

The books in this series are intended primarily for use in university courses, at both the undergraduate and graduate levels. The editors also expect that all of the books will serve as valuable reference material for practicing engineers.

T. William Lambe and Robert V. Whitman

樁承基礎之分析與設計

PILE FOUNDATION ANALYSIS AND DESIGN

H. G. POULOS
E. H. DAVIS
The University of Sydney

虹橋書店
Rainbow-Bridge Book Co.

中華民國七十年十月十六日第一版
局版臺業字第二四〇一號
發行人：孫國仁
住址：臺北市峨眉街107號
發行所：虹橋書店有限公司
發行所地址：臺北市峨眉街107號
印刷所：合興彩色印刷有限公司
印刷所地址：台北市西園路2段261巷34弄44號

PREFACE

This book deals with methods of analysis that may be useful in design of pile foundations. Many excellent textbooks are concerned with the more practical aspects of pile foundations, such as the factors influencing the selection of the type of pile, the techniques of installation, and practical details of construction and maintenance of piles. No attempt has been made to duplicate this type of information. The aims of the present book are to:

1. Present a consistent theoretical approach to the prediction of pile deformation and load capacity.
2. Present parametric solutions for a wide range of cases.
3. Demonstrate how such solutions can be used for design purposes.
4. Review the applicability of these approaches to practical problems.

In any theory, a certain amount of idealization is necessary to obtain a tractable mathematical solution; this is especially so when dealing with problems involving soil. In dealing with the deformations of pile foundations in this book, we have generally considered the soil as an elastic material, with allowances made for pile-soil slip and soil yield where appropriate. Although real soils possess few, if any, of the attractive attributes of an ideal homogeneous isotropic elastic material, they nevertheless can often be treated as elastic over a limited range of stress, provided that the "elastic" parameters are determined for this stress range. When used in this manner, with due discretion and a measure of engineering judgment, elastic-based theory has had considerable success in predicting the deformation of both shallow and deep foundations. Although other simple soil models have also been successfully used for various aspects of pile analysis (for example, the theory of subgrade reaction as applied to laterally loaded piles), elastic theory provides a unified basis for the analysis of all types of foundation; it also makes possible identification of the parameters that exercise a significant influence on pile performance. Since elastic theory allows consideration of stress transmission through a mass, it can be used to analyze the interaction between two or more piles and, therefore, to examine the behavior of groups of piles.

The material contained in this book is organized as follows:

1. The behavior of piles under vertical loads (Chapters 2 to 6).
2. The behavior of piles under lateral loading (Chapters 7 and 8) and under combined vertical and lateral loading (Chapter 9).
3. The behavior of piled rafts (Chapter 10).
4. Piles subjected to vertical or lateral soil movements (Chapters 11 to 13).
5. Miscellaneous topics such as pile buckling, dynamic loading, and pile load tests (Chapters 14 to 16).

Although the text deals with a relatively wide range of topics, it is by no means exhaustive. Furthermore, since geotechnical analysis is advancing at a very rapid rate, there may well be cases in which the analytical techniques we describe may have been superseded by more versatile methods capable of modeling real soil behavior more realistically. Nevertheless, we feel that the techniques and solutions presented in this book can be usefully applied to most practical problems and provide a basic series of results against which the results of more sophisticated analyses may be checked.

Some worked examples are given to illustrate the application of the solutions to practical problems. Because units are by no means standardized as yet, some of the examples are worked in SI units, some in British units, and a few in the Continental metric system.

We thank the many people who have contributed to this book and in particular Dr. N. S. Mattes, of the Electricity Commission of New South Wales, who obtained a considerable number of the elastic solutions presented, Dr. J. R. Booker and Dr. P. T. Brown of the University of Sydney, who provided a great deal of assistance with various aspects of the theoretical analyses, Mr. P. J. N. Pells who provided valuable information on the subject of piles

to rock, and Dr. T. J. Wiesner, who obtained some of the solutions presented in Chapter 10. The Civil Engineering Graduates Association of the University of Sydney gave financial support for the post-graduate course on pile foundations that formed the basis of this book. Grateful acknowledgement is given to Professor J. W. Roderick, former Head of the Department of Civil Engineering, who made the facilities of the Department available to us, to C. J. Peiti, B. Crook, J. Kilpatrick, S. Picken, J. Knight and B. Rocke who undertook the typing and assembly of the manuscript, and R. Brew and H. Papallo who prepared many of the diagrams.

H. G. Poulos
E. H. Davis

CONTENTS

PILE FOUNDATION ANALYSIS AND DESIGN

1

GENERAL PRINCIPLES

1.1 INTRODUCTION

The use of piles is man's oldest method of overcoming the difficulties of founding on soft soils. Although it dates back to prehistoric lake villages, until the late nineteenth century, the design of pile foundations was based entirely on experience, or even divine providence. Modern literature on piles can be said to date from the publication of *Piles and Pile Driving*, edited by Wellington of the *Engineering News* (later to become the *Engineering News-Record*) in 1893, in which the widely known *Engineering News* pile-driving formula was proposed. Since this first attempt at a theoretical assessment of the capacity of a pile, a great volume of field experience and empirical data on the performance of pile foundations has been published. In recent years, the increasing demand on the foundation engineer to predict reliably the behavior of his pile designs has stimulated more-sophisticated theoretical research into the interaction between a pile or piles and the embedding soil, so that a large volume of empirical knowledge is now balanced by a comparable theoretical understanding.

This balance between empiricism and theory is a common feature of progress in many engineering fields. Any engineering design or solution to a practical problem can be imperfect in two ways. It can be imperfect because it is inadequate: that is, parts of the structure fail or deform excessively; in the present context, the design involves too few, too-slender, or too-short piles. But it can also be imperfect because it is more than adequate (too many, too-long, or too-substantial piles) and therefore is an excessively costly design. Design based on empiricism alone tends to focus attention on the former, because recorded experience generally only distinguishes between unsatisfactory and trouble-free performance and rarely between economical and uneconomical design. Only by understanding the behavior of the engineering structure in an analytical as well as empirical sense can engineers reasonably expect to achieve designs that are neither inadequate nor overadequate. In other words, to obtain the full benefit of experience of actual engineering behavior, it is important to have a sound theoretical understanding of the problem. Of course, it is equally important that engineering theory should be based initially on experience and extended or modified in the light of further experience.

1.2 STRUCTURAL APPROACH

It is only too convenient to divide the design of major buildings into two components: the design of the structure and the design of the foundations. The structure for its own

reasons alone is assumed to produce certain column loads, and the foundations are merely required to carry these predetermined loads. In reality, for complicated structures, the loads on the foundations determine their movement, but this movement affects the loads imposed by the structure; there is inevitably interaction between structure and foundation. In fact, the whole complex of structural frame, foundation components (footings, piles, pile caps, raft, etc.), and soil or rock forming the founding material, together comprise one interacting structural system. The interaction between a pile and its embedding soil, and that between one pile and another pile, provide subsets of the larger set of all interacting structural components.

If an overall structural approach is to be successful, we need to know much more about a particular pile than that it can be classified as, say, a 50-ton pile. We need to know its load-settlement behavior up to failure, possibly its behavior under lateral load and moment, and how its behavior is modified by adjacent piles. This is analogous to saying that we need the complete load-deformation characteristics of beams and columns, not just their load capacities, before we can analyze complete structural frameworks.

Most of this book is concerned with bringing the analytical treatment of the load-deformation and the failure behavior of pile foundation systems to the same level of sophistication as similar analytical treatments available for systems of structural frames. With this achieved, it is a relatively simple matter with modern computer programs to combine the structural and foundation systems into one—but that matter is outside the scope of this book.

1.3 BASIC THEORY REQUIRED

Piles embeded in soil provide a reinforcement to the soil, increasing its load capacity and modifying its deformation behavior in much the same way as the steel reinforces the concrete in reinforced or prestressed concrete members. Unfortunately, although a sufficiently accurate analysis of the effects of reinforcement in concrete members can usually be obtained by adaptation of the simple theory of bending, the extended-continuum nature of the embedding soil around piles makes the corresponding analysis of the reinforcement effect of piles much more difficult.

1.3.1 Failure Theory

In the present state of knowledge, it is generally only possible to consider failure as something that occurs mainly at the interface between the sides of the pile and the soil, ignoring the details of failure within the soil, although for the pile base, ordinary bearing-capacity theories may be applicable. Thus for vertical failure, the shear stress at the shaft-soil interface attains a limiting value (possibly varying with depth and soil type), and for horizontal failure resulting from lateral load or moment, the normal stress at the interface attains a limiting value (again, possibly varying with depth). In such a simplified approach, any reduction in failure load for a particular pile because of the presence of a nearby pile cannot be taken into account, except that the failure load for a group of closely spaced piles can sometimes be calculated from bearing-capacity theory for buried footings on the assumption that the piles and soil between them act as one solid block. This load can be taken as the answer if it is less than the sum of the failure loads for the piles, calculated individually.

1.3.2 Elastic Theory

Soil and rock are not ideal elastic materials in that stress and strain are not linearly related, strains are not fully recoverable on reduction in stress, and strains are not independent of time. However, at least it can be said that strains in soil increase as stresses increase. Furthermore, the assumption of anything more complicated than a linearly elastic material for the soil in the pile-soil continuum situation would generally lead to unduly complicated theory lacking useful generality. The use of linear elastic theory is therefore expedient and should be sufficiently accurate for engineering purposes, provided that elastic "constants" are employed that are appropriate to the particular problem. That is, they have either been backfigured from field tests on piles in similar situations, or determined from laboratory tests employing stress changes similar to the average changes in the soil mass in the particular case.

The basic elastic response of the soil from which the solutions for elastic piles in elastic soil can be derived is given by Mindlin's set of equations for the stresses and displacements throughout an elastic half-space resulting from horizontal or vertical point load applied at a point beneath the surface. As will be explained in subsequent chapters, this basic response can be integrated to give the pile-soil interface stresses in such a way that the displacements of the pile and soil are compatible. Modifications to take account of failure at some parts of the interface are then relatively easy to make.

Alternatively, the elastic response can be assumed to be that of a series of unconnected springs, that is, a Winkler medium or the subgrade reaction assumption. In spite of what is said by some of the protagonists of this approach, it must fundamentally be inferior to the elastic continuum approach of the Mindlin equations, since it ignores the

very real interconnection among elements throughout the soil mass. However, it does have the advantages of computational simplicity and perhaps more-ready adaptation to complications such as change in soil type. On the other hand, it can never take into account the important matter of interaction between adjacent piles.

1.3.3 Changes in Soil Type

Appropriate idealization of actual subsurface conditions frequently involves consideration of one or more distinct layers of material of different properties. Piles in soft clay are often driven to a stiffer stratum of sand, which may in turn overlie a different clay before encountering bedrock. Both the failure theory and the deformation theory should therefore be capable of coping with such changes in properties from layer to layer. The modification of the failure theory for this matter presents little difficulty, but the modification of the deformation theory may require a number of simplifying assumptions.

1.3.4 The Role of Idealization

Engineering theory can only give the behavior in an ideal situation. It must start from assumptions with regard to the properties of the materials and their disposition. In complicated problems such as that of pile behavior, the engineering theory itself is often not fully rigorous, since approximations have to be made to obtain numerical answers even for the ideal situation. Thus, there is a judgement to make about the extent to which a particular set of numerical answers is an accurate enough answer to the ideal problem. This judgement is largely the job of the research engineer. There is also a judgement to be made on the practical side, of the accuracy with which the idealized situation fits the real situation. This judgement is largely the job of the practicing engineer. It is important that the difference between these judgements should be recognized and that they should never be made as one. For example, the fact that predicted behavior is not verified by subsequent observation can mean either that the prediction was based on inaccurate theory, or that it was based on an unrealistic idealization, or even both.

1.4 EXAMPLES OF THEORETICAL PILE CALCULATIONS

As a foretaste of the types of prediction possible from the theory to be given in subsequent chapters, the results of calculations are given for different-example pile foundations, and for comparison, a surface pad footing.

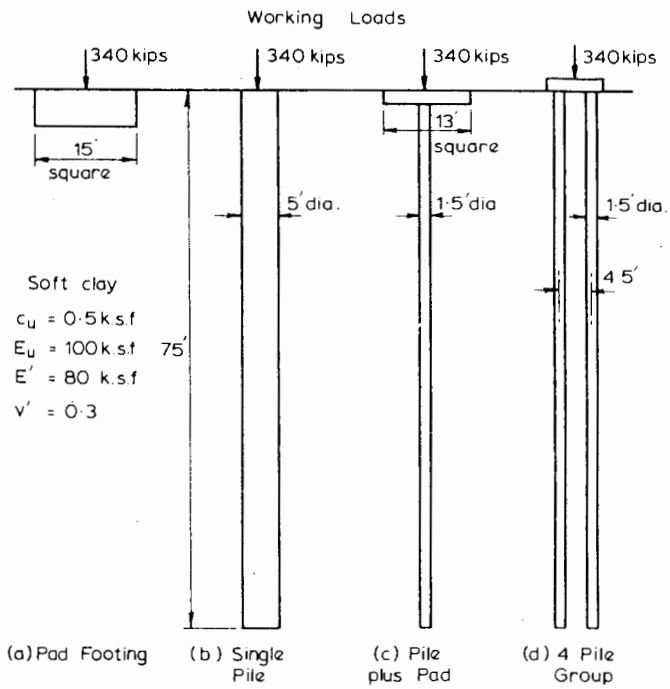

FIGURE 1.1 Example 1. Foundations on deep clay.

1.4.1 Vertically Loaded Foundations on Deep Clay

The foundations considered are shown in Fig. 1.1. All carry the same load and have the same factor of safety

TABLE 1.1 BEHAVIOR OF EXAMPLE FOUNDATIONS ON DEEP CLAY[a]

Example		1*a* Pad footing	1*b* Single Pile	1*c* Pile + pad	1*d* 4-Pile Group
Factor of Safety		2	2	2	2
Percent of Failure load taken by:	Pad or cap	100	-	73	14
	Shaft	-	87	26	83
	Pile base	-	13	1	3
Percent of working load taken by:	Pad or cap	100	-	45	5
	Shaft	-	92	53	93
	Pile base	-	8	2	2
Settlements at working load	Immediate	4.1 in.	0.9 in.[b]	2.3 in.	0.8 in.[c]
	Percent of immed. resulting from yield	56%	0%	36%	0%
	Consolidation	1.2 in.	0.1 in.	0.4 in.	0.2 in.
	Total final	5.3 in.	1.0 in	2.7 in.	1.0 in.

[a] See Fig. 1.1.
[b] Elastic shortening of pile as a column = 0.04 in.
[c] Elastic shortening of pile group as columns = 0.11 in.

against ultimate failure. The calculated behavior is given in Table 1.1, from which it can be seen that the surface pad footing, an unlikely choice for a comparatively heavy load on a soft clay, settles what would probably be an excessive amount. Furthermore, a high proportion of the settlement is irrecoverable, so that variations in load might produce further settlement. The single large-diameter pile and the four-pile group have similar behaviors and may even involve settlements that are more than satisfactorily small. The case of a pad with one small-diameter pile is unusual but represents an interesting intermediate case between pad only and piles only. At the working load, the pile is carrying its full failure-load but nevertheless succeeds in reducing the settlement well below that of the pad on its own.

1.4.2 Vertically Loaded Foundations on Clay over Gravel

The cases of a surface pad footing and a pile driven to a stiff gravel base under the soft clay are illustrated in Fig. 1.2. Again, each foundation carries the same load and has the same factor of safety. The results of calculation are given in Table 1.2. The behavior of the pad footing is unaffected by the gravel, since the clay has a depth of five times the footing breadth. The pile, being "end-bearing," can be of smaller diameter than before; in fact,

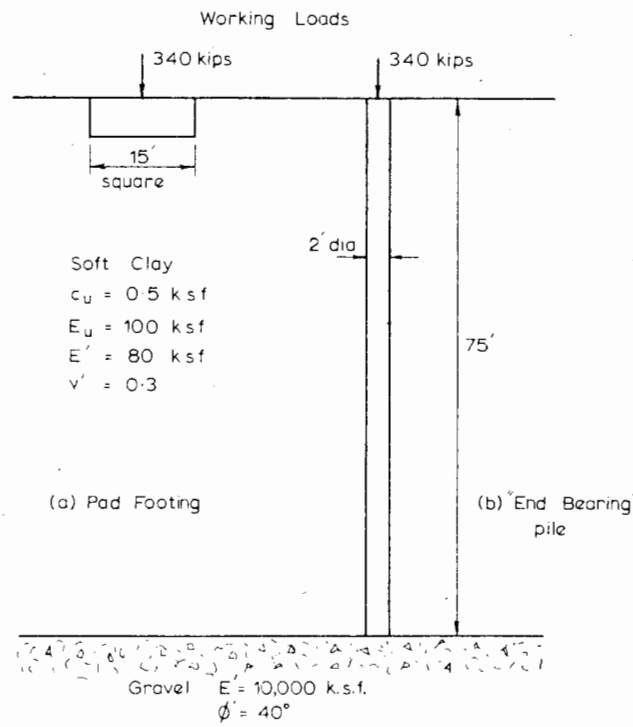

FIGURE 1.2 Example 2. Foundations on clay over gravel.

it is the strength of the concrete of the pile which determines its diameter, rather than soil properties. The settlement of the pile is now even smaller, as would be expected, although still greater than the straight column compression. It is interesting to note that although the pile is classified as "end-bearing," a third of the load is in fact taken by side shear on the shaft. For more slender piles, the proportion of the load taken by the shaft can be even higher. The fact that "end-bearing" piles are far from 100 percent end-bearing has been verified in the field in several instances.

TABLE 1.2 BEHAVIOR OF EXAMPLE FOUNDATIONS ON CLAY OVER GRAVEL[a]

Example		2a Pad footing	2b "End-bearing" Pile
Factor of Safety		2	2 (concrete strength governs)
Percent Failure load taken by:	Pad	100	-
	Shaft	-	13
	Pile base	-	87
Percent working load taken by:	Pad	100	-
	Shaft	-	33
	Pile base	-	67
Settlements at working load	Immediate	4.1 in.	0.5[b] in.
	Percent immed. resulting from yield	56%	0
	Consol.	1.2 in.	0
	Total final	5.3 in.	0.5 in.

[a] See Fig. 1.2.
[b] Elastic shortening of pile as a column = 0.25 in.

1.4.3 Foundations subject to Rotation

For the same vertical load as in the previous examples, but also with a horizontal load and á moment applied, a pad and pier are compared in the third example (Fig. 1.3). The results of calculations are given in Table 1.3. In order to carry even a relatively small moment, the pad footing has had to be enlarged to an inordinate size, and in view of the movements and rotations at the working loads, it would unlikely to be considered a satisfactory solution. The length and diameter of the pier have been selected so that the factor of safety against failure resulting from the vertical load is the same as that against failure resulting from the horizontal load and moment.

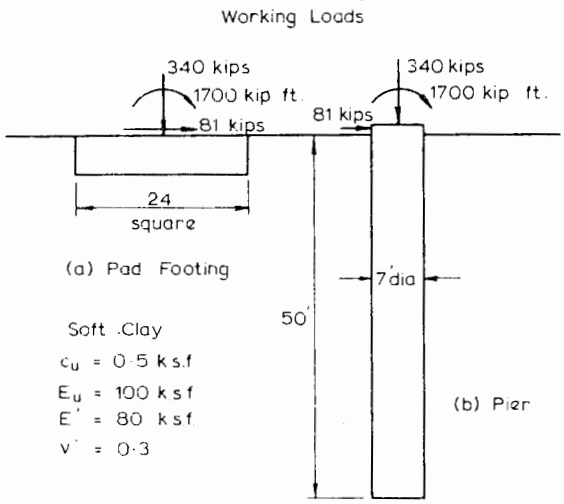

FIGURE 1.3 Foundations subject to rotation.

TABLE 1.3 BEHAVIOR OF EXAMPLE FOUNDATIONS SUBJECT TO ROTATION[a]

Example		3a Pad Footing	3b Single Pier
Factor of Safety		2	2
Settlement	Immediate	2.7 in.	1.0 in.
	Consol.	0.6 in.	0.2 in.
	Total final	3.3 in.	1.2 in.
Horizontal displacement	Immediate	1.4 in.	0.8 in.
	Consol.	0.3 in.	0.2 in.
	Total final	1.7 in.	1.0 in.
Rotation	Immediate	0.45°	0.16°
	Consol.	0.10°	0.04°
	Total final	0.55°	0.20°
Percent immediate movement resulting from local yield		56%	0

[a] See Fig. 1.3.

2

EFFECTS OF INSTALLATION OF PILES

2.1 INTRODUCTION

Piles may be classified in a number of ways, the common methods being

(a) By the material of which they are formed.
(b) By the method of installation.

The commonly used materials for piles are concrete, steel, and timber; discussions on the relative practical merits of each type of pile for various applications may be found in many references, for example, Chellis (1962), Tomlinson (1975), Bowles (1977), and Whitaker (1970). In terms of installation method, piles may be classified as

(a) Driven piles.
(b) Bored or cast-in-situ piles.
(c) Driven and cast-in-situ piles.
(d) Screw piles.

Detailed descriptions of these methods and equipment used in installation may also be found in the above four references.

The method of installation of a pile may have a profound effects on its behavior under load. It may also determine the severity of effect on nearby structures, including undesirable movements, vibrations, or even structural damage. Much of the available data on installation effects is concerned with driven piles, since pile driving generally creates more disturbance than other methods. Relatively little is known of the effects of constructing bored piles.

In this chapter, the effects of pile driving in clays are examined, with particular emphasis on the pore pressures developed around the pile and the resulting influence on the surrounding soil. Piles driven into sand are then considered, and finally, a brief review, largely qualitative, of the effects of installing bored piles is given.

It should be emphasized that this chapter is concerned with the extent to which installation changes the properties of the soil surrounding piles from those existing prior to installation, which are presumably determinable by normal methods of site investigation, sampling, and laboratory or in-situ testing. Furthermore, it is concerned with the manner in which such changes, at least with clays, may subsequently become modified the longer the loading of the installed pile is delayed. The change in bearing capacity of a loaded pile as a clay consolidates under the stresses produced by the load on the pile is not dealt with here, but is considered in Chapter 3. It is important to maintain a clear distinction between these two matters.

2.2 EFFECTS OF PILE DRIVING IN CLAYS

The effects of pile driving in clays have been classified into four major categories by de Mello (1969):

(a) Remolding or partial structural alteration of the soil surrounding the pile.
(b) Alteration of the stress state in the soil in the vicinity of the pile.
(c) Dissipation of the excess pore pressures developed around the pile.
(d) Long-term phenomena of strength-regain in the soil.

Some data is available on all the above effects, although the state of knowledge, particularly in relation to (d), is generally limited.

2.2.1 Influence on Soil Shear Strength and Pile Capacity

Early investigations into the effects of pile driving on the properties of clays were made by Housel and Burkey (1948) and Cummings, Kerkhoff, and Peck (1950). Based on the evidence from load tests to failure carried out on piles at different times after their installation, it can be inferred that the undrained strength of a clay is initially decreased considerably because of driving, but that significant regain of strength occurs with elapsed time between driving and pile testing. Generally, it may be expected that the driving of piles into clay will initially cause some (or even considerable) loss in undrained strength of the clay because of remolding at constant water content. Subsequently, the strength will usually increase because of a combination of two factors: thixotropic regain of undrained strength as the structural bonds destroyed by remolding are at least partially restored, and increase resulting from local consolidation of the clay produced by dissipation of excess pore-water pressures that arise from the increase in stress in the soil surrounding the pile. Conceivably, there would be situations in which the consolidation was negative (i.e., a swelling with time), thus producing a weakening in addition to that caused by remolding—for example, for stiff, overconsolidated clays.

Although investigations into the extent of the disturbance around a pile caused by driving have produced somewhat conflicting results, the available evidence (de Mello, 1969) suggests that immediately after driving, the amount of remolding decreased from about 100% at the pile-soil interface to virtually zero at about 1.5 to 2.0 diameters from the pile surface. Investigations by Orrje and Broms (1967) of concrete piles in a sensitive clay

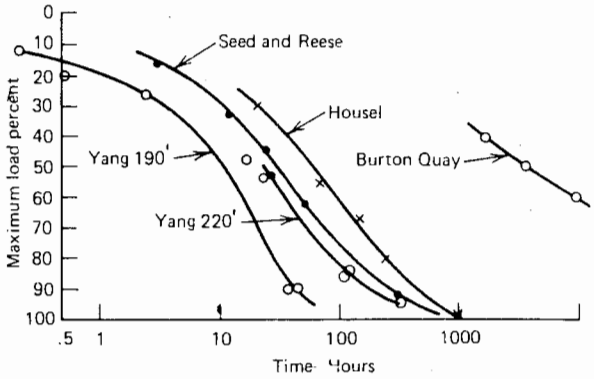

FIGURE 2.1 Increase of load capacity with time (Soderberg, 1962).

showed that the undrained strength had almost returned to its original value after nine months, except when piles were spaced at less than about 4.0 diameters, in which case little strength-regain (and in some cases a further loss) was noted with time.

Other than for thixotropic regain, the rate of increase of soil strength subsequent to pile driving is related to the rate of dissipation of excess pore pressure. Data presented by Soderberg (1962) showed that the increase in ultimate load capacity of a pile (and hence, shear strength of the soil) was very similar in character to the rate of dissipation of excess pore pressure with time (see Fig. 2.1). Some estimate of the "set-up" time may be obtained from a knowledge of the excess pore pressures developed around the pile, and the rate of dissipation of these pore pressures.

2.2.2 Pore Pressures Developed during Driving

A number of measurements of the excess pore pressure developed in a soil because of pile driving have been made; for example, Bjerrum et al. (1958), Bjerrum and Johannessen (1960), Milligan et al. (1962), Lambe and Horn (1965), Lo and Stermac (1965), Orrje and Broms (1967), Hanna (1967), Koizumi and Ito (1967), D'Appolonia and Lambe (1971). Results of measurements of pore pressure at the pile face in many of these papers have revealed that the excess pore pressures may become equal to or even greater than the effective overburden stress. However, the induced excess pore pressures decrease rapidly with distance from the pile and generally dissipate very rapidly.

A summary of some measurements of the variation with radial distance of the excess pore pressures around a single driven pile are given in Fig. 2.2. The excess pore pressure Δu is expressed dimensionlessly as $\Delta u/\sigma'_{vo}$, where σ'_{vo} is the vertical effective stress in-situ prior to driving, while

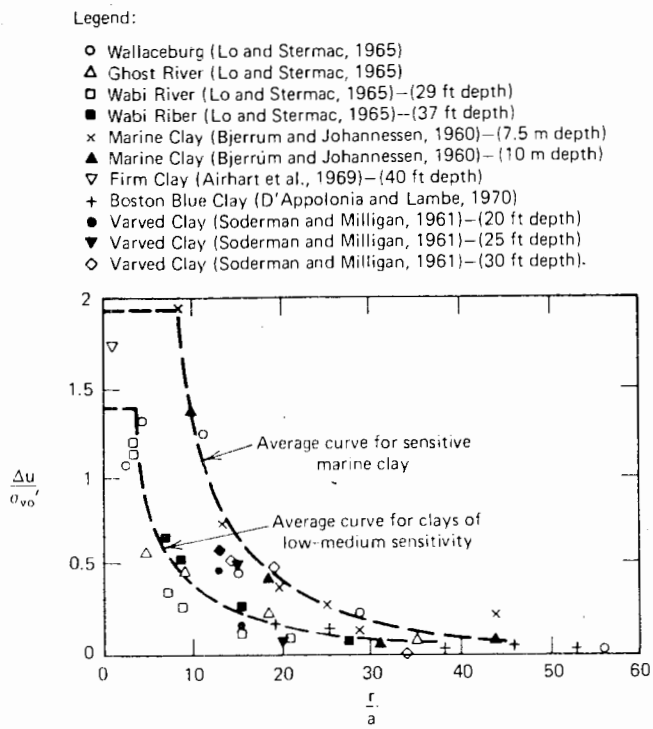

FIGURE 2.2 Summary of measured pore pressures.

the radial distance r from the pile is expressed in terms of the pile radius a. There is a considerable scatter in the points in this figure resulting largely from differences in soil type, the larger pore pressures being associated with the more sensitive soils.

In the vicinity of the pile, very high excess pore pressures are developed, in some cases approaching 1.5 to 2.0 times the in-situ vertical effective stress. Data presented by Airhart et al. (1969) suggests that near the pile tip, even greater pore pressures may be developed, amounting to 3 to 4 times the in-situ vertical effective stress.

Beyond r/a of about 4 for normal clays, and about 8 for sensitive clays, a rapid decrease in pore pressure with distance occurs, and beyond $r/a = 30$ the excess pore pressures are virtually negligible.

A further consequence of the development of pore pressures around a pile during driving has been reported by Fellenius and Broms (1969), who found that significant negative friction and downdrag forces were induced in a pile because of reconsolidation of the soil around the pile. This aspect is discussed further in Chapter 11.

Estimation of Pore Pressures

A number of methods have been developed to predict the excess-pore-pressure distribution around a driven pile. For cases in which it is sufficient to estimate only the maximum pore pressure developed near the pile surface, Lo and Stermac (1965) derived an expression from the consideration of failure of a radial zone of soil around the pile. D'Appolonia and Lambe (1971) derived an alternative form of Lo and Stermac's equation, namely,

$$\frac{\Delta u_m}{\sigma'_{vo}} = \left[(1 - K_o) + \frac{2 s_u}{\sigma'_{vo}} \right] A_f \qquad (2.1)$$

where

Δu_m = maximum excess pore pressure
K_o = in-situ coefficient of earth pressure at rest
s_u = undrained shear strength
A_f = pore-pressure coefficient A at failure
σ'_{vo} = initial vertical effective stress in soil

Comparisons, reported by Lo and Stermac (1965) and Lo (1968), between measured pore pressures and those calculated from Eq. (2.1), showed generally good agreement. Within the failure zone of the soil surrounding the pile, the pore pressures were a maximum and constant, and driving of adjacent piles only increased the pore pressure slightly. Outside the failure zone, the pore pressure decreased rapidly with distance and was negligible at a radial distance of about 16 diameters from the pile (see Fig. 2.2). Driving of adjacent piles developed pore pressures in this outer zone that added up directly until the maximum value was reached. Thus, the *maximum* pore pressures induced by driving a number of piles in a pile foundation may be predicted simply as the value of Δu_m from equation (2.1). The data presented by Lo and Stermac (1965) suggests a radius of the failure zone of about 4-pile radii, which is consistent with the extent of remolding around the pile, discussed in the previous section.

Theoretical methods of estimating the distribution of excess pore pressure with distance from the pile have been developed by Nishida (1962) and Ladanyi (1963). The former method is based on an elastoplastic analysis, while the latter is an adaption of the theory of expansion of a cylindrical cavity in a mass for use with the measured undrained stress-strain behavior of a soil. Although the latter method is versatile and relates to real soil behavior, it requires considerable computation. Furthermore, it relies on the details of laboratory stress-strain curve, the accuracy of which is liable to be affected by such factors as sampling disturbance and the initial stress condition of the sample.

As a rapid, practical means of estimating the excess-pore-pressure distribution, the following procedure is suggested:

(a) The Lo and Stermac expression (Eq. 2.1) is used to obtain the maximum pore pressure Δu_m, from the face of the pile to a distance R from the face. On the basis of Fig. 2.2 and also the analysis of Nishida (1962), R varies from $3a$ to $4a$ for insensitive clays, to $8a$ for sensitive clays.
(b) Beyond the distance R, the excess pore pressure is assumed to vary inversely as the square of the distance r from the pile, that is,

$$\Delta u = \Delta u_m / \left(\frac{r}{R}\right)^2 \tag{2.2}$$

The inverse variation is predicted from elastic theory, as utilized by Ladanyi (1963) and Nishida (1962).
(c) For pile groups, the pore pressure distributions around individual piles may be superposed, except that the pore pressure cannot exceed Δu_m, as found by Lo and Stermac (1965).

The excess pore pressures around a pile in sensitive clay as calculated by the above procedure, agree well with the average observed curve in Fig. 2.2.

2.2.3 Dissipation of Excess Pore Pressures

A relatively simple solution for the rate of dissipation of excess pore pressures around a driven pile has been proposed by Soderberg (1962a). It is assumed that dissipation occurs radially only, the vertical dissipation that may occur near the top and tip of the pile being ignored. The relevant equation of consolidation is then

$$\frac{\partial u}{\partial t} = c_h \left[\frac{\partial^2 u}{\partial r^2} + \left(\frac{1}{r}\right)\left(\frac{\partial u}{\partial r}\right)\right] \tag{2.3}$$

where

c_h is the two-dimensional coefficient of consolidation for horizontal drainage
u is excess pore pressure

The above equation may readily be written in finite difference form (e.g., see Gibson and Lumb, 1953), and solved for the appropriate drainage condition at the pile and initial pore-pressure distribution. Solutions for the excess pore-pressure dissipation at the pile face, for an impermeable pile, were obtained by Soderberg, who found that the form of the initial pore-pressure distribution had a relatively small influence on this solution.

A reasonable measure of the rate of strength or adhesion-regain after driving appears to be to consider the rate of consolidation within a limited area in the vicinity of the pile. Such solutions are shown in Fig. 2.3, assuming an initial excess pore-pressure distribution as suggested in Section 2.2.2 and a failure zone having ratios of radius R to pile radius a of 3 and 5. The degree of consolidation within a radius of R is shown for both a permeable and an impermeable pile.

It is interesting to compare these theoretical solutions with an empirical relationship suggested by Radugin (1969).

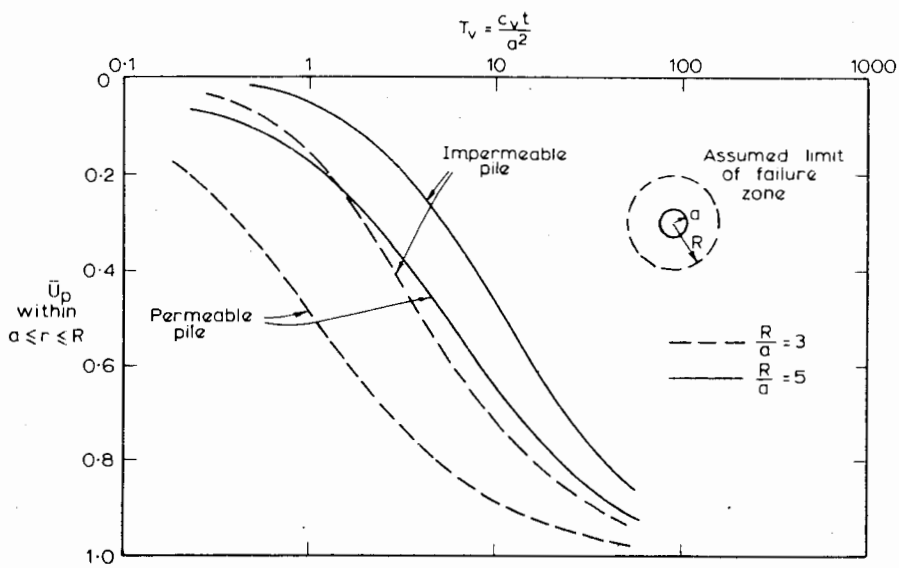

FIGURE 2.3 Theoretical solutions for rate of consolidation near a driven pile.

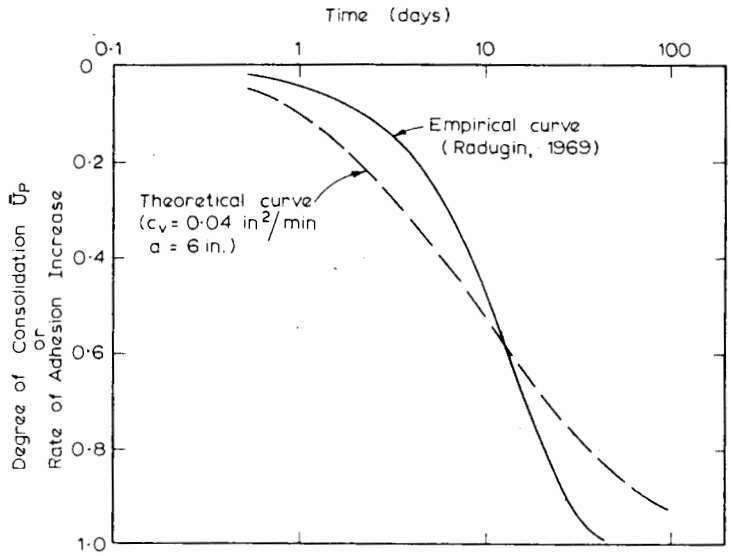

FIGURE 2.4 Comparison between empirical and theoretical solutions for rate of adhesion increase.

Assuming $R/a = 5$, $c_h = 0.04$ sq in./min (typical of a medium clay), and a permeable concrete pile of 6-in. radius, Fig. 2.4 compares the theoretical degree of consolidation versus time curve and Radugin's empirical curve, assuming the rate of consolidation is the same as the rate of adhesion increase in Radugin's relationship. There is some difference between the shape of the curves, but they are generally in sufficient agreement to suggest that the simple consolidation analysis provides a reasonable estimate of the rate of increase of load capacity.

From a practical point of view, solutions such as those in Fig. 2.3 are of most use in giving an estimate of the time that should elapse after driving before a load test is carried out, if a reliable estimate of the ultimate undrained load capacity and load-settlement behavior is to be obtained.

A more rigorous analysis of the stress changes, excess pore pressures, and subsequent consolidation around a driven pile in clay has been presented by Wroth et al. (1979). The pile-driving process is modeled as the creation of a long cylindrical cavity by radial soil movement. Values of stress and pore-pressure change have been obtained using a finite-element analysis incorporating a work-hardening soil model (the Cam-clay model). It is concluded that the total and effective stresses adjacent to the pile just after driving may be related directly to the original undrained strength of the soil, and are essentially independent of the overconsolidation ratio. The final stress state after consolidation is similar to that in an oedometer (K_o) test, except that the radial stress is now the major principal stress.

2.2.4 Displacement Caused by Driving

Pile driving generally causes a heave of the clay surrounding the pile, followed by consolidation of the clay. This movement caused by pile driving may have a significant effect on adjacent structures and may also cause the piles driven earlier in a multiple-pile installation to rise during the driving of the later piles. Under these circumstances, redriving of the earlier piles is often considered necessary, or may lead to a decision to use bored rather than driven piles. The limited data available on the magnitude of the heave is rather conflicting, although much of the conflict may arise from differences in soil types in the various investigations. The ratio of the total volume of initial heave to the total volume of driven piles *within* a foundation has been found to be about 100% by Adams and Hanna (1970) for steel H-piles in a firm till, 50% for piles in clay by Hagerty and Peck (1971), 60% by Avery and Wilson (1950), and 30% by Orrje and Broms (1967) for precast concrete piles in a soft, sensitive, silty clay. The latter investigators found that the heave near the edge of the foundation was about 40% of the value at the center. Outside the edge of the group, only very small heaves were noted by Adams and Hanna, and Orrje and Broms. Adams and Hanna measured radial and tangential movements as well as vertical heave, and found that the maximum radial movement was about 1.5 in., and the maximum tangential displacement about 0.4 in.—both these values being considerably less than the average vertical heave of

about 4.5 in. As with vertical heave, very small lateral movements occurred beyond the edge of the group.

Measurements of the movement of an existing building as a result of driving of piles for the foundations of a new building were reported by Lambe and Horn (1965). It was found that, at the near corners of the existing building, a heave of about 0.3 in. occurred during driving, but that by the end of construction, a net settlement of about 0.35 in. had occurred. Despite the fact that the piles were preaugered to within about 30 ft of their final elevation, high excess pore-pressures (maximum of about 40 ft of water) were measured near the corner of the existing building, even before a substantial building load was carried by the piles.

Figure 2.5 shows some measurements of heave and settlement of buildings caused by pile driving, as reported by D'Appolonia and Lambe (1971). The settlement data plotted are for net settlement one to three years after the end of construction. Larger movements than those measured by Lambe and Horn were found, although the piles were again preaugered to within 20 to 30 ft of the final tip elevation.

From measurements of displacements resulting from pile driving in clays, Hagerty and Peck (1971) concluded that the soil displacements are less for piles driven in sensitive clays than for corresponding piles in insensitive clays, and that when piles penetrate alternating strata of fine-grained soil and granular materials, the observed surface-heave may be much less than that which would have occurred in insensitive clay soils. It was also found that if the sequence of pile driving involved driving piles first along the perimeter of the foundation, the heave of the soil surface in the central area of the foundation is increased and that of the surrounding area correspondingly decreased. Observations also were made of lateral movements, and it was found that driven piles tended to be displaced away from subsequent driving, with movements continuing for a considerable length of time after completion of driving. Where large differences in elevation existed within the foundation area, pile driving often displaced the soil preferentially toward the areas in which the lower elevations occurred.

Estimation of Displacements

Lambe and Horn (1965) proposed a method of estimating the heave and subsequent settlement of the surface of soil near a pile resulting from driving of the pile. Although the method was found to predict movements considerably larger than those measured, it appears to be a logical procedure and worthy of further application. The method

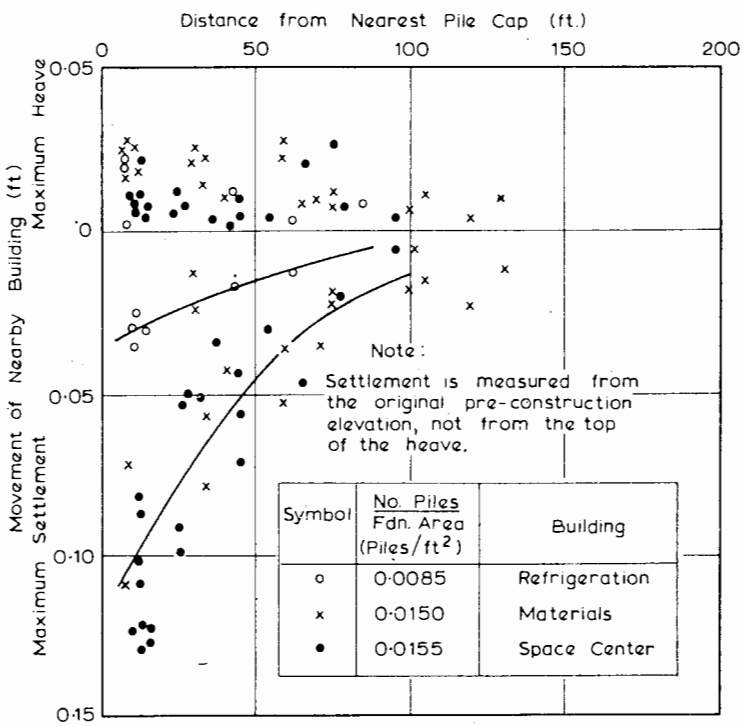

FIGURE 2.5 Movements of nearby buildings caused by piledriving operations (D'Appolonia and Lambe, 1971).

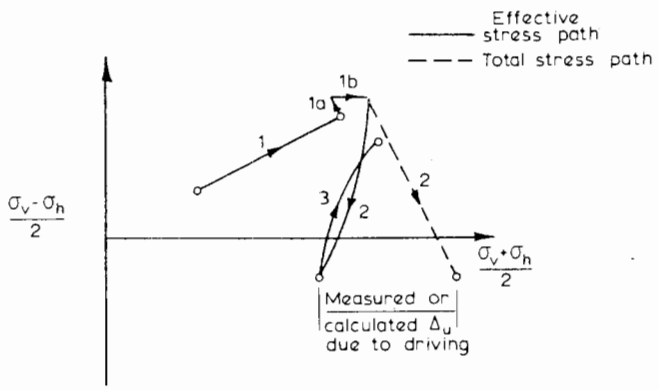

Step 1	Deposit formation
Steps 1a,1b	Undrained loading and consolidation due to building (if applicable)
Step 2	Pile driving simulation
Step 3	Dissipation subsequent to driving

FIGURE 2.6 Test procedure for displacement calculation (Lambe and Horn, 1965). (© Canada, 1965 by University of Toronto Press.)

is based on the stress-path approach advocated by Lambe (1964). It consists of estimating the effective stress-path for an "average" element in the compressible soil layer, running a laboratory test on a sample of this soil such that the loading follows the stress path estimated for the field element, and using the laboratory-measured value of vertical strain to estimate the building heave and settlement.

There are essentially three steps in the procedure, which is shown diagrammatically in Fig. 2.6:

1. Consolidation of the sample (usually under K_o conditions) to the in-situ stresses in the layer prior to pile driving. Where the element under consideration is beneath an existing building, as it was in the case described by Lambe and Horn, this first stage involves simulation of the undrained loading caused by construction of the building followed by consolidation, after initial K_o consolidation of the element to the field stress state.
2. Increasing the total lateral stress at constant total vertical stress until the pore pressure in the element equals that measured by the field piezometers or that calculated on the basis of Section 2.2.2. The vertical strain measured during this stage allows the heave to be computed.
3. Dissipation of the pore pressures developed by the pile driving, that is, consolidation of the sample. Lambe and Horn suggest that this process might take place under conditions of no lateral strain, but this suggestion appears questionable. The movement measured in this stage will enable the total consolidation, subsequent to the heave, to be computed.

The choice of a single "average" element, however, appears to be a difficult task. Obviously, a more satisfactory procedure, although it involves considerably more testing, is to divide the soil into a number of layers, test samples from each of these layers, and add up the resulting displacements computed for each layer to obtain the overall displacement.

Of course, the movement of the surface of the soil, discussed above, is not necessarily the same as the movement of the top of an existing pile caused by the installation of an adjacent pile. A very simple approximate procedure for estimating the heave of an existing pile was proposed by Hagerty and Peck (1971). This procedure was based on the concept that inextensible vertical piles embedded in the clay would be lifted by the relative rise of the soil along the upper part of the pile, but that along the lower part of the pile, a downward force would act, tending to reduce the total uplift of the pile (Fig. 2.7). A surface *a-a* can be found at which the relative movement between soil and pile is zero. The pile heave is considered to be approximately equal to the heave of the soil, on the assumption that no heave takes place below *a-a*; that is,

$$\text{Pile heave} = \frac{(L - d_h)}{L} \text{ (Soil heave)} \qquad (2.4)$$

The depth, d_h, is estimated by balancing the potential upward and downward adhesive forces on the upper and lower parts of the pile.

For simple distributions of pile-soil adhesion, d_h may be calculated directly (for example, for uniform adhesion, $d_h = 0.5L$), so that the pile heave would be estimated as one half of the soil heave; while for linearly increasing adhesion, from zero at the surface, $d_h = 0.67L$, and the pile heave is estimated as one third of the soil heave.

Hagerty and Peck found good agreement between observed pile heave and estimates based on the above simple approach.

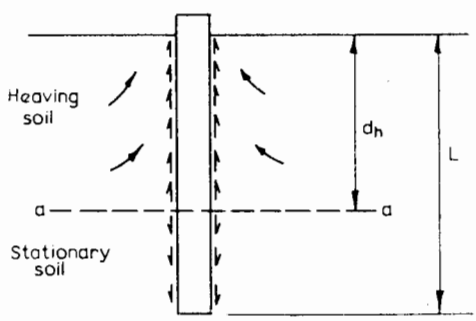

FIGURE 2.7 Balance of forces along driven pile (Hagerty and Pecl 1971).

A more refined analysis of pile movement caused by adjacent pile-driving may be made using the approach described in Chapter 12 for piles in swelling or shrinking soils.

2.3 EFFECTS OF PILE DRIVING IN SANDS

2.3.1 Single Piles

When a pile is driven into sands and cohesionless soils, the soil is usually compacted by displacement and vibration, resulting in permanent rearrangement and some crushing of the particles. Thus, in loose soils, the load capacity of a pile is increased as a result of the increase in relative density caused by the driving, and installation by driving rather than boring has distinct advantages. Detailed investigations of the extent of compaction of sand and the increase in relative density around the pile have been carried out by Meyerhof (1959) and Robinsky and Morrison (1964).

Robinsky and Morrison conducted a careful series of model-pile tests in sand in which the displacement and compaction around the piles was studied by means of radiography techniques. It was found that in an initially very loose sand (relative density D_r = 17%), soil movement extended 3 to 4 pile diameters from the side of the pile and 2.5 to 3.5 diameters below the pile tip. In a medium dense sand ($D_r \simeq 35\%$), the extent of movement was somewhat larger, extending 4.5 to 5.5 diameters from the side and 3.0 to 4.5 diameters below the tip. These figures are in broad agreement with those found by Meyerhof (1959).

The tests of Robinsky and Morrison also showed that the process of sand displacement and compaction below a pile tip is followed by sand movements adjacent to the pile sides. These movements tend to decrease the sand density in the immediate vicinity of the sides and thus nullify some of the benefits gained by the primary compaction. The pattern of displacements around a typical pile, as found from the radiographs, is shown in Fig. 2.8, while the strain pattern deduced from these displacements is shown in Fig. 2.9 (Vesic, 1967). The decrease in density occurring above the tip is clearly reflected in the tensile strains, which amount to about half of the maximum compressive strains below the tip. The above remarks apply to a straight-sided pile, but Robinsky and Morrison found that the same process occurs with a tapered pile. Their tests did not indicate that the loosening effect was markedly compensated by the wedging action of the pile-taper compacting the surrounding sand. The higher load capacity of a tapered pile can probably be attributed mainly to the greater normal stresses developed between the pile and the soil when loaded by the foundation.

On the basis of an empirical correlation among density, penetration resistance, and friction angle, Meyerhof (1959) devised a method of estimating the extent of the zones of increased density, and hence increased friction angle,

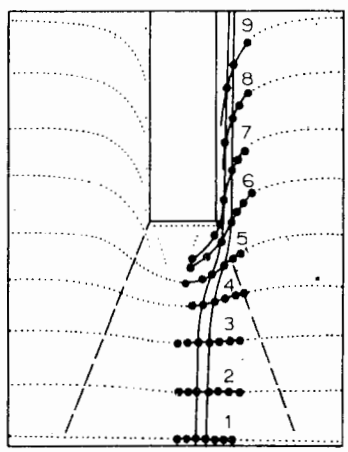

FIGURE 2.8 Displacements around driven pile in sand (after Robinsky and Morrison, 1964). (Reproduced by permission of the National Research Council of Canada from the Canadian Geotechnical Journal, Vol. 1, 1964, p. 81.)

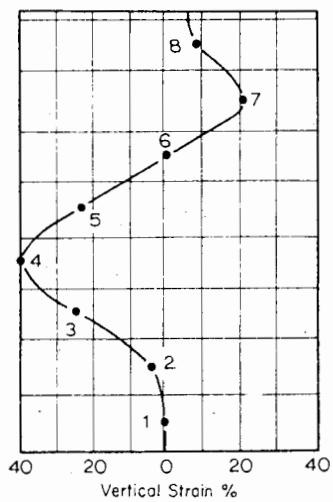

FIGURE 2.9 Strains around driven pile in sand (after Robinsky and Morrison, 1964). (Reproduced by permission of the National Research Council of Canada from the Canadian Geotechnical Journal, Vol. 1, 1964, p. 81.)

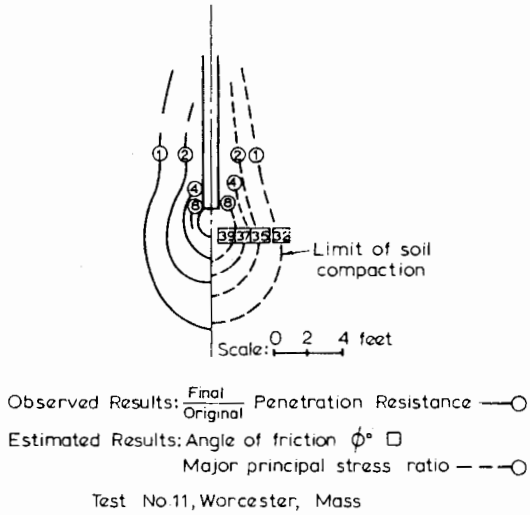

FIGURE 2.10 Observed vs. computed compaction of sand near pile (after Meyerhof, 1959).

around a pile driven in sand; a typical result compared with observations is shown in Fig. 2.10. These results are in broad agreement with those of Robinsky and Morrison (1964), but according to Meyerhof, the amount of compaction near the tip is greater, and that near the top of the shaft is less.

A simpler method of estimating the effects of driving a pile in loose sand in the vicinity of the tip is that proposed by Kishida (1967). On the basis of field and model test-results, he assumes that the diameter of the compacted zone around a pile is $7d$. Within this zone, he further assumes that the angle of friction ϕ' changes linearly with distance from the original value of ϕ_1' at a radius $r = 3.5d$ to a maximum value of ϕ_2' at the pile tip, as shown in Fig. 2.11.

The relationship between ϕ_1' and ϕ_2' is taken to be

$$\phi_2' = \frac{\phi_1' + 40^\circ}{2} \tag{2.6}$$

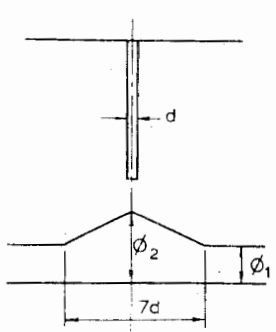

FIGURE 2.11 Effect of driving on ϕ (Kishida, 1967).

When $\phi_1' = 40^\circ$ in Eq. (2.6), there is no change in relative density due to pile driving.

2.3.2 Pile Groups

When groups of piles are driven into a loose sand, the soil around and between the piles becomes highly compacted, and if the pile spacing is sufficiently close (less than about six diameters), the ultimate load capacity of the group may be greater than the sum of the capacities of the individual piles—that is, the efficiency of the group is greater than 1. On the other hand, if the sand is so dense that pile driving causes loosening rather than compaction, the group efficiency may be less than 1.

An estimate of the effects of driving a group of piles into loose sand may be made by application of the approach suggested by Kishida (1967) for single piles, assuming that superposition of the effects of single piles is applicable. In applying Eq. (2.6), the value of ϕ_1' is the changed value caused by previous piles. By application of this approach, a rough estimate may be made of the effect on ultimate load capacity of the order of installation of the piles. It has been found in practice that piles driven later have a greater load capacity than those driven earlier.

Some field measurements of the amount of compaction caused by the driving of a group in a granular soil, in which standard penetration tests have been carried out before and after driving of groups have been reported by Philcox (1962). The test results are shown in Fig. 2.12. In case (a), the standard penetration number, N, near the center of a four-pile group, was more than doubled by driving. In case (b), the increase in N for a point a little away from the center of a nine-pile group shows a relatively smaller increase (average about 75%). Cases (c) and (d) show that the increase in N becomes less as the point considered becomes more distant from the center of the group. Another point apparent from Figs. 2.12b and 2.12c is that the effect on driving on N, and hence on soil density, is greater below the tip than along the shaft.

In order to relate the increase in N to the increase in ϕ, Kishida (1967) suggests that ϕ_1' and N may be related by the following expression:

$$\phi_1' = \sqrt{20N} + 15^\circ \tag{2.7}$$

The differences between the degree of densification at various points within a group, as shown in Fig. 2.12, suggest that the load capacity of piles near the center of the group may be greater than those near the edge of the group, and that the load distribution, even at working loads, may be nonuniform, with larger loads being carried by the center piles—as predicted by Kishida's approach.

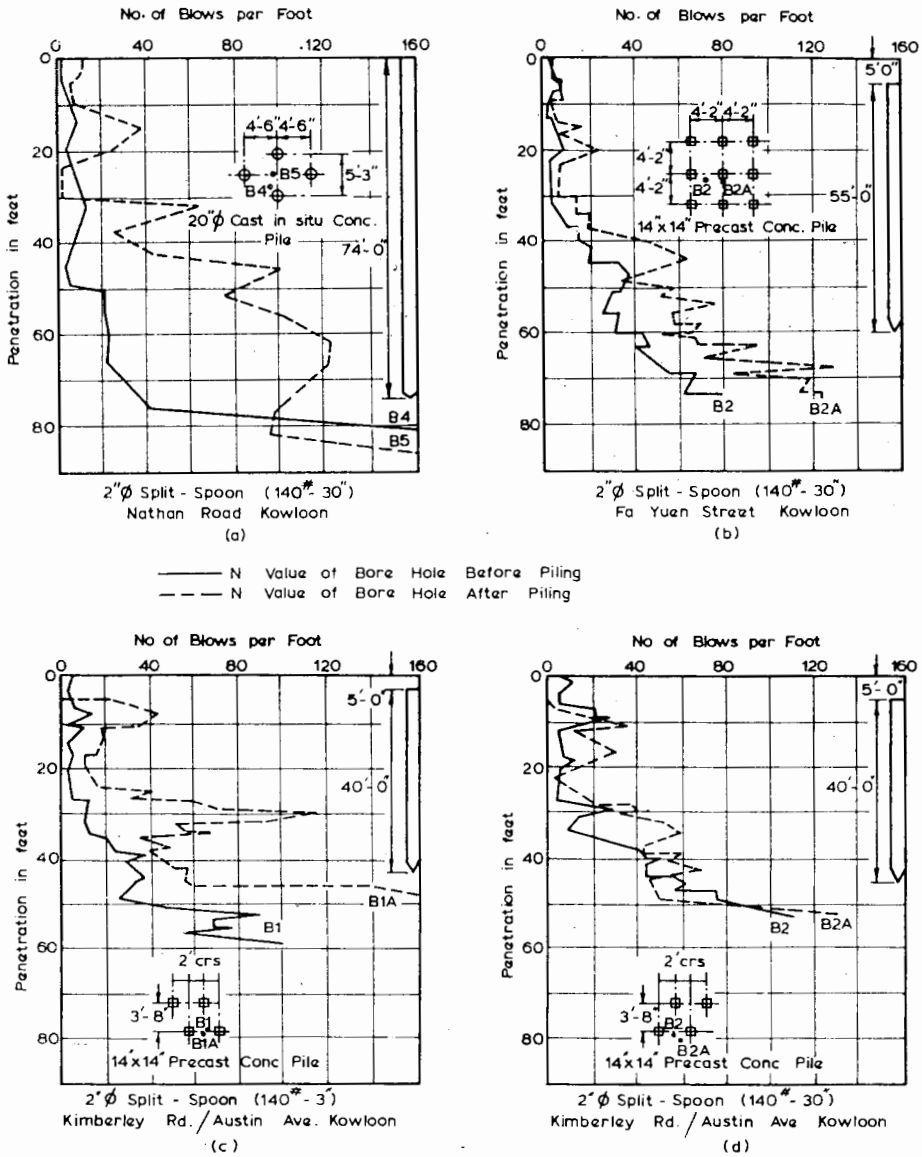

FIGURE 2.12 A comparison of N Values–before and after driving piles (Philcox, 1962). (Reproduced by permission of the Institution of Structural Engineers, London.)

This behavior, which is in contrast to that usually observed for groups in clay, has been observed in tests carried out by Hanna (1963) and Beredugo (1966). As suggested by Kishida (1967), the effects of differing compaction may also explain the dependence of pile-load distribution on the order of driving piles in sand.

2.4 EFFECTS OF INSTALLING BORED PILES

2.4.1 Clay Soils

The effects of installing bored piles in clay have been studied largely in relation to the adhesion between the pile and the soil. The adhesion has been found to be less than the undrained cohesion before installation, mainly because of softening of the clay immediately adjacent to the soil surface. This softening may arise from three causes:

(a) Absorption of moisture from the wet concrete.
(b) Migration of the water from the body of the clay toward the less highly-stressed zone around the borehole.
(c) Water poured into the boring to facilitate operation of the cutting tool.

Factor (c) may be eliminated by good drilling technique, and (b) can be minimized by carrying out the drilling and

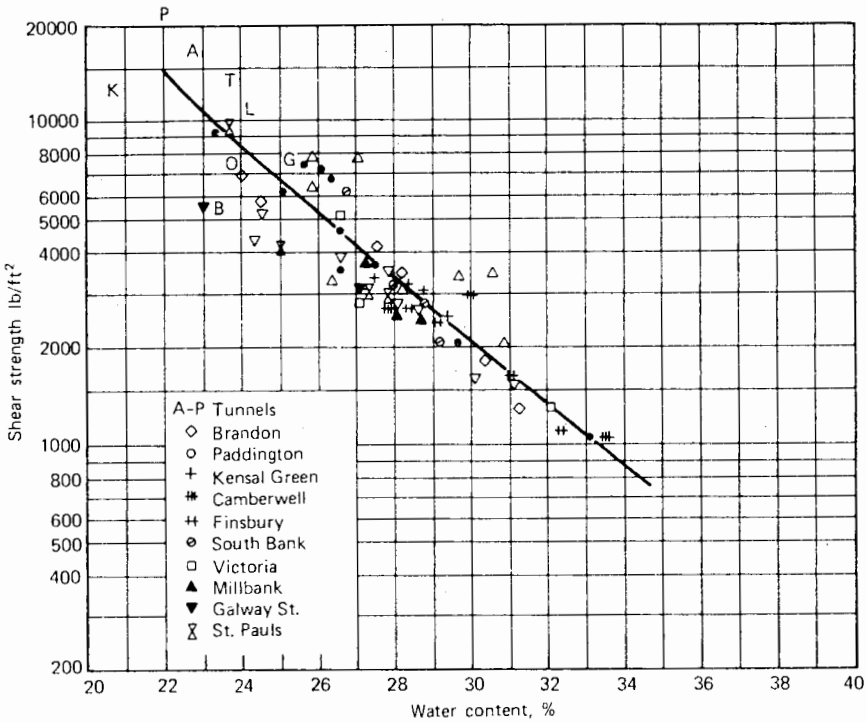

FIGURE 2.13 Relation between shear strength and water content for London clay (Liquid Limit, 70–85) (Skempton, 1959).

concreting operations as rapidly as possible. Some effects from factors (a) and (b) are considered to be inevitable by Skempton (1959), but their seriousness will depend largely on the technique employed, whether or not casing or drilling fluid is used to support the walls during construction, and the time taken for construction of the pile. Palmer and Holland (1966) contend that softening in overconsolidated London clay is minimized if drilling and concreting is carried out within one or two hours.

Meyerhof and Murdock (1953) measured the water contents of the clay immediately adjacent to the shaft of a bored pile in London clay and found an increase of nearly 4% at the contact surface, although at a distance of 3 in. from the shaft, the water contents had not altered. This increase should be a maximum value, as the hole was drilled by hand and took two to three days to complete. An estimate of the effect of the increase in water content can be made if information is available on the relation between shear strength and water content. Such a relationship for London clay has been presented by Skempton (1959) and is reproduced in Fig. 2.13. These results show that an increase in water content of only 1% results in a 20% change in the ratio c_a/c_u, of undrained adhesion c_a to original undrained strength c_u, while for a 4% increase in water content, c_a/c_u is reduced to about 0.3. Values of c_a/c_u for bored piles are discussed in detail in Section 3.2.

A further effect of installing a bored pile is that the clay just beneath the pile base may be disturbed and softened by the action of the boring tools. The effects of this disturbance may result in increased settlements, especially for belled piers, in which the base carries a major proportion of the load; hence, it is important to clean out the base thoroughly. However, as stated by Skempton (1959), base disturbance and softening should have a negligible effect on the ultimate bearing capacity of the base because of the comparatively large mass of clay involved when the base penetrates the clay. In contrast, the shearing process developed in the clay along the pile shaft is probably restricted to the narrow softened zone.

Construction problems may also arise with bored piles, and a number of these have been described by Pandey (1967) in relation to the foundations for a heavy industrial building, including the following:

(a) Caving of the borehole, resulting in necking or misalignment of the pile.
(b) Aggregate separation within the pile.
(c) Buckling of the pile reinforcement.

Such structural defects may be difficult to detect, since a load test may not reveal any abnormal behavior, especially if the load is only taken to the design load.

Barker and Reese (1970) investigated the influence of drilling fluids on the performance of bored piers. They

concluded that when proper construction techniques are employed, drilling mud has no detrimental effects on the load-carrying characteristics of a bored shaft. The concrete properties and the concrete-placement procedure are the two most critical factors involved in the construction process. Elimination of the effects of the drilling mud is accomplished when it is completely displaced by the concrete, resulting in a vigorous scouring of the borehole wall by the rising concrete. Should drilling mud be trapped between the concrete and borehole wall, it would virtually eliminate the development of any shear-load transfer in the vicinity of the trapped drilling mud. The use of casing in placing the concrete involves a greater risk of trapping drilling mud than does the procedure of placing the concrete under the drilling mud by the use of a tremie or concrete pump. Barker and Reese suggested that reduction factors of 0.6 for clay and 0.8 for sand and silts should be applied to the shear strength in the design of drilled shafts. However, no reliance should be placed on load transfer developing within three shaft diameters of the surface or one diameter of the base.

2.4.2 Sands

There is relatively little quantitative information on the effects of installing bored piles in sands or cohesionless soils. Such piles usually require casing or drilling fluid to support the walls of the hole and sinking of the hole, and subsequent withdrawal of the casing while concreting the shaft is likely to disturb and loosen the soil to some extent. Also, some loosening is liable to occur at the bottom of the pile as a result of baling or "shelling-out" the hole, and when this is done under water, the upward surge on withdrawal of the baler or shell can loosen the soil for several feet below and around the pile. Thus, in calculating the load capacity of a bored pile in sand, Tomlinson (1975) suggests that the ultimate value of angle of shearing resistance ϕ should be used, unless the pile is formed in a dense gravel when the "surging" effect may not take place. If heavy compaction can be given to the concrete at the base of the piles, then the disturbed and loosened soil may be recompacted and the value of ϕ for the dense state used. However, if the shaft is obstructed by the reinforcing cage, such compaction may not be possible.

Tests on bored piles in sand have been reported by Touma and Reese (1974) and Clemence and Brumund (1975). Touma and Reese found evidence of the arching that occurs around the pile with driven piles (see section 3.2) and that results in the development of limiting values of skin friction and base resistance at depth. It was also found that the skin resistance, for piles penetrating less than 25 ft, could be correlated with the integral around the pile periphery of $\sigma'_{vo} \tan \phi'$ (where σ'_{vo} = effective overburden pressure), using a reduction factor of about 0.7. There were indications that smaller reduction factors are appropriate for greater penetrations. From a large-scale test on a bored pier in sand bearing on a simulated rock base, Clemence and Brumund (1975) found that 20 to 30% of the design axial load in "end-bearing" drilled piers was carried by the pile skin. A roughly linear increase in skin friction with depth was measured, except near the lower part of the pier, where a sharp increase in skin friction was noted, presumably because of the confining effect of the rock base. It was found possible to use the results of direct shear tests for the soil-pier interface materials to predict the limiting skin friction, except near the tip, where the calculated skin friction was lower than that measured.

3

ULTIMATE LOAD CAPACITY OF PILES

3.1 INTRODUCTION

There are two usual approaches to the calculation of the ultimate load capacity of piles: the "static" approach, which uses the normal soil-mechanics method to calculate the load capacity from measured soil properties; and the "dynamic" approach, which estimates the load capacity of driven piles from analysis of pile-driving data. The first approach will be described in detail in this chapter, and the second in Chapter 4.

In this chapter, a general expression for the ultimate load capacity of a single pile is given and its application to piles in clay and sand is described. Approaches for groups of piles in clay and sand will then be outlined. Other topics include the design of piles to rock, the use of in-situ tests such as the standard penetration test and the static cone to estimate pile-load capacity, the calculation of uplift resistance of piles and groups, and the load capacity of bent piles.

3.2 ULTIMATE LOAD CAPACITY OF SINGLE PILES

3.2.1 General Expression

The net ultimate load capacity, P_u, of a single pile is generally accepted to be equal to the sum of the ultimate shaft and base resistances, less the weight of the pile; that is,

$$P_u = P_{su} + P_{bu} - W \qquad (3.1)^*$$

where

P_{su} = ultimate shaft resistance
P_{bu} = ultimate base resistance
W = weight of pile

P_{su} can be evaluated by integration of the pile-soil shear strength τ_a over the surface area of the shaft. τ_a is given by the Coulomb expression

$$\tau_a = c_a + \sigma_n \tan \phi_a \qquad (3.2)$$

where

τ_a = pile-soil shear strength
c_a = adhesion
σ_n = normal stress between pile and soil
ϕ_a = angle of friction between pile and soil

* It is an implicit assumption of Eq. 3.1 that shaft and base resistance are not interdependent. This assumption cannot be strictly correct, but there is little doubt that it is correct enough for practical purposes for all normal-proportion piles and piers.

σ_n is in turn frequently related to the vertical stress σ_v, as

$$\sigma_n = K_s \sigma_v \tag{3.3}$$

where

K_s = coefficient of lateral pressure

Thus,

$$\tau_a = c_a + \sigma_v K_s \tan \phi_a \tag{3.4}$$

and

$$P_{su} = \int_0^L C\tau_a dz$$

$$= \int_0^L C(c_a + \sigma_v K_s \tan \phi_a) dz \tag{3.5}$$

where

C = pile perimeter
L = length of pile shaft

It is usually accepted that the ultimate resistance P_{bu} can be evaluated from bearing-capacity theory as

$$P_{bu} = A_b(cN_c + \sigma_{vb}N_q + 0.5\gamma dN_\gamma) \tag{3.6}$$

where

A_b = area of pile base
c = cohesion of soil
σ_{vb} = vertical stress in soil at level of pile base
γ = unit weight of soil
d = pile diameter
N_c, N_q, N_γ = bearing capacity of factors, which are primarily functions of the angle of internal friction ϕ of the soil, the relative compressibility of the soil and the pile geometry

Rigorous solutions for the bearing capacity of surface footings using the methods of classical plasticity are now well-established (Prandtl, 1923; Sokolovskii, 1965; Cox, 1962; Lundgren and Mortensen, 1953; Davis and Booker, 1971), and the only doubts regarding the practical validity of these solutions lie in the possible effects of the differences between the behavior of real soil and that of the ideal material assumed in the theory. At the present time, there are few if any classical plasticity solutions that are relevant to a buried footing, and therefore, for the calculation of base resistance of piles, reliance has to be placed on approximate theoretical or semiempirical methods. With regard to sands, these methods have been reviewed by Vesic (1967), who found that the solution of Berezantzev et al. (1961) generally fitted experimental results best.

From Eqs. (3.1), (3.5), and (3.6),

$$P_u = \int_0^L C(c_a + \sigma_v K_s \tan \phi_a) dz$$
$$+ A_b(cN_c + \sigma_{vb}N_q + 0.5\gamma dN_\gamma) - W \tag{3.7}$$

Equation (3.7) is a general expression for the ultimate load capacity of a single pile. If the undrained or short-term ultimate load capacity is to be computed, the soil parameters c, ϕ, c_a, and γ should be values appropriate to undrained conditions, and σ_v and σ_{vb} should be the *total* stresses. If the long-term ultimate load capacity of piles in sand is required, the soil parameters should be drained values, and σ'_v and σ'_{vb} the effective vertical stresses. The vertical stresses are usually taken to be the overburden stresses, and for clays, this is probably true enough, even close to the piles. However, for sands, there is now clear evidence implying that the vertical stress near the pile may be less than the overburden. This matter is discussed in greater detail in Section 3.2.3.

For steel H-piles, two modes of failure of the shaft are possible: (a) the development of the limiting pile-soil shear strength along the entire surface area of the pile; and (b) the development of the limiting pile-soil shear strength along the outer parts of the flanges, plus the development of the full shear strength of the soil along the plane joining the tips of the flanges—that is, the soil within the outer boundaries of the pile effectively forms part of the pile shaft. Therefore, when using Eq. (3.7), the ultimate skin resistance, P_{su}, should be taken as the lesser of the two values.

3.2.2 Piles in Clay

3.2.2.1 UNDRAINED LOAD CAPACITY

For piles in clay, the undrained load capacity is generally taken to be the critical value unless the clay is highly overconsolidated. (Burland, 1973, contends, however, that an effective stress-drained analysis is more appropriate, as the rate of pore-pressure dissipation is so rapid that for normal rates of load application, drained conditions generally prevail in the soil near the pile shaft.) If the clay is saturated, the undrained angle of friction ϕ_u is zero, and ϕ_a may also be taken as zero. In addition, $N_q = 1$ and $N_\gamma = 0$ for $\phi = 0$, so that Eq. (3.7) reduces to

$$P_u = \int_0^L Cc_a dz + A_b(c_u N_c + \sigma_{vb}) - W \qquad (3.9)$$

where

c_u = undrained cohesion of soil at level of pile base
c_a = undrained pile-soil adhesion

Further simplification is possible in many cases, since for piles without an enlarged base, $A_b\sigma_{vb} \simeq W$, in which case

$$P_u = \int_0^L Cc_a dz + A_b c_u N_c \qquad (3.10)$$

Undrained Pile-Soil Adhesion c_a

The undrained pile-soil adhesion c_a varies considerably with many factors, including pile type, soil type, and method of installation. Ideally, c_a for a given pile at a given site should be determined from a pile-loading test, but since this is not always possible, resort must often be made to empirical values of c_a. Many attempts have been made to correlate c_a with undrained cohesion c_u, notably Tomlinson (1957, 1970), Peck (1958), Woodward et al. (1961), Coyle and Reese (1966), Vesic (1967), Morgan and Poulos (1968), McClelland et al. (1969), McClelland (1972), and McClelland (1974).

For driven piles, typical relationships between c_a/c_u and c_u, based on the summary provided by McClelland (1974), are shown in Fig. 3.1. It is generally agreed that for soft clays ($c_u \leqslant 24$ kPa), c_a/c_u is 1 (or even greater*); however, for driven piles in stiff clays, a wide scatter of

TABLE 3.1 DESIGN VALUES OF ADHESION FACTORS FOR PILES DRIVEN INTO STIFF COHESIVE SOILS[a]

Case	Soil Conditions	Penetration Ratio[b]	c_a/c_u
I	Sands or sandy soils overlying stiff cohesive soils	<20	1.25
		>20	See Fig. 3.2
II	Soft clays or silts overlying stiff cohesive soils	<20 (>8)	0.40
		>20	0.70
III	Stiff cohesive soils without overlying strata	<20 (>8)	0.40
		>20	See Fig. 3.3

[a] After Tomlinson (1970).

[b] Penetration ratio = $\frac{\text{Depth of penetration in stiff clay}}{\text{Pile diameter}}$

NOTE 1: Adhesion factors not applicable to *H*-section piles.

NOTE 2: Shaft adhesion in overburden soil for cases I and II must be calculated separately.

* For driven piles, the rapid dissipation of excess pore pressures due to driving may result in a locally overconsolidated condition, and hence a value of c_a even greater than c_u for the unaffected soil.

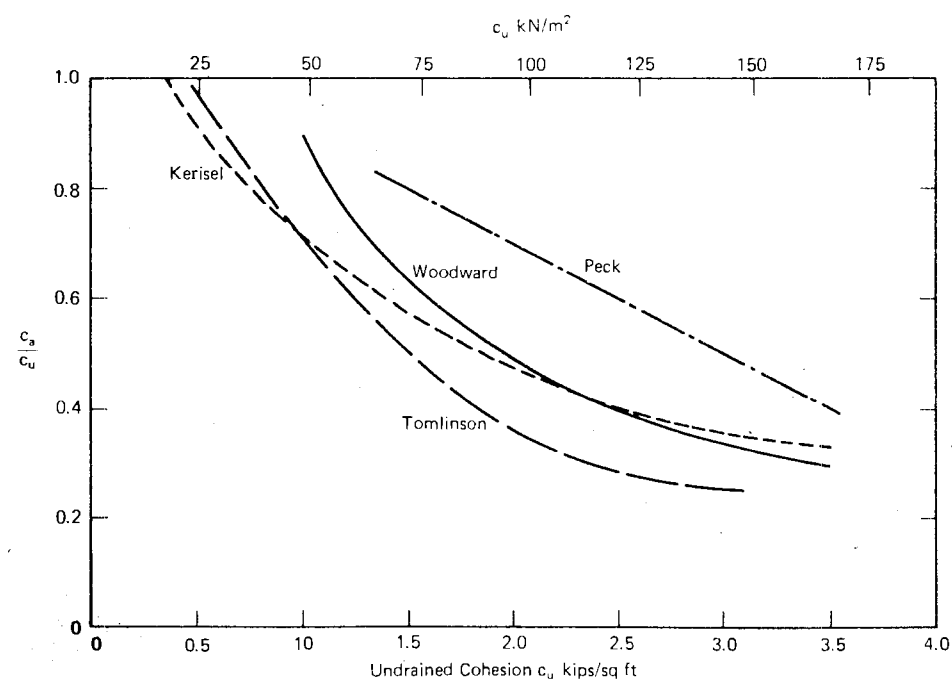

FIGURE 3.1 Adhesion factors for driven piles in clay (after McClelland, 1974).

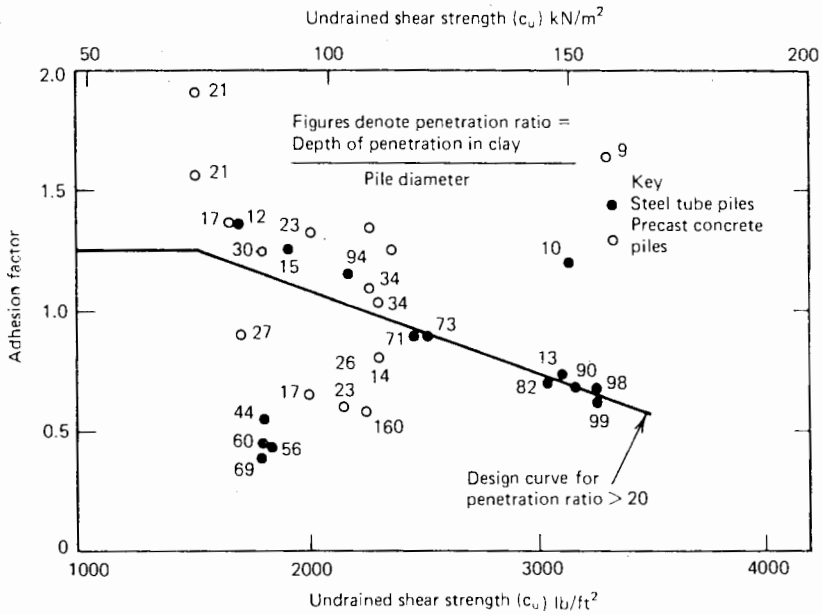

FIGURE 3.2 Adhesion factors for case I (sands and gravels overlying stiff to very stiff cohesive soils) (Tomlinson, 1970).

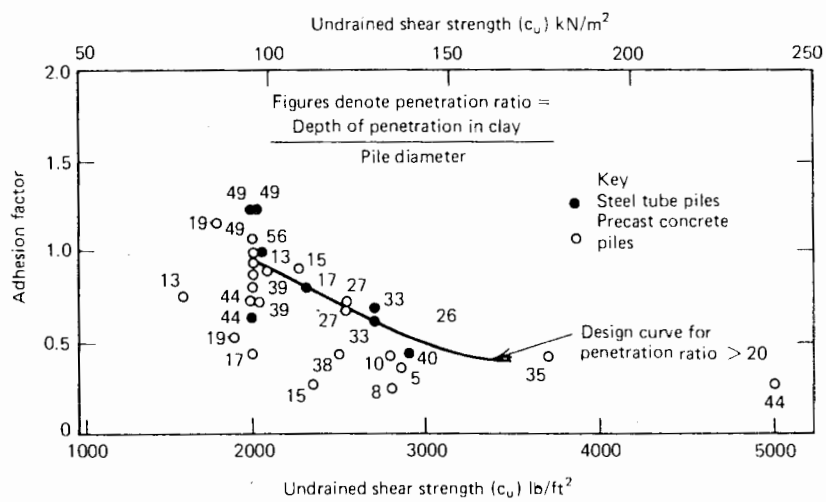

FIGURE 3.3 Adhesion factors for case III (stiff to very stiff clays without overlying strata) (Tomlinson, 1970).

values of $^{c}a/c_u$ is evident. This scatter is often attributed to the effects of "whip" during driving. A more complete investigation of adhesion for driven piles in stiff clay has been made by Tomlinson (1970), who found that $^{c}a/c_u$ may be markedly influenced by the soil strata overlying the clay, as well as by the value of c_u. Tomlinson has suggested the adhesion factors shown in Table 3.1 and Figs. 3.2 and 3.3 for $c_u \geqslant 1000$ lb/sq ft (48 kPa). The most notable feature of Tomlinson's results are the high values of $^{c}a/c_u$ for case I, where sand or sandy gravel overlies the clay, because of the "carrying down" of a skin of the overlying soil into the clay by the pile. There appears to be little data on appropriate values of c_a for driven piles founded in very sensitive clays, and the extent to which "set-up" compensates for remolding can at present only be determined by a load test.

For bored piles, the available data on $^{c}a/c_u$ is not as extensive as for driven piles, and much of the data that is available is related to London clay. Table 3.2 gives a summary of adhesion factors, one of which is expressed in terms of remolded strength, c_r, as well as the undisturbed undrained strength, c_u. Results obtained by Skempton (1959) and Meyerhof and Murdock (1953) suggest that an upper limit of c_a is 2000 lb/sq ft (96 kPa).

TABLE 3.2 ADHESION FACTORS FOR BORED PILES IN CLAY

Soil Type	Adhesion Factor	Value	Reference
London clay	c_a/c_u	0.25–0.7 Average, 0.45	Golder and Leonard (1954) Tomlinson (1957) Skempton (1959)
Sensitive clay	c_a/c_r	1	Golder (1957)
Highly expansive clay	c_a/c_u	0.5	Mohan and Chandra (1961)

A somewhat different approach to the calculation of the ultimate shaft capacity P_{su} has been adopted by Vijayvergiya and Focht (1972) for steel-pipe piles. From an examination of a number of loading tests on such piles, they concluded that P_{su} can be expressed as follows:

$$P_{su} = \lambda(\sigma'_m + 2c_m) A_s \qquad \textbf{(3.10}a\textbf{)}$$

where

σ'_m = mean effective vertical stress between ground surface and pile tip

c_m = average undrained shear strength along pile.

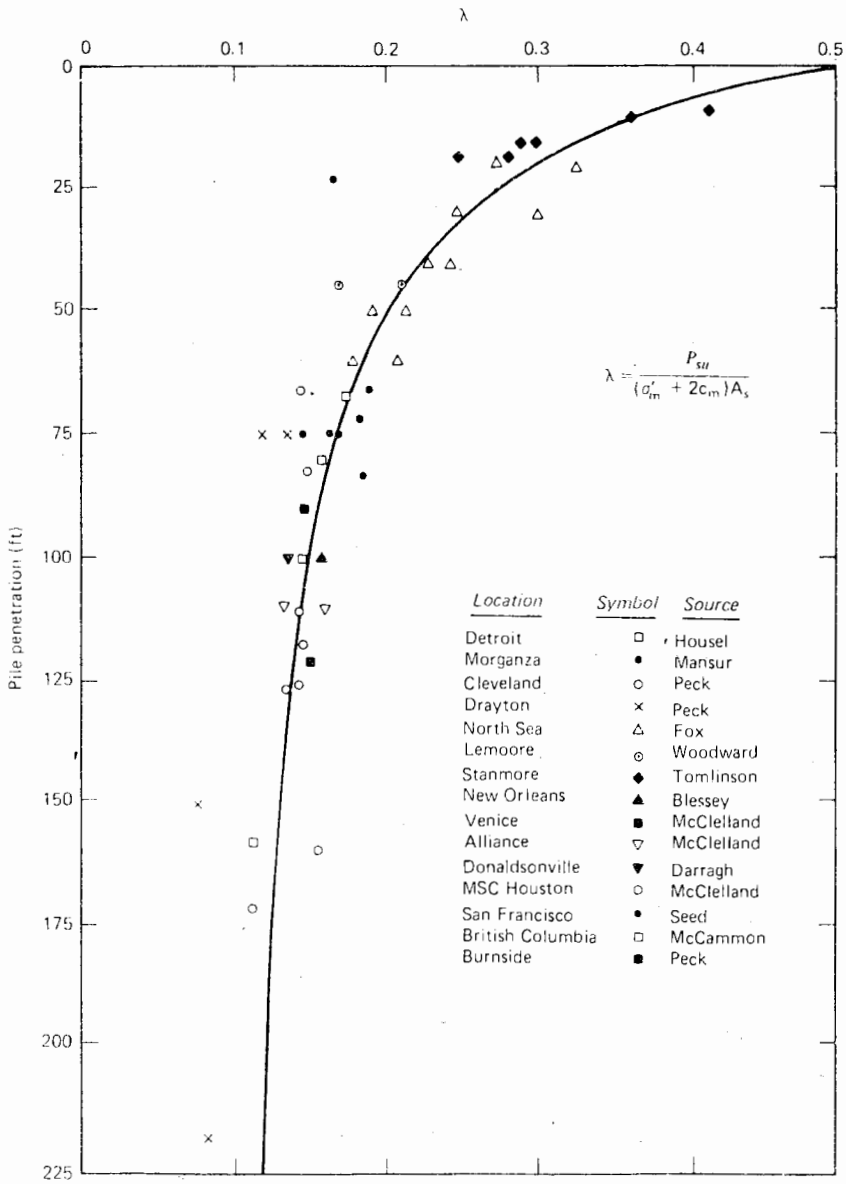

FIGURE 3.4 Frictional capacity coefficient λ vs. pile penetration (Vijayvergiya and Focht, 1972).

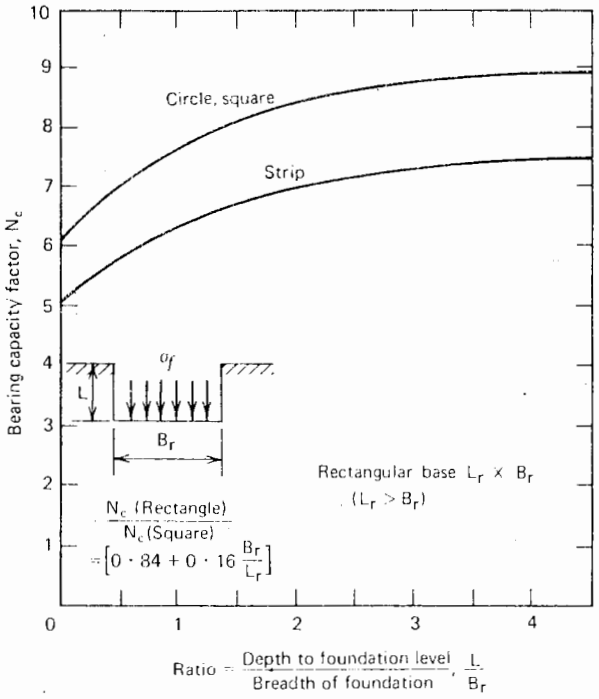

FIGURE 3.5 Bearing-capacity factors for foundations in clay ($\phi = 0$) (after Skempton, 1951).

A_s = pile surface area
λ = dimensionless coefficient

In effect, the average pile-soil adhesion factor is then

$$\frac{\bar{c}_a}{\bar{c}_m} = \lambda\left(\frac{\bar{\sigma}'_m}{\bar{c}_m} + 2\right) \tag{3.10b}$$

λ was found to be a function of pile penetration and is plotted in Fig. 3.4.

Equation (3.10*a*) has been used extensively to predict the shaft capacity of heavily loaded pipe-piles for offshore structures.

Bearing Capacity Factor N_c

The value of N_c usually used in design is that proposed by Skempton (1951) for a circular area, which increases from 6.14 for a surface foundation to a limiting value of 9 for length $\geq$ 4 diameters (Fig. 3.5). The latter value of N_c = 9 has been confirmed in tests in London clay (Skempton, 1959) and has been widely accepted in practice. However, differing values have been found by other investigators; for example, Sowers (1961) has found $5 < N_c < 8$ for model tests, and Mohan (1961) has found $5.7 < N_c < 8.2$ for expansive clays. The variations in the value of N_c may well be associated with the influence of the stress-strain behavior of the soil. From an analysis of the expansion of a cavity in a mass, Ladanyi (1963) found that for insensitive clays, $7.4 < N_c < 9.3$, depending on the stress-strain behavior of the soil. This analysis broadly confirmed the earlier analysis of Bishop et al. (1945), which gave the following result for a circular base (as quoted by Ladanyi).

$$N_c = 1 + \frac{4}{3}\left[1 + \ln\left(\frac{E_u}{3c_u}\right)\right] \tag{3.11}$$

3.2.2.2 DRAINED LOAD CAPACITY

For piles in stiff, overconsolidated clays, the drained load capacity, rather than the undrained, may be the critical value, and Vesic (1967, 1969) and Chandler (1966, 1968) have advocated an effective-stress approach in such cases. If the simplifying assumption is made that the drained pile-soil adhesion c'_a is zero and that the terms in Eq. (3.7) involving the bearing capacity factors N_c and N_γ can be ignored, the drained ultimate load capacity from Eq. (3.7) may be expressed as

$$P_u = \int_0^L C\sigma'_v K_s \tan \phi'_a \, dz + A_b \sigma'_{vb} N_q - W \tag{3.12}$$

where

σ'_v = effective vertical stress at depth z
σ'_{vb} = effective vertical stress at level of pile base
ϕ'_a = drained angle of friction between pile and soil

Burland (1973) discusses appropriate values of the combined parameter $\beta = K_s \tan \phi'_a$ and demonstrates that a lower limit for this factor for normally consolidated clay can be given as

$$\beta = (1 - \sin \phi') \tan \phi' \tag{3.13}$$

where

ϕ' = effective stress friction angle for the clay

For values of ϕ' in the range of 20 to 30 degrees, Eq. (3.13) shows that β varies only between 0.24 and 0.29. This range of values is consistent with values of $\beta = K_s \tan \phi'_a$ deduced from measurements of negative friction on piles in soft clay (see Figs. 11.26 and 11.27). Meyerhof (1976) also presents data that suggests similar values of β; however, there is some data to suggest that β decreases

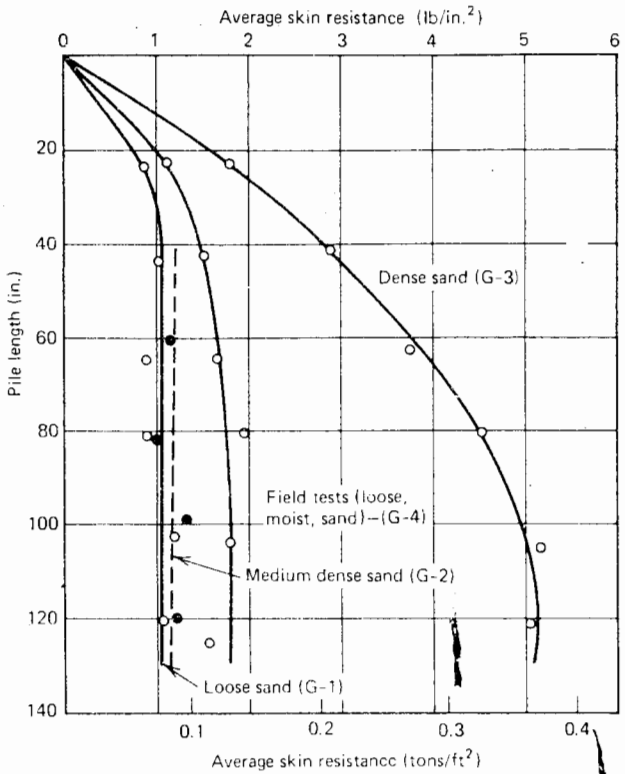

FIGURE 3.6 Variation of skin resistance with pile length (Vesic, 1967).

with increasing pile length, and that for long piles (in excess of about 60 m), β could be as low as 0.15.

For piles in stiff clays, Burland suggests that taking $K_s = K_o$ and ϕ'_a = the remolded friction angle, gives an upper limit to the skin friction for bored piles and a lower limit for driven piles. Meyerhof (1976) presents data indicating that K_s for driven piles in stiff clay is about 1.5 times K_o, while K_s for bored piles is about half the value for driven piles. For overconsolidated soils, K_o can be approximately estimated as

$$K_o = (1 - \sin \phi') \sqrt{OCR} \tag{3.14}$$

where

OCR = overconsolidation ratio

It is inferred that ϕ'_a can be taken as ϕ', the drained friction angle of the clay.

In the absence of contrary data, σ'_v and σ'_{vb} may be taken as the effective vertical overburden stresses. Values of N_q may be taken to be the same as for piles in sand; these values are plotted in Fig. 3.11.

3.2.3 Piles in Sand

Conventional methods of calculation of the ultimate load capacity of piles in sand (Broms, 1966; Nordlund, 1963)

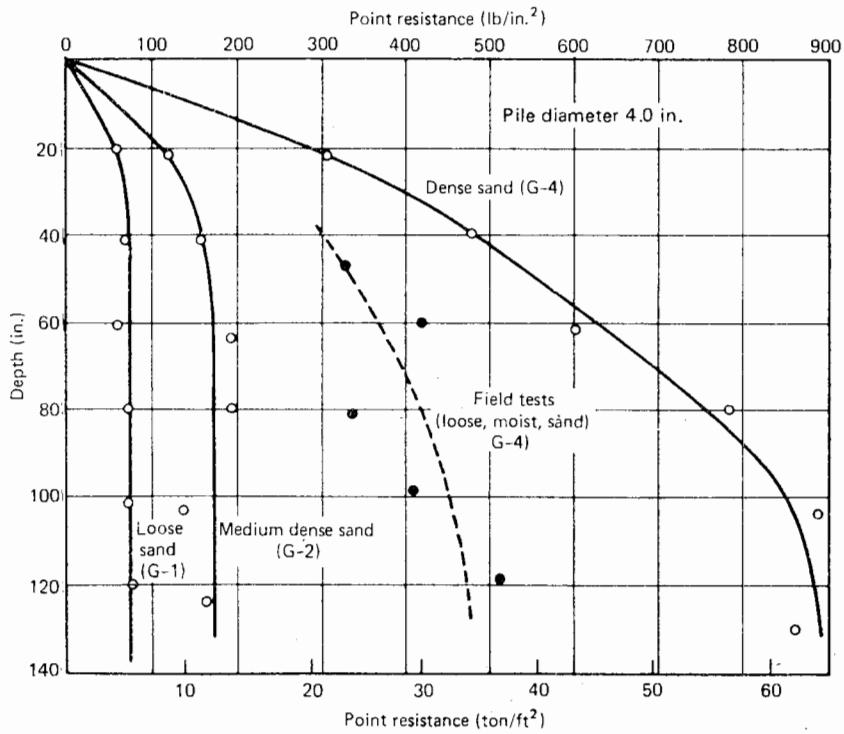

FIGURE 3.7 Variation of point resistance with pile length (Vesic, 1967).

assume that the vertical stresses σ_v and σ_{vb} in Eq. (3.7) are the effective vertical stresses caused by overburden. However, extensive research by Vesic (1967) and Kerisel (1961) has revealed that the unit shaft and base resistances of a pile do not necessarily increase linearly with depth, but instead reach almost constant values beyond a certain depth (Figs. 3.6 and 3.7). These characteristics have been confirmed by subsequent research (e.g., BCP Comm., 1971; Hanna and Tan, 1973). Vesic also found that the ratio of the limiting unit point and shaft resistances, f_b/f_s, of a pile at depth in a homogeneous soil-mass appears to be independent of pile size, and is a function of relative density of the sand and method of installation of the piles. Relationships between f_b/f_s and angle of internal friction (ϕ'), obtained by Vesic, are shown in Fig. 3.8. The above research indicates that the vertical effective stress adjacent to the pile is not necessarily equal to the effective overburden pressure, but reaches a limiting value at depth. This phenomenon was attributed by Vesic to arching and is similar to that considered by Terzaghi (1943) in relation to tunnels. There are however other hypotheses, such as arching in a horizontal plane, which might explain the phenomena shown in Figs. 3.6 and 3.7.

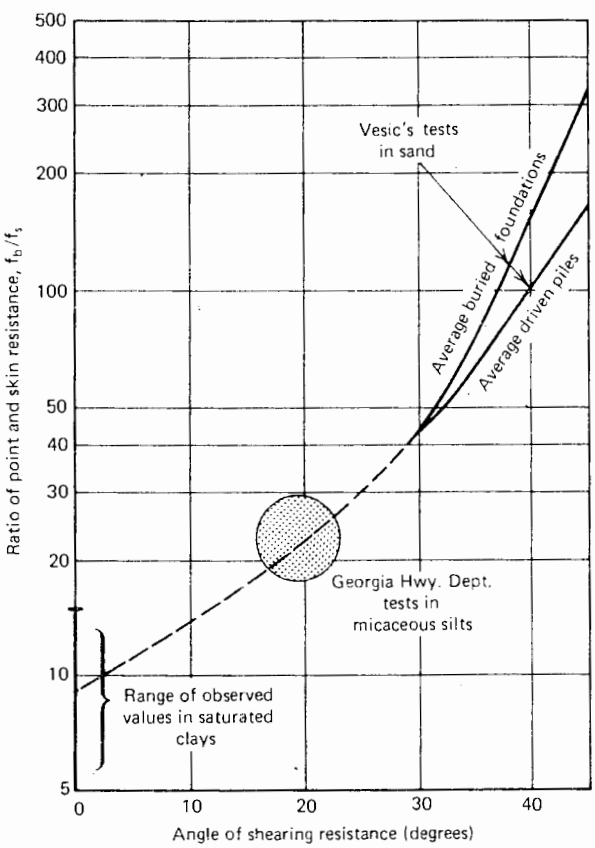

FIGURE 3.8 Variation of f_b/f_s with ϕ (Vesic, 1967).

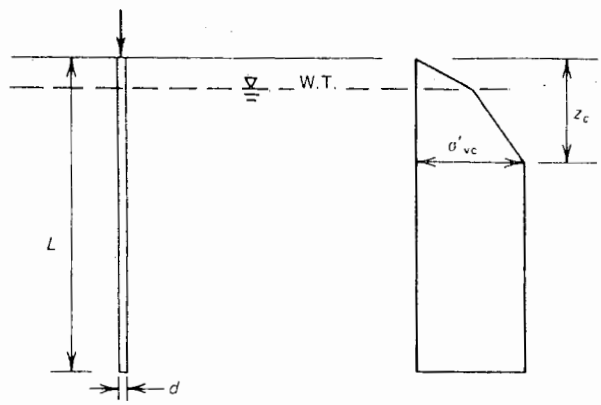

FIGURE 3.9 Simplified distribution of vertical stress adjacent to pile in sand.

Some design approaches have effectively incorporated Vesic's findings by specifying an upper limit to the shaft and base resistances. For example, McClelland et al. (1969) have suggested, for medium-dense clean sand the following design parameters: $\phi'_a = 30°$; $K_s = 0.7$ (compression loads) or 0.5 (tension loads), with a maximum value of shaft resistance f_s of 1 ton/ft^2 (96 kN/m^2); and $N_q = 41$, with a maximum base resistance f_b of 100 ton/ft^2 (9.6 MN/m^2). However, such approaches take little account of the nature of the sand and may not accurately reflect the variation of pile capacity with pile penetration, as the limiting resistances generally will only become operative at relatively large penetrations (of the order of 30 to 40 m).

In order to develop a method of ultimate load prediction that better represents the physical reality than the conventional approaches, and yet is not excessively complicated, an idealized distribution of effective vertical stress σ'_v with depth adjacent to a pile is shown in Fig. 3.9. σ'_v is assumed to be equal to the overburden pressure to some critical depth z_c, beyond which σ'_v remains constant. The use of this idealized distribution, although simplified, leads to the two main characteristics of behavior observed by Vesic: namely, that the average ultimate skin resistance and the ultimate base resistance become constant beyond a certain depth of penetration.

If the pile-soil adhesion c_a and the term cN_c are taken as zero in Eq. (3.7), and the term $0.5\gamma d\, N_\gamma$ is neglected as being small in relation to the term involving N_q, the ultimate load capacity of a single pile in sand may be expressed as follows:

$$P_u = \int_0^L F_\omega C\sigma'_v K_s \tan\phi'_a .dz + A_b \sigma'_{vb} N_q - W \quad (3.15)$$

where

σ'_v = effective vertical stress along shaft
= effective overburden stress for $z \leqslant z_c$ or limiting value σ'_{vc} for $z \geqslant z_c$
σ'_{vb} = effective vertical stress at level of pile base
F_ω = correction factor for tapered pile (= 1 for uniform diameter pile)

On the basis of the test results of Vesic (1967), values of $K_s \tan \phi'_a$ and the dimensionless critical depth z_c/d have been evaluated. Vesic's results are presented in terms of the relative density D_r of the sand, but the results may also be expressed in terms of the angle of internal friction ϕ', by using a relationship such as that suggested by Meyerhof (1956):

$$\phi' = 28 + 15D_r \tag{3.16}$$

Relationships between $K_s \tan \phi'_a$ and ϕ', and z_c/d and ϕ', are shown in Fig. 3.10. In a layered-soil profile, the critical depth z_c refers to the position of the pile embedded in the sand. It should be emphasized that these relationships may be subject to amendment in the light of further test results. For example, at present, the dependence of $K_s \tan \phi'_a$ on the pile material is not defined. Vesic's tests were carried out on steel tube piles, but the values of $K_s \tan \phi'_a$ derived from these tests appear to be applicable to other pile materials. However, in the light of future test results, it may be possible to derive different relationships for different pile materials.

For bored or jacked piles, the values of $K_s \tan \phi'_a$ in Fig. 3.10*b* are considered to be far too large, and it is suggested that values derived from the data of Meyerhof (1976) are more appropriate for design. These values are shown in Fig. 3.10*c*, and have been obtained by assuming $\phi'_a = 0.75\phi'$. The values for bored piles are reasonably consistent with, although more conservative than, those recommended by Reese, Touma, and O'Neill (1976). Also shown are values of $K_s \tan \phi'_a$ for driven piles, derived from Meyerhof's data; these latter values are considerably smaller (typically about one half) of the values given in Fig. 3.10*b*. Some of this difference may lie in the method of interpretation of the data of Vesic and others by Meyerhof, which leads to smaller values of $K_s \tan \phi'_a$ associated with larger values of z_c/d.

The bearing capacity factor N_q is plotted against ϕ in Fig. 3.11, these values being based on those derived by Berezantzev et al. (1961). Vesic (1967) has pointed out that there is a great variation in theoretical values of N_q derived by different investigators, but the values of Berezantzev et al. appear to fit the available test data best.

The solutions given by Berezantzev et al. indicate only a small effect of relative embedment depth L/d, and the curve in Fig. 3.11 represents an average of this small range. The curves given by Meyerhof (1976) show a larger effect

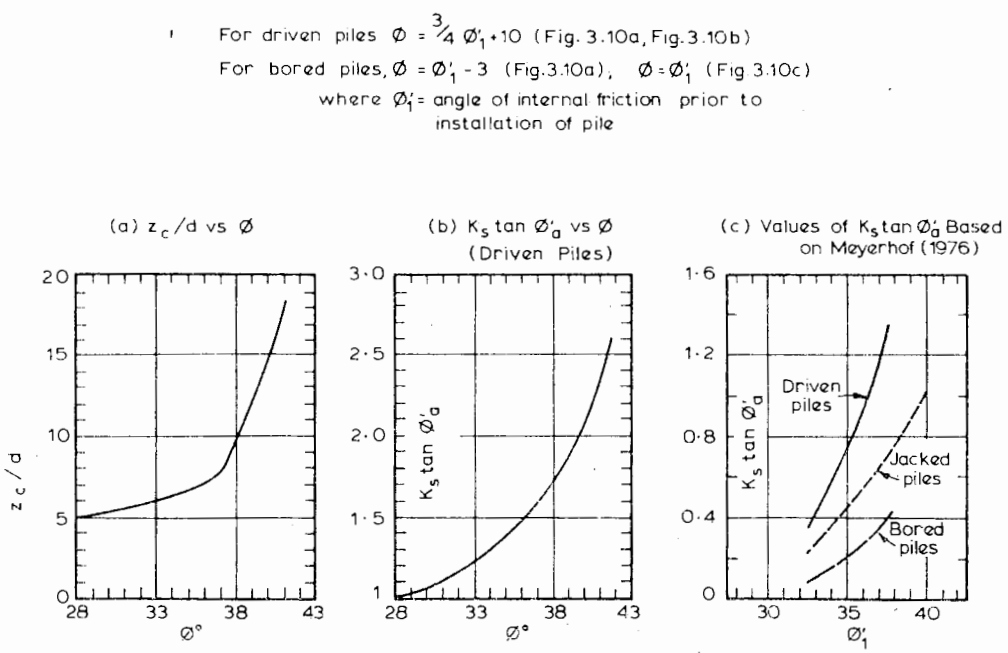

FIGURE 3.10 Values of z_c/d and $K_s \tan \phi'_a$ for piles in sand.

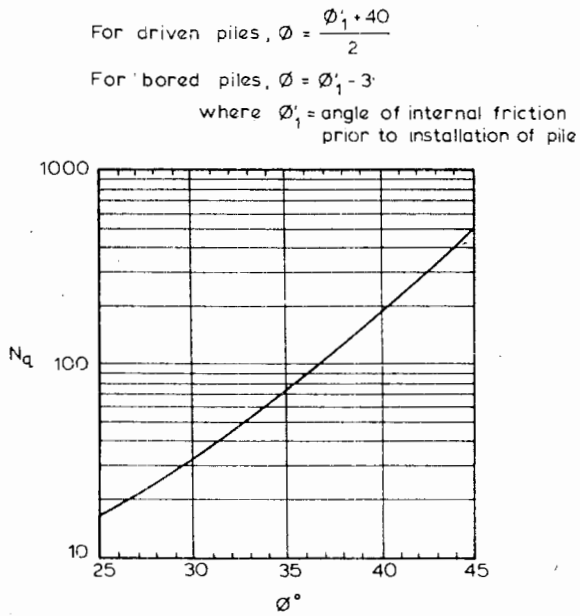

FIGURE 3.11 Relationship between N_q and ϕ (after Berezantzev et al., 1961).

of L/d; however, the curve of Fig. 3.11 also lies near the middle of Meyerhof's range.

Values of the taper correction factor F_ω are plotted against ϕ in Fig. 3.12 and have been derived from the results of the analysis developed by Nordlund (1963).

In applying the results in Fig. 3.10 to Fig. 3.12, it is suggested that the following values of ϕ be used to allow for the effects of pile installation.

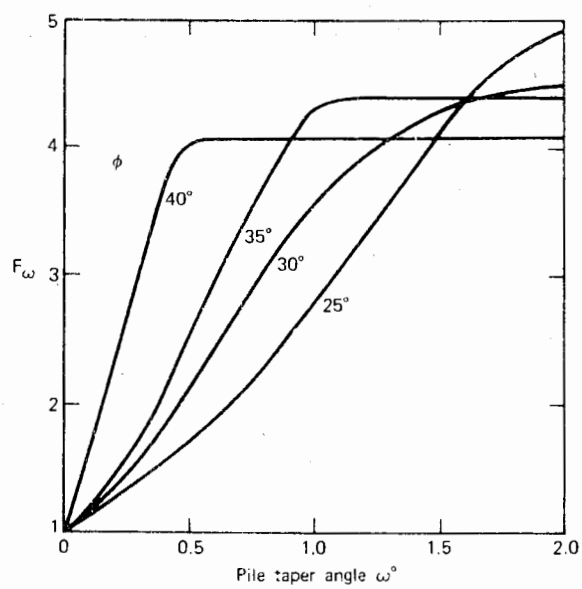

FIGURE 3.12 Pile taper factor F_ω (after Nordlund, 1963).

(a) Driven Piles

(a) For the determination of N_q, the values of ϕ beneath the pile top should be taken as the final value subsequent to driving, as given by Kishida (1967):

$$\phi = \frac{\phi'_1 + 40}{2} \tag{3.17}$$

where

ϕ'_1 = angle of internal friction prior to installation of the pile

(b) For the determination of $K_s \tan \phi'_a$ and z_c/d, the value of ϕ along the pile shaft should be taken as the mean of the values prior to, and subsequent to, driving; that is,

$$\phi = \frac{3}{4}\phi'_1 + 10 \tag{3.18}$$

(b) Bored Piles

(a) For the determination of N_q and z_c/d, it is suggested that the value of ϕ be taken as $\phi'_1 - 3$, to allow for the possible loosening effect of installation (see Section 2.4).
(b) For $K_s \tan \phi'_a$, Fig. 3.10*c* should be used, taking the value of ϕ'_1 directly.

The above suggestions may also require modification in the light of future investigations. Furthermore, if jetting is used in conjunction with driving, the shaft resistance may decrease dramatically and be even less than the value for a corresponding bored pile.

McClelland (1974) has reported tests in which the use of jetting with external return flow followed by driving reduced the ultimate shaft capacity by about 50%, while installation by jetting alone reduced the ultimate shaft capacity to only about 10% of the value for a pile installed by driving only.

Another case in which caution should be exercised is when piles are to be installed in calcareous sands. Such sands may show friction angles of 35° or more, but have been found to provide vastly inferior support for driven piles than normal silica sands. In such cases, McClelland (1974) suggests limiting the skin resistance to 0.2 tons/ft^2 (19 kN/m^2) and base resistance to 50 tons/ft^2 (4800 kN/m^2). In such circumstances, drilled and grouted piles may provide a more satisfactory solution than wholly driven piles.

In many practical cases, only standard penetration-test data may be available. The value of ϕ'_1 may be esti-

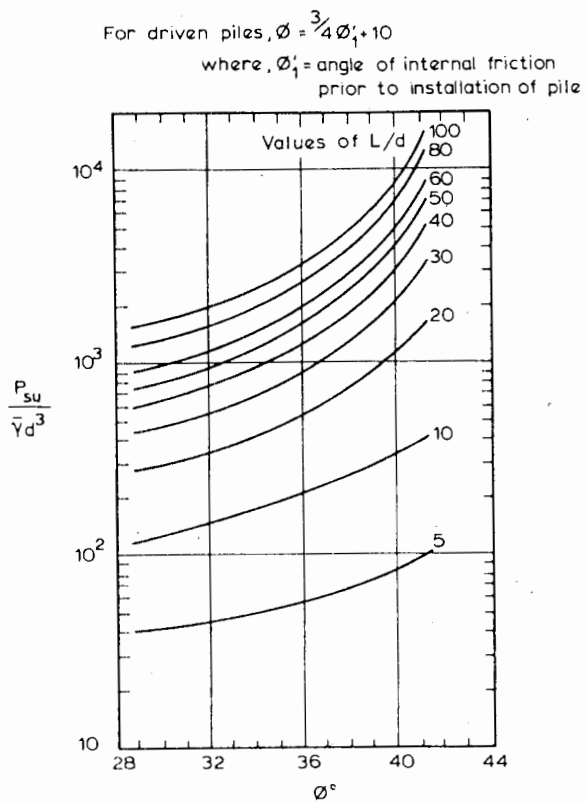

FIGURE 3.13 Dimensionless ultimate shaft-load capacity for pile in uniform sand.

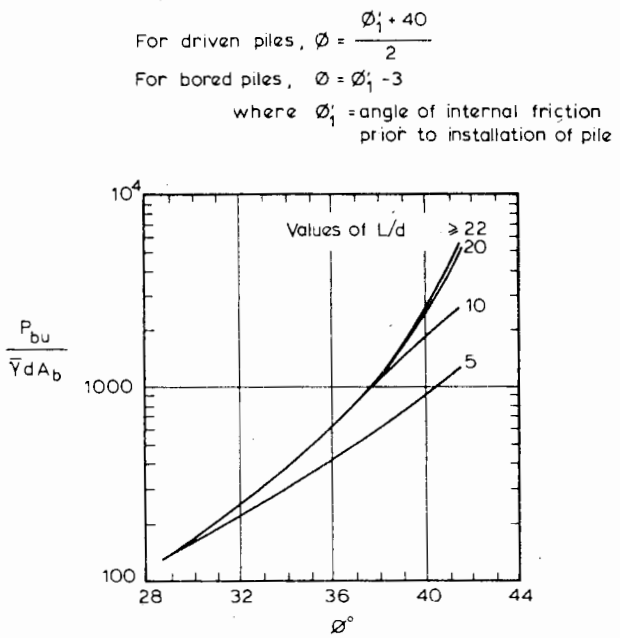

FIGURE 3.14 Dimensionless ultimate base-load capacity for pile in uniform sand.

mated from a correlation such as that given by Peck, Hansen, and Thorburn (1974), or by the following empirical relationship suggested by Kishida (1967):

$$\phi'_1 = \sqrt{20N} + 15^\circ \tag{3.19}$$

where

N = standard penetration number

A more detailed discussion of the relationship between ϕ'_1 and N, and also ϕ'_1 and relative density D_r, is given by de Mello (1971).

For the case of a driven pile in a uniform layer of sand, dimensionless values of the ultimate shaft load and ultimate base load may be derived using Eq. (3.15) and Figs. 3.10, 3.11, and 3.12. In Fig. 3.13, the dimensionless ultimate shaft load $P_{su}/\bar{\gamma}d^3$ is plotted against ϕ for various values of L/d; $\bar{\gamma}$ is the effective unit weight of the soil above the critical depth z_c. The marked increase in ultimate shaft load with increasing L/d and ϕ is clearly shown. The dimensionless ultimate base load $P_{bu}/\bar{\gamma}dA_b$ is plotted against ϕ in Fig. 3.14. The value of L/d does not generally have a marked effect on the ultimate base load unless ϕ is relatively large, that is, for dense sands.

The use of a high value of ϕ for very dense sands (say, $\phi > 40^\circ$) simultaneously for the shaft and the base, should also be treated with caution, since the full base resistance may well only be mobilized after a movement sufficient for the operative value of ϕ along the shaft to be significantly less than the peak.

If the pile is founded in a relatively thin, firm stratum underlain by a weaker layer, the ultimate base load may be governed by the resistance of the pile to punching into the weaker soil. Meyerhof (1976) shows that if the weaker layer is situated less than about 10 base diameters below the base, a reduction in base capacity can be expected; he suggests that in such cases, the ultimate point resistance can be taken to decrease linearly from the value at $10d_b$ above the weaker layer to the value at the surface of the weaker layer.

The suggested approach of ultimate load calculation has been applied to 43 reported load-tests on driven piles. The details of the parameters chosen for the calculations are given in Table 3.3, and the comparison between calculated and measured ultimate loads is shown in Fig. 3.15. The mean ratio of calculated to observed ultimate loads is 0.98, with a standard deviation of 0.21. It should be pointed out that the ultimate load of all piles considered in the comparison is less than 300 tons. The use of this

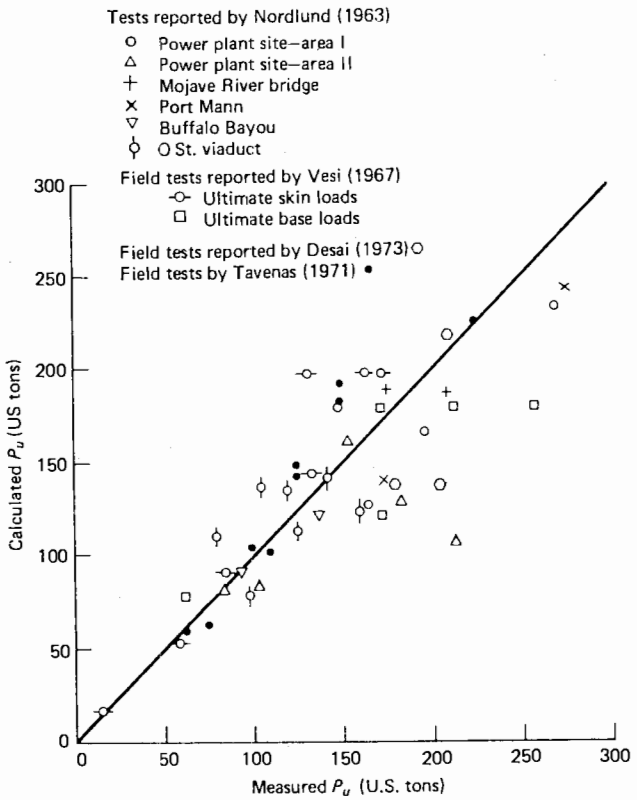

FIGURE 3.15 Comparison between calculated and measured ultimate load capacity of driven piles in sand.

approach for piles of much larger capacity—those used for offshore structures for example—should be treated with caution. Indeed, for relatively short, larger-diameter piles, the average values of shaft resistance given by this approach are considerably larger than those normally adopted for design purposes (for example, the values suggested by McClelland et al., 1969). These high values arise because of the combination of high values of K_s tan ϕ'_a (Fig. 3.10*b*) with a relatively large critical depth. In such cases, a more conservative estimate of shaft resistance may be desirable for design, based on the values of K_s tan ϕ'_a derived from Meyerhof (1976) and shown in Fig. 3.10*c*.

To illustrate the application of the suggested method of calculation, the following example details calculations for two of the pile tests reported by Nordlund (1963).

Illustrative Example

The piles considered are Piles B and A from the Power Plant Site, Area I, Helena, Ark. Pile B was a closed-end steel-pipe pile, 24.4 m long and 0.32 m in diameter, driven into fine sand grading to coarse and having an average

TABLE 3.3 SUMMARY OF COMPARISONS BETWEEN CALCULATED AND OBSERVED LOAD CAPACITY OF PILES IN SAND

Reference	Case	Remarks
Nordlund (1963)	Power Plant Site-Areas I & II	Values of ϕ'_1 suggested by Nordlund used
	Mojave River Bridge	Upper 14 ft of sand assumed to have lower ϕ'_1 (38°) than lower depths (ϕ'_1 = 40°) because of jetting during installation
	Port Mann	Values of ϕ'_1 suggested by Nordlund used
	Buffalo Bayou	Values of ϕ'_1 suggested by Nordlund used
	Interchange	Vertical stress due to soil above excavation level ignored
	O Street Viaduct	As above; H-pile treated as a square pile
Vesic (1967)	Piles H11-H16 & H2	From reported N values, following values of ϕ chosen: 0-12 ft, ϕ'_1 = 33°; 12-30 ft, ϕ'_1 = 38°; 30+ ft, ϕ'_1 = 42°
Desai (1973)	Piles 2,3,10	ϕ'_1 assumed to be 33°, constant with depth
Tavenas (1971)	Piles H2-6, J2-6	ϕ'_1 assumed to be 33°, constant with depth

standard penetration value, N, of about 16. The water table was 3.4 m below the surface. On the basis of the available data, the following values were adopted:

(a) Bulk unit weight above water table = 17.3 kN/m^3.
(b) Submerged unit weight below water table = 7.8 kN/m^3
(c) Angle of internal friction angle prior to installation:

ϕ'_1 = 25° (0 - 2.4 m)
ϕ'_1 = 32° (2.4 - 18.3 m)
ϕ'_1 = 30° (18.3 - 20.8 m)
ϕ'_1 = 33° (> 20.8 m)

Considering first the ultimate skin resistance, the values of ϕ given by Eq. (3.18) are as follows:

ϕ = 28.75° (0–2.4 m)
ϕ = 34° (2.4–18.3 m)

$\phi = 32.5^\circ$ (18.3–20.8 m)
$\phi = 34.75^\circ$ (> 20.8 m)

From Fig. 3.10b, the values of $K_s \tan \phi'_a$ are 1.00 (0–2.4 m), 1.30 (2.4–18.3 m), 1.18 (18.3–20.8 m), 1.35 (20.8 m). If it is assumed that the critical depth is less than 2.4 m below the surface, then for $\phi = 28.75^\circ$, $z_c/d = 5.0$, from Fig. 3.10a; that is, $z_c = 5.0 \times 0.32 = 1.56$ *m*. Thus, the assumption is justified.

At the critical depth, the effective overburden stress is

$$\sigma'_{vc} = 1.56 \times 17.3 = \mathbf{26.99\ kN/m^2}$$

Because the pile has uniform diameter, $F_\omega = 1$.

For the ultimate base resistance, the value of ϕ given by Eq. (3.17) is 36.5°. From Fig. 3.11, the value of N_q is 98.

Substituting into Eq. (3.15),

$$\begin{aligned} P_u = {} & \pi \times 0.32 \left\{ \left[\left(\frac{0 + 26.99}{2} \right) \times 1.56 + 26.99 \times (2.4 - 1.56) \right] \times 1.00 \right. \\ & + 26.99 \times (18.3 - 2.4) \times 1.30 + 26.99 \times (20.8 - 18.3) \\ & \left. \times 1.18 + 26.99 \times (24.4 - 20.8) \times 1.35 \right\} \\ & + 26.99 \times \pi \times \frac{0.32^2}{4} \times 98 \\ = {} & 816 + 213 \\ = {} & \mathbf{1029\ kN\ (115.6\ t)} \end{aligned}$$

This compares with the measured value of **1112 kN (125 t)**.

Pile A was a Raymond Standard pile, 10 m long, with a head diameter of 0.55 m and a tip diameter of 0.20 m. The pile taper ω is 1°. From Fig. 3.12, for $\omega = 1^\circ$, $F_\omega = 3.35$ (0–2.4 m), and $F_\omega = 4.1$ (2.4–18.3 m). The values of $K_s \tan \phi'_a$ are as for pile B. Assuming again that the critical depth is above 2.4 m, $z_c/d = 5.0$ as before, and taking an average value of d of 0.51, $z_c = 2.55$ m, that is, greater than 2.4 m. However, the difference is negligible and hence z_c will be taken as 2.55 m. At this level,

$$\sigma'_{vc} = 2.55 \times 17.3 = \mathbf{44.12\ kN/m^2}$$

At 2.4 m,

$$\sigma'_v = 2.4 \times 17.3 = 41.52\ \text{kN/m}^2$$

Since the pile tip is founded in the second stratum, ϕ from Eq. (3.17) is 36° and the corresponding value of N_q is 88.

Substituting into Eq. (3.15) and using, for simplicity, the mean diameter of the pile in the upper 2.4 m and the lower 7.6 m,

$$\begin{aligned} P_u = {} & \left(\frac{0 + 41.52}{2} \right) \times \pi \times 0.51 \times 3.35 \times 1.00 \times 2.4 \\ & + \left[\frac{(41.52 + 44.12)}{2} \times 0.15 + 44.12 \times (10 - 2.55) \right] \\ & \times \pi \times 0.33 \times 4.1 \times 1.30 + 44.12 \times \pi \times \frac{0.20^2}{4} \\ & \times 88 \\ = {} & 2243\ \text{kN (252.2t)} \end{aligned}$$

The measured ultimate load for this pile was **2400 kN (270 t)**.

3.3 PILE GROUPS

In examining the behavior of pile groups, it is necessary to distinguish between two types of group:

(a) A free-standing group, in which the pile cap is not in contact with the underlying soil.
(b) A "piled foundation," in which the pile cap is in contact with the underlying soil.

For both types, it is customary to relate the ultimate load capacity of the group to the load capacity of a single pile through an efficiency factor η, where

$$\eta = \frac{\text{ultimate load capacity of group}}{\text{sum of ultimate load capacities of individual piles}} \qquad (3.20)$$

3.3.1 Pile Groups in Clay

3.3.1.1 FREE-STANDING GROUPS

For free-standing groups of friction or floating piles in clay, the efficiency is unity at relatively large spacings, but decreases as the spacing decreases. For point-bearing piles, the efficiency is usually considered to be unity for all spacings—that is, grouping has no effect on load capacity, although in theory the efficiency could be greater than unity for closely-spaced piles that are point-bearing, for example, in dense gravel. For piles that derive their load capacity from both side-adhesion and end-bearing, Chellis (1962) recommends that the group effect be taken into consideration for the side-adhesion component only.

Several empirical efficiency formulas have been used to try and relate group efficiency to pile spacings, among which are the following:

(a) Converse-Labarre formula,

$$\eta = 1 - \xi \left[\frac{(n-1)m + (m-1)n}{mn}\right] /90 \qquad (3.21)$$

where

m = number of rows
n = number of piles in a row
ξ = arctan d/s, in degrees
d = pile diameter
s = center-to-center spacing of piles

(b) Feld's rule, which reduces the calculated load capacity of each pile in a group by 1/16 for each adjacent pile, that is, no account is taken of the pile spacing.
(c) A rule of uncertain origin, in which the calculated load capacity of each pile is reduced by a proportion I for each adjacent pile where

$$I = \frac{1}{8}d/s \qquad (3.22)$$

A comparison made by Chellis (1962), between these and other empirical formulas shows a considerable variation in values of η for a given group, and since there appears to be little field evidence to support the consistent use of any empirical formula, an alternative means of estimating group efficiency is desirable.

One of the most widely used means of estimating group-load capacity is that given by Terzaghi and Peck (1948), whereby the group capacity is the lesser of (a) The sum of the ultimate capacities of the individual piles in the group; or (b) the bearing capacity for block failure of the group, that is, for a rectangular block $B_r \times L_r$,

$$P_B = B_r L_r c N_c + 2(B_r + L_r) L\bar{c} \qquad (3.23)$$

where

c = undrained cohesion at base of group
L = length of piles
N_c = bearing capacity factor corresponding to depth L (see Fig. 3.5)
$\bar{c}$ = average cohesion between surface and depth L

Model tests on free-standing groups carried out by Whitaker (1957) confirmed the existence of the above two types of failure. For a given length and number of piles in a group, there was a critical value of spacing at which the mechanism of failure changed from block failure to individual pile failure. For spacings closer than the critical value, failure was accompanied by the formation of vertical slip planes joining the perimeter piles, the block of clay enclosed by the slip planes sinking with the pile relative to the general surface of the clay. For wider spacings, the piles penetrated individually into the clay. The critical spacing was found to increase as the number of piles in the group increased.

Although Whitaker's tests confirmed the existence of the above two types of failure, the transition between the ultimate group capacity as given by individual pile failure and that given by block failure was not as abrupt as the Terzaghi and Peck approach suggests. In order to obtain a more realistic estimate of the ultimate load capacity of a group, the following empirical relationship is suggested:

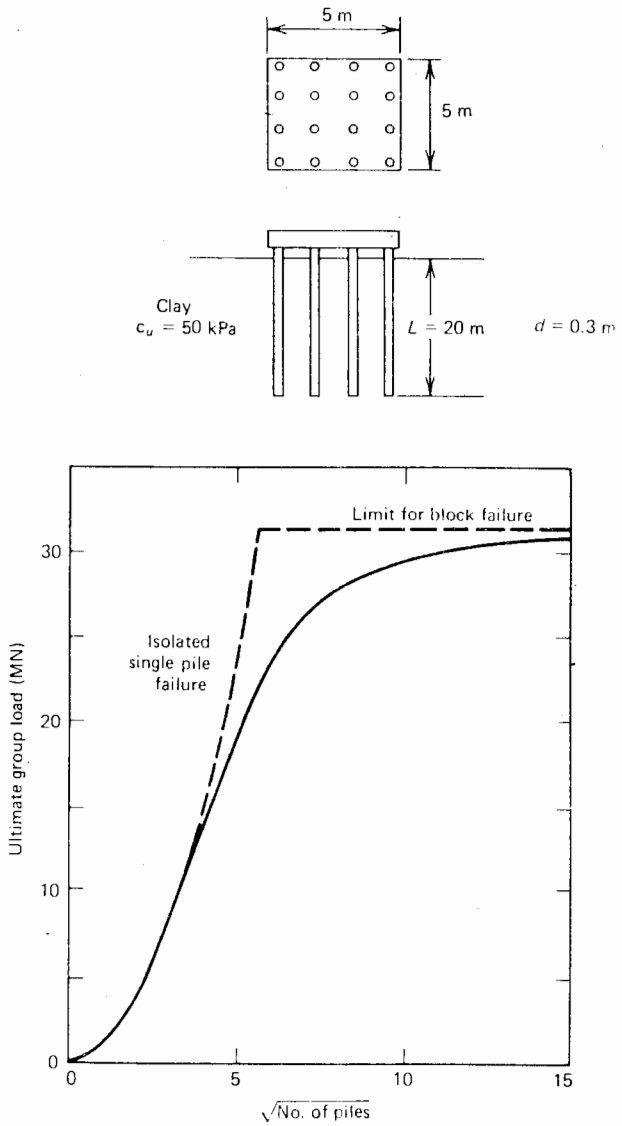

FIGURE 3.16 Example of relationship between number of piles and ultimate load capacity of group.

$$\frac{1}{P_u^2} = \frac{1}{n^2 P_1^2} + \frac{1}{P_B^2} \tag{3.24}$$

where

P_u = ultimate load capacity of group
P_1 = ultimate load capacity of single pile
n = number of piles in group
P_B = ultimate load capacity of block (Eq. 3.23)

Eq. (3.24) may be reexpressed as follows:

$$\frac{1}{\eta^2} = 1 + \frac{n^2 P_1^2}{P_B^2} \tag{3.25}$$

where

η = group efficiency

Figure 3.16 illustrates an example of the relationship between the ultimate load capacity of a group of specified dimensions and the number of piles in the group, calculated using Eq. (3.24). This figure shows the transition between single-pile failure and block failure as the number of piles increases. In the design of such a group, it is obvious that virtually no advantage is gained by using more piles than is required to cause failure of the group as a block; in the example in Fig. 3.16, increasing the number of piles beyond about 80 produces very little increase in ultimate load capacity.

A considerable number of model tests have been carried out to determine group efficiency factors in homogeneous clay—for example, Whitaker (1957), Saffery and Tate (1961), and Sowers et al. (1961). A summary of some of these tests has been presented by de Mello (1969) and is reproduced in Fig. 3.17. From this summary, it may be seen that higher efficiency factors occur for

(a) Piles having smaller length-to-diameter ratios.
(b) Larger spacings.
(c) Smaller numbers of piles in the group.

For spacings commonly used in practice (2.5d to 4d), η is on the order of 0.7 to 0.85, and little increase in η occurs beyond these spacings, except for large groups of relatively long piles.

Figures 3.18 and 3.19 show comparisons between the measured efficiency-spacing relationships from the tests of Whitaker (1957) and those calculated from Eq. (3.25). The agreement is generally quite good and the method of

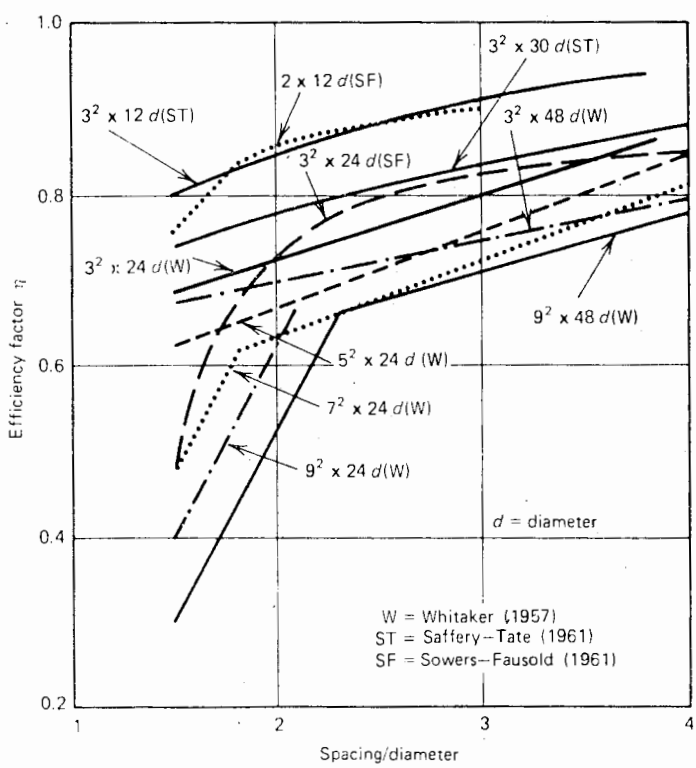

FIGURE 3.17 Relationships for freestanding groups of 2^2 to 9^2 piles of lengths 12d to 48d, from model tests (after de Mello, 1969).

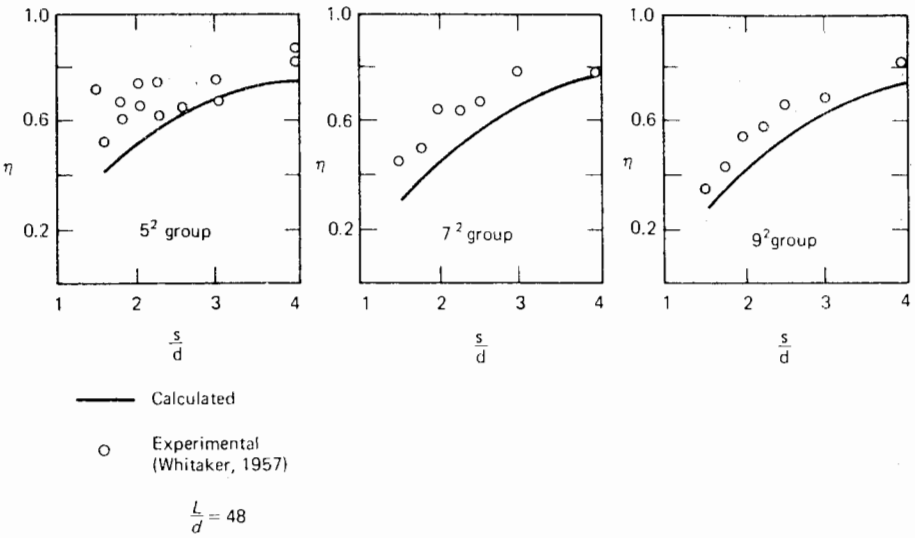

FIGURE 3.18 Experimental and calculated group efficiency, effect of group size.

calculation appears to predict with reasonable accuracy the effects of group size, pile spacing, and pile length.

It has often been assumed that all piles in a group are equally loaded. However, if the group supports a rigid cap, the load distribution within the group is generally not uniform, the outer piles tending to be more heavily-loaded than the piles near the center. Whitaker (1957) has measured the load carried by the piles in model free-standing groups in clay by introducing a small load gauge at the head of each pile. The results for a 3^2 group of piles at three different spacings are shown in Fig. 3.20, in which the average percentage of load taken by each pile is plotted against the group load as a percentage of the group load at failure. At spacings of $2d$ and $4d$, the corner piles take the greatest load (about 13 to 25% more than the average load) while the center pile takes the least (about 18 to 35% less than the average). At a spacing of $8d$, virtually no group action was observed and the load distribution was uniform. The load distribution for a 5^2 group, at a spacing of $2d$, is shown in Fig. 3.21. The corner piles reached their maximum load at about 80% of the ultimate group load, and carried a constant load thereafter. At failure, the corner piles carried about 28% more than the average load, while the center and lightest-loaded pile carried about 44% less. Therefore, there appears to be a tendency for the load distribution to become increasingly nonuniform as the number of piles in the group increases. A theoretical method for calculating the load distribution prior to ultimate failure is described in Chapter 6, and this method also confirms the trends displayed by Whitaker's tests.

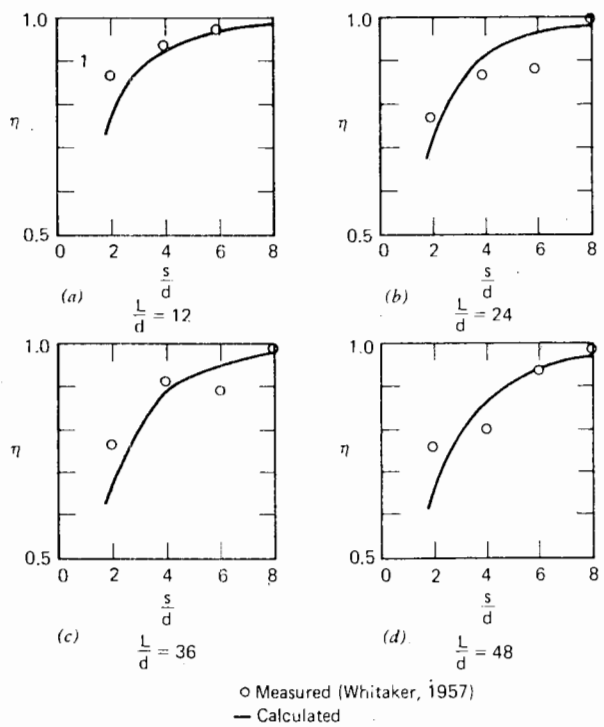

FIGURE 3.19 Effect of pile length on group efficiency.

3.3.1.2 PILED FOUNDATIONS

The ultimate load capacity of a piled foundation (i.e., a pile group having a cap cast on or beneath the surface of the soil) may be taken as the lesser of the following two values:

(a) The ultimate load capacity of a block containing the piles (Eq. 3.23) plus the ultimate load capacity of that portion of the cap outside the perimeter of the block.

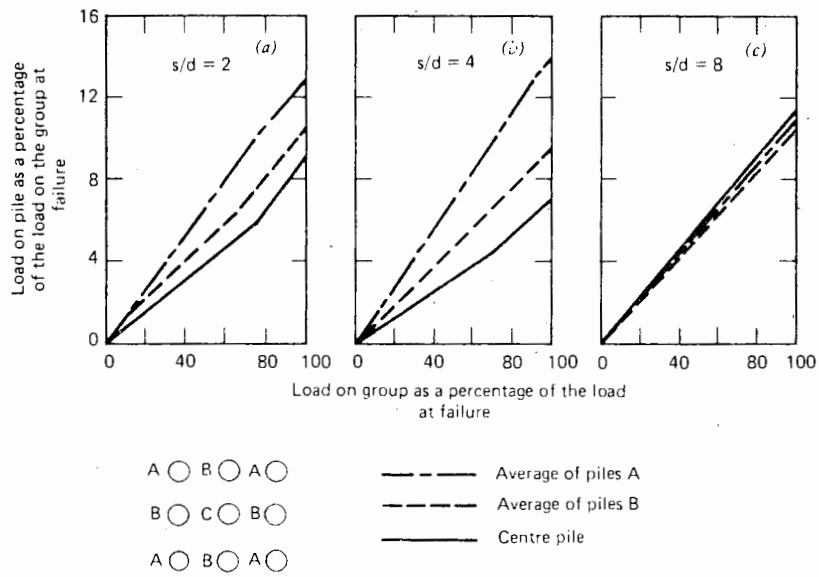

FIGURE 3.20 Load distribution in 3^2 pile group (Whitaker, 1970).

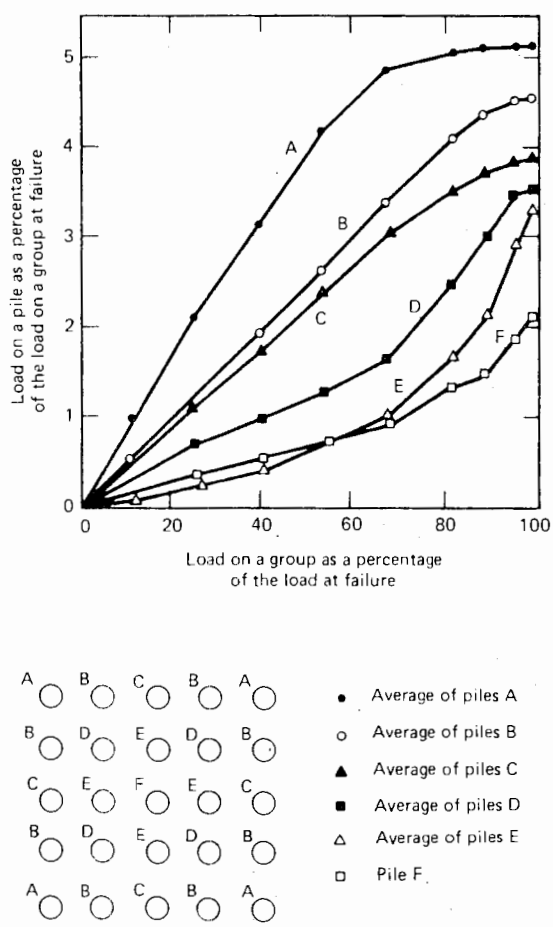

FIGURE 3.21 Load distribution in 5^2 pile group at $2d$ spacing (Whitaker, 1970).

(b) The sum of the ultimate load capacity of cap and the piles, acting individually, that is, for group of n piles of diameter d and length L, supported by a rectangular cap of dimensions $B_c \times L_c$,

$$P_u = n(\bar{c}_a A_s + A_b\, c_b\, N_c) + N_{cc} c_c \cdot (B_c L_c - n\pi d^2/4) \tag{3.26}$$

where

$\bar{c}_a$ = average adhesion along pile
c_b = undrained cohesion at level of pile tip
c_c = undrained cohesion beneath pile cap
N_c = bearing capacity factor for pile (see Fig. 3.5)
N_{cc} = bearing capacity factor for rectangular cap $B_c \times L_c$ ($L_c > B_c$) $\simeq 5.14\,(1 + 0.2\, B_c/L_c)$ (Skempton 1951)

The first value will apply for close pile-spacings while the second will apply at wider spacings when individual action can occur.

Whitaker (1960) carried out tests on model piled foundations in clay and found that at close spacings, block failure occurred, and that when the cap did not extend beyond the perimeter of the group, it added nothing to the efficiency of the group. At greater spacings, the efficiency-versus-spacing relationship was found to be an extension of the relationship for block failure, with the efficiency exceeding unity because of the effect of the cap. Good agreement was

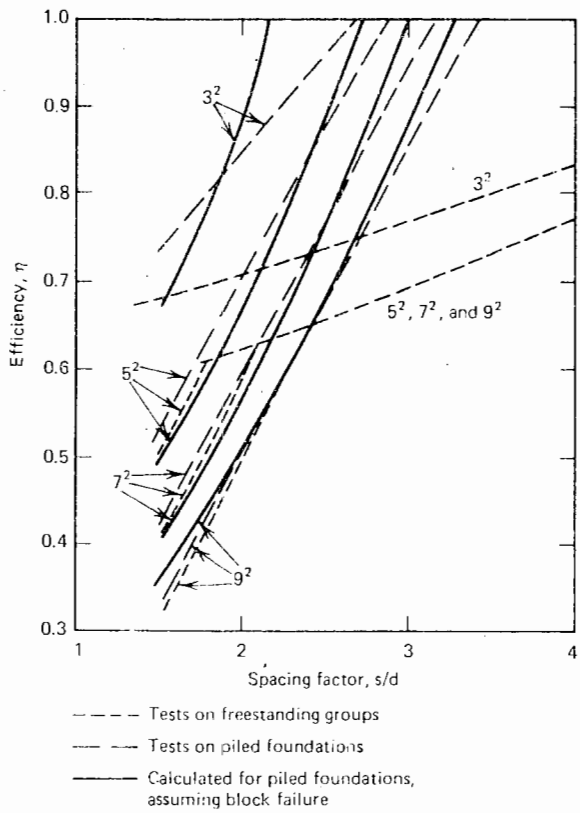

FIGURE 3.22 Efficiency of piled groups (Whitaker, 1970).

obtained between the model test results and the predicted efficiency from the block failure equation (Fig. 3.22).

The load-settlement behavior of piled foundations containing a relatively small number of piles to reduce settlement is considered in detail in Chapter 10.

3.3.1.3 ECCENTRIC LOADING

Model tests on groups with small eccentricities of load have been carried out by Saffery and Tate (1961), who found that for eccentricities up to two thirds of the spacing, the group efficiency is not noticeably affected. Meyerhof (1963) also reported that model tests on piled foundations showed that the load eccentricity had no effect on load capacity for eccentricities up to half the group width. This behavior is explained by the fact that the reduced base resistance is offset by mobilization of lateral resistance. The group capacity can therefore be calculated as for symmetrical vertical loading, except that for groups whose width is on the same order as the pile length, Meyerhof (1963) suggests that the shaft resistance can be ignored and the base resistance calculated in a fashion similar to eccentrically-loaded spread foundations, that is, using a reduced effective base area.

3.3.2 Pile Groups in Sand

3.3.2.1 FREESTANDING GROUPS

There is less information on pile groups in sand than on groups in clay, but it has been fairly well established that group efficiencies in sand may often be greater than 1. A summary of some of the available data on larger piles is given in Table 3.4.

A summary of some tests on model piles, presented by Lo (1967), is reproduced in Fig. 3.23. The data shown in this figure are reasonably consistent with the data in Table 3.4. Results of tests on somewhat larger model piles, in groups of four and nine, carried out by Vesic (1969), are shown in Fig. 3.24. Vesic measured the point load separately from the shaft resistance, and in the light of his measurements, he concluded that when the efficiency of closely spaced piles was greater than unity, this increase was in the shaft rather than the point resistance.

The broad conclusion to be drawn from the above data is that unless the sand is very dense or the piles are widely spaced, the overall efficiency is likely to be greater than 1. The maximum efficiency is reached at a spacing of 2 to 3 diameters and generally ranges between 1.3 and 2.

3.3.2.2 INFLUENCE OF PILE CAPS

As can be seen in Fig. 3.24, the pile cap can contribute significantly to the load capacity of the group, particularly in the case of the smaller four-pile groups. However, it seems likely that mobilization of the bearing capacity of the full area of the cap requires considerably greater movement than that required to mobilize the capacity of the piles themselves. This is the implication of tests by Vesic, and for practical purposes, the contribution of the cap can be taken to be the bearing capacity of a strip footing of half-width equal to the distance from the edge of the cap to the outside of the pile.

3.3.2.3 ECCENTRIC LOADING

The influence of eccentric loading on the load capacity of pile groups in sand has been studied by Kishida and Meyerhof (1965) in a series of model tests. These tests showed that small eccentricities of load have no significant influence on the bearing capacity of freestanding groups and piled groups because the applied moment is resisted mainly by the earth pressure moment on the sides of the group. At larger eccentricities, the load capacity decreases rapidly because of smaller point resistance of the group by a reduction of the effective base area.

In estimating load capacity, Kishida and Meyerhof suggest that the moment caused by a load V at eccentricity

TABLE 3.4 SUMMARY OF TEST DATA ON LARGE-SCALE PILE GROUPS IN SAND

Reference	Soil	Pile Length L	Pile Diameter d	L/d	Group	Spacing d	Group Efficiency η	Remarks
Press (1933)	Medium-grained moist, dense sand	6–10 ft	5 & 6 in.	12–20	2–8	Various	> 1	Driven piles. Max. η of 1.5 at $s/d \cong 2$
		23 ft	16 in.	17	2	Various	< 1.	Bored piles
Cambefort (1953)	Humus/stiff clay/sand/ gravel	100 in.	2 in.	50	2–7	2	1.39	Driven piles Average values of η.
						3	1.64	
						5	1.17	
						9	1.07	
Kezdi (1957)	Moist fine sand	80 in.	4 in. (square)	20	4 (In line)	2	2.1	Driven piles. Max. η at $s/d \cong 2$. η greater for square group.
						3	1.8	
						4	1.5	
						6	1.05	
					4 (square)	2	2.1	
						3	2.0	
						4	1.75	
						6	1.1	

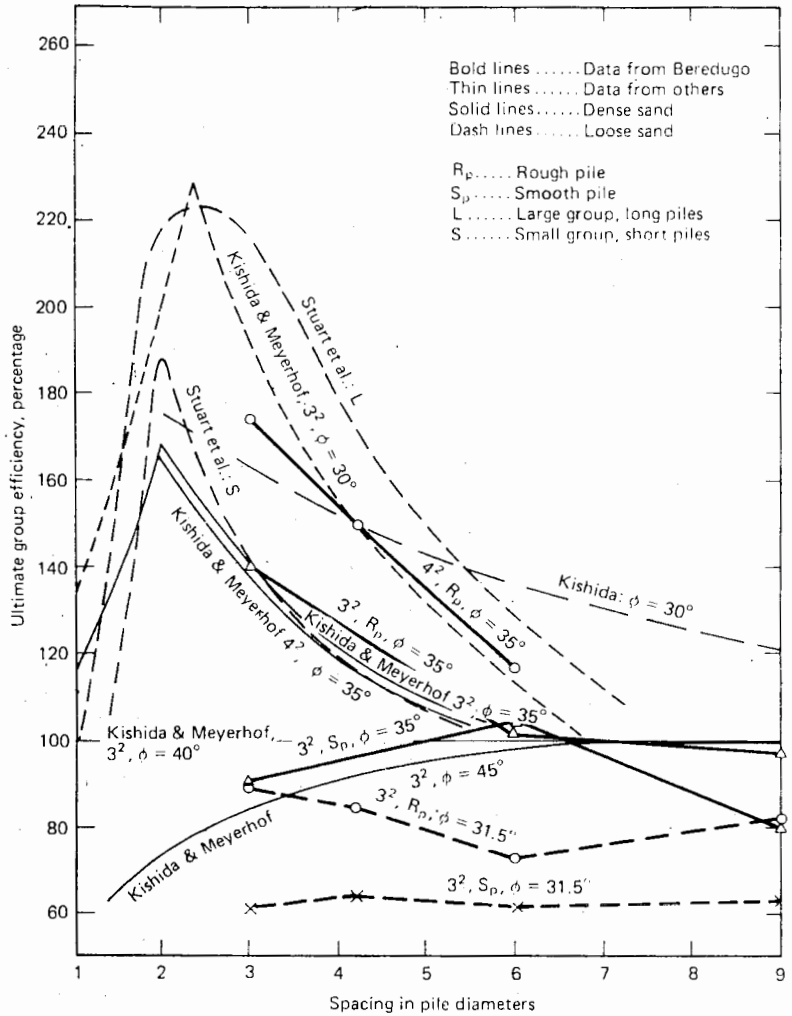

FIGURE 3.23 Measured values of group efficiency in sands–model tests (Lo, 1967). (Reproduced by permission of the National Research Council of Canada from the Canadian Geotechnical Journal, Vol. 4, 1967, pp. 353-354.)

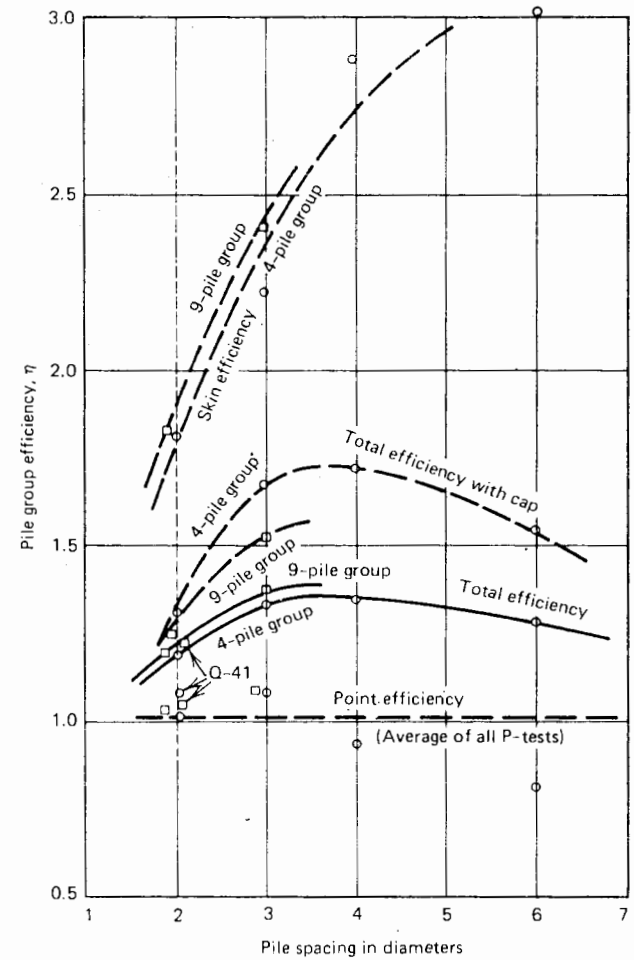

FIGURE 3.24 Pile group efficiencies (Vesic, 1969).

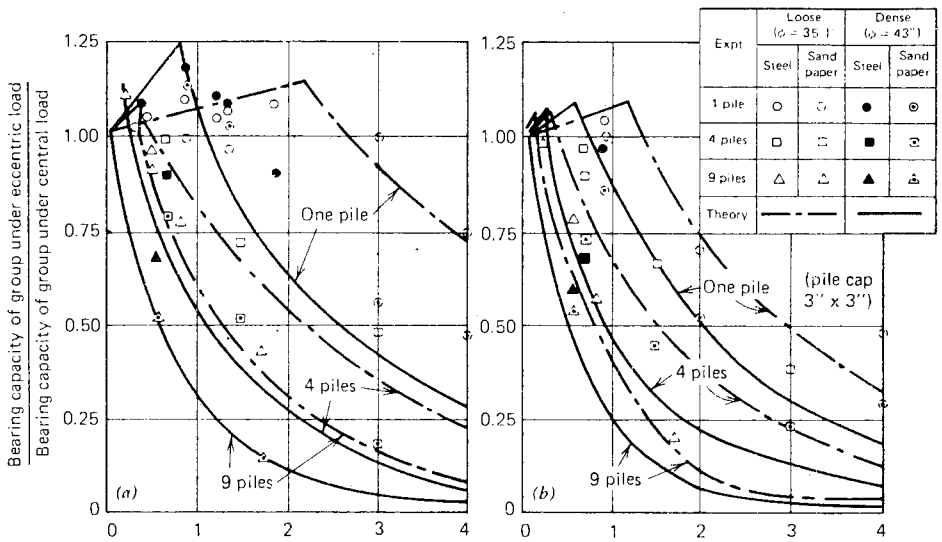

FIGURE 3.25 Bearing capacity of model pile groups under eccentric load in sand: (a) freestanding pile groups; (b) piled foundations (Kishida and Meyerhof, 1965). (Copyright Canada, 1965 by University of Toronto Press.)

e is balanced by the moment caused by lateral forces on the sides of the group until it reaches the maximum value corresponding to the coefficient of passive earth pressure. Within this limit, the eccentricity of load is assumed to have no effect on the point resistance. When the moment Ve is greater than can be resisted by side pressure on the outer piles, the extra is considered to be taken by an eccentric base resistance for the case of block failure; or, for individual pile failure, by the development of uplift resistance of some piles. The total bearing capacity then decreases with further increase in eccentricity.

Comparisons between the theoretical and measured effect of load eccentricity on load capacity are shown in Fig. 3.25 for the tests carried out by Kishida and Meyerhof (1965), and there is fair agreement for tests in both loose and dense sands.

3.3.2.4 LOAD DISTRIBUTION IN GROUP

The most detailed data available on load distribution within groups in sand is that reported by Vesic (1969), who made axial load measurements in individual piles during group placement, as well as during loading tests. For the four-pile groups tested, the measured load distribution was almost uniform, as expected; the maximum deviation from the average was 3 to 7%. For the nine-pile groups, significant nonuniformity of load was measured. The center pile carried about 36% more load than the average, while the corner piles carried about 12% less and the edge piles 3% more. Other tests on similar groups showed a similar trend, with the center piles carrying between 20% and 50% more than the average. These results are in contrast to the load distribution in groups in clay, where the center pile carries the least load and the corner piles the most.

The influence of the order of driving piles in a group on the load distribution has been studied by Beredugo (1966) and Kishida (1967). They found that when the load on the group was relatively small, piles that had been installed earlier carried less load than those that have been installed later; but when the failure load of the group was approached, the influence of driving order diminished, and the position of the pile in the group became the dominant factor. At this stage, the piles near the center took the most load and the corner piles the least, as in Vesic's experiments.

Beredugo also investigated the effects of repeated loading and found that there was a progressive reduction of the influence of driving order, and that for the third and subsequent loadings, the pile position was the dominant factor at all loads up to the ultimate of the group.

3.4 PILES TO ROCK

3.4.1 Point-Bearing Capacity

There are a number of possibl approaches to the estimation of point-bearing capacity of piles to rock, including:

(a) The use of bearing-capacity theories to calculate the ultimate point-bearing capacity p_{bu}.
(b) The use of empirical data to determine the allowable point pressure p_{ba}.
(c) The use of in-situ tests to estimate either ultimate point capacity p_{bu} or allowable point pressure p_{ba}.

Bearing-Capacity Theories

Pells (1977) has classified theoretical approaches into three categories:

1. Methods that essentially assume rock failure to be "plastic" and either use soil mechanics-type bearing-capacity analyses or modifications thereof to account for the curved nature of the peak failure envelope of rock.
2. Methods that idealize the zones of failure beneath a footing in a form that allows either the brittleness-strength ratio or the brittleness-modular ratio to be taken into account.
3. Methods based on limiting the maximum stress beneath the loaded area to a value less than required to initiate fracture. These methods assume essentially that once the maximum strength is exceeded at any point in a brittle material, total collapse occurs.

For a typical sandstone having an effective friction angle ϕ' in excess of 45°, effective cohesion c′ of about one-tenth of the uniaxial strength, q_{um}, and a ratio of Young's modulus-to-uniaxial strength of about 200, Pells shows that the various theories predict an ultimate point-bearing capacity ranging between $4.9q_{um}$ (incipient failure theory based on the modified Griffith theory) to $56q_{um}$ (classical plasticity theory). Various model tests on intact rock carried out by Pells and others indicate ultimate capacities ranging between 4 and 11 times q_{um}. Pells draws attention to the fact that the load-penetration curve for rocks of medium strength or less ($\leq$ 100 MPa) has a large "plastic" component, despite the brittle nature of the rock. The curve divides into two portions, with what appears to be a change of slope associated with the formation of a crushed zone beneath the footing. The displacements required to mobilize the full bearing capacity of such rocks are very large, and it seems that a factor of safety of 3 to 4 is required to limit the displacements to less than 2% of the footing diameter. Very brittle rocks (q_{um} > 150 MPa), do not exhibit this "plastic" load-penetration curve.

The presence of jointing in the rock will tend to reduce the ultimate bearing capacity. The presence of closely-spaced continuous tight joints may not reduce the bearing capacity much below that for the intact rock material. If there are open vertical joints with a spacing less than the width or diameter of the pile point, the point is essentially supported by unconfined rock columns and the bearing capacity may be expected to be slightly less than the average uniaxial strength of the rock. If the joint spacing is much wider than the footing width, Meyerhof (1953) suggests that the crushed zone beneath the footing splits the block of rock formed by the joints. Sowers and Sowers (1970) present a theory for this case that generally indicates a bearing capacity slightly greater than the uniaxial strength. Thus, in summary, theoretical considerations suggest that the ultimate bearing capacity is unlikely to be reduced much below the uniaxial strengtn of the intact rock, even if open vertical joints are present.

Use of Empirical Data

Allowable bearing pressures on rock have often been specified by various building codes and authorities, either based on a description of the rock, or in terms of the

TABLE 3.5 TYPICAL PROPERTIES OF ROCK (PECK, 1969)

Rock Type	Compressive Strength q_{um} (psi)	Shear Strength (psi)	E(10⁶psi)		Poisson's Ratio	
			Field	Lab.	Field	Lab.
Basalt	28,000–67,000		0.8–3.5	3.6– 5.9	0.30–0.32	0.26–0.28
Granite	10,000–38,700	2000–4260	5.6–11.6	5.4–11.8	0.25–0.27	0.17–0.29
Quartzite	16,000–44,800		3.1– 8.5	3.6–12.5	0.25–0.30	0.07–0.17
Limestone	2450–28,400	1200–2980		3.3–11.9		0.24–0.27
Marble	7900–27,000	1280–6530				
Sandstone	4900–20,000	284–2990	1.3– 5.6	1.0– 9.0	0.28–0.30	0.07–0.17
Slate	6950–31,000	1990–3550	1.0– 2.5	5.3– 8.4	0.30–0.32	0.24–0.25
Shale	500–6500				0.26–0.27	0.20–0.25
Concrete	2000–5000	400–1000	2.5– 4.0	2.5– 4.0	0.15	0.15

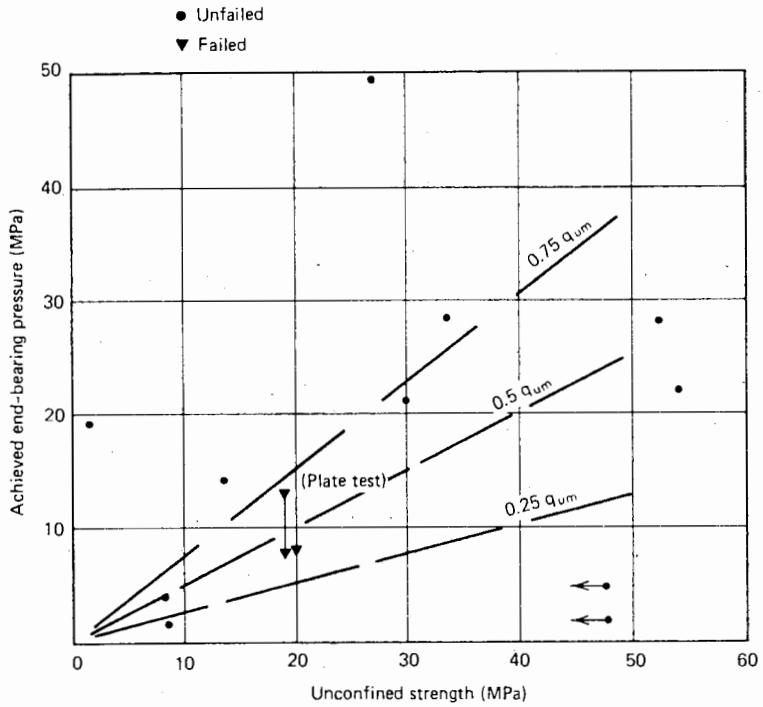

FIGURE 3.26 Achieved end-bearing pressures in field tests on piles to rock (Thorne, 1977).

uniaxial compressive strength q_{um}. Some typical values of q_{um} and other rock properties are summarized in Table 3.5. Typically, allowable pressures, p_{ba}, ranging between 0.2 and 0.5 times q_{um} have been stipulated. An example of stipulated bearing pressures related to rock types is provide by Ordinance No. 70 in New South Wales, Australia, in which values of p_{ba} range between 430 kN/m^2 for soft shale to 3210 kN/m^2 for hard sandstone free from defects to a depth of 900 mm.

Thorne (1977) has collected data on recorded values of bearing capacity, as shown in Fig. 3.26. These values vary from $0.3q_{um}$ to about $4q_{um}$, and most cases do not involve failure. The few recorded failures are in swelling shales and in fractured rocks, it is clear from these results that the fracture spacing has an effect on the bearing capacity, although the data is insufficient to quantify this effect.

On the basis of the available data, an allowable point-bearing pressure on the order of $0.3q_{um}$ would appear to be quite conservative for all but swelling shales. Reference to the theoretical solutions shows that such values generally imply a factor of safety of at least 3 in fractured or closely-jointed rocks and 12 or more for intact rocks.

The Use of In-Situ Tests

A number of methods of in-situ testing of rock have been developed in recent years. Plate-load tests have frequently been used but may be expensive if the rock is strong and large loads are required. Freeman et al. (1972) have described the use of the Ménard Pressuremeter to estimate the allowable point-bearing capacity, p_{ba}, of piles in rock, and suggest that p_{ba} may be taken as the value where the pressure-versus-volume relationship starts to become nonlinear. Satisfactory designs of caissons in sound shale bedrock using the above approach have been reported by Freeman et al., and design pressures considerably larger than those specified by empirical relationships or building codes have been used.

3.4.2 Pile-Rock Adhesion

When piles are socketed or driven into rock, some load transfer to the embedded portion of the shaft will usually occur. Theoretical solutions for load transfer are discussed in Section 5.3, and also by Ladanyi (1977). The distribution of applied load between side-adhesion and end-bearing at working loads, as given by theory, has been supported by in-situ measurements at a number of sites (Pells, 1977). There is not a great amount of data on ultimate values of pile-rock adhesion, but Thorne (1977) has summarized some of the available data, and this summary is reproduced in Fig. 3.27. These results show that a number of failures

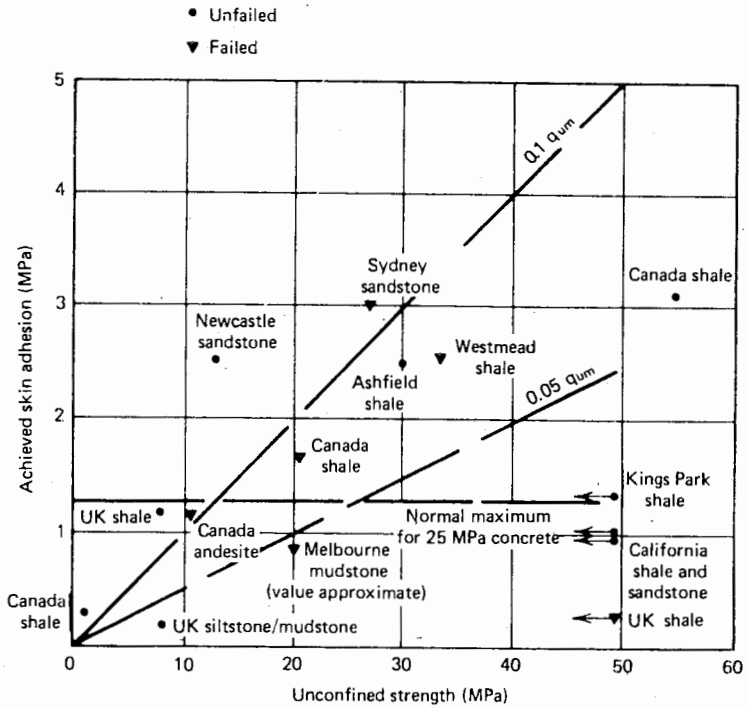

FIGURE 3.27 Adhesion attained in field tests on piles in rock (Thorne, 1977).

have occurred, even in relatively unjointed rocks, at values on the order of $0.1q_{um}$. It should be noted that in many instances, concrete strength will be the limiting factor, and in the few instances in which information is available on concrete strengths, failure has occurred at an average shear-stress of between 0.05 to 0.2 times the ultimate compressure strength of concrete, f'_c. However, the tests of Jaspar and Shtenko (1969) indicated that considerable caution must be exercised with piles in expansive shales that are likely to be affected by water; an adhesion of only about 11 psi (75 kPa) was measured in these tests. Freeman et al. (1972) suggest a design value of allowable pile-rock adhesion of 100 to 150 psi (700 to 1000 kPa), depending on the quality of the rock. With such a value, they recommended that the full calculated end-bearing capacity be added to obtain the total design-load capacity.

On the basis of the limited information available, it would appear reasonable to use as a design value an allowable adhesion of $0.05f'_c$ or $0.05q_{um}$, whichever is the lesser value. These values should not be applied to highly fractured rocks, for which values of adhesion between 75 and 150 kPa may be more appropriate. It must be emphasized that care should be exercised to remove all remolded soil from the socket zone. Furthermore, for uplift loads, a reduction of the above loads (e.g., by about 30%) appears to be desirable.

3.5 USE OF IN-SITU TESTS

3.5.1 Static Cone Penetrometer

The basis of the test is the measurement of the resistance to penetration of a 60° cone with a base area of 10 sq cm. Two types of cone are commonly used; the standard point, with which only point resistance can be measured; and the friction-jacket point, which allows both point resistance and local skin resistance to be measured (Begemann, 1953 and 1965).

In purely cohesive soils, it is generally accepted that the cone-point resistance, C_{kd}, is related to the undrained cohesion, c_u, as

$$C_{kd} = c_u N_c \tag{3.27}$$

As discussed in the previous section, the factor N_c may vary widely both theoretically and in practice, and values of N_c ranging from 10 to 30 have been suggested. The major causes of this variation are the sensitivity of the soil, the relative compressibility of the soil, and the occurrence of adhesion on the side of the cone. The variation in the rate of strain between the cone test and other testing methods also has an effect on the deduced value of N_c,

but the use of a constant-penetration rate minimizes variations from this cause. For design purposes, a value of N_c = 15 to 18 appears reasonable (Begemann, 1965; Thomas, 1965; Blight, 1967; Thorne and Burman, 1968).

Van der Veen (1957) suggested that the ultimate resistance of a pile point, of diameter d_b, could be derived from the corresponding cone-penetration curve by taking the average cone resistance over a distance bd_b below the pile point and ad_b above the point. Average values of a = 3.75 and b = 1 were suggested by Van der Veen.

The adhesion measured by the friction jacket may safely be taken as the skin friction for driven piles in clays (Begemann, 1965). Alternatively, but less desirably, the cohesion may be estimated from the point resistance and an appropriate reduction made to obtain the pile-soil adhesion (see Section 3.2.1).

For piles in sand, various attempts have been made to relate the cone-point resistance to the angle of friction and relative density of the sand (Meyerhof, 1956; Shultze and Mezler, 1965; Plantema, 1957), but it has been found that cone resistance is very sensitive to changes in density. For practical use, the previously mentioned suggestion of Van der Veen (1957) may be adopted; namely, that the ultimate point resistance of the pile be taken as the average cone resistance C_{kd} within a distance 3.75 d_b above and d_b below the pile tip, where d_b is the diameter of the pile tip.

Full-scale tests carried out by Vesic (1967) showed that the point resistance of the piles tested is comparable with that of the penetrometer, but the shaft resistance of the piles was approximately double that measured by the penetrometer. Thus, the ultimate load capacity is given by

$$P_u = C_{kd}A_b + 2\overline{f_c}A_s \tag{3.28}$$

where

C_{kd} = measured cone-point resistance at base
$\overline{f_c}$ = average shaft friction along pile, as measured on the friction jacket

For driven steel H-piles, Meyerhof (1956) suggested that the above shaft resistance should be halved.

A comparison between the pile and penetrometer resistances for the tests reported by Vesic (1967) is shown in Fig. 3.28. The upper and lower limits of the penetrometer values are shown. Correlation with static cone tests

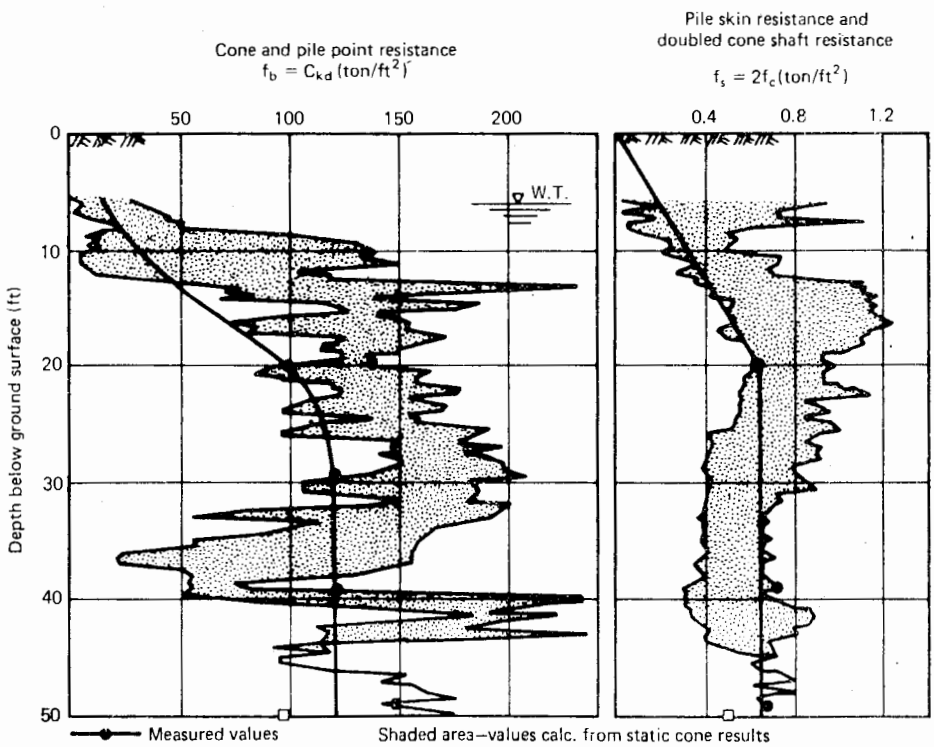

URE 3.28 Variation of point and skin resistances with depth (Vesic, 1967).

was found by Vesic to be better than with the results of standard penetration tests (see below).

For cases in which separate measurements of friction-jacket resistances are not made, Meyerhof (1956) suggested that for driven concrete or timber piles, the ultimate skin friction f_s could be estimated from the cone point resistance C_{kd} as follows:

$$f_s = 0.005 C_{kd} \tag{3.29}$$

For driven steel H-piles, Meyerhof suggested that the above value be halved. Some comparisons (Mohan et al., 1963; Thorne and Burman, 1968) indicate that Eq. (3.29) underestimates the skin friction by a factor of about 2 if C_{kd} is less than about 35 kgf/cm^2.

In sands, it is necessary to make a distinction between the skin friction for downward and upward loading. Modifications for uplift resistance are discussed in Section 3.7.

3.5.2 Standard Penetration Test

Meyerhof (1956) has correlated the shaft and base resistances of a pile with the results of a standard penetration test. For displacement piles in saturated sand, the ultimate load, in U.S. tons, is given by

$$P_u = 4N_p A_p + \frac{\bar{N} A_s}{50} \tag{3.30}$$

where

N_p = standard penetration number, N, at pile base
$\bar{N}$ = average value of N along pile shaft

For small displacement piles (e.g., steel H-piles),

$$P_u = 4N_p A_b + \frac{\bar{N} A_s}{100} \tag{3.31}$$

where

A_b = net sectional area of toe (sq ft)
A_s = gross surface area of shaft (sq ft) (area of all surfaces of flanges and web for H-piles)

In Eq. (3.30), the recommended upper limit of the unit shaft resistance ($\bar{N}/50$) is 1 ton/ft^2 and in Eq. (3.31), 0.5 ton/ft^2.

The above equations have also been used with some success in stiff clays (Bromham and Styles, 1971).

3.5.3 Pressuremeter Test

The use of the pressuremeter in foundation design has been developed extensively in France in recent years. Its application to the estimation of pile load capacity has been summarized by Baguelin et al (1978) who present curves relating ultimate base capacity to the pressuremeter limit pressure, for both driven and cast-in-situ piles. Relationships are also presented between ultimate skin resistance and limit pressure for steel or concrete piles in granular and cohesive soils, and for cast-in-situ piles in weathered rock. The following upper limits on the ultimate skin resistance are suggested by Baguelin et al for pressuremeter limit pressures in excess of 1500 kPa;

concrete displacement piles in granular soil	122 kPa
concrete displacement piles in cohesive soil, or steel displacement piles in granular soil	82 kPa
steel displacement piles in cohesive soil	62 kPa
non-displacement piles in any soil	40 kPa

3.6 SPECIAL TYPES OF PILE

3.6.1 Large Bored Piers

Large-diameter bored piles have come into increasing use in recent years as an alternative to pile groups. They have been constructed up to 10 ft in diameter and in lengths exceeding 100 ft, often with an underreamed or belled base. Such piles have found extensive use in London clay, and much of the research on large bored piers is based on their behavior in London clay. Empirical methods of design have been developed on the basis of extensive experience and research. One of the earliest investigations was in model tests on piles with enlarged bases, reported by Cooke and Whitaker (1961). These tests revealed that, whereas settlements on the order of 10 to 15% of the base diameter were required to develop the ultimate base capacity, the full shaft resistance was developed at very small settlements, on the order of 0.5 to 1.0% of the shaft diameter. (The theory given in Chapter 5 supports these findings.) A considerable amount of field-test evidence has subsequently been obtained (Whitaker and Cooke, 1966;

Burland et al., 1966), and the behavior of full-scale large bored piers has been found to be similar to that of the model piles.

Because of the different degrees of shaft-and base-load mobilization at a given pier settlement, it may be advisable to determine the working load on a large pier by applying separate factors to the ultimate shaft and base resistances; for example, Skempton (1966) suggested a safety factor of 1.5 for shaft resistance and 3.0 for base resistance, for piers with an enlarged base of diameter 6 ft or less. In many cases, the working load for bored piers, especially those with enlarged bases, will be determined by settlement considerations rather than ultimate capacity (Whitaker and Cooke, 1966; Burland et al., 1966). Settlement theory is discussed in Chapter 5.

3.6.2 Underreamed Bored Piles

Underreamed piles have been extensively used in India, both as load-bearing and anchor piles in expansive clays. For anchor piles, a single enlarged bulb is often used, while for load-bearing, one or more bulbs may be used. A single underreamed pile can be treated in a similar manner to a pile with an enlarged base, except that the bulb may be situated above the base of the pile. Mohan et al. (1967) suggest that the base and shaft resistance be added to give the ultimate load capacity. Thus, referring to Fig. 3.29, for a pile in clay,

$$P_u = c_a A_s + \frac{\pi d^2}{4} c_b N_{cb} + \frac{\pi}{4}(d_0^2 - d^2) c_0 N_{c0} \tag{3.32}$$

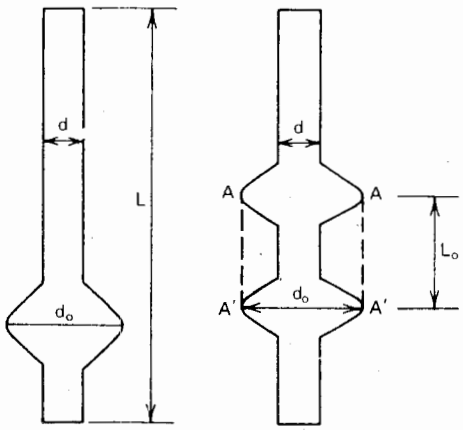

(a) Single underreamed pile (b) Double underreamed pile

FIGURE 3.29 Underreamed piles.

where

c_b = cohesion at pile base
c_0 = cohesion at level of base of bulb
N_{cb} = value of N_c at pile-base level
N_{c0} = value of N_c at level of base of bulb
c_a = average pile-soil adhesion
A_s = surface area of pile shaft
d_0 = bulb diameter

Values of c_a, N_{cb}, and N_{c0} can be obtained from Section 3.2.

For double or multiple underreamed piles with the bulbs suitably spaced, the soil between the bulbs tends to act as part of the pile, so that the full resistance of the soil can be developed on the surface A-A' of a cylinder with a diameter equal to that of the bulbs and height equal to their spacing. Model tests carried out by Mohan et al. (1967) have confirmed this behavior. Mohan et al. (1969) have suggested two methods for estimating the load capacity of multiple underreamed piles:

1. Summation of the frictional resistance along the shaft above and below the bulbs, shearing resistance of the cylinder circumscribing the bulbs, and the bearing capacity of the bottom bulb and base.
2. Summation of the frictional resistance along the shaft above the top bulb and below the bottom bulb, and the bearing capacity of all the bulbs and the base.

It was found that for a typical example of a pile in London clay, these methods give almost identical results. For other cases, the lesser of the two capacities given by the equations should be taken.

Mohan et al. (1967) suggest that the optimum spacing of the bulbs in a multiple underreamed pile lies between 1.25 and 1.5 times the bulb diameter for maximum efficiency. As an example of the economy in material that may be obtained by using underreamed piles, they calculated that a multiple underreamed pile in London clay can develop the same load capacity as a uniform pile of about four times the volume.

3.6.3 Screw Piles

Screw piles have been used in several countries for mast and tower foundations and for underpinning work. Load tests on model and full-scale screw piles have been reported by Wilson (1950) and by Trofimenkov and Mariupolskii (1965). Wilson (1950) developed a method of analysis of the load capacity of screw piles in both sand and clay,

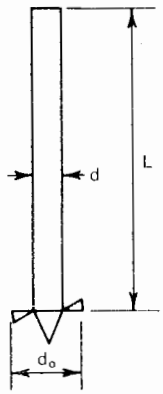

FIGURE 3.30 Idealized screw pile.

based on the use of elastic theory. In a relatively simple analysis for screw piles in clay proposed by Skempton (1950), the load capacity is taken to be the sum of the bearing capacity of the screw and the side resistance along the shaft, assuming no skin friction to be mobilized for a distance above the screw equal to its diameter. Thus, referring to Fig. 3.30.

$$P_u = N_c c_b A_b + \bar{c}_r \pi d(L - d_0) \tag{3.33}$$

where

$\bar{c}_r$ = average remolded shear strength along the shaft in the length $(L - d_0)$
c_b = average of undisturbed and remolded shear strength of soil beneath the screw
A_b = area of screw

The remolded strength of the soil is used because the clay adjacent to the shaft is likely to be almost fully remolded by the passage of the screw and by the lateral displacement caused by the cylinder.

A comparison made by Skempton between measured and predicted load capacities by the above method showed that the predicted ultimate loads were within 15% of the measured values, although always greater. Trofimenkov and Mariupolskii (1965) employed the same basis of calculation as the above and also obtained good agreement between measured and calculated load capacity.

3.7 UPLIFT RESISTANCE

3.7.1 Single Piles

Piles may be required to resist uplift forces—for example, in foundations of structures subjected to large overturning moments such as tall chimneys, transmission towers, or jetty structures. Methods of calculating the adhesion to resist uplift are the same as those used for bearing piles.

For a uniform pile in clay, the ultimate uplift resistance, P_{uu}, is

$$P_{uu} = \bar{c}_a A_s + W_p \tag{3.34}$$

where

W_p = weight of pile
$\bar{c}_a$ = average adhesion along pile shaft

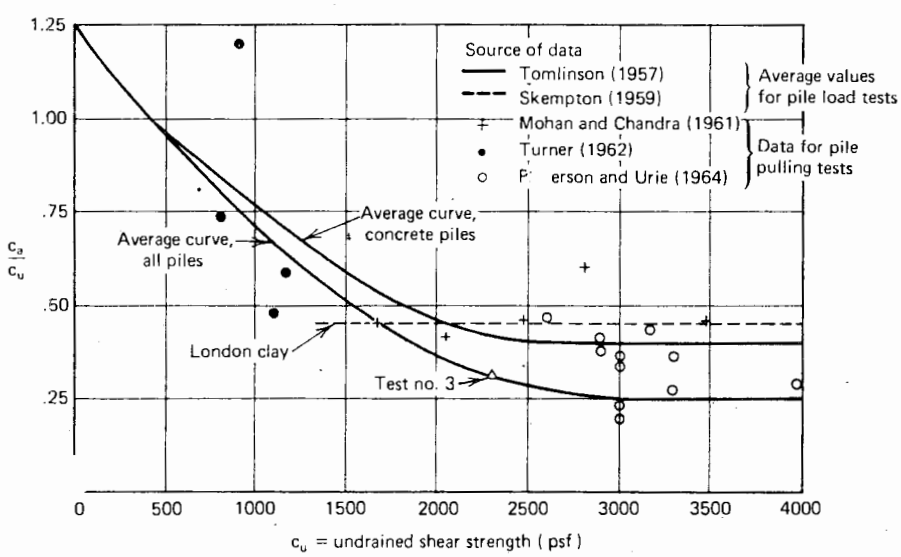

FIGURE 3.31 Relationship between c_a/c_u and undrained shear strength for pulling tests (Sowa, 1970). (Reproduced by permission of the National Research Council of Canada from the Canadian Geotechnical Journal, Vol. 7, 1970, pp. 482-493.)

Relatively few pulling tests on piles have been reported in the literature. A summary of some of the available results is given by Sowa (1970), who has found that the values of c_a/c_u agree reasonably well with the values for piles subjected to downward loading (Fig. 3.31).

For piles of uniform diameter in sand, the ultimate uplift capacity may be calculated as the sum of the shaft resistance plus the weight of the pile. There is, however, little data available on the skin friction for upward loading, and the available data is to some extent conflicting. For example, tests reported by Ireland (1957) on piles driven into fine sand suggest that the average skin friction for uplift loading is equal to that for downward loading, but data summarized by Sowa (1970) and Downs and Chieurzzi (1966) indicates considerable variations in average skin friction between different tests, although there is a tendency for the values to be lower than for downward loading, especially for cast-in-situ piles. In the absence of other information, a reduction to two thirds of the calculated shaft resistance for downward loading is recommended. However, a reliable estimate is best determined by carrying out a pulling test in-situ.

If static-cone-penetration tests are used as a basis for estimating ultimate uplift skin resistance, Begemann (1965) suggests that the calculated skin resistance for downward loading be adjusted by a reduction factor dependent on the soil and pile type. He also suggests reduced values of skin resistance be used if the uplift load is oscillating. Begemann's suggestions, however, should be viewed with considerable caution, as they are based on limited data.

Additional uplift resistance may be obtained by underreaming or enlarging the base of the pile, and in such cases, the pile shaft may have little or no influence on the uplift capacity. Traditional methods of design assume the resistance of the enlarged base to be the weight of a cone of earth having sides that rise either vertically or at 30° from the vertical. Neither of these methods has proved reliable in practice, however. The 30°-cone method is usually conservative at shallow depths but can give a considerable overestimate of uplift capacity at large depths (Turner, 1962). Parr and Varner (1962) showed that the vertical-failure-surface approach did not apply to piles in clay, although it could apply to backfilled footings. Alternative theories for uplift resistance of enlarged bases have been proposed by Balla (1961), MacDonald (1963), and Spence (1965)--these theories differing in the assumptions regarding the shape of the failure surface.

Meyerhof and Adams (1968) have developed an approximate approach based on observations made in laboratory model tests. They suggest that the short-term uplift capacity of a pile in clay (under undrained conditions) is given by the lesser of

(a) The shear resistance of a vertical cylinder above the base, multiplied by a factor k, plus the weight of soil and pile, W, above the base.
(b) The uplift capacity of the base plus W, that is,

$$P_{uu} = \frac{\pi(d_b^2 - d^2)}{4} c_u N_u + W \qquad (3.34)$$

where

N_u = uplift coefficient
$\cong N_c$ for downward load

Examination of the results of model and field tests led Meyerhof and Adams to suggest the following values of k:

Soft clays	$k = 1$–1.25
Medium clays	$k = 0.7$
Stiff clays	$k = 0.5$
Stiff fissured clays	$k = 0.25$

The low values of k in the stiffer clays are partly attributed by Meyerhof and Adams to the influence of tension cracks arising from premature tension-failure in the clay.

It has been found that negative pore pressures may occur in clays during uplift, particularly with shallow embedment depths. The uplift capacity under sustained loading may therefore be less than the short-term or undrained capacity, because the clay tends to soften with time as the negative pore pressures dissipate. The long-term uplift capacity can be estimated from the theory for a material with both friction and cohesion, using the drained parameters ϕ_d and c_d of the clay.

For a soil with both cohesion and friction, the following expressions were obtained by Meyerhof and Adams for the ultimate load capacity, P_{uu}, of a circular base:

(a) Shallow depths ($L < d_b$):

$$P_{uu} = \pi c d_b L + s\frac{\pi}{2}\gamma d_b L^2 K_u \tan\phi + W \qquad (3.35)$$

(b) Great depths ($L > H$):

$$P_{uu} = \pi c d_b H + s\frac{\pi}{2}\gamma d_b (2L - H) H K_u \tan\phi + W \qquad (3.36)$$

where

γ = soil unit weight*
s = shape factor

$= 1 + mL/d_b$, with a maximum value of $1 + mH/d_b$

K_u = earth-pressure coefficient (approximately 0.9 - 0.95 for ϕ values between 25° and 40°)

m = coefficient depending on ϕ

H = limiting height of failure surface above base

W = weight of soil and pile in cylinder above base*

The upper limit of the uplift capacity is the sum of the net bearing-capacity of the base, the side adhesion of the shaft, and the weight of the pile, that is,

$$P_{uu_{max}} = \frac{\pi}{4}(d_b^2 - d^2)(cN_c + \sigma'_{vb}N_q) \qquad (3.37)$$

$$+ A_s f_s + W$$

where

N_c, N_q = bearing-capacity factors

f_s = ultimate shaft-shear resistance

σ'_{vb} = effective vertical stress at level of pile base

Meyerhof and Adams suggest that the values of N_c and N_q for downward load can be used in this context, but theoretically this is incorrect, and somewhat lower values may be appropriate to upward loading. However, the theory for failure of anchor piles with enlarged bases, or of anchor plates more generally, has yet to be fully developed.

For use in Eqs. (3.35) and (3.36), values of H/d_b, s, and m, obtained from tests results by Meyerhof and Adams, are shown in Table 3.6. The ultimate uplift capacity should be taken as the lesser value of that given by Eq. (3.37) and the appropriate equations 3.35 or 3.36.

The results of model tests in clays, reported by Meyerhof and Adams (1968), are shown in Fig. 3.32. Both the undrained and long-term pullout loads are shown, and the

* Buoyant or total, as appropriate.

TABLE 3.6 FACTORS FOR UPLIFT ANALYSIS[a]

$\phi°$	20	25	30	35	40	45	48
H/d_b	2.5	3	4	5	7	9	11
m	0.05	0.1	0.15	0.25	0.35	0.5	0.6
s	1.12	1.30	1.60	2.25	3.45	5.50	7.60

[a] From Meyerhof and Adams (1968). (Reproduced by permission of the National Research Council of Canada from the *Canadian Geotechnical Journal*, Vol. 5, 1968, pp. 225-244.)

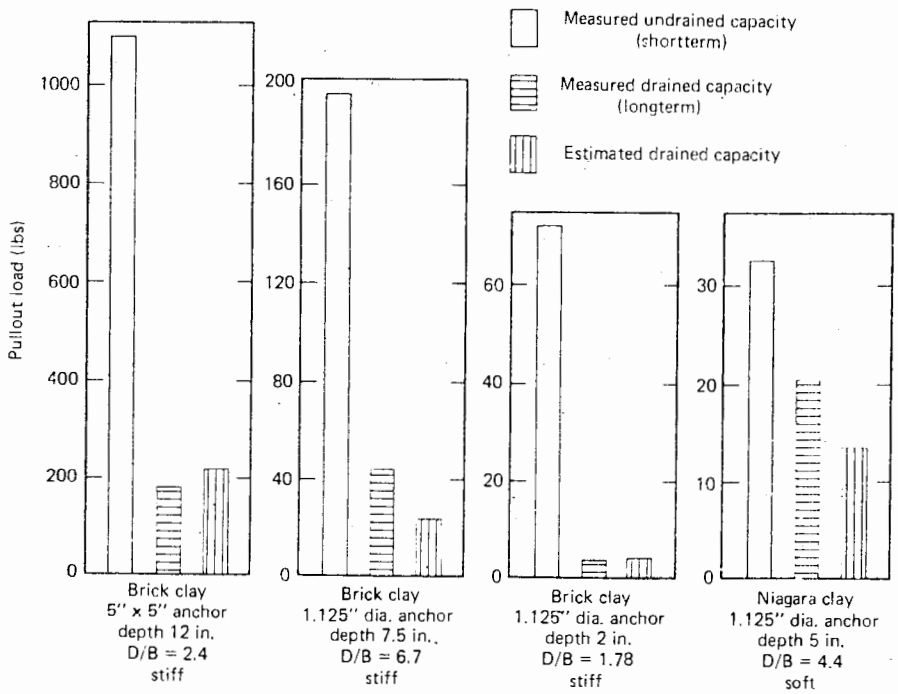

FIGURE 3.32 Comparison of short-term and long-term pull-out tests in clay (Meyerhof and Adams, 1968). (Reproduced by permission of the National Research Council of Canada from the Canadian Geotechnical Journal, Vol. 5, 1968, pp. 225-244.)

considerable reduction in load capacity with time can clearly be seen. The extent of the load-capacity decrease becomes greater as the soil becomes stiffer. The predicted long-term capacities of the piles show reasonable agreement with the measured values.

The above theory can also be used to estimate the uplift capacity of piles in sand. Meyerhof and Adams have compared predicted and measured uplift capacities for buried footings in sand and have found fair agreement, although there is a relatively wide scatter of points.

3.7.2 Pile Groups

Meyerhof and Adams (1968) suggest that the ultimate uplift load of a group be calculated as the lesser of

(a) The sum of the uplift of the individual footings.

(b) The uplift load of an equivalent pier foundation consisting of the footings and enclosed soil mass.

Meyerhof and Adams (1968) have presented some data on the uplift efficiency of groups of two and four model circular footings in clay. The results indicate that the uplift efficiency increases with the spacing of the footings or bases and as the depth of embedment decreases, but decreases as the number of footings or bases in the group increases. The uplift efficiencies are found to be in good agreement with those found by Whitaker (1957) for freestanding groups with downward loads.

For uplift loading on pile groups in sand, there appears to be little data from full-scale field tests. However, Meyerhof and Adams (1968) have carried out tests on small groups of circular footings and rough circular shafts, and have analyzed the group efficiencies. For a given sand density, the uplift efficiencies of the groups increase roughly linearly with the spacing of the footings or shafts,

TABLE 3.7 SUMMARY OF REPORTED PILE-BENDING MEASUREMENTS

Reference	Pile Type	Pile Length	Soil Type	Out-of-Alignment at Tip	Type of Bend
Parsons and Wilson (1954)	Composite: lower 85 ft, 10¾-in. pipe, top 55 ft, corrugated pipe	140 ft	20 ft fill, layers of organic silt, medium sand, fine sand, silt with clay layers, gravel, bedrock	4.4 ft	Gentle sweep over lower length
Bjerrum (1957)	Steel H-section	30 ft	Clay	1.2 ft	Gentle sweep
Johnson (1962)	Composite: lower 40 ft, 10¾ in. upper 50 ft, corrugated taper pipe	40 ft	20 ft silt overlying medium sand	8 ft	Gentle sweep over lower length
Mohr (1963)	10¾-in. pipe	85 ft	80 ft soft silt, stiff sand clay, medium dense sand	10.25 ft	Gentle sweep
National Swedish Council (1964)	Precast hexagonal, Hercules jointed	60m	50m soft clay, 10m clay, silt, sand, rock at 70m	11m	Gentle
Hanna (1967)	Steel H-section 14 BP73	140 ft	34 ft stiff clay, 50 ft soft clay, 64 ft stiff clay, shale	3.0 ft	Triple curvature. relatively sharp direction changes
	Steel H-section 14 BP 89	138 ft		6.0 ft	Double curvature, relatively sharp direction changes

and increase as the depth of embedment becomes smaller. The uplift efficiency decreases as the number of footings or shafts in the group increases and as the sand density increases.

3.8 LOAD CAPACITY OF BENT PILES

A number of cases have been reported in which long, slender piles have become bent during driving. A summary of these measurements is shown in Table 3.7. For concrete-filled steel shell piles, load tests indicated that the piles could tolerate significant out-of-verticality and still carry their design load with safety. This, however, may largely be caused by the neglect of the structural strength of the pile shell in the design. Long, precast, hexagonal test piles have also been found to perform satisfactorily, but Hanna (1967) has found that for steel H-piles, large stresses are induced because of bending during driving. Pile bending is attributed by Hanna to the development of asymmetrical stresses in the pile as a result of the eccentric pile-tip reaction and eccentric driving inherent in all pile-driving work. These eccentric stresses are considered to be sufficient to initiate bending, which causes the pile to drive off vertical. Reverse curvature of the pile may subsequently occur, and this is believed to result primarily from the vertical-weight component of the inclined pile forcing the pile to bend.

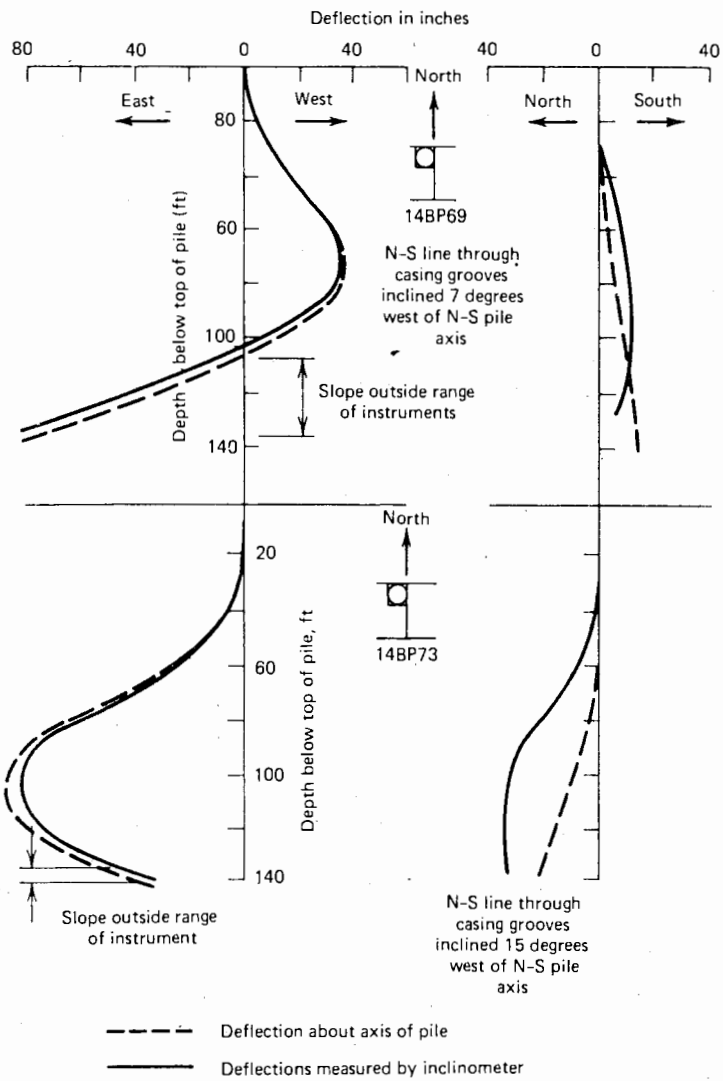

FIGURE 3.33 Measured deflection components of driven pile (Hanna, 1968). (Reproduced by permission of the National Research Council of Canada from the Canadian Geotechnical Journal, Vol. 5, 1968, pp. 150-172.)

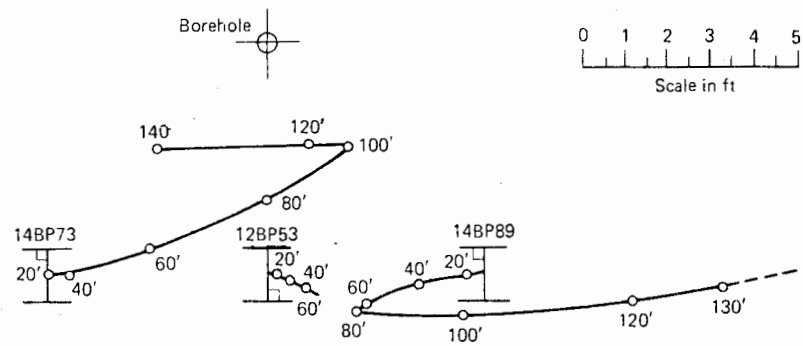

FIGURE 3.34 Driven position of pile tips (Hanna, 1968). (Reproduced by permission of the National Research Council of Canada from the Canadian Geotechnical Journal, Vol. 5, 1968, pp. 150-172.)

Typical deflection profiles, reported by Hanna (1967), are shown in Fig. 3.33. These profiles have been obtained from measurements on an inclinometer installed within the H-piles. The as-driven positions of the pile tips for every 20 ft of depth are shown in Fig. 3.34. For the two piles considered, minimum computed radii of curvature were on the order of 170 ft and 190 ft at depths of 100 ft and 70 ft; these values are about six times less than the suggested safe minimum value for steel H-piles of 1200 ft (Bjerrum, 1957).

Methods of estimating the stresses in a pile due to nonverticality have been proposed by Johnson (1962), Broms (1963), Parsons and Wilson (1954), and Madhav and Rao (1975). Typical of these methods is that of Broms, who by expressing the deflected shape of the pile as a Fourier sine series and assuming the soil to be a Winkler medium, was able to derive a simple approximate equation for the buckling load on the pile (the subject of buckling is discussed more fully in Chapter 14). Provided that some information of the departure from straightness of the actual piles is available, the maximum soil pressure along the pile and the maximum bending moment can then be calculated. As design criteria, Broms suggested that

(a) The calculated maximum soil pressure along the pile should not exceed one third of the ultimate value.
(b) The maximum stress (axial plus bending) in the pile should be less than the allowable value.

The first criterion leads to an allowable load P given by

$$P = \frac{p_{max} P_{cr}}{k\rho_{max} + p_{max}} \tag{3.38}$$

where

p_{max} = maximum allowable soil pressure
P_{cr} = buckling load of pile
k = modulus of subgrade reaction
ρ_{max} = maximum lateral deflection (deviation of the center line of the pile from a straight line connecting the pile tip and the point at which curvature of the pile begins)

For the second criterion to be satisfied, the allowable load P is

$$P = 0.5\,(b - \sqrt{b^2 - 4c}) \tag{3.39}$$

where

$$b = P_{cr} + A\sigma_{max}$$

$$c = A\sigma_{max} - \frac{AE_pI_p}{ZR_{min}} \tag{3.39}$$

P_{cr} = pile-buckling load
A = area of pile
σ_{max} = allowable maximum stress in pile
E_p = Young's modulus of pile
I_p = moment of inertia of pile
Z = pile section-modulus
R_{min} = minimum radius of curvature along pile

From Eq. (3.39), it may be deduced that the load-carrying capacity will be reduced to zero if $c \leq 0$, that is, if

$$R_{min} \leq \frac{E_pI_p}{Z\sigma_{max}} \tag{3.40}$$

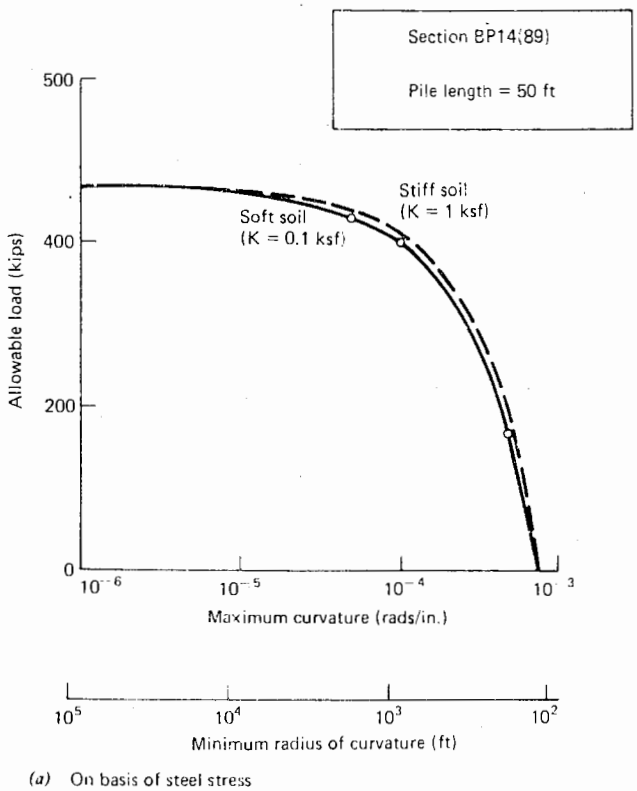

(a) On basis of steel stress

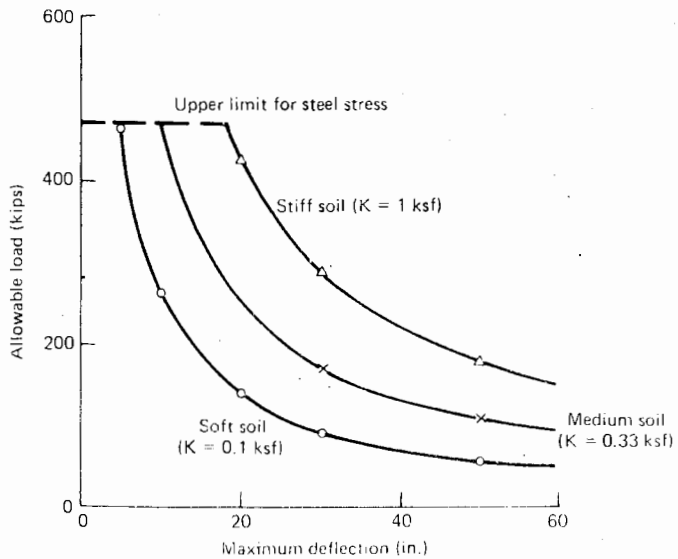

(b) On basis of soil pressure

FIGURE 3.35 Allowable loads for bent piles (from Broms' analysis).

For a typical steel H-pile section in clay, the allowable loads from Eqs. (3.38) and (3.39) are plotted in Fig. 3.35. For the limiting-soil-pressure criterion, the allowable load increases as the stiffness of the soil increases (K=kd = 33 times the cohesion, has been assumed) but is almost independent of pile length. For the limiting steel-stress criterion, an allowable steel stress of 18 kips/sq ft has been adopted. The allowable load is insensitive to change in soil subgrade-reaction modulus or pile length.

4

LOAD CAPACITY BY DYNAMIC METHODS

4.1 INTRODUCTION

Perhaps the oldest and most frequently used method of estimating the load capacity of driven piles is to use a driving formula, or dynamic formula. All such formulas relate ultimate load capacity to pile set (the vertical movement per blow of the driving hammer) and assume that the driving resistance is equal to the load capacity of the pile under static loading. They are based on an idealized representation of the action of the hammer on the pile in the last stage of its embedment. There are a great number of driving formulas available, of varying degrees of reliability. Smith (1960) states that the editors of the *Engineering New Record* have on file 450 such formulas. In Section 4.2, a summary of the most common formulas is given and their reliability is discussed. The derivation of most of these formulas is discussed by Whitaker (1970), while details of some of the parameters required are available in Chellis (1961).

The primary objectives in using a pile-driving formula are usually either to establish a safe working load for a pile by using the driving record of the pile, or to determine the driving requirements for a required working load. The working load is usually determined by applying a suitable safety factor to the ultimate load calculated by the formula. This safety factor, however, varies considerably, depending on the formula used and the type of pile being driven. Also, because pile driving formulas take no account of the nature of the soil, the appropriate safety factor may vary from one site to another.

A relatively recent improvement in the estimation of load capacity by dynamic methods has resulted from the use of the wave equation to examine the transmission of compression waves down the pile, rather than assuming that a force is generated instantly throughout the pile, as is done in deriving driving formulas. The main objective in using the wave-equation approach is to obtain a better relationship between ultimate pile-load and pile-set than can be obtained from a simple driving formula. As well as providing a means of load capacity estimation, this relationship allows an assessment to be made of the driveability of a pile with a particular set of equipment. Moreover, this approach also enables a rational analysis to be made of the stresses in the pile during driving and can therefore be useful in the structural design of the pile. The application of this technique is described in Section 4.3.

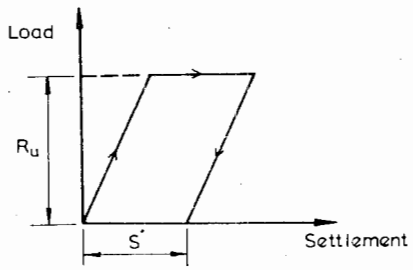

FIGURE 4.1 Assumed load-settlement curve for pile.

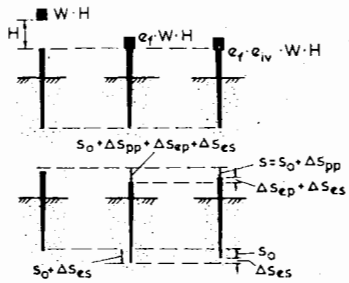

FIGURE 4.2 Transfer of energy and penetration of pile during one blow of the pile-driving hammer.

4.2 PILE-DRIVING FORMULAS

4.2.1 Derivation of General Formula

Pile-driving formulas attempt to relate the dynamic to the static resistance of a pile, and have been established on an empirical or a theoretical basis. Several of the latter are based on Newton's law of impact, modified in some cases for energy losses during impact and stress propagation.

The assumed relationship between pile resistance and downward movement of the pile is shown in Fig. 4.1. The materials of the pile and the driving cushion are assumed to be perfectly elastic, and inertia forces in the soil and energy losses stemming from irreversible deformations (except of the soil) are disregarded.

The derivation of a general pile-driving formula has been given by Taylor (1948) and quoted by Flaate (1964). This derivation will be reproduced below and the various versions of this general formula will be discussed subsequently. The following symbols are used in the derivation:

S = pile penetration for last blow, or "set"
ΔS_{pp} = plastic deformation of pile
ΔS_{ep} = elastic deformation of pile
ΔS_{es} = elastic deformation of soil
$S_0 = S - \Delta S_{pp}$
W = Weight of hammer
H = drop of hammer
e_f = efficiency factor for hammer
e_{iv} = efficiency factor for impact
W_p = weight of pile
A = cross-section of pile
L = pile length
E_p = modulus of elasticity of pile
v = hammer velocity before impact
u = hammer velocity after impact
v_p = pile velocity before impact
u_p = pile velocity after impact
g = gravitational acceleration
R_u = load capacity of pile (just after driving)
E_1 = energy reaching pile
E_2 = energy left after impact.

The process of energy transfer and pile penetration during one blow of the hammer is shown in Fig. 4.2. The energy reaching the pile is

$$E_1 = e_f W H = \frac{W v^2}{2g} \tag{4.1}$$

The efficiency of impact is

$$e_{iv} = \frac{(W/2g)u^2 + (W_p/2g)u_p^2}{(W/2g)v^2 + (W_p/2g)v_p^2} = \frac{E_2}{E_1} \tag{4.2}$$

The law of impulse gives:

$$\frac{W}{g}(v - u) = -\frac{W_p}{g}(v_p - u_p) \tag{4.3}$$

The coefficient of elastic restitution, n, is

$$n = \frac{u_p - u}{v - v_p} \tag{4.4}$$

Assuming $v_p = 0$, and eliminating u, u_p, and v,

$$e_{iv} = \frac{W + n^2 W_p}{W + W_p} \tag{4.5}$$

The energy left after impact is

$$E_2 = e_f e_{iv} W H = e_f W H \left(\frac{W + n^2 W_p}{W + W_p}\right) \tag{4.6}$$

The work done during impact is approximately

$$E_2 \simeq R_u(S + \Delta S_{pp} + \tfrac{1}{2}\Delta S_{ep}) \tag{4.7}$$

Neglecting the elastic deformation of the soil, and introducing Hooke's Law for the pile,

$$\Delta S_{ep} = C\frac{R_u L}{AE_p} \tag{4.8}$$

where

C = ratio between actual displacement at pile top and that given by Hooke's Law

From Eqs. (4.6), (4.7), and (4.8), the following equation is obtained:

$$R_u = \frac{e_f WH}{S + (CR_u L)/(2AE_p) + \Delta S_{pp}} \times \left(\frac{W + n^2 W_p}{W + W_p}\right) \tag{4.9}$$

4.2.2 Practical Driving Formulas

Although the above general formula takes most practical factors into account, the validity of the law of impact is very questionable, since the pile is by no means the free body that the law of impact assumes. As pointed out by Terzaghi (1943), "Newton himself warned against the application of his theory to problems involving for instance the impact produced by 'the stroke of a hammer.'" In addition to this basic criticism, the general formula is not readily applicable in practice, since many of the quantities are extremely difficult to measure or estimate reliably. Consequently, most practical pile-driving formulas are simplifications of the general equation, often incorporating empirical "constants" and coefficients. Most of these formulas can be expressed in the following form:

$$e_h e_f WH = \zeta\frac{1}{2}\left(\frac{R_u{}^2 L}{AE}\right) + R_u S \tag{4.10}$$

where

e_h = efficiency of impact
e_f = efficiency of hammer blow
ζ = factor allowing for elastic compression of soil and driving cushion

The left-hand side of Eq. (4.10) represents the energy of the hammer blow, the first term on the right-hand side is the energy consumed by the elastic compression of the pile, computed as a static compression under the force R_u, and he second term is the energy absorbed by the plastic deformation of the soil.

A summary of various practical formulas is given in Table 4.1. Tables 4.2, 4.3, and 4.4 give typical values of various quantities required for these formulas.

4.3.2 Reliability of Dynamic Formulas

Several investigations have been carried out to determine the reliability of the various pile-driving formulas by comparing the load capacity computed from the appropriate formula with the measured capacity from a pile loading test. Some of the most comprehensive investigations have been reported by Sorensen and Hansen (1957), Agerschou (1962), Flaate (1964), Housel (1966), and Olsen and Flaate (1967).

Sorensen and Hansen used data from 78 load tests on concrete, steel, and wooden piles, most of these having their points bearing on sand (a few were founded on hard moraine clay). The results of their comparisons are shown in Fig. 4.3, in which the ratio, μ, of the measured to the computed load-capacity is plotted against the percentage of load tests smaller than μ. This plot is a probability plot, and a straight line on this plot represents a normal or Gaussian distribution of results. Figure 4.3 shows that all the formulas considered, with the exception of the Eytelwein formula, follow approximately a Gaussian distribution. There is very little difference in the accuracy of the Danish, Hiley, and Janbu formulas, and the theoretical

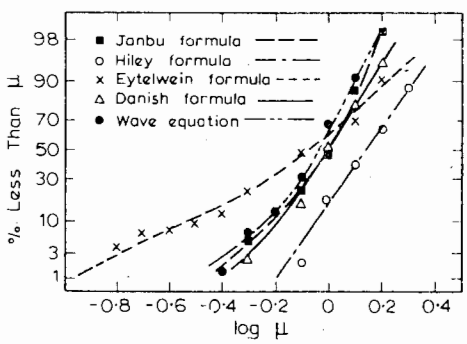

FIGURE 4.3 Statistical distribution of load test results (Sorensen and Hansen, 1957). (This figure is reproduced from the proceedings of the Fourth International Conference on Soil Mechanics and Foundation Engineering. Butterworths, London, 1957.)

TABLE 4.1 SUMMARY OF PILE-DRIVING FORMULAS

Formula	Equation for R_u	Remarks
Sanders	$\frac{WH}{S}$	
Engineering News	$\frac{WH}{S+C}$	C = 1.0 in. for drop hammer 0.1 in. for steam hammer 0.1 W_p/W in. for steam hammer on very heavy piles
Eytelwein (Dutch)	$\frac{WH}{S} \cdot \frac{W}{W+W_p}$	
Weisbach	$-\frac{SAE_p}{L} + \sqrt{\left(\frac{2WHAE_p}{L}\right) + \left(\frac{SAE_p}{L}\right)^2}$	
Hiley	$\frac{e_f WH}{S+\frac{1}{2}(C_1+C_2+C_3)} \cdot \frac{W+n^2W_p}{W+W_p}$	See Tables 4.2, 4.3 and 4.4 for values of e_f, C_1, C_2, C_3, and n.
Janbu	$\left(\frac{1}{k_u}\right)\left(\frac{WH}{S}\right)$	$k_u = C_d(1+\sqrt{1+\gamma e/C_d})$ $C_d = 0.75+0.15\ W_p/W$ $\lambda e = WHL/AES^2$
Danish	$\frac{e_f WH}{S+(2e_f WHL/AE_p)^{1/2}}$	See Table 4.2 for e_f values.
Gates	$5.6\sqrt{e_f WH}\log_{10}(10/S)$	Units are inches and tons (short).
	$4.0\sqrt{e_f WH}\log_{10}(25/S)$	Units are metric tons (1000 kg) and centimeters.

TABLE 4.2 VALUES OF HAMMER EFFICIENCY, e_f[a]

Hammer Type	e_f
Drop hammer released by trigger	1.00
Drop hammer actuated by rope and friction winch	0.75
McKiernan-Terry single-acting hammers	0.85
Warrington-Vulcan single-acting hammers	0.75
Differential-acting hammers	0.75
McKiernan-Terry, Industrial Brownhoist, National & Union double-acting hammers	0.85
Diesel hammers	1.00

[a] From *Pile Foundations* by R. D. Chellis. © 1961 McGraw-Hill Book Company, Inc. Used with permission of McGraw-Hill Book Company.

curves derived from the wave equation (see Section 4.3), but the Eytelwein formula is very inaccurate.

Agerschou's investigation concentrated on the *Engineering News* formula but also broadly confirmed the conclusions of Sorensen and Hansen regarding the Hiley, Janbu, and Danish formulas. Agerschou showed that despite its popularity, the *Engineering News* formula is unreliable. It has the highest standard deviation, and 96% of the allowable loads determined by this formula will have actual safety factors ranging between 1.1 and 30.0. Flaate (1964) investigated the accuracy of the Janbu, Hiley, and *Engineering News* formulas for 116 tests on timber, concrete, and steel piles in sand. The conclusions reached by Agerschou regarding the unreliability of the *Engineering News* formula are reinforced by Flaate's results. There is relatively little difference between the Janbu and Hiley formulas, although the former is perhaps the more reliable overall and gives

TABLE 4.3 VALUES OF C_1, C_2, C_3 FOR HILEY FORMULA[a]

(a) *Values of* C_1

Temporary Compression Allowance C_1 for Pile Head and Cap

Material to Which Blow Is Applied	Easy Driving: P_1 = 500 psi on Cushion or Pile Butt If No Cushion (in.)	Medium Driving: P_1 = 1000 psi on Head or Cap (in.)	Hard Driving: P_1 = 1500 psi on Head or Cap (in.)	Very Hard Driving: P_1 = 2000 psi on Head or Cap (in.)
Head of timber pile	0.05	0.10	0.15	0.20
3–4 in. packing inside cap on head of precast concrete pile	0.05 + 0.07[b]	0.10 + 0.15[b]	0.15 + 0.22[b]	0.20 + 0.30[b]
1/2–1 in. mat pad only on head of precast concrete pile	0.025	0.05	0.075	0.10
Steel-covered cap, containing wood packing, for steel piling or pipe	0.04	0.08	0.12	0.16
3/16–in. red electrical fiber disk between two 3/8–in. steel plates, for use with severe driving on Monotube pile	0.02	0.04	0.06	0.08
Head of steel piling or pipe	0	0	0	0

(b) *Value of* C_2 — $C_2 = R_u L/AE_p$ (Include additional value for followers.)

(c) *Values of* C_3 — C_3 is temporary compression allowance for quake of ground. Nominal value = 0.1 inches. Range = 0.2 for resilient soils to 0 for hardpan

[b] The first figure represents the compression of the cap and wood dolly or packing above the cap, whereas the second figure represents the compression of the wood packing between the cap and the pile head.

[a] From *Pile Foundations*, by R. D. Chellis, © 1961 McGraw-Hill Book Company, Inc. Used with permission of McGraw-Hill Book Company.

good results for timber and concrete piles. Hiley's formula is also reasonable for timber piles.

The tests undertaken by the Michigan Department of State Highways at Belleville, and reported by Housel (1966), are compared in Table 4.5 with predictions from a large number of pile-driving formula. The *Engineering News* formula gives predictions of ultimate load of between 2 and 6 times the measured values, the Hiley formula gives 7 to 30 times the measured values, and the Eytelwein formula gives 5 to 25 times the measured values. In comparison with the previous comparisons, the spread of results of the Hiley formula is greater and that of the *Engineering News* formula is less. This difference may well stem from the fact that the results in Table 4.5 are predominantly for piles in sand, whereas the Belleville site consists largely of clay. Consequently, the reliability of pile-driving formulas at this site is likely to be poor, as significant frictional resistance may be mobilized along the pile, whereas this resistance is not directly considered in the formulas. It is also interesting to note that the Belleville results are consistent with the analyses performed by Forehand and Reese (1964), which suggest that the *Engineering News* formula may be less un-

TABLE 4.4 VALUES OF COEFFICIENT OF RESTITUTION, n[a]

Pile Type	Head Condition	Drop, Single-acting, or Diesel Hammers	Double-acting Hammers
Reinforced concrete	Helmet with composite plastic or greenheart dolly and packing on top of pile	0.4	0.5
	Helmet with timber dolly, and packing on top of pile	0.25	0.4
	Hammer direct on pile with pad only	–	0.5
Steel	Driving cap with standard plastic or greenheart dolly	0.5	0.5
	Driving cap with timber dolly	0.3	0.3
	Hammer direct on pile	–	0.5
Timber	Hammer direct on pile	0.25	0.4

[a] After Whitaker (1970).

TABLE 4.5 SUMMARY OF SAFETY-FACTOR RANGE FOR EQUATIONS USED IN THE MICHIGAN PILE-TEST PROGRAM[a]

Formula	Upper and Lower Limits of $SF = R_u/R_d$[b] Range of R_u, kips: 0–200	200–400	400–700	Nominal Safety Factor
Engineering News	1.1–2.4	0.9– 2.1	1.2– 2.7	6
Hiley	1.1–4.2	3.0– 6.5	4.0– 9.6	3
Pacific Coast Uniform Building Code	2.7–5.3	4.3– 9.7	8.8–16.5	4
Redtenbacher	1.7–3.6	2.8– 6.5	6.0–10.9	3
Eytelwein	1.0–2.4	1.0– 3.8	2.2– 4.1	6
Navy-McKay	0.8–3.0	0.2– 2.5	0.2– 3.0	6
Rankine	0.9–1.7	1.3– 2.7	2.3– 5.1	3
Canadian National Building Code	3.2–6.0	5.1–11.1	10.1–19.9	3
Modified *Engineering News*	1.7–4.4	1.6– 5.2	2.7– 5.3	6
Gates	1.8–3.0	2.5– 4.6	3.8– 7.3	3
Rabe	1.0–4.8	2.4– 7.0	3.2– 8.0	2

[a] After Housel (1966).
[b] R_u = ultimate test load
R_d = design capacity, using the nominal safety factor recommended for the equation

reliable for cases in which considerable side friction occurs (e.g., piles in soft clay) than for point-bearing piles.

Olsen and Flaate (1967) extended the comparisons reported by Flaate (1964) and examined the reliability of various pile-driving formulas for the timber, concrete, and steel friction piles in sand considered by Flaate. It was concluded that Janbu's formula was the most accurate for timber and steel piles, although none of the formulas was clearly best for the precast concrete piles. The three formulas that yielded the highest average correlation coefficients were the Danish, Janbu, and Gates formulas. The *Engineering News* formula was found to be quite unsatisfactory. As a rapid and accurate means of estimation of load capacity, Olsen and Flaate suggested the following adjusted versions of the Gates formula:

Timber piles:

$$R_u = 7.2\sqrt{e_f WH} \times \log_{10}(10/S) - 17 \qquad (4.11a)$$

Precast concrete piles:

$$R_u = 9.0\sqrt{e_f WH} \times \log_{10}(10/S) - 27 \qquad (4.11b)$$

Steel piles:

$$R_u = 13.0\sqrt{e_f WH} \times \log_{10}(10/S) - 83 \qquad (4.11c)$$

where R_u and W are in tons, and H and S are in inches.

A summary of the statistical analyses of Flaate, Agerschou, Olsen and Flaate, and Sorensen and Hansen is given in Table 4.6. This table contains standard deviations for different formulas, the standard deviation being defined as the difference between the values of $\log \mu$ corresponding to 83.5% and 16.5% on the curve. The nominal safety factor is the value to be applied to each formula if only 2% of the formula loads are allowed to have an actual safety factor less than 1.0, and is equal to 1 divided by the value of μ corresponding to 2%. The upper limit of the safety factor for 96% of the formula loads, also included in Table 4.6, is calculated as the μ value for 96% multiplied by the nominal safety factor. The reliability of the various formulas can best be judged from the upper limit of the safety factor for 96% safety; the higher this value, the less reliable is the formula (higher values of this quantity are also associated with higher standard deviations). It is obvious from Table 4.6 that for the formulas considered, the most reliable are the Janbu and the Danish formulas.

TABLE 4.6 SUMMARY OF STATISTICAL ANALYSES

Formula		Standard Deviation on μ	Upper Limit of 96% Safety if Lower Limit Is 1.0	Nominal Safety Factor	Number of Load Tests
Engineering News	A	0.78	26.0	0.86	171
	F	0.70	17.5	5.8	116
Hiley	S & H	0.27	3.8	1.4	50
	F	0.37	10.1	2.4	116
Janbu	S & H	0.25	3.6	2.3	78
	F	0.22	3.2	2.0	116
Danish	S & H	0.26	3.8	2.0	78
	O & F	0.28	4.1	3.0	55
	A	0.30	4.2	2.3	123
Eytelwein	S & H	0.57	17.0	7.1	78
Weisbach	A	0.36	6.0	2.6	123
Gates	O & F	0.35	5.1	2.3	55

Legend: S & H = Sorensen and Hansen (1957)
A = Agerschou (1962)
F = Flaate (1964)
O & F = Olsen and Flaate (1967) (steel piles in sand)
μ = ratio of measured to computed load capacity

The overall conclusions from the above comparisons are that, if driving formulas are to be used, those which involve the least uncertainty are the Janbu, Danish and Hiley formulas, while the most uncertain is the Engineering News formula.

In conclusion, it is interesting to note the remarks made by Terzaghi (1943): "In spite of their obvious deficiencies and their unreliability, the pile formulas still enjoy a great popularity among practicing engineers, because the use of these formulas reduces the design of pile foundations to a very simple procedure. The price one pays for this artificial simplification is very high. In some cases the factor of safety of foundations designed on the basis of the results obtained by means of pile formulas is excessive and in other cases significant settlements have been experienced. On account of their inherent defects all the existing pile formulas are utterly misleading as to the influence of vital conditions, such as the ratio between the weight of the pile and the hammer, on the result of the pile driving operations. In order to obtain reliable information concerning the effect of the impact of the hammer on the penetration of the piles it is necessary to take into consideration the vibrations which are produced by the impact."

4.3 PILE-DRIVING ANALYSIS BY THE WAVE EQUATION

The realization that pile driving could not accurately be analyzed by rigid-body mechanics led to the development of an analysis that utilizes wave theory. This analysis takes account of the fact that each hammer-blow produces a stress wave that moves down the length of the pile at the speed of sound, so that the entire length of the pile is not stressed simultaneously, as assumed in the conventional dynamic formulas.

As previously stated, the wave-equation approach is primarily used to yield a relationship between ultimate pile load and pile set, although the stresses set up in the pile during driving are also calculated. In addition, this approach enables a rational analysis to be made of the effects of var-

ious factors in the driving process, such as pile characteristics, hammer characteristics, and cushion stiffness. It therefore provides a convenient and logical means of determining the suitability of a given driving system for driving a given pile, and of choosing an optimum system to obtain a desired load capacity without damaging the pile. It has been widely used for piles supporting offshore structures (McClelland et al., 1969; McClelland, 1974).

Although the safe working load of the pile is again determined by applying a safety factor to the calculated ultimate-load capacity, the fact that some account is taken of the soil characteristics removes at least part of the uncertainty in ascribing a suitable safety factor to a particular site.

The method of solution of the wave equation to obtain the ultimate load versus set relationship is described below, and typical values of the requisite soil-data input are discussed. Some solutions from the wave-equation approach showing the effect of various factors are given in Section 4.4, and a discussion of the reliability of the wave equation is given in Section 4.5.

The use of the wave equation was considered by Isaacs (1931) and Glanville et al. (1938), but it was not until the work of Smith (1960) that the method was fully developed. Considerable refinements of Smith's analysis have been made, notably by Samson, Hirsch and Lowery (1963), and Forehand and Reese (1964). Scanlan and Tomko (1969) have also applied wave theory, in a somewhat different approach, to estimate pile capacity. In the development of the method described below, the nomenclature and notation of Samson et al. (1963) and Lowery et al. (1969) will generally be employed.

4.3.1 The Wave Equation

The wave equation may be derived from consideration of the internal forces and motion produced on a segment of a freely-suspended prismatic bar subjected to an impact at one end. The resulting equation is

$$\frac{\partial^2 D}{\partial t^2} = \left(\frac{E}{\rho}\right)\left(\frac{\partial^2 D}{\partial x^2}\right) \tag{4.12}$$

where

D = longitudinal displacement of a point of the bar from its original position
E = modulus of elasticity of bar
ρ = density of bar material
t = time
x = direction of longitudinal axis

For a pile, the resistance of the surrounding soil must also be considered; in which case, Eq. (4.12) becomes

$$\frac{\partial^2 D}{\partial t^2} = \left(\frac{E}{\rho}\right)\left(\frac{\partial^2 D}{\partial x^2}\right) \pm R \tag{4.13}$$

where

R = soil-resistance term.

Equation (4.13) may be solved, for the appropriate initial and boundary conditions, to determine the relationship among displacement, time, and position in the pile, from which the stress variation in the pile may be determined. Because of the complications involved in practical piling problems, analytical solutions to Eq. (4.13) generally are not feasible, and resort must be made to numerical means of solution. A convenient numerical method has been described by Smith (1960). A simple computer program is listed in Bowles (1977).

4.3.2 Smith's Idealization

The method developed by Smith is a finite-difference method in which the wave equation is used to determine the pile-set for a given ultimate pile load. The pile system is idealized as shown in Fig. 4.4. and consists of

1. A ram, to which an initial velocity is imparted by the pile driver.

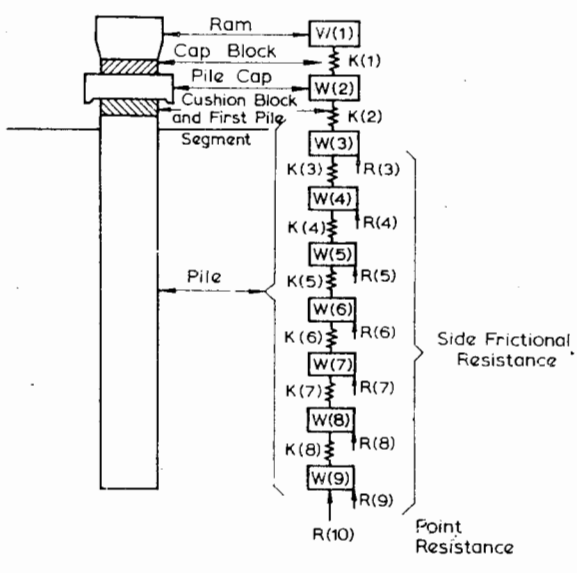

FIGURE 4.4 Idealization of pile.

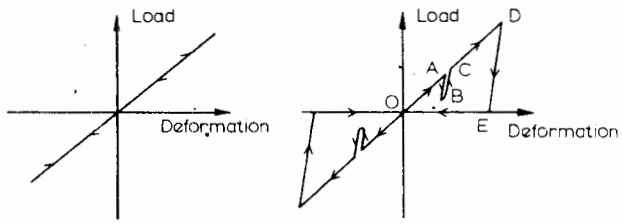

FIGURE 4.5 Load-deformation relationships for internal springs.

2. A capblock (cushioning material).
3. A pile cap.
4. A cushion block (cushioning material).
5. The pile.
6. The supporting soil.

The ram, capblock, pile cap, cushion block, and pile are represented by appropriate discrete weights and springs. The frictional resistance on the side of the pile is represented by a system of springs and dashpots (see Fig. 4.6), while the point resistance is represented by a single spring and dashpot. The characteristics of the components are considered subsequently. If the actual situation differs from that shown in Fig. 4.4—that is, if the cushion block is not used or if an anvil is placed between the ram and capblock—the idealization of the system can of course be modified.

Pile Model–Internal Springs

The ram, capblock, pile cap, and cushion block may be considered to consist of internal springs, although the ram and pile cap can often be treated as rigid bodies. The load-deformation behavior of these elements is most simply taken to be linear (Fig. 4.5*a*) although internal damping may also be considered (e.g., as shown in Fig. 4.5*b*), for components such as the capblock and the cushion block. It should be noted that the spring $K(2)$ in Fig. 4.4 represents both the cushion block and the top element of the pile, and its stiffness may be obtained from Kirchoff's equation as

$$\frac{1}{K(2)} = \frac{1}{K(2)_{\text{cushion}}} + \frac{1}{K(2)_{\text{pile}}} \tag{4.14}$$

Soil Model–External Springs

Smith's model of the load-deformation characteristics of the soil, represented as external springs, subjected to static loading, is shown in Fig. 4.6. The path *OABCDEFG* represents loading and unloading in side friction. For the point, only compressive loading is considered and the loading and unloading path is *OABCF*. The quantities defining this static behavior are Q and R_u where

Q = "quake," the maximum soil deformation that may occur elastically
R_u = ultimate static soil-resistance

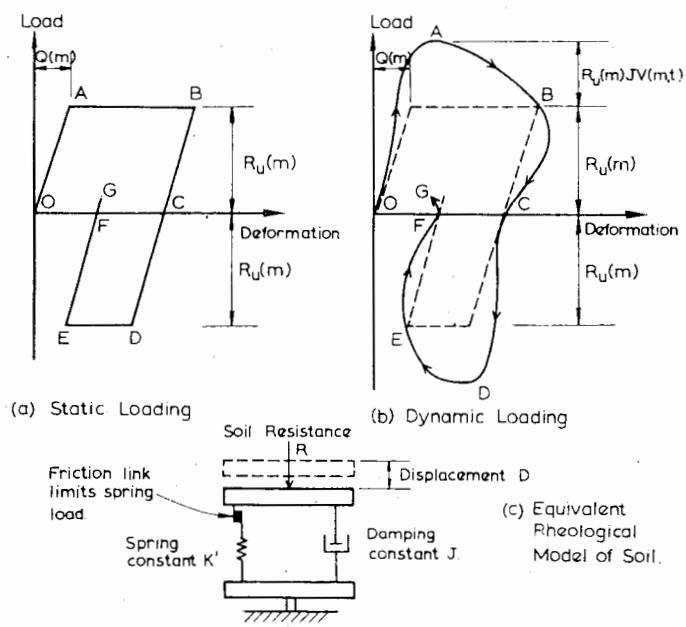

FIGURE 4.6 Load-deformation relationships for soil.

A load-deformation diagram such as Fig. 4.6 may be established separately for each spring, so that

$$K'(m) = \frac{R_u(m)}{Q(m)} \tag{4.15}$$

where $K'(m)$ is the spring constant during elastic deformation for external spring m.

To allow for the effects of dynamic loading during driving in increasing the instantaneous resistance of the soil, the dynamic load-settlement behavior of the soil is taken to be that shown in Fig. 4.6*b*, which as pointed out by Lowery et al. (1969), corresponds to a Kelvin rheological model. This dynamic behavior is characterized by a further parameter J, the damping constant. The dashpot in the model produces an additional resisting force proportional to the velocity of loading (V).

4.3.3 Basic Equations

In solving the wave equation numerically, Eq. (4.13) could be expressed in finite-difference form for each element, and then the resulting equations, incorporating the appropriate boundary conditions, could be solved simultaneously for each time-interval considered. This method is the conventional method of solving such equations and has been suggested for this problem by Soderberg (1962*b*); it may also be applied to problems involving periodic dynamic loading of the pile. However, it has been shown by Smith (1960) that the finite-difference form of the wave equation may be replaced by a system of five simpler equations, and this form of expression of the wave equation has generally been adopted for pile-driving analysis. The basic equations are as follows:

$$D(m, t) = D(m, t-1) + \Delta t \cdot V(m, t-1) \tag{4.16}$$

$$C(m, t) = D(m, t) - D(m+1, t) \tag{4.17}$$

$$F(m, t) = C(m, t) \cdot K(m) \tag{4.18}$$

$$R(m, t) = [D(m, t) - D'(m, t)] \cdot K'(m) \cdot [1 + J(m) \cdot V(m, t-1)] \tag{4.19}$$

$$V(m, t) = V(m, t-1) + [F(m-1, t) + W(m) - F(m, t) - R(m, t)] \cdot \frac{g\Delta t}{W(m)} \tag{4.20}$$

where

m = element number
t = time
Δt = time interval
$C(m, t)$ = compression of internal spring m at time t
$D(m, t)$ = displacement of element m at time t
$D'(m, t)$ = plastic displacement of external spring m at time t
$F(m, t)$ = force in internal spring m at time t
g = acceleration caused by gravity
$J(m)$ = soil-damping constant at element m
$K(m)$ = spring constant for internal spring m
$K'(m)$ = spring constant for external spring m
$R(m, t)$ = force exterted by external spring m on element m at time t
$V(m, t)$ = velocity of element m at time t
$W(m)$ = weight of element m

Equation (4.18) applies for the elastic pile elements for which internal damping is ignored. For elements such as the capblock and the cushion block, in which internal damping should be considered, the following equation should be used instead of Eq. (4.18):

$$F(m, t) = \frac{K(m)}{[e(m)]^2} \cdot C(m, t) - \left\{\frac{1}{[e(m)]^2} - 1\right\} \cdot K(m) \cdot C(m, t)_{\max} \tag{4.21}$$

where

$e(m)$ = coefficient of restitution of internal spring m
$C(m, t)_{\max}$ = temporary maximum value of $C(m,t)$

The above equation characterizes the path $OABCDEO$ shown in Fig. 4.5*b*. For a pile cap or cushion block, no tensile forces can exist and hence only this part of the diagram applies. Intermittent unloading-loading is typified by path ABC, established by control of $C(m, t)_{\max}$ in Eq. (4.17). The slope of lines AB, BC, and DE depends on the value of $e(m)$.

Smith (1960) notes that Eq. (4.19) produces no damping when $D(m, t) - D'(m, t)$ becomes zero, and suggests an alternate equation to be used after $D(m, t)$ first becomes equal to $Q(m)$, where $Q(m)$ is the "quake" for element m:

$$R(m, t) = [D(m, t) - D'(m, t)] \cdot K'(m) + J(m) \cdot R_u(m) \cdot V(m, t-1) \tag{4.22}$$

where $R_u(m)$ is the ultimate static soil-resistance of element m.

Equations (4.16) to (4.22) are solved for each of the pile elements involved, $m = 1$ to $m = p$ (point), for a succes-

sion of time intervals starting when the hammer [$W(1)$] travelling with known velocity touches the first spring. The solution of these equations continues until the permanent set or plastic displacement of the soil at the point $D'(p, t)$ is a maximum.

Before commencing the computations, the following values must be determined:

1. The initial velocity of the ram at initial impact, v_r, which can be calculated as

$$v_r = \sqrt{E_r E_h \frac{2g}{W_h}} \tag{4.23}$$

where

E_r = manufacturer's hammer-energy rating
E_h = pile-driver hammer efficiency
W_h = weight of hammer

2. Values of the internal spring constants, $K(m)$, of the pile and other elements, where

$$K(m) = \frac{AE}{\Delta L}$$

where

A = cross-sectional area of element m
E = Young's modulus of element m
ΔL = length of element m

3. Values of the external spring constants, $K'(m)$, of the soil. This necessitates the assumption of a total pile resistance R_u, the percentage of pile resistance to be used as side resistance, and the distribution of side resistance along the pile. If known, the soil strength and adhesion properties may provide a guide to the selection of the above quantities (see Chapter 3).

If it is assumed that the proportion of load carried by the pile point is ξ, then the internal spring constant, $K(p)$, for the pile tip is

$$K(p) = \frac{\xi R_u}{Q(p)} \tag{4.25}$$

where $Q(p)$ = quake at the pile point. Also, if, for example, the shaft resistance is assumed to be distributed uniformly along the shaft, the external spring constant, $K(m)$, at the element m is

$$K(m) = \frac{(1-\xi) R_u}{nQ(m)} \tag{4.26}$$

where

$Q(m)$ = quake at element m
n = number of elements along the pile

4. Values of the quakes $Q(m)$ and $Q(p)$ and the damping factors $J(m)$ and $J(p)$. These quantities are discussed in Section 4.3.4.

In performing the computations, the following sequence of operations is carried out:

1. The initial velocity, v_r, is calculated from Eq. (4.23). Other time-dependent quantities are initialized at zero or to produce equilibrium of forces under gravity.
2. The displacements $D(m,t)$ are calculated from Eq. (4.16) where for the first time-step, $V(1,0)$ is the initial velocity of the ram.
3. The total plastic deformation of the soil, $D'(m, t)$, remains constant [starting at $D'(m, t) = 0$] unless it is changed by the following condition (see Fig. 4.7*a*):

$$D'(m, t) \leftarrow D(m, t) - Q(m) \tag{4.27a}$$
$$D'(m, t) \rightarrow D(m, t) + Q(m) \tag{4.27b}$$

These comparisons are made in each time-interval, Δt, and $D'(m, t)$ is adjusted accordingly.

4. The plastic deformation of the pile tip, $D'(p, t)$, remains constant, starting at zero, unless changed by the condition (see Fig. 4.7*b*).

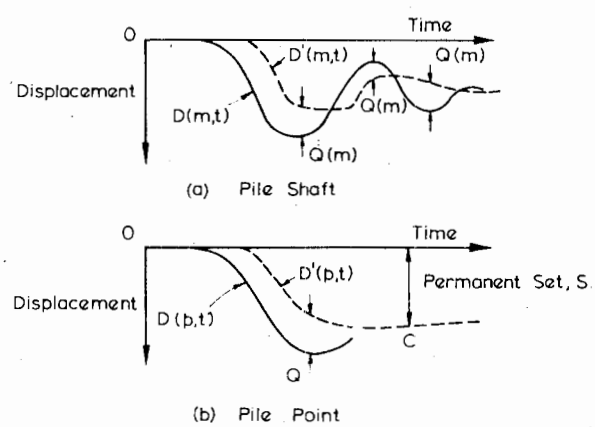

FIGURE 4.7 Displacements of pile vs. time.

$$D'(p, t) \leq D(p, t) - Q(p) \tag{4.28}$$

This comparison is made at each time-interval and $D'(p, t)$ is adjusted accordingly.

5. The soil resistances $R(m, t)$ for $m = 3$ to p are calculated from Eq. (4.19). If desired, when $D(m, t) - D'(m, t)$ first becomes zero, Eq. (4.22) may be used.

6. The spring compressions $C(m, t)$ for $m = 1$ to $p - 1$ are calculated from Eq. (4.17).

7. The forces in the pile elements, $F(m, t)$, are calculated from Eq. (4.18) for the pile elements in which no internal damping occurs, or from Eq. (4.21) for the capblock and cushion block ($m = 1$ and 2). For the capblock, which is not attached to the pile, $F(1, t)$ can never be less than zero. For the pile cap, two cases are possible:

(a) $F(2, t) \geq 0$ if cap is not properly attached.
(b) $F(2, t)$ can be negative if cap is attached to pile.

Case (a) or (b) must be specified at the start of the problem.

8. The velocity $V(m, t)$ is calculated for $m = 1$ to p from Eq. (4.20).

9. The cycle is repeated for successive time-intervals until the pile segments reach their maximum downward movement and rebound upward. Unless Eq. (4.22) is used for $R(m, t)$, the computation can be terminated when

(a) $D'(p, t) - D'(p, t - 1) = 0$.
(b) $V(1, t)$ to $V(p, t)$ are all simultaneously negative or zero.

The permanent set of the pile tip as a result of the ram blow is the maximum value of $D'(p, t)$.

10. If the relationship between permanent set (or its reciprocal, the blow count), and the ultimate resistance R_u of the pile is required, various values of R_u are chosen and the procedure repeated. A plot of R_u versus permanent set (or blow count) may thus be obtained.

It is obvious that the above procedure requires the use of a computer for practical problems. A simple computer program has been given by Bowles (1977).

In employing the numerical procedure described above, the accuracy of the resulting solution will depend on the values of Δt and ΔL chosen. It has been shown that for free longitudinal vibrations in a continuous elastic bar, the discrete element solution is an exact solution of the partial differential equation when

$$\Delta t = \frac{L}{\sqrt{E/\rho}} \tag{4.29}$$

Because inelastic springs and material of different densities and elastic moduli are usually involved in practical problems, Samson et al. (1963) recommended a value of Δt of about half the value given by Eq. (4.29). The accuracy of the solution is more sensitive to the choice of Δt if the pile is divided into only a few elements. The solutions of Samson et al. suggest that $\Delta L = L/10$ is generally a reasonable division of the pile. Smith's original suggestions on Δt and ΔL were 1/4000 sec. and 8 to 10 ft, respectively, for most practical piles, which are consistent with the values recommended above.

Modification for Effect of Gravity

Smith's original procedure does not account for the static weight of the pile since all springs, internal and external, are assumed to exert zero force at $t = 0$: that is, $F(m, 0) = R(m, 0) = 0$. If the effect of gravity is to be included, these forces must be given initial values to reproduce equilibrium of the system; in fact, these initial values should be those in effect as a result of the previous blow, but this refinement appears unjustified (Samson et al., 1963).

Studies by Samson et al. (1963) indicate that the gravity effect is relatively small, and in a typical case, the effect of gravity was to increase the permanent set by about 10%. For practical purposes, it does not appear necessary to include the effect of gravity in the wave-equation analysis.

4.3.4 Values of Soil Parameters

The soil parameters required for the wave-equation analysis are the ultimate soil resistance, R_u; quake, Q; and damping factor, J.

Ultimate soil resistance, R_u

Various values of R_u are input into the computer program and the corresponding permanent set determined. The main problem with R_u is to determine the relative proportions of shaft and base resistance. A reasonable estimate of these proportions may be made by estimating the static shaft and base resistances from the known or assumed soil properties, as described in Chapter 3. A typical example of the effect of varying the proportions of shaft and base resistance is shown in Fig. 4.8. A somewhat higher ultimate resistance for a given driving resistance is obtained if some shaft resistance is considered, rather than only end-bearing. As a rough guide where other information is not available, values of the percentage of shaft resistance suggested by Forehand and Reese (1964) are shown in Table 4.7.

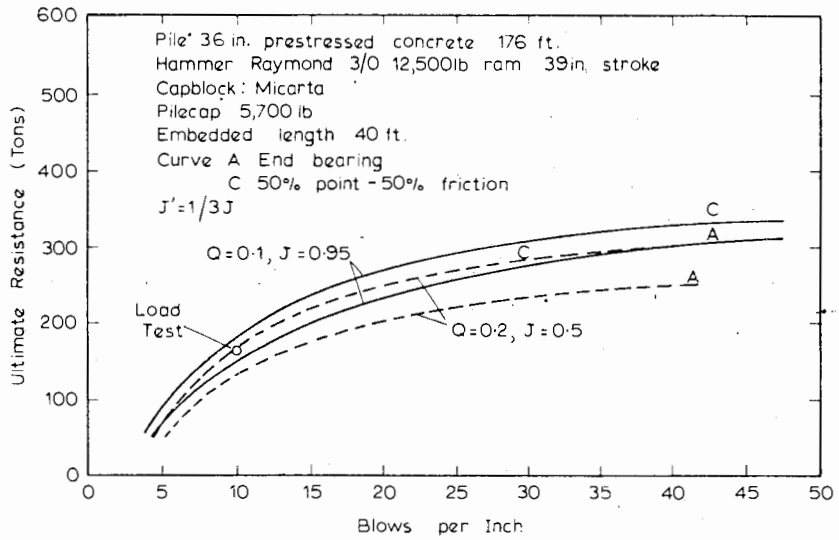

FIGURE 4.8 Resistance vs. set curves for 36-in.-diameter prestressed concrete Pile. Effect of percentage point load (Forehand and Reese, 1964).

TABLE 4.7 EMPIRICAL VALUES OF Q, J, AND PERCENT SIDE ADHESION[a]

Soil	Q (in.)	$J(p)$ (sec/ft)	Side Adhesion (% of R_u)
Coarse sand	0.10	0.15	35
Sand gravel mixed	0.10	0.15	75–100
Fine sand	0.15	0.15	100
Sand and clay or loam, at least 50% of pile in sand	0.20	0.20	25
Silt and fine sand underlain by hard strata	0.20	0.20	40
Sand and gravel underlain by hard strata	0.15	0.15	25

[a] After Forehand and Reese (1964).

Quake, Q

Values of Q have been obtained empirically to date, and the single empirical values of Q for all elements of the pile suggested by Forehand and Reese (1964) are shown in Table 4.7. It is, however, also possible to derive values of Q theoretically from pile-settlement theory if the "elastic" soil parameters are known (see Chapter 5). On the basis of this theory, the value of Q varies along the pile, with the value at the pile tip being greater than the values along the shaft. Alternatively, Q could also be estimated from the soil-resistance curves employed by Seed and Reese (1957) and Coyle and Reese (1966).

An example of the effect of varying Q on the R_u versus driving-resistance curve is shown in Fig. 4.9. The curves have been obtained by Hirsch et al. (1969) for a steel-pipe pile in a layered-soil profile consisting mainly of clays. R_u tends to decrease as Q increases.

Damping factor, J

Empirical correlations between J and soil type obtained by Forehand and Reese (1964) are shown in Table 4.7. The values in this table are for the pile point [i.e., $J(p)$]. The average value for the sides of the pile $J(m)$ have been found

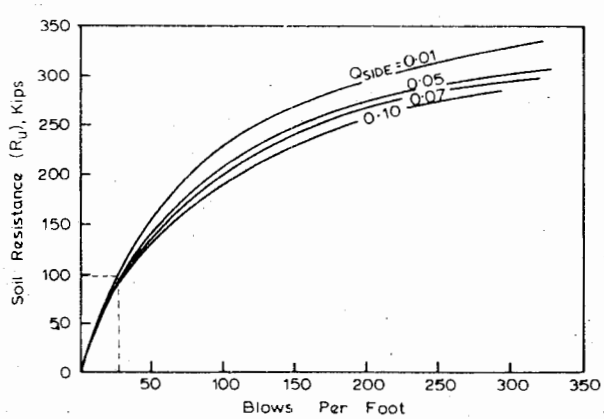

FIGURE 4.9 Effect of varying Q_{side} (Hirsch et al., 1969).

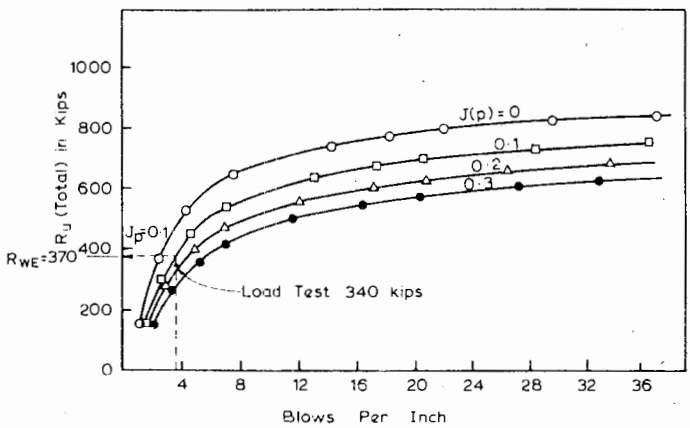

FIGURE 4.10 Effect of J (Hirsch et al., 1969). Arkansas load test, pile 4.

to be less than $J(p)$, and for practical purposes, it has been suggested that

$$J(m) = \frac{1}{3}J(p) \tag{4.30}$$

A typical example of the effect of $J(p)$ $[J(m) = \frac{1}{3}J(p)]$ is shown in Fig. 4.10 for a pipe pile in a relatively dense medium to fine sand with some thin seams of clay (Arkansas Test Piles, Hirsch et al., 1970). For a given blow count, R_u decreases as $J(p)$ increases.

Various attempts have also been made to measure $J(p)$ from static and dynamic tests on triaxial specimens (Coyle and Gibson, 1970). It has been found, however, that $J(p)$ is dependent on the velocity of deformation for both sands and clays, decreasing as velocity increases. Coyle and Gibson

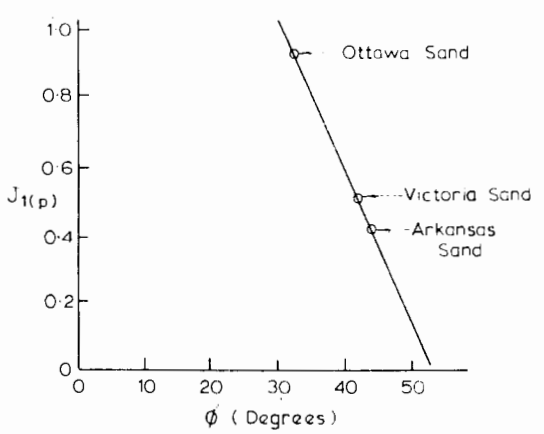

FIGURE 4.11 Effective angle of internal shearing resistance vs. damping constant for sand (Coyle and Gibson, 1970).

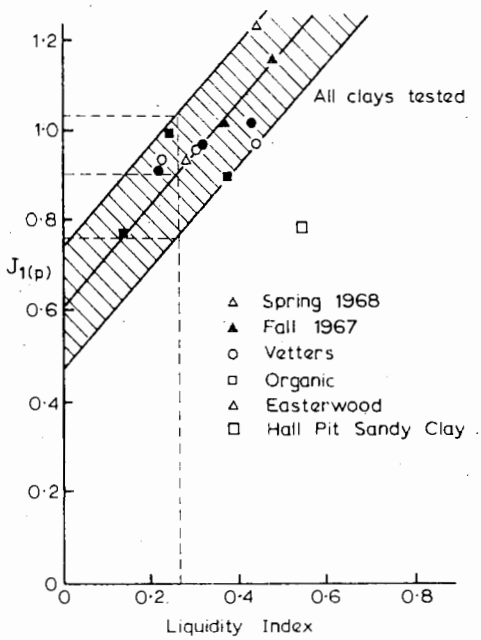

FIGURE 4.12 Liquidity index vs. damping constant for clays (Coyle and Gibson, 1970).

suggest that this problem can be overcome by rewriting Smith's original Eq. (4.19) as follows:

$$R(m, t) = [D(m, t) - D'(m, t)] \times K'(m) \{1 + J_1(m) [V(m, t-1)]^N\} \tag{4.31}$$

where $J_1(m)$ is a modified damping factor and the exponent N is less than 1.

The most suitable values were found to be

$N = 0.20$ for sands
$N = 0.18$ for clays

On the basis of the above modified equation, Coyle and Gibson found $J_1(p)$ to be almost independent of velocity, and reasonable correlations between $J_1(p)$ and soil properties could be obtained. The relationship between $J_1(p)$ and ϕ' for sands is shown in Fig. 4.11, while the relationship between $J_1(p)$ and the liquidity index for clays is shown in Fig. 4.12.

4.3.5 The Effect of "Set-Up"

As described in Chapter 2, driving a pile into normally consolidated clay results in the creation of excess pore pres-

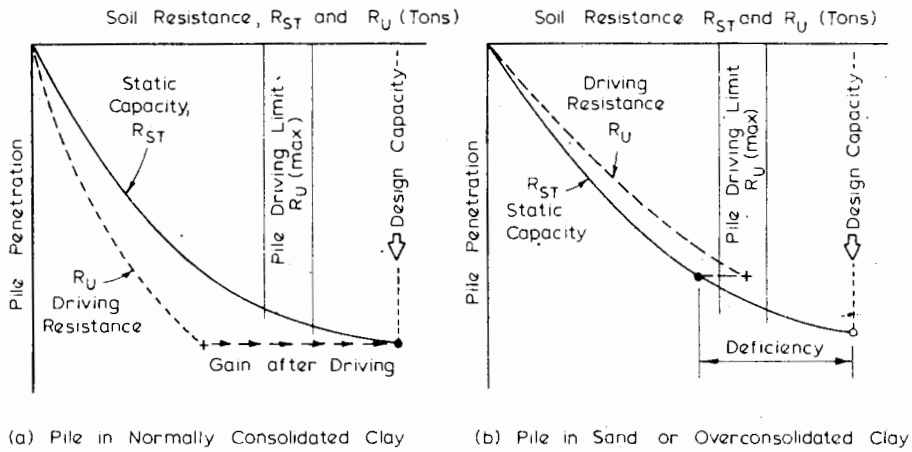

(a) Pile in Normally Consolidated Clay (b) Pile in Sand or Overconsolidated Clay

FIGURE 4.13 Effect of pile characteristics (McClelland et al., 1969).

sures and subsequent consolidation and possible regain in soil strength and pile-soil adhesion. As shown in Fig. 4.13*a* (McClelland et al., 1969), under these circumstances, a pile hammer with a driving limit less than design capacity may successfully drive a pile to design penetration. A prediction of the pile capacity on the basis of the wave equation, however, will only give the pile capacity immediately after driving; thus, if the pile capacity some time after driving is required, some knowledge of the amount of "set-up" (i.e., increase in soil strength and adhesion with time) is required. If the "set-up" factor (the ratio of soil strength a considerable time after driving to that immediately after driving) can be estimated, the final load capacity, R_{uF}, can be calculated as follows:

$$R_{uF} = \sum_{i=1}^{l} \Delta R_i s k_i \tag{4.32}$$

where

ΔR_i = immediate soil resistance in soil type i, as calculated from the wave equation
sk_i = set-up factor for soil type i
l = number of soil layers through which the pile is driven

Lowery et al. (1969) tentatively suggest that a set-up factor of 3 might be appropriate for soft clays, 2 for firm and stiff clays, and 1 for other soils.

McClelland et al. (1969), on the other hand, consider that for piles driven into hard clay or sand, a decrease of soil strength and adhesion with time could occur. The final static resistance of the pile would then be less than the resistance during driving (see Fig. 4.13*b*), and under these circumstances, the driving limit of the hammer may be reached before design penetration is reached.

4.4 TYPICAL SOLUTIONS FROM WAVE-EQUATION ANALYSIS

4.4.1 Resistance versus Set Curves

Effects of Pile Characteristics

Typical solutions showing the effect of various pile characteristics on the resistance versus set curves have been presented by McClelland et al. (1969). The problem considered is shown in Fig. 4.14, together with the effects of pile length above the ground, embedded length, distribution of soil resistance, and pile wall thickness. The effects of the first two factors are relatively small, while as previously indicated in Fig. 4.8, the ultimate resistance increases as the proportion of load taken by the pile point decreases. The effect of pile wall thickness is quite marked, with the ultimate resistance increasing as the wall thickness increases. Bender, Lyons, and Lowery (1969) have found that a pile having a varying wall thickness along its length may be adequately replaced by a pile of equivalent uniform thickness.

Effect of Hammer Characteristics

For the same problem shown in Fig. 4.14, the effect of the hammer energy is shown in Fig. 4.15. The resistance increases as the hammer energy increases, but doubling the energy leads only to an increase of about 28% in this case. For the 60,000–ft-lb hammer, which is widely used in the

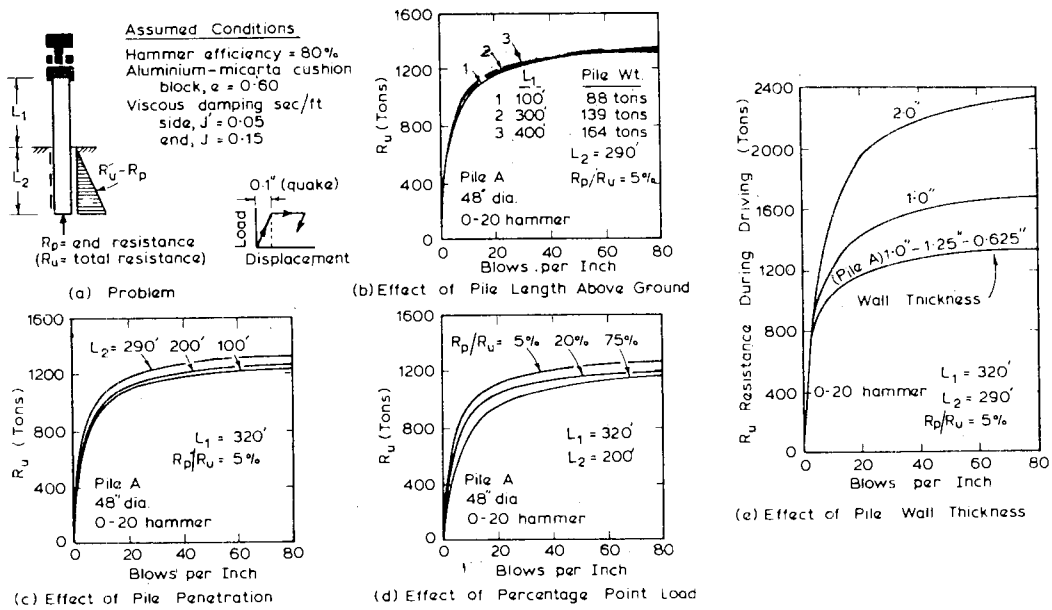

FIGURE 4.14 Effect of pile characteristics (McClelland et al., 1969).

United States, the maximum pile-load capacity for the pile considered is on the order of 1200 tons for a practical driving limit of 40 blows per in. For offshore pile installations, capacities in excess of 2000 tons may be required, and under these circumstances, using a large blow count or increasing the energy rating of the hammer are not efficient solutions. As shown in Fig. 4.14, increasing the pile wall thickness may be effective. Alternatively, McClelland et al. (1969) suggest four possible solutions:

(a) Driving an insert pile through an initially installed, larger pile.

(b) Grouting a pile into an oversized hole.

(c) Driving a pile concentrically with an undersized pilot hole.

(d) Driving a pile with the aid of uncontrolled drilling or jetting.

These four procedures are illustrated in Fig. 4.16.

The effect of ram shape and hammer efficiency has been examined by Bender, Lyons, and Lowery (1969). For a given ram weight and fall, a longer ram was found to be slightly more effective than a shorter one, although the

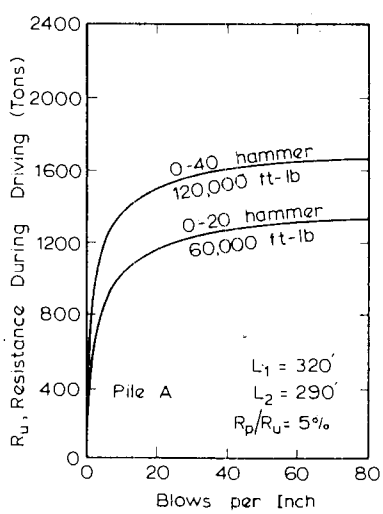

FIGURE 4.15 Effect of hammer energy (McClelland et al., 1969).

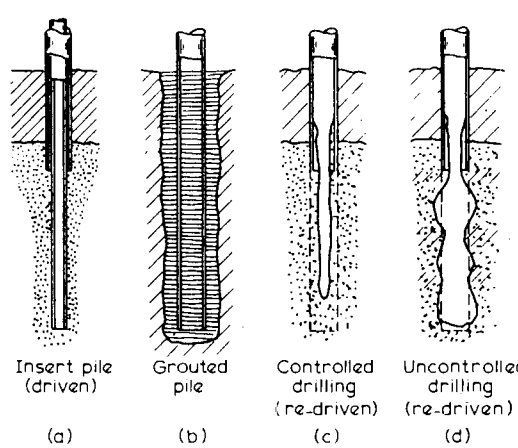

FIGURE 4.16 Installation procedures currently in use for piles that cannot be installed by driving alone (McClelland et al., 1969).

presence of a cushion tended to reduce the effect of hammer shape. A reduction in hammer efficiency was found to result in considerably more blows being required to drive to a given resistance when the resistance is high. At lower resistances, this effect is not as pronounced; however, the net increase in total driving time per pile can be quite significant, and the possibility of not being able to drive the pile to design penetration must be considered. Thus, neglect of hammer maintenance can seriously reduce hammer capabilities.

The effects of both hammer and pile characteristics on the resistance versus set curves have also been examined by Mosley and Raamot (1970), who give a series of solutions for various sizes of steel and concrete piles driven by two different hammers.

Effect of Cushion Stiffness

An example of the effect of cushion stiffness is shown in Fig. 4.17 (Bender, Lyons, and Lowery, 1969). As the cushion stiffness decreases, the ability to drive against soil resistance decreases. Figure 4.17 suggests that there is an optimum cushion stiffness that can provide adequate protection for the hammer and pile while not seriously affecting the driving capability of the system. For example, increasing the cushion stiffness above about 1000 kip/in. when driving against 800-kips resistance does not lower the number of blows per foot and will lead to higher driving stresses with no gain in driveability. It is clear that in practice the cushion should be inspected at regular intervals, so that a deteriorated cushion, which might adversely affect the driving process, may be detected and replaced.

Effect of Soil Characteristics

The effects of varying the quake Q and damping factor J have been shown previously, in Figs. 4.9 and 4.10, while the effect of relative shaft and point resistances has been shown in Figs. 4.8 and 4.14.

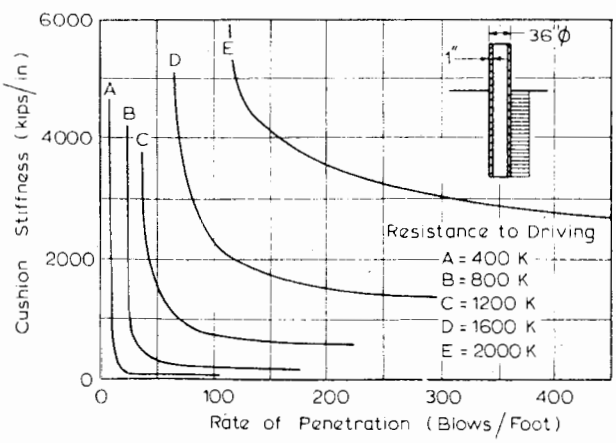

FIGURE 4.17 Effect of cushion stiffness (Bender et al., 1969).

4.4.2 Pile Stresses

Effect of Pile Characteristics

For typical cases involving prestressed concrete piles, Samson et al. (1963) have investigated the influence of the Young's modulus of the pile and the stiffness of the cushion block on the maximum tensile and compressive stresses in the pile. Higher compressive and tensile stresses are developed for higher values of pile modulus or increasing stiffness of the cushion block. The high tensile stresses are of considerable interest, especially for a prestressed concrete pile, and could significantly influence the design of the pile and the specification of driving conditions. Samson et al. (1963) have noted that the time for a tensile wave to be reflected back along a typical pile is less than 0.02 sec, whereas the time interval between successive blows, for a typical rate of 105 blows per min, is 0.57 sec—that is, about 28 times greater than the time for tensile-wave reflection. Thus, successive blows cannot be relied upon to reduce tensile stresses.

Effect of Hammer Characteristics

Samson et al. (1963) have also investigated the effects on pile stresses of ram velocity and weight, and of explosive pressure (as might be encountered in certain types of diesel hammers). The ram velocity is of primary importance, the stresses increasing with increasing velocity. However, the effects of ram weight and explosive pressure are relatively minor.

Effect of Soil Characteristics

From Figs. 4.9 and 4.10, it will be seen that an increase in both quake Q and damping J lead to a decrease in R_u and hence to lower driving stresses in a given pile.

4.5 RELIABILITY OF WAVE EQUATION

Investigations of the reliability of the wave equation in predicting ultimate resistance have been made by Sorensen and Hansen (1957) and Lowery et al. (1969). A statistical analysis of the above comparisons is summarized in Table 4.8. Despite differences in application of the wave equation in the two cases, the results are reasonably consistent and indicate that the wave equation is at least as good as the best of the pile-driving formulas (see Section 4.2). Lowery et al.

TABLE 4.8 STATISTICAL ANALYSES OF WAVE-EQUATION RELIABILITY

Reference	Standard Deviation on μ	Upper Limit for 96% Safety if Lower Limit Is 1.0	Nominal Safety Factor	Number of Load Tests
Hansen & Sorensen (1957)	0.23	4.0	2.7	78
Lowery et al. (1969)	0.26	3.4	2.0	31

μ = ratio of measured to computed load capacity

(1969) consider that load capacity is predicted by the wave equation to an accuracy as follows:

Piles in sand: ± 25%
Piles in clay: ± 40%
Piles in sand & clay: ± 15%

Some comparisons have also been made between measured and predicted stresses in the pile during driving, a detail that cannot be predicted by conventional pile-driving formulas. A typical comparison made by Samson et al. (1963) is shown in Fig. 4.18 for a point 9.5 ft below the pile head. Fair agreement is found when internal damping is considered.

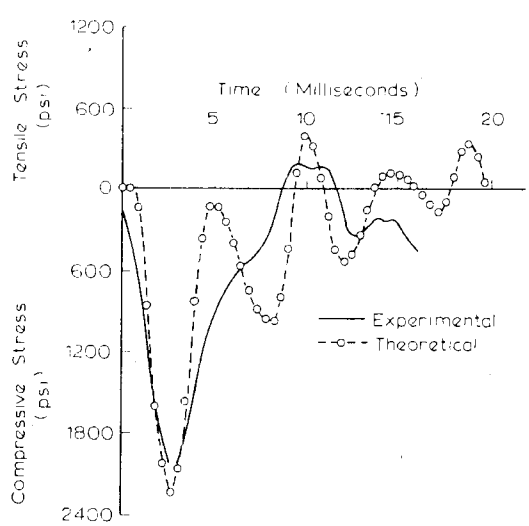

FIGURE 4.18 Comparison of theoretical and test results: pile IV (Samson et al., 1963).

Despite the above comparisons, care should be taken when attempting to use any dynamic approach, whether it be a pile-driving formula or the wave equation, for estimating the static bearing capacity of a pile, since such approaches strictly only predict the pile capacity just after driving. In soft clays, "set-up" can greatly affect the load capacity of a pile subsequent to driving, as described in Section 4.3.5, and unless an appropriate allowance is made, serious errors in predicted capacity could result. Also, if piles are driven through a compressible soil that may consolidate under its own weight or may be subjected to fill or embankment loading, a downdrag force is transmitted to the pile by "negative friction" acting on the pile surface. In considering the safe load that can be applied to such piles, account should be taken of this downdrag force, which may in some cases be a significant part of the ultimate load capacity of the pile. The calculation of downdrag forces caused by negative friction is treated in detail in Chapter 11.

4.6 PILE IMPEDANCE

Parola (1970) used the concept of impedance to motion to examine energy transmission from the ram to the pile, as a function of system impedance. His simplified analysis simulated ram-drive head impact and energy transmission to an infinite elastic rod. From a series of analyses employing a range of hammer-cushion-pile properties commonly used in practice, Parola found that a range of pile/hammer impedance values would assure at least 90% efficient energy-transfer to the pile, this range being expressed as:

$$\rho cA = (0.6 \text{ to } 1.10)\sqrt{\frac{W_{\text{ram}}}{g}(K)} \qquad (4.33)$$

where

ρ = mass density of pile
c = wave velocity in pile $= \sqrt{E/\rho}$
E = Young's modulus of pile
A = cross-sectional area of pile
W_{ram} = ram weight
K = axial stiffness of pile cushion
g = acceleration as a result of gravity

The quantity ρcA is defined as the pile impedance, and the term $\sqrt{\frac{W_{\text{ram}}}{g}(K)}$ represents the driving impedance.

The implications of this concept are as follows. Too stiff a pile, and hence too large a pile impedance, will cause the ram to rebound, reflecting input energy. Piles having too low an impedance absorb only a portion of the ram energy, as the ram will follow the pile and retain energy. Either condition causes inefficient driving and may cause pile damage. Pile impedance also has a significant influence on peak driving stresses. Higher impedance piling (heavier and/or stiffer sections) induces higher peak stresses and shorter impact durations under otherwise similar conditions.

Along with matching the impedance of the pile and driving system, consideration must also be given to the shape of the transmitted stress wave in order to ensure the most efficient driving system. Parola found that pile driveability is directly influenced by stress-wave shape. For easy driving conditions (low resistance to penetration), it was found that longer impact duration (longer stress-wave length) was more effective in increasing penetration per blow than was the magnitude of the impact stress. Conversely, for hard driving conditions, pile penetration was increased more effectively by increased stress amplitude than by increased impact duration. Thus, in the latter case, use of a lighter ram at higher impact velocity, a stiffer cushion, and a higher impedance pile all tend to produce a higher stress wave of shorter duration, and this stress-wave shape will drive piling more efficiently under hard driving conditions. Under easy driving conditions, the selection of the opposite trend in any of the above variables will produce more penetration per blow. The judicious selection of a compatible hammer-pile-soil system may therefore optimize driveability and minimize installation cost. It is in pursuing this aim that the wave-equation analysis probably enjoys its greatest success.

5

SETTLEMENT ANALYSIS OF SINGLE PILES

5.1 INTRODUCTION

Traditional methods of calculating the settlement of a pile rely on either an arbitrary assumption of the stress distribution along the pile and the use of conventional one-dimensional theory (Terzaghi, 1943), or on empirical correlations. Typical of these correlations are those proposed by Meyerhof (1959) for piles in sand and Focht (1967) for piles in clay. From an analysis of a number of load tests, Meyerhof has suggested that at loads less than about one third of the ultimate, the settlement of ρ of a pile could be estimated as follows (provided that no softer layers exist beneath the pile):

$$\rho = \frac{d_b}{30F} \tag{5.1}$$

where

d_b = diameter of pile base
F = factor of safety (>3) on ultimate load

Focht (1967) has examined data from a number of load tests and has related the observed settlement, ρ, at the working load to the computed column deformation ρ_{col} at the working load. Focht has defined a "movement ratio" as ρ/ρ_{col}, and has found that for relatively long highly-stressed piles having $\rho_{col} > 8$ mm, the movement ratio is on the order of 0.5, whereas for relatively rigid piles, having $\rho_{col} < 8$ mm, the movement ratio is larger, on the order of 1.0.

With the advent of computers, more-sophisticated methods of analysis have been developed to predict the settlement and load distribution in a single pile. Such methods may be classified into three broad categories:

1. "Load-transfer" methods, which use measured relationships between pile resistance and pile movement at various points along the pile.
2. Methods based on the theory of elasticity that employ the equations of Mindlin (1936) for subsurface loading within a semi-infinite mass.
3. Numerical methods; and in particular, the finite-element method.

This chapter describes these methods and discusses their advantages and limitations. Attention is then concentrated on solutions obtained from the elastic-based analysis and their use in predicting the load-settlement behavior of piles. The estimation of the required soil parameters is then discussed, and finally, some comparisons between observed and theoretical pile behavior are presented.

5.2 THEORETICAL METHODS OF ANALYSIS

5.2.1 Load-Transfer Method

This method, proposed by Coyle and Reese (1966), utilizes soil data measured from field tests on instrumented piles and laboratory tests on model piles. The relevant soil data required in this method are curves relating the ratio of the adhesion (or load transfer) and the soil shear strength to the pile movement. Such curves were first developed by Seed and Reese (1957), and a typical relationship is shown in Fig. 5.1. In actual problems, a number of such relationships may be required to describe the load transfer along the whole length of the pile.

The load-transfer method may be summarized as follows:

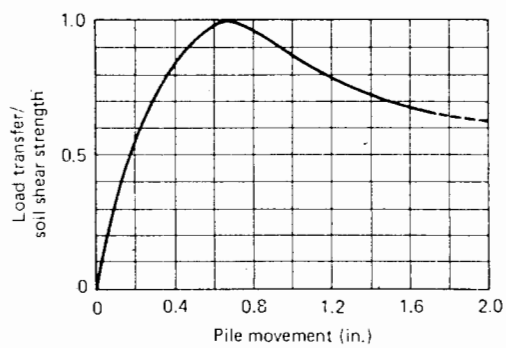

FIGURE 5.1*a* Typical shear stress vs. pile movement curve (after Coyle and Reese, 1966).

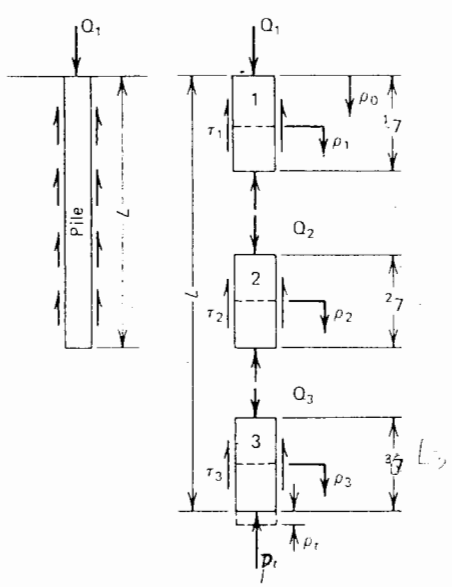

FIGURE 5.1*b* Load-transfer analysis (after Coyle and Reese, 1966)

1. The pile is divided into a number of segments (for simplicity, three segments are shown in Fig. 5.1*b*).
2. A small tip movement, ρ_t, is assumed (zero may be selected, but generally the tip undergoes some movement, except for end-bearing piles on rock).
3. The point resistance, P_t, caused by this movement is calculated. This may be done approximately by assuming the pile tip to be a rigid circular area and employing the Boussinesq theory:

$$P_t = \frac{2dE\rho_t}{(1-\nu^2)} \tag{5.2}$$

where

E, ν are the average deformation parameters of the material beneath the tip, estimated from triaxial tests or other data

4. A movement, ρ_3, in the bottom segment at midheight is assumed (for the first trial, assume $\rho_3 = \rho_t$).
5. Using the estimated ρ_3, the appropriate curve of load-transfer/soil-shear-strength versus pile movement (e.g., as in Fig. 5.1) is used to find the appropriate ratio.
6. From a curve of shear-strength versus depth, the strength of the soil at the depth of the segment is obtained.
7. The load transfer or adhesion is then calculated as τ_a = (ratio × shear strength). The load Q_3 on the top of segment 3 can then be calculated as

$$Q_3 = P_t + \tau_a L_3 P_3 \tag{5.3}$$

where

L_3 = length of segment 3
P_3 = average perimeter of segment 3

8. The elastic deformation at the midpoint of the pile segment (assuming a linear variation of load in the segment) is calculated as

$$\Delta'\rho_3 = \left(\frac{Q_m + P_t}{2}\right)\left(\frac{L_3}{2A_3E_p}\right) \tag{5.4}$$

where

$$Q_m = \frac{Q_3 + P_t}{2}$$

A_3 = area of segment 3
E_p = pile modulus

9. The new midheight movement is then given by

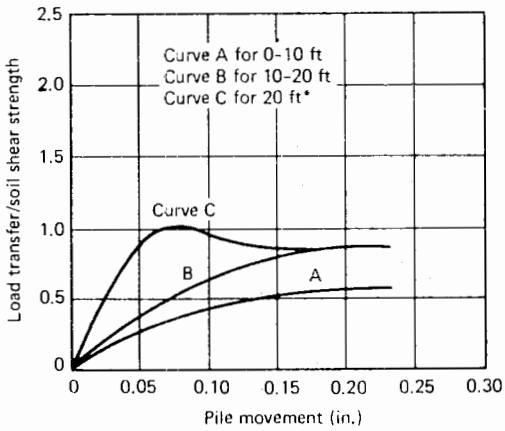

FIGURE 5.2 Design load-transfer curves for pipe piles in clay (Coyle and Reese, 1966).

$$\rho_3' = \rho_t + \Delta\rho_3' \tag{5.5}$$

10. ρ_3' is compared with the estimated value of ρ_3 from step (4).

11. If the computed movement ρ_3' does not agree with ρ_3 within a specified tolerance, steps (2) to (10) are repeated and a new midpoint movement calculated.

12. When convergence is achieved, the next segment up is considered, and so on, until a value of load (Q_0) and displacement (ρ_0) for the top of the pile are obtained.

The procedure is then repeated using different assumed tip movements until a series of values of Q_0 and ρ_0 are obtained. These values can then be used to plot a computed load-settlement curve.

On the basis of field data on instrumented piles and laboratory tests on model piles, Coyle and Reese derived a series of three average curves of load transfer, shear-strength versus pile-movement curves for various depths, which are shown in Fig. 5.2. The interpretation of the tests on instrumented piles to obtain these curves is described in detail by Coyle and Reese (1966). The curves in Fig. 5.2 are limited to the case of steel-pipe friction piles in a clay soil with an embedded depth not exceeding 100 ft, and the soil shear strengths in these curves have been obtained from unconfined compression tests.

From a series of tests on instrumented pile in sand, Coyle and Sulaiman (1967) have presented data on the load-transfer-versus-movement characteristics for steel piles in saturated sand, a summary of which is shown in Fig. 5.3. This data suggests that for depths of 0 to 20 ft, curve A, with an upper limit of skin friction of twice the shear strength, can be used (considerably higher values were obtained at shallow depths). For depths greater than 20 ft, the measured relationships approach curve B, with an upper limit of skin friction of 0.5 times the shear strength.

Reese et al. (1969) carried out load tests to study the load transfer along bored piles in clay. On the basis of a curve-fitting analysis of these test results, the following relationship between load transfer (adhesion) and pile movement was developed:

$$\tau_{az} = \tau_{a\max}\left[2.0\sqrt{\frac{\rho}{s_0}} - \left(\frac{\rho}{s_0}\right)\right] \tag{5.6}$$

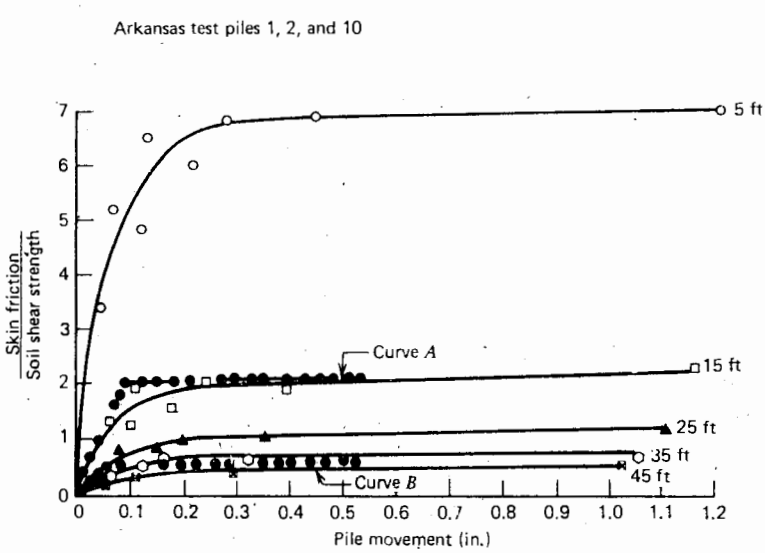

FIGURE 5.3 Design load-transfer curves for piles in sand (after Coyle and Sulaiman, 1967).

where

τ_{az} = adhesion at depth z (tons/ft^2)
$\tau_{a\max}$ = maximum adhesion that can occur at any depth (tons/ft^2)
ρ = downward movement of pile at depth z (in.)
s_0 = $2d\epsilon$ (in.)
d = pile diameter
ϵ = average failure strain, in percent, obtained from stress-strain curves for unconfined compression tests run on soil samples near the pile tip

Although the load-transfer method has gained quite wide acceptance, the following theoretical and practical limitations should be recognized:

(a) In using the load-transfer curves, it is inherently assumed that the movement of the pile at any point is related only to the shear stress at that point and is independent of the stresses elsewhere on the pile. This inherent assumption is equivalent to that made when the theory of subgrade reaction is used to analyze laterally loaded piles. Thus, no proper account is taken of the continuity of the soil mass.
(b) The load-transfer method, because of its inherent disregard for continuity of the soil, is not suitable for analyzing load-settlement characteristics of pile groups.
(c) In order to obtain load-transfer curves at a site, considerably more instrumentation is required on a pile than for a normal pile-load test. Extrapolation of test data from one site to another may not always be entirely successful.

5.2.2. Analysis Based on Elastic Theory

Elastic-based analyses have been employed by several investigators: for example, D'Appolonia and Romualdi (1963), Thurman and D'Appolonia (1965), Salas and Belzunce (1965), Nair (1967), Poulos and Davis (1968), Mattes and Poulos (1969), Poulos and Mattes (1969a), Butterfield and Banerjee (1971*a*, 1971*b*), Banerjee and Davies (1977), Randolph and Wroth (1978). In most of these approaches, the pile is divided into a number of uniformly-loaded elements, and a solution is obtained by imposing compatibility between the displacements of the pile and the adjacent soil for each element of the pile. The displacements of the pile are obtained by considering the compressibility of the pile under axial loading. The soil displacements are obtained in most cases by using Mindlin's equations for the displacements within a soil mass caused by loading within the mass.

The main difference between the various methods lies in the assumptions made regarding the distribution of shear stress along the pile. D'Appolonia and Romualdi, Thurman and D'Appolonia, and Salas and Belzunce assume the shear stress at each element to be represented by a single-point load acting on the axis at the center of each element. Nair assumes a uniformly-loaded circular area at the center of each element. Poulos and Davis, Mattes and Poulos, and Poulos and Mattes consider a shear stress distributed uniformly around the circumference of the pile. The latter appears to be the most satisfactory of those mentioned, especially for shorter piles. However, for relatively slender piles, there is very little difference between solutions based on the three above representations of shear stress. In the derivations described below, the method of Poulos and Davis (1968), among others, is followed. The basic problems of a floating or friction pile in a semi-infinite mass and an end-bearing pile are considered in detail and modifications to these analyses are described.

5.2.2.1 BASIC ANALYSIS FOR SINGLE FLOATING PILE

The pile is considered to be a cylinder, of length L, shaft diameter d, and base diameter d_b, and loaded with an axial force P at the ground surface. For the purposes of the analysis, the pile is acted upon by a system of uniform vertical shear stresses p around the periphery, and the base is acted upon by a uniform vertical stress p_b, as shown in Fig. 5.4. The sides of the pile are assumed to be rough. The soil is initially considered to be an ideal homogeneous isotropic elastic half-space, having elastic parameters E_s and ν_s that are not influenced by the presence of the pile. Modifications for more realistic representation of soil behavior will be discussed later. Unless otherwise stated, d_b will be taken to be equal to d.

As in almost all methods of pile-settlement analysis, it is assumed, that the pile and soil are initially stress-free, and that no residual stresses exist in the pile resulting from its installation. Holloway et al. (1975) emphasize the importance of residual pile-soil stresses on pile behavior and on the interpretation of pile-load tests, and suggest a method for evaluating such stresses. However, in order to reduce the complexity of the analysis here, the assumption of an initially stress-free pile is adopted; as subsequently will be demonstrated for predicting pile settlements, the influence of the residual stresses may be adequately taken into account by choosing appropriate values of the soil modulus.

If conditions at the pile-soil interface remain elastic and no slip occurs, the movements of the pile and the adjacent soil must be equal. The correct values of the stress

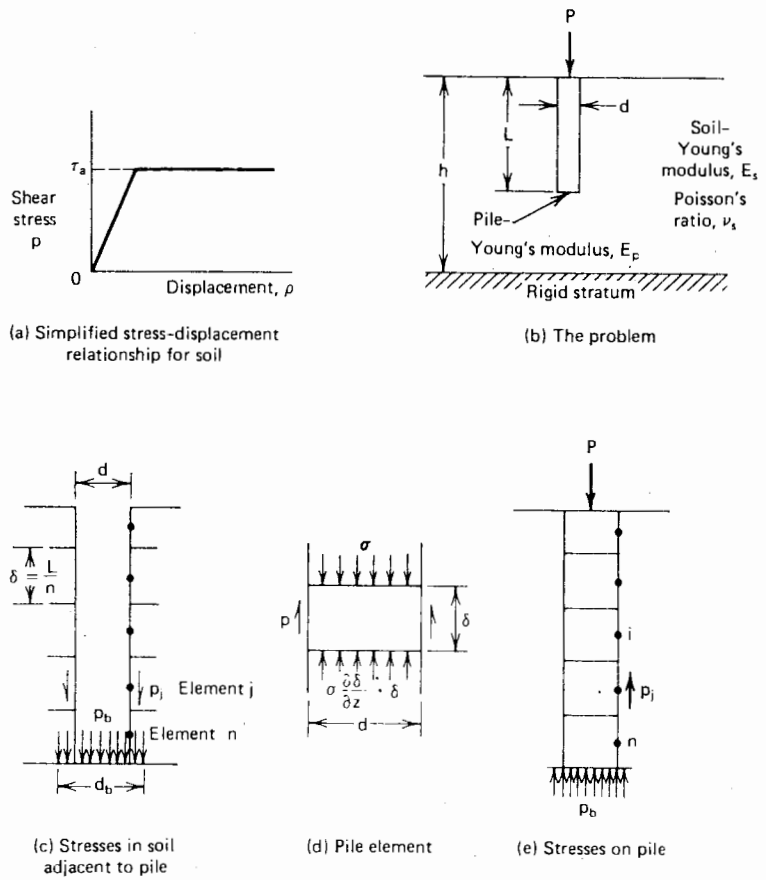

(a) Simplified stress-displacement relationship for soil

(b) The problem

(c) Stresses in soil adjacent to pile

(d) Pile element

(e) Stresses on pile

FIGURE 5.4 Analysis of floating pile.

system p^* and base stress p_b will be those that satisfy this condition of displacement compatibility. Ideally, consideration should be given to compatibility of both vertical and radial displacements, and a normal stress system σ should also then be imposed on the pile elements. However, as will be discussed, this more-complete analysis gives solutions that are generally almost identical with those from a simpler analysis that considers only vertical displacement compatibility: therefore, only the simpler analysis is described in detail. Details of the more complete analysis are given by Butterfield and Banerjee (1971) and by Mattes (1972). It has also been shown by Mattes (1972) that an even more refined analysis, one recognizing the difference between the fictitious and the real stress-systems, gives for piles and piers of normal proportions very similar solutions to those from the simple analysis described below.

In order to obtain a solution for the values of p, p_b, and the displacement of the pile, it is necessary to obtain expressions for the vertical displacement of the pile and the soil at each element in terms of the unknown stresses on the pile, impose the compatibility condition, and solve the resulting equations.

Soil Displacement Equations

Considering a typical element i in Fig. 5.4, the vertical displacement of the soil adjacent to the pile at i resulting from the stress p_j on an element j can be expressed as

$$s\rho_{ij} = \frac{d}{E_s} I_{ij} p_j \tag{5.7}$$

where

I_{ij} = vertical-displacement factor for element i due to shear stress at element j

* The shear stresses (p) are fictitious in that they represent tractions applied to the boundaries of the imaginary surface in the half-space representing the pile surface, and are not necessarily the actual stresses acting on the real-pile surfaces. Once the values of p are determined, the actual stresses and displacements they produce anywhere in the half-space, including the real-pile boundaries, may be calculated.

As a result of all n elements and the base, the soil displacement at i is

$$ {}_s\rho_i = \frac{d}{E_s}\sum_{j=1}^{n}(I_{ij}p_j) + \left(\frac{d_b}{E_s}I_{ib}\right)p_b \tag{5.8} $$

where

I_{ib} = vertical displacement factor for element i due to uniform stress on the base

A similar expression may be written for the base; and for all elements on the pile, the soil displacements may be written as

$$ \{s^\rho\} = \frac{d}{E_s}[I_s]\{p\} \tag{5.9} $$

where

$\{s\rho\}$ = soil-displacement vector
$\{p\}$ = pile stress vector
$[I_s]$ = $n+1$ square matrix of soil-displacement factors factors

$$ [I_s] = \begin{bmatrix} I_{11}\,I_{12} & \cdots & I_{1n}\,I_{1b}\cdot\frac{d_b}{d} \\ I_{21}\,I_{22} & \cdots & I_{2n}\,I_{2b}\cdot\frac{d_b}{d} \\ \cdots & \cdots & \cdots \\ \cdots & \cdots & \cdots \\ I_{n1}\,I_{n2} & \cdots & I_{nn}\,I_{nb}\cdot\frac{d_b}{d} \\ I_{b1}\,I_{b2} & \cdots & I_{bn}\,I_{bb}\cdot\frac{d_b}{d} \end{bmatrix} $$

Evaluation of the elements of I_s is most conveniently carried out by integration of the Mindlin equations (Mindlin, 1936) for the displacement caused by a point load within a semi-infinite mass. Details of the relevant integration are given in Appendix A.

Pile Displacement Equations

The pile material is assumed to have a constant Young's modulus E_p and area of pile section A_p. It is convenient to define the area ratio, R_A, as

$$ R_A = \frac{A_p}{\pi d^2/4} \tag{5.10} $$

= ratio of area of pile section A_p to area bounded by outer circumference of pile

For a solid pile, $R_A = 1$.

In calculating the displacement of the pile elements, only the axial compression of the pile is considered. Referring to Fig. 5.4*d*, consideration of vertical equilibrium of a small cylindrical pile element yields

$$ \frac{\partial\sigma}{\partial z} = \frac{-4p}{R_A d} \tag{5.11} $$

where

σ = axial stress in pile (average over the cross section)
p = shear stress on pile surface

The axial strain of this element is

$$ \frac{\partial_p\rho}{\partial z} = \frac{-\sigma^*}{E_p} \tag{5.12} $$

where

${}_p\rho$ = displacement of pile

From Eq. (5.11) and (5.12),

$$ \frac{\partial^2_p\rho}{\partial z^2} = \left(\frac{4p}{d}\right)\left(\frac{1}{E_p R_A}\right) \tag{5.13} $$

This equation can be written in finite-difference form and applied to the points $i = 1$ to n. Equation (5.11) may similarly be applied to the top of the pile, where $\sigma = P/A_p$, and Eq. (5.12) to the base of the pile, where $\sigma = p_b$. The following relationship is then obtained for the pile displacements (Mattes and Poulos, 1969):

$$ \{p\} = \frac{d}{4\delta^2}E_p R_A[I_p]\{{}_p\rho\} + \{Y\} \tag{5.14} $$

where

$\{p\}$ = $n+1$ shear-stress vector
$\{{}_p\rho\}$ = $n+1$ pile-displacement vector
$[I_p]$ = pile-action matrix, $(n+1)$ by $(n+1)$

$$ = \begin{bmatrix} -1 & 1 & 0 & 0 & \cdots & 0 & 0 & 0 & 0 \\ 1 & -2 & 1 & 0 & \cdots & 0 & 0 & 0 & 0 \\ 0 & 1 & -2 & 1 & \cdots & 0 & 0 & 0 & 0 \\ \cdots & \cdots & \cdots & \cdots & \cdots & \cdots & \cdots & \cdots & \cdots \\ \cdots & \cdots & \cdots & \cdots & \cdots & \cdots & \cdots & \cdots & \cdots \\ 0 & 0 & 0 & 0 & \cdots & 0 & 1 & -2 & 1 \\ 0 & 0 & 0 & 0 & \cdots & 2 & 2 & -5 & 3.2 \\ 0 & 0 & 0 & 0 & \cdots & 0 & \frac{-4f}{3} & 12f & \frac{-32f}{3} \end{bmatrix} $$

* This equation involves the approximating assumption that the pile is undergoing pure compression under a uniform axial stress σ.

$$f = \frac{L/d}{nR_A}$$

$$\{Y\} = \begin{Bmatrix} \left(\frac{P}{\pi d^2}\right)\left(\frac{n}{L/d}\right) \\ 0 \\ 0 \\ \cdot \\ \cdot \\ \cdot \\ \cdot \\ \cdot \\ \cdot \\ 0 \\ 0 \\ 0 \end{Bmatrix}$$

Displacement Compatability

When purely elastic conditions prevail at the pile-soil interface (i.e., no slip), the displacements of adjacent points along the interface are equal, that is,

$$\{_p\rho\} = \{_s\rho\} \tag{5.15}$$

Equations (5.9), (5.14), and (5.15) give

$$\{p\} = \left[[I] - \left(\frac{n^2}{4(L/d)^2}\right)(K[I_p])([I_s])\right]^{-1} \cdot \{Y\} \tag{5.16}$$

where $[I]$ = unit matrix of order (n + 1).

$$K = \frac{E_p R_A}{E_s} \tag{5.17}$$

= *pile stiffness factor*

K is a measure of the relative compressibility of the pile and the soil. The more relatively compressible the pile, the smaller the value of K.

Approximate Treatment for Nonuniform Soil

The foregoing analysis assumes constant soil-deformation parameters at all points within the soil. An approximate allowance may be made for the effects of varying soil-deformation moduli along the length of the pile by assuming that the stress distribution within the soil remains the same as if the soil were homogeneous, but that the soil displacement at a point adjacent to the pile is a function of the soil-deformation moduli at that point. With this assumption, the soil-displacement equation (5.9) is modified as follows:

$$\{_s\rho\} = d\left\{\frac{1}{E_s}\right\}[I_s]\{p\} \tag{5.18}$$

where

$\left\{\frac{1}{E_s}\right\}$ = vector of reciprocal values of soil Young's modulus along the pile

For a point i, the elements of $[I_s]$ are calculated for the value of ν_s at i.

The pile-displacement equation (5.14) remains unchanged, so that combining of Eqs. (5.18) and (5.14) yields the analogous equation to (5.16), which may be solved for stresses and displacements along the pile.

Although the above approach is only approximate, it should give sufficiently accurate solutions for practical purposes, unless sudden large variations in soil moduli occur along the pile length. In such cases, a better solution is obtained if the soil modulus E_s is taken as the mean of the value at point i and the influencing element j. This procedure leads to lower settlements that are in reasonable agreement with finite-element solutions (Poulos, 1979).

Approximate Treatment for Finite Layer Depth

The elements of $[I_s]$ calculated as previously described apply only for a soil mass of inifinite depth. For soil layers of finite depth, the elements of I_s may be obtained approximately by employing the Steinbrenner approximation (Steinbrenner, 1934). For a point i in a layer of depth h, the displacement-influence factor $I_{ij(h)}$ is then

$$I_{ij(h)} = I_{ij(\infty)} - I_{hj(\infty)} \tag{5.19}$$

where

$I_{ij(\infty)}$ = displacement-influence factor for i caused by stress on element j, in a semi-infinite mass

$I_{hj(\infty)}$ = displacement-influence factor for a point within the semi-infinite mass directly beneath i, at a depth h below the surface, caused by stress on element j

Using these adjusted elements of $[I_s]$, Eq. (5.16) may be solved for the stress and displacement distributions along the pile.

For the case of $h = L$—that is, an end-bearing pile resting on a rigid or stiffer stratum—an alternative, and probably more reliable approach is described below.

5.2.2.2 PILE RESTING ON A STIFFER STRATUM

A great number of piles are installed such that the tip bears on to a stratum that is stiffer than the soil along the shaft of the pile. Such piles are often designated as "end-bearing"

or "point-bearing," but the results of several analyses and field and laboratory measurements have shown that a significant proportion of the load may be transferred from the pile shaft to the surrounding soil.

To analyze the behavior of such piles, the analysis described in the preceding section, for a floating pile, must be modified to allow for the effect of the stiffer bearing-stratum. The same assumptions are again made for the pile and soil behavior, but in addition the bearing stratum is assumed to be an ideal elastic half-space with constant parameters E_b and ν_b. The problem is defined in Fig. 5.5*a*. To obtain the solution for the unknown stresses on the pile shaft and tip, and the corresponding pile movements, compatibility of the vertical displacements of the pile and adjacent soil are again considered.

Soil Displacement Equations

To properly determine the displacement in the soil surrounding the pile, it would be necessary to use equations for loading within a two-layer elastic system. Since suitable analytical solutions to this problem are not available, Mindlin's equations for displacements caused by loading within a half-space may be utilized in an approximate manner. To allow for the reduction in soil displacements because of the presence of the bearing stratum, a method is used that is an extension of the "mirror-image" approximation suggested by D'Appolonia and Romualdi (1963) for piles bearing on rock. Referring to Fig. 5.5*b*, pile element j is mirrored in the soil-bearing stratum interface by an imaginary pile element j', which is acted on by stress kp_j in the opposite direction to the stress p_j on the real element j. The

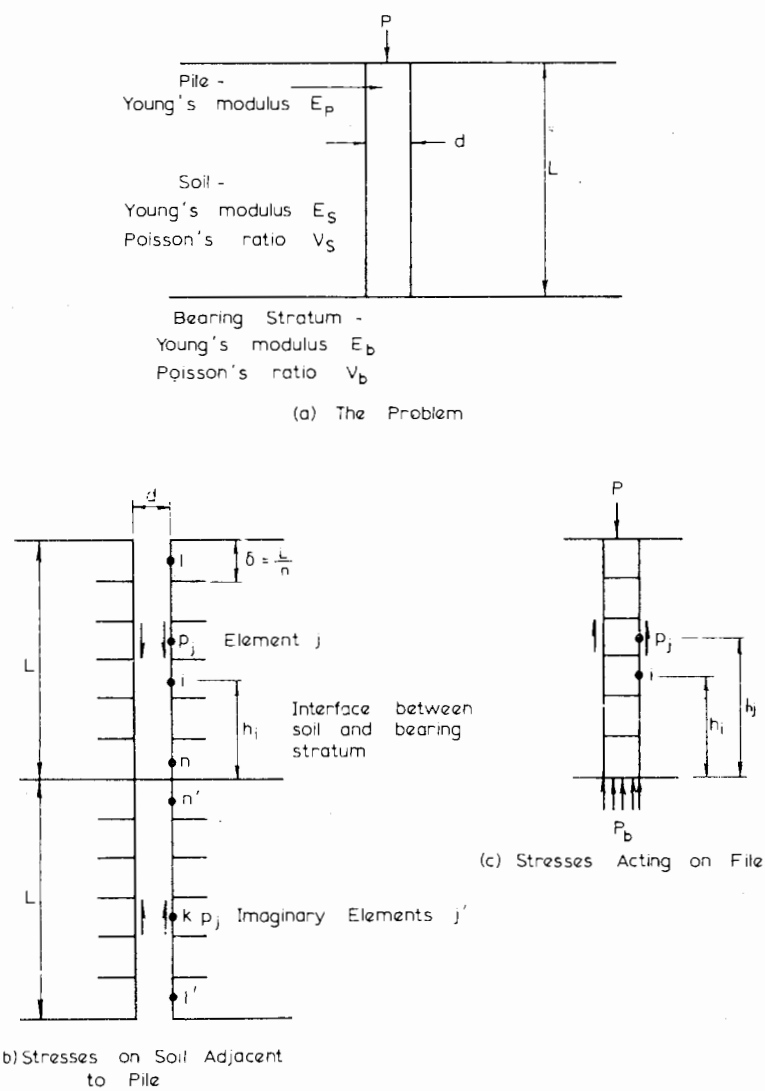

FIGURE 5.5 Analysis of end-bearing pile.

limiting values of k are $k = 0$ for a floating pile where $E_b = E_s$, in which case the stratum has no effect on soil displacements; and $k = 1$ for a pile resting on a rigid bearing-stratum ($E_b = \infty$), in which case the condition of zero tip-displacement is satisfied. In general, k must be determined as part of the analysis, and it is one of the assumptions of the analysis that it has the same value for all imaginary elements.

Taking downward displacements of the soil as positive, the displacement ${}_s\rho_{ij}$ of the soil at i because of the stress on the real element j and the imaginary element j', is

$$ {}_s\rho_{ij} = \frac{d}{E_s} p_j (I_{ij} - kI'_{ij}) \tag{5.20} $$

where

I_{ij} = vertical displacement factor for i due to shear stress on element j, as before
I'_{ij} = vertical displacement factor for i due to shear stress on imaginary element j' (calculated for a distance $L + h_i$ from the imaginary soil surface)

If we make the simplifying assumption that the influence of the stress on the pile tip has a negligible effect on the soil displacement at i, ${}_s\rho_i$, then

$$ {}_s\rho_i = \left(\frac{d}{E_s}\right) \sum_{j=1}^{n} \left(p_j (I_{ij} - kI'_{ij}) \right) \tag{5.21} $$

and for all n elements along the pile shaft (not including the pile tip),

$$ \{{}_s\rho\} = \frac{d}{E_s} [I_s - kI'_s] \{p\} \tag{5.22} $$

where

$\{{}_s\rho\}$ and $\{p\}$ = vectors of soil-displacement and shear-stress, respectively (of order n)
$[I_s - kI'_s]$ = $n \times n$ matrix of values of $I_{ij} - kI'_{ij}$

Equation (5.22) is analogous to Eq. (5.9) for a floating pile.

The soil displacement at the pile tip will be considered subsequently when dealing with compatability requirements.

The values of I_{ij} and I'_{ij} are evaluated from the Mindlin equation as described in the previous section.

Pile Displacement Equation

The displacement of each element of the pile itself may be divided into three components: displacement caused by shear stresses along the pile, displacement caused by applied axial load P, and displacement caused by the finite compressibility of the bearing stratum. Again assuming only axial compression of the pile, it may be shown (Poulos and Mattes, 1969*a*) that the displacement vector $\{{}_p\rho\}$ for the n elements along the shaft is

$$ \{{}_p\rho\} = -\left\{ \frac{1}{E_p R_A} [D_p] + \left(\frac{\pi(1-\nu_b^2)}{E_b}\right)\left(\frac{L}{n}\right)\left(\frac{d}{d_b}\right)[X] \right\} \cdot \{p\} + \frac{4P}{E_p R_A \pi d^2} \{h\} + \left(\frac{P}{d}\right)\left(\frac{(1-\nu_b^2)}{E_b}\right)\left(\frac{d}{d_b}\right) \cdot \{W\} \tag{5.23} $$

where

$[D_p]$ = $n \times n$ matrix of pile displacement factors, with
$D_{p_{ij}} = 4\delta h_j d$ for $i \leqslant j$

or

$D_{p_{ij}} = 4\delta h_i d$ for $i \geqslant j$
$\delta = L/n$
h_i, h_j = distances from bearing stratum to points i and j (see Fig. 5.5*c*)
$\{h\}$ = n column vector of values of h_i
$[X]$ = $n \times n$ matrix, every term of which is unity
$\{p\}$ = n column vector of p_j values
$\{W\}$ = n column vector of values of unity
R_A = area ratio of pile (Eq. 5.10)

Displacement Compatibility

Assuming again no slip at the pile-soil interface, $\{{}_p\rho\} = \{{}_s\rho\}$, so that from Eqs. (5.22) and (5.23),

$$ \left[\frac{1}{Kd} [D_p] + \frac{\pi(1-\nu_b^2)}{n} \left(\frac{L}{d_b} - \frac{E_s}{E_b}\right)[X] + [I - kI'] \right] \cdot \{p\} = \frac{P}{d^2} \left[\frac{4}{\pi K d} \{h\} + (1-\nu_b^2) \times \left(\frac{E_s}{E_b}\right)\left(\frac{d}{d_b}\right)\{W\} \right] \tag{5.24} $$

where

K = pile-stiffness factor, as defined in Eq. (5.17)

For a chosen initial value of k, Eq. (5.24) may be solved to give the n unknown stresses p_j. The stress acting on the

pile base may then be evaluated from the equilibrium equation

$$P = \frac{\pi d_b^2}{4} p_b + \pi d \frac{L}{n} \sum_{j=1}^{n} p_j \tag{5.25}$$

Having obtained the solutions for the chosen value of k, a closer estimate of k for the particular pile, soil, and base parameters being considered may be obtained by examining compatibility between the displacements of the soil and the bearing stratum at the pile base. The soil displacement at the pile base is, from Eq. (5.24),

$$_s\rho_b = \left(\frac{d}{E_s}\right) \sum_{j=1}^{n} [p_j(I_{bj} - kI'_{bj})] \tag{5.26}$$

where

I_{bj}, I'_{bj} = vertical-displacement factors for the center of the pile base.

However, from symmetry, $I_{bj} = I'_{bj}$, so that

$$_s\rho_b = \left[\frac{d(1-k)}{E_s}\right] \sum_{j=1}^{n} (p_j I_{bj}) \tag{5.27}$$

Making the simplifying assumption that, as far as the bearing stratum is concerned, the displacement at the pile base is caused by the base stress p_b alone and is given by the Boussinesq equation for the vertical displacement of a rigid circular disc on a half space, it then follows that

$$\rho_b = \frac{(\pi p_b)(d_b)(1 - \nu_b^2)}{4E_b} \tag{5.28}$$

Thus, by equating Eqs. (5.27) and (5.28), the next approximation for the value of k is as follows:

$$k = 1 - \left(\frac{\pi}{4}\right)\left(\frac{E_s}{E_b}\right)\left(\frac{d_b}{d}\right)\left[\frac{(1-\nu_b^2)p_b}{\sum_{j=1}^{n}(p_j)(I_{bj})}\right] \tag{5.29}$$

Equations (5.24) and (5.25) may now be solved again, using this new value of k, and the process repeated until convergence in the value of k is obtained. The soil and bearing stratum displacements along the pile may then be calculated from Eqs. (5.22) or (5.23). It has been found that in many cases, only two or three iteration cycles give adequate convergence of k.

5.2.2.3 MODIFICATION TO BASIC ANALYSES FOR SINGLE PILE

Pile-Soil Slip

The analyses described above require that no slip occurs at the pile-soil interface. However, since real soils have a finite shear strength and the pile-soil interface has a finite adhesive strength, slip or local yield will occur when the shear stress reaches the adhesive (or yield) strength. By use of a method similar to that described by D'Appolonia and Romualdi (1963), Salas (1965), and Poulos and Davis (1968), the elastic analyses can be modified to take account of possible slip, provided that the following assumptions are made:

1. Local yield or slip occurs at the pile-soil interface when the average shear stress on any pile element, calculated from the elastic analysis, reaches the limiting value τ_a.
2. Although compatibility of pile and soil displacements at a yielded element is no longer possible, displacements anywhere in the soil caused by the limiting stress τ_a are still given by elastic theory.
3. Failure of the tip or base of the pile occurs when the base pressure reaches the ultimate bearing capacity of the base, the displacements of the soil elsewhere resulting from this pressure still being given by elastic theory.

In carrying out the modified analysis, it is convenient to restate the elastic equation governing pile behavior in terms of displacement rather than shear stress. Thus, using the floating pile analysis as an example, Eq. (5.16), in terms of the shear-stress vector $\{p\}$, alters to the following form in terms of the displacement vector $\{\rho\}$:

$$\frac{E_s}{d}\left[[I_s]^{-1} - \left(\frac{Kd^2n^2}{4L^2}\right)[I_p]\right]\{\rho\} = \{Y\} \tag{5.30a}$$

or

$$[Z] \cdot \{\rho\} = \frac{d}{E_s}\{Y\} \tag{5.30b}$$

where

$$[Z] = [I_s]^{-1} - \left(\frac{Kd^2n^2}{4L^2}\right)[I_p]$$

The analysis is carried out incrementally, increasing the applied load P successively. For any stage of loading, Eq. (5.30*b*) is solved on the assumption that all elements are

elastic. From the resulting solution for $\{\rho\}$, the shear-stress vector $\{p\}$ is calculated from Eq. (5.14) or Eq. (5.9). These shear stresses are then compared with the specified limiting stresses τ_a. At an element where the computed stress exceeds τ_a, the displacement-compatibility equation for that element (i.e., the appropriate row of the matrix [Z] in Eq. 5.30*b*) is replaced by the pile-displacement equation for that element (i.e., the appropriate row of the matrix in equation 5.14), putting the shear stress at that element equal to τ_a. For example, if an element i has slipped, the elements Z_{ij} in row i of the matrix Z in Eq. (5.30*b*) are replaced by the elements ${}_pI_{ij}$ of matrix ${}_pI$, while the element $\frac{d}{E_s} Y_i$ on the right-hand side is replaced by $\frac{4L^2}{E_p R_A dn^2} - (\tau_{ai} - Y_i)$, where τ_{ai} is the value of τ_a at element i.

The modified system of equations is now resolved and the procedure is repeated until the computed values of shear stress do not exceed the limiting values τ_a.

By successively increasing the applied load P until all elements have failed, a load-settlement curve to failure may be obtained.

Analyses taking account of pile-soil slip along the shaft have revealed that for normal piles having length-to-diameter ratios greater than about 20 and for constant τ_a, the load-settlement curve is substantially linear until a load of at least 50% of the failure load is reached. For the prediction of settlement at working loads for such piles, a linear-elastic analysis is therefore adequate. For larger-diameter piles or piers, full shaft slip may occur at relatively low loads. For such cases, a simplified procedure for obtaining the load-settlement curve, described in Section 5.4., has been developed.

Other Modifications

The basic analyses have been formulated in terms of a uniform pile with provision for a thin enlarged base. However, extensions may readily be made to allow for cases in which the shaft is not of uniform diameter or in which the pile is attached to a pile cap resting on the soil surface.

For piles having nonuniform shaft diameter, the relative diameters of the various shaft elements are considered when calculating the pile and soil displacements. In those cases where the shaft diameter of an element is less than that of the element above it, the stress on the annular area at the junction of the two elements must be included as an additional unknown. Examples of the analysis of underreamed and step-taper piles using the above approach have been given by Poulos (1969). For piles with an enlarged base of relatively large volume, the shaft elements near the base can be considered to have an increased diameter; this approach is more accurate than considering only a thin, enlarged base.

For the case of a pile with a rigid cap resting on the soil surface, uniformly loaded annular elements are included in the analysis, to represent the pile cap. Compatibility of pile and soil displacements is considered at these cap elements, as well along the pile. Details of such an analysis are given by Poulos (1968*b*) and Butterfield and Banerjee (1971*b*). The effects are discussed later in this chapter and again in Chapter 10.

5.2.2.4 ACCURACY OF ELASTIC SINGLE-PILE SOLUTIONS

Investigations into the sensitivity of the solutions on the number of elements used in the analysis have shown that the use of 10 elements to divide the pile shaft leads to answers of acceptable accuracy unless the pile is relatively long ($L/d > 50$) or very compressible ($K < 100$), in which case 15 or 20 elements may be desirable. For short, stiff piles, even the use of 5 elements gives accurate solutions. The use of a single base element and the application of a rigidity-correction factor (see Appendix A) also appears to be quite satisfactory, as the solutions are almost identical with those obtained by the use of 5 annular elements to divide the base.

Complete solutions for the settlement of a pile, in which both vertical and radial displacement compatibility are considered, have been presented by Butterfield and Banerjee (1971*a*), and Mattes (1969; 1972). Comparisons between the complete solutions and solutions in which only vertical-displacement compatibility is considered, are shown in Fig. 5.6 for the shear stress along the pile (Mattes, 1969) and in Table 5.1 for the top displacement of the pile (Mattes, 1972). Only for relatively short piles ($L/d < 25$) does the inclusion of radial-displacement compatibility have any effect on the solutions, and even in such cases, the effect is unimportant from a practical point of view. It therefore appears quite adequate to employ analyses in which only compatibility of vertical displacements is considered.

Although the analysis described in Section 5.2.2.2 is primarily developed for end-bearing piles, it may be used to obtain solutions for a floating pile in a uniform mass by putting $E_b/E_s = 1$. The possible errors involved in the analysis are a maximum for $E_b/E_s = 1$, so that by comparing this solution with the corresponding solution from the floating-pile analysis described in Section 5.2.2.1, an estimate may be made of the maximum error of the end-bearing pile analysis. Comparisons of the settlements of the top and tip of a pile obtained from the two solutions have been made by Poulos and Mattes (1969*a*), and rela-

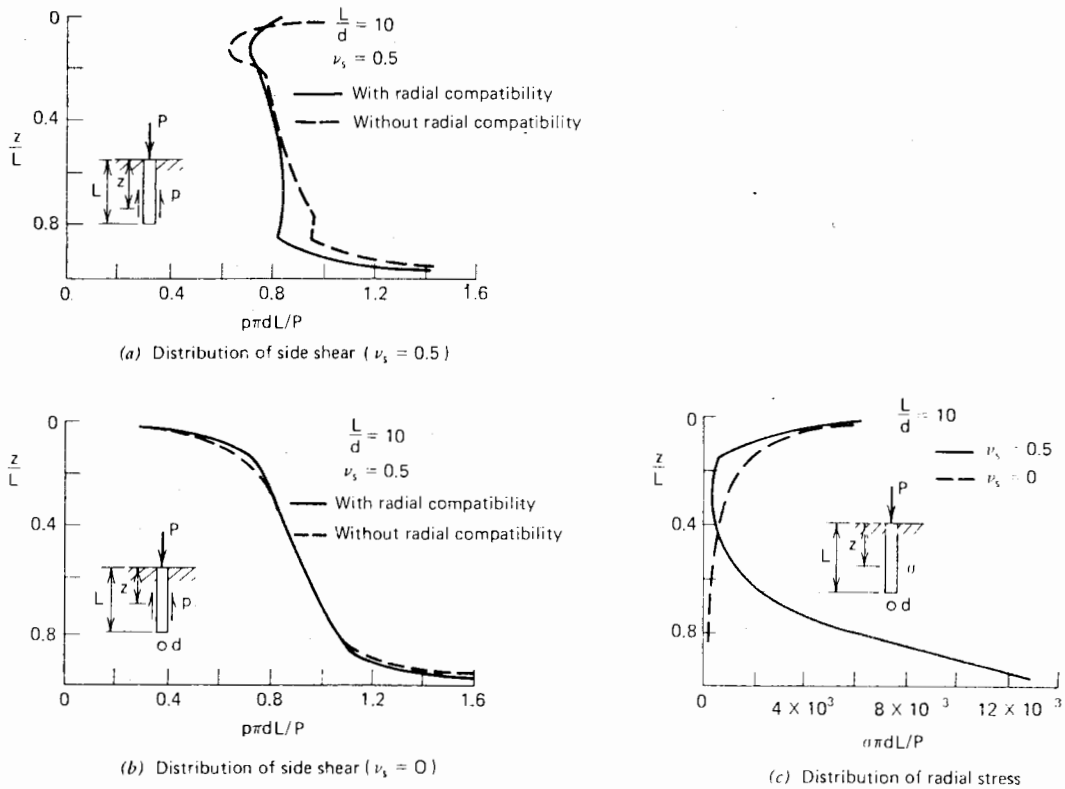

FIGURE 5.6 Effect of inclusion of radial displacement compatibility (Mattes, 1969).

TABLE 5.1 EFFECT ON PILE DISPLACEMENT OF CONSIDERING RADIAL DISPLACEMENT COMPATABILITY

L/d	K	Top Displacement Influence Factor, I_ρ	
		Vertical Displacement Compatability Only	Vertical and Radial Displacement Compatability
10	100	1.793	1.782
	1000	1.378	1.448
25	100	3.559	3.542
	1000	3.181	3.160
100	100	10.670	10.488
	1000	5.220	5.140
	20,000	2.758	2.712

$$\text{Displacement } \rho = \frac{P}{LE_s} I_\rho$$

tively close agreement has been found (see Figs. 5.24 and 5.25). The end-bearing analysis, when applied to the floating pile, results in a slight underestimate of settlement (maximum effect about 10%) and a slight overestimate of the amount of load in the pile. From a practical point of view, the errors involved in the end-bearing pile analysis are unlikely to be significant, especially for $E_b/E_s > 1$.

5.2.3 Finite-Element Analysis

Detailed descriptions of the finite-element method have been given by Zienkiewicz (1971) and Desai and Abel (1972), and its use in geotechnical problems is discussed comprehensively in Desai and Christian (1977). The application of finite-element analysis to pile foundations has been described by several investigators. Ellison et al. (1971) have considered a multilinear soil stress-strain curve and have introduced special joint elements at the pile interface to allow for slip. Desai (1974) has considered a pile in sand with a hyperbolic stress-strain response and has also used special elements for the pile-soil interface. Hyperbolic stress-strain behavior has also been used by Esu and Ottaviani (1975) for analyzing a pile in clay. A very interesting result of their analysis is that the load-settlement behavior of a pile is substantially linear to a load well beyond half the failure load, despite the fact that the soil stress-strain response is nonlinear. This fact suggests that elastic theory, modified for slip as previously suggested, should provide an adequate basis for load-settlement prediction, provided appropriate values of soil modulus are used.

Lee (1973) and Valliappan et al. (1974) have done elastic parametric studies of the influence of soil layering on settlement behavior. The superior accuracy of isoparametric elements over conventional elements is also demonstrated.

Balaam et al. (1975, 1976) have used a different type of analysis, in which the finite-element method is used to analyze the pile and soil mass separately and then compatibility conditions are imposed to determine the nodal forces and deflections. This approach is thus a generalization of the elastic approaches described earlier in this chapter. The possibility of slip at the pile-soil interface is allowed for by specifying a limiting pile-soil shear strength, from which limiting values of nodal force can be calculated. Possible failure within the soil mass itself is allowed for by considering the soil as a bilinear elastic or elastic-plastic material. This type of approach appears to hold some advantage over the use of joint elements in that the rate of convergence of the solution is much more rapid when pile-soil slip or soil-yield has occurred. It also overcomes problems that may arise when there are extreme differences between the moduli of the pile and the soil. Balaam et al. (1975) used this analysis to investigate the effects on settlement of nonhomogeneity of the soil that might arise during installation of the pile. In a further application, Balaam et al. (1976) have used this approach to analyze the behavior of piles composed of gravel.

5.2.4. Comparisons between Solutions from Mindlin Approach and Finite-Element Analysis

Balaam et al. (1975) obtained elastic solutions for the case $L/d = 10$, $K = 1000$, $h/L = 2$, and $\nu_s = 0.45$. Twenty triangular elements were used for the pile and 160 triangular elements for the soil. A free outer boundary was assumed at 35 pile-diameters from the pile axis, the base underlying the soil was assumed at 35 pile-diameters from the pile axis, and the base underlying the soil was assumed to be rough and rigid. The settlement at the top of the pile was found to be only 2.0% less than that given by the previous analysis utilizing Mindlin's equations. Furthermore, the finite-element solution was identical with the conventional elastic-finite-element solution in which the pile and soil are analyzed together as a single mass. Decreasing the number of pile elements to 10 and the soil elements to 120 increases the discrepancy between the finite-element solution and the elastic solution to 3.5%. In a parametric study of the settlement of a pile presented by Lee (1973), the solutions are obtained from a finite-element analysis. Table 5.2 shows a comparison between Lee's solutions for a floating pile in a uniform mass and the corresponding solutions from the elastic analysis presented herein. In this case, the finite-element solutions are slightly greater, but generally there is close agreement between the two series of solutions and such difference as does exist may well arise from numerical inaccuracies in one or both of the solutions.

A further comparison with Lee's solutions is shown in Table 5.2, this time for a pile bearing on a stiffer stratum. The agreement is again reasonable, and these comparisons suggest that the analysis based on the Mindlin equation should give results of adequate accuracy for practical purposes, provided that severe variations in subsoil conditions do not occur along the pile (see Section 5.3.3 for further discussion of the effects of soil layering).

A comparison between computed load-settlement curves to failure for a pile in a purely cohesive soil is shown in Fig. 5.7 (P_u is the ultimate load capacity). The agreement is generally reasonable, but at loads approaching the ultimate, the settlements given by the finite-element analysis are greater than those from the "elastic" approach, probably because the latter uses elastic theory to calculate soil deflections after pile soil-slip has commenced.

TABLE 5.2 COMPARISONS BETWEEN ELASTIC- AND FINITE-ELEMENT SOLUTIONS FOR PILE SETTLEMENT

$K = 1000$ $\nu_s = 0.4$

(a) Floating Pile in Semi-infinite Mass

L/d	I_ρ	
	Finite Element[a]	Elastic Mindlin Approach
3.5	0.267	0.258
5.0	0.211	0.205
10.5	0.115	0.112
15.0	0.103	0.100
19.5	0.094	0.092

[a] Lee (1973).

(b) End-Bearing Pile

L/d	E_b/E_s	I_ρ	
		Finite Element[a]	Elastic Mindlin Approach
5	10	0.078	0.075
	100	0.014	0.016
15	100	0.020	0.020

[a] Lee (1973).

$$\rho = \frac{P}{dE_s} I_\rho$$

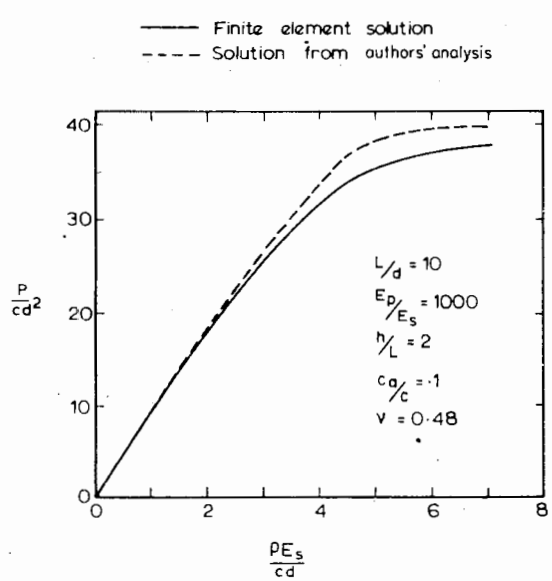

FIGURE 5.7 Comparison between load-settlement curves to failure.

5.3 THEORETICAL SOLUTIONS FOR SETTLEMENT AND LOAD DISTRIBUTION

To enable rapid practical estimates of pile-settlement behavior, it is extremely useful to have available dimensionless parametric solutions from which the effects of variations in pile and soil properties can readily be determined. In this section, a series of solutions is presented for the stress and load distribution in a pile, and for the settlement of a single pile. The soil is assumed to be homogeneous, having constant Young's modulus and Poisson's ratio. However, the influence of nonhomogeneity and soil layering is also discussed. The solutions described have been obtained from the analyses based on Mindlin's equations, and in most cases, 10 elements have been used to divide the pile shaft.

5.3.1 Stress and Load Distribution in Pile

For a floating pile in a uniform soil, the distribution of shear stress along the shaft is shown in Fig. 5.8 for $L/d = 25$. For $K = 5000$, the pile is almost incompressible and the shear stresses are relatively uniform, but for $K = 50$ (a very compressible pile), high shear-stresses occur near the top of the pile. Poisson's ratio of the soil, ν_s, has little influence on the shear stresses.

For a pile bearing on a stiffer stratum, the distribution of load in the pile is shown in Fig. 5.9 for various values of

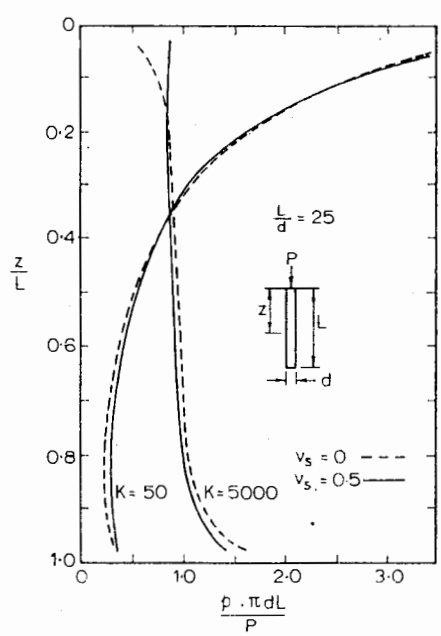

FIGURE 5.8 Distribution of shear stress along compressible pile.

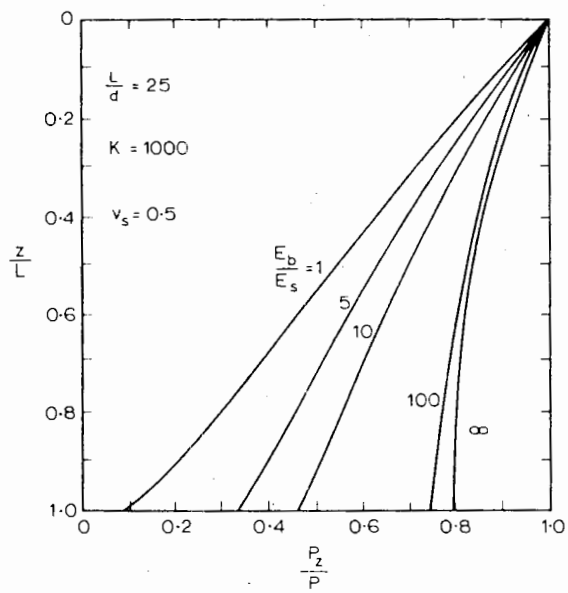

FIGURE 5.9 Load distribution along pile bearing on stiffer stratum.

E_b/E_s. Load transfer along the pile increases as the relative modulus of the bearing stratum decreases. Load transfer also increases as the pile-stiffness factor K decreases or as the length-to-diameter ratio L/d increases.

An example of the effect of pile-soil slip on the stress distribution along a floating pile is shown in Fig. 5.10. A constant pile-soil adhesion of $c_a = c_u$ (undrained cohesion) and a point resistance of $9c_u$ is assumed in this case. The progressive slip along the shaft with increasing load is clearly shown.

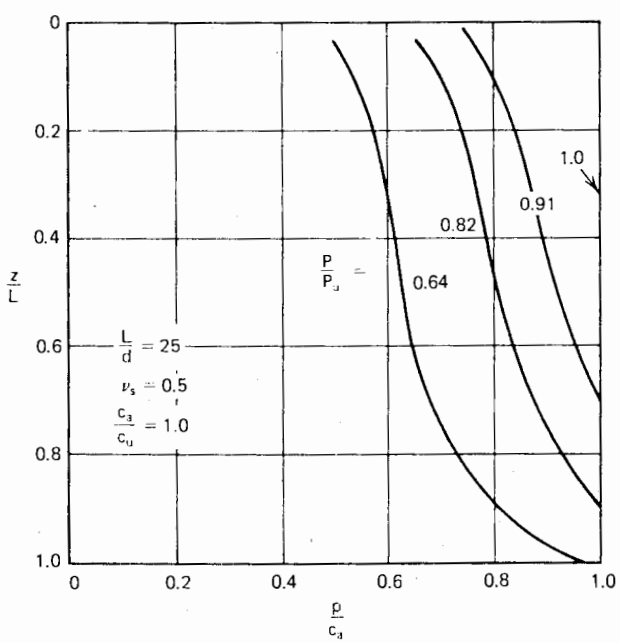

FIGURE 5.10 Influence of local yield on stress distribution along floating pile.

The effect of nonhomogeneity of the soil on the stress distribution is discussed by Randolph and Wroth (1978) and Poulos (1978). For a soil whose modulus increases linearly with depth from zero at the surface, the shear stresses increase approximately linearly with depth also.

5.3.2. Load Transferred to Pile Tip

In a simplified presentation given by Poulos (1972*d*), the proportion of load transferred to the pile tip, β, is expressed in terms of the value β_0 for an incompressible floating pile in a semi-finite mass, multiplied by correction factors to take account of pile compressibility and the relative stiffness of the bearing stratum.

a) Floating Pile

$$\beta = \beta_0 C_K C_\nu \tag{5.31}$$

where

$\beta = P_b/P$ = proportion of applied load transferred to pile tip
β_0 = tip-load proportion for incompressible pile in uniform half-space (Poisson's ratio = 0.5)
C_K = correction factor for pile compressibility
C_ν = correction factor for Poisson's ratio of soil

Values of β_0, C_K, and C_ν are plotted in Figs. 5.11, 5.12, and 5.13 for a wide range of parameters. The effect of pile compressibility is to decrease the amount of load transferred to the tip—that is, C_K is less than 1. The presence of an enlarged base increases β significantly. β is not significantly affected if the pile is situated in a finite layer rather than a half-space, provided the hard base of the layer is more than $0.2L$ below the bottom of the pile.

b) End-Bearing Pile on Stiffer Stratum

$$\beta = \beta_0 C_K C_b C_\nu \tag{5.32}$$

where

β, β_0 C_K, and C_ν are defined as above and to sufficient accuracy, may be assumed to take their previous values

C_b = correction factor for stiffness of bearing stratum

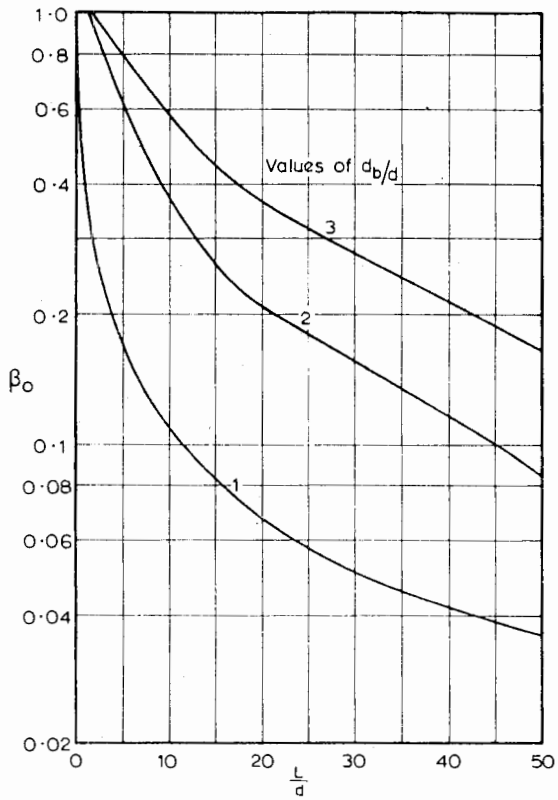

FIGURE 5.11 Proportion of base load, β_0.

Values of C_b are plotted in Fig. 5.14. The load at the pile tip increases as the relative modulus of the bearing stratum, E_b/E_s, increases. The effects of the bearing stratum are more pronounced as K or L/d increase.

The tip load may also be affected by other factors, such as the presence of enlarged bulbs along the pile, tapering of the pile, or the presence of a pile cap resting on the soil surface. For an incompressible floating pile in a homogeneous semi-infinite mass, the effect of these factors is shown in Figs. 5.15, 5.16, and 5.17. These figures may be used approximately to estimate the effects on tip load for compressible piles.

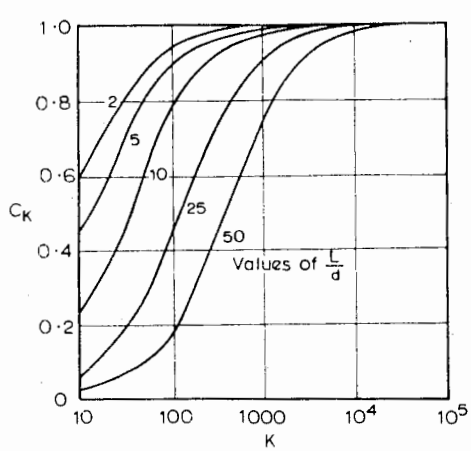

FIGURE 5.12 Compressibility correction factor for base load, C_K.

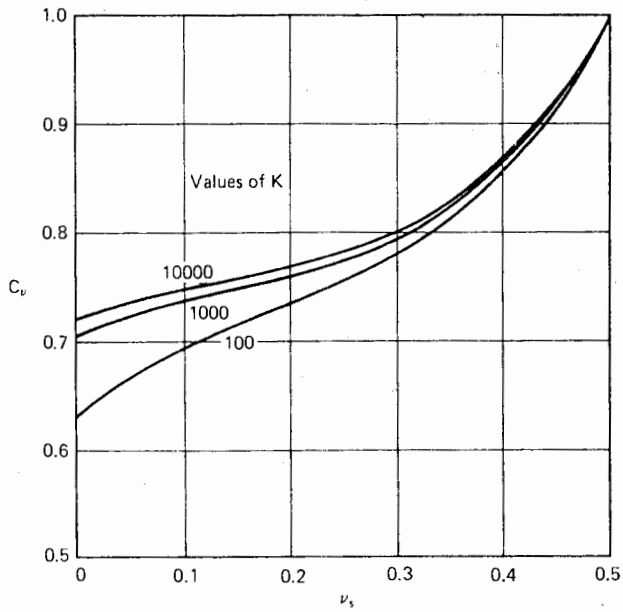

FIGURE 5.13 Poisson's ratio correction factor for base load, C_ν.

5.3.3 Settlement of Pile

As with the tip load on a pile, the settlement of the top of the pile may be expressed, to sufficient accuracy, in terms of the settlement of an incompressible pile in a half-space, with correction factors for the effects of pile compressibility, and so on. It is again convenient to consider two cases for a homogeneous soil mass having constant Young's modulus E_s and Poisson's ratio ν_s:

a) Floating Pile

$$\rho = \frac{PI}{E_s d} \tag{5.33}$$

where

$$I = I_0 R_K R_h R_\nu \tag{5.33a}$$

ρ = settlement of pile head
P = applied axial load
I_0 = settlement-influence factor for incompressible pile in semi-infinite mass, for $\nu_s = 0.5$.
R_K = correction factor for pile compressibility

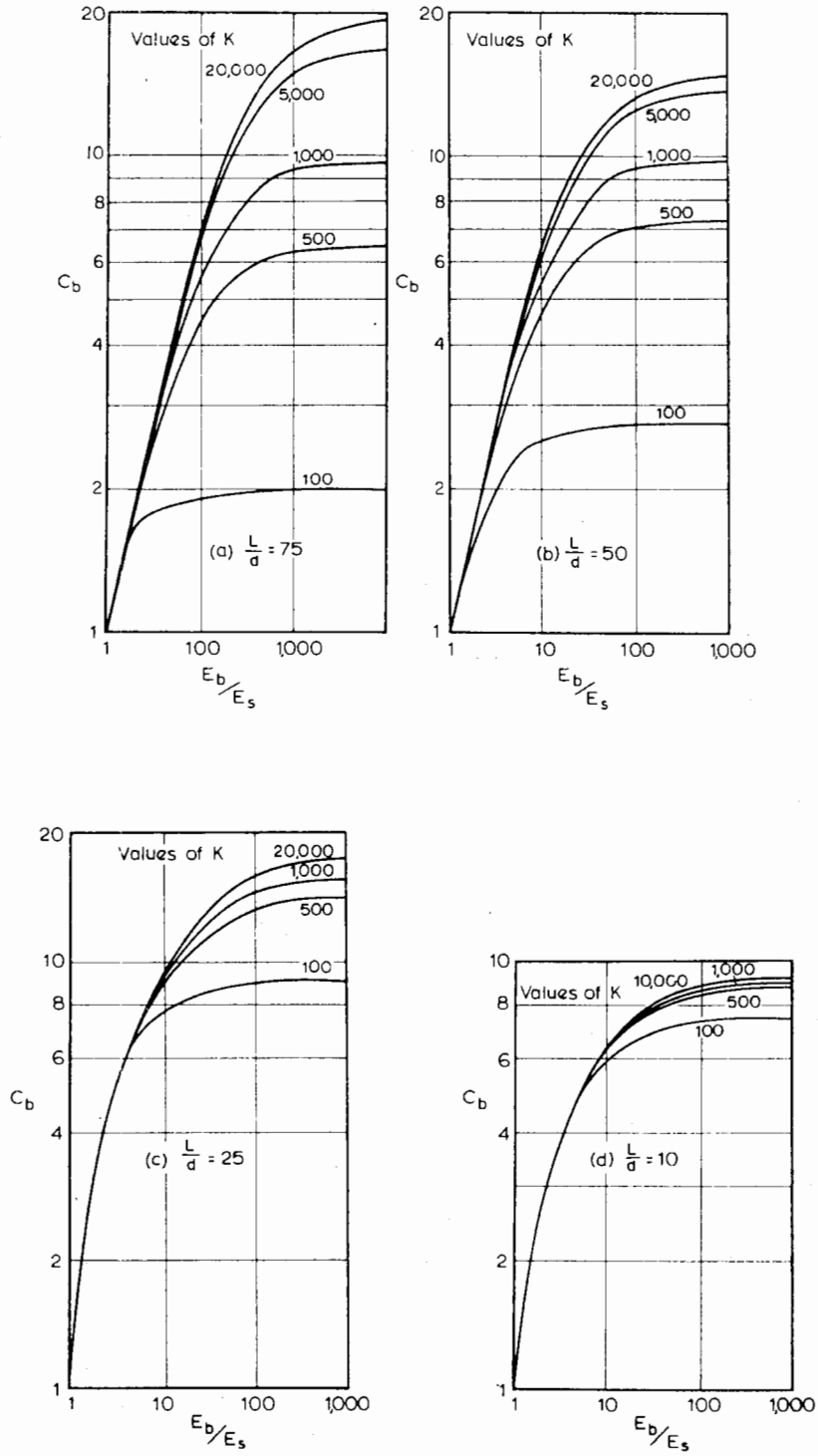

FIGURE 5.14 Base modulus correction factor for base load, C_b.

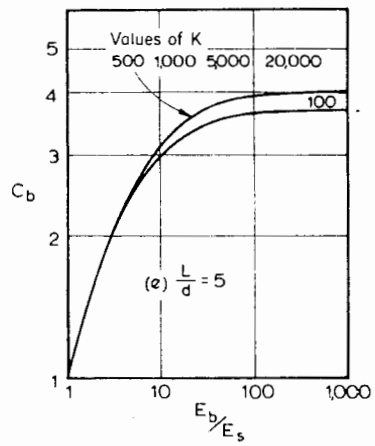

FIGURE 5.14 (continued).

R_h = correction factor for finite depth of layer on a rigid base
R_ν = correction for soil Poisson's ratio ν_s
h = total depth of soil layer

Values of I_0, R_K, R_h, and R_ν are plotted in Figs. 5.18, 5.19, 5.20, and 5.21. Figure 5.18 shows the decrease in settlement of a pile of constant diameter as the length increases. The presence of an enlarged base also decreases settlement, although the effect is only significant for relatively short piles. Pile compressibility increases settlement, especially for slender piles (Fig. 5.19), while the effect of having a finite layer is to decrease settlement (Fig. 5.20). [If the hard base is level with the pile tip, case (b) should be used.] A decrease in Poisson's ratio, ν_s, while maintaining E_s constant leads to a decrease in settlement, as shown in Fig. 5.21, although the effect is relatively small.

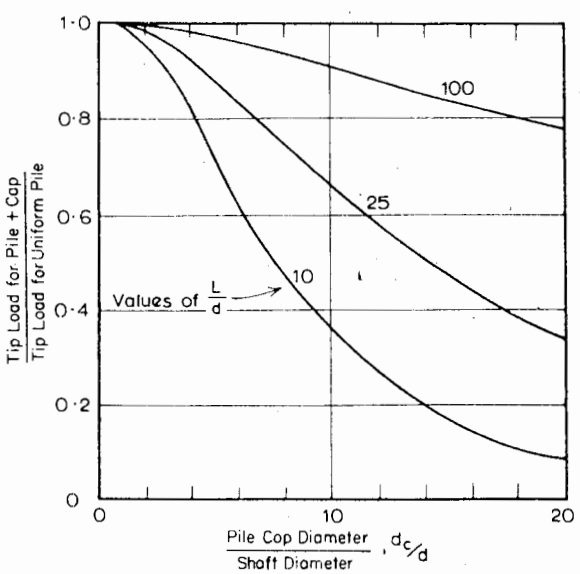

FIGURE 5.15 Influence of pile cap on tip load. Incompressible floating pile.

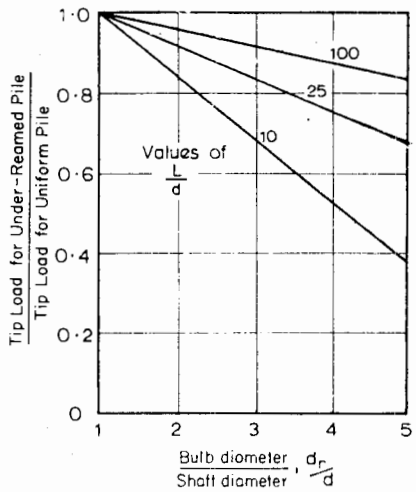

FIGURE 5.16 Influence of underreaming on tip load (incompressible floating pile with single central bulb, $0.2L$ long).

b) End-Bearing Pile on Stiffer Stratum

$$\rho = \frac{PI}{E_s d} \tag{5.34}$$

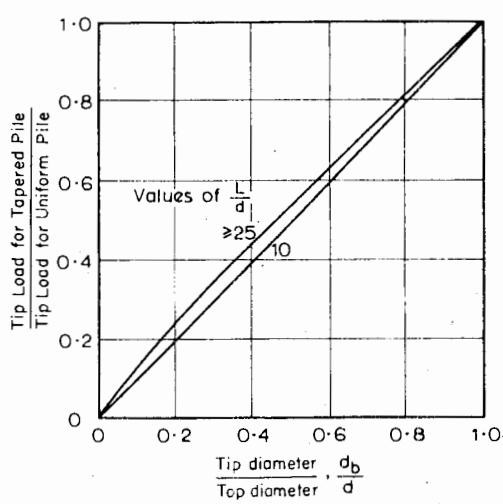

FIGURE 5.17 Influence of tapered or step-tapered pile on tip load (incompressible floating pile, top diameter = d).

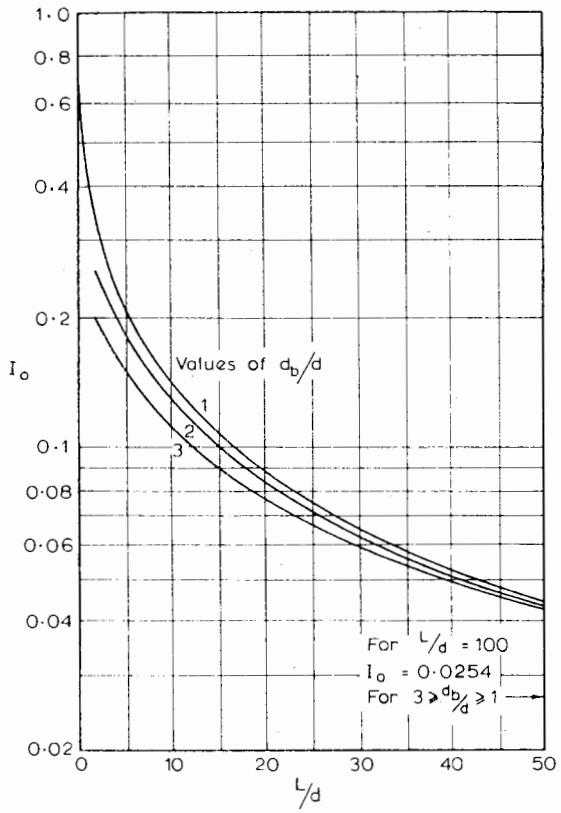

FIGURE 5.18 Settlement-influence factor, I_o.

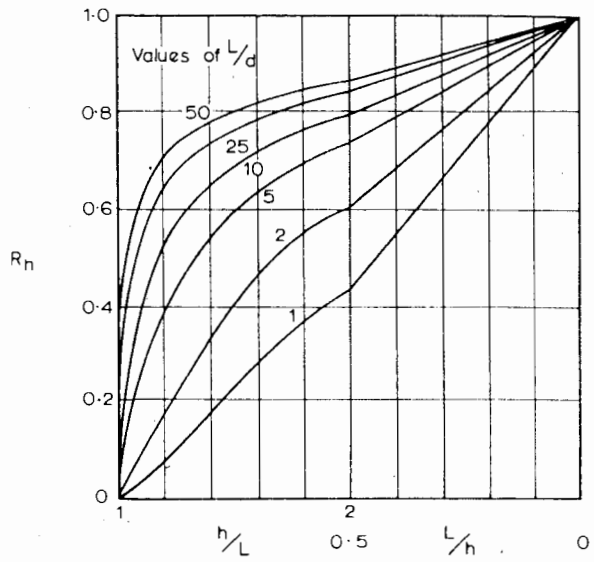

FIGURE 5.20 Depth correction factor for settlement, R_h.

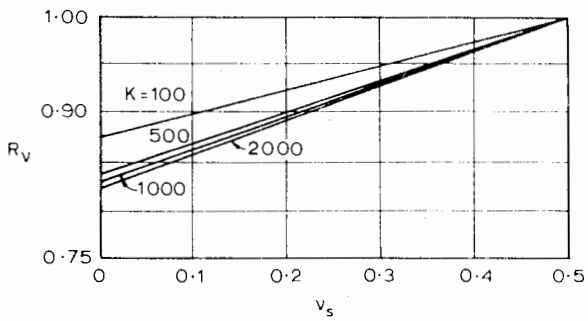

FIGURE 5.21 Poisson's ratio correction factor for settlement, R_v.

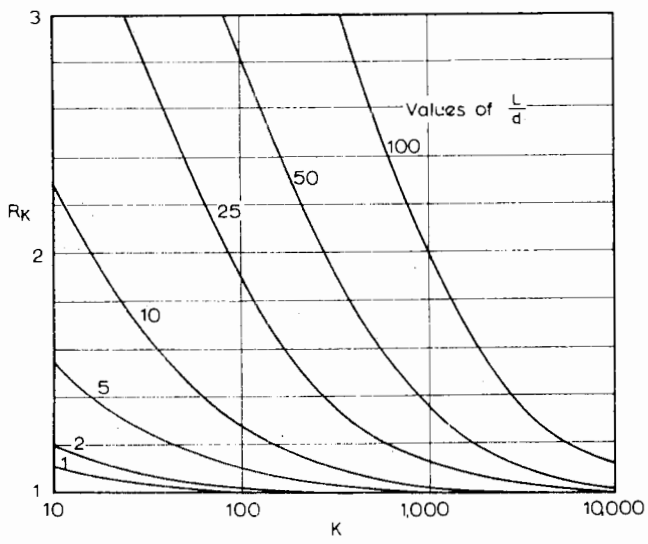

FIGURE 5.19 Compressibility correction factor for settlement, R_K.

where

$$I = I_0 R_K R_b R_v \qquad (5.34a)$$

(I_0, R_K, R_v are defined as for Eq. 5.33 and take the same values to sufficient accuracy)

R_b = correction factor for stiffness of bearing stratum

Values of R_b are plotted in Fig. 5.22. The effect of the bearing stratum is to decrease settlement, the effect being most pronounced for relatively short or stiff piles on a stiff bearing-stratum.

For very slender piles ($L/d \geqslant 100$), the properties of the bearing stratum have little effect on settlement (i.e., $R_b \simeq 1$) for most practical values of pile stiffness factor K.

It should be emphasized that the expressions for settlement in Eqs. (5.33) and (5.34) are only approximate because except where taken into account, some of the effects

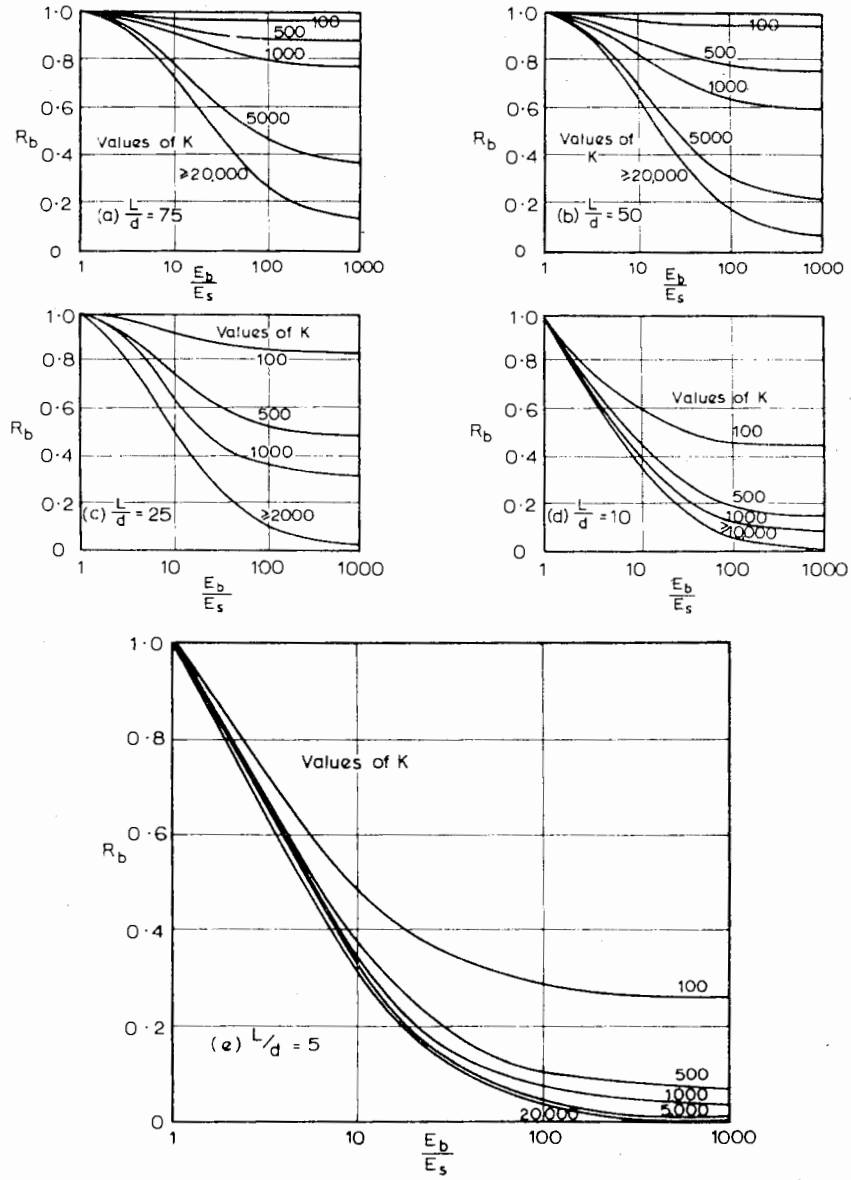

FIGURE 5.22 Base modulus correction factor for settlement, R_b.

are assumed to be mutually independent; for example, the effect of finite layer depth is assumed to be independent of pile stiffness factor K. While this may not be strictly correct, the use of the correction factor allows a convenient parametric presentation of results and should be of adequate accuracy for practical purposes.

5.3.3.1 MOVEMENT RATIOS

For some applications, it may be useful to reexpress the settlement of a pile bearing on a stiffer stratum in terms of the movement ratio M_R, where

$$M_R = \frac{\text{Settlement of pile}}{\text{Elastic shortening of pile}} \tag{5.35}$$

Theoretical values of M_R are shown in Fig. 5.23 for a pile on a rigid bearing-stratum and in Fig. 5.24 for a 25-diameter pile resting on a nonrigid stratum. The pile-head settlement is calculated as

$$\rho = \left(M_R\right)\left(\frac{PL}{E_p A_p}\right) \tag{5.36}$$

Focht (1967) has observed from actual tests that the ratio

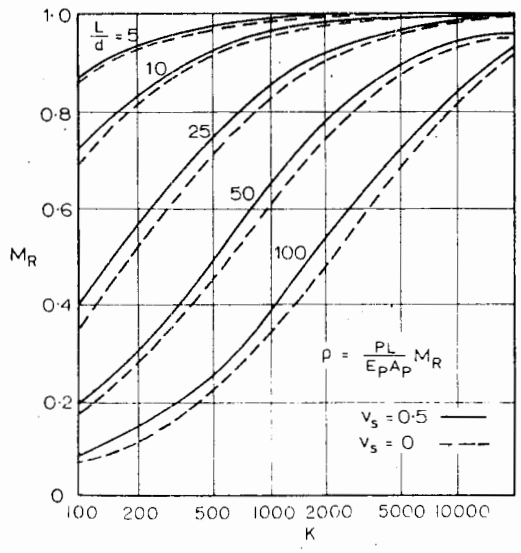

FIGURE 5.23 Movement ratio for end-bearing pile on rigid base.

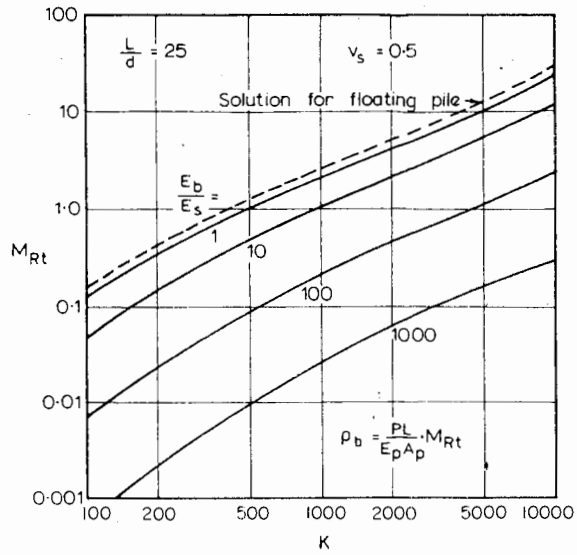

FIGURE 5.25 End-bearing pile on stiffer stratum. Pile-tip movement ratio.

M_R lies within the range 0.5 to 2 for most practical pile dimensions and this observation can be said to generally agree with the theoretical results in Figs. 5.23 and 5.24.

A plot of the theoretical movement ratio for the pile tip, M_{Rt}, is shown in Fig. 5.25.

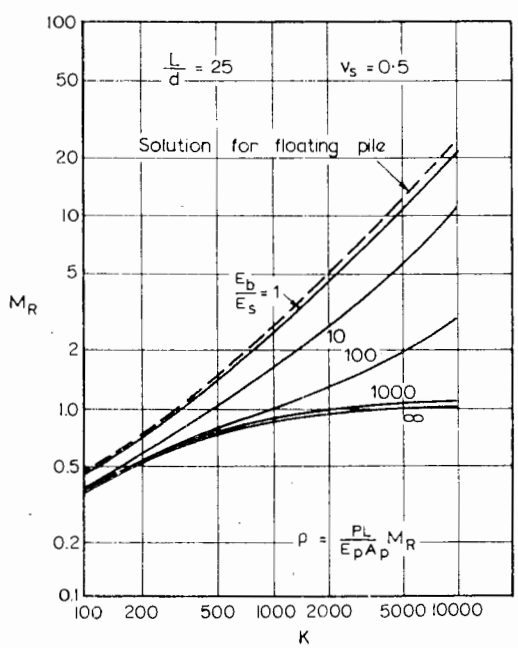

FIGURE 5.24 Movement ratio for end-bearing pile on stiffer stratum.

5.3.3.2 EFFECT OF PILE-SOIL SLIP

For a floating pile in a purely cohesive homogeneous soil, with constant adhesion c_a along the shaft, the influence of slip on settlement is shown in Figs. 5.26 and 5.27, in terms of plots of a slip factor M_s and the factor of safety against undrained failure, where

$$M_s = \frac{\text{Elastic settlement of pile}}{\text{Actual settlement of pile}} \qquad (5.37)$$

By first calculating the elastic settlement of the pile (Eq. 5.33), the actual settlement of the pile, including the

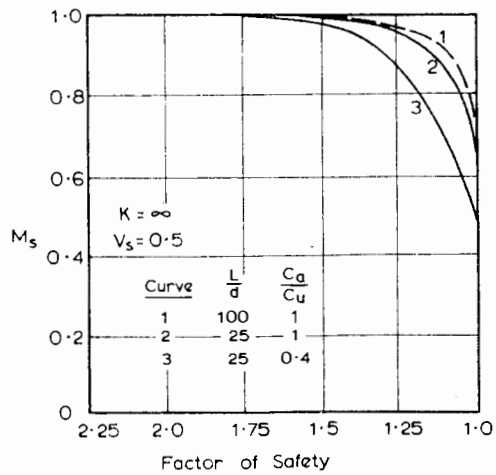

FIGURE 5.26 Settlement modification factor M_s for slip. Effect of L/d and adhesion factor.

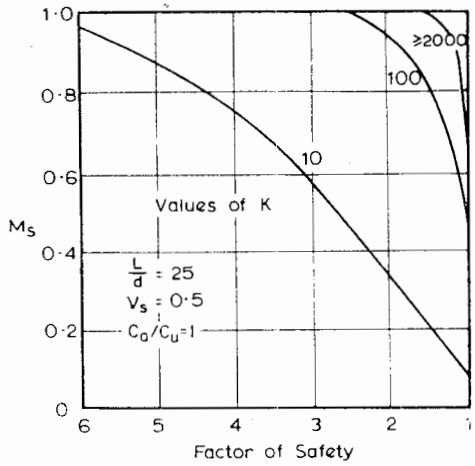

FIGURE 5.27 Settlement modification factor M_s for slip. Effect of K.

effects of slip, may be estimated from Figs. 5.26 and 5.27. The following observations can be made from these figures:

1. The effect of L/d is not very significant, provided that $L/d > 25$ (i.e., provided that the pile is relatively slender).
2. The effect of slip on settlement becomes more pronounced as c_a/c_u decreases.
3. For very low values of pile-stiffness factor K, small values of M_s can occur, indicating the very pronounced effect of slip.
4. Except for low values of K, slip has little or no effect on settlement at normal working loads. While this conclusion applies strictly only to piles in an ideal soil with a constant soil modulus, it has also been found to apply closely for soils with linearly-increasing modulus and strength with depth, and confirmation of this observation has been found in a considerable number of load-test results.

For piles bearing on a stiffer stratum, the effect of slip is generally less than that shown in Figs. 5.26 and 5.27. For the extreme case of a rigid bearing-stratum, computations by Poulos and Mattes (1969*a*) show that unless the pile is very compressible (K less than about 200), the load-settlement curve remains substantially linear up to full slip along the shaft. Beyond full shaft-slip, the load-settlement behavior of the pile depends on the elastic properties of the bearing stratum.

The above remarks apply for a uniform distribution of adhesion along the pile shaft. If the adhesion or skin friction increases linearly with depth, the effect of slip is more significant and the load-settlement curve prior to full shaft-slip departs from the purely elastic relationship at somewhat lower loads. Nevertheless, the effect of slip on settlement is relatively small in many cases, and it is therefore convenient to ignore the effects of shaft slip and assume that the relationship between shaft load and shaft settlement is linear. This assumption leads to a convenient method of predicting the load-settlement behavior of piles or piers in which a significant amount of base resistance is developed. This method will be discussed in detail in Section 5.4.

5.3.3.3 LAYERING AND NONHOMOGENEITY OF SOIL ALONG PILE

As previously mentioned, in Section 5.2.2, an approximate analysis of the behavior of a pile in a layered or nonhomogeneous soil may be carried out by using the Mindlin equations for a uniform mass but employing the appropriate value of Young's modulus and Poisson's ratio at various points along the pile. For a pile in soil whose modulus increases linearly with depth, detailed solutions for settlement are given by Randolph and Wroth (1978), Poulos (1979) and Banerjee and Davies (1977). Consideration will be given here to ways of utilizing the solutions for a homogeneous soil to obtain approximate solutions for non-homogeneous soil profiles.

A number of solutions have been obtained from this approximate analysis (which will be referred to here as the approximate computer analysis) for an incompressible pile

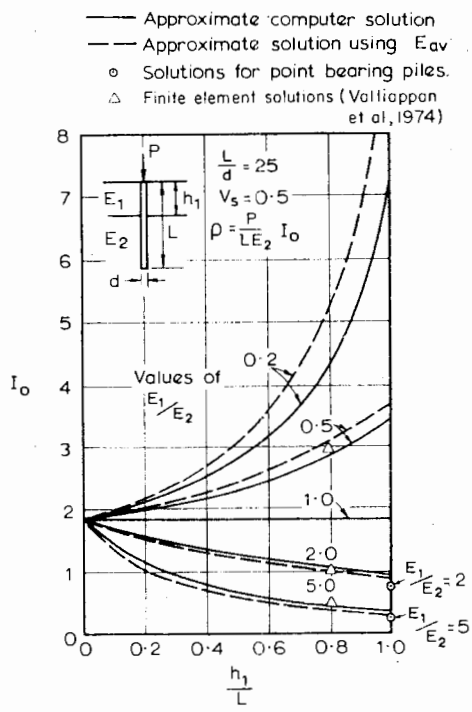

FIGURE 5.28 Settlement of pile in layered soil.

in a two-layer soil, the upper layer being of depth h_1 ($h_1 < L$) and the lower layer being of infinite extent. These approximate computer solutions for pile settlement are shown in Fig. 5.28 for $L/d = 25$. Also shown are the solutions for a point-bearing pile ($h_1 = L$) for $E_1/E_2 = 2$ and 5, obtained from the analysis described in Section 5.2.2, and finite element solutions from Valliappan et al. (1974). Finally, approximate solutions are shown that use the displacement-influence factor for a homogeneous soil and an average modulus, E_{av}, as follows:

$$E_{av} = \frac{E_1 h_1 + E_2 (L - h_1)}{L} \tag{5.38}$$

Figure 5.28 shows that at least for $E_2 > E_1$, the approximate computer solution for $h_1 = L$ overestimates the settlement somewhat, as compared with the point-bearing pile analysis, but the error is not great. Furthermore, the simple solutions employing the average modulus E_{av} are in reasonable agreement with the approximate computer solutions and in some cases are in fact in closer agreement with both the solutions for a point-bearing pile, and the finite-element solutions.

On the basis of the above evidence, it is suggested that where the soil modulus varies along the length of the pile (e.g., where a number of layers occur), and where the modulus variation between successive layers is not large, the settlement may be calculated from the expressions for a pile in uniform soil (Eq. 5.33 or Eq. 5.34) using an average soil modulus E_{av} as follows:

$$E_{av} = \left(\frac{1}{L}\right) \sum_{j=1}^{n} E_i h_i \tag{5.39}$$

where

E_i = modulus of layer i
h_i = thickness of layer i
n = number of different soil layers along pile length

Because the pile displacement is only slightly dependent on Poisson's ratio (ν_s) of the soil, variations of ν_s along the pile length may be ignored.

For the important case of a soil in which the modulus increases linearly with depth (a "Gibson soil"), comparisons between the solutions of Banerjee and Davies (1977) and the settlement calculated by using the average modulus together with the uniform soil solutions indicate that the errors involved in the latter approach are on the order of 10 to 15%.

In cases where the pile passes through distinct layers of soil, having large differences in soil modulus, the uniform soil solutions may be utilized in an alternative approximate fashion. For example, for the simple case of a pile penetrating one layer and founded in a second layer, the settlement may be estimated by treating the portion of the pile in the first layer as an end-bearing pile and determining the settlement of this portion and the amount of load in the pile at the interface of the two layers (say, P_2). The settlement is added to the previously calculated settlement of the upper portion to obtain the overall settlement of the pile head. Comparisons with the finite element solutions of Lee (1973) indicate that this approximate approach gives a settlement within 20% of the finite-element solution, the accuracy increasing as the modulus of the bearing stratum increases relative to that of the overlying soil.

Despite the apparent success with which the settlement of a pile in a nonhomogeneous soil may be estimated by approximate methods, it must be borne in mind that such methods will probably not give an accurate picture of the distribution of load and settlement along the length of pile; a more refined analysis is warranted and necessary if such a picture is required.

5.3.3.4 OTHER EFFECTS

The effects on settlement of enlarged bulbs, tapering of the pile and of a pile cap resting on the soil surface have been investigated for an incompressible pile in a semi-infinite mass (Poulos, 1968*a*; 1969). These effects are shown in Figs. 5.29, 5.30, and 5.31 in terms of the settlement of a uniform-diameter freestanding pile. The presence of en-

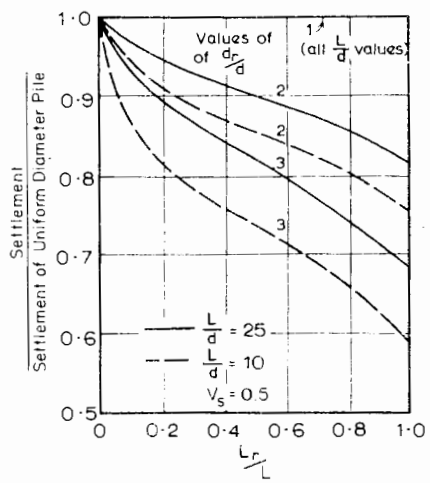

FIGURE 5.29 Influence of underreaming on pile settlement (incompressible pile in half-space; single central bulb, length L_r, diameter d_r).

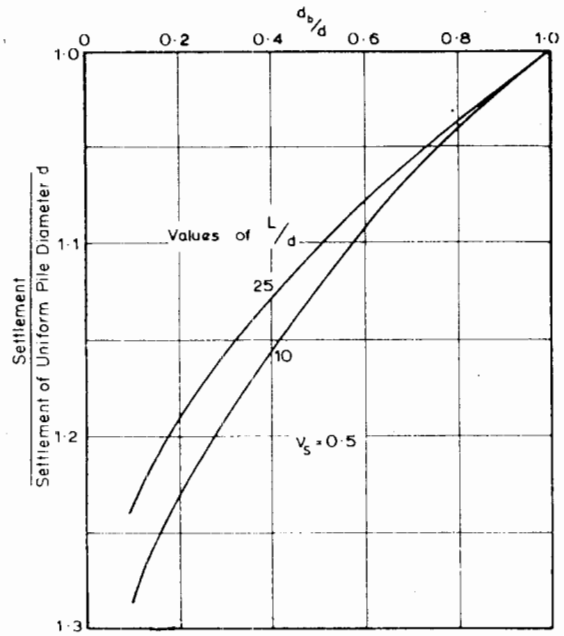

FIGURE 5.30 Effect of tapering or step-tapering on settlement (incompressible pile in half-space, tip diameter d_b).

larged bulbs along the pile shaft decreases settlement, as does a pile cap resting on the soil surface, but the effect is generally only significant for relatively short piles (e.g. $L/d \geqslant 10$). The position of an enlarged bulb has some influence on settlement, with the maximum effect being obtained when the bulb is near the pile tip. Tapering or step-tapering of a pile increases settlement as compared with a uniform pile of equal head diameter. However, the settlement of a step-taper or tapered pile may be closely approximated by the settlement of a uniform pile of diameter equal to the mean diameter. Poulos (1969) has shown that for a given volume and length of pile, an underreamed pile settles less than a uniform-diameter pile, which in turn settles less than a tapered or step-tapered pile. Although Figs. 5.29, 5.30, and 5.31 apply to incompressible piles, they may be used to give an indication of the likely effects on the settlement of compressible piles.

5.3.4 Settlements in a Soil Mass Resulting From a Pile

Once the stress distribution along a pile is known, the vertical displacement of any point within the soil mass may be determined by integrating the appropriate Mindlin equation around the various elements of the pile and the pile base. Results of such computations for a uniform semi-infinite soil mass have been presented by Poulos and Mattes (1971*a*) and Poulos and Davis (1974) for various values of L/d and K. Typical solutions for one value of K are shown in Figs. 5.32, 5.33, and 5.34 as a function of the dimensionless depth of a point below the surface, H/L, and the dimensionless distance from the pile axis, r/L. The displacement at any point in the mass is given by

$$\rho = \frac{P}{LE_s} \cdot I_\rho \tag{5.40}$$

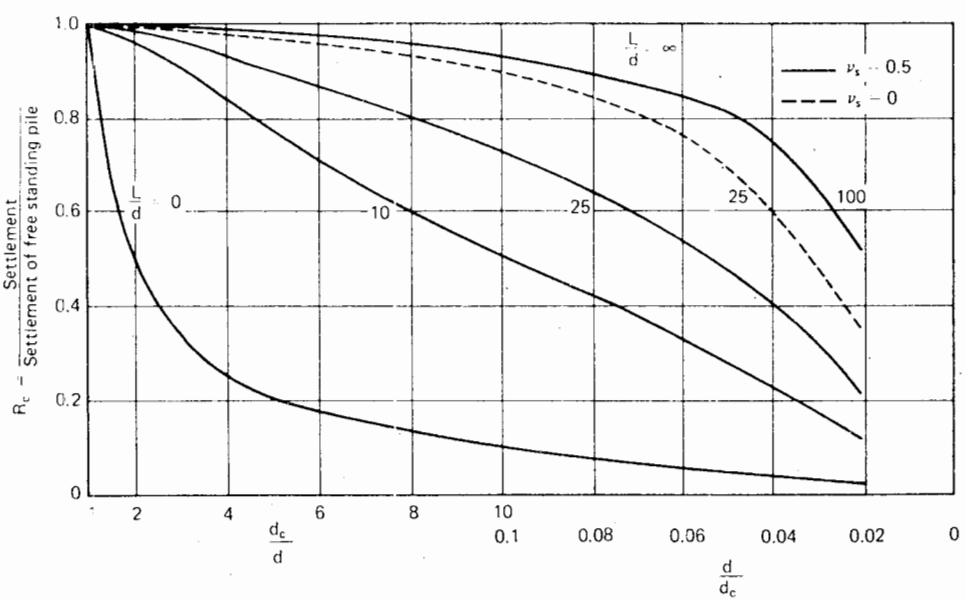

FIGURE 5.31 Effect of pile cap on settlement. Incompressible pile in half-space, rigid cap, diameter d_c.

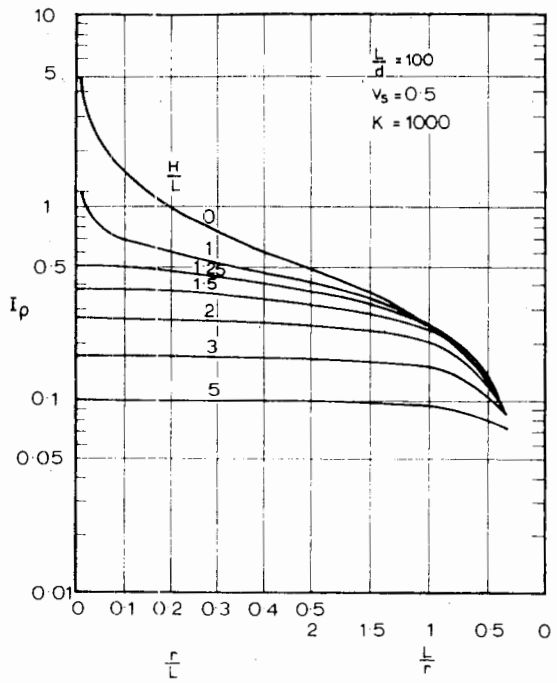

FIGURE 5.32 Displacement influence factors.

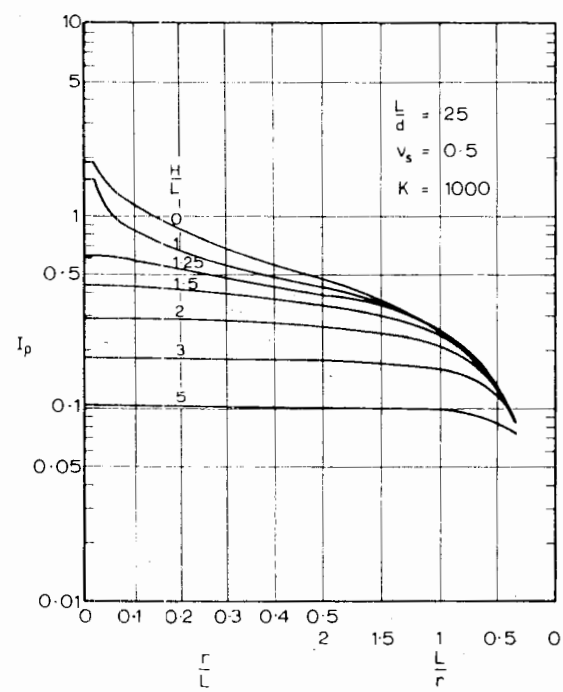

FIGURE 5.33 Displacement influence factors.

where

I_ρ = displacement-influence factor

Although I_ρ is only plotted for $\nu_s = 0.5$, ν_s has relatively little influence. If desired, Fig. 5.21 may be used to obtain a correction for other values of ν_s. Settlements near the pile are considerably influenced by the pile stiffness factor K (see Poulos and Davis, 1974), but at points remote from the pile (e.g., $H/L > 1.75$ or $r/L > 0.4$), settlements are almost independent of K. For points remote from the axis, the pile may be replaced by a point load of magnitude equal to the load on the pile, and acting at a depth $2L/3$ below the surface.

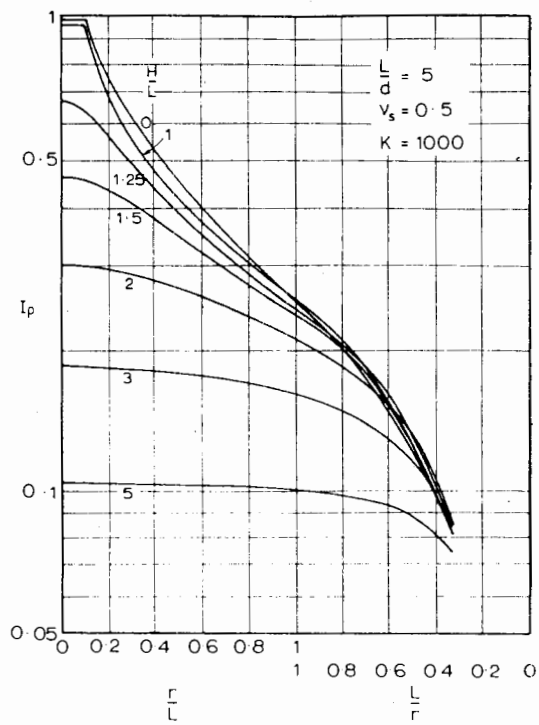

FIGURE 5.34 Displacement influence factors.

The solutions shown in Figs. 5.32, 5.33, and 5.34 may be used in the following ways:

(a) For calculating the settlements in the soil surrounding a single pile.
(b) For calculating the settlement of a pile resulting from underlying soil layers (see below).
(c) For calculating the settlements around and beneath a pile group (see Chapter 6, Section 6.4).

5.3.4.1 SETTLEMENT OF A PILE RESULTING FROM UNDERLYING SOIL LAYERS

The solutions for settlements within a uniform semi-infinite soil mass caused by a pile, described in the preceding section, may be used to estimate the settlement of a pile founded within the first layer of a system of m layers of

different soils. If the first layer is of depth h_1 ($h_1 > L$), the settlement ρ of the pile is given approximately as:

$$\rho = \rho_0 + \frac{P}{L}\left[\frac{I_m}{E_{sm}} + \sum_{j=2}^{m-1}\left(\frac{I_j - I_{j+1}}{E_{sj}}\right)\right] \qquad (5.41)$$

where

ρ_0 = settlement of a pile in a layer of depth $h = h_1$, obtained from Eq. (5.33)
I_j = displacement influence factor I_ρ on the pile axis at the level of the top of layer j
E_{sj} = Young's modulus of layer j

The first term of the above equation is the settlement of the pile in the founding layer (depth h_1, modulus E_{s1}) and the second term represents the summation of the displacements of the underlying layers caused by the pile. It should be noted that the value of $(I_j - I_{j+1})$ calculated for layer j should be that for a value of K corresponding to a soil modulus E_{sj}, although for deeper layers, the value of K used has almost no influence on the calculations.

For application of Eq. (5.41), it is convenient to have values of the influence factor I_ρ on the axis plotted against depth, and such a plot is shown in Fig. 5.35 for three values of L/d and for $\nu_s = 0.5$. The effect of L/d becomes insignificant for $H/L > 1.75$. The influence factors then become

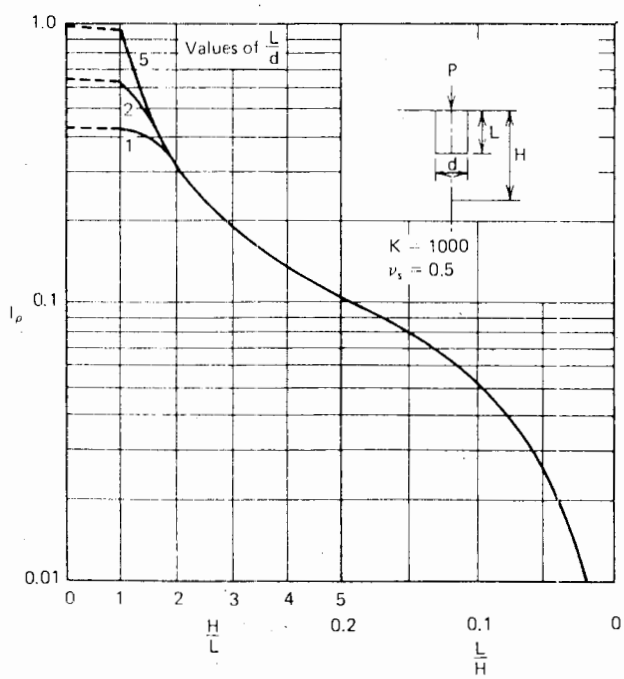

FIGURE 5.35 Influence factors for settlement beneath center of a pier.

identical with those given by the Mindlin equation for a point-load acting at a depth of $2L/3$ below the surface, that is,

$$I_\rho = \frac{(1+\nu_s)}{2\pi(1-\nu_s)}\left[\frac{(1-\nu_s)}{(\zeta - {}^2/_3)} + \frac{2(1-\nu_s)^2}{(\zeta + {}^2/_3)} + \left(\frac{2}{3}\right)\frac{\zeta}{(\zeta + {}^2/_3)^3}\right] \qquad (5.42)$$

where

$$\zeta = H/L.$$

Equation (5.41) is similar to that suggested by Nair (1967) for piles and that used by Egorov, Kuzmin, and Popov (1957) for surface foundations, and makes use of the Steinbrenner approximation that the stresses in a layered system are the same as those in a uniform mass. The use of this equation will generally lead to an overestimate of the settlement caused by the underlying layers if the modulus of the layers decreases with depth, but Poulos and Mattes (1971*b*) estimate that this error is not serious unless the modulus of successive layers varies by more than a factor of 10. If softer layers overlie stiffer layers, little error is involved in using Eq. (5.41).

For cases in which layering occurs along the pile as well as beneath the pile, an average value of E_{s1} should be estimated from Eq. (5.39).

5.3.5 Immediate and Final Settlements

For piles in sand or unsaturated soils, the final settlement (excluding possible creep movements) may be considered to occur immediately on application of the load, so that the values of E_s and ν_s used in calculating the settlement of the pile should be the drained values, that is, the moduli of the soil skeleton, E_s' and ν_s'. On the other hand, for piles in saturated clay, an immediate settlement, ρ_i, occurs under undrained conditions followed by a time-dependent consolidation settlement. After dissipation of the excess pore pressures resulting from loading of the pile is complete, the total settlement of the pile is ρ_{TF} ($\rho_{TF} = \rho_i + \rho_{CF}$, where ρ_{CF} = final consolidation settlement). The immediate settlement ρ_i is calculated from the theoretical solutions by using the undrained Young's modulus of the soil, E_u, and the undrained Poisson's ratio, ν_u, which is 0.5 for a saturated soil. The final settlement ρ_{TF} is calculated by using the drained Young modulus of the soil skeleton, E_s', and the drained Poisson's ratio ν_s'.

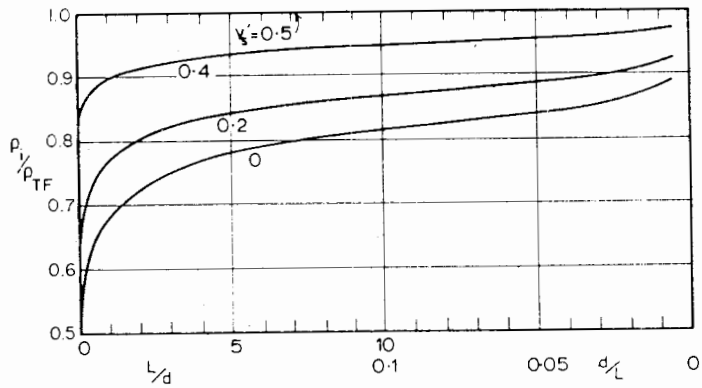

FIGURE 5.36 The relative importance of immediate settlement for an incompressible pile in a semi-infinite mass.

5.3.5.1 RELATIVE IMPORTANCE OF IMMEDIATE SETTLEMENT

It is possible to examine the relative magnitudes of the immediate and final settlements of a pile if the soil is assumed to be an ideal two-phase elastic homogeneous isotropic material. For such a material, the undrained and drained moduli may be shown to be related as follows:

$$E_u = \frac{3E_s'}{2(1+\nu_s')} \tag{5.43}$$

The ratio ρ_i/ρ_{TF} of immediate to final settlement can then be calculated as

$$\frac{\rho_i}{\rho_{TF}} = \frac{2(1+\nu_s')}{3} \cdot \frac{I_{0.5}}{I_\nu'} \tag{5.44}$$

where

$I_{0.5}$ = displacement-influence factor for $\nu = \nu_u = 0.5$
I_ν' = displacement-influence factor for $\nu = \nu_s'$

Figure 5.36 shows values of ρ_i/ρ_{TF} calculated by Poulos and Davis (1968) for an incompressible pile for various values of L/d and ν_s'. This figure shows that for a practical range of values of L/d, the immediate settlement contributes the major part of the final settlement, even for $\nu_s' = 0$. For example, for $\nu_s' = 0.2$ and $L/d = 25$, $\rho_i/\rho_{TF} = 0.89$, or in other words, 89% of the final settlement occurs immediately on application of the load, and only the remaining 11% is time-dependent consolidation settlement. Similar computations have been made by Mattes and Poulos (1969) for a compressible pile and Poulos and Mattes (1969*a*) for an end-bearing pile. The effect of pile compressibility on ρ_i/ρ_{TF} for a floating pile is shown in Fig. 5.37 for $L/d = 25$. The proportion of immediate settlement tends to decrease with increasing pile compressibility (i.e., decreasing K), but it still remains the most significant part of the final settlement. For end-bearing piles, virtually the entire settlement of the pile head is immediate settlement; only for compressible slender piles ($L/d > 50$, $K < 500$) does the consolidation movement exceed 10% of the total final movement.

Confirmation of the predominance of immediate settlement may be obtained from a considerable number of published results of maintained load tests on piles (e.g., Whitaker and Cooke, 1966) that show that at loads well below the ultimate, there is only a relatively small amount

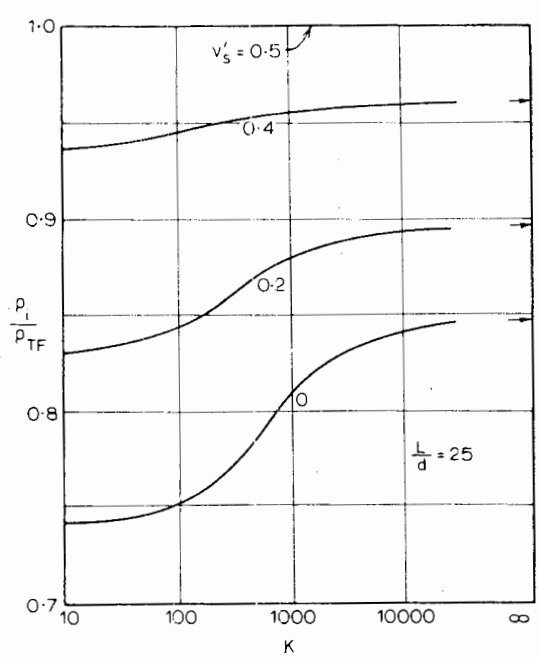

FIGURE 5.37 Relative importance of immediate settlement (compressible floating pile).

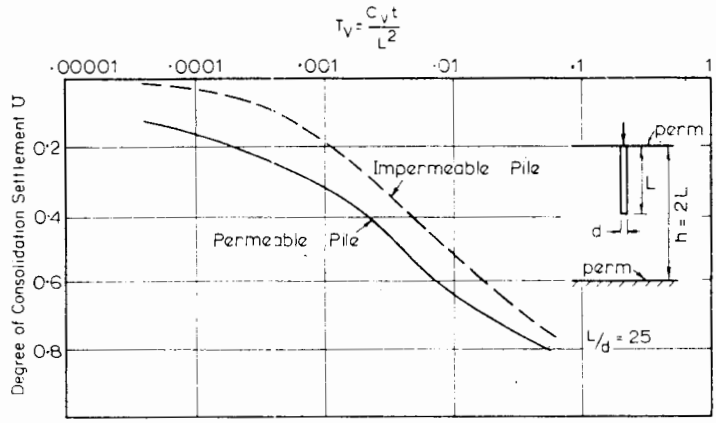

FIGURE 5.38 Approximate solutions for the rate of settlement of a single pile (Poulos and Davis, 1968).

of time-dependent settlement. At higher load levels, however, significant time-dependent settlements occur, primarily as a result of the effects of shear creep.

Figures 5.36 and 5.37 imply that in contrast to surface foundations, the consideration of the rate of settlement of a pile is of relatively minor importance. Figures 5.36 and 5.37 also show the fallacy of calculating settlements of single piles by using one-dimensional consolidation theory. However, it should be emphasized that consolidation settlement becomes more important for pile groups. A further implication in regard to pile-loading tests, is that sufficient information on the settlement behavior of a pile at normal working loads may be obtained from a constant-rate-of-penetration test, as suggested by Whitaker and Cooke (1966) (see Chapter 16).

Although the rate of consolidation for piles is generally not of great importance, some approximate solutions for the rate of consolidation settlement of an incompressible pile have nevertheless been obtained by Poulos and Davis (1968) and are shown in Figs. 5.38 and 5.39. For a given diameter, the rate of settlement decreases as L increases.

5.3.5.2 CREEP SETTLEMENTS

A number of long-duration pile tests have revealed that at loads above about one third of the ultimate, the settlement tends to increase with time, long after consolidation should have finished (e.g., Murayama and Shibata, 1960; Sharmnan, 1961; Yamagata, 1963; Cambefort and Chadeisson, 1961; Bromham and Styles, 1971). In several cases, it has been observed that the settlement appears to increase linearly with the logarithm of time, and consequently, some investigators have proposed empirical equations relating settlement and time (e.g., Cambefort and Chadeisson, 1961).

Theoretical analyses of a pile in a viscoelastic soil have been described by Booker and Poulos (1976*a*; 1976*b*). In the case of soil whose creep-response varies linearly with log time, it has been shown that the logarithmic creep rate C_r (the slope of the settlement-versus-log-time relationship) is given by

$$C_r = \frac{PI_\rho B}{d} \tag{5.45}$$

where

P = applied load
I_ρ = displacement-influence factor from elastic theory (Eqs. 5.33a or 5.34a)
B = parameter in the creep function $J(t)$ of the soil, in which

$$J(t) = A + B \log (1 + \alpha t) \tag{5.46}$$

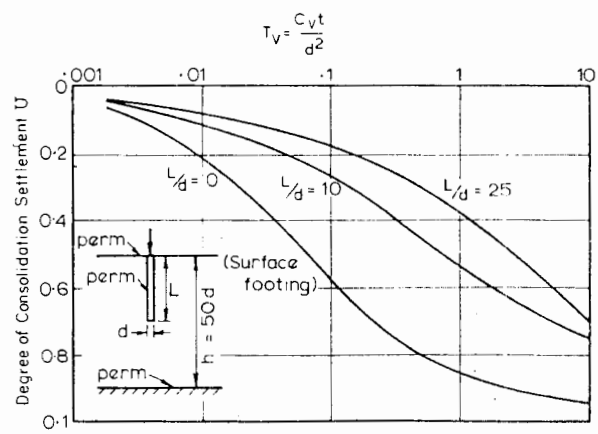

FIGURE 5.39 Comparison between rate of settlement of a pile and a surface footing (Poulos and Davis, 1968).

A, B, and α are experimentally determined parameters of the soil, and $J(t)$ is, in effect, an inverse Young's modulus that is time dependent. A is the inverse of the drained Young's modulus E_s' of the soil and the parameter B reflects the rate of decrease of modulus [or increase in $J(t)$] with log time. There is little available data on values of B, but from one test reported by Cambefort and Chadeisson (1961), backfigured values of B/A were found to increase very markedly with increasing load-level, from a value of about 0.3 at a load of about 30% of the ultimate to about 2.7 at a load of about 80% of the ultimate. Provided that an appropriate value of B can be established, the logarithmic creep rate can readily be estimated from Eq. 5.45, using the elastic solutions for I_ρ from Figs. 5.18, 5.19, 5.20, 5.21, and 5.22.

5.4 SIMPLIFIED METHOD FOR CONSTRUCTING LOAD-SETTLEMENT CURVE TO FAILURE

Analyses taking account of pile-soil slip along the shaft have revealed that for normal piles having a length-to-diameter ratio L/d, greater than about 20, the load-settlement curve is substantially linear until a load of about 50 to 70% of the failure load is reached. For the prediction of the settlement at working loads for such piles, a linear elastic analysis is therefore adequate. However, for large-diameter piles or piers, piles with an enlarged base, or some pile groups, full shaft slip may occur at a relatively low load (less than the working load), so that some account should then be taken of the effects of shaft slip on load-settlement behavior.

A simplified method of constructing the load-settlement curve for such cases has been described by Poulos (1972*d*) and is similar in principle to the methods suggested by Whitaker and Cooke (1966) and Burland et al. (1966). The overall load-settlement curve is constructed as a combination of the relationships between shaft load and settlement and base load and settlement, which are assumed to be linear up to failure of the shaft and the base, respectively. However, in contrast to the methods of Burland et al. and Whitaker and Cooke, which rely almost entirely on the use of empirical data to construct the shaft-load-versus-settlement and base-load-versus-settlement curves, the proposed method utilizes the elastic solutions described in this chapter. Consideration will be given first to the estimation of load-versus-immediate-settlement curves for piles in clay or load-versus-total-settlement curves for piles in sand. Consolidation settlements in clay will be considered subsequently.

Shaft Load versus Settlement

The amount of the load carried by the shaft, P_s, is related to the total applied load P as

$$P_s = P(1-\beta) \tag{5.47}$$

where

β = proportion of load carried by base, obtained from elastic theory, Eq. (5.31) or (5.32)

Assuming a linear shaft-load-versus-settlement relationship up to failure of the shaft, the relationship between settlement of the pile head ρ and P_s, up to the ultimate shaft resistance, P_{su}, can be expressed as

$$\rho = \frac{I}{E_s d} \cdot \frac{P_s}{(1-\beta)} \tag{5.48}$$

where

I = displacement-influence factor for pile, obtained from Eq. (5.33) or (5.34)

E_s = average soil modulus along the pile shaft.

Base Load versus Settlement

The load carried by the base, P_b, is related to the total load P as

$$P_b = \beta P \tag{5.49}$$

Assuming a linear relationship between base load and settlement up to failure of the base, the relationship between settlement and base load is

$$\rho = \frac{I}{E_s d} \cdot \frac{P_b}{\beta} \tag{5.50}$$

where

E_s = average soil modulus along the pile shaft

To the settlement in Eq. (5.50) should be added the compression of the pile shaft which occurs subsequent to the development of the ultimate shaft resistance.

Assuming that the pile material remains perfectly elastic, the additional compression of the shaft, $\Delta\rho$, is

$$\Delta\rho = \left[P_b - \frac{P_{su}\beta}{(1-\beta)} \right] \frac{L}{A_p E_p} \tag{5.51}$$

The base-load-versus-settlement relationship is therefore

$$\rho = \left(\frac{I}{E_s d}\right)\left(\frac{P_b}{\beta}\right) + \left[P_b - \frac{P_{su}\beta}{(1-\beta)}\right]\frac{L}{A_p E_p} \qquad (5.52)$$

It should be noted that the effect of having a modulus at the pile tip, E_b, greater than the average value along the shaft, E_s, is taken into account in determining the settlement-influence factor I, and not by using the value of E_b for E_s in the denominator of Eq. (5.52).

Overall Load versus Settlement

The overall load-settlement curve can be constructed by superposition of the shaft-load-versus-settlement and base-load-versus-settlement curves. If only the overall curve is required, it can readily be constructed as two linear portions (see Fig. 5.40):

1. The first extends from the origin to the load P_{y1} corresponding to full shaft yield, where

$$P_{y1} = \frac{P_{su}}{1-\beta} \qquad (5.53)$$

the settlement, ρ_{y1}, at this load being given by

$$\rho_{y1} = \left(\frac{I}{E_s d}\right)\left(P_{y1}\right) \qquad (5.54)$$

2. The second extends from the latter point to the ultimate bearing capacity of the pile, $P_u = P_{su} + P_{bu}$, at which the settlement, ρ_u, is given as

$$\rho_u = \left(\frac{I}{E_s d}\right)\left(\frac{P_{bu}}{\beta}\right) + \left[P_{bu} - \frac{P_{su}\beta}{(1-\beta)}\right]\frac{L}{A_p E_p} \qquad (5.55)$$

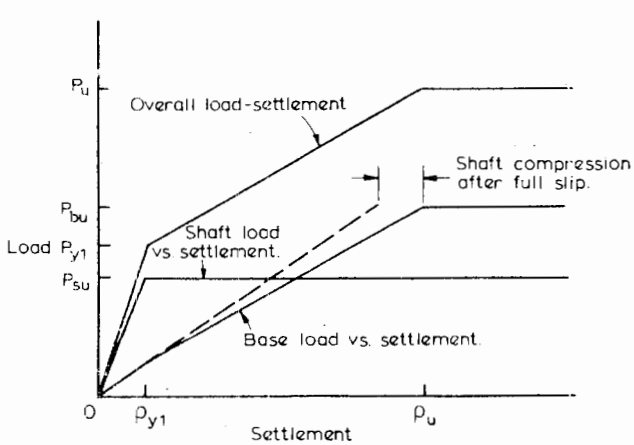

FIGURE 5.40 Construction of load-settlement curve.

The ultimate shaft and base resistances may be calculated from the methods described in Chapter 3.

Consolidation Settlement

To calculate consolidation settlements for piles in clay, it is convenient to assume that the consolidation process is entirely elastic, even if some yielding or slip has occurred under undrained conditions. A similar assumption is made in Chapter 10 in relation to pile-raft systems. Referring to Fig. 5.41, the final consolidation settlement, ρ_{CF}, is given by

$$\rho_{CF} = \rho_{CF(E)} = \rho_{TF(E)} - \rho_{i(E)} \qquad (5.56)$$

where

$\rho_{TF(E)}$ = total final settlement for the required working load, calculated on a purely elastic basis (no yield), and similarly for $\rho_{i(E)}$ and $\rho_{CF(E)}$

If values of undrained Young's modulus, E_{su}, and drained modulus, E'_s, of the soil are available, ρ_{CF} can be calculated as follows:

$$\rho_{CF} = \frac{P_w}{d}\left[\frac{I'}{E'_s} - \frac{I_{0.5}}{E_{su}}\right] \qquad (5.57)$$

where

P_w = working load on pile
I' = displacement-influence factor for the drained Poisson's ratio, ν'_s

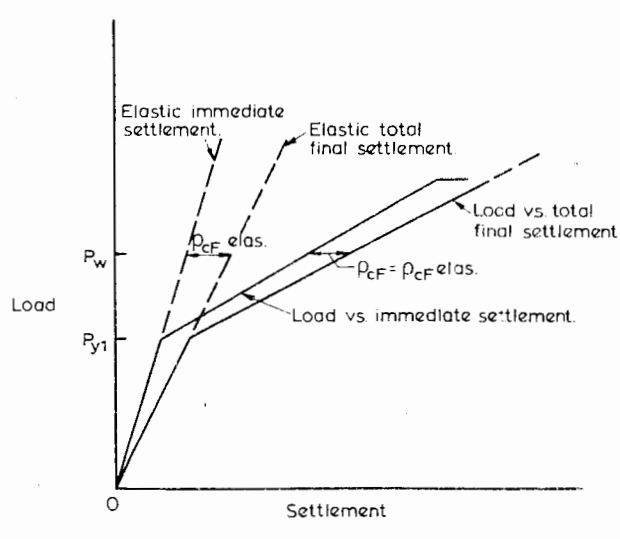

FIGURE 5.41 Suggested method of estimating consolidation settlement.

$I_{0.5}$ = displacement-influence factor for the undrained Poisson's ratio (0.5 for saturated clay)

If no data is available on the drained modulus E_s', a rough estimate of the consolidation settlement may be obtained from the ratios of immediate to total-final settlement plotted in Figs. 5.36 and 5.37 for an ideal elastic two-phase soil. On this basis,

$$\rho_{CF} = \rho_{i(E)}\left[\frac{1}{(\rho_i/\rho_{TF})} - 1\right] \qquad (5.58)$$

The total final settlement is obtained by adding the consolidation settlement, taken from either Eq. (5.57) or Eq. (5.58), to the immediate settlement calculated from the procedure previously described.

Illustrative Example

To illustrate the use of the simplified procedure described above, the case of a large bored pile in clay will be considered. The pile has been tested by Whitaker and Cooke (1966) and is denoted as Pile *F*. The pile details are as follows:

L = 39.9 ft (12.2 m) [shaft length = 36.5 ft (11.1 m)]
d = 2.0 ft (0.61 m)
d_b = 4.0 ft (1.2 m)
E_p = 3.0×10^6 lb/sq in. (19.3×10^4 tons/sq ft, 20.67×10^6 kN/m^2)

The soil details are as follows:

Along shaft, $\bar{c}_u$ = 1.2 tons/sq ft (129 kN/m^2)
At base, c_u = 1.4 tons/sq ft (150 kN/m^2)
Average E_s along shaft = 10,500 lb/sq in (675 tons/sq ft, 72,400 kN/m^2)— see Section 5-5-3
ν_s = 0.5 (assumed undrained conditions)

From the above data,

L/d = 19.5, d_b/d = 2.0
$K = 3 \times 10^6/1.05 \times 10^4 = 285$

Determination of I and β

From Fig. 5.18, I_0 = 0.085 (for L/d = 19.5 and d_b/d = 2.0)
From Fig. 5.19, R_K = 1.35 (for K = 285)
From Fig. 5.21, R_ν = 1.0

Treating the pile as a floating pile in a deep soil layer, R_h = 1.0

From Eq. (5.33a), $I = 0.085 \times 1.35 \times 1.0 \times 1.0 = 0.115$
From Fig. 5.11, β_0 = 0.215
From Fig. 5.12, C_k = 0.76
From Fig. 5.13, C_ν = 1.0
$\beta = 0.215 \times 0.76 \times 1 = 0.164$

Determination of Ultimate Shaft and Base Resistance

Assuming c_a/c_u = 0.33,
$P_{su} = \pi \times 2.0 \times 36.5 \times 1.2 \times 0.33$
= 92 tons (920 kN)
$P_{bu} = 9.0 \times 1.4 \times 12.6$
= 158 tons (1580 kN)

Determination of Overall Load-Settlement Curve

From Eq. (5.53), total load at ultimate shaft yield is

$$P_{YI} = \frac{92}{0.836} = 110 \text{ tons (1100 kN)}$$

From Eq. (5.54), settlement at ultimate shaft yield is

$$\rho_{YI} = \frac{0.115 \times 110 \times 12}{2.0 \times 675}$$
$$= 0.112 \text{ in. (2.8 mm)}$$

From Eq. (5.55), settlement at ultimate failure of pile [P_u = 92 + 158 = 250 tons (2500 kN)] is

$$\rho_u = \frac{0.115}{2.0 \times 675} \times \frac{158}{0.165} \times 12 + \left(158 - 92 \times \frac{0.165}{0.835}\right) \times \frac{39.5 \times 12}{3.14 \times 19.3 \times 10}$$
$$= 1.088 \text{ in. (27.6 mm)}$$

The load-settlement curve is thus drawn as two straight lines, the first joining the origin to the point P = 110 tons, ρ = 0.112 in., and the second joining the latter point to the point P = 250 tons, ρ = 1.088 in. This computed curve is compared with the measured curve in Fig. 5.46*c*.

5.5 DETERMINATION OF SOIL PARAMETERS

The application of the theoretical solutions described in this chapter to practical problems generally requires a knowledge of representative values of the deformation parameters E_u, E_s' and ν_s' of the soil and of the soil shear strength and the pile-soil adhesion. Methods of determining soil shear strength are well-established, and some data on the relationship between shear strength and pile-soil adhesion are given in Chapter 3. However, methods for determining the soil deformation parameters are not so well established. There appear to be three means of obtaining these parameters:

(a) From laboratory triaxial tests.
(b) From pile-loading tests.
(c) From empirical correlations based on previous experience.

5.5.1 Laboratory Triaxial Tests

The use of such tests for settlement predictions of pad foundations has been described by Davis and Poulos (1963), Lambe (1964), and Kerisel and Quatre (1966). In all cases, the stress paths of typical elements in the field are reproduced in the laboratory test and the resulting strains measured. However, for a pile foundation, such tests are complicated by the difficulty of determining the appropriate stress path, both during installation of the pile and resulting from the applied load on the pile.

Conventional types of triaxial tests such as those used for settlement prediction of shallow foundations (Davis and Poulos, 1963; 1968) have been found to give values of E_s that are much too low for piles. For example, Bromham and Styles (1971) obtained a value only about one third of that backfigured from a field-loading test, while Mattes (1972) obtained a value of only about one eighth of the backfigured value from a field-loading test. Attempts (Mattes, 1972) to simulate more closely the stress path of a soil element near a driven pile by failing the specimen in extension, allowing consolidation and then testing for the deformation parameters, led to higher values of E_s, but still lower than the backfigured values from model-pile tests. The conclusion, then, is that it is not possible to measure accurately the value of E_s appropriate to a pile in a conventional triaxial test, even with relatively refined testing procedures. At the present time, possibilities of other, more appropriate forms of laboratory testing remain to be explored.

5.5.2 Pile-Loading Tests

Because many uncertainties may be associated with small-scale laboratory tests, it is desirable where possible to deduce the deformation and strength parameters from a full-scale pile-loading test. Such factors as the method of installation of the pile and layering of the soil profile are then largely taken into account. In order to determine all three required deformation parameters from full-scale pile tests, it is theoretically necessary to carry out loading tests on two piles of different proportions and to use the appropriate theoretical solutions to backfigure these parameters. However, it is probably sufficient either to estimate the value of ν_s' or to determine it from a laboratory triaxial test (e.g., as described by Davis and Poulos, 1963, for pad footings). At low load levels (about one third of the ultimate), where little time-dependent settlements may occur, it may be possible to use a constant-rate-of-penetration (C.R.P.) test rather than a maintained loading test, and obtain a single value of soil modulus. The interpretation of a pile-loading test to obtain the deformation parameters is considered in detail in Chapter 16.

If the load test is carried to failure, the field value of pile-soil adhesion may also be determined, provided that the strength parameters can be estimated independently. Thus, a single pile-loading test may provide sufficient data to enable both the deformation and the strength parameters to be estimated.

5.5.3 Empirical Correlations

In order to provide some information on values of E_s for situations in which pile-loading test data are not available, a number of published pile-test results have been analyzed and values of E_s determined.

5.5.3.1 PILES IN CLAY

Where possible, the calculated values of E_s have been correlated with reported values of the undrained cohesion, c_u, of the clay, and these are plotted in Fig. 5.42. Mean relationships between E_s and c_u are plotted for bored and driven piles for which two trends can be observed:

1. For soft to medium clays [$c_u < 17$ lb/sq in. (120 kPa)], E_s for driven piles is greater than for bored piles, but for stronger clays, E_s for bored piles becomes greater. The first effect may be attributed to the higher excess pore pressures and greater subsequent reconsolidation for the driven piles in soft clay, while the second may be attributed to the effects of "whip" in the driving of piles in stiff clay.
2. For stiff clays, E_s appears to reach a limiting value—about 6000 lb/sq in. (40 MPa) for driven piles, and 12,000 lb/sq in. (80 MPa) for bored piles—although some tests on bored piles in London clay gave considerably higher values.

In many of the tests, it is not possible to determine whether the value of E_s is the undrained or the drained value. It is possibly reasonable to consider the values of E_s in Fig. 5.42 as drained values, E_s', and in the absence of other information, the undrained modulus E_u may be estimated from the following relationship for an ideal isotropic elastic two-phase soil:

$$E_u = \frac{3E_s'}{2(1+\nu_s')} \tag{5.59}$$

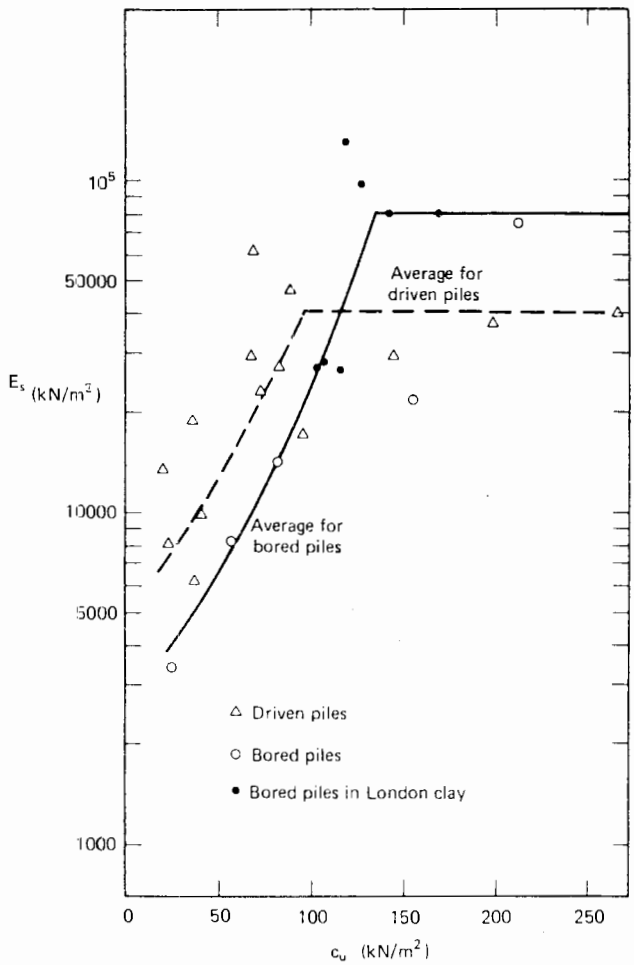

FIGURE 5.42 Backfigured soil modulus E_s for piles in clay.

The reliability of this relationship when applied to real soils is somewhat dubious; in relation to shallow foundations, it has been found to be reasonable for a remolded kaolin (Davis and Poulos, 1963) and a silty clay (Moore and Spencer, 1969) but to be most unreliable for Boston blue clay, probably because of anisotropy of the soil.

From a number of triaxial tests on various types of clay, the following typical ranges of values of ν_s' have been encountered (suggested average values are shown in brackets):

Stiff overconsolidated clays:	0.1 –0.2 (0.15)
Medium clays:	0.2 –0.35 (0.3)
Soft normally consolidated clays:	0.35–0.45 (0.4)

5.5.3.2 PILES IN SAND

In analyzing the results of pile tests in sand, E_s has been calculated on the assumption that the soil moduli remain constant with depth although the assumption of E_s varying linearly with depth might have been more appropriate. Most of the tests considered are for driven piles, and the suggested ranges of average values of E_s for such piles are summarized in Table 5.3.

TABLE 5.3 SUGGESTED AVERAGE VALUES OF E_s FOR DRIVEN PILES IN SAND

Sand Density	Range of Relative Density, D_r	Range of E_s (lbs/sq in.)	(MN/m^2)
Loose	< 0.4	4000–8000	27.5–55
Medium	0.4–0.6	8000–10,000	55 –70
Dense	> 0.6	10,000–16,000	70 –110

Values of Poisson's ratio, ν_s, obtained from triaxial tests generally lie between 0.25 and 0.35 at relatively low stress levels. An average value of 0.30 is reasonable when no test data are available.

While the use of a constant average modulus with depth of the sand may provide satisfactory settlement predictions for relatively slender piles in which only a small proportion of the load is taken by the base, it may lead to inaccuracy in load-settlement predictions for shorter piles or piers, as the soil modulus near the tip tends to be considerably greater than the average modulus along the shaft. A more detailed analysis of Vesic's tests together with an examination of the tests by Meyerhof (1959)—see Chapter 2—suggests that the soil modulus beneath the pile tip, E_b, is of the order of 5 to 10 times the average value along the shaft, E_s. The use of such a value of E_b/E_s (rather than assuming $E_b/E_s = 1$) leads to more satisfactory agreement between measured and predicted load-settlement behavior from Vesic's tests (Poulos, 1972*d*).

It is therefore suggested that for the prediction of load-settlement behavior of piles in sand, the value of the average soil modulus along the shaft, E_s, be estimated from Table 5.3 and that the ratio of E_b/E_s be taken between 5 and 10, the higher value being used for driven piles in dense sand and the lower value for bored piles in loose sand.

5.5.4 Typical Values of K

On the basis of the preceding values of soil modulus, average values of pile-stiffness factor K, calculated for various types of pile and soil, are given in Table 5.4.

TABLE 5.4 AVERAGE VALUES OF K FOR SOLID PILES

Soil Type	Pile Material		
	Steel[a]	Concrete	Timber
Soft clay	60,000	6000	3000
Medium clay	20,000	2000	1000
Stiff clay	3000	300	150
Loose sand	15,000	1500	750
Dense sand	5000	500	250

[a] For hollow or H-piles, multiply these values by area ratio R_A.

5.6 SOME COMPARISONS BETWEEN OBSERVED AND PREDICTED PILE SETTLEMENTS

Although the majority of published pile-loading test results are concerned primarily with ultimate load capacity, some tests are sufficiently well-documented to allow the settlement behavior to be analyzed and compared with that predicted from pile-settlement theory. A number of these cases are described below.

Tests by Darragh and Bell (1969)

Mattes (1972) has analyzed an interesting series of pile tests carried out by Darragh and Bell (1969) at the site of Gulf Oil Corporation's Faustina Works, on the banks of the Mississippi River. Brief details of the piles driven and of site subsurface conditions are given in Fig. 5.43. The site involved about 120 ft of natural levee and back-swamp deposits consisting of layers and laminations of clays, silts, and fine sands, which overlay a 70-ft deep layer of fine silt grading to sandy gravel with depth. Two pairs of step-taper piles and one pair of steel-tube piles were driven: step-taper piles 1B and 3 were friction piles driven to within 20 ft of the sandy stratum, step-taper piles 2A and 4 were end-bearing in the sandy stratum, tube pile 9 was a floating pile founded at a similar depth to 1B and 3, and tube pile 10 was end-bearing in the sand. Piles 1B and 3 gave very similar load-test results, and were analyzed as floating piles in a finite layer to derive a backfigured soil modulus for the back-swamp deposits. The relevant details of these piles are as follows:

Pile length, L:	108 ft
Average diameter, d:	13 in.
L/d:	100 (approx.)
Depth of founding layer, h:	120 ft
h/L:	1.1 (approx.)
Ultimate load:	160 tons
Settlement at 80 tons:	0.12 in.
Soil modulus E_s (backfigured):	6500 psi
Pile stiffness factor, K:	460–500

For the purpose of predicting the performance of the end-bearing piles 2A, 4, and 10, it was assumed that the base-soil modular ratio, E_b/E_s, was 2.

In Table 5.5, the observed settlements of piles 2, 4A, 9, and 10 are compared with those predicted by the elastic theory, using the soil modulus derived from the floating-

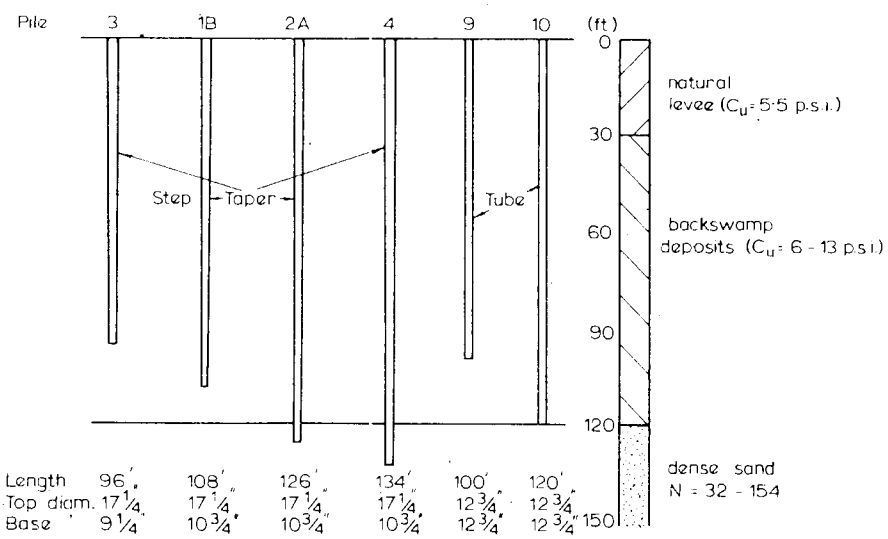

FIGURE 5.43 Details of tests by Darragh and Bell (1969).

TABLE 5.5 PREDICTED PILE PERFORMANCE–TESTS BY DARRAGH & BELL (1969)

Pile Number	2A	4	9	10
Floating or end-bearing	End-bearing	End-bearing	Floating	End-bearing
Length (ft)	126	132	100	120
Length/diameter (approx.)	120	120	80	95
Pile type	Steel step-taper (closed)	Steel step-taper (closed)	Closed Steel tube 0.188-in wall	Closed Steel tube 0.188-in. wall
E_s (psi)	6500	6500	6500	6500
E_b/E_s	2	2	1	2
K	500	500	270	270
Applied load (tons)	120	120	40	80
Predicted top settlement (in.)	0.25	0.25	0.09	0.16
Measured top settlement (in.)	0.20	0.24	0.10	0.17
Predicted base settlement (in.)	0.05	0.05	0.01	0.016
Measured base settlement (in.)	0.04	0.06	0.015	0.02

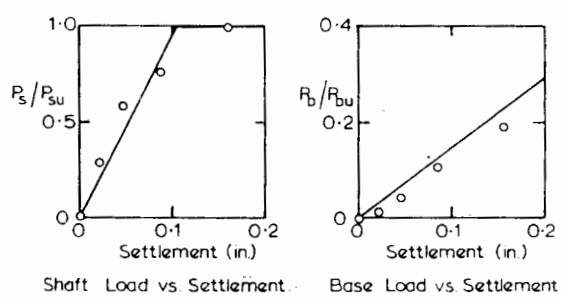

FIGURE 5.44 Comparisons between predicted and observed behavior. Tests of Whitaker and Cooke (1966).

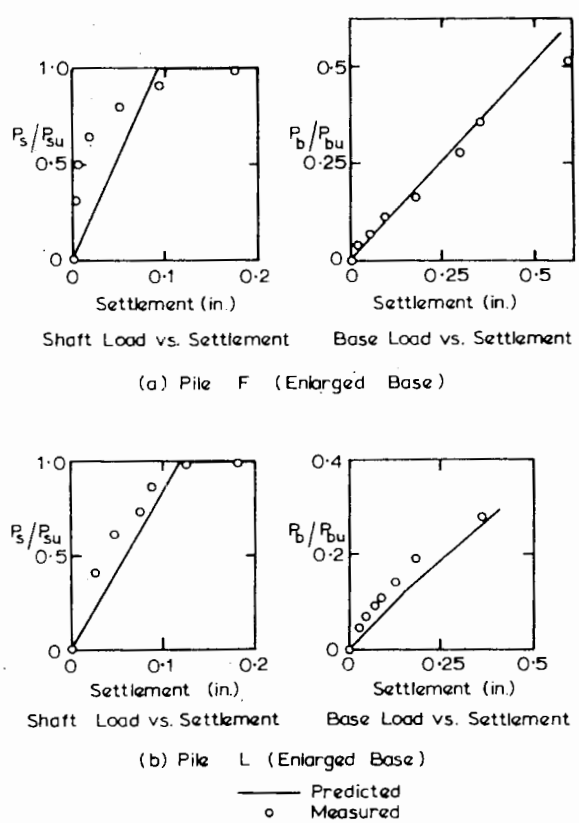

FIGURE 5.45 Comparisons between predicted and observed behavior. Tests of Whitaker and Cooke (1966).

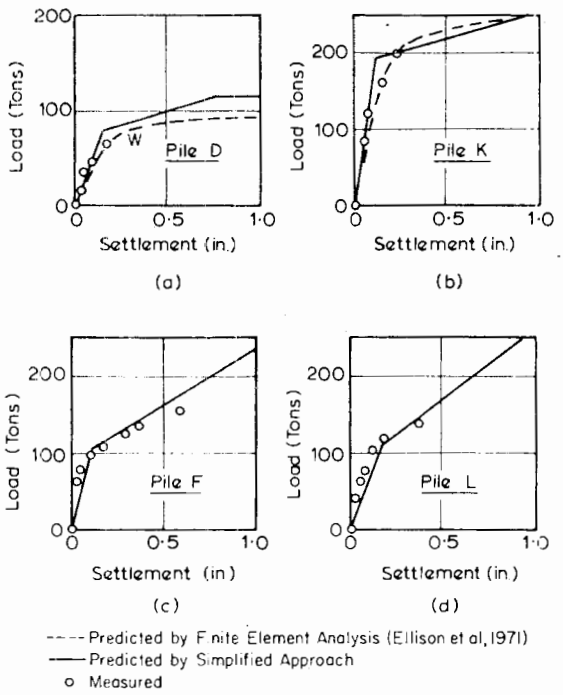

FIGURE 5.46 Comparisons between observed and predicted load-settlement curves. Tests of Whitaker and Cooke (1966).

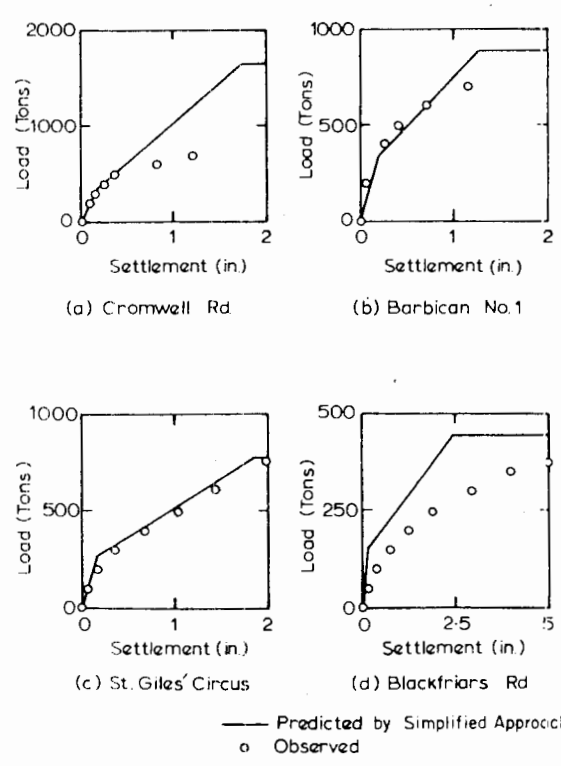

FIGURE 5.47 Comparisons between observed and predicted load-settlement curves. Tests of Burland et al. (1966).

pile tests 1B and 3, and it can be seen that the settlement performance of both the floating and end-bearing piles has been closely predicted.

Large Bored Piers

For some of the tests reported by Whitaker and Cooke (1966) and Burland et al. (1966) on bored piers in London clay, comparisons are shown in Figs. 5.44 and 5.45 between measured and predicted shaft load versus settlement, and base load versus settlement. The values of E_s in these comparisons have been obtained from the mean curve in Fig. 5.42. The agreement is generally reasonable and the linearity assumption of these relationships appears justified, at least over the range of load employed in these tests.

Comparisons of overall behavior are shown in Figs. 5.46 and 5.47 for the tests of Whitaker and Cooke (1966) and tests reported by Burland et al. (1966). Reasonable agreement again is found, and at least part of the discrepancy that exists can be attributed to the selection of E_s from the average curve in Fig. 5.42, rather than from the actual backcalculated value of E_s for the particular test. Also shown in Fig. 5.46 are the curves for piles and predicted by Ellison et al. (1971) from a finite-element analysis using a trilinear stress-strain curve for the London clay. These predicted curves agree well with the measured curves and are in reasonable agreement with those predicted by the approximate approach described herein.

Tests by Mansur and Kaufman (1956)

Six instrumented piles were driven into a fairly deep-layered system of silts, sandy silts, and silty sands with interspersed clay strata, underlain by a deep layer of dense, fine sand. All except pile number 5, a floating pile, were driven to end-bearing in the dense, fine sand. One of the end-bearing piles (pile 3) was an H-pile with a rectangular baseplate attached, and because of the disturbing effect of this plate during driving, pile 3 will not be considered further. The test results were analyzed as follows:

1. Using the theory for a floating pile in a finite layer (Section 5.2.2), a soil modulus, E_s, of 10,000 psi was backfigured from the test results for pile 5.
2. From the S.P.T. blow counts for the silty soils and the dense, fine sand, it was deduced that a ratio of bearing-stratum to soil moduli, E_b/E_s, of about 3 would be applicable for the end-bearing piles.
3. The analysis for a pile resting on a stiffer stratum (Section 5.2.2) was used to evaluate the load-distribution along and settlement of piles 1, 2, 4, and 6. In Table 5.6, the details of pile properties, settlements, and settlement predictions are given, while in Figs. 5.48a to 5.48e the predicted

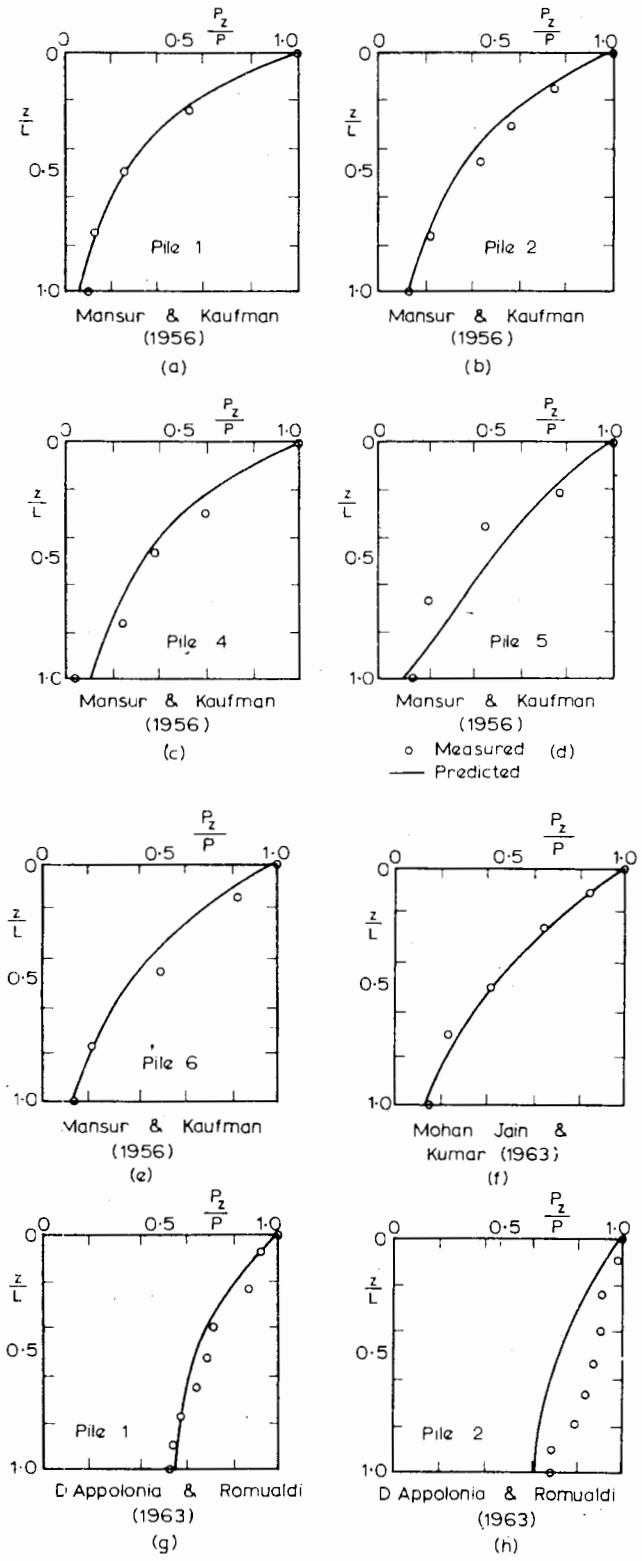

FIGURE 5.48 Comparisons between predicted and observed load distributions.

TABLE 5.6 TESTS BY MANSUR AND KAUFMAN (1956)

Pile number	1	2	4	5	6
Pile type	14-in. H-beam	21-in. pipe	17-in. pipe	17-in. pipe	19-in. pipe
Pile length (ft)	81	65	66	45	65
L/d	70	37	47	32	41
K	470	250	350	350	350
End-bearing (E.B.) or floating (F)	E.B.	E.B.	E.B.	F	E.B.
E_b/E_s	3	3	3	1	3
Load (tons)	125	125	125	75	125
Observed settlement (in.)	0.13	0.13	0.16	0.10	0.13
Predicted settlement (in.)	0.144	0.130	0.142	(0.100)	0.150
Predicted/observed settlement	1.10	1.00	0.89	(1.00)	1.15

NOTE: Soil type: alternating strata of silts, silty sands, sandy silts, with interspersed clay strata.
Bearing Stratum: Dense fine sand.
Pile 5 (floating) used as control pile for predictions.

and measured load-distributions along the piles are compared.

Figure 5.48 and Table 5.6 show that quite low values of K are possible when steel tubes or H-sections are used as piles. In such cases, it is likely that very little load does in fact reach the pile base, even in nominally end-bearing piles. In the case described here, the results of a floating-pile test, when combined with the results of a routine borehole test, have allowed the accurate prediction of the load distribution along and settlement of end-bearing piles on the same site.

Test by Mohan, Jain, and Kumar (1963)

A 14-in.-diameter cast in-situ pile of L/d = 33 was placed through a layered system of fill, medium sand, and silt to end-bearing on a bed of dense, fine sand. No satisfactory soil data were available in the test report, and so a value for K of 300 was assumed, based on an E_s value from Table 5.3, and a ratio of bearing stratum to soil modulus of 2 was adopted. The observed and calculated load-distributions shown in Fig. 5.48*f* reveal good agreement.

Tests by D'Appolonia and Romualdi (1963)

Tests on two instrumented H-piles were reported; the piles were about 45 ft long, and passed through layers of fill, sandy silt, sand and gravel, fine to medium sand, sand and gravel, and sandy silt, to end-bearing in shale. No satisfactory soil data was available, so a K value for solid steel piles of 3000 was adopted, based on an E_s value from Table 5.3.

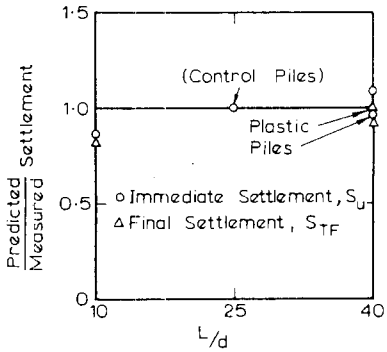

FIGURE 5.49 Comparison between measured and predicted settlements (Mattes and Poulos, 1971).

TABLE 5.7 TESTS BY D'APPOLONIA AND ROMUALDI (1963)

Pile number	1	2
Pile type	14 BP 89 (H-pile)	14 BP 119 (H-pile)
Length (ft)	44	45
Assumed L/d	33	34
Assumed area ratio (R_A)	0.143	0.186
K	430	560
E_b/E_s	∞	∞
Load (tons)	75	100
Observed settlement (in.)	0.07	0.11
Predicted settlement (in.)	0.06	0.09
Predicted/observed settlement	0.86	0.82

NOTE: Soil: layers of fill, sandy silt, sand and gravel, fine to medium sand, sand and gravel, and sandy silt.
Bearing stratum: shale.

The bearing stratum was assumed to be rigid. In Table 5.7, the pile properties and settlement details are listed, and comparisons based on the assumed soil properties are made. In Figs. 5.48*g* and 5.48*h*, the load distributions within the piles are compared with the calculated distributions. In each case, quite reasonable agreement between prediction and observation is obtained, although better agreement could possibly have been obtained if the soil had been considered to have a modulus that increased with depth.

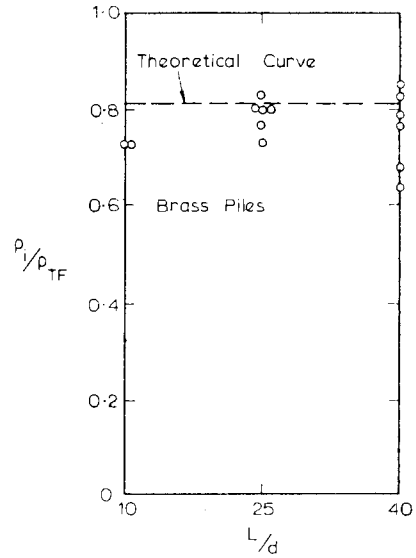

FIGURE 5.50 Comparison between observed and predicted ratio ρ_i/ρ_{TF} (Mattes and Poulos, 1971).

Model Tests

A series of carefully controlled model tests on piles in normally consolidated clay has been carried out by Mattes and Poulos (1971) in order to examine the effects on settlement of length-to-diameter ratio and pile compressibility, and the relative proportions of immediate and final settlement. Figure 5.49 shows the ratio of predicted to observed settlements for piles of various L/d, using brass piles having L/d = 25 as control piles and backfiguring the undrained and drained Young's moduli E_{su} and E'_s, from the measured settlements of these piles. The agreement between predicted and measured settlements for L/d = 10 and 40 is reasonably good, indicating that the theory predicts with adequate accuracy the effects of pile length on settlement. Also shown are comparisons for plastic piles, of about ten times the compressibility of the brass piles, having L/d = 40. Again, the good agreement indicates that the theory gives a good prediction of the effects of pile compressibility.

Figure 5.50 shows a comparison between measured and predicted ratios of immediate to final settlement of the model piles, and reveals fair agreement. The test results confirm the conclusion reached from the theory that the major part of the settlement of a pile occurs as immediate settlement and that consolidation settlement is relatively unimportant at normal working loads.

6

SETTLEMENT OF PILE GROUPS

6.1 INTRODUCTION

Until relatively recently, estimates of the settlement of pile groups were based either on empirical data or on simplified approaches based on one-dimensional consolidation theory. Among the empirical approaches are those for groups in sand devised by Skempton (1953), who on the basis of a limited number of field observations, suggested the following relationship between the settlement, ρ_G, of a group and the settlement, ρ_1, of a single pile-

$$\rho_G/\rho_1 = \frac{(4B + 9)^2}{(B + 12)^2} \tag{6.1}$$

where

B = width of pile group in feet

For driven piles and displacement caissons in sand, Meyerhof (1959) suggested the following relationship for a square group:

$$\rho_G/\rho_1 = \frac{s(5 - s/3)}{(1 + 1/r)^2} \tag{6.2}$$

where

s = ratio of spacing to pile-diameter

r = number of rows for square group

Among the simplified approaches based on one-dimensional theory is that in which the group is replaced by a flexible footing acting at the level of the pile tips, or more conservatively, at two thirds the depth of the pile. Bjerrum et al. (1957) compared these two approximations and found that both underestimated the settlement of a bridge foundation, although the second gave closer agreement. However, the comparison was complicated by an appreciable amount of settlement arising from secondary consolidation in the field.

More recently, analytical methods based on the theory of elasticity have been employed with some success. These analyses are extensions of those for a single pile (see chapter 5). Such analyses have been described by Pichumani and D'Appolonia (1967), Poulos (1968*b*), and Poulos and Mattes (1971*b*). Attention will be concentrated on the method in the latter two papers, which although similar in principle to that of Pichumani and D'Appolonia, is amenable to hand computation. In this chapter, the piles will be assumed to be freestanding. Thus, a pile cap will only influence the behavior of a group by controlling differential settlement between different piles in the group. The effect of contact between cap and soil is included in the analysis given in Chapter 10.

6.2 ANALYSIS OF GROUP SETTLEMENT

6.2.1 Two-Pile Interaction Analysis

The method described here is that described by Poulos (1968*b*) and Poulos and Mattes (1971*b*) for floating and end-bearing pile groups. A group of two identical, equally-loaded piles is considered, as shown in Fig. 6.1, and as with the single-pile analysis, each pile is divided into n cylindral elements and a uniformly-loaded circular base. If conditions remain purely elastic within the soil and no slip or yield occurs at the pile-soil interface, the pile and soil displacements at the center of each element may be equated. The equations for the pile displacement are identical with those for the single pile: that is, Eq. (5.14) for a fully floating pile, or Eq. (5.23) for a pile bearing on a stiffer stratum. The soil displacements for a floating pile may be written as follows:

$$\{_s\rho\} = \frac{d}{E_s}[_1I + {}_2I]\{p\} \tag{6.3}$$

$\{_s\rho\}$ = vector of soil displacement
$\{p\}$ = vector of shear stresses

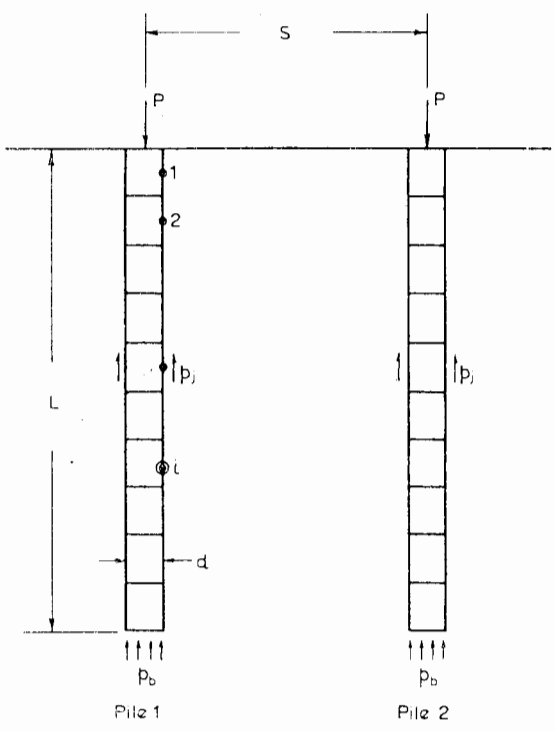

FIGURE 6.1 Group of two floating piles.

$[_1I + {}_2I]$ = $(n+1)$ by $(n+1)$ matrix of displacement-influence factors, containing elements $_1I_{ij} + {}_2I_{ij}$, where
$_1I_{ij}, {}_2I_{ij}$ = displacement-influence factors at element i on pile 1 caused by shear stress on element j of pile 1 and pile 2, respectively

The values of $_1I_{ij}$ and $_2I_{ij}$ may be obtained by integration of the Mindlin equation for the vertical displacement in a semi-infinite mass resulting from interior vertical loading. In the case of end-bearing piles, an allowance may be made for the effect of the stiffer underlying stratum, as outlined in Section 5.2.2.

The soil displacements thus obtained may be equated to the pile displacements and the resulting system of equations solved, to obtain the unknown shear-stresses and displacements along the piles. The analysis of a two-pile group is therefore identical with that of a single pile, except that the soil-displacement-influence matrix includes contributions from the second pile.

The results of the above analysis may be conveniently expressed in terms of an "interaction factor" α, where

$$\alpha = \frac{\text{Additional settlement caused by adjacent pile}}{\text{Settlement of pile under its own load}} \tag{6.4}$$

where the pile and the adjacent pile carry the same load. Solutions for α as a function of several variables are described below. The use of interaction factors to analyze the settlement of general pile groups is described in Section 6.2.3.

6.2.2 Interaction Factors

6.2.2.1 FLOATING PILES

Interaction factors α_F, for two floating piles in a homogeneous semi-infinite mass $\nu_s = 0.5$) have been obtained by Poulos and Mattes (1971*b*) and are shown, as a function of dimensionless pile spacing s/d, in Figures 6.2 to 6.5 for various values of L/d and K. The decreasing interaction with increasing spacing is clearly shown. Interaction increases as L/d increases and K increases, that is, as piles becomes more slender or stiffer.

Effect of Finite Layer

Solutions for the interaction factor for two incompressible piles in a finite layer have been obtained by Poulos (1968*b*). On the basis of these solutions, correction factors N_h to the interaction factors for piles in a semi-infinite mass are shown in Fig 6.6. The actual interaction factor α is then

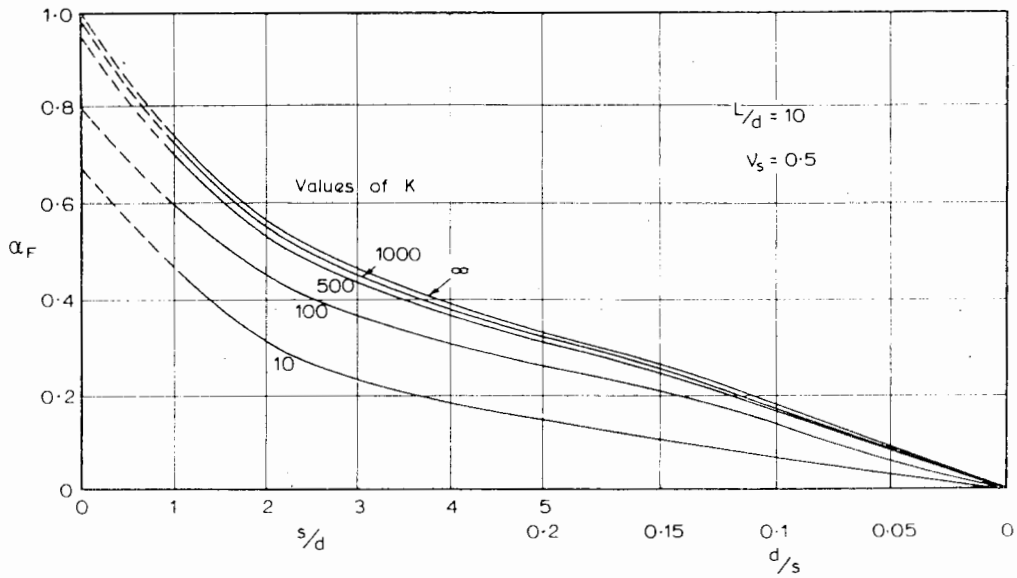

FIGURE 6.2 Interaction factors for floating piles, $\frac{L}{d} = 10$.

$$\alpha = \alpha_F N_h \tag{6.5}$$

where

α_F = interaction factor for semi-infinite mass

While the values of N_h in Fig. 6.6 are for the case $L/d = 25$ and $K = \infty$, they may be applied approximately to other values of L/d and K, bearing in mind that

1. As L/d decreases, the value of N_h decreases.
2. As K decreases, the value of N_h increases.

As examples of the effect of L/d and K on N_h, for $s/d = 5$ and $h/L = 2$, a decrease to $L/d = 15$ results in a 10% decrease in N_h, whereas for $L/d = 50$, N_h is increased by 22% compared with the value for $L/d = 25$. If K is decreased to 1000, the value of N_h for $L/d = 25$, $h/L = 2$, and $s/d = 5$ is decreased by 8%.

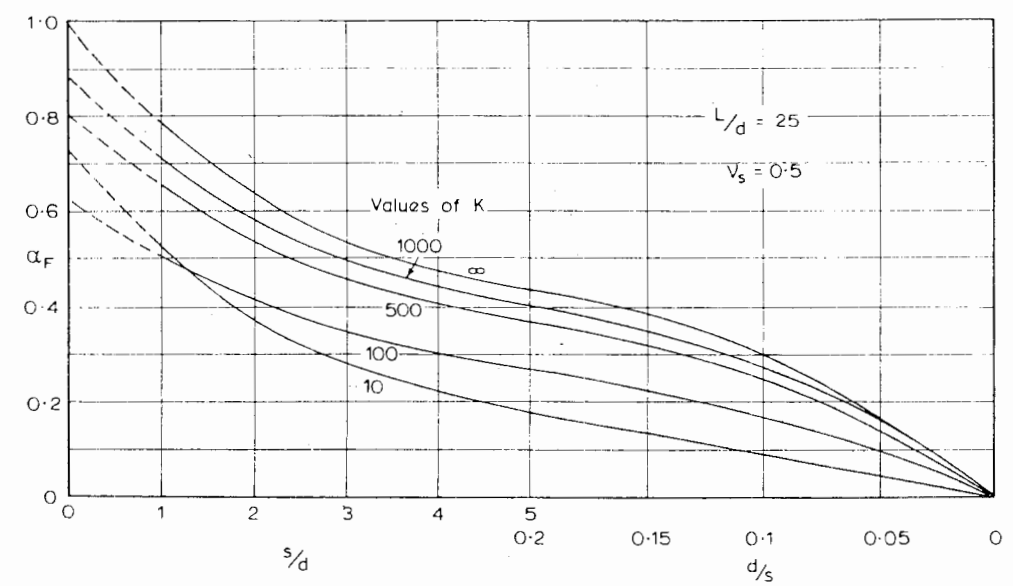

FIGURE 6.3 Interaction factors for floating piles, $\frac{L}{d} = 25$.

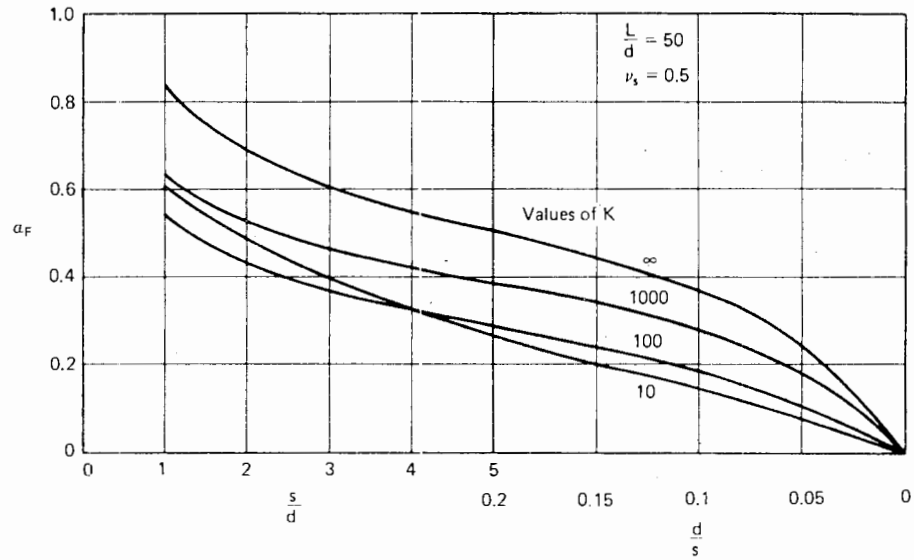

FIGURE 6.4 Interaction factors for floating piles, $\frac{L}{d} = 50$.

Effect of Enlarged Pile Base

Correction factors, N_{db}, to the interaction factors for uniform-diameter floating piles are shown in Fig. 6.7 for values of d_b/d of 2 and 3. The interaction factor for two enlarged-base piles is then

$$\alpha = N_{db}\alpha_F \tag{6.6}$$

where

α_F = interaction factor for $d_b/d = 1$, for relative spacing s/d

Interaction increases as the base diameter increases, this effect being most pronounced for relatively short piles. The values of N_{db} in Fig. 6.7 are for incompressible piles ($K = \infty$); for relatively compressible piles, the effect of the enlarged base is less, so that N_{db} is less than in Fig. 6.7.

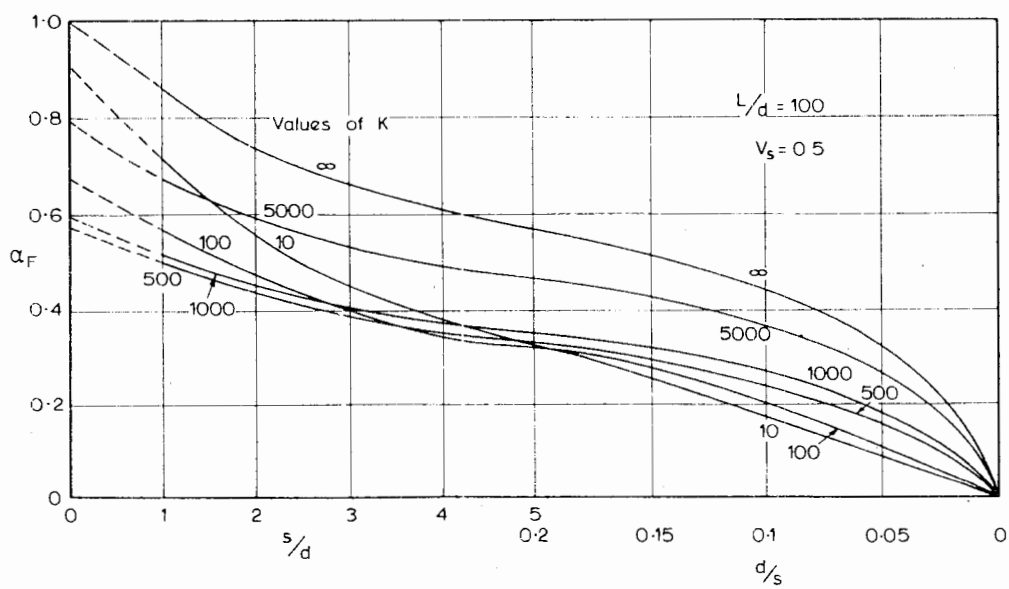

FIGURE 6.5 Interaction factors for floating piles, $\frac{L}{d} = 100$.

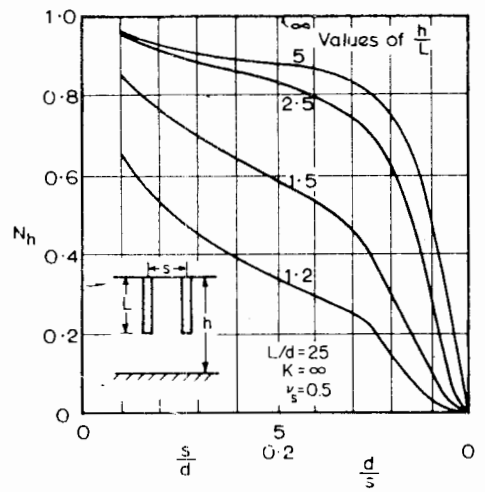

FIGURE 6.6 Correction factors N_h to interaction factors, for effect of finite layer depth.

Effect of Poisson's Ratio

The effect of Poisson's ratio, ν_s, of the soil is indicated in Fig. 6.8, where for $L/d = 50$ and $K = 1000$, a correction

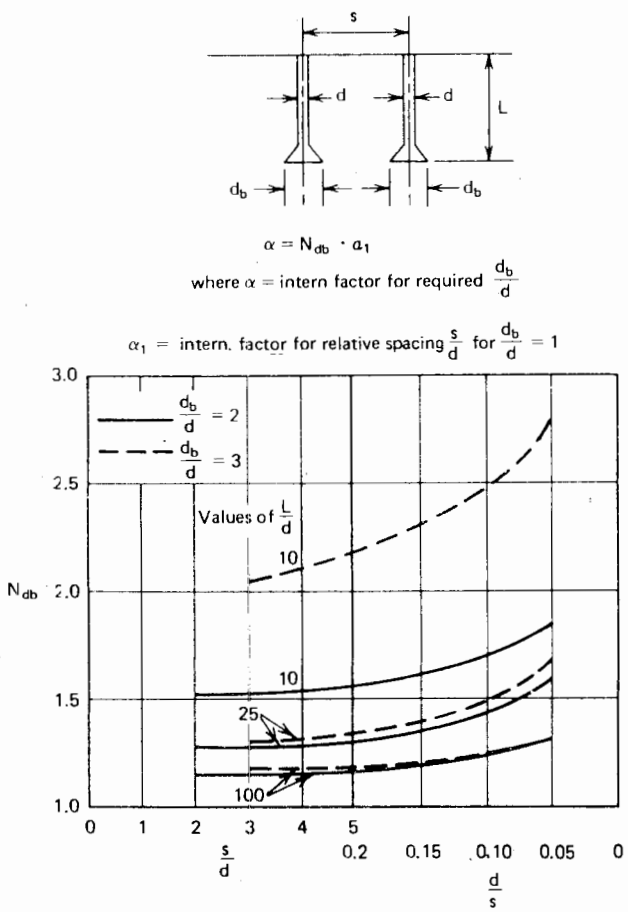

FIGURE 6.7 Correction factors N_{db} to interaction factors, for effect of finite layer depth.

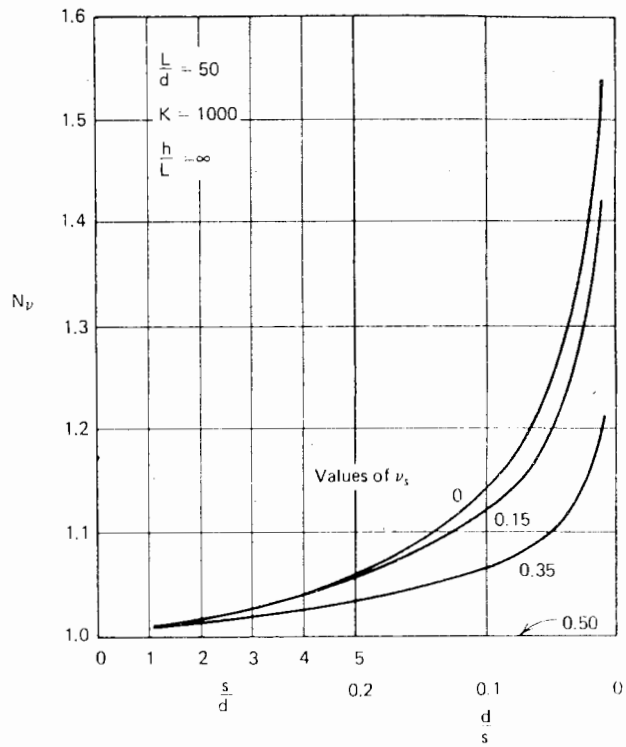

FIGURE 6.8 Correction factor N_ν for effect of Poisson's ratio.

factor N_ν is plotted for floating piles. The interaction factor for any value of ν_s is given by

$$\alpha = N_\nu \alpha_{0.5} \tag{6.7}$$

where

$\alpha_{0.5}$ = interaction factor for $\nu_s = 0.5$

N_ν, and hence interaction, increases as the value of ν_s decreases, this effect becoming more marked as the spacing increases.

Effect of Nonuniform Soil Modulus

The preceding solutions for interaction factors all assume a uniform soil-modulus along the pile shaft. In many cases, a closer approximation to reality is to consider the soil modulus as increasing linearly with depth. A typical interaction curve for this case is shown in Fig. 6.9, where it is compared with the corresponding curve for a uniform soil with the same average modulus. The value of α for the nonhomogeneous soil is 20 to 25% smaller than for the homogeneous soil at any given spacing. Thus, the use of interaction factors for a homogeneous soil may overestimate the settlement somewhat for cases in which the modulus increases with depth.

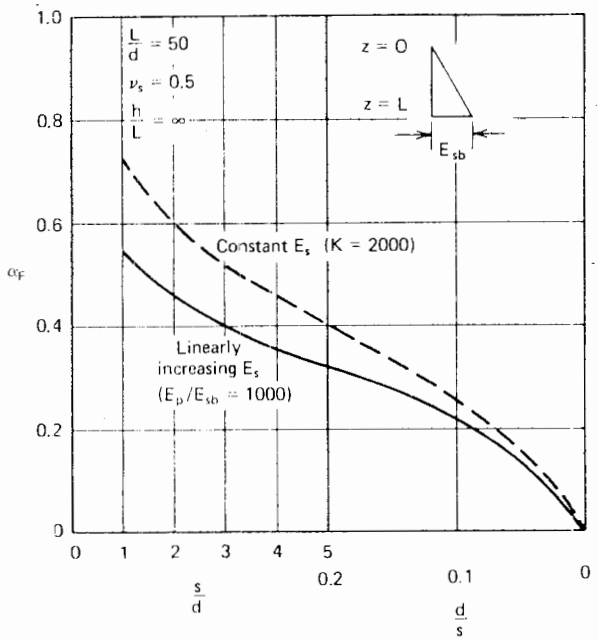

FIGURE 6.9 Effect of distribution of E_s on interaction factor.

Effect of Slip

As pointed out in Chapter 5, slip at the interface between the pile shaft and the soil plays a negligible role in the settlement behavior of single piles of normal proportions at the working load, but for piers having low values of L/d and for piles with enlarged bases, slip has some significance. However, extension of the above interaction-analysis to incorporate a moderate degree of slip shows that the value of α_F is not significantly changed.

6.2.2.2 END-BEARING PILES ON RIGID STRATUM

Interaction factors α_E for end-bearing piles on a rigid stratum are shown in Figs. 6.10 to 6.13 (Poulos and Mattes, 1971*b*). As s/d increases, α_E decreases, but in contrast to the floating piles, α_E generally decreases as K increases, and for $K = \infty$ (incompressible piles), no interaction occurs, since the entire load is transferred to the rigid base. Also, α_E decreases as L/d decreases, since less load-transfer then occurs. The effect of Poisson's ratio, ν_s, is again small in relation to the effects of L/d and K.

Effect of Finite Compressibility of Bearing Stratum

Interaction factors for a pile resting on a compressible stratum will lie between those for a floating pile in a homogeneous mass, α_F, and those for a pile resting on a rigid base, α_E, and may be expressed as

$$\alpha = \alpha_F - F_E(\alpha_F - \alpha_E) \tag{6.8}$$

where

F_E is a factor depending on K, L/d, and E_b/E_s.

Values of F_E for four values of L/d are shown in Fig. 6.14,

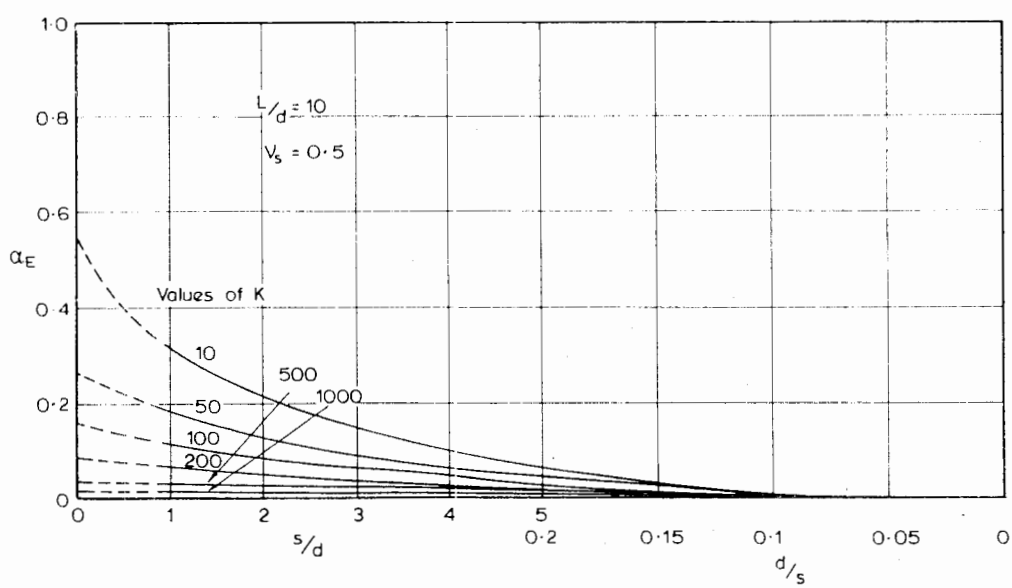

FIGURE 6.10 Interaction factors for end-bearing piles, $\frac{L}{d} = 10$.

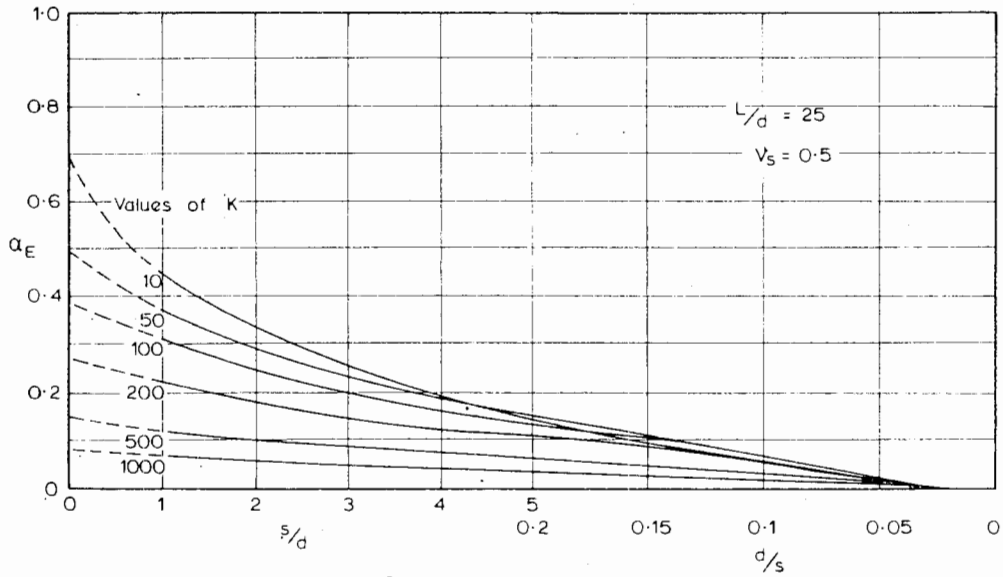

FIGURE 6.11 Interaction factors for end-bearing piles, $\frac{L}{d} = 25$.

which shows the transition from end-bearing to floating interaction with E_b/E_s and K. The smaller the value of K or the larger the value of L/d, the smaller the value of E_b/E_s for which F_E tends to 1 (i.e., the interaction factor tends to the rigid base value). Although the curves shown are for $s/d = 5$, they apply approximately for other values of s/d.

6.2.2.3 INTERACTION BETWEEN PILES OF DIFFERENT SIZE

For two piles—i and j in Fig. 6.15— of different size, it is reasonable to calculate the increase in settlement of pile i caused by pile j, $\Delta\rho_{ij}$, approximately as

$$\Delta\rho_{ij} = \rho_j \cdot \alpha_{ij} \tag{6.9}$$

where

ρ_j = settlement of pile j under its own load
α_{ij} = interaction factor corresponding to the spacing between piles i and j, and for the geometrical parameters (i.e., length and diameter) of pile j

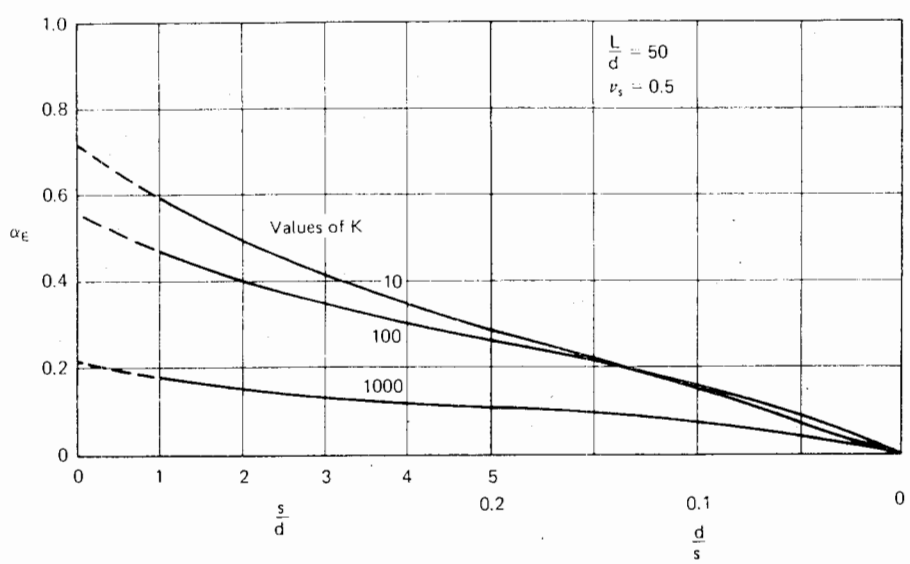

FIGURE 6.12 Interaction factors for end-bearing piles, $\frac{L}{d} = 50$.

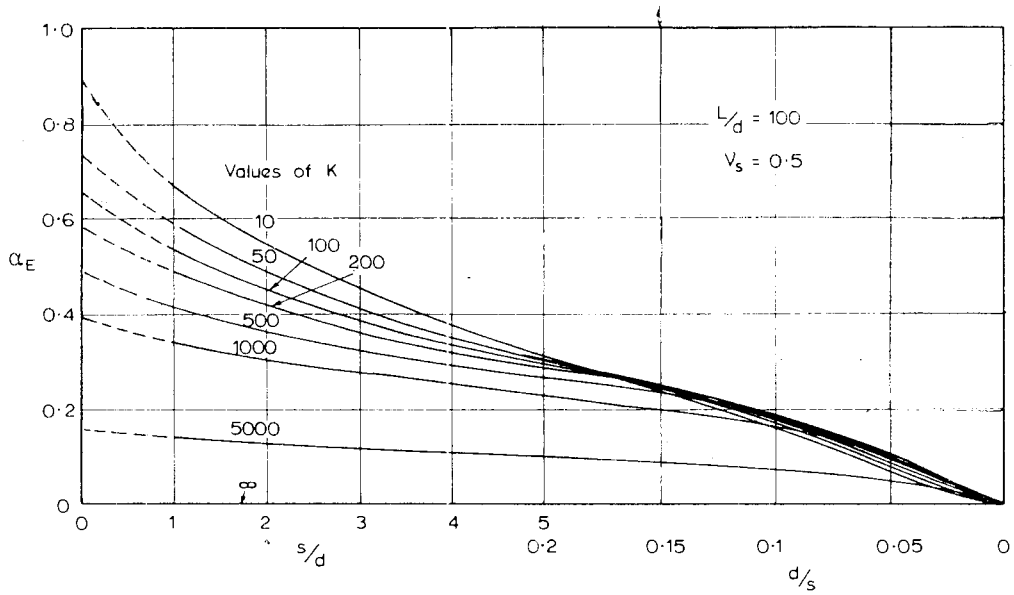

FIGURE 6.13 Interaction factors for end-bearing piles, $\frac{L}{d} = 100$.

Similarly, the increase in settlement of pile j caused by pile i, $\Delta\rho_{ji}$, is

$$\Delta\rho_{ji} = \rho_i \cdot \alpha_{ji} \tag{6.10}$$

where

ρ_i = settlement of pile i under its own load
α_{ji} = interaction factor corresponding to the spacing between piles i and j, and for the geometrical parameters of pile i.

In general, for equal loads on piles i and j, $\Delta\rho_{ij} \neq \Delta\rho_{ji}$.

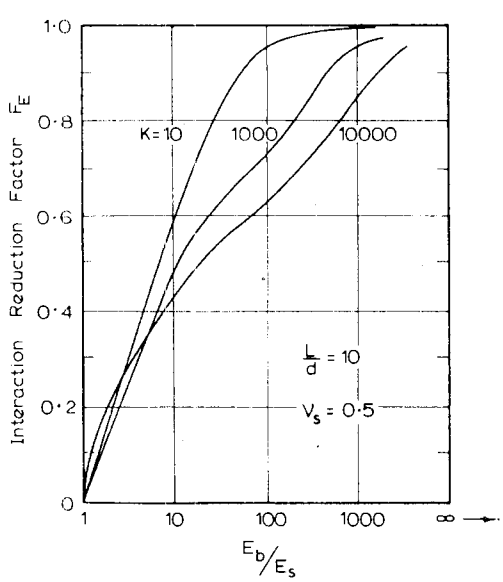

FIGURE 6.14*a* Interaction reduction factor F_E.

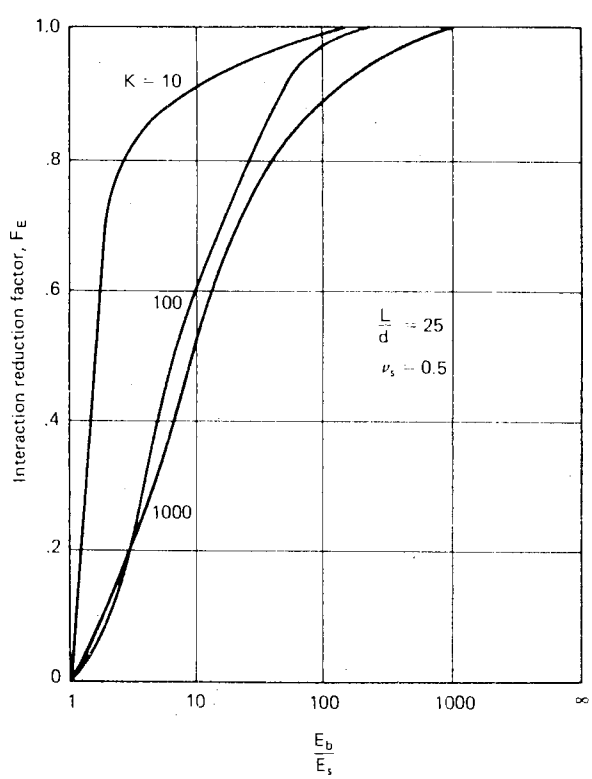

FIGURE 6.14*b* Interaction reduction factor F_E.

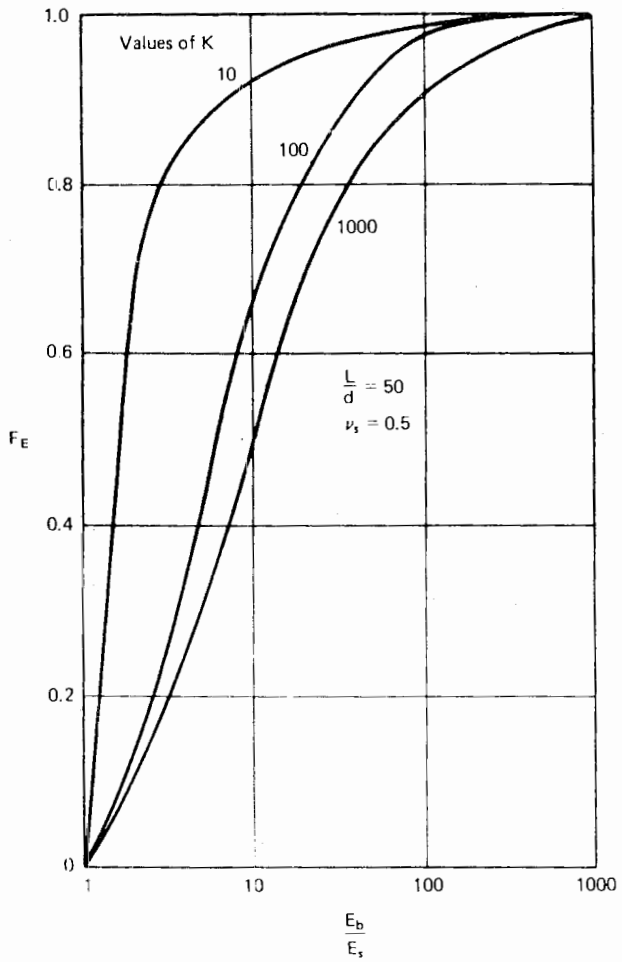

FIGURE 6.14*c* Interaction reduction factor F_E.

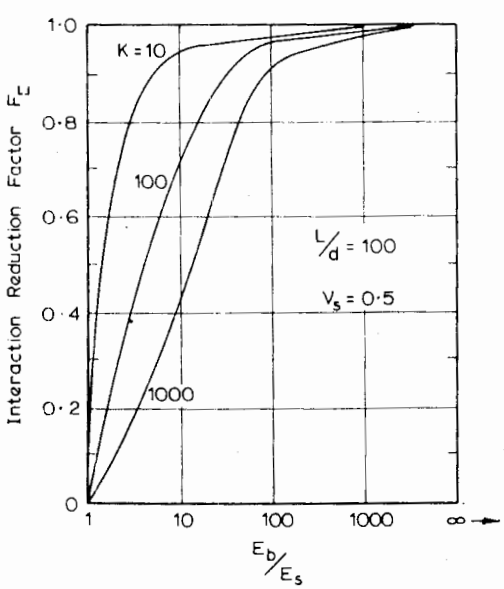

FIGURE 6.14*d* Interaction reduction factor F_E.

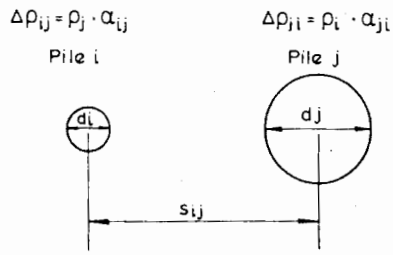

FIGURE 6.15 Interaction between two piles of different size.

6.2.3 Analysis of General Groups

The analysis for a two-pile group can be extended to any number of piles, provided that all piles in the group behave identically: that is, the piles are spaced equally around the circumference of a circle and each displaces equally and carries equal load (a "symmetrical group"). Solutions for such groups have revealed that the additional settlement of each pile in the group caused by the other piles is almost exactly equal to the sum of the displacement increases caused by each of the other piles in turn–that is, the individual interaction factors may be superposed*. Thus, for a group of three equally-loaded piles arranged in an equilateral triangle, the increase in group settlement over that of a single pile is twice that for a group of two piles at the same spacing, while for a square group of four piles, at a spacing of s diameters, the group displacement, ρ_G, is given by

$$\rho_G = P_1 \rho_1 (1 + 2\alpha_1 + \alpha_2) \qquad (6.11)$$

where

P_1 = load in each pile
ρ_1 = displacement of single pile under unit load
α_1 = interaction factor for spacing $s \cdot d$
α_2 = interaction factor for spacing $\sqrt{2}s \cdot d$

Although pile displacement increases can be superposed, it should be noted that the shear-stress distribution is slightly altered by interaction and the proportion of the load taken by the base increases as the number of piles in the group increases (Poulos, 1968*b*).

The applicability of the superposition principle to symmetrical groups suggests that it may be applied to general pile groups. Thus, for a group of n identical piles, the settlement ρ_k of any pile k in the group is given by superposition, as

* It should be noted that superposition cannot be rigorously correct because the addition of a pile involves a change in the overall elastic system as well as an additional load.

$$\rho_k = \rho_1 \sum_{\substack{j=1 \\ j \neq k}}^{n} (P_j \cdot \alpha_{kj}) + \rho_1 P_k \qquad (6.12)$$

where

ρ_1 = displacement of single pile under unit load
P_j = load in pile j
α_{kj} = interaction factor for spacing between piles k and j

For groups containing piles of different size or geometry, following upon Eq. (6.8) and (6.9), Eq. (6.11) may be expressed as

$$\rho_k = \sum_{\substack{j=1 \\ j \neq k}}^{n} (\rho_{1j} \cdot F_j \quad \alpha_{kj}) + \rho_{1k} \cdot P_k \qquad (6.13)$$

where

ρ_{1j} = displacement of single pile j under unit load
α_{kj} = interaction factor for spacing between piles k and j, and for the geometrical parameters of of pile j

Equations (6.12) or (6.13) may be written for all piles in the group, giving n displacement equations. Also, for vertical load equilibrium,

$$P_G = \sum_{j=1}^{n} P_j \qquad (6.14)$$

where

P_G = total group load

The $n+1$ equations thus obtained may be solved for two simple conditions:

1. Equal load (or known load) on all piles, corresponding to loading over a flexible pile cap.
2. Equal settlement of all piles, corresponding to a perfectly rigid cap on the piles.

For case **1**, $P_j = P_G/n$, and Eq. (6.12) may be used directly to calculate the settlement of each pile in the group and hence the differential settlement between the piles. For case 2, the settlements from the n equations (6.12) are equated, which together with Eq. (6.14) give $n+1$ simultaneous equations that can be solved for the unknown loads in the group and the group settlement. Frequently, in practice, the number of equations is reduced by the symmetry of the pile arrangement.

For most practical purposes, the proper consideration of a group with a rigid cap, as outlined above, is not necessary if the group settlement only is required. As in the example below, the average settlement of a group with equally loaded piles is approximately equal to that of a group with a rigid cap. Thus, the assumption of equal loading should be adequate in most cases, and it may be adequate if the settlement is calculated at a representative pile that is neither at the center nor at the corner of the group.

The above analysis of any general pile group therefore requires only a knowledge of the relationship between α and pile spacing for two-pile groups (see Section 6.2.2) and the settlement of a single pile. The results of this analysis for the group settlement can be expressed conveniently in two ways:

1. In terms of the settlement ratio R_s, where

$$R_s = \frac{\text{Average group settlement}}{\text{Settlement of single pile at same } \textit{average} \text{ load as a pile in the group}} \qquad (6.15)$$

2. In terms of the group reduction factor R_G, where

$$R_G = \frac{\text{Average group settlement}}{\text{Settlement of single pile at same } \textit{total} \text{ load as the group}} \qquad (6.16)$$

R_G is strictly meaningful only for an elastic soil, where there is a linear relationship between load and settlement and failure of the single pile under the group load does not develop.

The settlement ratio R_s is the more useful and familiar quantity for practical problems, but there is some advantage to using the group-reduction factor R_G for examining the comparative behavior of pile groups, since R_G in fact represents the settlement of a group if the settlement of the corresponding single pile is unity. Thus, R_G gives a direct measure of the relative settlement of groups containing different numbers of piles and subjected to the same total load. R_G lies in the range $1/n \leqslant R_G \leqslant 1$, and is related simply to R_s as follows:

$$R_s = nR_G \qquad (6.17)$$

Once F_s or R_G has been determined from the analysis, the group settlement, ρ_G, is then given by

$$\rho_G = R_s P_{av} \rho_1 \tag{6.18}$$

or

$$\rho_G = R_G P_G \rho_1 \tag{6.19}$$

where

P_{av} = average load on a pile in the group
P_G = total group load

It should be emphasized that the above analysis does not directly consider the influence of softer compressible layers which may lie beneath the piles unless the interaction factors and single pile settlement are computed to allow for such layers. A simple extension of the analysis to cover this problem is described in Section 6.4.

To illustrate the use of the superposition principle for calculating the settlement of a pile group, an example is described below. Solutions for square groups of piles are described in Section 6.3.

Illustrative Example

A freestanding group of six 12-in-diameter concrete piles is driven into a deep layer of medium clay, and is to be subjected to a load of 300 tons (see Fig. 6.16). A test on a single pile gives a final settlement of 0.60 in. under a load of 50 tons. Determine the final settlement of the six-pile group.

From Table 5.4, the value of K is about 2000. Piles 1, 3, 4, and 6 behave identically and will be called type A, while piles 2 and 5 will be called type B. The loads on types A and B are P_A and P_B, respectively. From Fig. 6.4 for $L/d = 25$, the interaction factors may be interpolated for $K = 2000$. The factors are tabulated in Table 6.1.

TABLE 6.1

	Pile 1 (Type A)		Pile 2 (Type B)	
Pile j	s/d	α_{1j}	s/d	α_{2j}
1	0	–	5	0.42
2	5	0.42	0	–
3	10	0.27	5	0.42
4	5	0.42	7.07	0.35
5	7.07	0.35	5	0.42
6	11.2	0.25	7.07	0.35

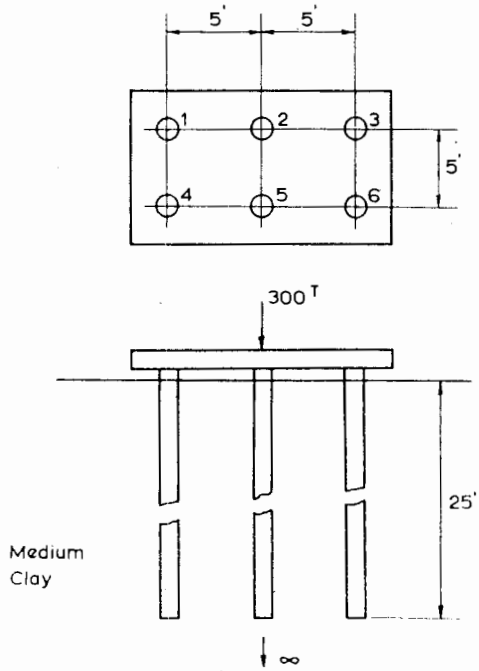

FIGURE 6.16 Pile group configuration in example.

The settlement of pile 1 (and all type A piles) is given by Eq. (6.12) as

$$\rho_A = \rho_1\{P_A (0.27 + 0.42 + 0.25) + P_B (0.42 + 0.35) + P_A\}$$

or,

$$\frac{\rho_A}{\rho_1} = 1.94 P_A + 0.77 P_B \tag{6.20}$$

where ρ_1 is the settlement of a single pile under unit load. Similarly, for pile 2 (and all type B piles),

$$\rho_B = \rho_1 \{P_A (0.42 + 0.42 + 0.35 + 0.35) + P_B (0.42) + P_B\}$$

or,

$$\frac{\rho_B}{\rho_1} = 1.54 P_A + 1.42 P_B \tag{6.21}$$

Also, from equilibrium,

$$4P_A + 2P_B = 300 \tag{6.22}$$

For a rigid cap, $\rho_A = \rho_B$.

The solving of Eqs. (6.20), (6.21), and (6.22) for this case yields the following solutions:

$$P_A = 57.4 \text{ tons}$$
$$P_B = 35.2 \text{ tons}$$
$$\frac{\rho_A}{\rho_1} = \frac{\rho_B}{\rho_1} = 134.4$$

From the pile-load test,

$$\rho_1 = \frac{0.60}{50} = 0.012 \text{ in./ton}$$

Therefore

$$\rho_A = \rho_B = 1.66 \text{ in.}$$

Settlement ratio

$$R_s = \frac{1.66}{0.60} = 2.77$$

Group-reduction factor

$$R_G = R_s/n = 0.46$$

If the pile cap is sufficiently flexible and the load is uniformly distributed so that all piles are equally loaded, then

$$P_A = P_B = 50 \text{ tons}$$
$$\rho_A = 50 \times 2.71 \times \rho_1 = 1.62 \text{ in.}$$
$$\rho_B = 50 \times 2.96 \times \rho_1 = 1.77 \text{ in.}$$

6.3 THEORETICAL SOLUTIONS FOR FREESTANDING GROUPS

6.3.1 Settlement of Floating and End-Bearing Groups

Theoretical values of settlement ratio R_s, determined from the analysis described above, are shown in Table 6.2 for floating-pile groups in a deep layer of uniform soil, and in Table 6.3 for pile groups bearing on a rigid stratum. These values apply to square groups of piles with a rigid cap in which the center-to-center spacing between adjacent piles in a row is s, and the length and diameter of each pile are L and d, respectively. The pile stiffness factor is K. In all cases, R_s increases as the spacing decreases and the number of piles increases. For floating groups, an increase in pile-stiffness factor K leads to an increase in R_s, whereas for the end-bearing groups, R_s decreases as K increases. The exact configuration of the piles in a group does not significantly influence R_s, so that values for other numbers of piles may be interpolated from Tables 6.2 and 6.3. For groups containing more than 16 piles, it has been found that R_s varies approximately linearly with the square root of the number of piles in the group. Thus, for a given value of pile spacing, K and L/d, R_s may be extrapolated from the values for a 16-pile group and a 25-pile group as follows:

$$R_s = (R_{25} - R_{16})(\sqrt{n} - 5) + R_{25} \tag{6.23}$$

where

R_{25} = value of R_s for 25-pile group
R_{16} = value of R_s for 16-pile group
n = number of piles in group

Figure 6.17 shows the group reduction factor, R_G, plotted against s/d for various groups. R_G, and hence group settlement, decreases as the number of piles increases. However, at relatively close spacings, the use of more piles to decrease settlement becomes increasingly ineffective if the same spacing between the piles is retained.

In general, it is found that the settlement of a group of piles in a relatively uniform stratum depends primarily on the breadth or width of the group; hence, within a group of given breadth or width, increasing the number of piles beyond a certain number will only marginally improve the settlement performance of the group, unless the original spacing within the group is greater than about six dia-

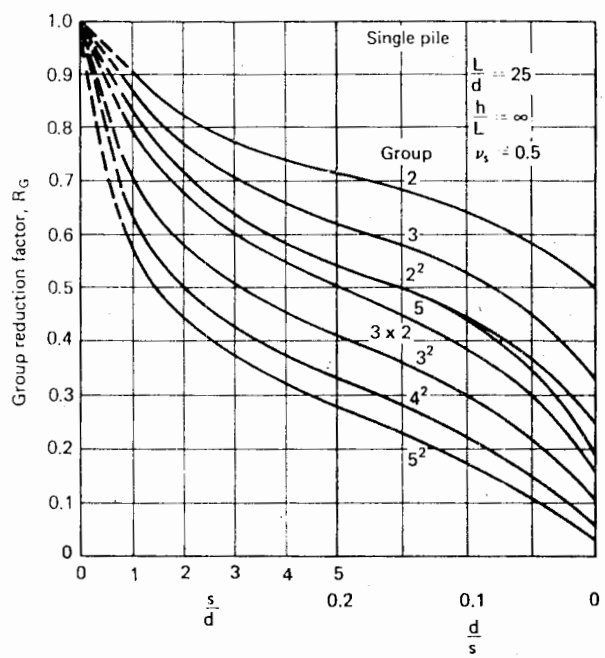

FIGURE 6.17 Influence of type of group on settlement—groups with rigid cap.

TABLE 6.2 THEORETICAL VALUES OF SETTLEMENT RATIO R_s FRICTION PILE GROUPS, WITH RIGID CAP, IN DEEP UNIFORM SOIL MASS

No of Piles in Group			4				9				16				25			
L/d	s/d	K	10	100	1000	∞	10	100	1000	∞	10	100	1000	∞	10	100	1000	∞
	2		1.83	2.25	2.54	2.62	2.78	3.80	4.42	4.48	3.76	5.49	6.40	6.53	4.75	7.20	8.48	8.68
10	5		1.40	1.73	1.88	1.90	1.83	2.49	2.82	2.85	2.26	3.25	3.74	3.82	2.68	3.98	4.70	4.75
	10		1.21	1.39	1.48	1.50	1.42	1.76	1.97	1.99	1.63	2.14	2.46	2.46	1.85	2.53	2.95	2.95
	2		1.99	2.14	2.65	2.87	3.01	3.64	4.84	5.29	4.22	5.38	7.44	8.10	5.40	7.25	9.28	11.25
25	5		1.47	1.74	2.09	2.19	1.98	2.61	3.48	3.74	2.46	3.54	4.96	5.34	2.95	4.48	6.50	7.03
	10		1.25	1.46	1.74	1.78	1.49	1.95	2.57	2.73	1.74	2.46	3.42	3.63	1.98	2.98	4.28	4.50
	2		2.43	2.31	2.56	3.01	3.91	3.79	4.52	5.66	5.58	5.65	7.05	8.94	7.26	7.65	9.91	12.66
50	5		1.73	1.81	2.10	2.44	2.46	2.75	3.51	4.29	3.16	3.72	5.11	6.37	3.88	4.74	6.64	8.67
	10		1.38	1.50	1.78	2.04	1.74	2.04	2.72	3.29	2.08	2.59	3.73	4.65	2.49	3.16	4.76	6.04
	2		2.56	2.31	2.26	3.16	4.43	4.05	4.11	6.15	6.42	6.14	6.50	9.92	8.48	8.40	10.25	14.35
100	5		1.88	1.88	2.01	2.64	2.80	2.94	3.38	4.87	3.74	4.05	4.98	7.54	4.68	5.18	6.75	10.55
	10		1.47	1.56	1.76	2.28	1.95	2.17	2.73	3.93	2.45	2.80	3.81	5.82	2.95	3.48	5.00	7.88

TABLE 6.3 THEORETICAL VALUES OF SETTLEMENT RATIO R_s: END-BEARING PILE GROUPS, WITH RIGID CAP, BEARING ON A RIGID STRATUM

No. of Piles in Group		4				9				16				25			
L/d	s/d K	10	100	1000	∞	10	100	1000	∞	10	100	1000	∞	10	100	1000	∞
	2	1.52	1.14	1.00	1.00	2.02	1.31	1.00	1.00	2.38	1.49	1.00	1.00	2.70	1.63	1.00	1.00
10	5	1.15	1.08	1.00	1.00	1.23	1.12	1.02	1.00	1.30	1.14	1.02	1.00	1.33	1.15	1.03	1.00
	10	1.02	1.01	1.00	1.00	1.04	1.02	1.00	1.00	1.04	1.02	1.00	1.00	1.03	1.02	1.00	1.00
	2	1.88	1.62	1.05	1.00	2.84	2.57	1.16	1.00	3.70	3.28	1.33	1.00	4.48	4.13	1.50	1.00
25	5	1.36	1.36	1.08	1.00	1.67	1.70	1.16	1.00	1.94	2.00	1.23	1.00	2.15	2.23	1.28	1.00
	10	1.14	1.15	1.04	1.00	1.23	1.26	1.06	1.00	1.30	1.33	1.07	1.00	1.33	1.38	1.08	1.00
	2	2.49	2.24	1.59	1.00	4.06	3.59	1.96	1.00	5.83	5.27	2.63	1.00	7.62	7.06	3.41	1.00
50	5	1.78	1.73	1.32	1.00	2.56	2.56	1.72	1.00	3.28	3.38	2.16	1.00	4.04	4.23	2.63	1.00
	10	1.39	1.43	1.21	1.00	1.78	1.87	1.46	1.00	2.20	2.29	1.71	1.00	2.62	2.71	1.97	1.00
	2	2.54	2.26	1.81	1.00	4.40	3.95	3.04	1.00	6.24	5.89	4.61	1.00	8.18	7.93	6.40	1.00
100	5	1.85	1.84	1.67	1.00	2.71	2.77	2.52	1.00	3.54	3.74	3.47	1.00	4.33	4.68	4.45	1.00
	10	1.44	1.44	1.46	1.00	1.84	1.99	1.98	1.00	2.21	2.48	2.53	1.00	2.53	2.98	3.10	1.00

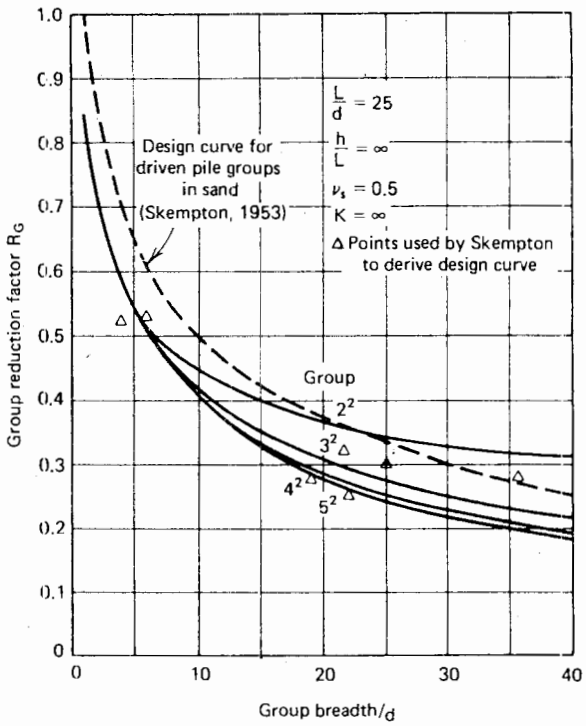

FIGURE 6.18 Settlement against breadth of group–rigid pile cap.

meters. This point is illustrated in Figs. 6.18 and 6.19, in which the group reduction factor, R_G, is plotted against total group breadth. These figures show that for larger groups, R_G does not vary greatly with the number of piles in the group. For groups containing more than 25 piles, it appears that a common limiting curve of R_G versus group breadth, coincident with the curve for the 5^2 group, can be used over a practical range of group breadths. The dependence of settlement on group width rather than number of piles has been confirmed in full-scale tests by Berezantzev et al. (1961), and from data collected by Skempton (1953) for driven piles in sand. The relationship suggested by Skempton (Eq. 6.1) between settlement ratio and group breadth, as reexpressed in terms of R_G and plotted in Fig. 6.18, agrees quite well with the theoretical curves. These results suggest, therefore, that if settlement is the sole criterion, it is more economical to use a smaller number of piles at a relatively large spacing, rather than a large number of piles at closer spacings.

6.3.1.1 EFFECT OF FINITE LAYER DEPTH

For floating-pile groups, the presence of an underlying rigid base below the soil layer tends to reduce the settlement ratio R_s. An indication of the extent of this decrease is given in Fig. 6.20, in which, for typical groups, a reduction coefficient, ξ_h, is plotted against the ratio of layer-depth h to pile-length L, ξ_h being defined as

$$\xi_h = \frac{R_s \text{ for finite layer of depth } h}{R_s \text{ for infinitely deep layer}} \tag{6.24}$$

Thus, ξ_h is a factor by which the values of R_s for an infinitely deep layer in Table 6.2 are multiplied to obtain R_s for a finite layer. Figure 6.20 shows that as would be expected, ξ_h decreases as h/L decreases, and that the effect of

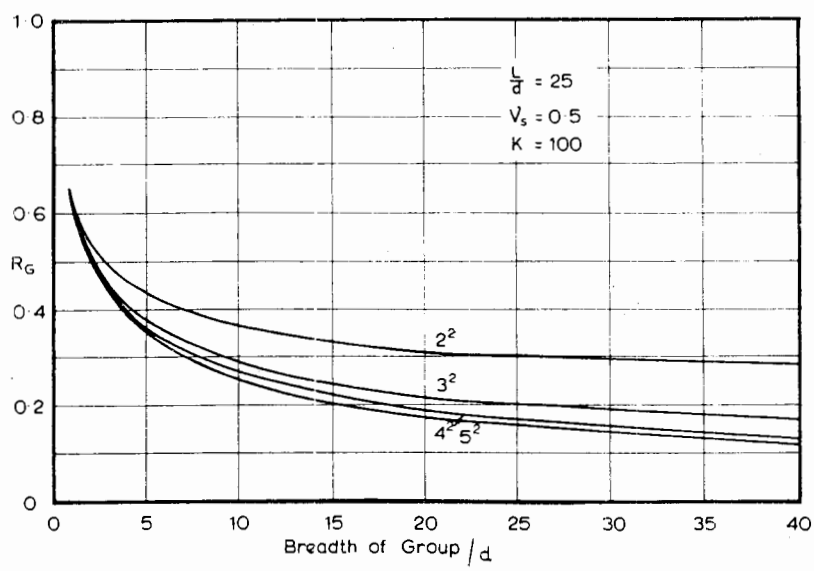

FIGURE 6.19 R_G vs. group breadth–Floating Groups.

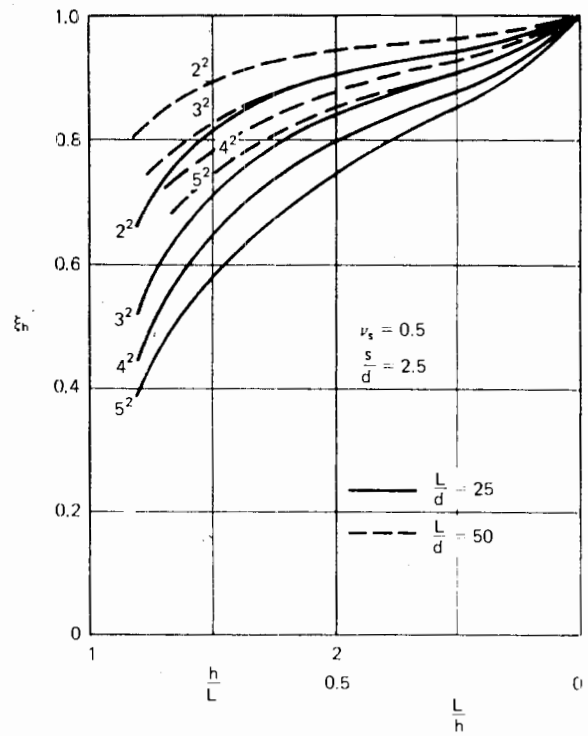

FIGURE 6.20 Reduction coefficient ξ_h for effect of finite layer.

the finite layer is more pronounced as the size of the group increases. ξ_h increases as the pile-stiffness factor K decreases. As L/d increases, the effect of the finite layer becomes less significant.

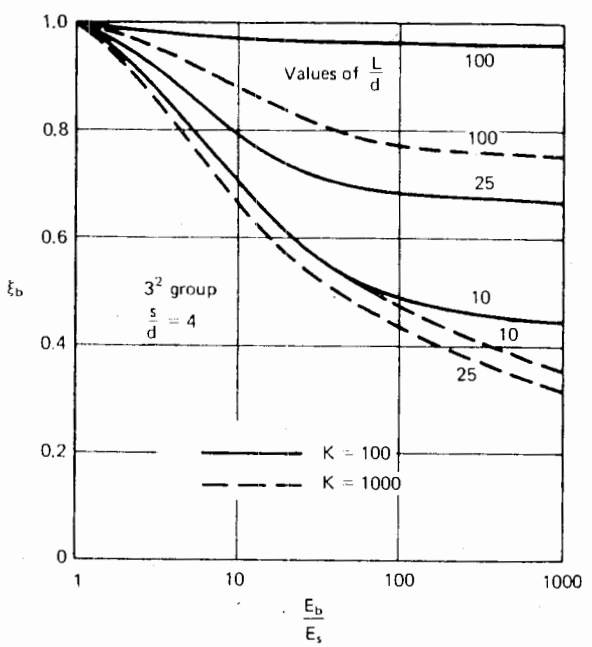

FIGURE 6.21 Reduction coefficient ξ_b for effect of bearing stratum.

6.3.1.2 EFFECT OF COMPRESSIBILITY OF BEARING STRATUM

An example of the influence of the stiffness of the bearing stratum on R_s is shown in Fig. 6.21 for the particular case of a 3^2 group with a pile spacing of four diameters. A reduction coefficient, ξ_b, is plotted against the ratio of the modulus E_b of the bearing stratum to the soil modulus E_s, ξ_b being defined as

$$\xi_b = \frac{R_s \text{ for group resting on bearing stratum}}{R_s \text{ for floating group on infinitely deep layer}} \qquad (6.25)$$

The following points are apparent from Fig. 6.21:

1. ξ_b, and hence settlement ratio R_s, decreases as the relative stiffness of the bearing stratum, E_b/E_s, increases, this effect being most pronounced for shorter, stiffer piles.
2. For slender piles (e.g., $L/d = 100$), unless the piles are quite stiff, the bearing stratum has little effect on settlements, because very little load reaches the pile tip under normal working-load conditions.

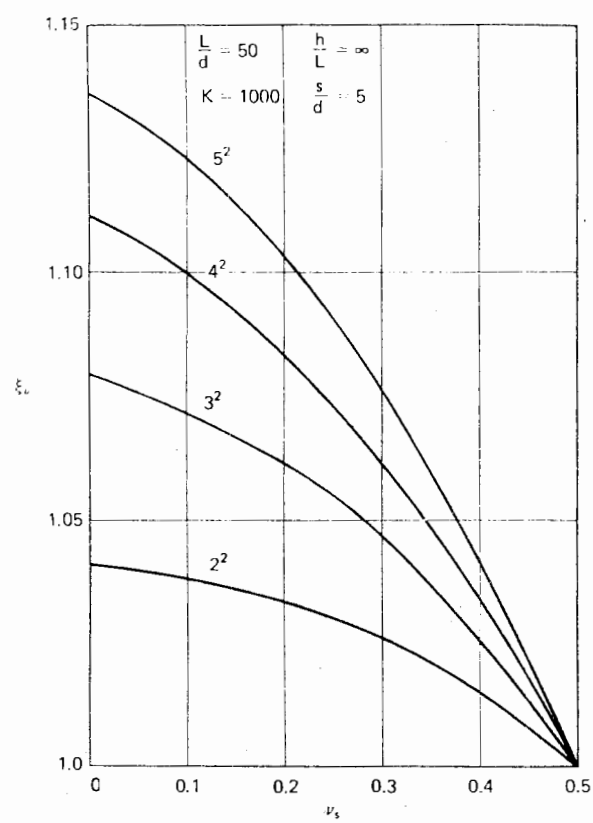

FIGURE 6.22 Correction factor ξ_ν for effect of ν_s.

As E_b/E_s approaches infinity, ξ approaches the ratio of R_s for the end-bearing group on a rigid base (Table 6.3) to the corresponding value for the floating group in a deep layer.

6.3.1.3 EFFECT OF POISSON'S RATIO, ν_s

The effect of ν_s on R_s is shown in Fig. 6.22, in which factor ξ_ν is plotted for a typical case, ξ_ν being defined as

$$\xi_\nu = \frac{R_s \text{ for specified value of } \nu_s}{R_s \text{ for } \nu_s = 0.5} \qquad (6.26)$$

ξ_ν increases as ν_s decreases, and this implies that as consolidation proceeds and ν_s decreases from the undrained value (0.5 for a saturated clay) to the drained value, the value of R_s will increase. The effect of ν_s becomes more pronounced as the number of piles in the group increases.

6.3.1.4 EFFECT OF SOIL-MODULUS DISTRIBUTION

Figure 6.23 shows the effect of the distribution of soil-modulus on R_s for a typical case. Two cases have been considered: a deep soil-layer having constant E_s, with depth; and a soil in which E_s varies linearly along the pile shaft, with the value at middepth of the pile being equal to the constant value in the first case. As expected from Fig. 6.9, larger values of R_s occur for the uniform soil, the difference becoming greater as the number of piles increases.

6.3.1.5 RATIO OF IMMEDIATE TO FINAL SETTLEMENT

For a pile group in an ideal, saturated, two-phase elastic soil mass, it is possible to calculate the ratio of immediate settlement to total final settlement, ρ_i/ρ_{TF}, as described in Section 5.3.5. For various groups of incompressible floating piles, the ratio ρ_i/ρ_{TF} is shown in Fig. 6.24. Poisson's ratio ν_s' of the soil skeleton has been taken as zero, so that Fig. 6.24 can be considered as representing the theoretical minimum relative importance of immediate settlement. As with a single pile, the predominant part of the total final settlement occurs as immediate settlement, although the time-dependent settlement does increase as the number of piles in the group increases. Pile compressibility has little influence on the ratio ρ_i/ρ_{TF}.

For end-bearing groups, the relative amount of immediate settlement is even greater than for floating groups, and in most cases likely to be met in practice, the consoli-

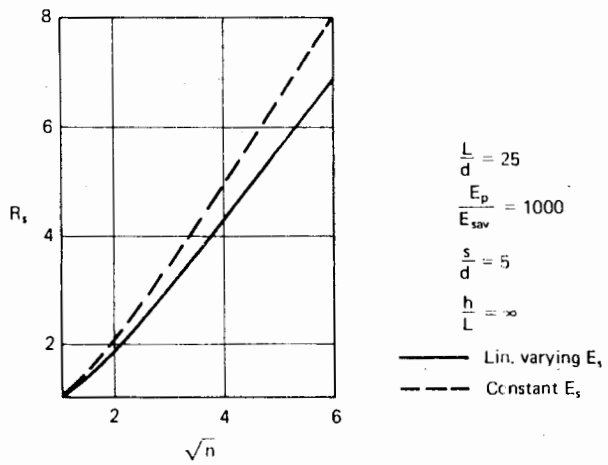

FIGURE 6.23 Effect of distribution of E_s on settlement ratio.

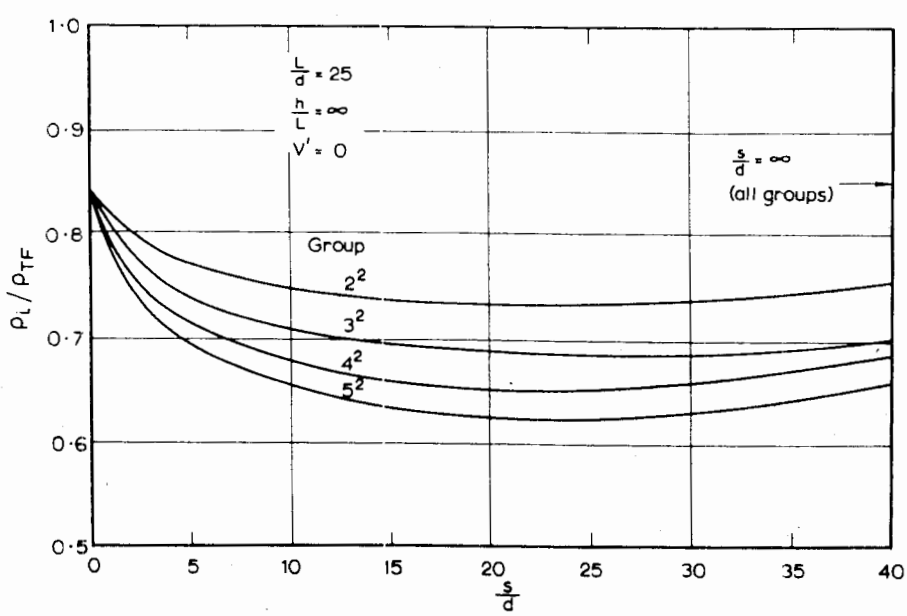

FIGURE 6.24 Relative importance of immediate settlement–pile groups with rigid cap.

dation settlement theoretically comprises less than 10% of the total final movement.

6.3.2 Load Distribution in Groups with Rigid Cap

For a wide range of values of L/d, s/d, K, and group size, load distributions within a floating-pile group are given in Tables 6.4*a* and *b*, the pile load being expressed as a fraction of the average load in the group. The key for identification of the piles in each group is shown in Fig. 6.25. The greatest loads occur at the corner piles, and the least at the center piles. The load distribution tends to become less uniform as the pile spacing decreases, the number of piles increases, L/d increases, or K increases. The load distribution is also influenced by the existence of a layer of finite depth, a typical example for a 3^2 group being shown in Fig. 6.26.

For pile groups bearing on a rigid stratum, load distributions are given in Tables 6.5*a* and *b*, while typical distributions for a 3^2 group are shown in Fig. 6.27. As with the floating groups, the load distribution generally becomes less uniform as L/d increases and spacing decreases, but in contrast to the corresponding floating groups, increasing the pile stiffness factor K causes the load distribution to become more uniform.

TABLE 6.4*a* LOAD DISTRIBUTIONS WITHIN 3^2 AND 4^2 FLOATING-PILE GROUPS: VALUES OF P/P_{av}

			Pile 1			Pile 2			Pile 3		
	L/d	K / s/d	100	1000	∞	100	1000	∞	100	1000	∞
3^2 group	10	2	1.28	1.47	1.56	0.84	0.75	0.72	0.52	0.16	−0.15
		5	1.20	1.25	1.26	0.91	0.88	0.88	0.57	0.47	0.45
		10	1.10	1.13	1.14	0.95	0.94	0.94	0.78	0.73	0.70
		20	1.04	1.05	1.06	0.98	0.97	0.97	0.91	0.88	0.88
	25	2	1.18	1.38	1.50	0.89	0.79	0.65	0.71	0.32	−0.35
		5	1.17	1.29	1.32	0.92	0.87	0.84	0.63	0.38	0.34
		10	1.11	1.18	1.21	0.95	0.91	0.89	0.77	0.61	0.55
		20	1.06	1.11	1.12	0.97	0.95	0.94	0.87	0.77	0.73
	100	2	1.24	1.11	1.70	0.86	0.93	0.66	0.58	0.84	−0.45
		5	1.22	1.17	1.37	0.90	0.92	0.81	0.53	0.61	0.24
		10	1.14	1.15	1.28	0.94	0.93	0.86	0.70	0.68	0.42
		20	1.07	1.10	1.21	0.97	0.95	0.90	0.86	0.79	0.55
4^2 group	10	2	1.68	2.00	2.14	0.97	0.95	0.95	0.38	0.09	−0.04
		5	1.42	1.51	1.52	1.01	1.00	1.00	0.56	0.48	0.47
		10	1.21	1.25	1.28	1.01	1.00	1.00	0.77	0.73	0.70
		20	1.10	1.13	1.12	1.00	1.00	1.00	0.89	0.86	0.86
	25	2	1.50	1.87	2.25	0.97	0.95	0.89	0.54	0.23	−0.05
		5	1.40	1.62	1.70	1.01	1.01	0.99	0.59	0.36	0.30
		10	1.25	1.41	1.48	1.00	1.01	1.00	0.74	0.57	0.50
		20	1.14	1.23	1.26	1.00	1.00	1.00	0.85	0.76	0.72
	100	2	1.56	1.35	2.30	0.96	0.97	1.01	0.52	0.70	−0.15
		5	1.50	1.45	1.84	1.02	1.01	0.98	0.47	0.52	0.18
		10	1.29	1.35	1.65	1.00	1.00	1.00	0.70	0.63	0.34
		20	1.15	1.24	1.42	1.00	1.01	1.00	0.83	0.75	0.56

TABLE 6.4*b* LOAD DISTRIBUTIONS WITHIN 5^2 FLOATING-PILE GROUPS VALUES OF P/P_{av}

			Pile 1			Pile 2			Pile 3			Pile 4			Pile 5			Pile 6		
	L/d	$\frac{K}{s/d}$	100	1000	∞	100	1000	∞	100	1000	∞	100	1000	∞	100	1000	∞	100	1000	∞
5^2 Group	10	2	2.12	2.48	2.65	1.18	1.19	1.12	1.05	1.07	1.20	0.42	0.21	−0.15	0.26	0.10	0.16	0.12	0.01	0.45
		5	1.64	1.75	1.79	1.13	1.14	1.15	1.07	1.09	1.10	0.60	0.53	0.49	0.55	0.49	0.46	0.49	0.45	0.42
		10	1.31	1.39	1.41	1.07	1.09	1.09	1.03	1.04	1.05	0.81	0.75	0.74	0.76	0.71	0.69	0.73	0.68	0.64
		20	1.18	1.22	1.19	1.05	1.06	1.05	1.01	1.02	1.02	0.90	0.87	0.89	0.86	0.83	0.85	0.82	0.79	0.82
	25	2	1.90	2.46	2.90	1.17	1.19	1.13	1.01	1.09	1.20	0.58	0.20	−0.20	0.38	0.12	0.09	0.24	0.04	0.25
		5	1.62	1.98	2.11	1.14	1.18	1.19	1.05	1.09	1.07	0.63	0.40	0.35	0.54	0.34	0.27	0.46	0.29	0.22
		10	1.39	1.63	1.73	1.10	1.14	1.16	1.04	1.05	1.07	0.77	0.64	0.56	0.70	0.55	0.47	0.64	0.45	0.37
		20	1.22	1.37	1.40	1.06	1.09	1.09	1.02	1.04	1.05	0.87	0.77	0.74	0.82	0.72	0.71	0.78	0.68	0.67
	100	2	2.06	1.75	3.00	1.15	1.14	1.10	1.08	1.00	1.20	0.41	0.65	−0.30	0.33	0.48	0.05	0.25	0.33	0.40
		5	1.77	1.78	2.34	1.18	1.18	1.22	1.07	1.06	1.09	0.54	0.55	0.21	0.48	0.42	0.14	0.33	0.30	0.07
		10	1.45	1.58	2.05	1.10	1.13	1.21	1.05	1.04	1.08	0.72	0.66	0.38	0.68	0.58	0.26	0.63	0.49	0.17
		20	1.25	1.41	1.78	1.17	1.10	1.13	1.02	1.02	1.02	0.85	0.77	0.55	0.80	0.70	0.50	0.75	0.62	0.52

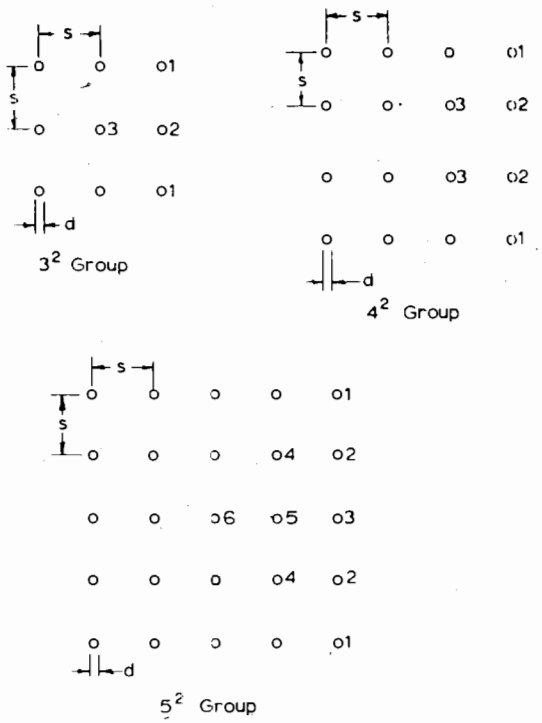

FIGURE 6.25 Identification of piles in square groups.

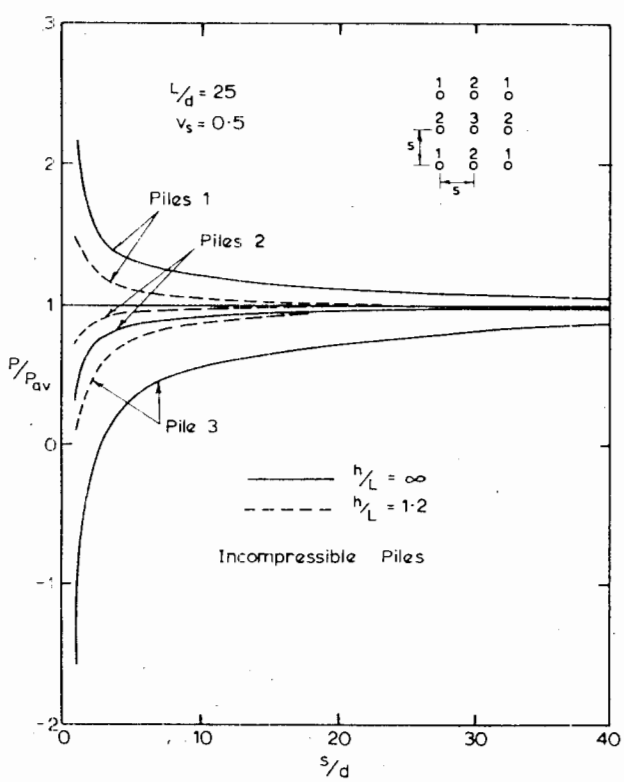

FIGURE 6.26 Influence layer depth on load distribution–3^2 group with rigid cap.

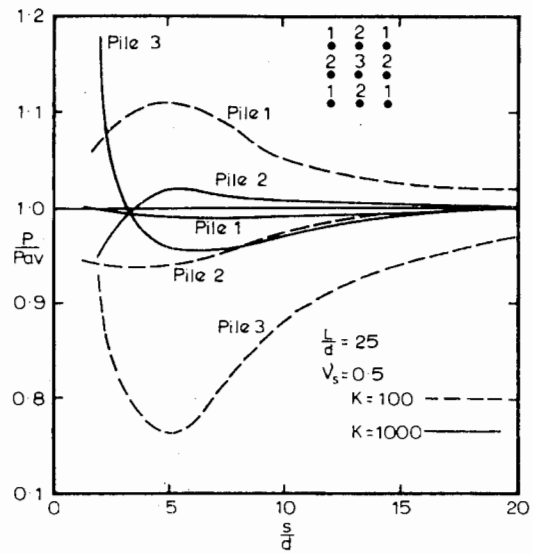

FIGURE 6.27 Load distributions in 3^2 end-bearing group.

Figure 6.28 shows a typical variation of pile loads within a 3^2 group with varying relative bearing-stratum modulus E_b/E_s. The load distribution becomes more uniform as E_b/E_s increases.

6.3.3 Groups with Equally Loaded Piles

For groups with equally loaded piles, the maximum settlement occurs at the center pile or piles, while the minimum settlement occurs at the corner piles. For some typical groups of incompressible floating piles, the ratio of the maximum settlement, ρ_{max}, to the settlement of the

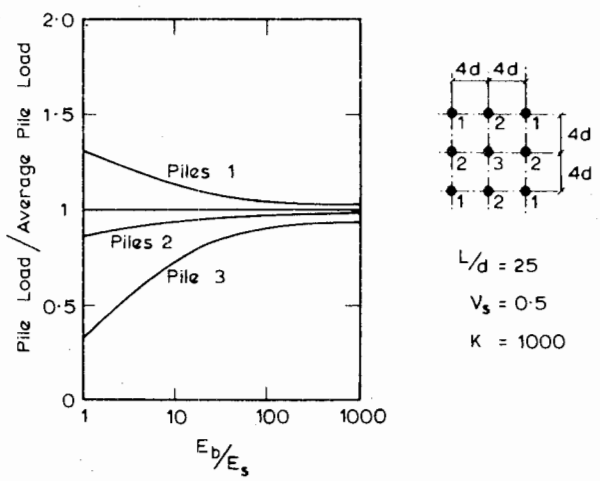

FIGURE 6.28 Influence of bearing stratum on load distribution in group.

TABLE 6.5*a* LOAD DISTRIBUTIONS WITHIN 3^2 AND 4^2 END-BEARING PILE GROUPS VALUES OF P/P_{av}

			Pile 1		Pile 2		Pile 3	
		K	100	1000	100	1000	100	1000
	L/d	s/d						
3^2 group	10	2	0.98	0.92	0.99	1.01	1.11	1.20
		5	1.02	1.00	0.99	1.00	0.94	1.00
		10	1.00	1.00	1.00	1.00	1.00	1.00
		20	1.00	1.00	1.00	1.00	1.00	1.00
	25	2	1.07	0.95	0.94	1.00	0.93	1.17
		5	1.11	1.02	0.94	0.99	0.76	0.96
		10	1.05	1.01	0.98	0.99	0.88	0.97
		20	1.02	1.00	1.00	1.00	0.97	1.00
	100	2	1.22	1.02	0.87	0.97	0.65	1.04
		5	1.21	1.13	0.90	0.94	0.53	0.73
		10	1.13	1.10	0.94	0.95	0.71	0.78
		20	1.06	1.06	0.97	0.97	0.88	0.87
4^2 group	10	2	1.04	0.88	0.98	0.98	1.00	1.17
		5	1.05	1.00	1.00	1.00	0.94	1.00
		10	1.00	1.00	1.00	1.00	0.99	1.00
		20	1.00	1.00	1.00	1.00	1.00	1.00
	25	2	1.26	0.95	0.98	0.98	0.77	1.10
		5	1.23	1.05	1.01	1.00	0.75	0.94
		10	1.10	1.02	1.00	1.00	0.88	0.98
		20	1.02	1.00	1.00	1.00	0.98	1.00
	100	2	1.61	1.19	0.97	0.98	0.44	0.86
		5	1.48	1.33	1.00	1.00	0.51	0.65
		10	1.27	1.23	1.00	1.00	0.72	0.75
		20	1.14	1.13	1.00	1.00	0.85	0.84

corresponding group with a rigid cap, ρ_R, is given in Table 6.6. The ratio ρ_{max}/ρ_R increases with increasing number of piles in the group, but is almost independent of spacing for a practical range of spacings. The value of K has little effect on ρ_{max}/ρ_R.

For groups of end-bearing piles on a rigid base, values of ρ_{max}/ρ_R are shown in Table 6.7, for $L/d = 25$ and $K = 100$. For such groups, ρ_{max}/ρ_R decreases rapidly as K increases and is unity for $K > 2000$, since no interaction then occurs.

The ratio ρ_d/ρ_{max}, of the maximum differential settlement to the maximum settlement, is shown in Fig. 6.29 for incompressible floating piles in a semi-infinite mass. This ratio increases with increasing spacing but decreases if the layer depth is decreased or L/d increased. The value of K has relatively little influence.

For typical groups of end-bearing piles on a rigid base, values of ρ_d/ρ_{max} are shown in Fig. 6.30 for $K = 100$. For such compressible piles, relatively large differential settlements may occur, expecially for large groups of slender piles. However, the relative differential settlement decreases rapidly with increasing K and is zero for piles that can be considered as incompressible.

6.3.4 Approximation of Group as a Single Pier

For calculations relating to large structures supported by a number of pile groups, it may often be useful to replace each pile group by an equivalent single pier that settles an equal amount. Such an approximation is useful, for example, if an analysis of intergroup interaction is desired,

TABLE 6.5*b* LOAD DISTRIBUTIONS WITHIN 5^2 END-BEARING PILE GROUPS VALUES OF P/P_{av}

			Pile 1		Pile 2		Pile 3		Pile 4		Pile 5		Pile 6	
	L/d	K / s/d	100	1000	100	1000	100	1000	100	1000	100	1000	100	1000
5^2 group	10	2	1.11	0.86	1.02	0.94	0.95	0.95	0.99	1.13	0.90	1.14	0.81	1.18
		5	1.06	1.01	1.02	1.00	1.01	1.00	0.96	1.00	0.95	1.00	0.94	1.00
		10	1.00	1.00	1.00	1.00	1.00	1.00	1.00	1.00	1.00	1.00	1.00	1.00
		20	1.00	1.00	1.00	1.00	1.00	1.00	1.00	1.00	1.00	1.00	1.00	1.00
	25	2	1.55	0.99	1.12	0.99	0.99	0.96	0.77	1.07	0.59	1.03	0.44	0.99
		5	1.37	1.09	1.09	1.03	1.04	1.00	0.77	0.95	0.72	0.92	0.67	0.87
		10	1.15	1.03	1.04	1.01	1.02	1.01	0.90	0.98	0.88	0.97	0.86	0.97
		20	1.02	1.00	1.00	1.00	1.00	1.00	0.98	1.00	0.98	1.00	0.98	1.00
	100	2	2.08	1.48	1.20	1.11	1.01	0.96	0.48	0.83	0.25	0.63	0.36	0.44
		5	1.75	1.55	1.16	1.13	1.08	1.04	0.53	0.68	0.46	0.58	0.39	0.47
		10	1.42	1.39	1.08	1.09	1.04	1.04	0.73	0.77	0.70	0.71	0.67	0.65
		20	1.21	1.22	1.05	1.05	1.01	1.01	0.88	0.87	0.83	0.82	0.79	0.78

TABLE 6.6 VALUES OF ρ_{max}/ρ_R FOR FLOATING-PILE GROUPS IN FINITE LAYER. $L/d = 25; \nu_s = 0.5$.

Group	3^2			4^2			5^2		
h/L / s/d	∞	1.5	1.2	∞	1.5	1.2	∞	1.5	1.2
1	1.13	1.15	1.15	1.13	1.17	1.18	1.18	1.25	1.26
2.5	1.13	1.17	1.16	1.14	1.20	1.17	1.19	1.30	1.24
5	1.13	1.18	1.13	1.15	1.20	1.15	1.21	1.30	1.23
10	1.14	1.15	1.10	1.16	1.16	1.11	1.24	1.20	1.11
20	1.14	1.05	1.01	1.13	1.05	1.01	1.18	1.04	1.02
40	1.03	1.00	1.00	1.06	1.00	1.00	1.17	1.00	1.00

TABLE 6.7 VALUES OF ρ_{max}/ρ_R FOR END-BEARING PILE GROUPS. $L/d = 25$, $K = 100, \nu_s = 0.5$.

Group / s/d	3^2	4^2	5^2
2	1.04	1.08	1.17
5	1.19	1.14	1.21
10	1.09	1.10	1.13
20	1.03	1.02	1.02
40	1.00	1.00	1.00

or if settlements caused by underlying compressible strata are to be estimated (see Section 6.4). Two types of approximation may be useful:

1. An equivalent single pier of the same circumscribed plan area as the group and of some equivalent length, L_e.
2. An equivalent single pier of the same length, L, as the piles, but having an equivalent diameter, d_e.

For incompressible floating groups, values of L_e/L for the first approximation, obtained by Poulos (1968*b*),

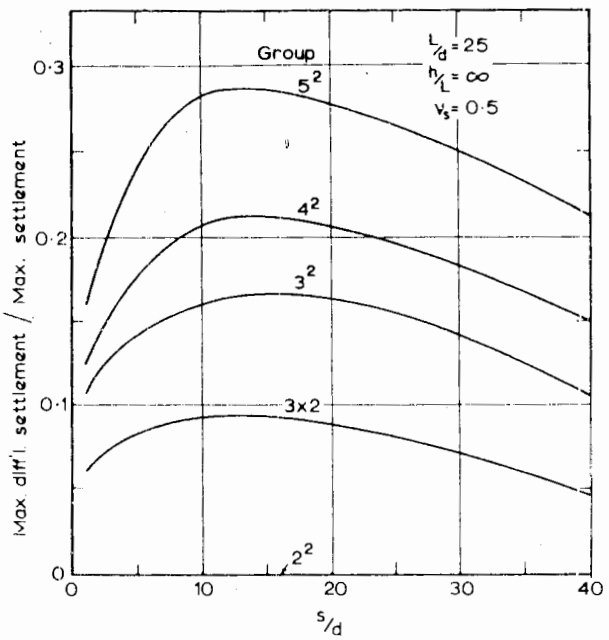

FIGURE 6.29 Differential settlement in floating pile groups with equally loaded piles.

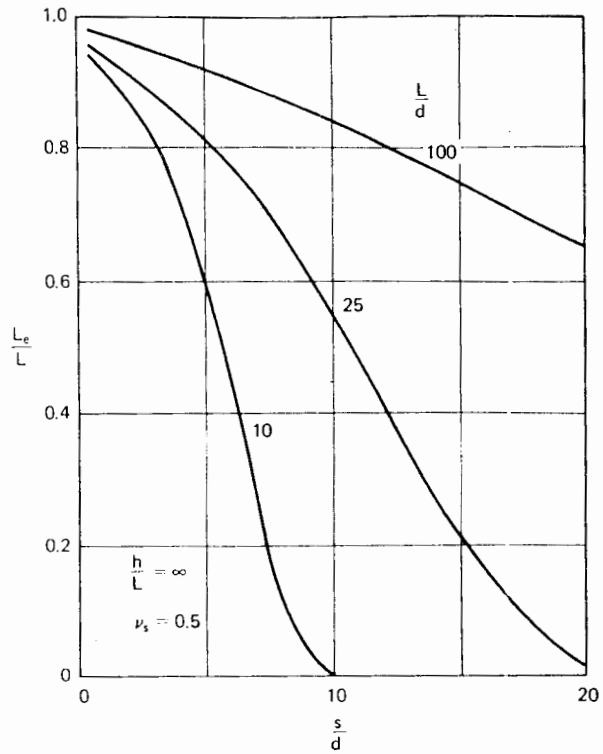

FIGURE 6.31 Equivalent length of single pier for same settlement as pile group.

are shown in Fig. 6.31. L_e/L depends both on spacing and L/d, but is virtually independent of the number of piles in the group. For most practical cases, L_e/L lies between 0.9 and 0.6.

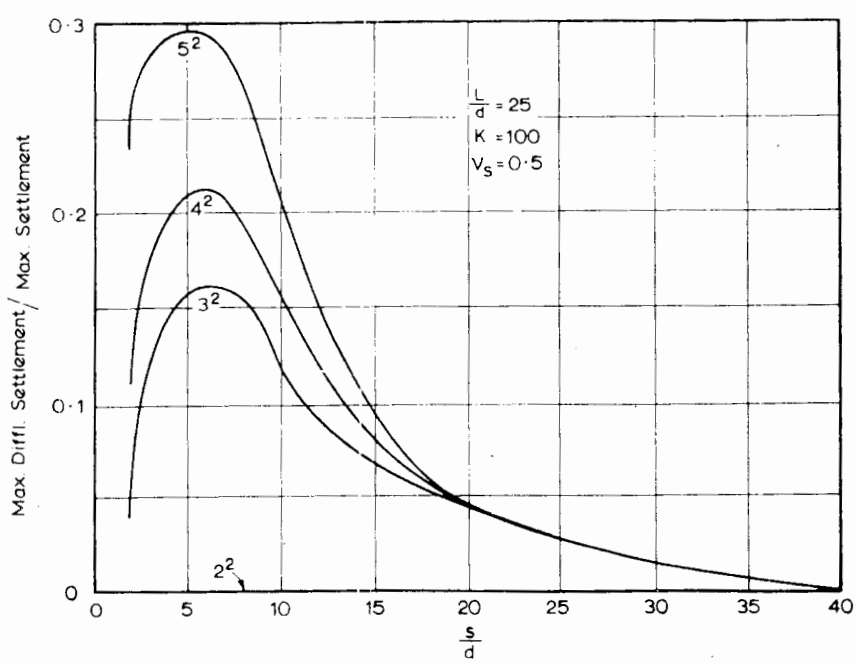

FIGURE 6.30 Differential settlement in end-bearing groups with equally loaded piles.

The second approximation is more appropriate when the piles pass through layered soils or are founded on very different material. Relationships between d_e/B and s/d are plotted in Fig. 6.32 for floating piles, where d_e = equivalent diameter of single pier of length L, and B = average width of group (i.e., the square root of the gross plan area of the group). Like L_e/L, d_e/B is almost independent of the group's size, but it does depend on L/d. The effect of the pile-stiffness factor K, also shown in Fig. 6.32, is considerable, especially for slender piles. The ratio d_e/B tends to decrease with increasing pile compressibility. It should be noted that the equivalent pier in Fig. 6.32 has the same value of K as the pile in the group.

Similar calculations could be done for end-bearing piles. For the limiting case of incompressible piles bearing on a rigid stratum, one obtains, by either method, an equivalent pier that has the same total area and the same length as the original piles. For compressible piles on a nonrigid base, the equivalent pier will be intermediate between this limiting case and that for the fully floating situation.

6.4 SETTLEMENT OF GROUPS CAUSED BY COMPRESSIBLE UNDERLYING STRATA

In practical cases in which the soil profile is layered and compressible strata are present below the piles, the settlement caused by these strata must be considered in calculating the overall settlement of the group. A method for calculating the settlement of single piles resulting from compressible strata has been described in Section 5.3.4. This method may be extended to a pile group by calculating the settlement of the group as the sum of the settlement of the group in the founding layer and the contributions to settlement of the underlying layers caused by all piles in the group (Poulos and Mattes, 1971*a*).

Poulos and Mattes found that little error results in assuming that the load distribution in the group is uniform, rather than considering the nonuniform distribution of load. Moreover, it was found that the replacement of the pile group by an equivalent pier (see Section 6.3.4 above) also leads to very similar answers. Thus, in practical calculations, it is convenient to employ the latter approach and calculate the settlement of the group as the sum of the settlement ρ_{GD} in the founding layer and the settlement caused by the underlying layers, using Eq. 5.41 and Fig. 5.35.

Illustrative Example

To demonstrate the application of this method to a practical case, the example shown in Fig. 6.33 will be considered. A 3^2 group of concrete piles with a rigid cap is founded in a clay layer underlain by two further layers, which are in turn underlain by rock. It is assumed that only a limited amount of soil data is available from the results of undrained triaxial tests and oedometer tests,

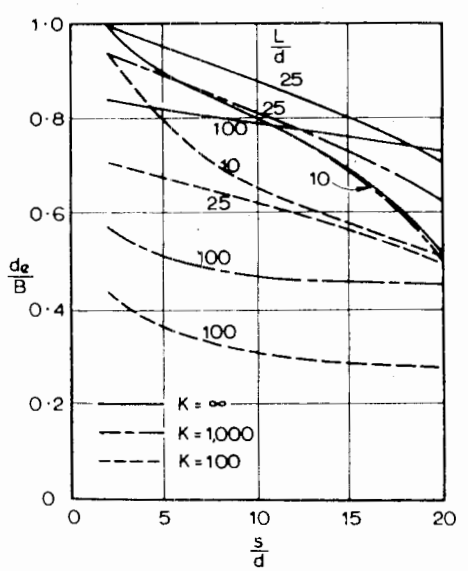

FIGURE 6.32 Diameter of equivalent pier to represent pile group.

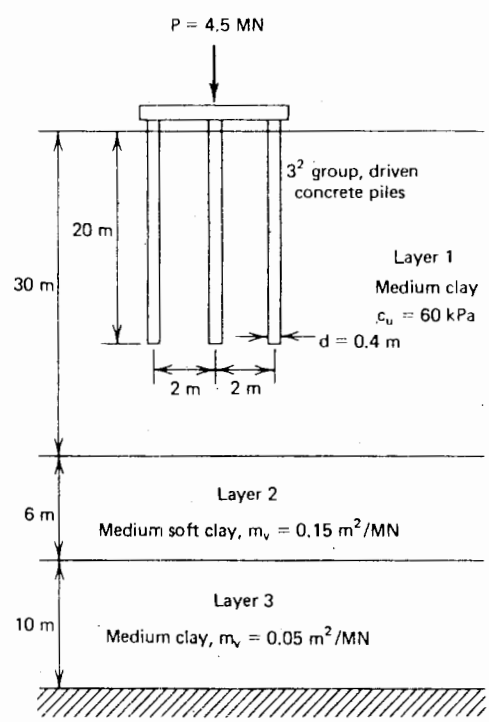

FIGURE 6.33 Illustrative example.

as indicated in Fig. 6.33. An estimate is required of the total final settlement of the pile group.

The first step is to estimate the drained Young's modulus and Poisson's ratio of each layer. For the first layer in which the piles are situated, interpolation from Fig. 5.42 for c_u = 60 kPa gives E'_s = 17.0 MPa. ν'_s is assumed to be 0.35. For the second and third layers, ν'_s is assumed to be 0.35 and 0.3, respectively. Using the specified values of m_v, and the following theoretical relationship between E'_s and m_v,

$$E'_s = \frac{(1 - 2\nu'_s)(1 + \nu'_s)}{(1 - \nu'_s)\, m_v} \qquad (6.27)$$

the values of E'_s for layers 2 and 3 are 4.2 MPa and 14.9 MPa, respectively.

Assuming Young's modulus of the concrete to be 17,000 MPa,

Pile-stiffness factor

$$K = \frac{17{,}000 \times 1.0}{17}$$

$$= 1000$$

The settlement of a single pile in the first layer may now be calculated, the relevant dimensionless parameters being L/d = 20/0.4 = 50, K = 1000, ν'_s = 0.35, h/L = 30/20 = 1.5. Using Eq. 5.33*a*, the single-pile influence factor I is found to be 0.046, and for the average pile load of 4.5/9 = 0.5 MN, the single-pile settlement is

$$\rho_{1av} = P_{av} \cdot \rho_1 = \frac{0.5}{0.4 \times 17.0} \times 0.046$$

$$= .0034 \text{ m}$$
$$= 3.4 \text{ mm}$$

The settlement ratio must now be determined. From Table 6.2, for a 3^2 group in a deep layer, with s/d = 2/0.4 = 5, K = 1000, and ν_s = 0.5, R_s = 3.51. Making allowance for the effect of the finite layer from Fig. 6.20 and for the effect of ν_s being 0.35 rather than 0.5 (Fig. 6.22), the required value of R_s is estimated to be 2.63. The settlement of the group in the founding layer, ρ_{GD}, is then given by Eq. (6.18) as

$$\rho_{GD} = 2.63 \times 3.4$$
$$= 8.9 \text{ mm}$$

The settlement contribution from the underlying layers must now be calculated. From Fig. 6.31, using the equivalent-length approach to represent the group, L_e is about $0.9L$, or, L_e = 0.9 × 20 = 18 m. The plan area of the group is 4.4 × 4.4 = 19.36 m^2, and hence the diameter of the equivalent pier is d_e = 4.96 m—say, 5 m. Thus, for the equivalent pier, L_e/d_e = 18/5 = 3.6. The calculations to evaluate the settlement of layers 2 and 3, using Eq. (5.41), are tabulated in Table 6.8. It is assumed that the rock beneath layer 3 is rigid. From Table 6.8, the settlement caused by the underlying layers is 8.3 mm, so that the estimated final settlement of the group is

$$\rho = 8.9 + 8.3$$
$$= 17.2 \text{ mm}$$

If the equivalent-diameter approach is used, the settlement caused by the underlying layers is calculated to be 9.7 mm, compared with the above value of 8.3 mm.

TABLE 6.8 CALCULATION OF ADDITIONAL SETTLEMENT CAUSED BY UNDERLYING LAYERS

Layer (k)	$\frac{H_k}{L_e}$ [a]	I_k [b]	$\frac{H_{k+1}}{L_e}$	I_{k+1} [b]	E_{sk} (MN/m^2)	$\frac{I_k - I_{k+1}}{E_{sk}}$ (m^2/MN)
2	1.67	0.428	2.0	0.308	4.2	0.0279
3	2.0	0.308	2.55	0.230	14.9	0.0052
					Σ =	0.0331

[a] L_e = 18 m.
[b] From Fig. 5.35.
∴ Settlement caused by layers 2 and 3 = $\frac{4.5}{18.0} \times 0.0331$
= .0083 m
= 8.3 mm

6.5 PREPARATION AND USE OF DESIGN CHARTS

The theoretical solutions presented in this chapter can be used to prepare design charts to assist in the selection of the necessary number and spacing of piles to support a given load with a specified maximum settlement and factor of safety against failure. The procedure is best described with reference to the following simple example.

A load of 5 MN is to be supported on a deep layer of clay having the following average properties: c_u = 50 kPa, pile-soil adhesion c_a = 45 kPa, E' = 15 MPa, ν' = 0.3. It is proposed to use driven 20-m-long concrete piles, 0.4 m in diameter, for which E_p = 15,000 MPa. It is required to examine the combinations of number and spacing of piles that satisfy the criterion of a factor of safety of 2.5 against failure and a maximum final settlement of 15 mm.

Considering first the settlement criterion, the results for R_s in Table 6.2, together with the solutions for single-pile settlement (Chapter 5) may be used to prepare plots of settlement, S, versus number of piles, n, for various

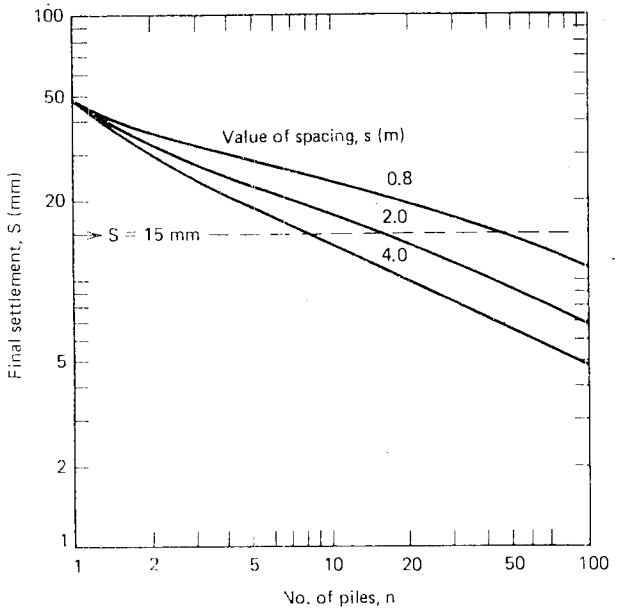

FIGURE 6.34 Design chart for settlement of pile groups in example.

pile spacings, s. The resulting plot is shown in Fig. 6.34. From this plot, the values of s and n that satisfy the criterion of 15-mm settlement may be obtained and replotted as curve 1 on Fig. 6.36. Combinations of s and n to the *right* of curve 1 will give settlements less than 15 mm, while those to the *left* will give greater settlements. If desired, a series of such curves could be constructed for different allowable settlements. It is assumed here that as previously mentioned, the settlement is dependent almost entirely on the number and spacing of piles and not on the exact group configuration.

A similar plot to Fig. 6.34 may be made of factor of safety, FS, versus n for various values of pile spacing. In obtaining these curves, the relationship in Eq. (3.22) for ultimate group-load capacity has been used.

The resulting curves of FS versus n for three values of spacing s are shown in Fig. 6.35. From Fig. 6.35, the values of s and n giving the required value of $FS = 2.5$ have been plotted as curve 2 in Fig. 6.36. Again, combinations of s and n to the right of curve 2 have a factor of safety greater than 2.5, while combinations to the left have FS less than 2.5. The minimum combination that satisfies both the settlement and the factor-of-safety criteria is given by the intersection of curves 1 and 2—in this case, $n = 12$ piles at about 2.8-m spacing.

Of course, other requirements may dictate the final design—for example, requirements for design of the pile cap, or limits on the area of the group. In such cases, Fig. 6.36 gives a rapid appreciation of the consequences of other constraints; for example, if the spacing had to be no greater than 1 m, a total of about 38 piles would be required to satisfy the settlement criterion, whereas 16 would be adequate for bearing-capacity purposes.

The use of design charts such as Figs. 6.34, 6.35, and 6.36 can therefore give a ready appreciation of the effects on group settlement and safety factor of changes in spacing, number of piles, pile length, and soil and pile proper-

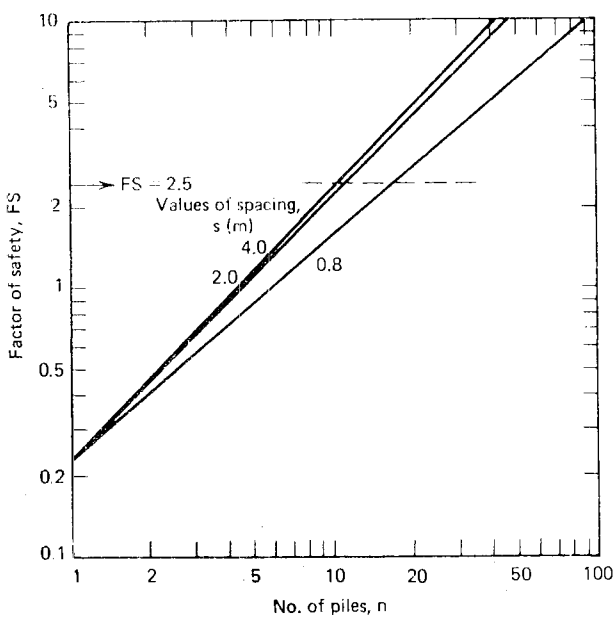

FIGURE 6.35 Design chart for factor of safety of pile groups in example.

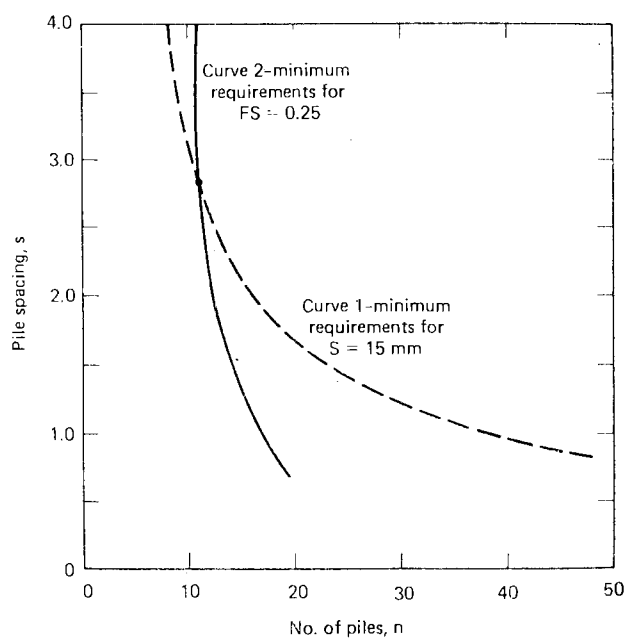

FIGURE 6.36 Composite design chart for pile group example.

ties. It is the simplicity and rapidity of construction of such charts—as compared with, say, a "one-off" finite-element solution—that make the elastic parametric solutions so useful in designing pile groups.

6.6 SURFACE SETTLEMENTS AROUND A GROUP

The preceding sections have dealt with the settlements directly beneath the pile group. In some cases, it may also be of interest to estimate the settlement of the ground surface at some distance away from the group—for example, in determining the additional settlement of an existing building caused by a new structure. Such an estimate may be obtained by using the solutions in Figs. 5.32, 5.33, and 5.34 for the settlement distribution around a pile. As with the calculation of settlements caused by compressible underlying strata, it is convenient to consider the group either as having a uniform load distribution among the piles, or as an equivalent single pier. An example of the surface-displacement profile caused by a 3^2 group with a rigid cap in a uniform semi-infinite mass, as given by Poulos and Mattes (1971*a*), is shown in Fig. 6.37. Profiles were obtained by considering:

1. The correct distribution of pile loads P_i.
2. A uniform distribution of loads P_i.
3. A single equivalent pier.

There is close correspondence between all three settlement profiles, except in the immediate vicinity of the groups, in which case the consideration of a uniform pile-load distribution leads to nonuniform settlement of the group. The satisfactory nature of the equivalent-pier approximation is evident from Fig. 6.37.

Further examples showing the effects of pile-stiffness factor K, length-to-diameter ratio L/d, and relative layer-depth h/L, on the surface-displacement profiles surrounding a 2^2 group, are shown in Figs. 6.38, 6.39, and 6.40.

6.7 OBSERVED AND THEORETICAL GROUP BEHAVIOR

6.7.1 Settlements

A number of comparisons between measured and theoretical values of settlement ratio for floating-pile groups were made by Poulos and Mattes (1971*b*). A summary of the cases considered is given in Table 6.9, and the comparisons are shown in Fig. 6.41. In all cases, the load level corresponds to a factor of safety of at least 2 against ultimate failure of the group. With the exception of the model tests by Hanna (1963) in loose sand, the agreement is generally satisfactory for both large and small values of K. The poor agreement for the tests in loose sand may be attributed to

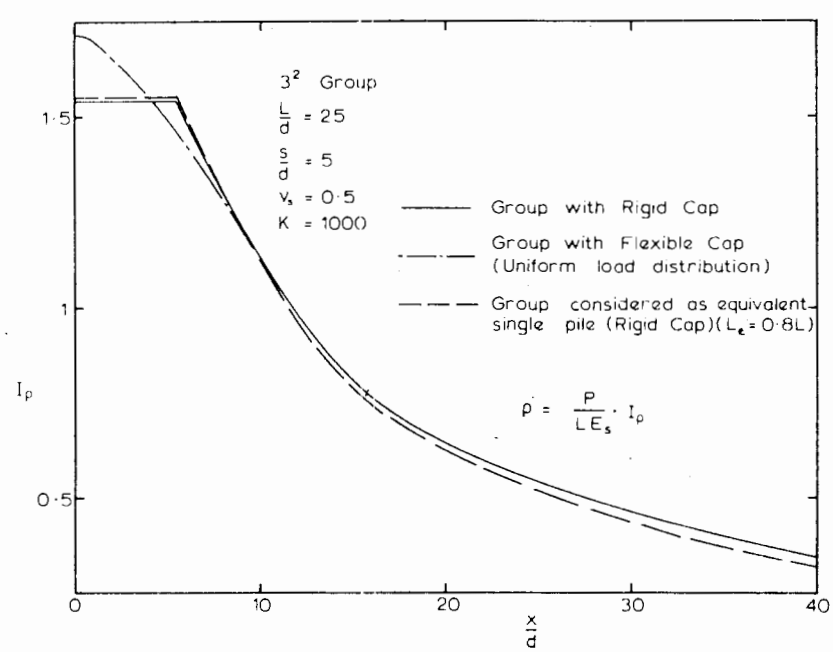

FIGURE 6.37 Comparison between correct and approximate surface-displacement profiles.

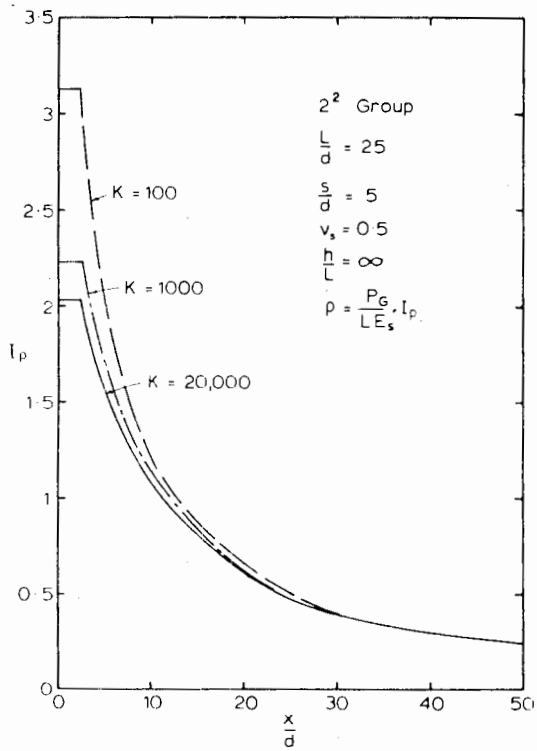

FIGURE 6.38 Influence of K on surface-displacement profiles.

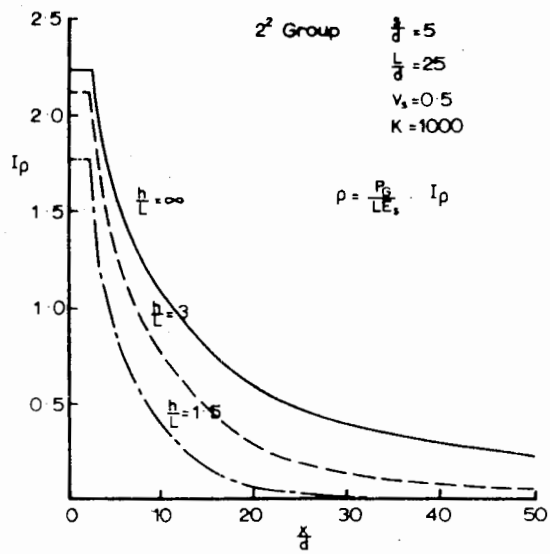

FIGURE 6.40 Influence of layer depth on surface-displacement profiles.

the effects of the greater densification of the loose sand by the pile group, as compared with the single pile. These comparisons, therefore, indicate that the theoretical approach should be satisfactory in practical cases, except for pile groups in loose sand.

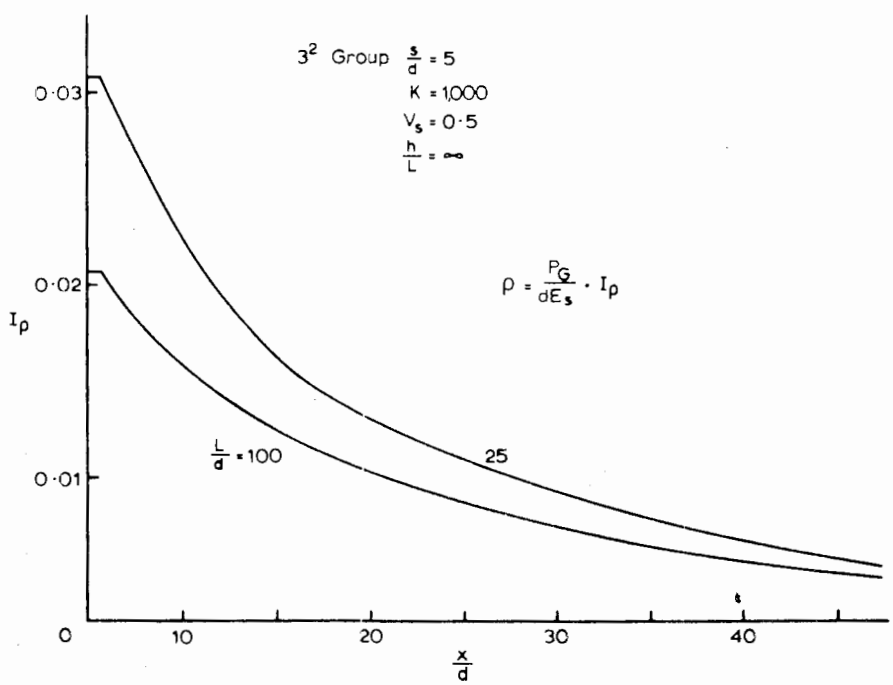

FIGURE 6.39 Influence of $\frac{L}{d}$ on surface-displacement profiles.

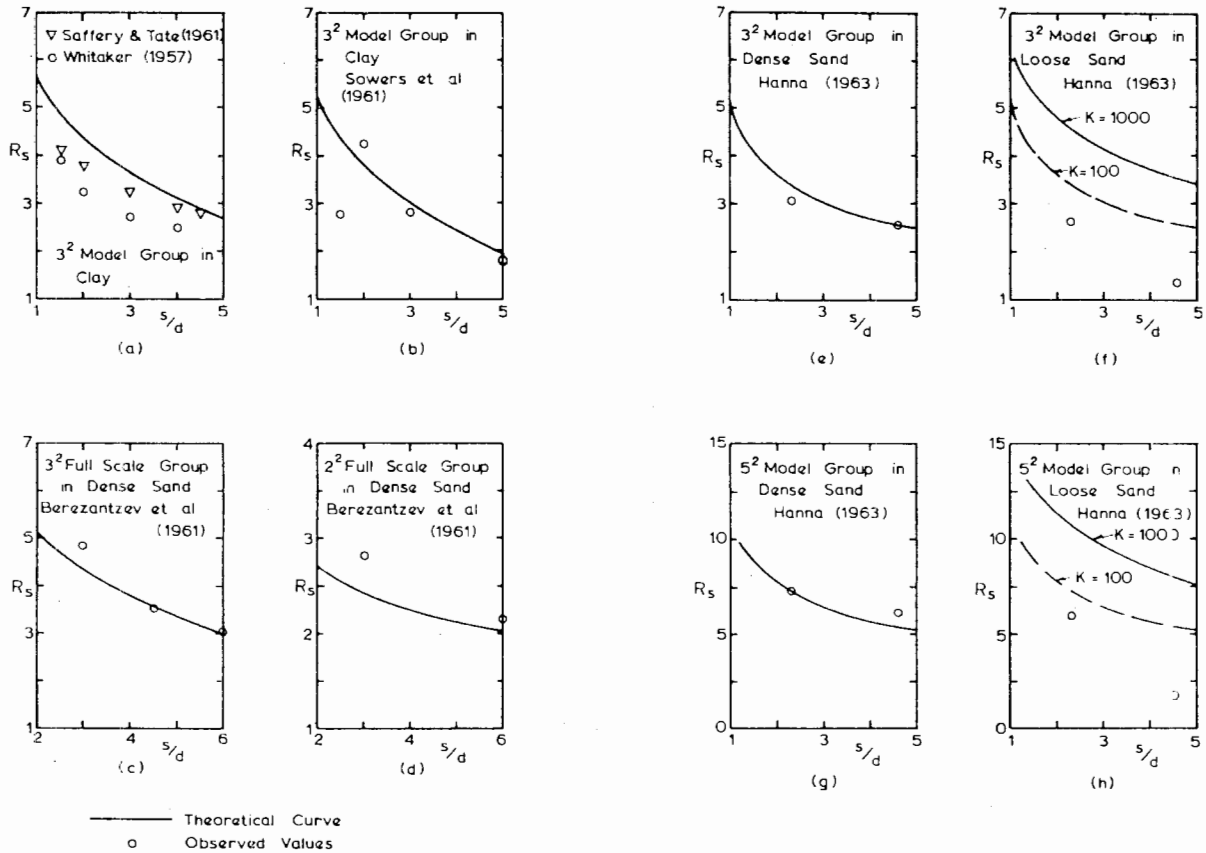

FIGURE 6.41 Comparison between theoretical and observed settlement-ratios.

TABLE 6.9 SUMMARY OF DATA ON FLOATING-PILE GROUP TESTS

Test	Pile Material	Soil Type	Assumed Parameters for Comparisons			Remarks
			L/d	K	Layer Depth/L	
Whitaker (1957)	Brass	Remolded London clay	24	∞	2	Model tests
Saffery and Tate (1961)	Stainless steel	Remolded clay	20	∞	2	Model tests
Sowers et al. (1961)	Aluminium tube	Remolded bentonite	24	2000	2	Model tests
Berezantzev et al. (1961)	Concrete	Dense sand	20	1000	∞	Field tests. K estimated for quoted values of E_s.
Hanna (1963)	Wood	Dense sand	33	100	2	Model tests.
Hanna (1963)	Wood	Loose sand	33	1000	2	K estimated from Table 5.4

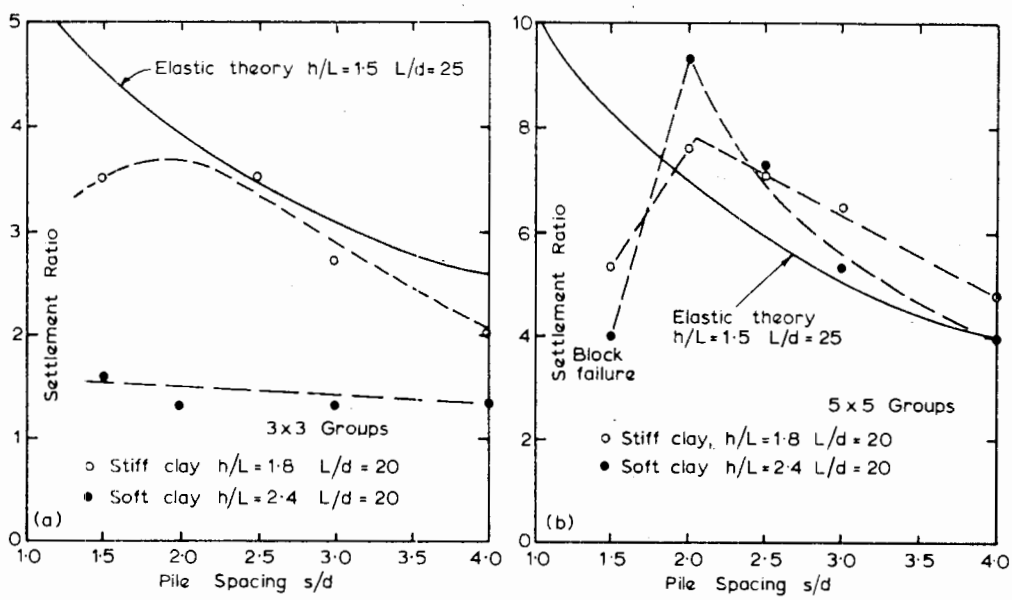

FIGURE 6.42 Theoretical and measured settlement-ratios. (Barden and Monckton, 1970).

Further evidence of the applicability of the theoretical approach can be found in the comparisons between theory and the data collected by Skempton, 1953 (Fig. 6.18) and Barden and Monckton, 1970 (Fig. 6.42). With the exception of the 3^2 groups in soft clay, the results of Barden and Monckton are in fair agreement with theory.

For two buildings at M.I.T., founded on end-bearing piles passing through a deep deposit of clay and bearing on rock, comparisons between measured and theoretical settlements have been made by Poulos (1972*b*). A typical soil profile is shown in Fig. 6.43. The calculated values were based on a value of modulus backfigured from the results of pile-loading tests, and a typical load-test result is shown in Fig. 6.44. For each building, the foundation consisted of a number of pile groups, so that in obtaining the theoretical settlement ratios, both the interaction between the piles of

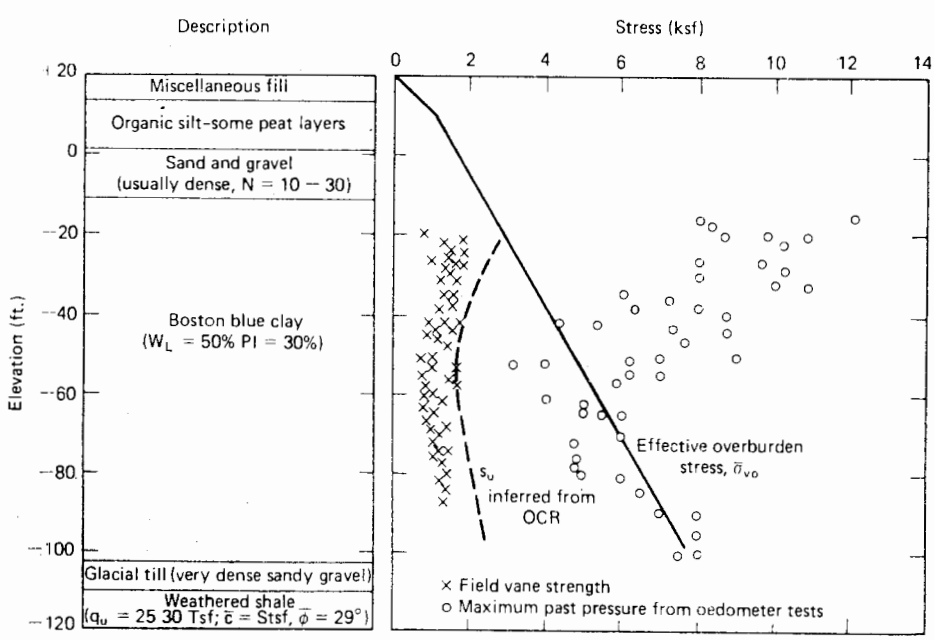

FIGURE 6.43 Typical soil profile, MIT buildings. (After D'Appolonia and Lambe, 1971).

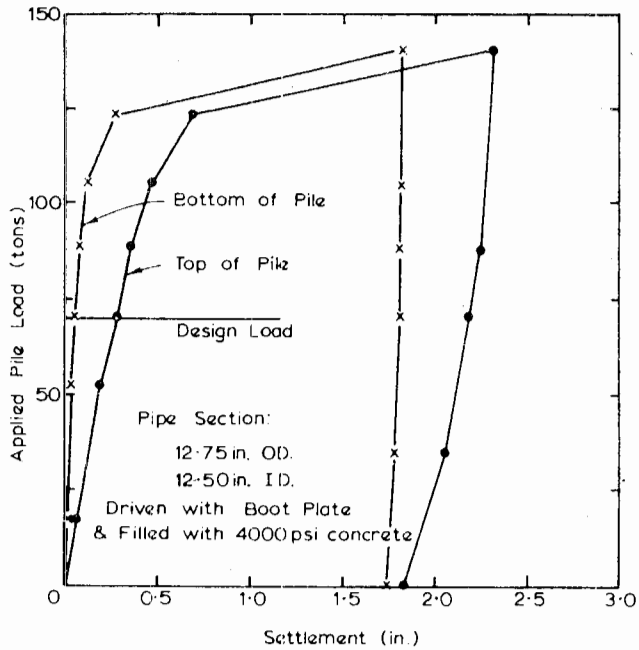

FIGURE 6.44 Load-settlement curves from pile load test (after D'Appolonia and Lambe, 1971).

an individual group and the intergroup interaction have been considered. Comparisons between measured and calculated settlements, shown in Figs. 6.45 and 6 46, reveal reasonable overall agreement. The discrepancies that occur at some columns possibly result from neglect of the structural rigidity in estimating the column loads, and errors in assessing the settlements that occurred prior to commencement of the settlement measurements–especially in the case of the eastern (right-hand) side of the Space Center Building.

Poulos (1972*b*) presented a further comparison between predicted and observed settlements by comparing the theoretical relationship between settlement and number of piles in the group with measured values reported by D'Appolonia and Lambe (1971) for four buildings on the M.I.T. campus. An average pile length of 100 ft was assumed in deriving the theoretical relationship, which is virtually linear and is an fair agreement with the observed relationship. This comparison is reproduced in Fig. 6.47.

6.7.2 Load Distribution

Comparisons between measured and theoretical load-distributions within a model pile group with a rigid cap have been made by Poulos (1968*b*). These are shown in Figs.

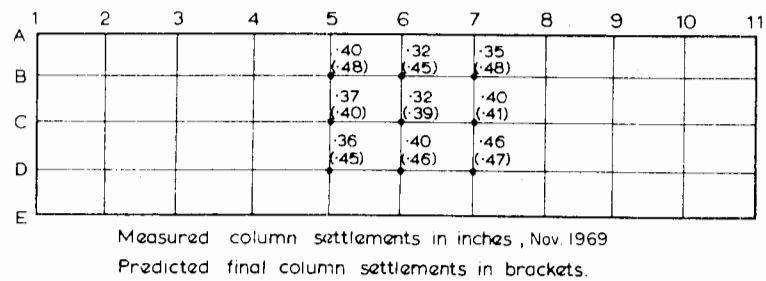

FIGURE 6.45 Comparison between predicted and observed column settlements, Materials Science Building.

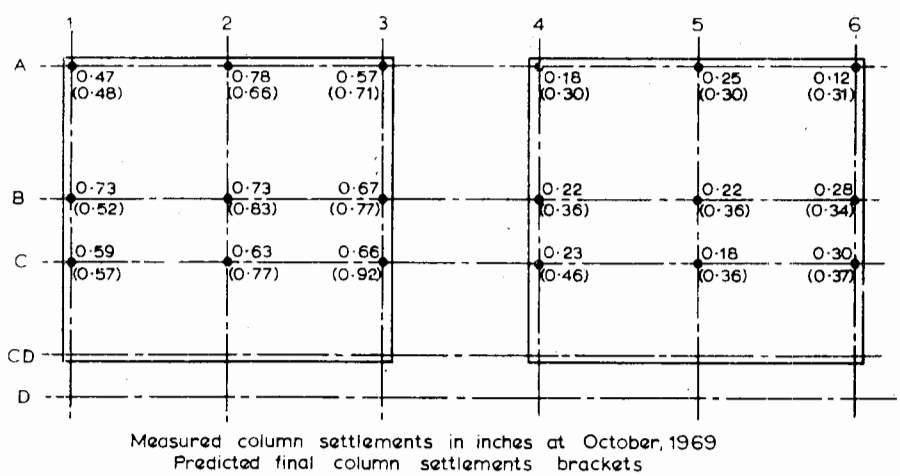

FIGURE 6.46 Comparisons between predicted and observed column settlements, Space Center.

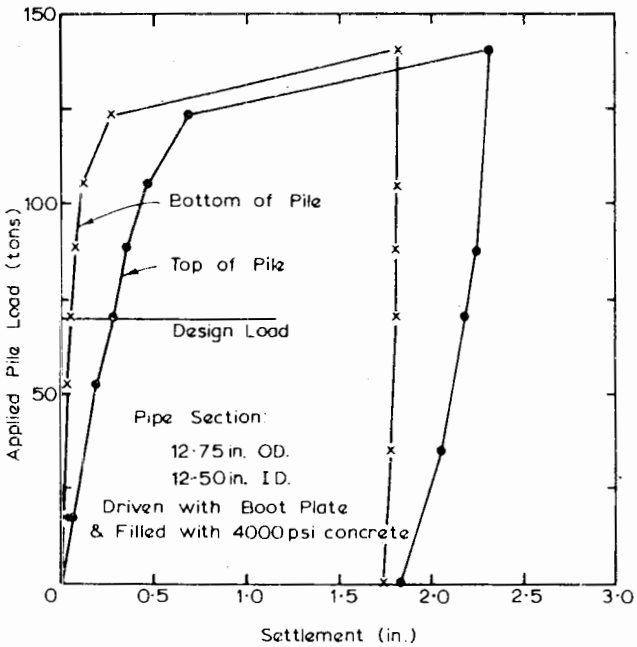

FIGURE 6.44 Load-settlement curves from pile load test (after D'Appolonia and Lambe, 1971).

an individual group and the intergroup interaction have been considered. Comparisons between measured and calculated settlements, shown in Figs. 6.45 and 6 46, reveal reasonable overall agreement. The discrepancies that occur at some columns possibly result from neglect of the structural rigidity in estimating the column loads, and errors in assessing the settlements that occurred prior to commencement of the settlement measurements–especially in the case of the eastern (right-hand) side of the Space Center Building.

Poulos (1972*b*) presented a further comparison between predicted and observed settlements by comparing the theoretical relationship between settlement and number of piles in the group with measured values reported by D'Appolonia and Lambe (1971) for four buildings on the M.I.T. campus. An average pile length of 100 ft was assumed in deriving the theoretical relationship, which is virtually linear and is an fair agreement with the observed relationship. This comparison is reproduced in Fig. 6.47.

6.7.2 Load Distribution

Comparisons between measured and theoretical load-distributions within a model pile group with a rigid cap have been made by Poulos (1968*b*). These are shown in Figs.

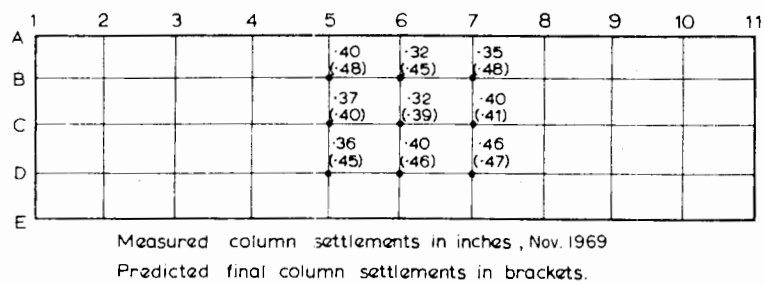

FIGURE 6.45 Comparison between predicted and observed column settlements, Materials Science Building.

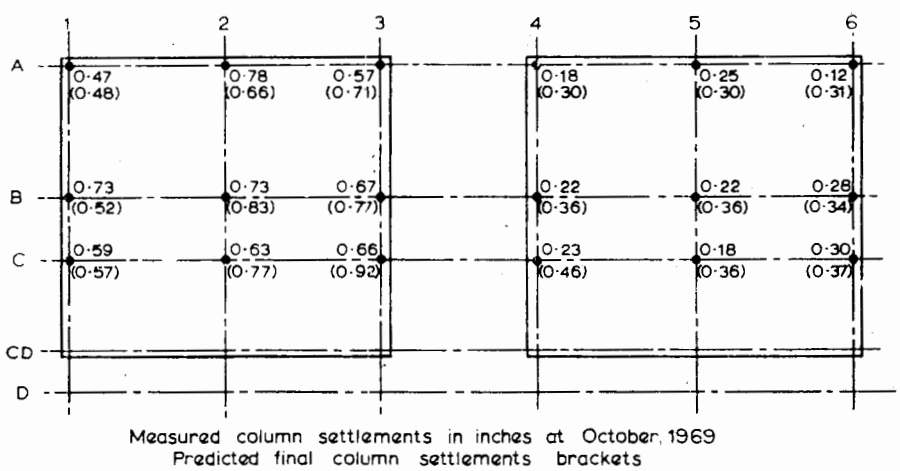

FIGURE 6.46 Comparisons between predicted and observed column settlements, Space Center.

but nevertheless exhibits similar trends. For the 5^2 group, both the magnitude of the loads, and their variation with spacing, are predicted more closely by the theory.

6.7.3 Group Behavior Predicted from Single-Pile Test Results

Tests by Koizumi and Ito (1967)

A series of full-scale tests by Koizumi and Ito (1967) offers an excellent opportunity to study the prediction of pile-group performance from the results of a single-pile test. A single floating-pile and a nine-pile rigid-capped group of similar piles were founded in a thick uniform layer of silty clay overlain by a thin layer of sandy silt. The piles were closed-end steel tubes instrumented to allow pile loads, earth pressures, and pore pressures to be measured. Provision was also made for measuring displacements and pressures in the soil remote from the piles. Details of the foundations and site conditions are given in Fig. 6.50.

By using the single-pile load-test results, a soil modulus of 2500 psi was backfigured, corresponding to a pile-stiffness factor of 500, at a load factor against failure of approximately 2.5. From the theoretical solutions presented in this chapter, the settlement of the rigid-capped group (at the same load factor) was calculated and compared with the measured settlement, as follows:

Group	3^2, floating, rigid cap
L/d	18.5 (individual piles)
Spacing	3 pile diameters center-to-center
Group load, P_G	90 tons
Group-reduction factor, R_G	0.40
Single pile settlement at unit load, ρ_1	0.20 mm/ton
Predicted settlement of group, $P_G \rho_1 R_G$	7.2 mm
Measured settlement of group	7.1 mm

Although the cap of this group was in contact with the soil, the effect of the cap on group settlement calculated on the basis of the analysis in Chapter 10 is in this case negligible. It will be seen that there is excellent agreement between predicted and measured group settlement. The measured and theoretically-predicted load distributions within the group also agree well, as is shown in Table 6.10.

Soil displacements near the group were recorded mainly

TABLE 6.10 THEORETICAL AND MEASURED LOAD DISTRIBUTION TESTS OF KOIZUMI AND ITO (1967)

Pile Location	Pile Load/Average Pile Load	
	Theoretical	Measured[a]
Centre	0.35	0.46
Mid-Side	0.82	0.86
Corner	1.35	1.20

[a] Group load 120 tons.

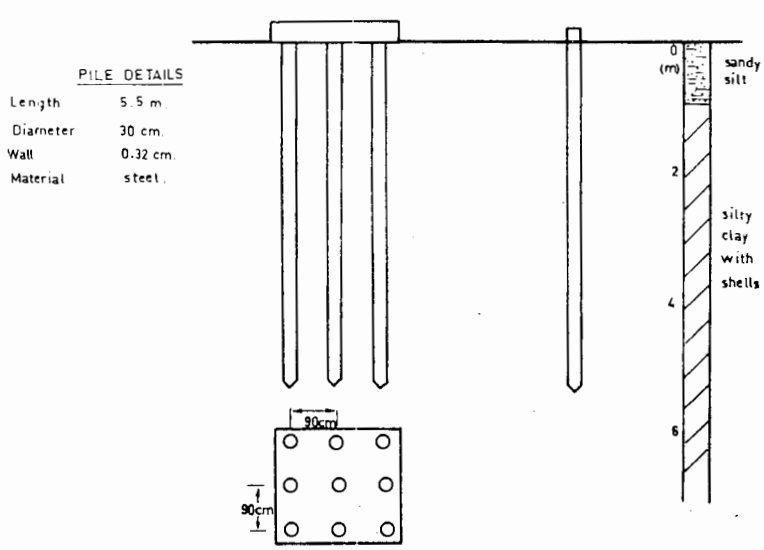

FIGURE 6.50 Pile group test (Koizumi and Ito, 1967).

in connection with ultimate-bearing-capacity investigations and at working loads, are considerably smaller than those predicted theoretically.

Model-Group Tests by Mattes and Poulos (1971)
Tests were carried out on 3 × 3 and 6 × 1 floating pile groups with piles of $L/d = 25$, at a pile spacing of two diameters. In Table 6.11, the measured settlements are compared with those predicted from the results of single-pile tests carried out under the same conditions, and it can be seen that there is good agreement between observed and predicted settlements.

TABLE 6.11 MODEL PILE GROUP TESTS[a]

Group size		3 × 3	6 × 1
Total group load (*lb*)		50	40
Theoretical group settlement ratio R_S		4.77	3.24
Settlement of single pile at average pile load (predicted from average soil modulus backfigured from single pile tests) (in. × 10^{-4})	Immediate	3.82	4.41
	Final	4.98	5.56
Immediate settlement of group (in. × 10^{-4})	Predicted	18.2	14.3
	Observed	15.3	15.0
	Ratio of predicted to observed settlement	1.19	0.95
Final settlement of group (in. × 10^{-4})	Predicted	23.4	18.0
	Observed	24.2	20.0
	Ratio of predicted to observed settlement	0.98	0.90

[a] After Mattes and Poulos (1971).

7

ULTIMATE LATERAL RESISTANCE OF PILES

7.1 INTRODUCTION

Piles are frequently subjected to lateral forces and moments: for example, in quay and harbor structures, where horizontal forces are caused by the impact of ships during berthing and wave action; in offshore structures subjected to wind and wave action; in pile-supported earth-retaining structures; in lock structures; in transmission-tower foundations, where high wind forces may act; and in structures constructed in earthquake areas such as Japan or the West Coast of the United States, where some building codes specify that piles supporting such structures should have the ability to resist a lateral force of 10% of the applied axial load. In the design of such pile foundations, two criteria must be satisfied: first, an adequate factor of safety against ultimate failure; and second, an acceptable deflection at working loads. As in other fields of soil mechanics, these two criteria are generally treated separately, and the design is arranged to provide the required safety margins independently.

In this chapter, methods of estimating the ultimate lateral resistance of single piles and pile groups are described. In many practical cases, the design of piles for lateral loading will be dependent on satisfying a limiting lateral-deflection requirement that may result in the specificiation of allowable lateral loads much less than the ultimate lateral capacity of the piles. For such cases, the estimation of lateral deflections caused by lateral loads is discussed in Chapter 8, while the general problem of a pile or pile-group subjected to both axial and lateral loading is considered in Chapter 9. Consideration in the present chapter will be confined to situations where the lateral deflection is not an important consideration. It must, however, be emphasized that in many cases, the ultimate load will be reached at very large deflections, especially in the case of relatively flexible piles. For such cases, it may be desirable to carry out a complete elastoplastic analysis, as outlined in Section 8.3. However, for relatively rigid piles, the method described herein will generally be applicable. The chapter concludes with a brief consideration of the effects of piles on slope stability, and of methods of increasing lateral load capacity.

7.2 SINGLE PILES

In this section, methods of estimating the ultimate lateral resistance of relatively-slender vertical floating piles having negligible base resistance are considered first, and a number

of possible approaches are described. The effects of socketing the tip and of pile-batter are then discussed, and the "thin-pile" analysis is extended to piers with significant base resistance.

7.2.1 Conventional Statical Approach

The simplest method of estimating the ultimate lateral resistance of a floating pile is to consider the statics of a pile, as shown in Fig. 7.1 for a pile with an unrestrained (or "free") head. The pile is subjected to a horizontal force H and a moment M, and the ultimate soil pressure at any depth z below the soil surface is p_u. The limiting combination of H and M, H_u and M_u, to cause failure—that is, to mobilize the ultimate soil resistance along the pile, assuming the pile to be rigid—may be obtained by considering equilibrium of horizontal forces and moments, and solving the resulting simultaneous equations for the unknown depth of rotation, z_r, and the ultimate horizontal load H_u (taking the moment M_u as He, where e = eccentricity of loading). Treating the pile as a thin strip of diameter or width d, these equations, in general form, are

$$H_u = \int_0^{z_r} p_u \, dz - \int_{z_r}^{L} p_u \, dz \tag{7.1}$$

$$M_u = H_u e = -\int_0^{z_r} p_u \, dz\,dz + \int_{z_r}^{L} p_u \, dz\,dz \tag{7.2}$$

In the case of a uniform distribution of soil resistance with depth along the whole length of the pile—that is, $p_0 = p_L = p_u$—the above equations yield the following solutions for the depth of rotation, z_r, and the ultimate lateral load H_u:

$$z_r = \frac{1}{2}\left(\frac{H_u}{p_u d} + L\right) \tag{7.3}$$

$$\frac{M_u}{p_u dL^2} = \frac{H_u e}{p_u dL^2} = \frac{1}{4}\left[1 - \left(\frac{2H_u}{p_u dL}\right) - \left(\frac{H_u}{p_u dL}\right)^2\right] \tag{7.4}$$

$$\frac{H_u}{p_u dL} = \sqrt{\left(1 + \frac{2e}{L}\right)^2 + 1} - \left(1 + \frac{2e}{L}\right) \tag{7.5}$$

$\frac{H_u}{p_u dL}$ is plotted against e/L in Fig. 7.2.

For the case of a linear variation of soil resistance with depth, from p_0 at the ground surface to p_L at the pile tip, the following equations may be derived:

$$4\left(\frac{z_r}{L}\right)^3 + \left[6\left(\frac{z_r}{L}\right)^2\right]\left[\frac{e}{L} + \frac{p_0}{p_L - p_0}\right] + \left(\frac{12p_0}{p_L - p_0}\right)\left(\frac{e}{L}\right)\left(\frac{z_r}{L}\right) - \left(3\frac{e}{L}\right)\left(\frac{p_0 + p_L}{p_L - p_0}\right) - \left(\frac{2p_L + p_0}{p_L - p_0}\right) = 0 \tag{7.6}$$

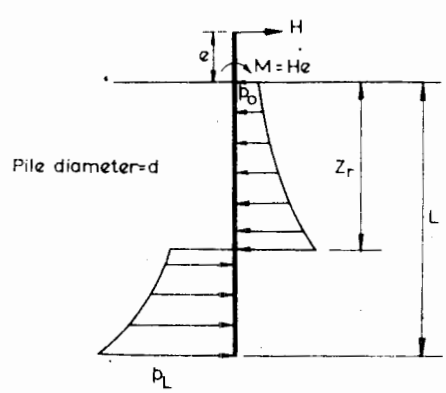

FIGURE 7.1 Unrestrained laterally-loaded pile.

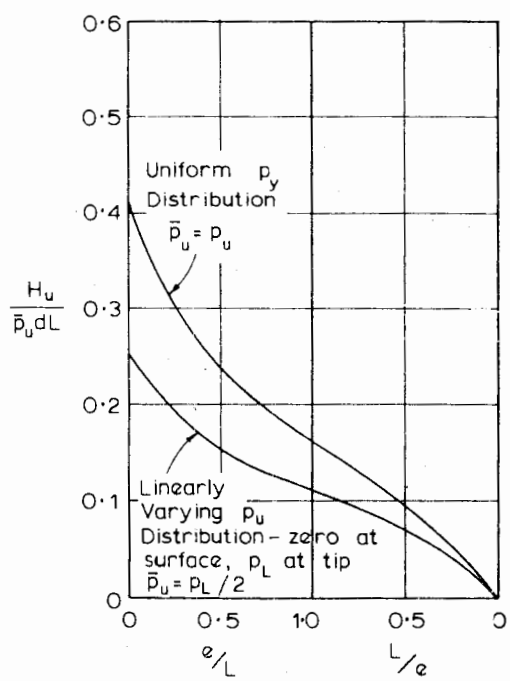

FIGURE 7.2 Ultimate lateral resistance of unrestrained rigid piles.

$$\frac{H_u}{p_L dL} = \left(1 - \frac{p_0}{p_L}\right)\left(\frac{z_r}{L}\right)^2 + \left(2\frac{p_0}{p_L}\right)\left(\frac{z_r}{L}\right) - \frac{1}{2}\left(1 + \frac{p_0}{p_L}\right) \quad (7.7)$$

$\frac{H_u}{p_L dL}$ is plotted against e/L in Fig. 7.2 for the case $p_0 = 0$. General solutions for failure load and moment combinations are shown in Fig. 7.3.

For any general distribution of soil resistance with depth, it is convenient to employ the procedure recommended by Brinch Hansen (1961). In this procedure, the center of rotation is determined by trial and error, such that the resulting moment, taken about the point of application of the load, is zero. When the center of rotation is determined, the ultimate lateral resistance can be obtained from the horizontal-equilibrium equation.

An extension of the above analysis for the case of a pile near a slope has been described by Poulos (1976).

Nonrigid Piles

The above derivations assumed that the pile is sufficiently rigid that failure of the soil will occur before failure of the pile itself. However, for relatively long piles, the ultimate lateral resistance may be determined by the yield moment of the pile, which may be reached before full mobilization of the ultimate soil resistance. In such cases, the maximum moment (occurring at the point of zero shear for a free-head pile) should be calculated, as described above, assuming full mobilization of the soil resistance above this point. Since this maximum moment cannot exceed the yield moment of the pile section, the ultimate lateral resistance is the lesser of:

1. The horizontal load required to cause failure of the soil along the whole length of the pile (i.e., the pile then is essentially rigid and its capacity is governed by the soil resistance).
2. The horizontal load required to produce a maximum moment equal to the yield moment of the pile section (i.e., the lateral capacity of the pile is governed primarily by the pile characteristics).

A more detailed consideration of the ultimate resistance of both rigid and nonrigid free-head piles is given in Section 7.2.2, together with consideration of the load capacity of piles having a restrained head.

Ultimate Soil Resistance

For a purely cohesive soil, the ultimate lateral resistance p_u increases from the surface down to a depth of about three pile diameters and remains constant for greater depths. This is shown diagrammatically in Fig. 7.4. When p_u becomes constant, lateral failure involves plastic flow of the soil around the pile in the horizontal plane only and the value of p_u can be determined by plasticity theory. The value of the lateral resistance factor K_c ($p_u = K_c c$) depends on the ratio of pile adhesion to cohesion c_a/c and on the shape of the pile section, the most significant property of the shape being the aspect ratio d/b. The influence of the aspect ratio on the value of K_c is shown in Fig. 7.5 for

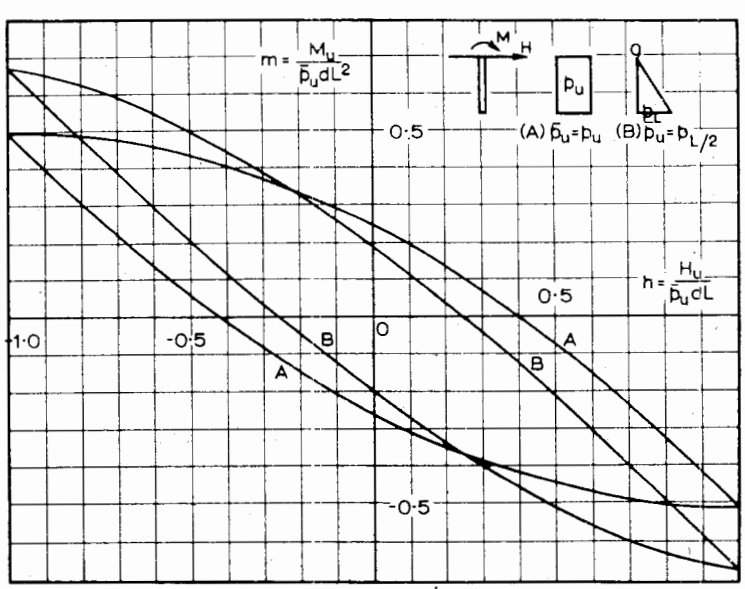

FIGURE 7.3 Ultimate lateral resistance of unrestrained rigid piles.

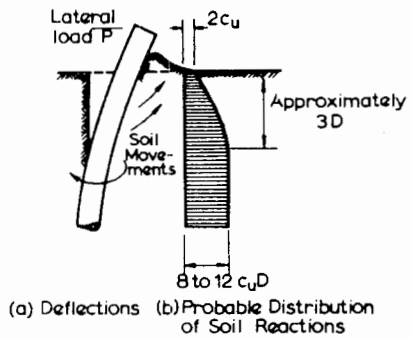

FIGURE 7.4 Distribution of lateral resistance.

$c_a/c = 1$ and $c_a/c = 0$ and, to sufficient accuracy, the solution for any intermediate value of c_a/c can be obtained by linear interpolation. The curves in Fig. 7.5 have been obtained by plasticity theory using limit analysis. (The upper bound obtained in this analysis generally only exceeded the lower bound by 10 to 15% and the curves are for the average of the two bounds). The analysis assumed the pile section to be a rhomb and may be slightly conservative for other convex shapes of the same aspect ratio. Elsewhere in this chapter the lateral resistance at depth in purely cohesive soil is usually taken as $9c$, whatever the shape of the pile and value of c_a/c, see for example Brom's approach to ultimate pile capacity detailed in 7.2.2.1 below. Fig. 7.5 confirms the reasonableness of this simple assumption.

For the more general case of a $c - \phi$ soil, an alternative derivation of the ultimate lateral soil resistance, based essentially on earth-pressure theory, has been given by Brinch Hansen (1961), who also considers the variation of resistance with depth along the pile. The ultimate resistance at any depth, z, below the surface is expressed as

$$p_u = qK_q + cK_c \tag{7.8}$$

where

q = vertical overburden pressure
c = cohesion
K_c, K_q = factors that are a function of ϕ and z/d

K_c and K_q are plotted in Fig. 7.6, while the limiting values for the ground surface and for infinite depth are plotted in Fig. 7.7.

7.2.2 Broms's Theory

The theory developed by Broms (1964*a* and *b*) is essentially the same as that described in the preceding section, except that simplifications are made to the ultimate soil-resistance distribution along the pile and also that full consideration is given to restrained or fixed-head piles as well as

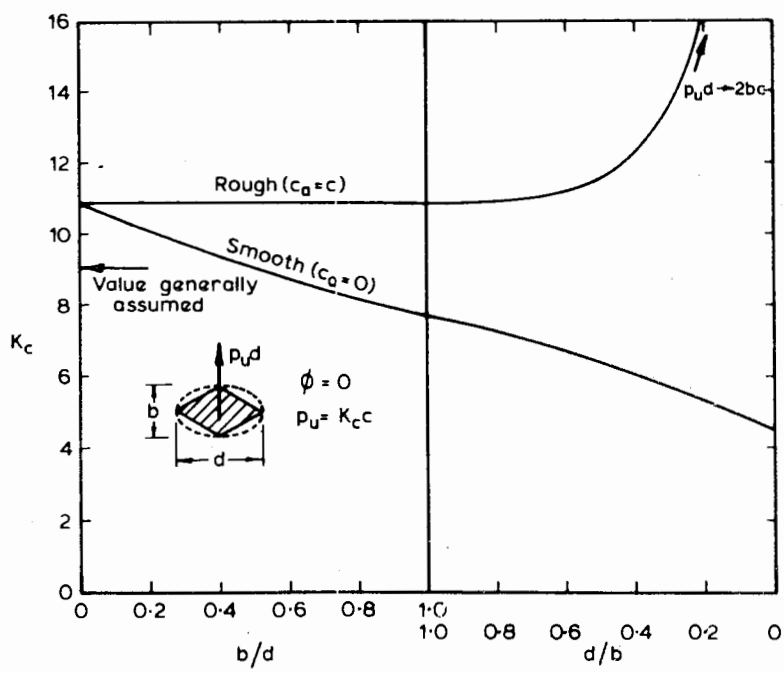

FIGURE 7.5 Effect of aspect ratio and adhesion ratio on lateral resistance for purely cohesive soil.

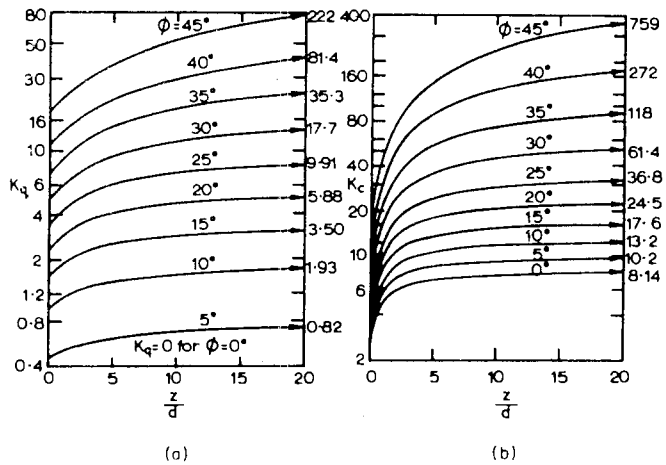

FIGURE 7.6 Lateral resistance factors K_q and K_c (Brinch Hansen, 1961).

unrestrained or free-head piles. For convenience, piles in purely cohesive soils and in purely frictional soils will be considered separately.

7.2.1 *PILES IN COHESIVE SOILS*

As discussed previously (Fig. 7.4), the ultimate soil resistance for piles in purely cohesive soils increases with depth from $2c_u$ at the surface (c_u = undrained shear-strength) to 8 to 12 c_u at a depth of about three pile-diameters ($3d$) below the surface. Broms (1964*a*) suggested a simplified distribution of soil resistance as being zero from the ground surface to a depth of $1.5d$ and a constant value of $9c_u$ below this depth. This assumes also that pile movements will be sufficient to generate this reaction in the critical zones, the location of which will depend on the failure mechanism.

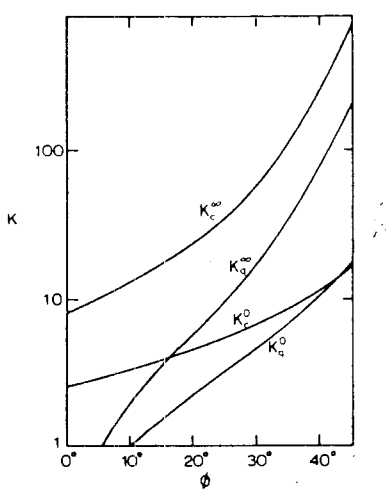

FIGURE 7.7 Lateral resistance factors at ground surface (O) and at great depth (∞) (Brinch Hansen, 1961).

Unrestrained or Free-Head Piles

Possible failure mechanisms for unrestrained piles are shown for "short" and "long" piles in Fig. 7.8, together with the soil-reaction distributions. "Short" piles (termed *rigid piles* in the preceding sections) are those in which the lateral capacity is dependent wholly on the soil resistance, while "long" piles are those whose lateral capacity is primarily dependent on the yield moment of the pile itself. In Fig. 7.8, f defines the location of the maximum moment, and since the shear there is zero,

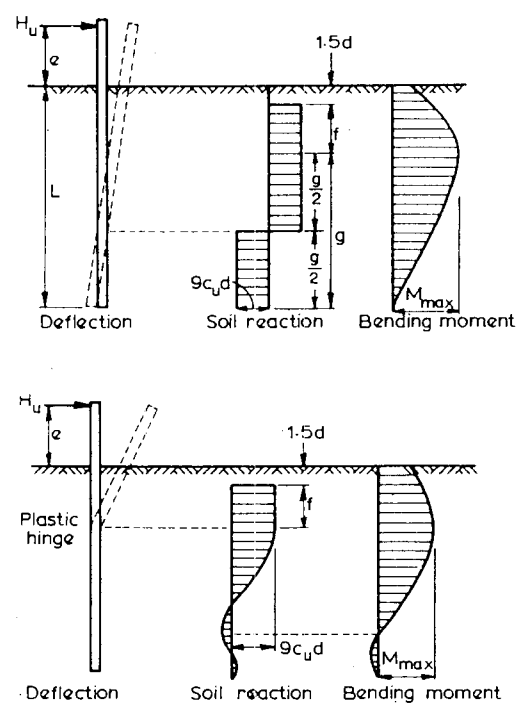

FIGURE 7.8 Failure mechanisms for piles in cohesive soil (Broms, 1964*a*).

$$f = \frac{H_u}{9c_u d} \tag{7.9}$$

Also, taking moments about the maximum moment location,

$$M_{\max} = H_u (e + 1.5d + 0.5f) \tag{7.10a}$$

also,

$$M_{\max} = 2.25dg^2c_u \tag{7.10b}$$

Since $L = 1.5d + f + g$, Eqs. (7.9) and (7.10) can be solved for the ultimate lateral load, H_u. The solution is plotted in Fig. 7.9*a* in terms of dimensionless parameters L/d and $H_u/c_u d^2$, and applies for short piles in which the yield moment $M_y > M_{\max}$, the inequality being checked by using Eqs. (7.9) and (7.10*a*).

For long piles, Eq. (7.10*b*) no longer holds, and H_u is obtained from Eqs. (7.9) and (7.10*a*) by setting $M_{\max}$ equal to the known value of yield moment, M_y. This solution is plotted in Fig. 7.9*b* in terms of dimensionless parameters $H_u/c_u d^2$ and $M_y/c_u d^3$. It should be noted that Broms's solution for short piles can easily be recovered from the simple statical solution for uniform soil described in Section 7.2, by using an equivalent length of pile equal to $L - 1.5d$, and an equivalent eccentricity of loading equal to $e + 1.5d$.

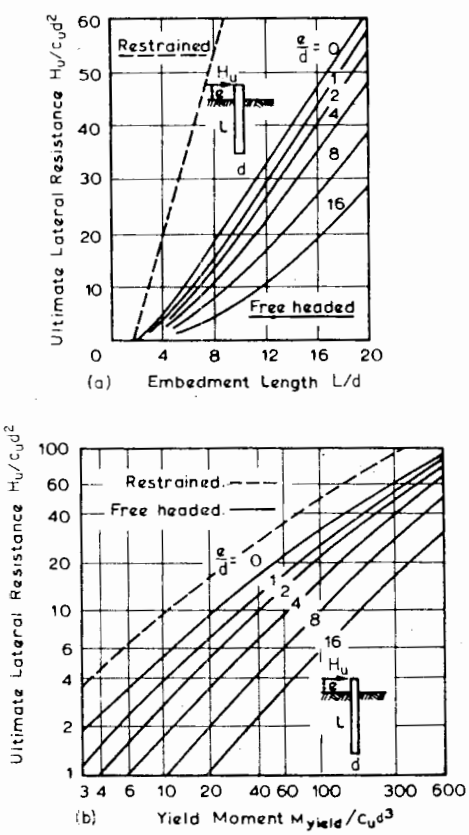

FIGURE 7.9 Ultimate lateral resistance in cohesive soils: (a) short piles; (b) lon piles (Broms, 1964*a*).

Restrained or Fixed-Headed Piles

Possible failure mechanisms for restrained piles are shown in Fig. 7.10, together with the assumed distributions of soil reaction, and moments. The changeover points from one failure-mode to another depend again on the yield moment of the pile. It is assumed that moment-restraint equal to the

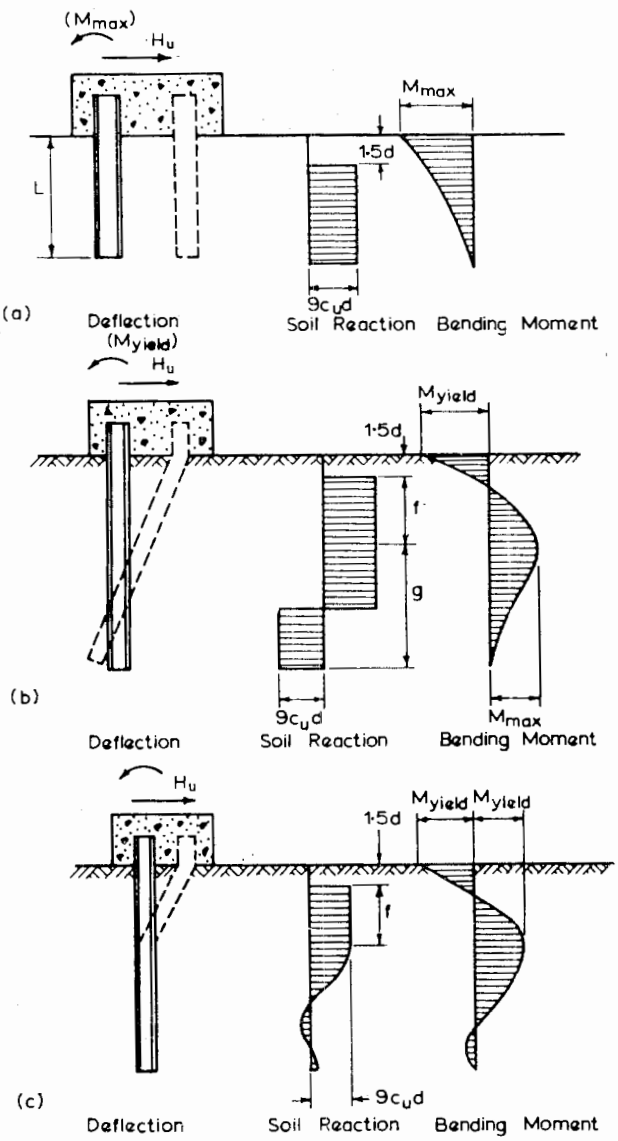

FIGURE 7.10 Restrained piles, in cohesive soil: (a) short; (b) intermediate; (c) long (after Broms, 1964*a*).

moment in the pile just below the cap is available*. In Fig. 7.10*a*, the following relationships hold for "short" piles:

$$H_u = 9c_u d\,(L - 1.5d) \tag{7.11}$$

$$M_{\max} = H_u\,(0.5L + 0.75d) \tag{7.12}$$

Solutions in dimensionless terms are shown in Fig. 7.9*a*.

For "intermediate" piles (i.e., first yield of pile occurs at the head) in Fig. 7.10*b*, Eq. (7.9) holds, and taking moments about the surface,

$$M_y = 2.25\,c_u d g^2 - 9c_u d f(1.5d + 0.5f) \tag{7.13}$$

This equation, together with the relationship $L = 1.5d + f + g$, may be solved for H_u. It is necessary to check that the maximum positive moment, at depth $f + 1.5d$, is less than M_y; otherwise, the failure mechanism for "long" piles illustrated in Fig. 7.10*c* holds. For the latter mechanism, the following relationship applies:

$$H_u = \frac{2M_y}{(1.5d + 0.5f)} \tag{7.14}$$

Dimensionless solutions are shown in Fig. 7.9*b*.

7.2.2.2 *PILES IN COHESIONLESS SOILS*

The following assumptions are made in the analysis by Broms (1964*b*):

1. The active earth-pressure acting on the back of the pile is neglected.
2. The distribution of passive pressure along the front of the pile is equal to three times the Rankine passive pressure.
3. The shape of the pile section has no influence on the distribution of ultimate soil pressure or the ultimate lateral resistance.
4. The full lateral resistance is mobilized at the movement considered.

The simplified assumption of an ultimate soil resistance, p_u, equal to three times the Rankine passive pressure is based on limited empirical evidence from comparisons between predicted and observed ultimate loads made by Broms; these comparisons suggest that the assumed factors of 3 may in some cases be conservative, as the average ratio of predicted to measured ultimate loads is about two thirds. The distribution of soil resistance is

$$p_u = 3\sigma_v' K_p \tag{7.15}$$

where

σ_v' = effective vertical overburden pressure
$K_p = (1 + \sin\phi')/(1 - \sin\phi')$
ϕ' = angle of internal friction (effective stress)

The analysis resulting from the assumption of the above factor of 3 is much simpler than that which would follow using Brinch Hansen's variable factor K_q (Fig. 7.6). Broms's approach is equivalent to assuming that Brinch Hansen's $K_q = 3K_p$ for all depths. From Fig. 7.7, it can be seen that for values of ϕ likely to obtain in sands, $3K_p$ lies between Brinch Hansen's surface and deep values of K_q.

Unrestrained or Free-Head Piles

Possible failure-modes, soil-resistance distributions, and bending-moment distributions for "long" and "short" piles are shown in Fig. 7.11 (for constant soil unit weight γ along the pile). As before, the pile will act as a "short" pile if the maximum moment is less than the yield moment of the section. In Fig. 7.11*a*, the rotation is assumed to be about a point close to the tip, and the high pressures acting near this point are replaced by a single concentrated force at the tip. Taking moments about the toe,

$$H_u = \frac{0.5\,\gamma d L^3 K_p}{e + L} \tag{7.16}$$

This relationship is plotted in Fig. 7.12*a* using the dimensionless parameters L/d and $H_u/K_p\gamma d^3$. The maximum moment occurs at a distance f below the surface, where

$$H_u = \frac{3}{2}\gamma d K_p f^2 \tag{7.17}$$

that is,

$$f = 0.82\sqrt{\left(\frac{H_u}{dK_p\gamma}\right)}$$

The maximum moment is

$$M_{\max} = H_u\left(e + \frac{2}{3}f\right) \tag{7.18}$$

If after use of Eq. (7.16), the calculated value of H_u results in $M_{\max} > M_y$ ($M_{\max}$ from Eq. 7.18), then the pile

* If only limited head-restraint is available, solutions may be obtained by application of statical considerations similar to those described in this and the previous section.

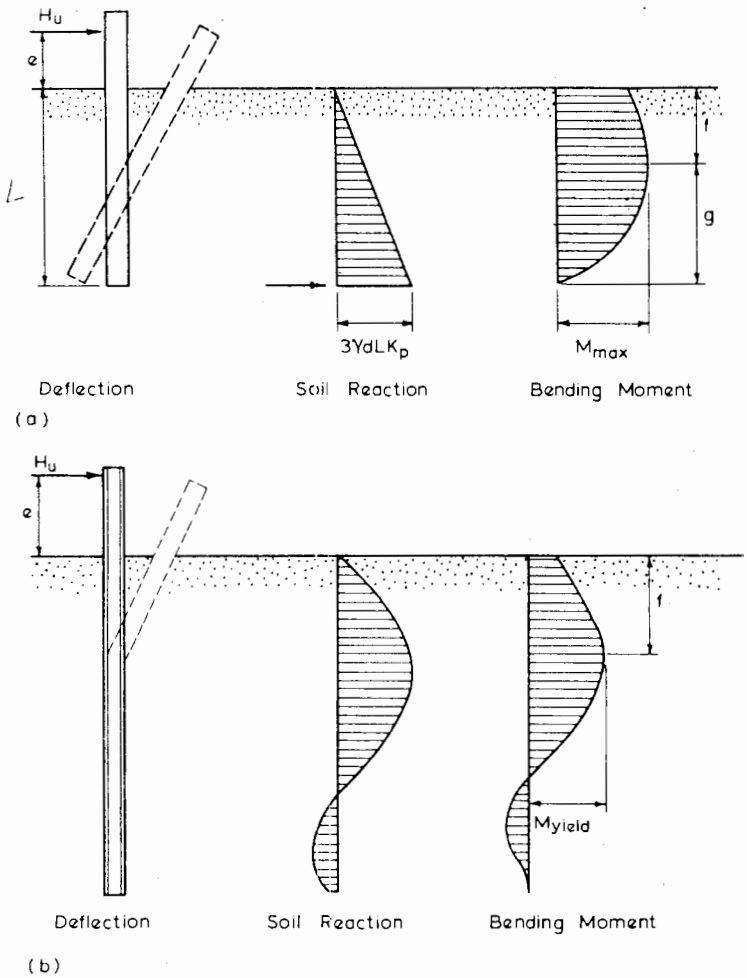

FIGURE 7.11 Free-head piles in a cohesionless soil: (a) short, (b) long (after Broms, 1964*b*).

will act as a "long" pile, and H_u may then be calculated from Eqs. (7.17) and (7.18), putting $M_{max} = M_y$. The solutions for H_u for "long" piles are plotted in Fig. 7.12*b*, in terms of $H_u/K_p\gamma d^3$ and $M_y/d^4\gamma K_p$.

For short piles, comparisons reveal that Broms's assumptions lead to higher values of ultimate load than the simple analysis given in Section 7.2. For example, for $L/d = 20$ and $e/L = 0$, Broms's solution gives a load 33% more than that derived from the simple statical analysis.

Restrained or Fixed-Head Piles

The assumption of an available moment-resistance at the top cap of at least M_y is again made. Possible failure modes for "short," "intermediate," and "long" piles are shown in Fig. 7.13. For a "short" pile (Fig. 7.13*a*), horizontal equilibrium gives

$$H_u = 1.5\gamma L^2 dK_p \tag{7.19}$$

This solution is plotted in dimensionless form in Fig. 7.12*a*. The maximum moment is

$$M_{max} = \frac{2}{3}H_u L \tag{7.20}$$

If M_{max} exceeds M_y, then the failure mode in Fig. 7.13*b* is relevant. From Fig. 7.13*b*, for horizontal equilibrium:

$$F = \left(\frac{3}{2}\gamma dL^2 K_p\right) - H_u \tag{7.21}$$

Taking moments about the top of the pile, and substituting for F from Eq. (7.21):

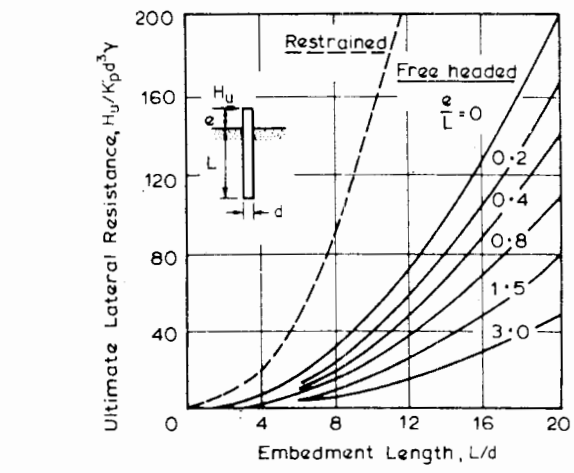

(a)

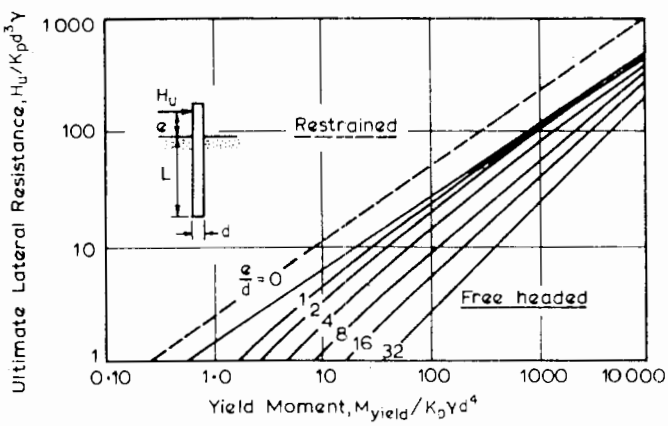

(b)

FIGURE 7.12 Ultimate lateral resistance of piles in cohesionless soils: (a) short; (b) long (after Broms, 1964*b*).

$$M_y = (0.5\gamma d\, L^3 K_p) - H_u L \tag{7.22}$$

Hence, H_u may be obtained.

This equation only holds if the maximum moment at depth f is less than M_y, the distance f being calculated from Eq. (7.17).

For the situation shown in Fig. 7.13*c*, where the maximum moment reaches M_y at two locations, it is readily found that

$$H_u\left(e + \frac{2}{3}f\right) = 2M_y \tag{7.23}$$

Dimensionless solutions from this equation are shown in Fig. 7.12*b*.

Comparisons have been made by Broms between maximum bending moments calculated from the above approach and values determined experimentally in a considerable number of tests reported in the literature. For cohesive soils, the ratio of calculated to observed moment ranged between 0.88 and 1.19, with an average value of 1.06. For cohesionless soils, this ratio ranged between 0.54 and 1.61, with an average value of 0.93. While good agreement was obtained, it was pointed out by Broms that the calculated maximum moment is not sensitive to small variations in the assumed soil-resistance distribution.

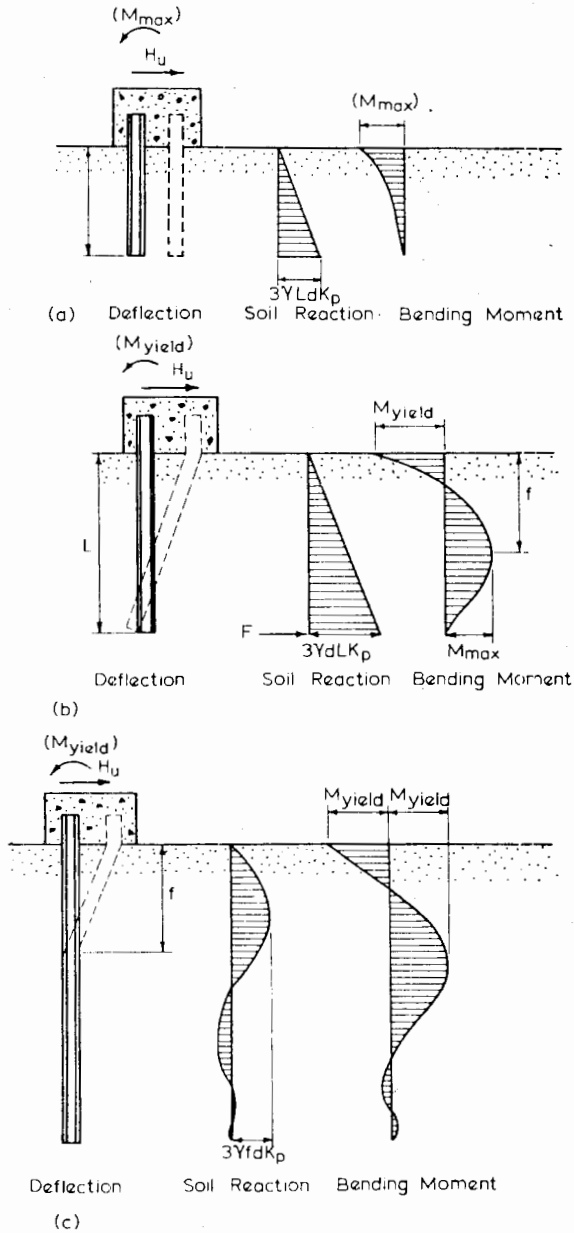

FIGURE 7.13 Restrained piles in a cohesionless soil: (a) short; (b) intermediate; (c) long.

7.2.3 Plane Strain Solutions

Solutions for a perfectly-rigid free-head plate in a purely-cohesive weightless soil have been obtained by Davis (1961) for plane-strain conditions. If it is assumed that there can be no tension between the soil and plate and that the plate is smooth, the soil pressure will act normally over the right-hand side of a portion AB of the plate, and over the left-hand side of BC, as shown in Fig. 7.14.

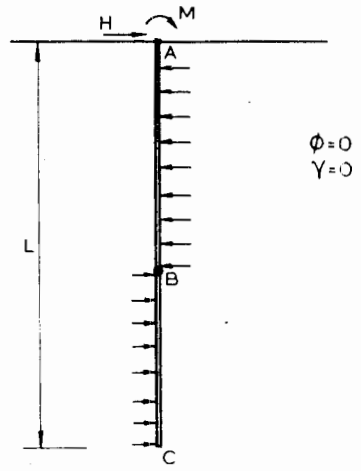

FIGURE 7.14 Plasticity analysis for laterally loaded plate.

Solutions for the failure of a strip footing near a vertical edge are then utilized. At failure, the pressure on AB is $2c$, while that on BC is given by the solution for a strip of width BC, distant AB from a vertical edge (Davis and Booker, 1973). Upper- and lower-bound solutions obtained in this way are shown in Fig. 7.15, and for practical purposes, these upper and lower bounds coincide or are only a slight distance apart. A similar approach can be employed in the case of a rough plate, by considering a rough footing under various inclinations of load (it is still assumed there is no tension between soil and plate.) A lower-bound solution for the rough-plate case is also shown in Fig. 7.15. The roughness of the plate only has an appreciable effect over a limited range of moment and load combinations. It should be emphasized that the solutions in Fig. 7.15 are for a weightless soil and will tend to be conservative for soil having appreciable weight. Also, plane-strain conditions are assumed with failure occurring in a vertical plane in contrast to failure in a horizontal plane in the analysis in Fig. 7.5. Model tests (Douglas, 1958) show satisfactory confirmation of the theory.

Comparisons between the solutions in Fig. 7.15 and those obtained from Broms's theory (Fig. 7.9) show that the ultimate lateral resistance calculated from plasticity theory is much less than that from Broms's theory—for example, for $L/d = 12$ and $e/L = 0$, the calculated ultimate loads differ by a factor of 3. This difference arises largely from the lower ultimate-soil-resistances used in the plasticity approach (a value of $2c_u$ for the portion AB and a maximum value of $5.14c_u$ for portion BC, as against Broms's value of $9c_u$), as a consequence of the assumption of plane-strain conditions.

The plasticity solutions in Fig. 7.15, while unduly conservative for normal proportions of pile, are relevant to the case of shallowly-embedded sheet piling and may be

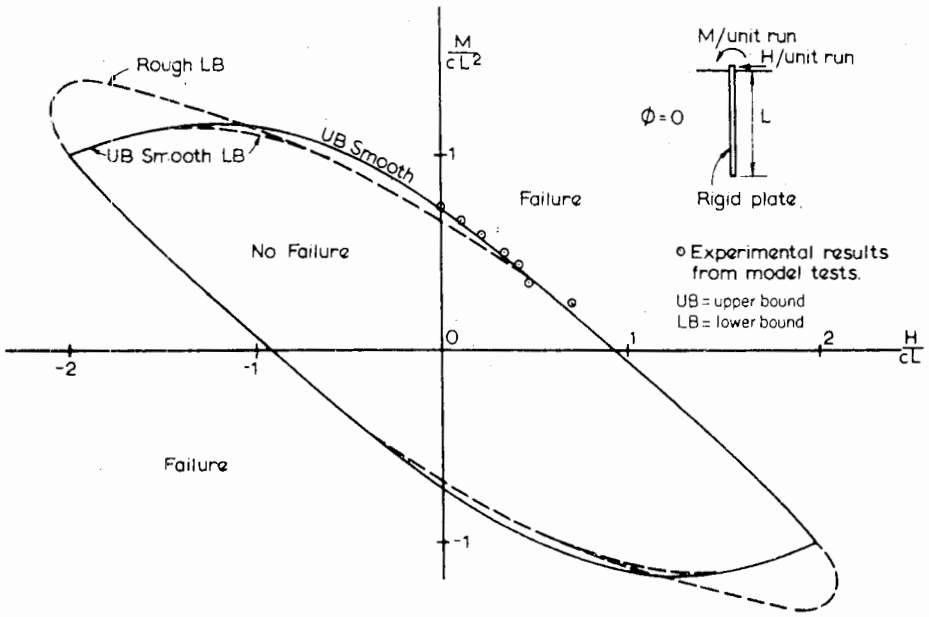

FIGURE 7.15 Failure of a rigid vertical plate under moment and horizontal load (Davis, 1961).

relevant to a group of piles closely spaced in a single long row. For the latter, the plane-strain plasticity analysis plays an analogous role for the loadings considered in this chapter to the role played by the block-bearing-capacity analysis in consideration of groups of piles subject to vertical load (Chapter 3).

7.2.4 Piles with Significant Base Resistance

Satisfactory theoretical solutions to this problem have not yet been obtained. For relatively long piles, it may be adequate, if conservative, to add the shearing resistance of the base of the pile to the ultimate lateral resistance of the pile calculated from the preceding sections. For relatively short piers, the base may provide significant moment-resistance, and this can be estimated from bearing-capacity theory for eccentric and inclined loading (e.g., Meyerhof, 1953). As the length-to-diameter ratio decreases, the center of rotation moves downward toward the base of the pile and may even be located outside the pile. In such cases, it may be desirable to consider alternative failure-mechanisms and adopt the one giving the minimum ultimate-lateral-resistance of the pier.

A reasonable engineering approach has been suggested by Roscoe (1957), who considers the presence of a horizontal shear-resistance at the interface between the base and the soil and the effect of an eccentric vertical reaction acting on the base. This reaction is balanced by the applied vertical load, the pile weight, and the vertical component of the lateral forces on the front and back of the pile. Consideration of these forces, together with those acting on the front and back of the pile, leads to a quartic expression for the position of the center of rotation. Solution of this equation enables the ultimate lateral load to be calculated. Roscoe also describes a similar analysis for tied piers, restrained to rotate about the center of the pile at the ground surface. In both analyses, however, it was assumed that the ultimate lateral pressure on the pile was the difference between the Ranking passive and active pressures; this assumption may be conservative unless the pile or pier is shallow.

7.2.5 Socketed Piles

For piles that are socketed into rock or whose tip is embedded in a firmer stratum, a modification of the preceding analyses for floating piles is necessary. A typical case is illustrated in Fig. 7.16, for a free-head pile. Here, assumed failure-modes and moment-distributions are shown together with an arbitrary distribution of ultimate soil resistance, p_u. The actual distribution of p_u may be estimated from the theories described in Section 7.2.1. It is again assumed that the effect of the high pressures near the tip may be replaced by a single force, since the center of rotation is obviously close to the tip. Considering "short" piles first: Taking moments about the tip gives

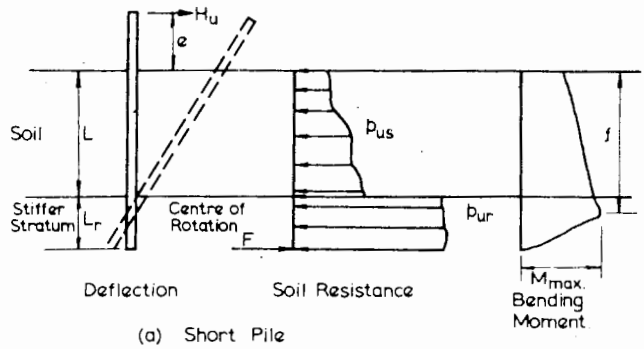

(a) Short Pile

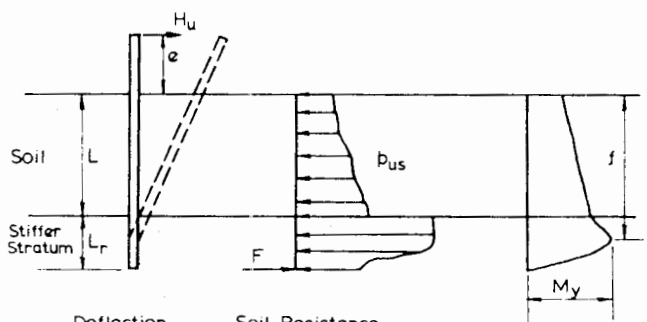

(b) Long Pile

FIGURE 7.16 Free-head socketed piles.

$$H_u = \frac{d}{(e+L)} \left(\int_0^{L_r} p_{ur}\bar{z}\,dz + \int_{L_r}^{L+L_r} p_{us}\bar{z}\,dz \right) \tag{7.24}$$

where

p_{ur} = ultimate lateral resistance of stiffer stratum
p_{us} = ultimate lateral resistance of soil
$\bar{z}$ = vertical distance, measured upward from the tip

For the value of H_u thus calculated, the maximum moment, M_{max}, must be checked. If $M_{max} < M_y$, the pile will fail as a short pile. If $M_{max} > M_y$, then the pile will fail as a long pile, and M_{max} must be equal to M_y. The position of M_{max} (distance f below the surface) may be determined by the condition of zero shear there; that is, when

$$H_u = d \int_0^f (p_{us} + \langle p_{ur} \rangle) dz \tag{7.25}$$

where

z = vertical distance, measured downward from the surface

The bracketed term $\langle p_{ur} \rangle$, in Eq. (7.25) applies only if f extends below the top of the stiffer stratum. The maximum moment is then

$$M_{max} = M_y = d \int_0^f (p_{us} + \langle p_{ur} \rangle) z dz \tag{7.26}$$

H_u may then be determined from Eqs. (7.25) and (7.26).

For piles with a restrained or fixed head, similar analyses may be carried out; these cases may be treated as extensions of the restrained-pile analyses of Broms, 1964*a* and *b* (Section 7.2.2).

7.2.6 Piles Subjected to Inclined Loading

The ultimate load capacity in this case is a function of both the lateral resistance and the vertical load capacity of the pile. When the applied load deviates only slightly from the

axial direction, failure will occur essentially by axial slip (and also bearing failure of the tip for downward loading). Lateral failure will occur when the inclination of the applied load is large, that is, as the load becomes perpendicular to the pile axis. The above two modes of failure will occur as follows:

1. Axial failure will occur when the ultimate lateral capacity exceeds the horizontal component of the ultimate inclined load: that is, when

$$H_u > Q_u \sin \delta,$$

or

$$H_u > P_u \tan \delta \tag{7.27}$$

where

Q_u = ultimate inclined-load capacity of pile
H_u = ultimate lateral capacity of pile (calculated as described earlier in this chapter)
P_u = ultimate axial-load capacity of pile (see Chapter 3)
δ = angle of inclination of load from vertical

2. Lateral failure will occur when the ultimate lateral capacity is less than the horizontal component of the ultimate inclined load: that is, when

$$H_u < P_u \tan \delta$$

For cohesive soils, it is reasonable to assume that the ultimate axial capacity of the pile is independent of the lateral component of load and that the lateral load capacity is independent of the axial component of load. The inclined-load capacity, Q_u, can then be calculated as the lesser of the following two values:

1. For axial failure,

$$Q_u = P_u \sec \delta \tag{7.29}$$

2. For lateral failure,

$$Q_u = H_u \operatorname{cosec} \delta$$

For a typical example involving a bored pier in a medium clay, the variation of ultimate load capacity with inclination of load is shown in Fig. 7.17.

7.2.6.1 *COHESIONLESS SOILS*

Yoshimi (1964) has employed the same approach as described above for cohesive soils. However, Broms (1965) has extended this approach to consider the influence of the lateral component of load on the axial load capacity. In Broms's method, the two modes of failure, axial failure and lateral failure, are again considered.

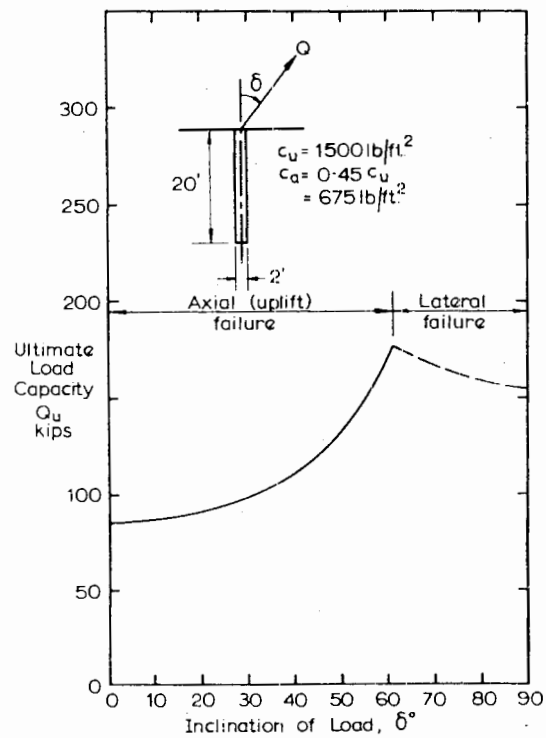

FIGURE 7.17 Example of variation of load capacity with inclination. Pier in cohesive soil.

Axial Failure

In a cohesionless soil, the lateral component of load will influence the axial load capacity of a pile. An illustration of the change in lateral pressure caused by inclination of the applied load is given in Fig. 7.18*a*. When the inclination is small, the increases in lateral pressure are small, the largest increases occurring near the top and tip of the pile. The lateral pressure is assumed to increase linearly near the surface as failure in the soil occurs, and is three to nine times the Rankine passive pressure. An idealized distribution of this change in earth pressure is shown in Fig. 7.18*b*. It is assumed by Broms that the high lateral-earth-pressure near the pile tip can be replaced by a concentrated load, and that the ultimate soil resistance is equal to five times the Rankine passive value to a depth g below the ground surface. This assumption is less conservative than Broms's earlier assumption of three times the Rankine passive value in deriving solutions for laterally-loaded vertical piles in cohesionless soils (see Section 7.2.2).

The axial load capacity, P_u, can be calculated as

$$P_u = P_{u0} + \Delta P_u \tag{7.31}$$

where

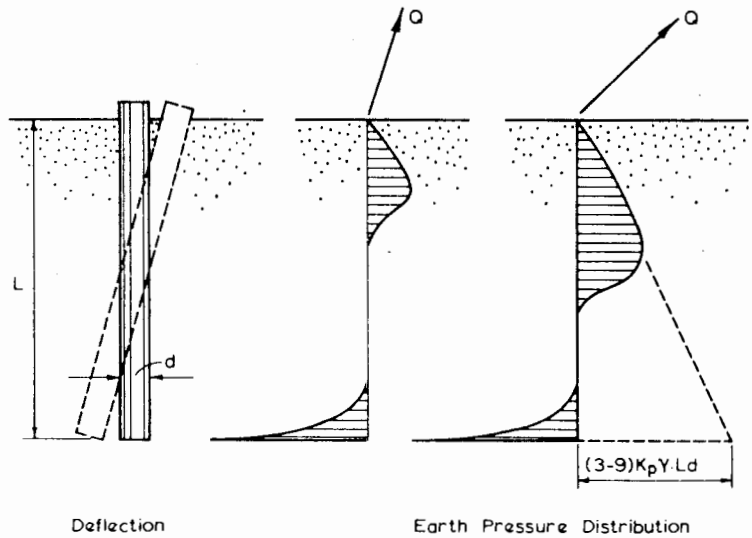

FIGURE 7.18*a* Earth-pressure distribution for oblique pull (Broms, 1965).

P_{u0} = axial capacity when the applied load acts along the pile axis

ΔP_u = increase in pullout resistance caused by the two lateral forces, T and R, in Fig. 7.18*b*

The ultimate inclined-load capacity is then

$$Q_u = P_u \sec \delta \tag{7.32}$$

Consideration of the statics of the pressure distribution in Fig. 7.18*b* enables ΔP_u, and hence Q_u, to be determined.

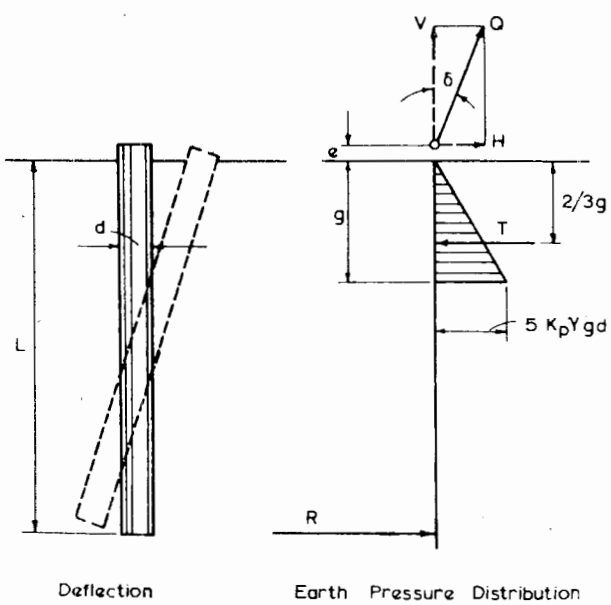

FIGURE 7.18*b* Assumed earth-pressure distribution (Broms, 1965).

Lateral Failure

If it is assumed that the vertical component of load does not affect the lateral resistance of the pile, then

$$Q_u = H_u \operatorname{cosec} \delta \tag{7.33}$$

where

H_u = ultimate lateral resistance for horizontal loading

The actual load capacity is then the lesser of the values calculated for axial and lateral failure.

For piles with a restrained head, or "long" piles (which may fail by failure of the pile itself), the approach outlined above may be extended in a similar manner to that described in Section 7.2.2.

Broms (1965) has compared predicted ultimate load capacities with those measured in the tests by Yoshimi (1964) and found reasonably good agreement. An example is shown in Fig. 7.19 for an 18-in.-long model pile in sand subjected to a load inclined at an angle of 30° to the vertical, the pile being battered at an angle β to the vertical (the pile is treated as a vertical pile loaded at an angle $\beta + 30°$ to the vertical—see next section). Also shown is the predicted ultimate load if no allowance is made for the increase in uplift capacity caused by lateral load. The latter prediction is obviously very conservative.

7.2.7 Battered Piles

The geometry of the problem is illustrated in Fig. 7.20*a*. For the normal range of pile batters employed in practice, it is reasonable to assume that the ultimate axial and normal

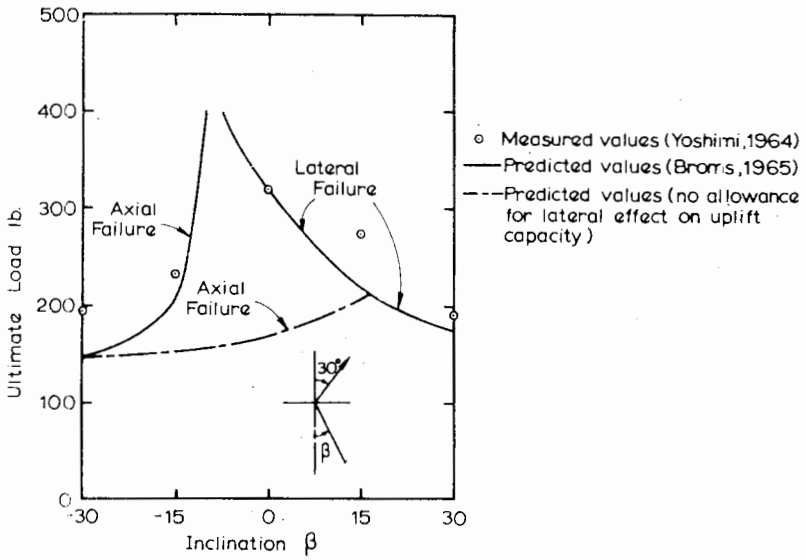

FIGURE 7.19 Predicted and observed inclined-load capacity–model pile in sand.

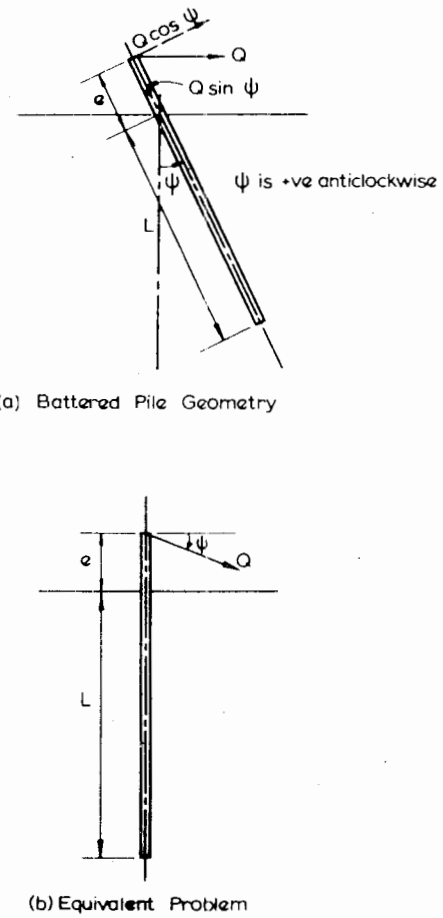

FIGURE 7.20 Battered pile.

loads are not seriously affected because of the inclination of the soil surface relative to the pile axis, so that the battered pile may be considered as an equivalent vertical pile subjected to inclined loading (Fig. 7.20*b*). The angle of inclination, δ, of the load to the vertical, as defined in Fig. 7.17, is then

$$\delta = 90^\circ + \psi \tag{7.34}$$

The ultimate load capacity, Q_u, of a battered pile can then be calculated in exactly the same manner as described in the previous section for vertical piles subjected to inclined loading.

Model tests to determine the effect of pile batter on pile-load capacity have been reported by Tschebotarioff (1953), Yoshimi (1964), and Awad and Petrasovits (1968). The similarity between the behavior of a battered pile subjected to a vertical load and a vertical pile subjected to an inclined load, as demonstrated by the latter investigators, is shown in Fig. 7.21

7.3 PILE GROUPS

7.3.1 Groups of Vertical Piles

In estimating the lateral load capacity of a pile group, an approach similar to that adopted for the calculation of vertical load capacity can be taken. The group capacity for a group of n piles is, ther., the lesser of

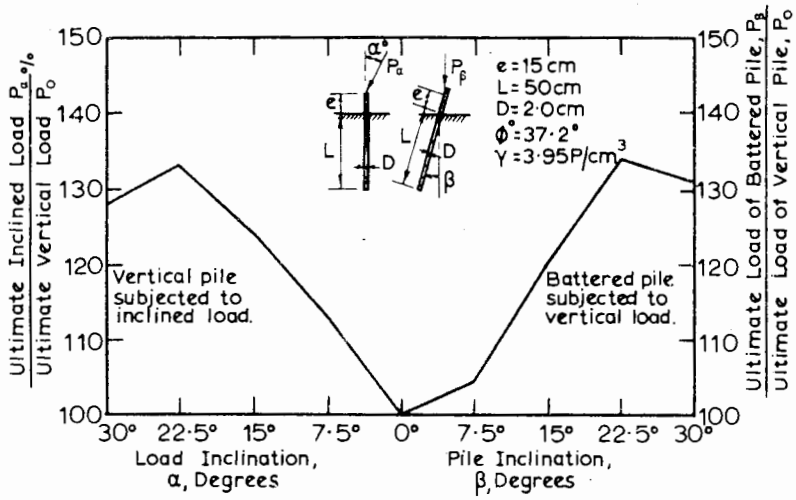

FIGURE 7.21 Load capacity of battered piles and piles subjected to inclined load (Awad and Petrasovits, 1968).

1. n times the lateral load capacity of a single pile.
2. The lateral load capacity of an equivalent single block containing the piles in the group and the soil between them.

The first value, representing individual pile failure, can be obtained by the methods described in Section 7.2. The second value, representing block failure and occurring at relatively close spacings, can be obtained as described in Section 7.2.4 for an equivalent single pile of diameter or width equal to the breadth of the group perpendicular to the direction of loading. However, in using Broms's theory for a pile group in clay, it is clearly absurd to allow a "dead" zone of zero soil-reaction of 1.5 times the group breadth, while ignoring such a zone may be unduly optimistic. A reasonable compromise is to use a "dead" zone of the lesser of $1.5d$ (d = individual pile diameter) or $0.1L$ (L = embedded length of piles). Results of a limited series of model tests suggest that the above procedure gives a reasonable estimate of the group capacity at close spacings. It the group is relatively narrow, and loaded perpendicular to the longer direction, the ultimate lateral load for block failure may be estimated from the plasticity solutions in Fig. 7.15. For a group of fixed-head piles, with the head embedded in a massive cap, the ultimate load for block failure can be calculated as the sum of the resistance of a short restrained pile (e.g., see Fig. 7.9 and 7.12) and the shear resistance of the base. Some allowance may also be made for side shear resistance of the block.

The concept of a group efficiency for lateral loading, η_L, can be employed as with group efficiency for vertical loading, where for a group of n piles,

$$\eta_L = \frac{\text{Ultimate lateral-load capacity of group}}{n \times \text{ultimate lateral load capacity of single pile}} \qquad (7.35)$$

A relatively small amount of data is available for values of η_L. A series of tests on model pile groups in clay was carried out by Prakash and Saran (1967) while Oteo (1972) carried out similar tests in sand; the values of η_L derived from these test results are shown in Fig. 7.22. η_L decreases with increasing numbers of piles in a group or with decreasing

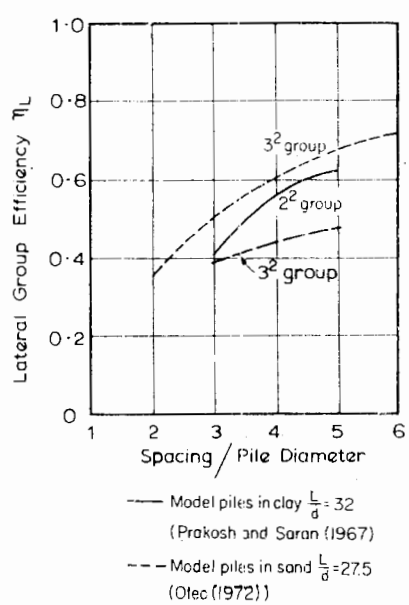

FIGURE 7.22 Lateral group efficiency from model tests.

spacing. Comparison with the efficiency values (η) for axially loaded groups shows that $\eta_L < \eta$, or in other words, that groups are less efficient under lateral loading than under axial loading. Model tests on three- and seven-pile dolphins embedded in sand overlying silty clay have been described by Tschebotarioff (1953). For the three-pile group (a central vertical pile and two outer battered at 10°), and efficiency η_L of 0.77 was calculated, the pile spacing at the ground line being about nine diameters. For the seven-pile dolphin, containing a central vertical pile surrounded by piles battered at 5°, with a spacing at the ground line of about three diameters, η_L = 0.52. Because of the effects of pile batter and the layered soil profile, direct comparison between Tschebotarioff's results and those shown in Fig. 7.22 is not possible; nevertheless, the values of η_L in the two series of tests appear to be reasonably consistent.

Finite-element analyses provide a means of theoretically estimating the lateral efficiency of a pile group. By carrying out a plane-strain analysis of the pile group in plan, and employing a nonlinear stress-strain relationship for the soil, a load-deflection curve may be obtained for the pile group (on the assumption that the piles are infinitely long). By comparing the maximum load capacity from this analysis with the corresponding value for a single pile, an estimate of the group lateral efficiency may be made. Analyses of this type have been performed by Yegian and Wright (1973) and Moser (1973). The solutions obtained by Yegian and Wright show that the efficiency of two or more piles in a row is considerably less when the horizontal loading is in a direction parallel to the line joining the piles than when it is perpendicular. For example, for two piles at center-to-center spacing of two diameters, the efficiency is about 0.72 for loading parallel to the piles, but 0.90 for loading perpendicular to the piles.

In designing the individual piles in the group, it is desirable to determine the load distribution within the group. Methods for such determinations are described in Chapter 9 for groups subjected to a general system of loading, and although these methods are strictly valid only for working-load conditions, they probably give a reasonable estimate of the failure load distribution. In practice, a widely used and relatively simple design-method of determining the load distribution in a group with a rigid cap is to assume that the piles in the group carry equal proportions of the applied horizontal and vertical load, together with additional vertical loads that are proportional to the distances of the piles from the group's center of gravity and thereby balance the applied moment. This approach ignores the effect of the soil and considers the pile group simply as a structural system.

7.3.2 Groups Containing Battered Piles

As with groups of vertical piles, the ultimate lateral-load capacity of groups containing battered piles may be taken as the lesser of

1. The sum of the lateral load capacities the individual piles in the group.
2. The load capacity of the group acting as a single block.

The first value can be estimated from Section 7.2.1 or Section 7.2.2 for vertical piles and Section 7.2.4 for battered piles. The second value can be estimated in a similar fashion to that described for vertical groups, but now allowing for the battered piles. If an analysis of the type described by Roscoe (1957) is employed, such allowance may be made by considering the resultant forces on the front and back of the group to act on inclined surfaces, if the front and back piles are battered. The base shear-resistance may also be assumed to act over the plan area of the group at the level of the pile tips. Alternatively, and more simply, an equivalent block with vertical sides may be considered. Both of these approaches imply that if the group fails as a single block, the ultimate lateral-load capacity of the group depends on the batter of the outer piles only, and not on the batter of interior piles. Some confirmation that this implication is reasonable may be seen from the results of model-pile tests in clay carried out by Simek (1966), who found that little benefit was

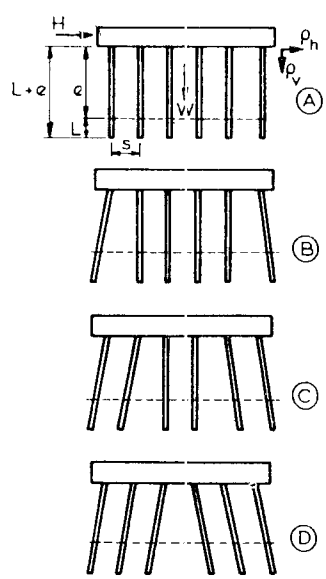

FIGURE 7.23 Model groups tested by Simek (1966).

derived by having battered piles additional to those at the end of the group. The benefits of having the end piles battered were found to be particularly marked when the piles were embedded in the soil for only a relatively small distance. Four group-configurations were tested by Simek, as shown in Fig. 7.23, and the results of these tests are summarized in Table 7.1. The ultimate lateral load capacity, H_u, is expressed as a percentage of the total weight, W, of the group, and it is seen from Table 7.1 that H_u/W increases significantly with increasing embedded length. Also, as indicated above, the effect of batter in increasing lateral-load capacity decreases as the embedded length increases, and for 75% embedment, has virtually no effect.

TABLE 7.1 SUMMARY OF MODEL GROUP TESTS OF SIMEK (1966)

Group	Relative Embedded Length, $L/(L+e)$	Relative Load Capacity, H_u/W	Relative Lateral Movement at Failure, $(\rho/s)\%$
	0.25	0.42	3.5
A	0.50	1.90	5.0
	0.75	5.70	7.0
	0.25	0.98	5.0
B	0.50	2.02	6.0
	0.75	5.62	7.0
	0.25	1.09	5.0
C	0.50	2.10	6.0
	0.75	5.55	7.0
	0.25	1.10	5.0
D	0.50	2.58	6.0
	0.75	5.10	7.0

7.4 USE OF PILES TO INCREASE SLOPE STABILITY

Broms (1972) describes the use of inclined timber piles to increase the slope stability of very soft clays, while large-diameter cast-in-place piles have been used in the United States to stabilize active landslide areas in stiff clays and shales through dowel action. The diameter of these piles varies between 1.0 and 1.5 m. In Japan, 300-mm-diameter steel-pipe piles reinforced with steel H-piles have been used for the same purpose. The piles are generally placed in predrilled holes close to the bottom of the slope, where the shear deformations in the soil are largest. Fukuoka (1977) describes further uses of piles to stabilize landslides and presents a method for analyzing the resulting moments and deflections in the pile. The possibilities of a finite-element analysis of this form of stabilization have been discussed by Rowe and Poulos (1979), who have employed the technique for analyzing soil-structure interaction described by Rowe et al., (1978).

In order to make an approximate estimate of the influence of piles on the factor of saftety against slope failure, the theory for ultimate lateral resistance presented in this chapter may be utilized. Referring to Fig. 7.24, if

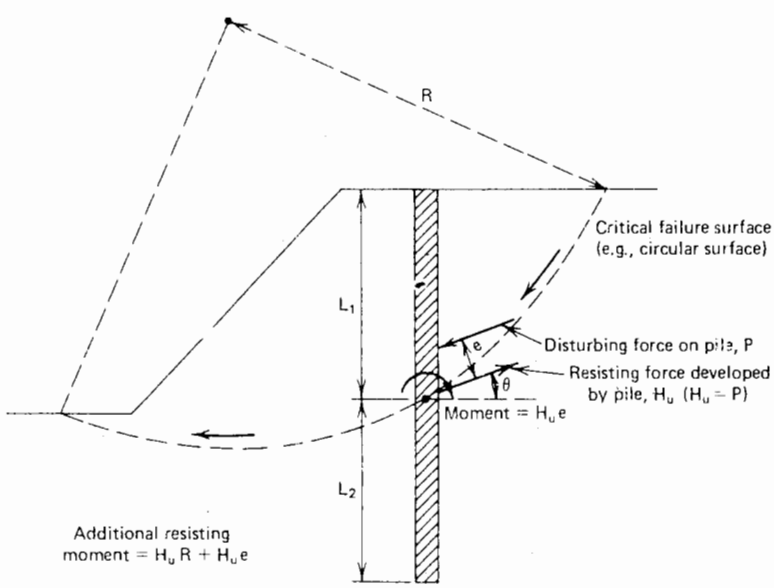

FIGURE 7.24 Analysis of effect of pile on slope stability.

a pile is installed in the slope, the portion of the pile (length L_1) above the assumed failure surface will be subjected to an inclined disturbing force P at some eccentricity e above this surface. Ignoring any axial resistance for simplicity, this disturbing force can be considered to be resisted by the lower portion of the pile (length L_2) below the critical failure surface. The maximum value of this resisting force, H_u, is given by the least of the following four values:

1. The ultimate lateral resistance of a "short" pile of length L_2 loaded at an eccentricity e.
2. The ultimate lateral resistance of a "long" pile loaded at an eccentricity e (this value will depend on the yield moment of the pile).
3. The ultimate load that can be developed along the upper part (length L_1) of the pile if the soil flows past the pile and the ultimate pile-soil pressure is developed along this portion of the pile.
4. The shear resistance of the pile section itself.

The values in 1, 2, and 3 may be obtained from the analysis presented in Section 7.2, once the ultimate pile-soil pressure distribution has been determined. Approximate allowance can be made for the inclination, as outlined in Section 7.2.6. The eccentricity e can, as a first approximation, be estimated by assuming full mobilization of the pile-soil pressure above the assumed failure surface.

Once the value of H_u has been thus determined, the additional resisting moment or force caused by the pile can be determined, and hence the effect on the safety factor can be evaluated (see Fig. 7.24). The procedure must be repeated for a series of trial failure surfaces to find the one with the lowest safety factor. Consideration should also be given to a surface that passes below the pile tips.

With groups of piles, adjustments can be made to the ultimate pile-soil pressures to allow for group effects, and the influence of each pile can be added up to determine the effect of the group on slope stability.

7.5 METHODS FOR INCREASING THE LATERAL RESISTANCE OF PILES

Broms (1972) has discussed some methods of increasing the lateral resistance of piles. As shown in Fig. 7.25, most of

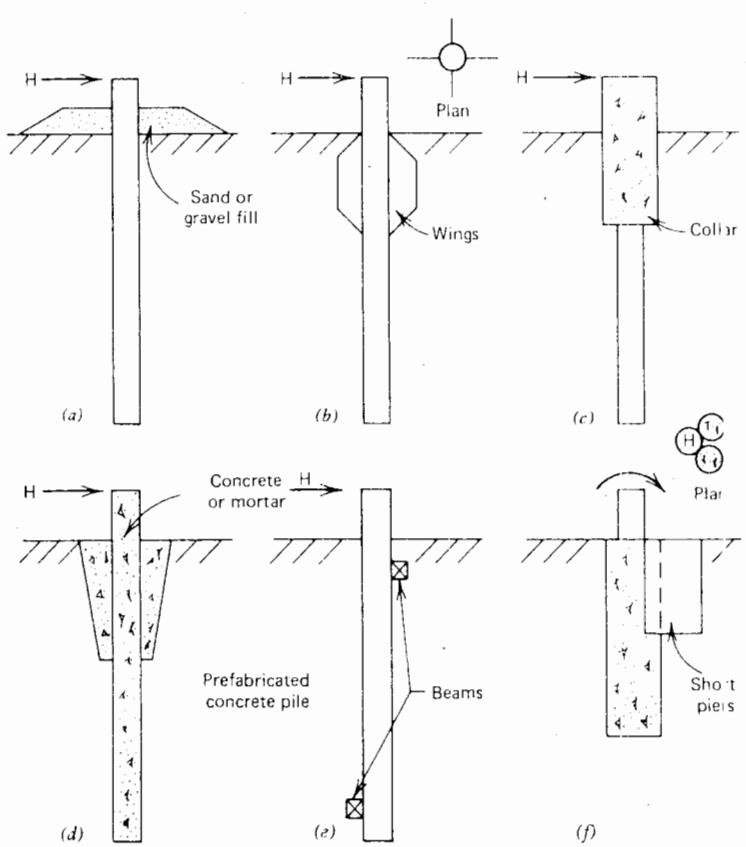

FIGURE 7.25 Methods used to increase the lateral resistance of piles.

these methods rely on increasing the dimensions and/or stiffness of the piles near the ground surface. The use of a sand or gravel fill placed around a pile (Fig. 7.25*a*) is very effective for soft clays when the piles are subjected to cyclic loads. The fill gradually works itself down into the clay and increases the effective diameter of the piles. The height of the fill around the piles is limited, however, by the bearing capacity of the underlying soil.

8

LOAD-DEFLECTION PREDICTION FOR LATERALLY LOADED PILES

8.1 INTRODUCTION

In designing pile foundations to resist lateral loads, the criterion for design in the majority of cases is not the ultimate lateral capacity of the piles, but the maximum deflection of the piles. The allowable deflection may be relatively large for temporary structures or tied retaining walls, but only small movements can be tolerated in such structures as tied abutments to bridges, or in the foundations of tall structures. Design practice in the past has frequently made use of empirical information for pile design; for example, that provided by McNulty (1956) from full-scale lateral-load tests, as shown in Table 8.1. In recent years, however, theoretical approaches for predicting lateral movements have been developed extensively. Two approaches have generally been employed:

1. The subgrade-reaction approach, in which the continuous nature of the soil medium is ignored and the pile reaction at a point is simply related to the deflection at that point,
2. The elastic approach, which assumes the soil to be an ideal elastic continuum.

TABLE 8.1 SUGGESTED SAFE ALLOWABLE LATERAL FORCES[a] ON VERTICAL PILES, KIPS (MCNULTY, 1956)

Pile Type	Medium Sand	Fine Clay	Medium Clay
Free-head timber, 12-in. dia.	1.5	1.5	1.5
Fixed-head timber, 12-in. dia.	5.0	4.5	4.0
Free-head concrete, 16-in. dia.	7.0	5.5	5.0
Fixed-head concrete, 16-in. dia.	7.0	5.5	5.0

[a] Based on a safety factor of 3 applied to the load required for 0.25-in. deflection.

The subgrade-reaction model of soil behavior, which was originally proposed by Winkler in 1867, characterizes the soil as a series of unconnected linearly-elastic springs, so that deformation occurs only where loading exists. The obvious disadvantage of this soil model is the lack of continuity; real soil is at least to some extent continuous,

since the displacements at a point are influenced by stresses and forces at other points within the soil. A further disadvantage is that the spring modulus of the model (the modulus of subgrade reaction) is dependent on the size of the foundation. In spite of these drawbacks, the subgrade-reaction approach has been widely employed in foundation practice because it provides a relatively simple means of analysis and enables factors such as nonlinearity, variation of soil stiffness with depth, and layering of the soil profile to be taken into account readily, if only approximately. In addition, despite the many difficulties in determining the modulus of subgrade reaction of real soil, a considerable amount of experience has been gained in applying the theory to practical problems, and a number of empirical correlations are available for determining the modulus.

From a theoretical point of view, the representation of the soil as an elastic continuum is more satisfactory, as account is then taken of the continuous nature of soil. The use of this model for the analysis of the settlement of piles and pile groups, as described in Chapters 5 and 6, has been found to provide a convenient and relatively reliable means of describing pile behavior under axial loading. While the elastic model is an idealized representation of real soil, it can be modified to make allowance for soil yield and can also be used to give approximate solutions for varying modulus with depth and for layered systems. In addition, it has the important advantage over the subgrade-reaction approach of enabling analysis to be made of group action of piles under lateral loads; also, it provides a means of analyzing the behavior of battered piles subjected to a general system of loading (Chapter 9). A further advantage of the elastic model is that it enables consistent analysis of both immediate movements and total final movements. The major drawback to the application of the elastic method to practical problems is the difficulty of determining the appropriate soil moduli; however, this difficulty also exists to a certain extent with the subgrade-reaction method.

The exact solution of the problem of a laterally loaded flexible pile in an elasto-plastic soil mass is a complicated and difficult one in three-dimensional continuum mechanics and does not appear to have been satisfactorily solved at present. Some attempts include two-dimensional finite element treatments in the horizontal plane (Yegian and Wright, 1973; Baguelin and Frank, 1979; Rowe and Poulos, 1979); a special finite element technique which is capable of dealing with general three-dimensional loading for axi-symmetric geometries, but only for elastic conditions (Randolph, 1977; Banerjee and Davies, 1978); and general three-dimensional elastic finite element analysis but with allowance for axial slip via the use of joint elements (Desai and Appel, 1976). Such analyses are too restrictive (for example only elastic), or too time consuming, or too uncertain with regard to accuracy to be entirely suitable for parametric studies.

In this chapter, the application of both the subgrade-reaction and elastic approaches to the analysis of a single pile is described in detail, and in each case, the available data on the relevant soil parameters is reviewed. The extension of the elastic approach to the estimation of group movements is then described.

8.2 SUBGRADE-REACTION ANALYSIS

8.2.1 Basic Theory

In the Winkler soil model, the pressure p and deflection ρ at a point are assumed to be related through a modulus of subgrade reaction, which for horizontal loading, is denoted as k_h. Thus,

$$p = k_h \rho \tag{8.1}$$

where k_h has the units of force/length^3. Equation (8.1) has been restated frequently (e.g., Reese and Matlock, 1956; Davisson and Gill, 1963) as

$$w = K\rho \tag{8.1a}$$

where

w = soil reaction per unit-length of pile
K = subgrade-reaction modulus, in units of force/length^2 ($K = k_h d$)
d = diameter or width of pile

The pile is usually assumed to act as a thin strip whose behavior is governed by the beam equation

$$E_p I_p \frac{d^4\rho}{dz^4} = -pd \tag{8.2}$$

where

E_p = modulus of elasticity of pile
I_p = moment of inertia of pile section
z = depth in soil
d = width or diameter of pile

As in the simple theory of bending of beams, the effect of axial load in the pile is ignored. (The effect of

axial load in relation to buckling is discussed in Chapter 14.) From Eqs. (8.1) and (8.2), the governing equation for the deflection of a laterally loaded pile is

$$E_p I_p \frac{d^4\rho}{dz^4} + k_h d\rho = 0 \tag{8.3}$$

Solutions to the above equation may be obtained either analytically or numerically Analytical solutions are only available in convenient f . 1 for the case of constant k_h along the pile. For other distributions of k_h, solutions are most conveniently obtained by a numerical finite-difference method (Palmer and Thompson, 1948; Gleser, 1953).
In this method, the basic differential equation (8.3) is written in finite-difference form; for a typical point i, this equation is (referring to Fig. 8.1)

$$E_p I_p \left[\frac{\rho_{i-2} - 4\rho_{i-1} + 6\rho_i - 4\rho_{i+1} + \rho_{i+2}}{\delta^4}\right] + (k_i d\rho_i) = 0 \tag{8.4}$$

that is,

$$\rho_{i-2} - 4\rho_{i-1} + a_i\rho_i - 4\rho_{i+1} + \rho_{i+2} = 0 \tag{8.4a}$$

where

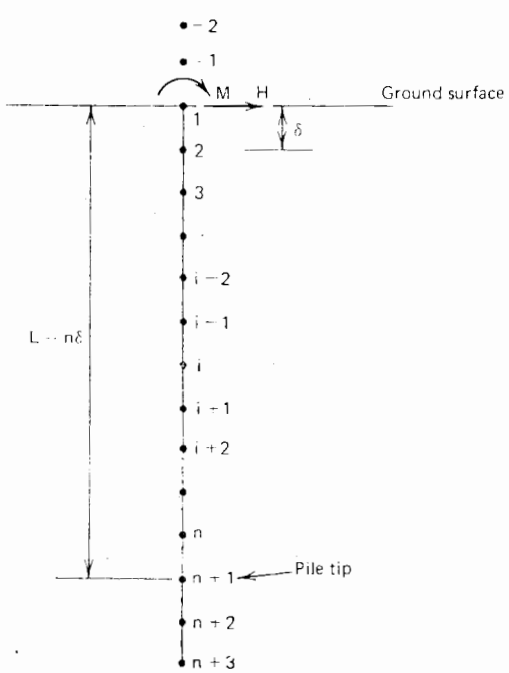

FIGURE 8.1 Finite-difference analysis of laterally loaded piles.

$$a_i = 6 + \frac{k_i L^4 d}{E_p I_p n^4}$$

n = number of intervals along pile
k_i = modulus of subgrade reaction k_h at i

Equation (8.4*a*) may be applied to points 2 to n to give $n - 1$ equations.

Four further equations may be obtained from the boundary conditions at the top and tip of the pile. At the top of the pile, two conditions may be considered;

1. A free-head pile, for which

$$\text{shear} = E_p I_p\left(\frac{d^3\rho}{dz^3}\right) = H$$

that is,

$$-\rho_{-2} + 2\rho_{-1} - 2\rho_2 + \rho_3 = \frac{HL^3}{E_p I_p n^3} \tag{8.5}$$

$$\text{and moment} = E_p I_p\left(\frac{d^2\rho}{dz^2}\right) = M$$

that is,

$$\rho_2 - 2\rho_1 + \rho_{-1} = \frac{ML^2}{E_p I_p n^2} \tag{8.6}$$

2. A fixed-head pile, for which Eq. (8.5) still applies, and also,

$$\text{rotation} = E_p I_p \frac{d\rho}{dz} = 0$$

that is,

$$\rho_2 - \rho_{-1} = 0 \tag{8.7}$$

At the tip of the pile, assuming a floating pile with a free tip

$$\text{shear} = E_p I_p \frac{d^3\rho}{dz^3} = 0$$

that is,

$$-\rho_{n-1} + 2\rho_n - 2\rho_{n+2} + \rho_{n+3} = 0 \tag{8.8}$$

$$\text{and moment} = E_p I_p \frac{d^2\rho}{dz^2} = 0$$

that is,

$$p_n - 2p_{n+1} + p_{n+2} = 0 \tag{8.9}$$

The final two equations required come from equilibrium of horizontal forces and moments. A system of $n + 5$ simultaneous equations is obtained for the $n + 5$ unknown displacements (those at points -2, -1, $n + 2$, and $n + 3$ are of course fictitious).

As an alternative to the above procedure, the shear equations at the top and tip of the pile (Eqs. 8.5 and 8.8) may be omitted, thus omitting the unknown displacements at points -2 and $n + 3$. In this case, only $n + 3$ equations are solved. This procedure has been found to give almost identical solutions to the previous procedure.

By using the finite-difference method, any variations of k_h with depth may be considered. Distributions of k_h relevant to various types of soil are discussed below. Solutions for various linear distributions of k_h are described in Section 8.2.2.

8.2.1.1 COEFFICIENT OF SUBGRADE REACTION, k_h

The analysis of pile behavior using the subgrade-reaction approach requires a knowledge of the variation of k_h along the pile. Several distributions of k_h have been employed, the most widely used being that developed by Palmer and Thompson (1948), which is of the form

$$k_h = k_L\left(\frac{z}{L}\right)^n \tag{8.10}$$

where

k_L = value of k_h at the pile tip ($z = L$)
n = an empirical index equal to or greater than zero

The most common assumptions are that $n = 0$ for clay—that is, that the modulus is constant with depth—and that $n = 1$ for granular soils—that is, that the modulus increases linearly with depth.

Davisson and Prakash (1963) suggest, however, that $n = 0.15$ is a more realistic value for clays (presumably under undrained conditions), as this has the effect of including some allowance for plastic soil behavior at the surface.

As an alternative to using $n = 0.15$ for clays, Davisson (1970) suggests that an equivalent solution may be obtained by considering the soil as a two-layer system, the upper layer having a value of k_h of 0.5 times the value for the lower layer, and a thickness equal to $0.4R$, where $R = (E_p I_p / k_0 d)^{1/4}$, k_0 being the coefficient of subgrade reaction for the lower layer.

For the case $n = 1$, it is convenient to reexpress the variation of k_h as follows:

$$k_h = n_h\left(\frac{z}{d}\right) \tag{8.11}$$

where

n_h = coefficient of subgrade reaction (units of force/length^3)
z = depth below surface
d = pile width or diameter

For real soils, the relationship between soil pressure p and deflection ρ is nonlinear, with the soil pressure reaching a limiting value when the deflection is sufficiently large (in some cases, "strain-softening" may subsequently occur). The most satisfactory approach to deflection prediction is to carry out a nonlinear analysis of the type described in Section 8.2.4. However, if linear theory is to be used, it is necessary to choose appropriate secant values of the subgrade modulus. Reese and Matlock (1956) argue that the adoption of a linearly increasing modulus of subgrade reaction with depth takes some account of soil yield and nonlinearity, as values of the secant modulus near the top of the pile are likely to be very small, but will increase with depth because of both a higher soil strength and lower levels of deflection. Reese and Matlock's argument is most relevant to piles in sand and soft clay. In some cases—for example, relatively stiff piles in overconsolidated clay at relatively low load-levels—the assumption of a constant subgrade modulus with depth may be more appropriate.

Solutions for the simple cases of constant subgrade modulus with depth, and linearly increasing modulus with depth, are described below.

8.2.2 Solutions to Linear Theory

8.2.2.1 CONSTANT k_h WITH DEPTH

Solutions to Eq. (8.3) in closed form have been obtained by Hetenyi (1946). For horizontal load H applied at ground level to a free-head or unrestrained pile of length L, the following solutions are given by Hetenyi for horizontal displacement ρ, slope θ, moment M, and shear Q at a depth z below the surface:

$$\rho = \frac{2H\beta}{k_h d} \times \left[\frac{\sinh \beta L \cos \beta z \cosh \beta(L - z) - \sin \beta L \cosh \beta z \cos \beta(L - z)}{\sinh^2 \beta L - \sin^2 \beta L}\right] \tag{8.12}$$

$$= \frac{2H\beta}{k_h d} \cdot K_{\rho H} \tag{8.12a}$$

$$\theta = \left(\frac{2H\beta^2}{k_h d}\right)\left(\frac{1}{\sinh^2 \beta L - \sin^2 \beta L}\right) \times \tag{8.13}$$

$$\Big(\sinh \beta L[\sin \beta z \cosh \beta(L - z) + \cos \beta z \sinh \beta(L - z)]$$

$$+ \sin \beta L[\sinh \beta z \cos \beta(L - z) + \cosh \beta z \sin \beta(L - z)]\Big)$$

$$= \frac{2H\beta^2}{k_h d} \cdot K_{\theta H} \tag{8.13a}$$

$$M = -\left(\frac{H}{\beta}\right) \times \tag{8.14}$$

$$\left[\frac{\sinh \beta L \sin \beta z \sinh \beta(L - z) - \sin \beta L \sinh \beta z \sin \beta(L - z)}{\sinh^2 \beta L - \sin^2 \beta L}\right].$$

$$= -\frac{H}{\beta} \cdot K_{MH} \tag{8.14a}$$

$$Q = -\left(\frac{H}{\sinh^2 \beta L - \sin^2 \beta L}\right)\Big(\sinh \beta L[\cos \beta z \tag{8.15}$$

$$\sinh \beta(L - z) - \sin \beta z \cosh \beta(L - z)] - \sin \beta L[\cosh \beta z$$

$$\sin \beta(L - z) - \sinh \beta z \cos \beta(L - z)]\Big)$$

$$= -H \cdot K_{QH} \tag{8.15a}$$

where

$$\beta = (k_h d/4E_p I_p)^{1/4} \tag{8.16}$$

The corresponding expressions for moment loading M_0 applied at the ground surface are

$$\rho = \frac{2M_0\beta^2}{k_h d}\left(\frac{1}{\sinh^2 \beta L - \sin^2 \beta L}\right)\Big(\sinh \beta L \tag{8.17}$$

$$[\cosh \beta(L - z) \sin \beta z - \sinh \beta(L - z) \cos \beta z] + \sin \beta L$$

$$[\sinh \beta z \cos \beta(L - z) - \cosh \beta z \sin \beta(z - L)]\Big)$$

$$= \frac{2M_0\beta^2}{k_h d} \cdot K_{\rho M} \tag{8.17a}$$

$$\theta = \left(\frac{4M_0\beta^3}{k_h d}\right) \times \tag{8.18}$$

$$\left[\frac{\sinh \beta L \cosh \beta(L - z) \cos \beta z + \sin \beta L \cosh \beta z \cos \beta(L - z)}{\sinh^2 \beta L - \sin^2 \beta L}\right]$$

$$= \frac{4M_0\beta^3}{k_h d} \cdot K_{\theta M} \tag{8.18a}$$

$$M = \frac{M_0}{\sinh^2 \beta L - \sin^2 \beta L}\Big(\sinh \beta L[\sinh \beta(L - z) \tag{8.19}$$

$$\cos \beta z + \cosh \beta(L - z) \sin \beta z] - \sin \beta L[\sinh \beta z \cos$$

$$\beta(L - z) + \cosh \beta z \sin \beta(L - z)]\Big)$$

$$= M_0 \cdot K_{MM} \tag{8.19a}$$

$$Q = \frac{-2M_0\beta}{\sinh^2 \beta L - \sin^2 \beta L}[\sin \beta L \sin \beta(L - z) \tag{8.20}$$

$$\sin \beta z + \sin \beta L \sinh \beta z \sin \beta(L - z)]$$

$$= -2M_0\beta \cdot K_{QM} \tag{8.20a}$$

Solutions for the case of a fixed-head or restrained pile may be obtained from the above solutions for a free-head pile by adding to the solutions for horizontal loading H, the solutions for an applied moment of

$$M_0 = -\left(\frac{H}{2\beta}\right)\left[\frac{K_{\theta H}(z = 0)}{K_{\theta M}(z = 0)}\right] \tag{8.21}$$

(This is the applied moment required to produce zero slope at the pile head—i.e., the fixing moment).

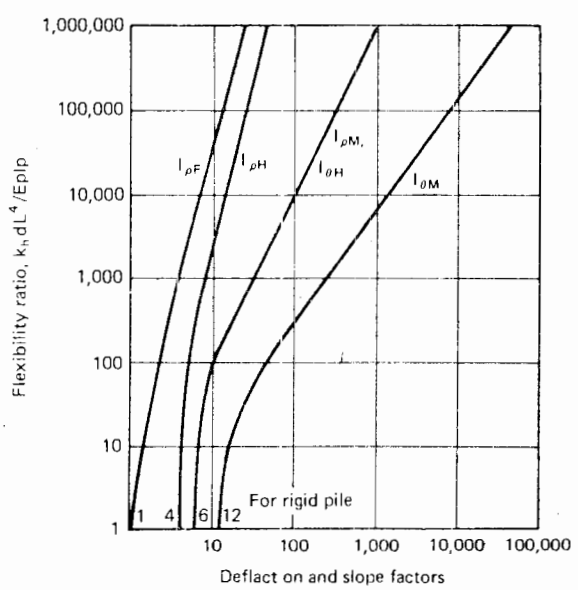

FIGURE 8.2 Top deflection and rotation for lateral loads on vertical piles for constant k_h (after Barber, 1953). (Reprinted by permission of the American Society for Testing and Materials, © 1953.)

Values for the dimensionless coefficients $K_{\rho H}$, $K_{\theta H}$, and so on, are given in Table 8.2. For deflections and rotations at the soil surface, convenient plots presented by Barber (1953) are shown in Fig. 8.2. For a free-head or unrestrained pile,

$$\text{deflection, } \rho = \left(\frac{H}{k_h dL}\right) \cdot I_{\rho H} + \left(\frac{M}{k_h dL^2}\right) \cdot I_{\rho M} \quad (8.22)$$

$$\text{rotation, } \theta = \left(\frac{H}{k_h dL^2}\right) \cdot I_{\theta H} + \left(\frac{M}{k_h dL^3}\right) \cdot I_{\theta M} \quad (8.23)$$

For a fixed-head pile, which is free to translate, but not to rotate,

$$\text{deflection, } \rho = \frac{H}{k_h dL} \cdot I_{\rho F} \quad (8.24)$$

In Eqs. (8.23) and (8.24),

H = applied horizontal force at ground level
M = moment at ground level
d = pile diameter
L = pile length
$I_{\rho H}, I_{\rho M}, I_{\theta H}, I_{\theta M}, I_{\rho F}$ = deflection- and rotation-influence factors in Fig. 8.2 (by the reciprocal theorem, $I_{\theta H} = I_{\rho M}$).

For a free-head pile, of embedded length L, subjected to a horizontal load H at an eccentricity e above the ground surface, the following limiting solutions apply for horizontal displacement and rotation at the ground line:

1. Rigid pile (holds if $\beta L < 1.5$):

$$\rho = \frac{4H(1 + 1.5e/L)}{k_h dL} \quad (8.25)$$

$$\theta = \frac{6H(1 + 2e/L)}{k_h dL^2} \quad (8.26)$$

2. Infinitely long pile (holds if $\beta L > 2.5$):

$$\rho = \frac{2H\beta(e\beta + 1)}{k_h d} \quad (8.27)$$

$$\theta = \frac{2H\beta^2(1 + 2e\beta)}{k_h d} \quad (8.28)$$

For a fixed-head pile, the limiting solutions are

1. Rigid pile ($\beta L < 0.5$)

$$\rho = \frac{H}{k_h dL} \quad (8.29)$$

2. Infinitely long pile ($\beta L > 1.5$):

$$\rho = \frac{H\beta}{k_h d} \quad (8.30)$$

8.2.2.2 SOLUTIONS FOR LINEARLY VARYING k_h WITH DEPTH

Convenient closed-form solutions are not available for this case, but the following limiting-solutions apply for free-head piles (Barber, 1953):

TABLE 8.2 INFLUENCE FACTORS FOR CONSTANT k_h

βL	z/L	$K_{\rho H}$	$K_{\theta H}$	K_{MH}	K_{QH}	$K_{\rho M}$	$K_{\theta M}$	K_{MM}	K_{QM}
2.0	0.	1.1376	1.1341	0.	1.0000	−1.0762	1.0762	1.0000	0.
2.0	0.0625	0.9964	1.1200	0.1080	0.7333	−0.8807	0.9519	0.9836	0.1256
2.0	0.1250	0.8586	1.0828	0.1848	0.5015	−0.6579	0.8314	0.9397	0.2214
2.0	0.1875	0.7264	1.0298	0.2347	0.3035	−0.4644	0.7178	0.8751	0.2913
2.0	0.2500	0.6015	0.9673	0.2620	0.1377	−0.2982	0.6133	0.7959	0.3387
2.0	0.3125	0.4848	0.9004	0.2704	0.0021	−0.1569	0.5192	0.7073	0.3669
2.0	0.3750	0.3764	0.8333	0.2637	−0.1054	−0.0376	0.4366	0.6138	0.3788
2.0	0.4375	0.2763	0.7695	0.2452	−0.1868	0.0624	0.3658	0.5191	0.3771
2.0	0.5000	0.1838	0.7115	0.2180	−0.2442	0.1463	0.3068	0.4262	0.3639
2.0	0.5625	0.0981	0.6610	0.1851	−0.2793	0.2168	0.2591	0.3379	0.3411
2.0	0.6250	0.0182	0.6192	0.1491	−0.2937	0.2767	0.2220	0.2564	0.3101
2.0	0.6875	−0.0571	0.5865	0.1125	−0.2887	0.3286	0.1946	0.1834	0.2722
2.0	0.7500	−0.1288	0.5628	0.0776	−0.2654	0.3747	0.1757	0.1208	0.2282

TABLE 8.2 Continued

βL	z/L	$K_{\rho H}$	$K_{\theta H}$	K_{MH}	K_{QH}	$K_{\rho M}$	$K_{\theta M}$	K_{MM}	K_{QM}
2.0	0.8125	−0.1981	0.5474	0.0468	−0.2245	0.4171	0.1640	0.0698	0.1787
2.0	0.8750	−0.2659	0.5389	0.0222	−0.1665	0.4572	0.1578	0.0318	0.1241
2.0	0.9375	−0.3330	0.5356	0.0059	−0.0916	0.4963	0.1554	0.0082	0.0645
2.0	1.0000	−0.3999	0.5351	0.	−0.0000	0.5351	0.1551	0.0000	0.
3.0	0.	1.0066	1.0004	0.	1.0000	−1.0004	1.0068	1.0000	0.
3.0	0.0625	0.8210	0.9695	0.1543	0.6575	−0.6589	0.8183	0.9690	0.1545
3.0	0.1250	0.6459	0.8919	0.2508	0.3829	−0.3854	0.6433	0.8913	0.2514
3.0	0.1875	0.4832	0.7870	0.3018	0.1709	−0.1743	0.4857	0.7862	0.3029
3.0	0.2500	0.3515	0.6698	0.3184	0.0141	−0.0184	0.3493	0.6684	0.3202
3.0	0.3125	0.2371	0.5514	0.3101	−0.0956	0.0905	0.2352	0.5491	0.3127
3.0	0.3750	0.1444	0.4394	0.2850	−0.1664	0.1607	0.1429	0.4360	0.2887
3.0	0.4375	0.0716	0.3389	0.2496	−0.2063	0.2002	0.0710	0.3339	0.2544
3.0	0.5000	0.0164	0.2528	0.2091	−0.2223	0.2162	0.0168	0.2458	0.2150
3.0	0.5625	−0.0242	0.1823	0.1673	−0.2205	0.2147	−0.0222	0.1728	0.1744
3.0	0.6250	−0.0529	0.1271	0.1272	−0.2057	0.2011	−0.0489	0.1148	0.1353
3.0	0.6875	−0.0727	0.0864	0.0908	−0.1819	0.1793	−0.0661	0.0709	0.0995
3.0	0.7500	−0.0861	0.0584	0.0594	−0.1519	0.1524	−0.0763	0.0396	0.0684
3.0	0.8125	−0.0953	0.0411	0.0340	−0.1178	0.1227	−0.0816	0.0189	0.0426
3.0	0.8750	−0.1021	0.0321	0.0154	−0.0807	0.0916	−0.0839	0.0069	0.0225
3.0	0.9375	−0.1077	0.0287	0.0039	−0.0414	0.0599	−0.0846	0.0014	0.0083
3.0	1.0000	−0.1130	0.0282	0.	−0.0000	0.0282	−0.0847	0.0000	0.
4.0	0.	1.0008	1.0015	0.	1.0000	−1.0015	1.0021	1.0000	0.
4.0	0.0625	0.7550	0.9488	0.1926	0.5616	−0.5624	0.7567	0.9472	0.1929
4.0	0.1250	0.5323	0.8247	0.2907	0.2411	−0.2409	0.5344	0.8229	0.2910
4.0	0.1875	0.3452	0.6693	0.3218	0.0234	−0.0220	0.3478	0.6673	0.3219
4.0	0.2500	0.1979	0.5101	0.3093	−0.1108	0.1136	0.2010	0.5082	0.3090
4.0	0.3125	0.0890	0.3641	0.2717	−0.1810	0.1855	0.0926	0.3626	0.2705
4.0	0.3750	0.0140	0.2403	0.2226	−0.2055	0.2118	0.0178	0.2397	0.2206
4.0	0.4375	−0.0332	0.1419	0.1715	−0.1996	0.2079	−0.0295	0.1430	0.1671
4.0	0.5000	−0.0590	0.0682	0.1243	−0.1758	0.1858	−0.0558	0.0720	0.1176
4.0	0.5625	−0.0692	0.0163	0.0843	−0.1432	0.1545	−0.0674	0.0242	0.0749
4.0	0.6250	−0.0687	−0.0176	0.0529	−0.1084	0.1200	−0.0696	−0.0043	0.0406
4.0	0.6875	−0.0615	−0.0379	0.0299	−0.0756	0.0858	−0.0665	−0.0178	0.0149
4.0	0.7500	−0.0505	−0.0488	0.0147	−0.0475	0.0538	−0.0616	−0.0206	−0.0025
4.0	0.8125	−0.0376	−0.0536	0.0057	−0.0255	0.0242	−0.0568	−0.0166	−0.0122
4.0	0.8750	−0.0239	−0.0552	0.0014	−0.0101	−0.0033	−0.0535	−0.0096	−0.0148
4.0	0.9375	−0.0101	−0.0555	0.0001	−0.0016	−0.0296	−0.0520	−0.0029	−0.0106
4.0	1.0000	0.0038	−0.0555	−0.	0.0000	−0.0555	−0.0517	−0.0000	−0.
5.0	0.	1.0003	1.0003	0.	1.0000	−1.0003	1.0002	1.0000	0.
5.0	0.0625	0.6964	0.9214	0.2249	0.4711	−0.4715	0.6964	0.9211	0.2250
5.0	0.1250	0.4342	0.7476	0.3131	0.1206	−0.1210	0.4343	0.7472	0.3133
5.0	0.1875	0.2317	0.5479	0.3155	−0.0842	0.0840	0.2320	0.5472	0.3158
5.0	0.2500	0.0901	0.3628	0.2716	−0.1817	0.1818	0.0907	0.3620	0.2720
5.0	0.3125	0.0013	0.2121	0.2093	−0.2079	0.2084	0.0022	0.2111	0.2095
5.0	0.3750	−0.0466	0.1013	0.1461	−0.1919	0.1930	−0.0455	0.1002	0.1461
5.0	0.4375	−0.0659	0.0277	0.0915	−0.1556	0.1575	−0.0644	0.0267	0.0910
5.0	0.5000	−0.0671	−0.0157	0.0494	−0.1133	0.1163	−0.0654	−0.0161	0.0482
5.0	0.5625	−0.0584	−0.0368	0.0203	−0.0738	0.0778	−0.0567	−0.0361	0.0180
5.0	0.6250	−0.0456	−0.0435	0.0026	−0.0412	0.0461	−0.0444	−0.0409	−0.0012
5.0	0.6875	−0.0321	−0.0419	−0.0063	−0.0169	0.0223	−0.0321	−0.0365	−0.0117
5.0	0.7500	−0.0197	−0.0369	−0.0088	−0.0008	0.0055	−0.0221	−0.0276	−0.0159
5.0	0.8125	−0.0090	−0.0317	−0.0075	0.0081	−0.0059	−0.0150	−0.0175	−0.0157
5.0	0.8750	0.0002	−0.0279	−0.0044	0.0108	−0.0139	−0.0110	−0.0086	−0.0125
5.0	0.9375	0.0086	−0.0261	−0.0014	0.0079	−0.0201	−0.0094	−0.0023	−0.0072
5.0	1.0000	0.0167	−0.0259	−0.	0.0000	−0.0259	−0.0091	−0.0000	−0.

1. Rigid pile ($Z_{max} < 2.0$):

$$\rho = \frac{18H(1 + 1.33e/L)}{L^2 n_h} \tag{8.31}$$

$$\theta = \frac{24H(1 + 1.5e/L)}{L^3 n_h} \tag{8.32}$$

2. Infinitely long pile ($Z_{max} > 4.0$):

$$\rho = \frac{2.40H}{(n_h)^{3/5}(E_p I_p)^{2/5}} + \frac{1.60He}{(n_h)^{2/5}(E_p I_p)^{3/5}} \tag{8.33}$$

$$\theta = \frac{1.60H}{(n_h)^{2/5}(E_p I_p)^{3/5}} + \frac{1.74He}{(n_h)^{1/5}(E_p I_p)^{4/5}} \tag{8.34}$$

For fixed-head piles:

1. Rigid pile:

$$\rho = \frac{2H}{L^2 n_h} \tag{8.35}$$

2. Infinitely long pile ($Z_{max} > 4.0$):

$$\rho = \frac{0.93H}{(n_h)^{3/5}(E_p I_p)^{2/5}} \tag{8.36}$$

For the above equations, Z_{max} is defined as

$$Z_{max} = L/T \tag{8.37}$$

where

$$T = \left(\frac{E_p I_p}{n_h}\right)^{1/5} \tag{8.38}$$

and

e = eccentricity of applied load H, (i.e., He = applied moment)

Solutions for pile-head deflection and slope, obtained by Barber (1953), are plotted in Fig. 8.3. The actual deflection and slope are given by Eqs. (8.22), (8.23), and (8.24), except that $k_h d$ is now replaced by $n_h L$ in the denominator of these equations.

A comprehensive series of solutions for deflection, rotation, moment, shear, and pressure along a pile have been presented by Reese and Matlock (1956). For the case

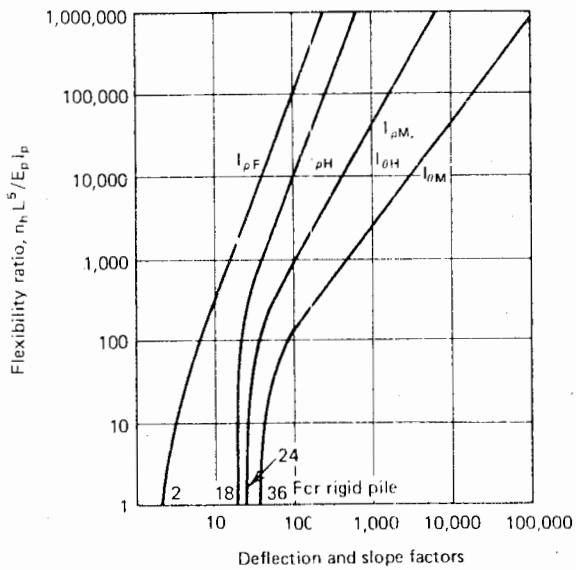

FIGURE 8.3 Top deflection and rotation for lateral loads on vertical piles for k_h proportional to depth (after Barber, 1953). (Reprinted by permission of the American Society for Testing and Materials, © 1953.)

of very long piles (i.e., $Z_{max} > 4.0$), Matlock and Reese (1961) give the following solutions for deflection ρ and moment M_z along the pile:

$$\rho = C_y \cdot \frac{HT^3}{E_p I_p} \tag{8.39}$$

$$M_z = C_m \cdot HT \tag{8.40}$$

Values of C_y and C_m are plotted in Figs. 8.4 and 8.5 for various values of M/HT, where M = applied moment, H = applied load, and T is defined in Eq. (8.38). The depth coefficient, Z, is

$$Z = z/T \tag{8.41}$$

where

z = distance below ground surface

Depending on the angular restraint provided by the cap, values of M/HT will range from zero for a free-head case to -0.93 for the case where the cap prevents any rotation of the pile head—in other words, the fixed-head case. Davisson (1970) suggests that the degree of fixity that can usually be developed is $M/HT = -0.4$ to -0.5; for this case, the positive and negative moments in the pile are approximately equal.

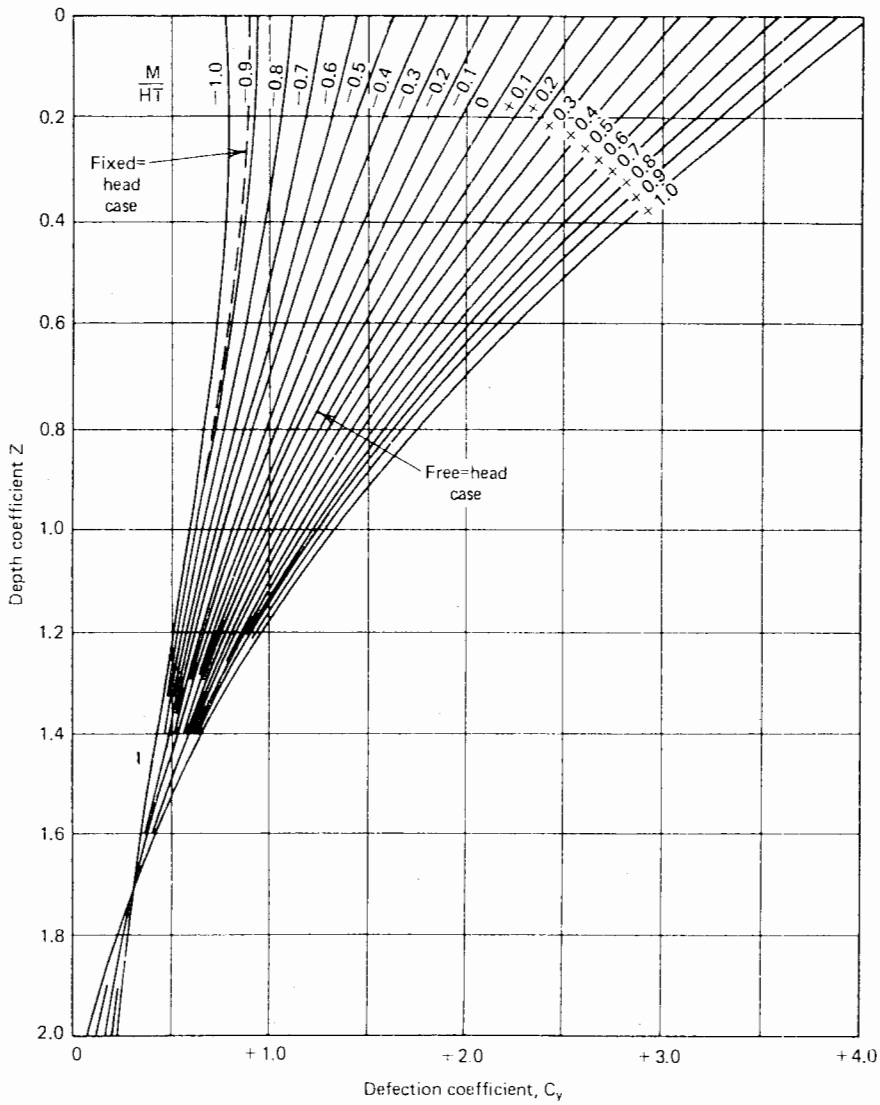

FIGURE 8.4 Curves of deflection coefficient C_y for long piles (after Matlock and Reese, 1961).

8.2.2.3 GENERAL DISTRIBUTION OF k_h WITH DEPTH

Cases involving a general distribution of k_h with depth, of the form $k_h = n_h z^n/d$ or $k_h d = k_0 + k_1 z + k_2 z^2$, have been considered by Matlock and Reese (1960). Larger deflections and moments are associated with larger values of n. Matlock and Reese also give solutions for the case $k_h d = k_0 + k_1 z$. Both deflections and moments decrease as k_0 increases.

8.2.2.4 LAYERED SOILS

Solutions for piles in a two-layer system have been presented by Davisson and Gill (1963) and Reddy and Valsangkar (1968). The influence of the upper layer on the deflection factors $I_{\rho H}$, $I_{\rho M}$, and $I_{\rho F}$ for uniform k is shown in Figs. 8.6, 8.7, and 8.8 as a function of the ratio of thickness of upper layer, h_1, to length L, and the ratio of modulus of upper layer, k_1, to that of the lower layer, k. These results have been derived from those of Davisson and Gill (1963) and apply to a pile of intermediate flexibility ($kdL^4/E_pI_p = 256$); they may be used as factors to correct the uniform layer influence factors in Fig. 8.2.

The results of Davisson and Gill's analysis may be summarized as follows:

1. With respect to reducing surface deflection and maximum moment, there is little benefit to be gained from a stiff surface layer exceeding a depth of $0.2R$ (a depth of the

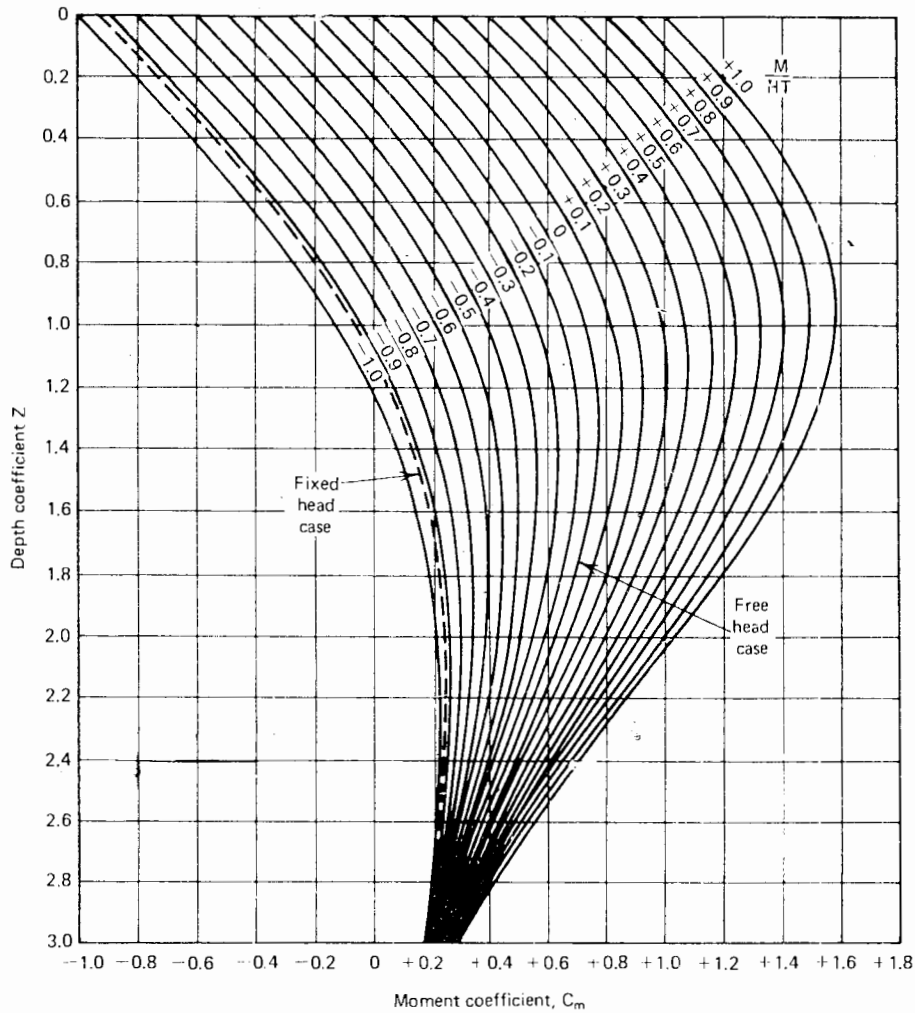

FIGURE 8.5 Curves of moment coefficient C_m for long piles (Matlock and Reese, 1961).

order of a few pile-diameters) or from a modulus ratio exceeding 5, where

$$R = [E_p I_p / kd]^{1/4}$$

2. The soil from the ground surface to depths of $0.2R$ to $0.4R$ exerts a controlling influence on pile behavior, so that investigations to determine k_h should be most thorough in this area. In addition, seasonal variations in moisture content may affect the upper part of the soil profile and hence influence the pile behavior.
3. Use of analytical results for a constant k_h with depth may lead to underestimates of moment and deflection by a factor of 2.

A further analysis of pile behavior in a layered system has been made by Reddy and Valsangkar (1968), who consider a distribution of k_h in each layer of the form $k_h d = k_0 + k_1 z + k_2 z^2$. The conclusions from this analysis are identical with those of Davisson and Gill.

8.2.3. Modulus of Subgrade Reaction

Determination of the modulus of subgrade reaction is generally carried out by one of the following methods:

1. Full-scale lateral-loading test on a pile.
2. Plate-loading tests.
3. Empirical correlations with other soil properties.

The most direct means of using pile-loading tests is to instrument the pile so that the soil pressures and pile deflections along the pile can be measured directly. This

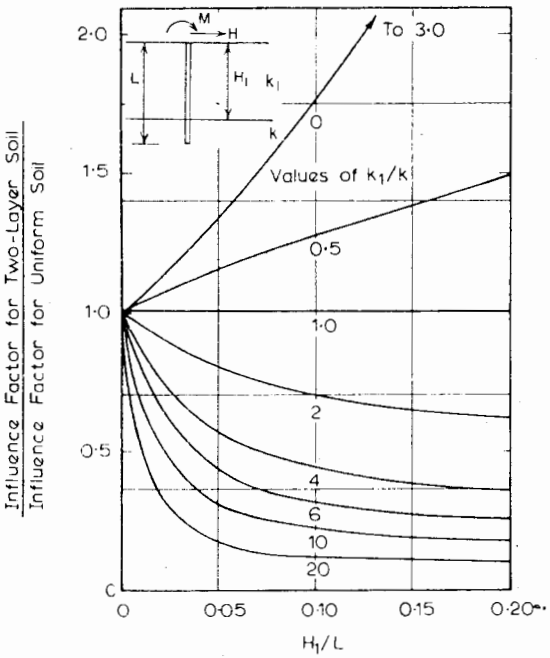

FIGURE 8.6 Effect of layered soil on deflection-influence factor $I_{\rho H}$ (after Davisson and Gill, 1963).

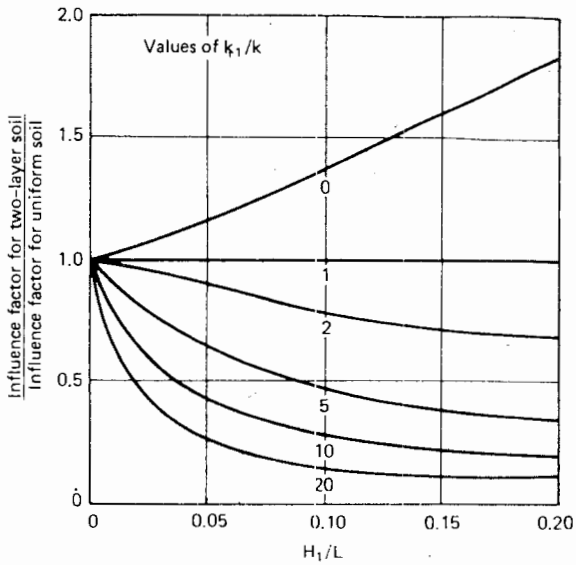

FIGURE 8.8 Effect of layered soil on deflection-influence factor $I_{\rho F}$ (after Davisson and Gill, 1963).

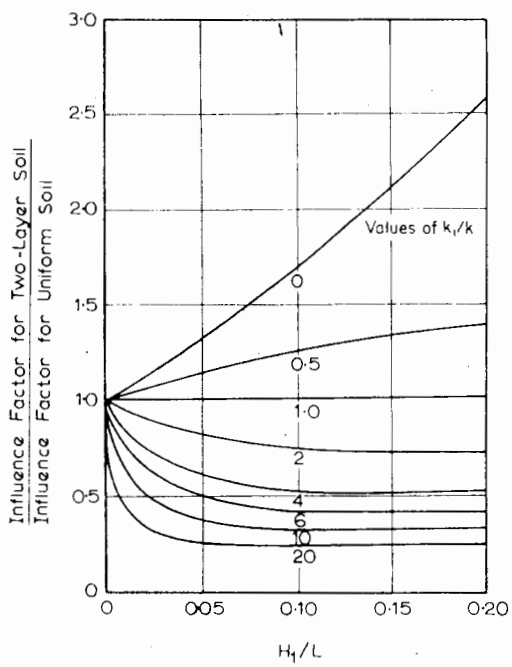

FIGURE 8.7 Effect of layered soil on deflection-influence factor $I_{\rho M}$ (after Davisson and Gill, 1963).

method has been used for a number of piles (e.g., Matlock and Ripperberger, 1958) but is time-consuming, requires care, and is relatively expensive. A more convenient procedure is to measure the ground-line deflection and/or rotation and to backfigure the value of k_h, assuming an appropriate distribution with depth. Reese and Cox (1969) describe the interpretation of tests in which both deflection and rotation is measured.

The use of plate-loading tests has been discussed by Terzaghi (1955) and Broms (1964). The main problem with this approach is the extrapolation of the results for a plate to a pile. Terzaghi (1955) considered that for clays, the modulus of subgrade reaction is essentially the same both horizontally and vertically and is independent of depth, and he suggested the following conservative relationship for k_h:

$$k_h = \left(\frac{1}{1.5d}\right)\left(\bar{k}_{s1}\right) \tag{8.42}$$

where

$\bar{k}_{s1}$ = modulus for horizontal square plate, 1 ft wide

d = breadth or diameter in feet

Typical values of $\bar{k}_{s1}$ for overconsolidated clays, suggested by Terzaghi, are shown in Table 8.3.

TABLE 8.3 VALUES OF $\bar{k}_{s1}$ TONS/FT³ FOR SQUARE PLATES, 1 × 1 FT, ON OVERCONSOLIDATED CLAY[a]

Consistency of Clay	Stiff	Very Stiff	Hard
Undrained shear strength c_u ton/ft²	0.5-1	1-2	2
Range for $\bar{k}_{s1}$	50-100	100-200	200
Proposed values of $\bar{k}_{s1}$	75	100	300

[a] After Terzaghi (1955).

Vesic (1961) analyzed an infinite horizontal beam on an elastic foundation and by comparing the results with those obtained by the use of subgrade-reaction theory, related the modulus of subgrade reaction k to the elastic parameters E_s and ν_s of the mass, as follows:

$$k = \left(\frac{0.65}{d}\right)\sqrt[12]{\frac{E_s d^4}{E_p I_p}}\left(\frac{E_s}{1-\nu_s^2}\right) \tag{8.43}$$

where

$E_p I_p$ = pile stiffness
d = pile diameter

The application of pressuremeter test results to the determination of k_h has been summarized by Baguelin et al (1978). k_h is related to the pressuremeter modulus and a factor dependent on the soil type.

A number of empirical correlations for k_h are available. For clays, assuming a constant k_h with depth, Broms (1964*a*) has related k_h to the secant modulus E_{50} at half the ultimate stress in an undrained test as

$$k_h = 1.67E_{50}/d \tag{8.44}$$

Using a value of E_{50} equal to 50 to 200 times the undrained shear strength c_u (Skempton, 1951),

$$k_h = (80 - 320)c_u/d \tag{8.45}$$

Davisson (1970) suggests a more conservative value of

$$k_h = 67\, c_u/d \tag{8.46}$$

For softer cohesive soils, it is usually assumed that k_h increases linearly with depth, that is, $k_h = n_h \cdot z/d$. Typical values of n_h for such soils are shown in Table 8.4.

TABLE 8.4 TYPICAL VALUES OF n_h FOR COHESIVE SOILS

Soil Type	n_h (lb/in.³)	Reference
Soft N/C clay	0.6-12.7	Reese and Matlock, 1956
	1.0-2.0	Davisson and Prakash, 1963
N/C organic clay	0.4-1.0	Peck and Davisson, 1962
	0.4-3.0	Davisson, 1970
Peat	0.2	Davisson, 1970
	0.1-0.4	Wilson and Hilts, 1967
Loess	29-40	Bowles, 1968

For piles in sand, assuming that the modulus of elasticity depends only on the overburden pressure and the density of the sand, Terzaghi (1955) showed that

$$n_h = \frac{A\gamma}{1.35}\ (\text{tons/ft}^3) \tag{8.47}$$

Typical values of the factor A and n_h are shown in Table 8.5. For comparison, values of n_h of 2.5 tons/ft³ and 1.5 tons/ft³ (cyclic loading) for loose, dry sand, and 79 tons/ft³ and 86 tons/ft³ for dense, dry sand, have been reported by Rowe (1956) and Davisson and Prakash (1963).

TABLE 8.5 VALUES OF n_h (TON/FT³) FOR SAND[a]

Relative Density	Loose	Medium	Dense
Range of values of A	100-300	300-1000	1000-2000
Adopted values of A	200	600	1500
n_h, dry or moist sand	7	21	56
n_h, submerged sand	4	14	34

[a] After Terzaghi, 1955.

8.2.3.1 EFFECT OF PILE DEFLECTION

Because of the nonlinearity of observed horizontal load-deflection curves for laterally-loaded piles, resulting from local yielding of the soil long before ultimate failure occurs, the overall modulus of subgrade reaction depends largely on the deflection of the pile, or the applied load level. An example of the variation of n_h with deflection for piles in sand is shown in Fig. 8.9, where the value of n_h, expressed as a fraction of n_h for a dimensionless pile displacement

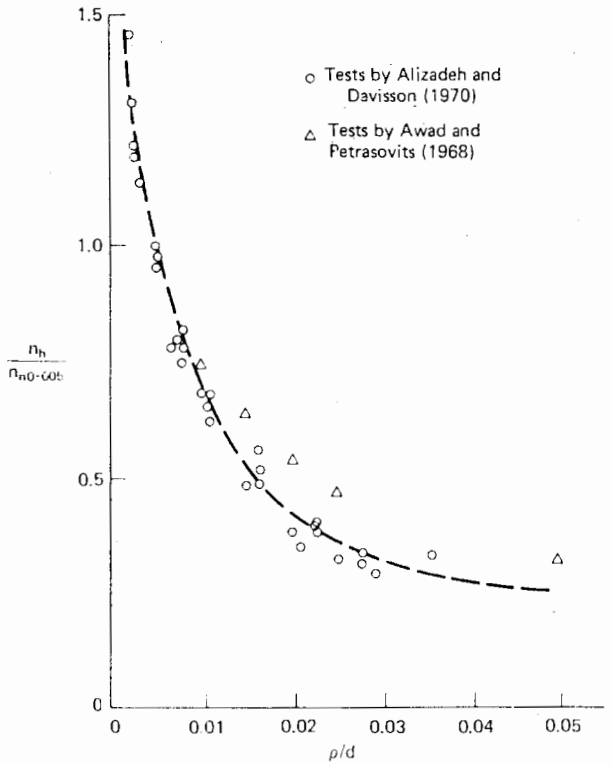

FIGURE 8.9 Effect of pile displacement on subgrade modulus n_h for piles in sand.

ρ/d of 0.005, is plotted against ρ/d. Data from full-scale tests reported by Alizadeh and Davisson (1970) and model tests by Awad and Petrasovits (1968) are plotted, and the rapid variation of n_h within the range ρ/d = 0.003 to 0.015 is clearly shown. Similar variations in k_h are found for piles in clay. Figure 8.9 therefore provides an approximate basis for taking account of the nonlinearity of soil behavior.

8.2.3.2 GROUP EFFECTS AND REPEATED LOADING

When using subgrade-reaction theory to predict group movements, an empirical correction must be made to the value of k_h used in the analysis. Davisson (1970) states that the spacing in the direction of the load is of primary importance, and that at a center-to-center spacing of $8d$ or more, there is essentially no influence of one pile on another, provided that the spacing normal to the load direction is at least $2.5d$. When the spacing parallel to loading is less than $8d$, the effective value of k_h (k_{eff}) is less than for an isolated pile, and from model tests on piles in sand (Prakash, 1962) k_{eff} was found to be about $0.25k_h$ at a spacing of $3d$. Jampel (1949) obtained expressions relating k_h to Young's modulus of the soil, E_s, for a single pile and a pile group. On the basis of these expressions, the following values of k_{eff}/k_h are suggested for normal spacings:

Two piles: $k_{\text{eff}}/k_h = 0.5$.
Three or four piles: $k_{\text{eff}}/k_h = 0.33$.
Five or more piles: $k_{\text{eff}}/k_h = 0.25$.

Repeated loading causes some deterioration of the soil resistance, effectively reducing k_h. Davisson (1970) states that the net effect is that the deflection observed under first application of a load is essentially doubled if the load is cycled 50 times or more. Moments are also increased and occur over an increased depth of embedment. Repeated loading has the effect of reducing k_h to approximately 30% of the value applicable to initial loading.

The combination of group effects and repeated loading can reduce k_{eff} to a value as low as 10% of that applicable to initial loading of an isolated pile (Prakash, 1962).

Further information on the effects of repeated loading is summarized by Reese (1975) in relation to the nonlinear "p-y" analysis (see Section 8-2-4).

8.2.3.3 EFFECT OF CONSOLIDATION AND CREEP

As a result of consolidation and creep of the soil surrounding a laterally loaded pile, an increase of the lateral deflections and a redistribution of soil reactions will occur with time. Only a small amount of data is available on the consequent reduction in the value of k_h, but Broms (1964*a*) tentatively suggests values of k_{eff}/k_h of 1/2 to 1/4 for stiff to very stiff clays, and 1/3 to 1/6 for soft and very soft clays. For sands, k_{eff}/k_h may be taken as 1.

A more satisfactory assessment of the effects of consolidation is possible with the use of elastic theory (Section 8.3).

8.2.3.4 EFFECT OF BATTERED PILES

All the preceding values of k_h and n_h have been obtained for vertical piles. The effect of pile batter on pile deflections, and hence the effective values of k_h and n_h, has been investigated by Kubo (1965) for model piles in clay and Awad and Petrasovits (1968) for model piles in sand. Deflection decreases for positive batter (i.e., batter in the direction of load) and increases for negative batter. More detailed consideration of the behavior of batter piles is given in Chapter 9.

8.2.4 Nonlinear Analysis

As discussed previously, the relationship between pressure and deflection at any point along a pile is nonlinear. Several approaches have been developed to account for this non-

linearity. Madhav et al. (1971) have employed an elasto-plastic Winkler model, while Kubo (1965) has employed the following nonlinear relationships between pressure p, deflection ρ, and depth z:

$$p = kz^m \rho^n \tag{8.48}$$

where

k, m, n = experimentally determined coefficients

However, the most widely-employed approach appears to be the so-called "p-y" approach developed by Reese and his coworkers (here, p = pressure, y = deflection). In this method, a finite-difference solution is obtained to the following equation:

$$\frac{d^2M}{dz} + (P_z)\frac{d^2\rho}{dz^2} - p = 0 \tag{8.49}$$

where

ρ = deflection
M = moment at depth z in pile
z = depth
P_z = axial load on pile at depth z
p = soil-reaction per unit length (i.e., p here is, in effect, an equivalent line loading)

This equation is a more general form of Eq. (8.3), in which the effects of axial load and variations of pile stiffness with depth can be incorporated. Equation (8.49) can be written in finite-difference form, and a full description of the resulting equations are given by Reese (1977), who also describes a computer program that solves these equations. The equations are a generalized version of those given in Section 8.2.1.

The solution requires input of a series of "p-y" curves (in the present notation of this book, p-ρ curves) for various points along the pile. Such a set is illustrated diagrammatically in Fig. 8.10. As in the normal subgrade-reaction approach, the curves shown in Fig. 8.10 imply that the behavior of the soil at a particular depth is independent of the soil behavior at other locations. While not strictly true, Reese states that experiments indicate that this assumption is sufficiently true for practical purposes. Since there is no restriction on the shape of the p-ρ curves, an iterative solution of the finite difference equations is necessary in order to obtain compatible values of p and ρ at all points along the pile.

Design procedures for constructing p-ρ relationships based on the results of field measurements on full-size instrumented piles, have been developed by Matlock (1970) for saturated soft clays subjected to either short-term static loading or cyclic loading. Other cases have subsequently been treated by Reese and his co-workers and are summarized by Reese (1975). As an example of these procedures, the case of soft saturated clays is outlined below.

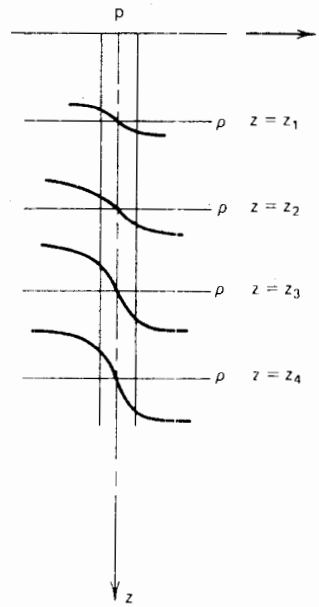

FIGURE 8.10 Concept of $p - \rho$ curves.

1. Short-term static loading.

(a) Values are obtained for the variation of shear strength and effective unitweight with depth, together with a value of ϵ_{50}, the strain corresponding to one half the maximum principal stress difference. (Values of ϵ_{50} typically range from 0.005 for stiff clays to 0.02 for soft clays.)

(b) The ultimate soil resistance per unit length of shaft, p_u, is computed, using the lesser of the following values:

$$p_u = (3 + \gamma z/c_u + 0.5z/d)c_u d \tag{8.50a}$$

or

$$p_u = 9c_u d \tag{8.50b}$$

where

γ = average effective unit weight from ground surface to the required depth z
c_u = undrained shear-strength at depth z
d = width or diameter of pile

The value of p_u is computed at each depth for which a p-ρ curve is required.

(c) The deflection, ρ_{50}, at one half the ultimate soil resistance is calculated as

$$\rho_{50} = 2.5\epsilon_{50}d \tag{8.51}$$

(d) Finally, points describing the p-ρ curve are computed from the following relationship:

$$p/p_u = 0.5\,(\rho/\rho_{50})^{1/3} \tag{8.52}$$

The value of p is taken to remain constant beyond $\rho = 8\rho_{50}$.

2. Cyclic loading.

(a) The p-ρ curve is constructed in the same manner as for short-term static loading, for values of p less than $0.72p_u$.
(b) Equations (8.50*a*) and (8.50*b*) are solved simultaneously to find the transition depth, z_r. For constant unit weight and shear strength in the upper zone,

$$z_r = \frac{6c_u d}{(\gamma d + 0.5c_u)} \tag{8.53}$$

(c) If the depth of the point in question is greater than or equal to z_r, then p is equal to $0.72p_u$ for all values of ρ greater than $3\rho_{50}$.
(d) If the depth is less than z_r, then the value of p decreases from $0.72p_u$ at $\rho = 3\rho_{50}$ to the value given by the expression below at $\rho = 15\rho_{50}$:

$$p = 0.72p_u(z/z_r) \tag{8.54}$$

The value of p remains constant beyond $\rho = 15\rho_{50}$.

Other cases for which p-ρ curve-construction procedures have been recommended are:

1. Stiff clays above the water table (Reese and Welch, 1975)
2. Stiff clays below the water table (Reese et al., 1975).
3. Sands, short-term and cyclic loading (Reese et al., 1974).

A unified approach for constructing p-ρ curves for piles in clay has been developed by Sullivan et al (1979).

An alternative and perhaps more generally applicable approach to determining p-ρ curves was described by Frydman et al. (1975), who made use of pressuremeter test results. The p-ρ curves were obtained by assuming that if the same pressure is applied to the soil by the pressuremeter and a pile, the ratio between the lateral movement of the soil next to the pile to that next to the pressuremeter is equal to the ratio of their diameters, or widths. The lateral movement of the soil next to the pressuremeter is equal to the increase in radius of the pressuremeter and is obtained from the volume change measurements. Using this approach, Frydman et al. were able to reproduce with quite good accuracy the measured deflection profiles of two prestressed-concrete test piles. Baguelin et al (1977) also discuss the use of pressuremeter test results to obtain p-ρ curves and describe a number of reasonably successful applications of this technique to instrumented piles.

8.3 ELASTIC ANALYSIS FOR SINGLE PILES

8.3.1 Basic Theory

Analyses in which the soil has been considered as an elastic continuum have been described by Douglas and Davis (1964); Spillers and Stoll (1964); Lenci, Maurice, and Madignier (1968); Matthewson (1969); Banerjee (1978); Banerjee and Davies (1978); and Poulos (1971*a*, 1972). All these analyses are similar in principle, the differences arising largely from details in the assumptions regarding the pile action. The analyses of Poulos (1971*a*) for a floating pile and Poulos (1972) for a socketted pile are described below.

8.3.1.1 FLOATING PILES

Referring to Fig. 8.11, the pile is assumed to be a thin rectangular vertical strip of width d, length L, and constant flexibility E_pI_p (in applying the results of the analysis to a circular pile, d can be taken as the pile diameter). To

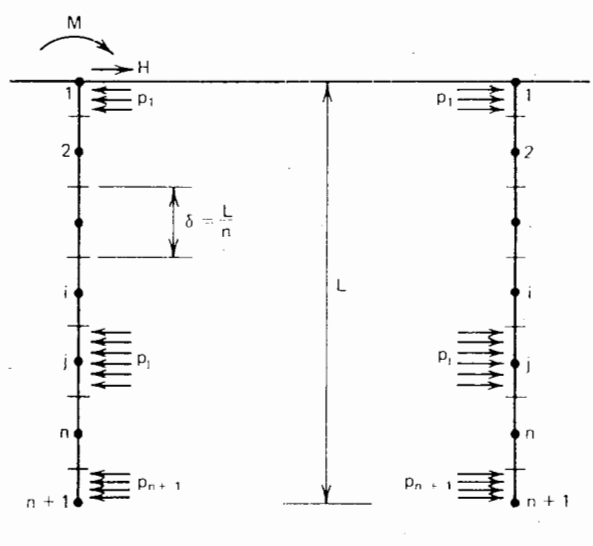

FIGURE 8.11 Floating pile. Stresses acting on (*a*) pile; (*b*) soil adjacent to pile.

simplify the initial analysis, possible horizontal shear-stresses developed between the soil and the sides of the pile are not taken into account. The pile is divided into $n + 1$ elements, all being of length δ except those at the top and tip, which are of length $\delta/2$. Each element is acted upon by a uniform horizontal stress p, which is assumed constant across the width of the pile. The soil is assumed to be an ideal, homogeneous, isotropic, semi-infinite elastic material, having Young's modulus, E_s, and Poisson's ratio, ν_s, which are unaffected by the presence of the pile. It is also assumed that the soil at the back of the pile near the surface adheres to the pile. This assumption is discussed further in this section, when an approximate method of allowing for pile-soil separation is outlined.

If purely elastic conditions prevail within the soil, the horizontal displacements of the soil and the pile are equal. In this analysis, these displacements are equated at the element centers, except for the two extreme elements, for which displacements are calculated at the top and the tip of the pile (i.e., the collocation points are equally spaced). The soil displacements for all points along the pile may be expressed as

$$\{{}_s\rho\} = \frac{d}{E_s}\,[I_s]\{p\} \tag{8.55}$$

where $\{{}_s\rho\}, \{p\}$ are the $n + 1$ column vectors of horizontal soil displacement and horizontal loading between soil and pile. (The stress between pile and soil caused by external loads on the pile is $p/2$ compression on one side and $p/2$ tension on the other side.) $[I_s]$ is the $n + 1$ by $n + 1$ matrix of soil-displacement-influence factors.

Elements I_{ij} of $[I_s]$ are evaluated by integration over a rectangular area of the Mindlin equation for the horizontal displacement of a point within a semi-infinite mass caused by horizontal point-load within the mass. This integration is described by Douglas and Davis (1964), and their solution is reproduced in Appendix B. Although Eq. (8.55) is for a soil with uniform E_s, the case of a varying E_s along the pile (e.g., for a pile in sand) may also be considered by assuming that the soil deflection at a point is given by the Mindlin equation and using the value of E_s at that point.

In determining the pile displacements, use is made of the differential equation for bending of a thin beam (Eq. 8.2). This equation can be written in finite-difference form, for the points 2 to n, and by using the appropriate boundary conditions at the top and tip of the pile to eliminate fictitious displacements at points outside the pile, the following equations may be derived for the cases of a free-head pile and a fixed-head pile:

a) Free-Head or Unrestrained Pile

$$-\{p\} = \frac{E_p I_p n^4}{dL^4}\,[D]\{{}_p\rho\} + \frac{E_p I_p}{dL^4}\,\{A\} \tag{8.56}$$

where

$\{{}_p\rho\}$ is the $n - 1$ column vector of pile displacements

$[D]$ = $n - 1$ by $n + 1$ matrix of finite difference coefficients.

$$= \begin{bmatrix} -2 & 5 & -4 & 1 & 0 & 0 & \cdots & 0 & 0 & 0 & 0 & 0 \\ 1 & -4 & 6 & -4 & 1 & 0 & \cdots & 0 & 0 & 0 & 0 & 0 \\ 0 & 1 & -4 & 6 & -4 & 1 & \cdots & 0 & 0 & 0 & 0 & 0 \\ \cdots & \cdots & \cdots & \cdots & \cdots & \cdots & \cdots & \cdots & \cdots & \cdots & \cdots & \cdots \\ \cdots & \cdots & \cdots & \cdots & \cdots & \cdots & \cdots & \cdots & \cdots & \cdots & \cdots & \cdots \\ 0 & 0 & 0 & 0 & 0 & 0 & \cdots & 1 & -4 & 6 & -4 & 1 \\ 0 & 0 & 0 & 0 & 0 & 0 & \cdots & 0 & 1 & -4 & 5 & -2 \end{bmatrix}$$

$$\{A\} = \begin{Bmatrix} \dfrac{ML^2}{n^2 E_p I_p} \\ 0 \\ 0 \\ \cdot \\ \cdot \\ \cdot \\ \cdot \\ \cdot \\ \cdot \\ 0 \\ 0 \\ 0 \end{Bmatrix},$$

Equating the soil and pile displacements from Eqs. (8.55) and (8.56)—that is, putting ${}_s\rho = {}_p\rho$,

$$\left[[I] + K_R n^4\,[D] \cdot [I_s]\right] \cdot \{p\} = \{B\} \tag{8.57}$$

where

$$\{B\} = \begin{Bmatrix} \dfrac{-Mn^2}{dL^2} \\ 0 \\ 0 \\ \cdot \\ \cdot \\ 0 \\ 0 \end{Bmatrix}$$

TABLE 8.6 TYPICAL VALUES OF PILE FLEXIBILITY FACTOR K_R FOR VARIOUS SOILS

Pile type	Soft Clay		Medium Clay		Stiff Clay		Loose Sand		Dense Sand	
	Pile Length (ft)									
	20	50	20	50	20	50	20	50	20	50
1-ft diam. concrete	6.2×10^{-3}	1.6×10^{-4}	3.1×10^{-3}	8.0×10^{-5}	1.2×10^{-3}	3.1×10^{-5}	3.7×10^{-3}	9.5×10^{-5}	9.2×10^{-4}	2.4×10^{-5}
3-ft diam. concrete	5.0×10^{-1}	1.3×10^{-2}	2.5×10^{-1}	6.4×10^{-3}	9.4×10^{-2}	2.4×10^{-3}	3.0×10^{-1}	7.7×10^{-3}	7.5×10^{-2}	1.9×10^{-3}
1-ft (average) diam. timber	3.1×10^{-3}	7.9×10^{-5}	1.5×10^{-3}	3.8×10^{-5}	6.0×10^{-4}	1.5×10^{-5}	1.8×10^{-3}	4.6×10^{-5}	4.7×10^{-4}	1.2×10^{-5}
14-in. × 14-in. × 117-lb steel H-pile	2.7×10^{-2}	6.9×10^{-4}	1.3×10^{-2}	3.4×10^{-4}	5.0×10^{-3}	1.3×10^{-4}	1.6×10^{-2}	4.1×10^{-4}	4.0×10^{-3}	1.0×10^{-4}

NOTE: Above values of K_R are derived from secant values of E_s at normal working loads.

$[I]$ = unit matrix ($n - 1$ by $n + 1$)

$$K_R = \frac{E_p I_p}{E_s L^4}$$

= the pile-flexiblity factor

K_R is a dimensionless measure of the flexibility of the pile relative to the soil and has limiting values of ∞ for an infinitely rigid pile and zero for an infinitely long pile. As a rough guide to practical values of K_R, Table 8.6 gives typical values for various types of piles and soils. These have been derived using secant values of E_s (see Section 8.5) and should be regarded as approximate only and applicable when a purely elastic analysis is used (lower values of K_R may be relevant when an elastoplastic analysis is employed).

The horizontal-load and moment-equilibrium equations provide the remaining two equations required for the analysis, and these may be written as

$$\{E\} \cdot \{p\} = \frac{nL}{d} \cdot \frac{H}{L^2} \tag{8.58}$$

where

$\{E\}$ is an $n + 1$ row vector,

with

$$E_j = 1 \text{ for } 1 < j < n + 1$$
$$E_j = 0.5 \text{ for } j = 1, n + 1$$

$$\{F\} \cdot \{p\} = -n^2 \left(\frac{L}{d}\right) \frac{M}{L^3} \tag{8.59}$$

where

$\{F\}$ is an $n + 1$ row vector,

with

$$F_j = j - 1 \text{ for } 1 < j < n + 1$$
$$F_1 = 0.125$$
$$F_{n+1} = 0.5n - 0.125$$

Equations (8.57), (8.58), and (8.59) may be solved for the $n + 1$ unknown stresses, whereby the displacements may be calculated from Eq. (8.55). The rotations, moments, and shears can subsequently be evaluated.

(b) Fixed-Head or Restrained Pile

The analogous equation to Eq. (8.56) is now

$$\left[[I] + K_R n^4 [D_1][I_s]\right]\{p\} = 0 \tag{8.60}$$

where

$[D_1]$ = $n - 1$ by $n + 1$ matrix of finite-difference coefficients

$$= \begin{bmatrix} -4 & 7 & -4 & 1 & 0 & \ldots & 0 & 0 & 0 & 0 & 0 \\ 1 & -4 & 6 & -4 & 1 & \ldots & 0 & 0 & 0 & 0 & 0 \\ \cdots & \cdots & \cdots & \cdots & \cdots & \cdots & \cdots & \cdots & \cdots & \cdots & \cdots \\ \cdots & \cdots & \cdots & \cdots & \cdots & \cdots & \cdots & \cdots & \cdots & \cdots & \cdots \\ 0 & 0 & 0 & 0 & 0 & \ldots & 1 & -4 & 6 & -4 & 1 \\ 0 & 0 & 0 & 0 & 0 & \ldots & 0 & 1 & -4 & 5 & 2 \end{bmatrix}$$

The horizontal-equilibrium equation is identical with that for the free-head pile (Eq. 8.58), but the moment equation must be altered to take account of the fixing moment at the pile head. This equation then becomes

$$\{G\} \cdot \{p\} = 0 \tag{8.61}$$

where

$\{G\}$ is an $n + 1$ row vector,

with

$$G_j = F_j + \left(\frac{2}{3} K_R n^4\right)(-I_{2j} + I_{3j})$$

and

F_j is defined in Eq. (8.59)

Equations (8.60), (8.58), and (8.61) may again be solved for the pressures, displacements, and so on.

Solutions obtained from the above analyses are given in the following sections (8.3.2 and 8.3.3). For these solutions, 21 elements were used to divide the pile. This number was generally found to give results of adequate accuracy, except for very slender or flexible piles, in which case, deflections and rotations may be underestimated. Evangelista and Viggiani (1976) and Poulos and Adler (1978) have examined the accuracy of such solutions and conclude that greater accuracy and economy may be achieved by formulating the beam equation for pile bending in terms of unequal spacings between adjacent nodes. This leads to different matrices $[D]$ and $[D_1]$ in Eqs. (8.56) and (8.60). Smaller elements can be used near the top of the pile, where displacement, pressure, and moment gradients are steep, and larger elements used along the lower part of the pile.

An alternative formulation of the analysis, using a finite element discretization of the pile, is described by Poulos and Adler (1978). Non-uniform pile sections are readily-handled with this analysis.

The extension of the analyses to cover the case of yield of the soil is described later in this section. Modifications for battered piles are discussed in Chapter 9.

8.3.1 2 SOCKETED PILES

The assumptions made regarding pile and soil behavior are similar to those made in relation to floating piles, but the soil is now assumed to be underlain by a rough, rigid bearing stratum, and a force H_f and a tip moment M_f act at the tip, which is restrained from moving horizontally. The solution for the case of purely-elastic soil behavior is again obtained by equating pile and soil displacements at the node points. The pile displacements are again obtained by expressing the beam equation in finite-difference form, which yields the following equation (for points 2 to n):

$$-\{p\} = \{C\} + \frac{E_p I_p n^4}{dL^4}[D_2]\{_p\rho\} \tag{8.62}$$

where

$\{p\}, \{_p\rho\}$ are $n - 1$ column vectors for loading and pile displacement

$[D_2]$ is an $n - 1$ by $n + 1$ matrix of finite-difference coefficients

$\{C\}$ is an $n - 1$ column vector

The elements of $[D_2]$ and $\{C\}$ depend on the head and tip boundary conditions. The following conditions are considered:

Free-head:	moment at head	= applied moment M
Fixed-head:	head rotation	= 0
Pinned-tip:	tip displacement	= 0
	tip moment, M_f	= 0
Fixed-tip:	tip displacement	= 0
	tip rotation	= 0

The boundary conditions may be expressed in finite-difference form and the first and last rows of $[D_2]$ and $\{C\}$ may be determined. The inner rows are identical with those of $[D]$ and $[D_1]$ for the floating pile.

The soil displacements at all elements along the pile may be written as

$$\{_s\rho\} = \frac{d}{E_s}[I_s]\{p\} \tag{8.63}$$

where

$\{_s\rho\}$ = the $n + 1$ column vector of soil displacements

$[I_s]$ = the $n + 1$ by n + 1 matrix of soil-displacement-influence factors

In evaluating the elements of $[I_s]$, allowance should be made for the effect of the rigid base in reducing soil movements, and a convenient approximate means of making this allowance is to introduce a fictitious "mirror image" of the pile, loaded by equal and opposite horizontal stresses (see Fig. 8.12). This procedure is analogous to that used in the analysis of axially-loaded end-bearing piles (Chapter 5). The displacements at all points along the pile, resulting from both the real and imaginary elements, are again evaluated from the expressions derived by Douglas and Davis (1964).

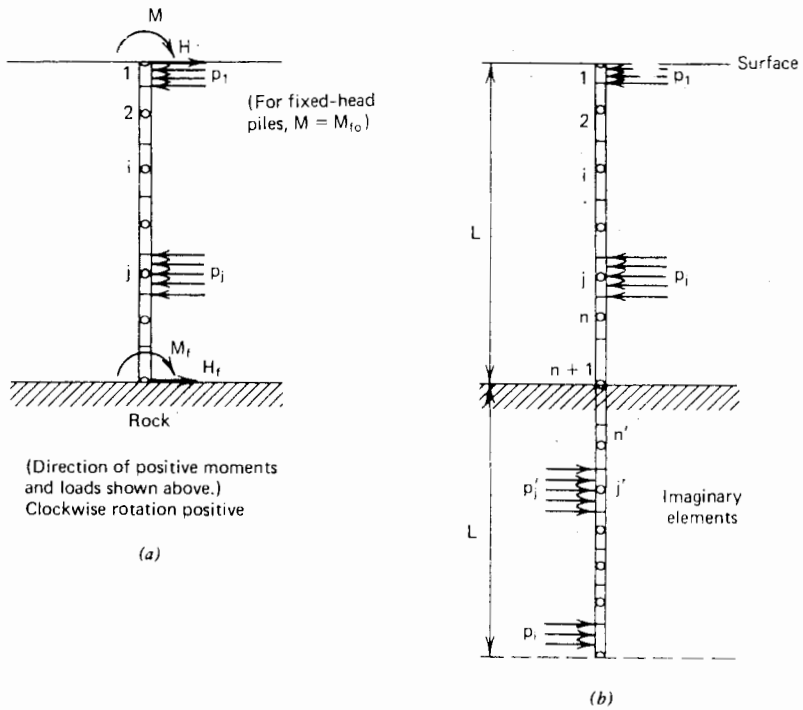

FIGURE 8.12 Socketed pile.

The pile and soil displacements from Eqs. (8.62) and (8.63) can be equated, and the resulting equations, together with the appropriate equilibrium equations, solved for the unknown pressures and displacements as well as the tip force H_f and tip moment M_f.

Solutions from the above analysis are given in Section 8.3.4, while the extension of the elastic analysis to account for local yield of the soil is described below.

8.3.1.3 *ANALYSIS FOR LOCAL YIELD OF SOIL*

Because the elastic analysis shows that high pressures are developed near the top of the pile, real soils are likely to yield at relatively low loads, and consequently, increased displacements will occur. Modifications of the elastic analysis to take account of soil yield have been described by Spillers and Stoll (1964) and Poulos (1971*a*). For a specified load and moment, a solution is first obtained assuming the soil to be elastic, and the soil pressures thus obtained are compared with the specified yield (ultimate lateral) pressures, p_y, at each point (see Chapter 7 for a discussion of values of p_y, denoted as p_u therein). At elements where the elastic pressure exceeds p_y, the displacement-compatibility equation is replaced by the condition that the pressure equals p_y. The solution is then recycled and the procedure repeated until the yield pressures are nowhere exceeded along the pile. Then by increasing the loads and moments, the entire load-deflection curve for the pile may be obtained. This analysis assumes that at elements at which the soil has not yielded, the soil displacement caused by elements that have yielded is still given by elastic theory. This assumption should not involve serious error when only a few elements have yielded, but is likely to lead to inaccuracy in the load-deflection curve as the ultimate load or moment is approached.

The above analysis is best carried out by reexpressing the equations in terms of the unknown deflections rather than the unknown pressures, so that difficulties regarding displacements at yielded elements are eliminated.

8.3.1.4 *ANALYSIS OF PILE-SOIL SEPARATION NEAR SURFACE*

The elastic analysis assumes that the soil behind the pile adheres to the pile at all times. However, because soil has limited ability to take tension, it is likely that separation will occur near the top of the pile, where large stresses, compressive in front of the pile and tensile behind the pile, are developed. This separation and local yield are the main causes of the marked nonlinearity in load-deflection behavior that is observed in lateral loading tests, even at low load levels. Douglas and Davis (1964) state that this effect could lead to an increase in displacements and rotations of 100% in the extreme case, but in practical cases involving stiff piles, an increase of 30 to 40% appears to be a more reasonable allowance.

Approximate allowance for the effects of separation may be made in the elastic analysis in the following manner:

1. From the initial elastic analysis, the stresses along the pile are obtained. Assuming in-situ horizontal stress to be $K_s\sigma_v$, where σ_v is the vertical overburden stress and K_s is a coefficient of horizontal pressure (see Chapters 2 and 3), the elements at which the resulting stress at the back of the pile, $K_s\sigma_v - 0.5\ p_j$, is negative (i.e., tensile) are determined (the factor of 0.5 arises because half the total force on a pile element is compressive at the front of the element and half is tensile at the back of the pile).
2. Assuming the soil to have zero tensile strength (if justifiable, a certain small tensile strength could be considered), separation is assumed to occur at these elements and the displacements caused by these elements are recalculated, assuming these displacements to be twice the values given by the Mindlin equations. The factor of 2 is correct for loading in an infinite mass, and at the soil surface (provided that $\nu_s = 0.5$).
3. A new solution is obtained, and the procedure repeated until no resulting net-tensile stresses exist at the back of the pile.

Solutions showing the effect of separation are discussed in Section 8.3.2.

This procedure may also be combined with the analysis for local yield of the soil to obtain a more accurate load-deflection relationship to failure for a laterally-loaded pile.

8.3.1.5 RELATIONSHIP BETWEEN ELASTIC AND SUBGRADE-REACTION ANALYSES

Having completed the description of the elastic method, it is now possible to consider its relationship to the subgrade-reaction analysis. Considering first the linear analyses, comparison between Eqs. (8.1) and (8.55) reveals that the subgrade-reaction method can be formulated in precisely the same manner as the elastic method; however, the off-diagonal components of the soil-influence-factor matrix $[I_s]$ are all zero in the subgrade-reaction analysis, and the diagonal components in the elastic theory ($\frac{d}{E_{si}} I_{ii}$ for an element i) are replaced by $1/k_i$. The presence of the off-diagonal elements of $[I_s]$ in the elastic theory is caused by the ability of an elastic material to transmit stress, in contrast to a Winkler material.

The elastic analysis modified for local yield is equivalent to a nonlinear subgrade-reaction analysis in which the p-ρ curves are linear up to the yield pressure p_y, but in which the linear portion of these curves depends on the pressures on all the elements rather than on the pressure at one element only. It should be noted that it would be possible to use other types of p-ρ relationships in conjunction with elastic theory, although it is doubtful whether the added complications in such an analysis would be justified in view of the approximations involved in using the Mindlin equations.

8.3.2 Solutions for Floating Pile in Uniform Soil

8.3.2.1 DISPLACEMENT AND ROTATION

Solutions have been obtained for the case of a free-head floating pile, loaded by a horizontal force H acting at an eccentricity e above the ground line. A soil having a uniform modulus E_s and limiting pressure p_y is considered; such an idealization is generally considered to be applicable to piles in overconsolidated clay. In the solutions, the influence of local yield of the soil adjacent to the pile is taken into account, but no allowance is made for the effects of pile-soil separation. A value of ν_s of 0.5 has been chosen; however, ν_s has relatively little influence on the solutions.

The ground-line displacement, ρ, and rotation, θ, for a free-head pile may be expressed as follows (Poulos, 1973):

$$\rho = \frac{H}{E_s L}(I_{\rho H} + \frac{e}{L} I_{\rho M})/F_\rho \tag{8.64}$$

$$\theta = \frac{H}{E_s L^2}(I_{\theta H} + \frac{e}{L} I_{\theta M})/F_\theta \tag{8.65}$$

where

H = applied horizontal load
e = eccentricity of load = M/H
M = applied moment at ground line
$I_{\rho H}$, $I_{\rho M}$ = elastic influence factors for displacement caused by horizontal load and moment, respectively, for constant E_s
$I_{\theta H}$, $I_{\theta M}$ = elastic influence factors for rotation caused by horizontal load and moment, respectively, for constant E_s ($I_{\theta H} = I_{\rho M}$ from the reciprocal theorem)
F_ρ = yield-displacement factor = ratio of pile displacement in elastic soil to pile displacement in yielding soil, for constant E_s and p_y

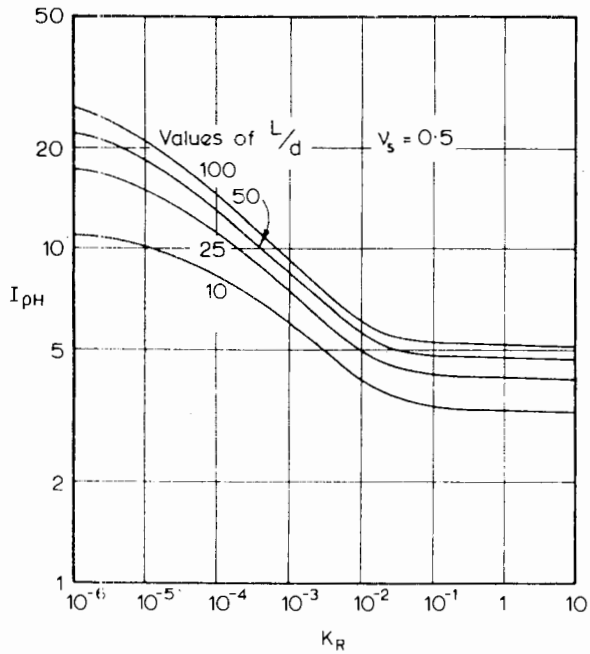

FIGURE 8.13 Values of $I_{\rho H}$–free-head floating pile, constant soil modulus.

F_θ = yield-rotation factor = ratio of pile rotation in elastic soil to pile rotation in yielding soil, for constant E_s and p_y

p_y = limiting soil pressure (also termed 'yield pressure' or 'ultimate lateral pressure' elsewhere in this book)

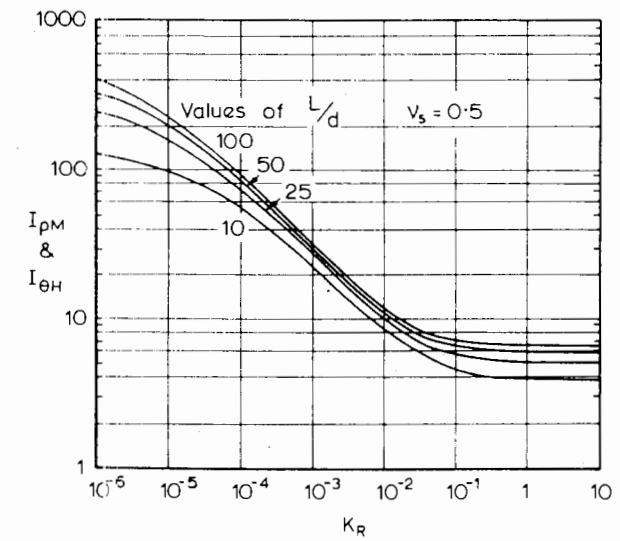

FIGURE 8.14 Values of $I_{\rho M}$ and $I_{\theta H}$–free-head floating pile, constant soil modulus.

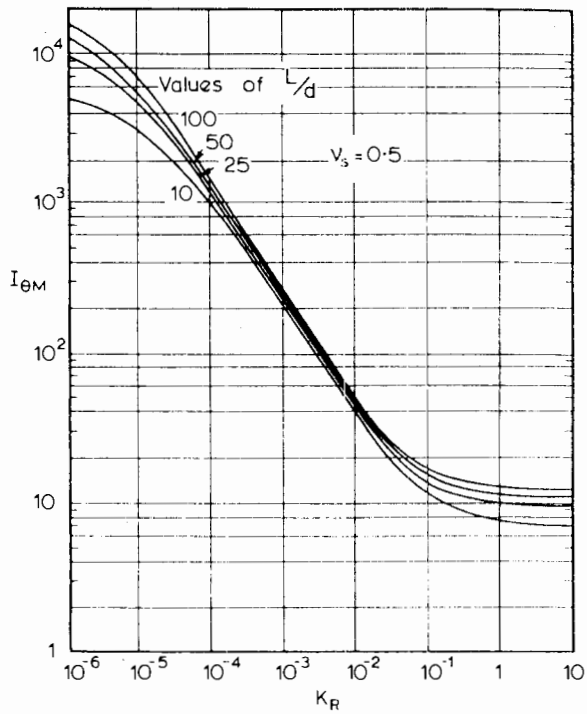

FIGURE 8.15 Values of $I_{\theta M}$–free-head floating pile, constant soil modulus.

The elastic influence factors $I_{\rho H}$, $I_{\rho M}$ (= $I_{\theta H}$), and $I_{\theta M}$ have been given by Poulos (1971*a*) and are reproduced in Figs. 8.13, 8.14, and 8.15. Because of the limited number of elements used, the solutions may be somewhat inaccurate for piles that are very slender or very flexible, and may lead to underestimates of deflection and rotation. The yield factors F_ρ and F_θ are functions primarily of the relative eccentricity of the load, e/L, the pile-flexibility factor, K_R, and the applied load level, which may be conveniently expressed dimensionlessly as H/H_u, where H_u is the ultimate lateral-load capacity of the pile if failure occurs by failure of the soil (i.e., if the pile is rigid). Values of F_ρ and F_θ are shown in Figs. 8.16 and 8.17 as functions of e/L, K_R, and H/H_u, for $L/d = 50$. Both F_ρ and F_θ decrease (i.e., the effect of soil yield increases) as H/H_u increases or as K_R decreases. However, for relatively rigid piles ($K_R > 10^{-2}$), the effect of soil yield is not great at ordinary working loads. An indication of the effect of L/d for one value of K_R and for $e/L = 0$ is given in Fig. 8.18. F_ρ decreases as L/d decreases.

The values of F_ρ and F_θ in Figs. 8.16 and 8.17 are for $e/L \geqslant 0$–that is, moment and load acting in the same direction. Values could also be derived for the case where moment and load act in opposite directions–that is, $e/L < 0$.

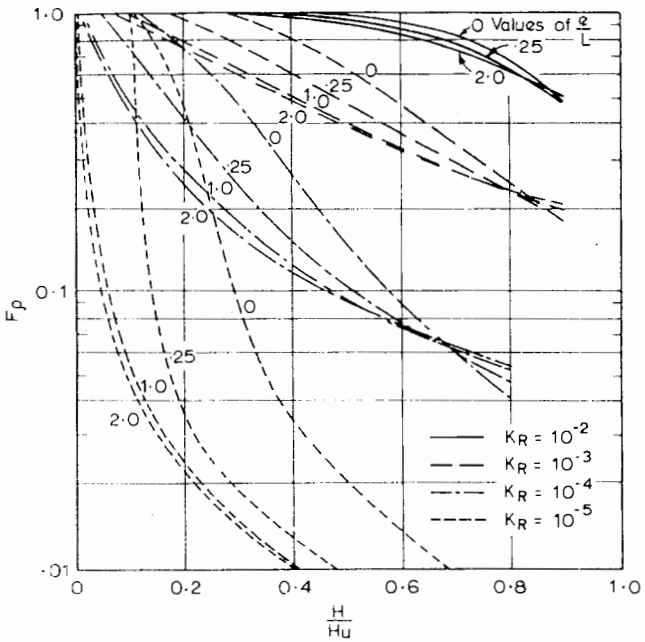

FIGURE 8.16 Yield-displacement factor F_ρ–free-head floating pile, uniform E_s and p_y.

H_u may be obtained from statical considerations, and it is shown as a function of e/L in Fig. 7.2. It should be emphasized that the presentation of the theoretical results in terms of H_u does not necessarily imply that the actual ultimate load could reach H_u, since for very flexible piles

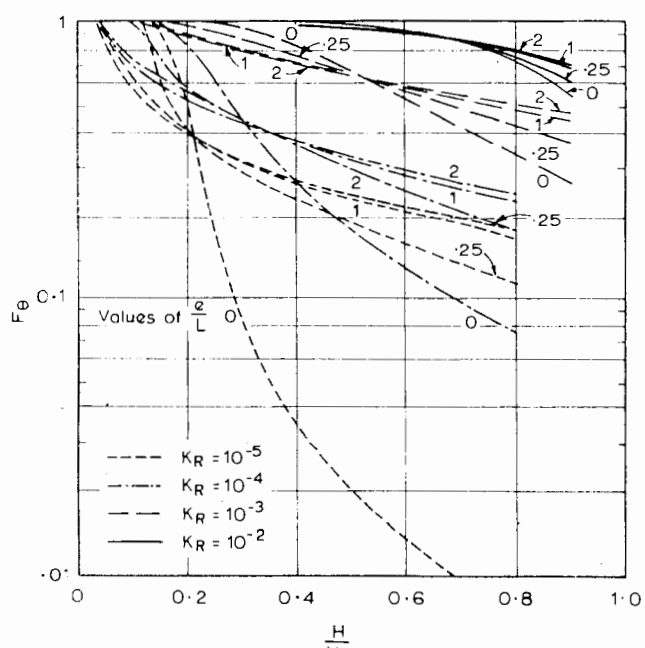

FIGURE 8.17 Yield-rotation factor F_θ–free-head floating pile, uniform E_s and p_y.

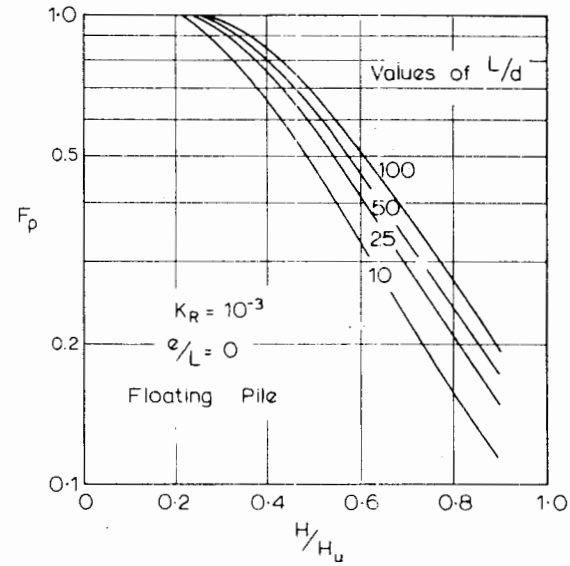

FIGURE 8.18 Effect of L/d on F_ρ.

(i.e., small K_R values), a pile may deflect excessively or fail by yielding of the pile before this value of H_u can be developed.

For a purely elastic soil the displacement ρ and the rotation θ at the ground line may be expressed as follows:

$$\rho = I_{\rho H}\left(\frac{H}{E_s L}\right) + I_{\rho M}\left(\frac{M}{E_s L^2}\right) \tag{8.66}$$

$$\theta = I_{\theta H}\left(\frac{H}{E_s L^2}\right) + I_{\theta M}\left(\frac{M}{E_s L^3}\right) \tag{8.67}$$

where M is the applied moment at ground line. In applying the above equations to practical problems, the value of E_s to be used should be a secant value appropriate to the working load level. However, the expression of the results as in Eqs. (8.64) and (8.65) enables a more rational account to be taken of the effects of soil yielding and allows the use of a single tangent value of E_s, irrespective of the load level. The relationship between solutions from the above two approaches is discussed later in this section. Appropriate values of E_s are discussed in Section 8.5.

For a fixed-head pile subjected to a lateral load H, the ground-line displacement can be expressed as

$$\rho = I_{\rho F}\left(\frac{H}{E_s L}\right)/F_{\rho F} \tag{8.68}$$

where

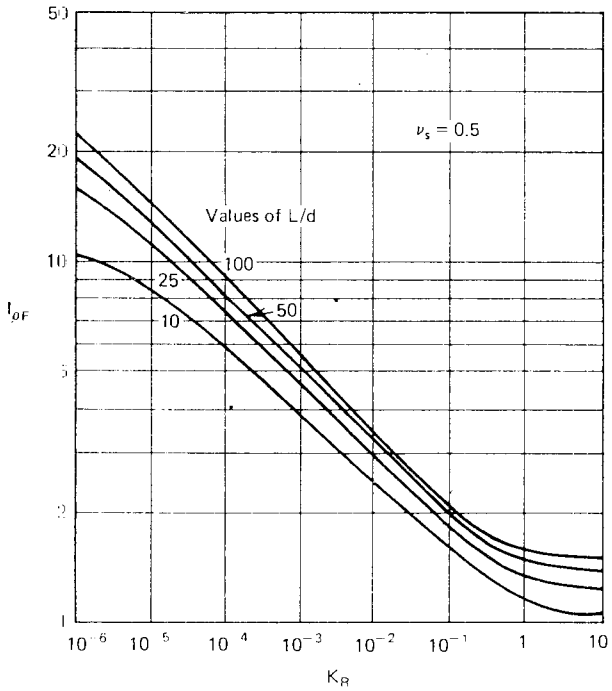

FIGURE 8.19 Influence factor $I_{\rho F}$–fixed-head floating pile, constant soil modulus.

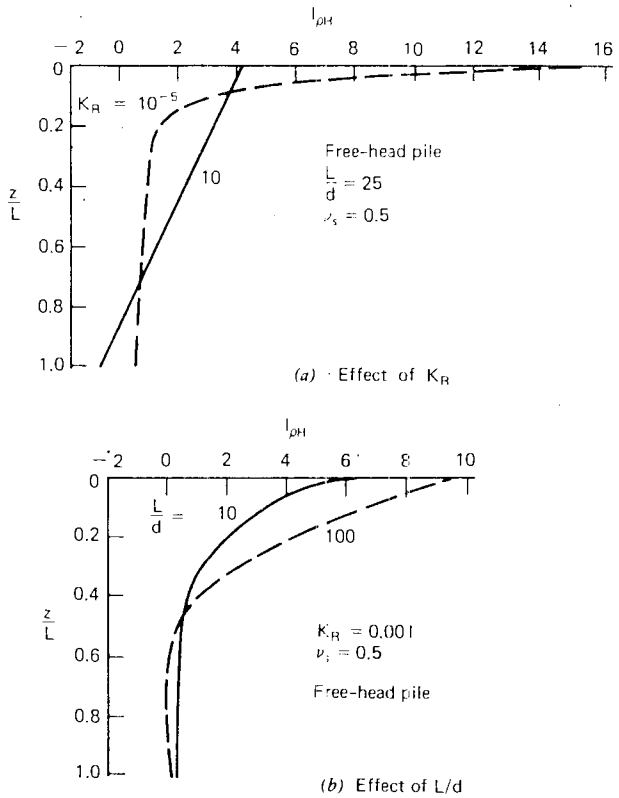

FIGURE 8.21 Typical displacement profiles along pile.

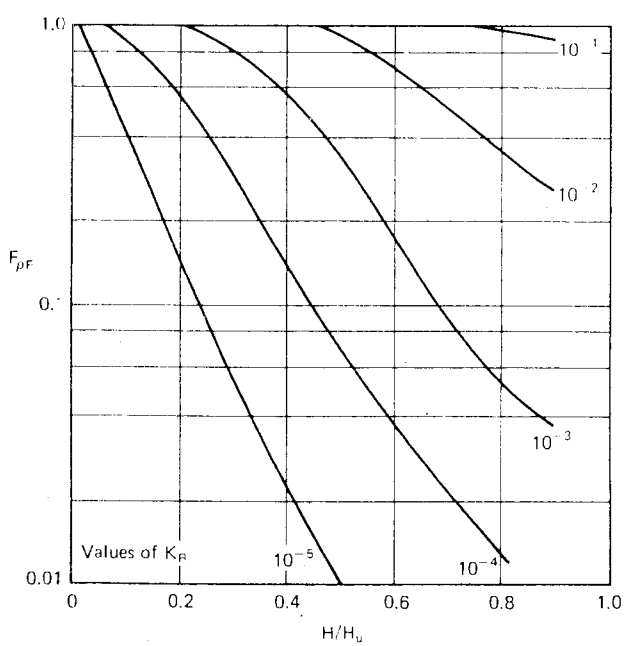

FIGURE 8.20 Yield-deflection factor $F_{\rho F}$–fixed-head pile, uniform E_s and p_y.

$I_{\rho F}$ = displacement-influence factor for horizontal load on fixed-head pile

$F_{\rho F}$ = yield-rotation factor for fixed-head pile

Values of $I_{\rho F}$ and $F_{\rho F}$ are plotted in Figs. 8.19 and 8.20. For this case, the ultimate load, H_u, is defined as

$$H_u = p_y dL \tag{8.69}$$

Typical displacement profiles along a pile showing the effects of L/d and K_R are shown in Fig. 8.21 for the case of a purely elastic soil.

An example of the effects of pile length and soil modulus on the horizontal movement is shown in Fig. 8.22 for a free-head concrete pile 1 ft in diameter, in a purely elastic soil and subjected to horizontal load only. For the soft soil, a rapid reduction in displacement occurs as pile length increases, up to a length of about 30 ft. Further increasing the length results in little or no reduction in displacement, a result that is consistent with the concept of effective length frequently employed in subgrade-reaction analysis. Similar characteristics are shown by the piles in stiffer soils, except that the relative reduction in displacement with increasing pile length becomes less as E_s in-

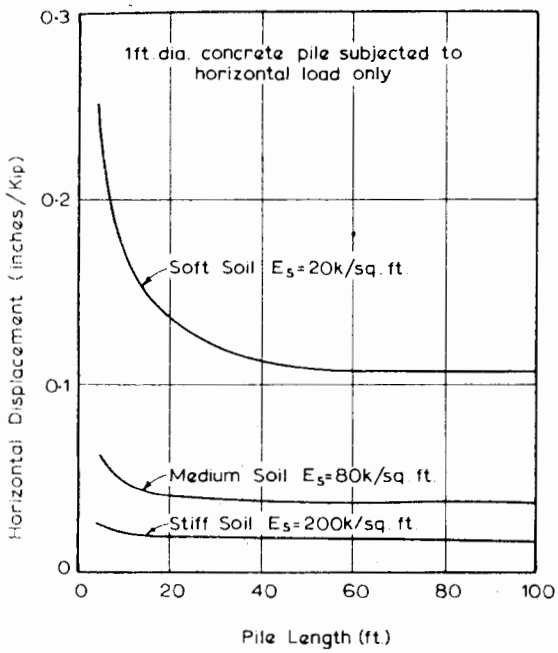

FIGURE 8.22 Influence of pile length and soil modulus on pile displacement.

creases. Figure 8.22 also gives some indication of the possible order of error in predicted movements caused by errors in estimating E_s.

For relatively short and rigid free-head plates, Douglas and Davis (1964) have presented corresponding elastic-displacement and rotation-influence factors. These factors, which are shown in Fig. 8.23, should be more accurate than the corresponding values for short, rigid piles in Figures 8.13, 8.14, and 8.15, because the transverse distribution of pressure is not assumed to be constant across the width, as is the case with the present analysis. For $L/d > 15$, the difference between the two sets of solutions is negligible. By the reciprocal theorem, $I_{\theta H} = I_{\rho M}$. The small discrepancy in Fig. 8.23 results from minor inaccuracy in the numerical analysis. Because the pile is idealized as a thin strip, these solutions will tend to overestimate deflections and rotations for a pile of finite thickness. The errors involved in the 'thin-strip' idealization are discussed by Randolph (1977), and are generally less than 15%.

The elastic analysis enables determination of the relative amounts of undrained movement ρ_i and final movement ρ_{TF} of the pile. ρ_i is calculated by using E_s =

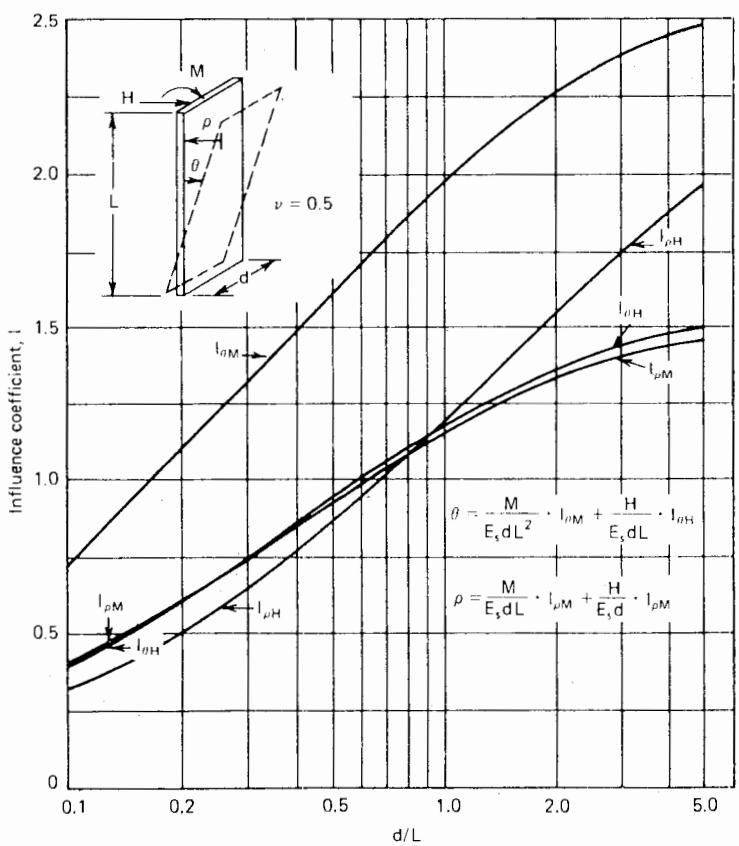

FIGURE 8.23 Influence coefficients for rotation and translation of rigid plate (Douglas & Davis, 1964).

E_u, the undrained Young's modulus of the soil, and the influence factors for $\nu_s = 0.5$ (the undrained Poisson's ratio of the saturated soil); ρ_{TF} is calculated by using $E_s = E'$, the drained modulus of the soil, and the influence factors for $\nu_s = \nu_s'$ (the drained Poisson's ratio). For an ideal two-phase soil, $E_u = 3E'/2(1 + \nu')$, and ratios of ρ_i/ρ_{TF} are shown in Fig. 8.24 as a function of K_R, for $\nu_s' = 0$. For practical values of L/d and K_R, ρ_i/ρ_{TF} is considerably greater than 0.5. Furthermore, for most soils, ν_s' is likely to be significantly greater than zero, and thus ρ_i/ρ_{TF} may be 0.7 or more. It can therefore be concluded that, as with axially loaded piles, the time-dependent displacement is not likely to be of major importance. Some confirmation of the above conclusion is provided by the model pile tests reported by Prakash and Saran (1967), in which a ratio of ρ_i/ρ_{TF} of about 0.75 was obtained for a relatively stiff pile having $L/d = 32$. This conclusion applies only at relatively low load levels, since time-dependent movements caused by creep may become significant at loads approaching failure.

In addition to the displacement and rotation of the pile at the ground surface, the solutions presented may be used to calculate the displacement of a pile at a point above the level of the ground surface. For example, for a free-head pile subjected to load H at a distance e above the surface, the displacement at the point of application of the load is given by

$$\rho = \left(\frac{H}{E_s L}\right)\left(I_{\rho H} + \frac{e}{L} I_{\rho M}\right)/F_\rho + \left(\frac{He}{E_s L^2}\right)\left(I_{\theta H} + \frac{e}{L} I_{\theta M}\right)/F_\theta + \frac{He^3}{3E_p I_p} \tag{8.70}$$

For the case of a pile projecting a distance e above the ground surface and having a fixed head, an equation may be derived for the fixing moment M_f at the pile head by obtaining an expression for the pile-head rotation in terms of M_f and the applied lateral load H, and equating this expression to zero. Knowing M_f, the pile-head deflection can be calculated. Further consideration is given to this case in Section 9.3.3.

8.3.2.2 *EFFECT OF PILE-SOIL SEPARATION*

An example of the effects of pile-soil separation is shown in Fig. 8.25. The ratio ρ_e/ρ of the displacement from a purely elastic analysis to the displacement including separation effects is plotted against dimensionless horizontal load $H/\gamma L^3$. Even at relatively low loads, ρ_e/ρ is less than one: that is, displacements are affected by separation, this effect being generally more pronounced for more flexible piles. For normal working loads, the analysis indicates that separation occurs to a depth of about $0.2L$ for flexible piles and up to $0.4L$ for rigid piles. Figure 8.25 indicates that for practical purposes, the effect of separation is to

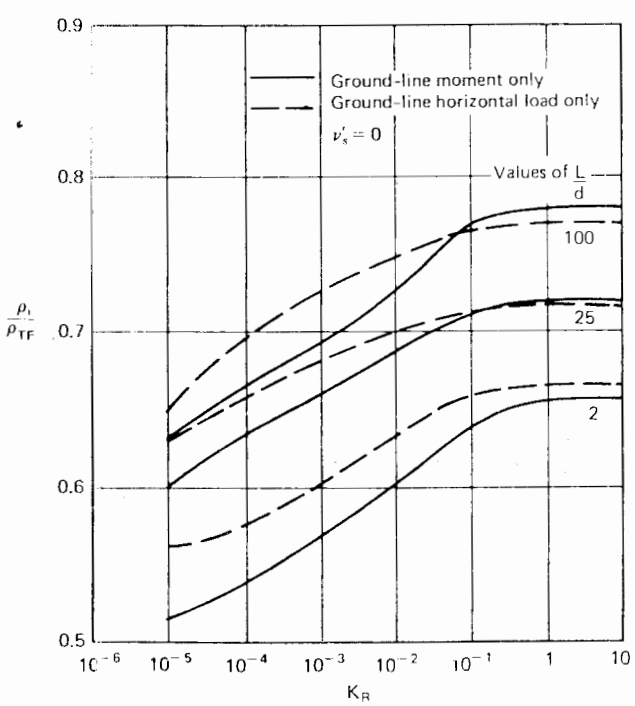

FIGURE 8.24 Theoretical ratio of immediate to total-final displacement.

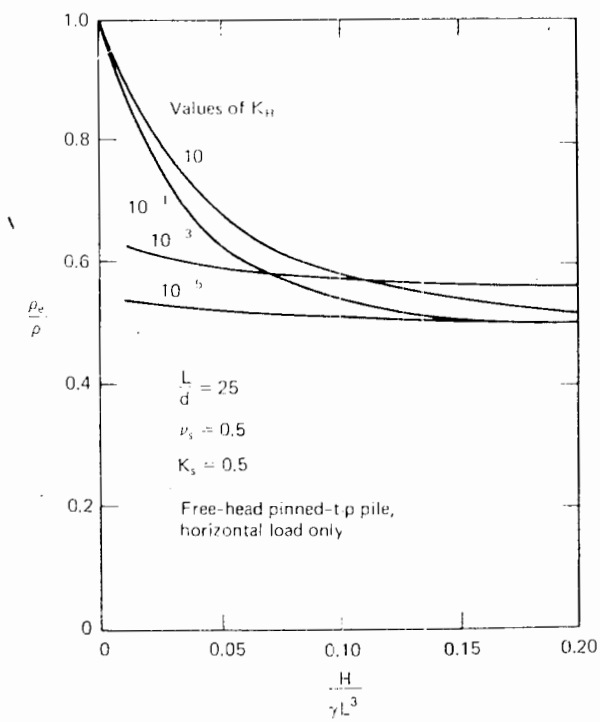

FIGURE 8.25 Example of effect of pile-soil separation on head movement.

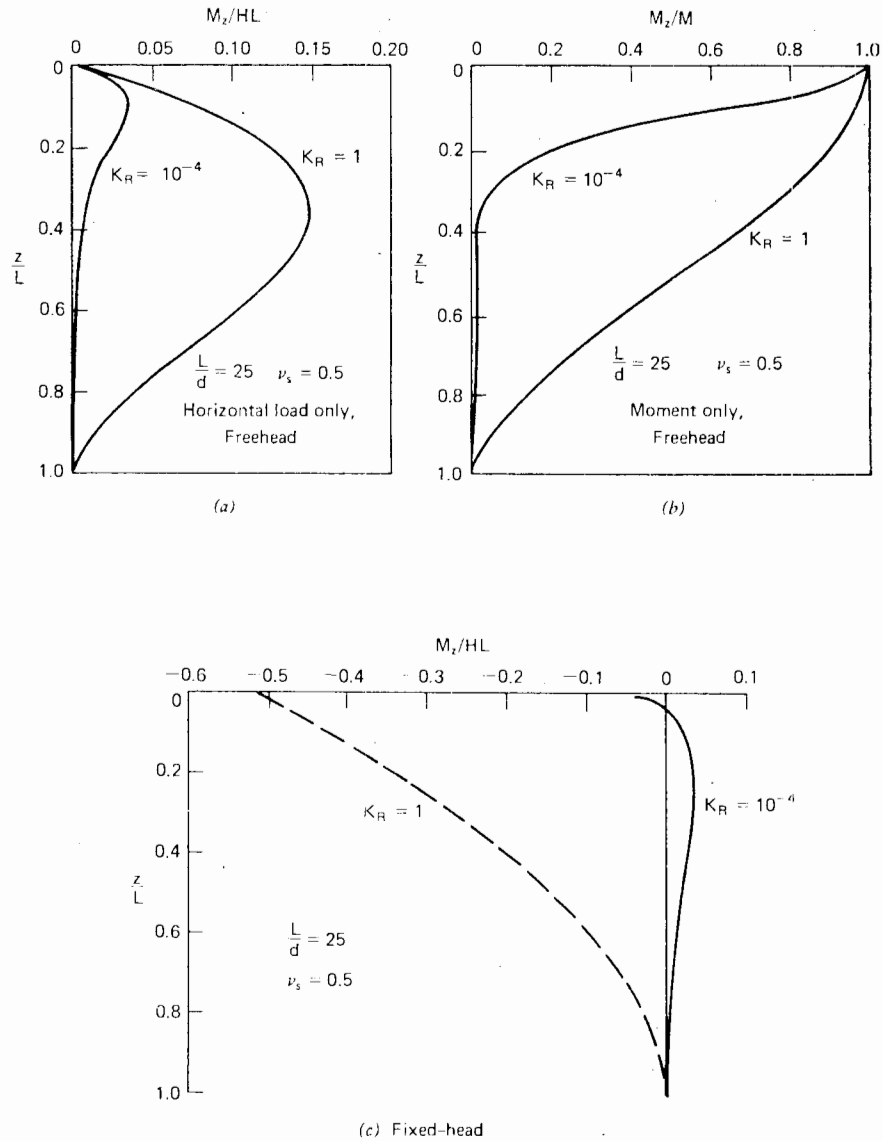

FIGURE 8.26 Typical moment distributions.

virtually double the deflection of the pile head under elastic conditions. This effect may also be considered as approximately equivalent to reducing the soil modulus by a factor of about 2.

8.3.2.3 MOMENTS IN PILE

Typical moment distributions along a pile in a purely elastic soil are shown in Fig. 8.26. The variation with K_R and L/d of the maximum moment in a free-head pile in an elastic soil subjected to horizontal load is shown in Fig. 8.27. This maximum moment typically occurs at a depth of between $0.1L$ and $0.4L$ below the surface, the larger depths occurring for stiffer piles. For moment-loading only, the maximum moment always occurs at the surface and equals the applied moment.

For a fixed-head pile, unless the pile is very flexible ($K_R < 10^{-5}$), the maximum moment occurs at the pile head where the restraint is provided. The variation of this restraining moment with K_R and L/d is shown in Fig. 8.28 for the case of an elastic soil.

An example of the influence of local yield on the moments in a pile is shown in Fig. 8.29. At failure, the maximum value of dimensionless moment M_z/HL in this case is about twice the elastic value (i.e., that for $H/H_u < 0.38$). It should be noted that the elastic distribution of

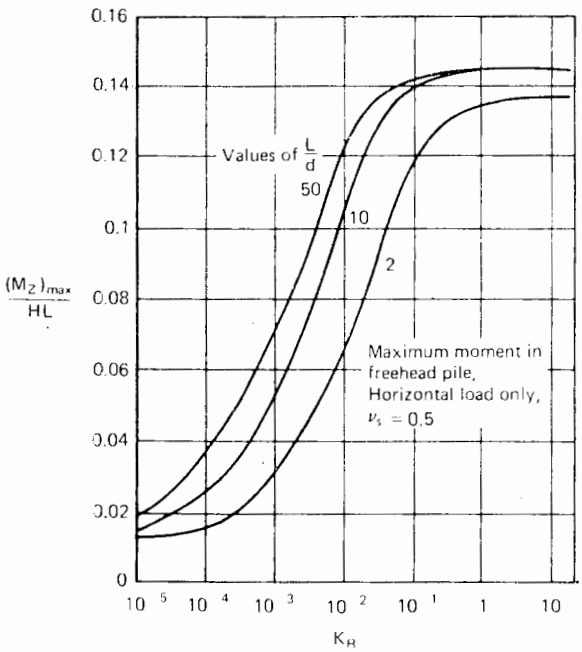

FIGURE 8.27 Maximum moment in free-head pile.

moment is largely dependent on the pile flexibility, K_R, whereas the distribution at failure is independent of K_R. It therefore follows that the largest increases in moment during local yielding may occur in relatively flexible piles in which the moments under elastic conditions are small.

8.3.2.4 COMPARISONS WITH SUBGRADE-REACTION THEORY

To compare solutions from elastic theory with those from subgrade-reaction theory, it is necessary to establish a relationship between Young's modulus, E_s, and the modulus of subgrade reaction, k_h. The most reasonable method appears to be to equate the elastic and subgrade-reaction solutions for the displacement of a stiff fixed-head pile. Assuming $\nu_s = 0.5$ and using values of $I_{\rho F}$ from Fig. 8.19, for $L/d = 25$, $k_h = 0.82\, E_s/d$.

Comparisons between the elastic and subgrade-reaction solutions for displacement and rotation factors are shown in Fig. 8.30 for $L/d = 25$. In all cases, the values from subgrade-reaction theory are greater than those from elastic theory. For $L/d < 25$, the difference between the two theories is greater than that shown in Fig. 8.30. Thus, subgrade-reaction theory tends to overestimate displace-

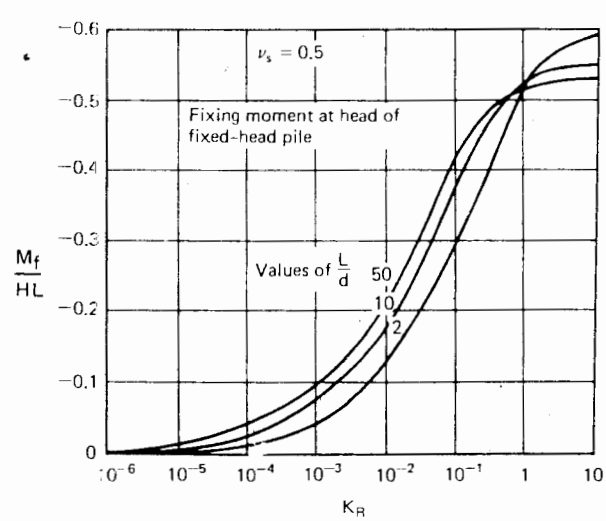

FIGURE 8.28 Fixing moment at head of fixed-head pile.

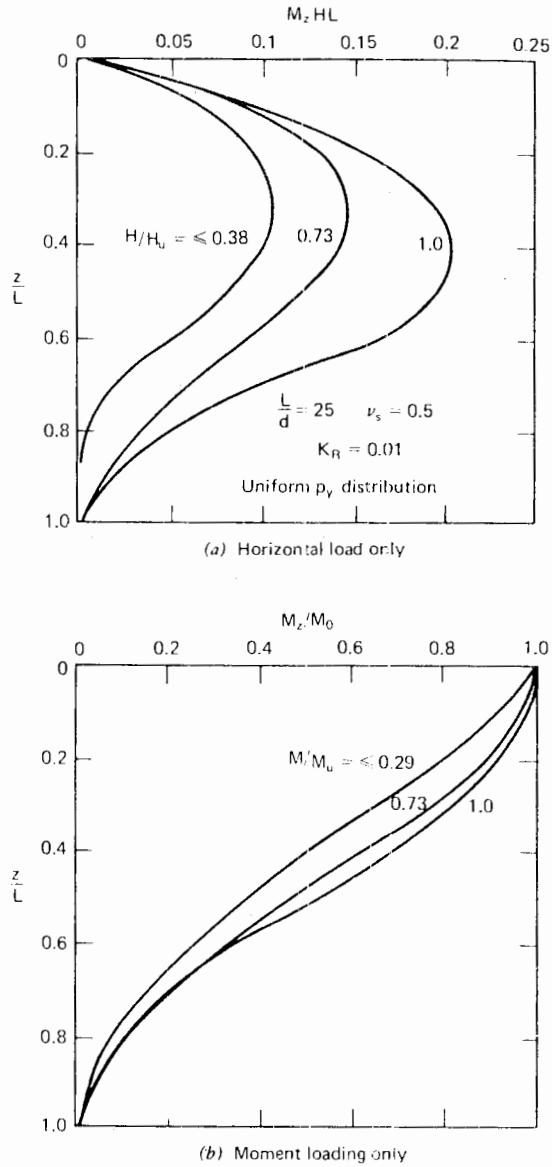

FIGURE 8.29 Influence of local yield on moments in pile.

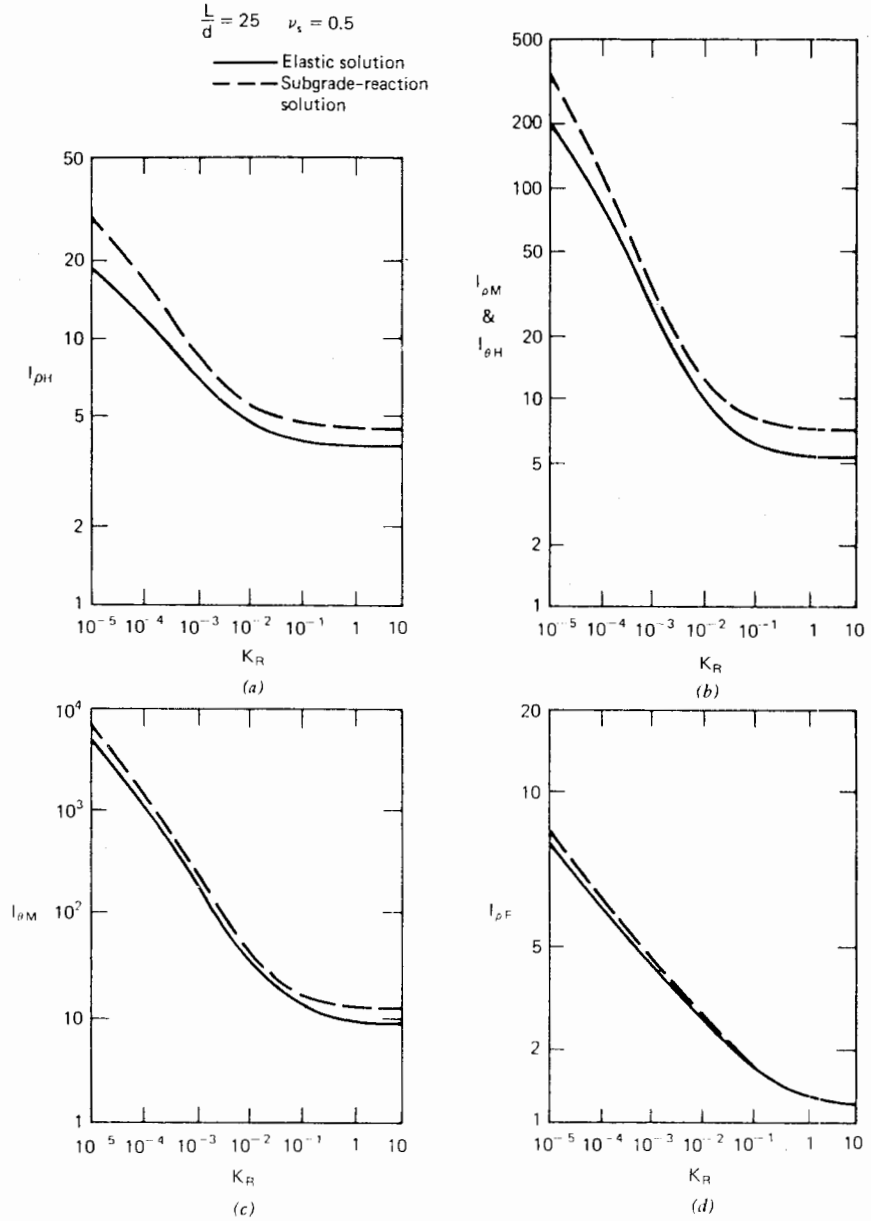

FIGURE 8.30 Comparison of elastic and subgrade-reaction solutions for displacements and rotations, constant E_s.

ments and rotations if k_h and E_s are related as described above. The discrepancy between the two theories will be decreased if the relationship between k_h and E_s is varied as the relative flexibility of the pile varies, as suggested by Vésic (1961) for strip foundations.

Comparisons between elastic and subgrade-reaction solutions for moments are shown in Fig. 8.31. The largest difference again occurs for relatively flexible piles, for which subgrade-reaction theory overestimates the moments. However, the two solutions are in reasonable agreement for stiffer piles and the overall agreement is better than for displacements and rotations.

8.3.2.5 COMPARISONS WITH SOLUTIONS FROM A "SECANT MODULUS" APPROACH

In practical predictions of lateral deflection of piles, it has been customary practice to use the solutions obtained from an analysis in which no soil yield is assumed to occur, together with an appropriately-chosen secant modulus of the soil. It is obvious that in such an approach, the secant

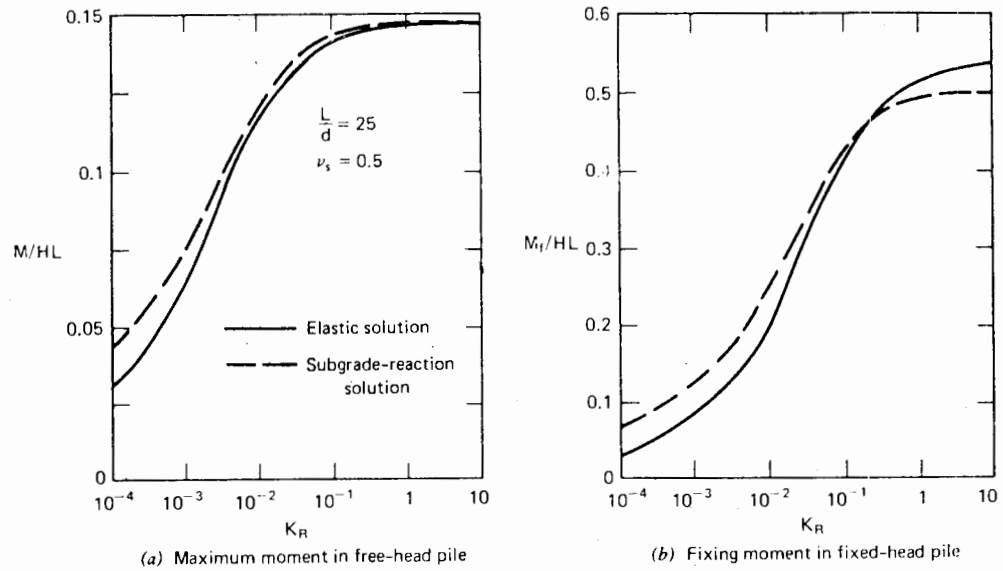

FIGURE 8.31 Comparison of elastic and subgrade-reaction solutions for moments, constant E_s.

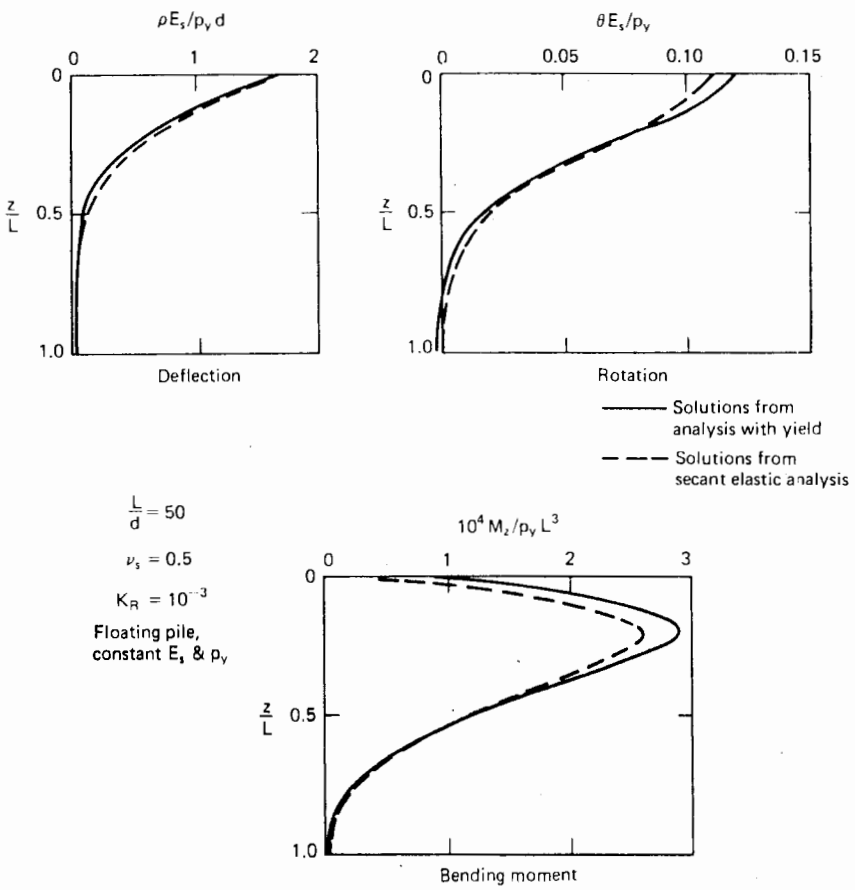

FIGURE 8.32*a* Comparisons between solutions with soil yield and secant-elastic solutions, $H/H_u = 0.4$.

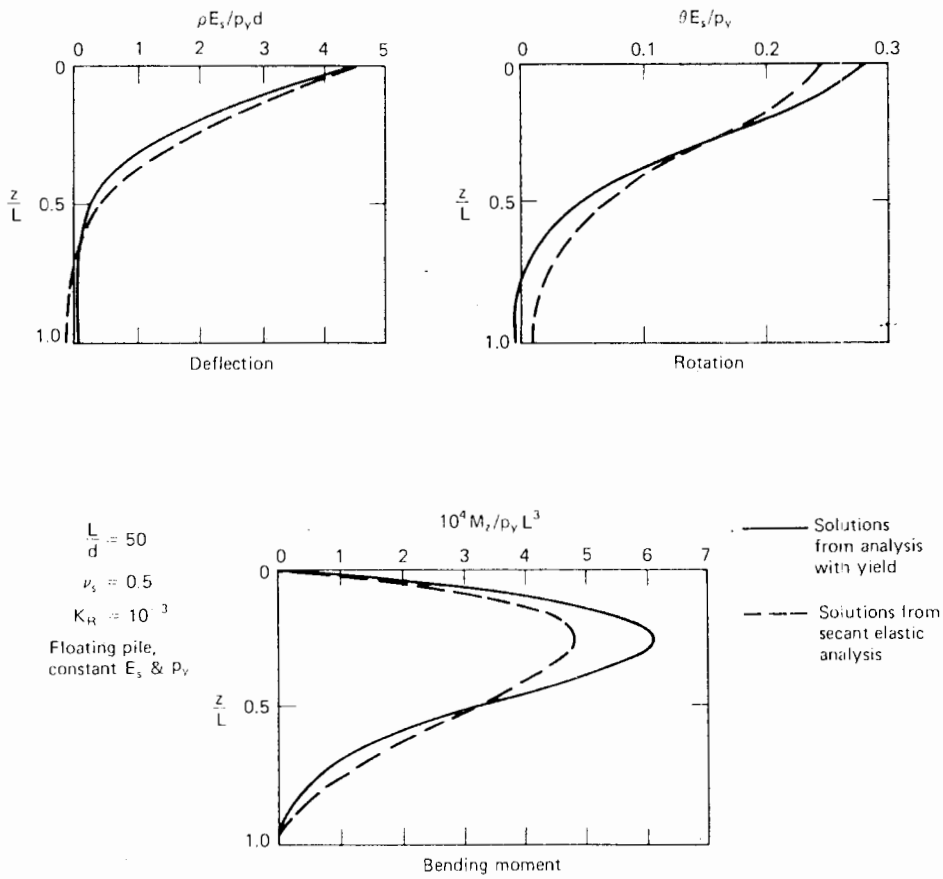

FIGURE 8.32*b* Comparisons between solutions with soil yield and secant-elastic solutions, $H/H_u = 0.6$.

modulus (whether it be a modulus of subgrade reaction or an elastic modulus) will decrease as the load on the pile increases. It is of some interest now to examine the relationship between solutions for pile behavior obtained from this "secant elastic approach" with those obtained from the analysis incorporating the effects of pile-soil yield, as described above.

Comparisons are shown in Figs. 8.32*a*, 8.32*b* and 8.32*c* for a typical floating pile in a uniform soil, subjected to a lateral force H at the ground line. Solutions are expressed in dimensionless form, E_s being the original "true" elastic modulus of the soil. The secant-elastic modulus for each load level has been obtained by fitting the elastic and yield solution for ground-line deflection of the pile, and determining the equivalent soil modulus, as described in Section 8.5. Figure 8.32 shows that the solutions, although generally similar, do differ significantly as the applied force approaches the ultimate. The main differences are that the secant-elastic approach underestimates the ground-line rotation and the maximum bending moment. However, at normal working-load levels (e.g., $H/H_u = 0.4$), the differences are not great, and it would appear that the secant-elastic approach will not be in serious error unless a significant amount of local yield occurs along the pile.

8.3.3 Solutions for Floating Pile in Soil with Linearly Increasing Modulus

For sands and soft normally consolidated clays solutions for linearly increasing soil modulus with depth are required since the assumption of one constant modulus may lead to solutions of unacceptable inaccuracy. As previously mentioned the Mindlin equation can still be used when the modulus is not constant although the resulting solutions will only be approximate, and will tend to over-estimate groundline deflections and rotations somewhat (Banerjee and Davies, 1978). In the solutions described below, the soil modulus E_s is assumed to increase linearly with depth, from zero at the ground surface, so that at any depth z, the modulus is

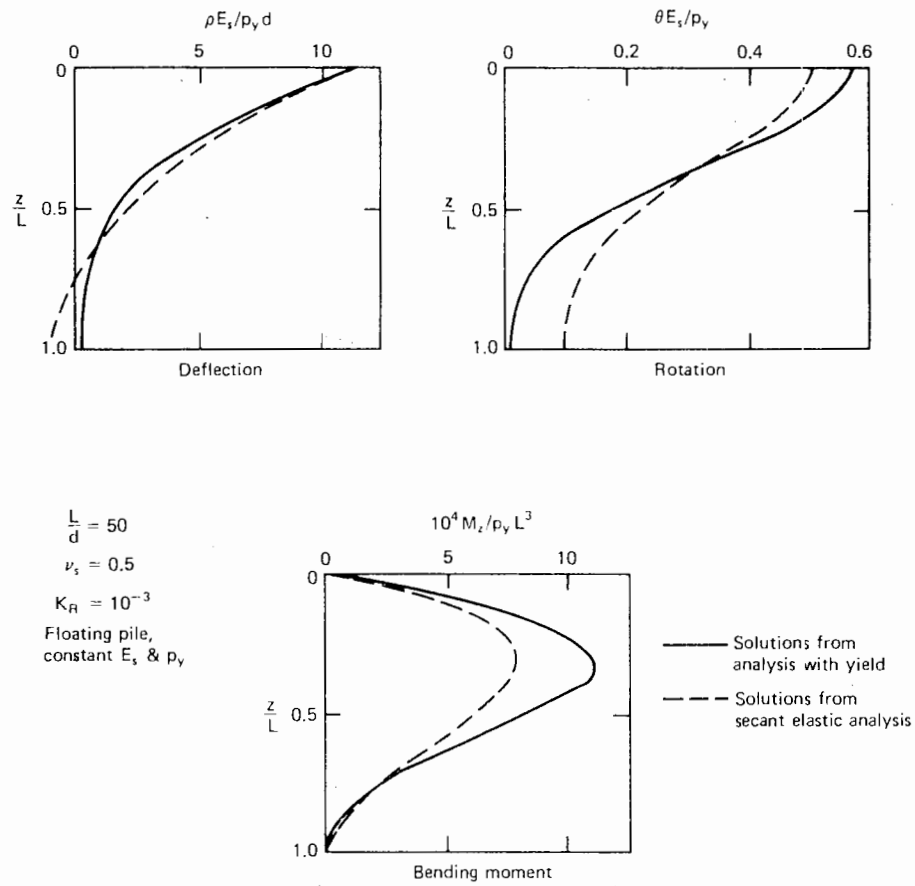

FIGURE 8.32*c* Comparisons between solutions with soil yield and secant-elastic solutions, $H/H_u = 0.8$.

$$E_s = N_h z \tag{8.71}$$

where

N_h = rate of increase of E_s with depth

N_h is analogous to n_h (Eq. 8.11) in subgrade-reaction theory, and if E_s and k_h are assumed to increase with depth at the same rate, then

$$N_h = n_h \tag{8.72}$$

The pile-flexibility factor is now defined as

$$K_N = \frac{E_p I_p}{N_h L^5} \tag{8.73}$$

The soil-yield strength, p_y, is also assumed to vary linearly with depth, from zero at the surface to a value of p_L at the level of the pile tip.

8.3.3.1 DISPLACEMENT AND ROTATION

The ground-line displacement, ρ, and rotation, θ, of a free-head pile may be expressed as follows:

$$\rho = \frac{H}{N_h L^2}\left(I'_{\rho H} + \frac{e}{L} \cdot I'_{\rho M}\right)/F'_\rho \tag{8.74}$$

$$\theta = \frac{H}{N_h L^3}\left(I'_{\theta H} + \frac{e}{L} \cdot I'_{\theta M}\right)/F'_\theta \tag{8.75}$$

where

$I'_{\rho H}, I'_{\rho M}$ = elastic-influence factors for displacement caused by horizontal load and moment, respectively, for linearly varying E_s, and similarly for $I'_{\theta H}$ and $I'_{\theta M}$

F'_ρ = yield-displacement-factor = ratio of pile displacement in elastic soil to pile displacement in yielding soil, for linearly increasing E_s and p_y, and similarly for F'_θ.

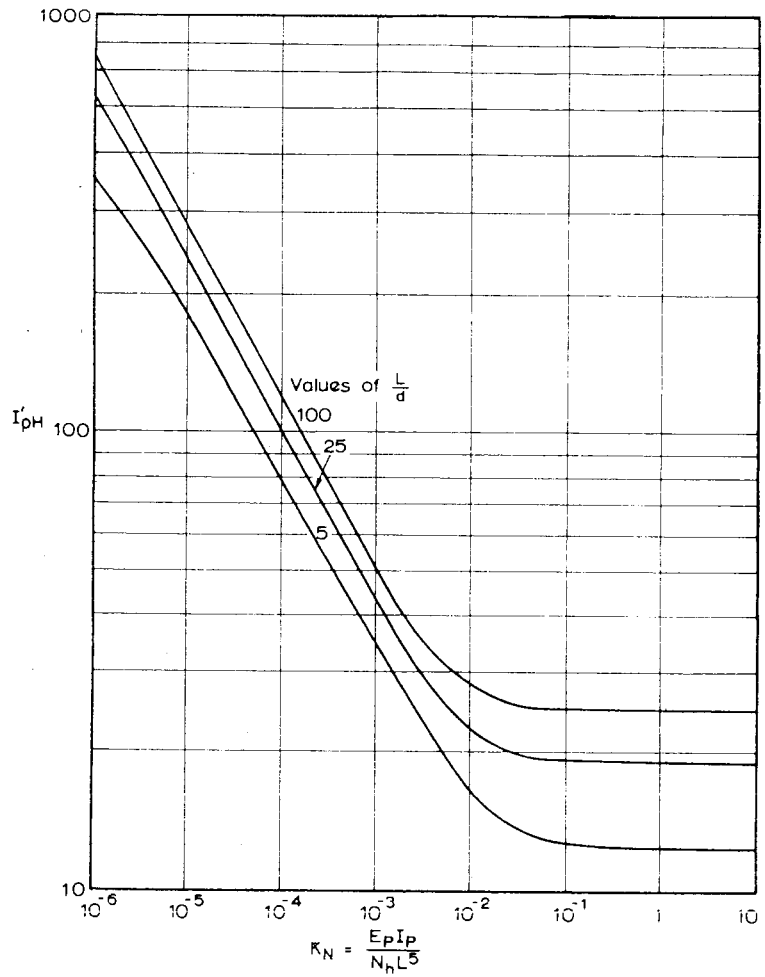

FIGURE 8.33 Values of I'_{pH}–free-head floating pile, linearly-varying soil modulus.

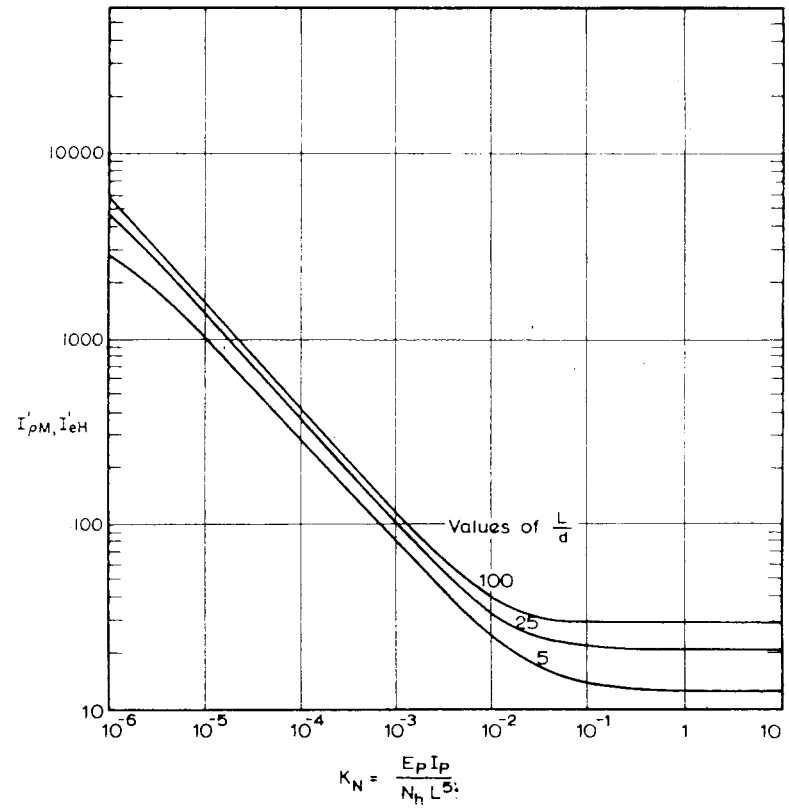

FIGURE 8.34 Values of I'_{pM} and $I'_{\theta H}$–free-head floating pile, linearly-varying soil modulus.

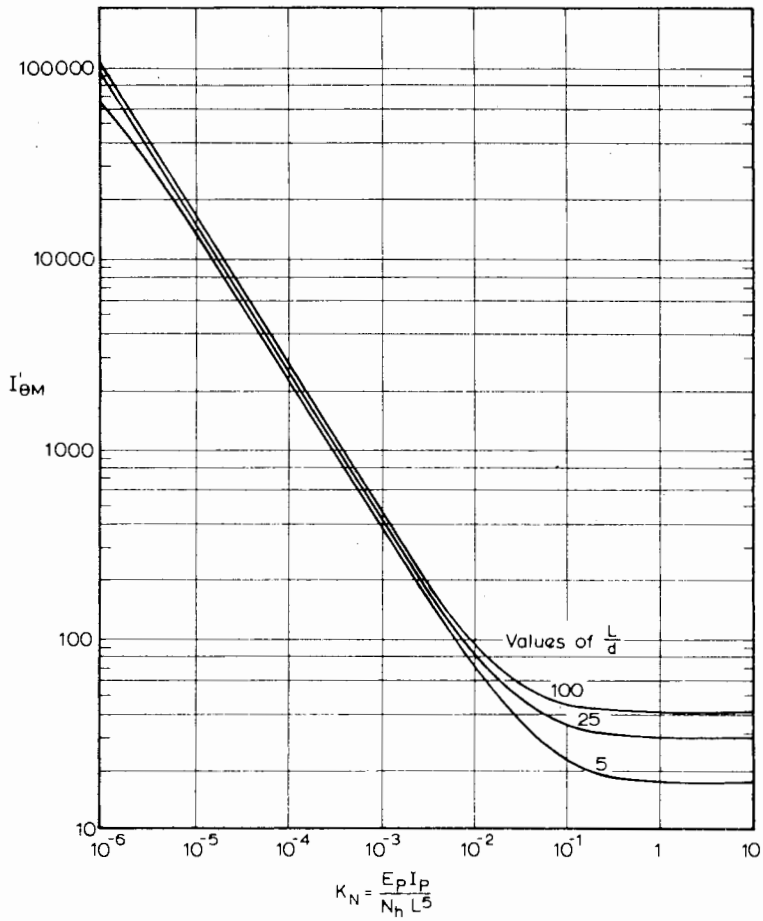

FIGURE 8.35 Values of $I'_{\theta M}$–free-head floating pile, linearly-varying soil modulus.

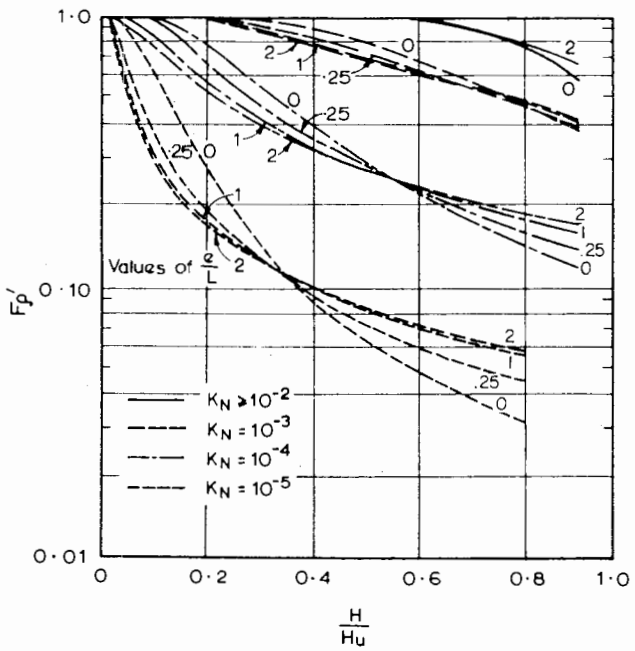

FIGURE 8.36 Yield-displacement factor F'_p–free-head floating pile, linearly-varying E_s and p_y.

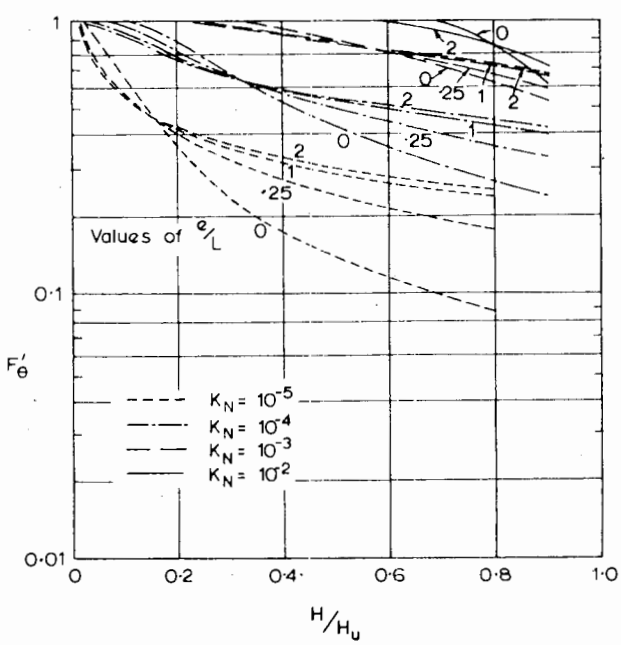

FIGURE 8.37 Yield-rotation factor F'_θ–free-head floating pile, linearly varying E_s and p_y.

The elastic influence factors $I'_{\rho H}$, etc., are given in Figs. 8.33, 8.34, and 8.35. The yield factors F'_{ρ} and F'_{θ} are, again, functions primarily of e/L, K_N, and H/H_u; they are shown in Figs. 8.36 and 8.37. H_u, which in this case, may again be obtained from statical considerations, is shown in dimensionless form in Fig. 7.2 as a function of e/L.

For a fixed-head pile, the ground-line deflection is given by

$$\rho = \frac{H}{N_h L^2} I'_{\rho F} / F'_{\rho F} \tag{8.76}$$

The elastic influence factor $I'_{\rho F}$ is plotted in Fig. 8.38, while the yield-displacement factor $F'_{\rho F}$ is plotted in Fig. 8.39. In the latter figure, H_u is given by $0.5 p_L dL$.

Illustrative Example of Construction of Load-Deflection Curve for Single Pile

The application of the theory is illustrated in the following example. The case considered is a free-head steel-tube pile, 40-cm O.D. and 2-cm wall thickness, situated in a medium-dense sand. The pile is 14-m long, embedded 10 m in the sand, and loaded at the top—that is, at an eccentricity of 4 m above the ground surface. The sand is assumed to have strength parameters $c'=0$ and $\phi' = 34°$, a saturated unit weight of 1.91×10^{-3} kg/cm^3, and a Young's modulus that varies linearly with depth. From Terzaghi's correlation (Table 8.5), the coefficient of subgrade reaction, n_h, is 0.5 kg/cm^3 and the rate of increase of Young's modulus with depth, N_h, will be taken as equal to n_h.

The relationship between applied horizontal load and ground-line deflection will be computed. For the pile,

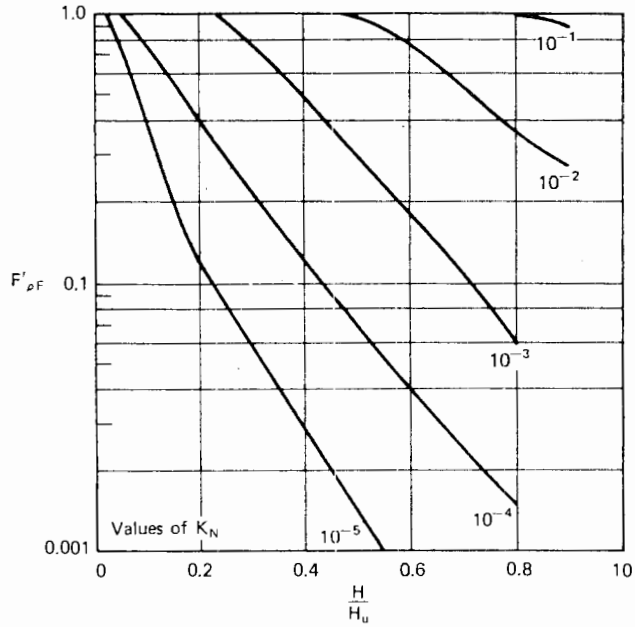

FIGURE 8.39 Yield-displacement factor $F'_{\rho F}$—fixed-head floating pile, linearly-varying E_s and p_y.

$$I_p = \frac{\pi}{64}(40^4 - 36^4)$$

$$= 2.33 \times 10^4 \text{ cm}^4$$

Taking

$$E_p = 2.05 \times 10^6 \text{ kg/cm}^2$$

then,

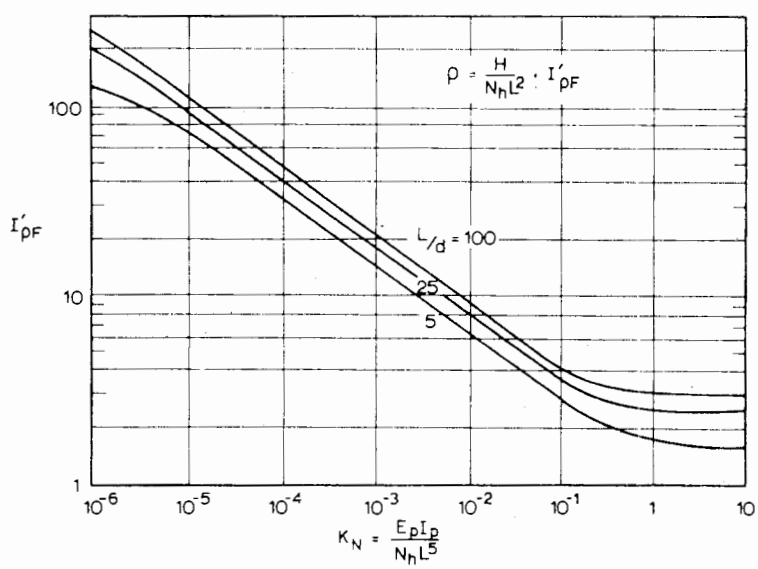

FIGURE 8.38 Values of $I'_{\rho F}$—fixed-head floating pile, linearly-varying soil modulus.

$$E_pI_p = 4.78 \times 10^{10} \text{ kg/cm}^2$$

$$K_N = \frac{E_pI_p}{N_hL^5} = \frac{4.78 \times 10^{10}}{0.5 \times 1000^5} = 9.56 \times 10^{-5}$$

Now,

$$L/d = 1000/40 = 25$$

$$e/L = 4/10 = 0.4$$

From Figs. 8.33 and 8.34,

$$I'_{\rho H} = 101$$

$$I'_{\rho M} = 395$$

Ground-line deflection from Eq. (8.74) is

$$\rho = \frac{H}{N_hL^2}\left[I'_{\rho H} + \frac{e}{L}I'_{\rho M}\right]/F'_p$$

$$= 0.518H/F'_\rho \text{ cm } (H \text{ in tonnes}) \quad (8.77)$$

The ultimate load, H_u, for failure of the soil will now be computed. From Fig. 7.2,

$$\frac{H_u}{\bar{p}_y dL} = 0.169$$

In this case, $\bar{p}_y$ is the yield pressure halfway along the embedded part of the pile. It will be assumed, as suggested by Broms, that $p_y = 3p_p = 3K_p\sigma'_v$

$$\bar{p}_y = 3 \times \tan^2(45 + 34/2) \times 500 \times (1.91 - 1.00) \times 10^{-3}$$

$$= 4.83 \text{ kg/cm}^2$$

$$H_u = 0.169 \times 4.83 \times 40 \times 1000$$

$$= 32{,}600 \text{ kg}$$

$$= 32.6 \text{ tonnes}$$

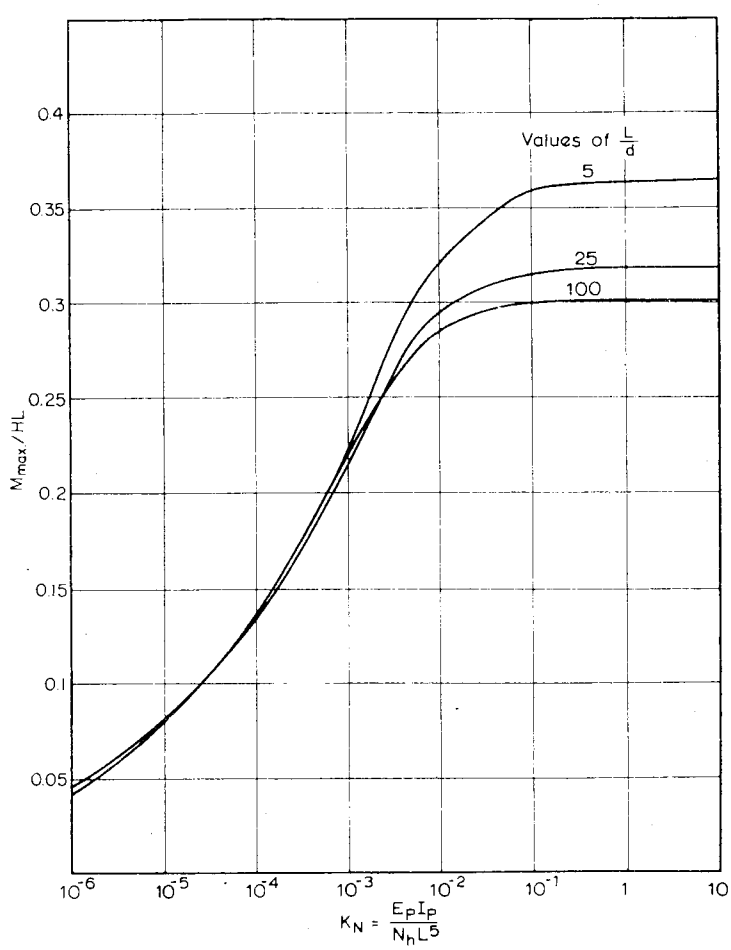

FIGURE 8.40 Maximum moment in free-head pile–linearly-varying soil modulus.

The subsequent calculations for the load-deflection curve are tabulated in Table 8.7.

TABLE 8.7

H (tonnes)	$\frac{H}{H_u}$	F_ρ (Fig. 8.36)	ρ (cm) (Eq. 8.77)
5	0.152	0.76	3.4
10	0.304	0.44	11.8
15	0.456	0.305	25.5
20	0.608	0.23	45.0
25	0.760	0.18	72.0
30	0.912	0.155	100.3

8.3.3.2 MOMENTS IN PILE

For free-head piles, the maximum moment caused by horizontal load only is shown in Fig. 8.40 as a function of L/d and of the pile flexibility factor, K_N. These moments are greater than for a uniform E_s with depth (Fig. 8.27), and occur typically at depths of $0.1L$ to $0.45L$ below the surface, the larger depths being for stiff piles.

The fixing moment at the head of a fixed-head pile is plotted as a function of K_N in Fig. 8.41. Comparison with Fig. 8.28 shows that larger moments are again developed for a linearly-increasing soil modulus.

8.3.3.3 COMPARISONS WITH SUBGRADE-REACTION THEORY

In relating elastic and subgrade-reaction theories, N_h and n_h have been equated. For the displacement factors $I_{\rho H}$, comparisons shown in Fig. 8.42 reveal somewhat closer agreement than with the case of constant modulus. Similar comparisons are found for the other influence factors. The subgrade-reaction solution does not directly take account of the effect of L/d, but in fact corresponds relatively closely to the elastic solutions for $L/d = 25$.

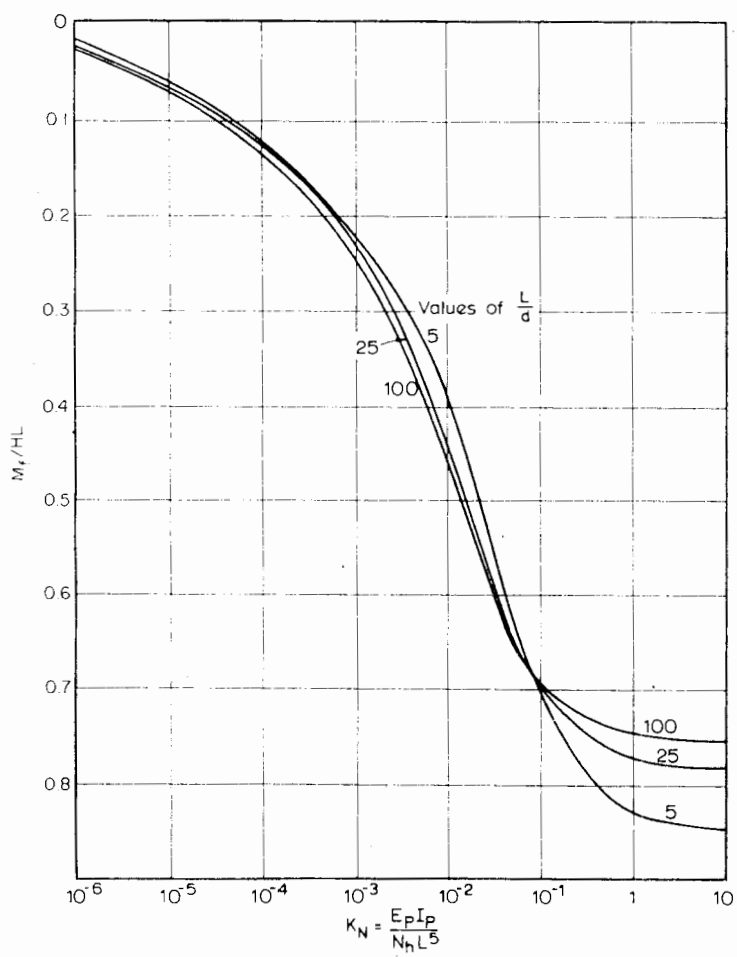

FIGURE 8.41 Fixing moment in fixed-head pile–linearly-varying soil modulus.

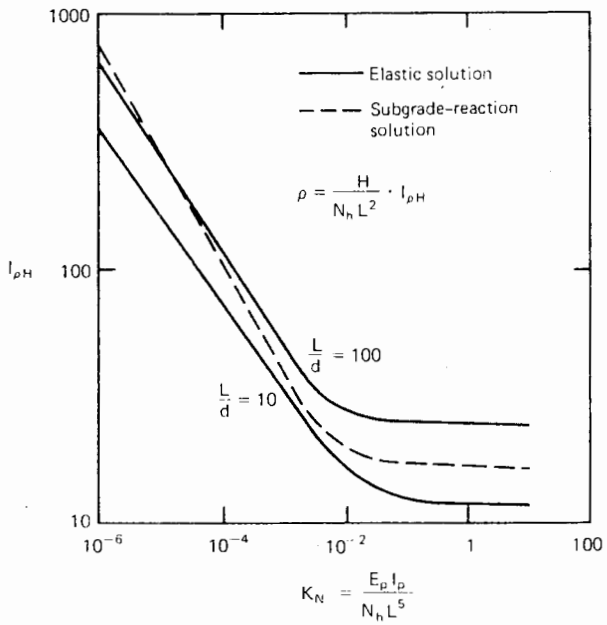

FIGURE 8.42 Comparison between elastic and subgrade-reaction solutions–free-head pile.

8.3.4 Solutions for Socketed Piles

8.3.4.1 DISPLACEMENTS AND ROTATIONS

For a socketed pile in a uniform soil, subjected to a horizontal force H at an eccentricity e above the surface, the displacement and rotation at the ground line may be calculated from the same expressions as for a floating pile (Eqs. 8.64 and 8.65, or Eqs. 8.66 and 8.67); but now, different elastic-influence factors, $I_{\rho H}$, $I_{\rho M}$, $I_{\theta H}$, and $I_{\theta M}$, are used. These factors are plotted in Figs. 8.43, 8.44, and 8.45 for both a pinned tip and a fixed tip. The tip boundary condition has virtually no effect on these factors unless the pile is relatively stiff ($K_R > 10^{-2}$). For smaller values of K_R, the displacement- and rotation-influence factors are almost identical with those for a floating pile. Similarly, for a given load H, the yield factors F_ρ and F_θ for a floating pile may be applied to a socketed pile if K_R is less than 10^{-2}. For larger values of K_R, the effects of local yield at normal working loads are very small, and F_ρ and F_θ may be taken as unity.

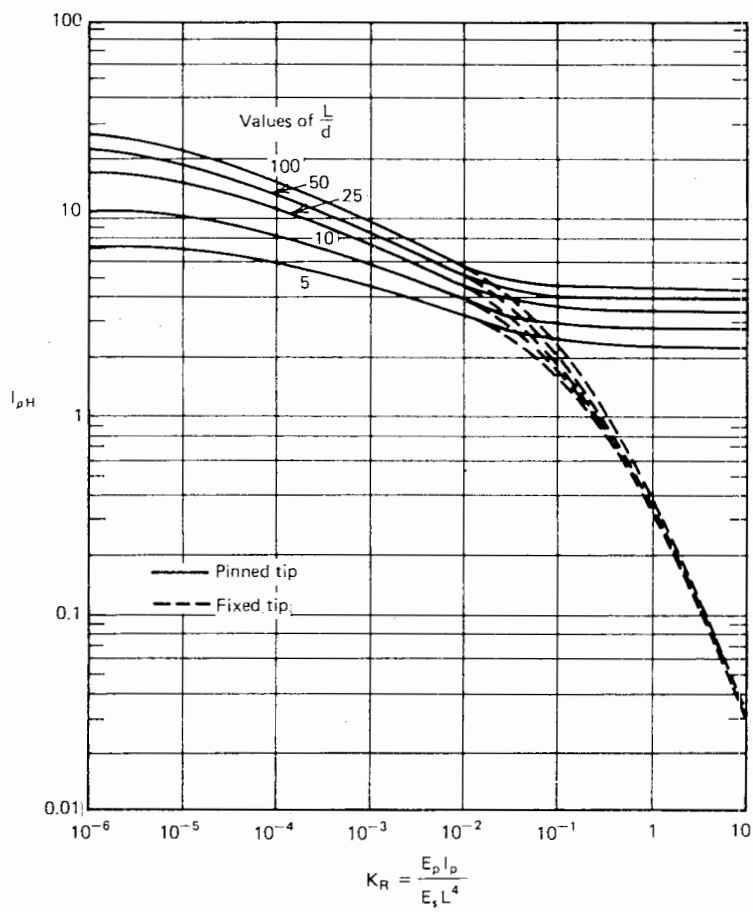

FIGURE 8.43 Influence factors $I_{\rho H}$ for free-head socketed piles in uniform soil.

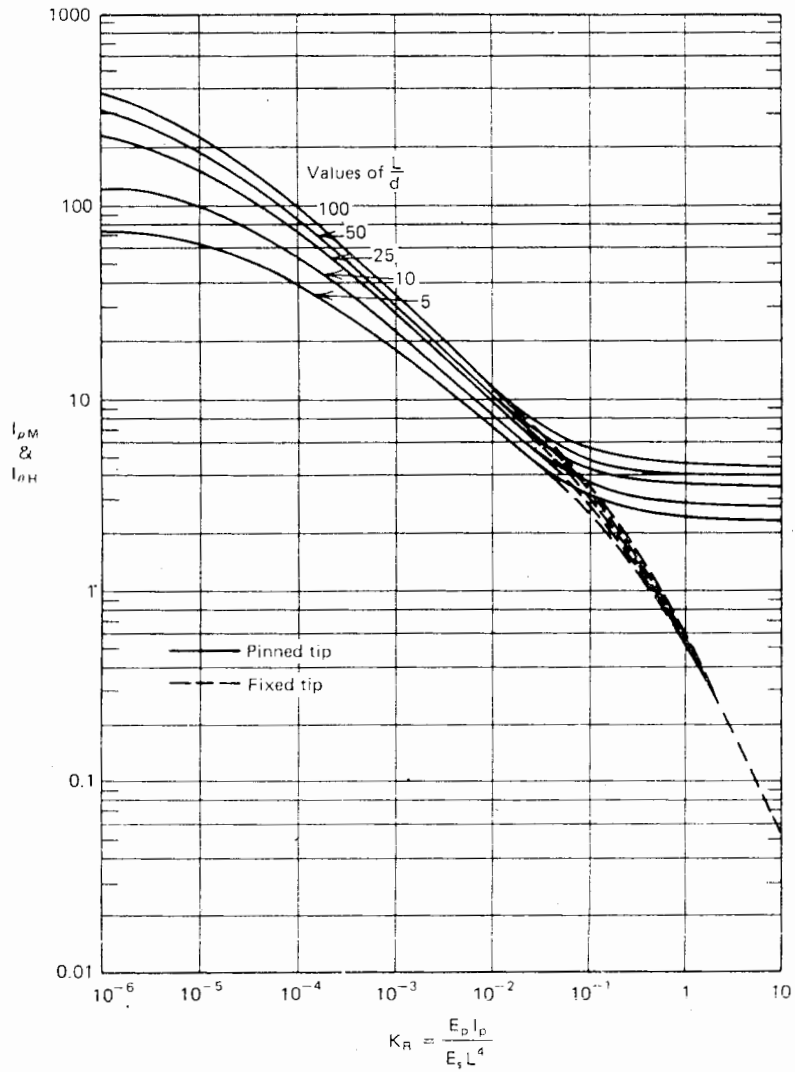

FIGURE 8.44 Influence factors $I_{\rho M}$ and $I_{\theta H}$ for free-head socketed piles in uniform soil.

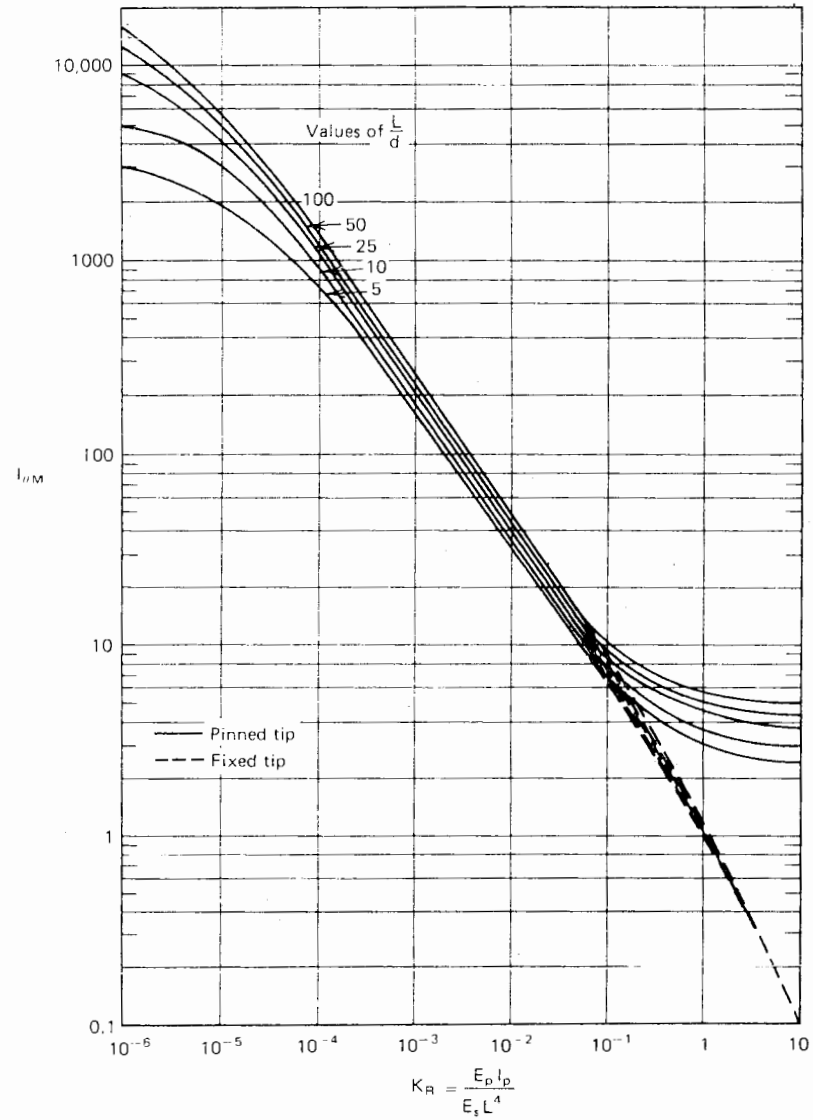

FIGURE 8.45 Influence factors $I_{\theta M}$ for free-head socketed piles in uniform soil.

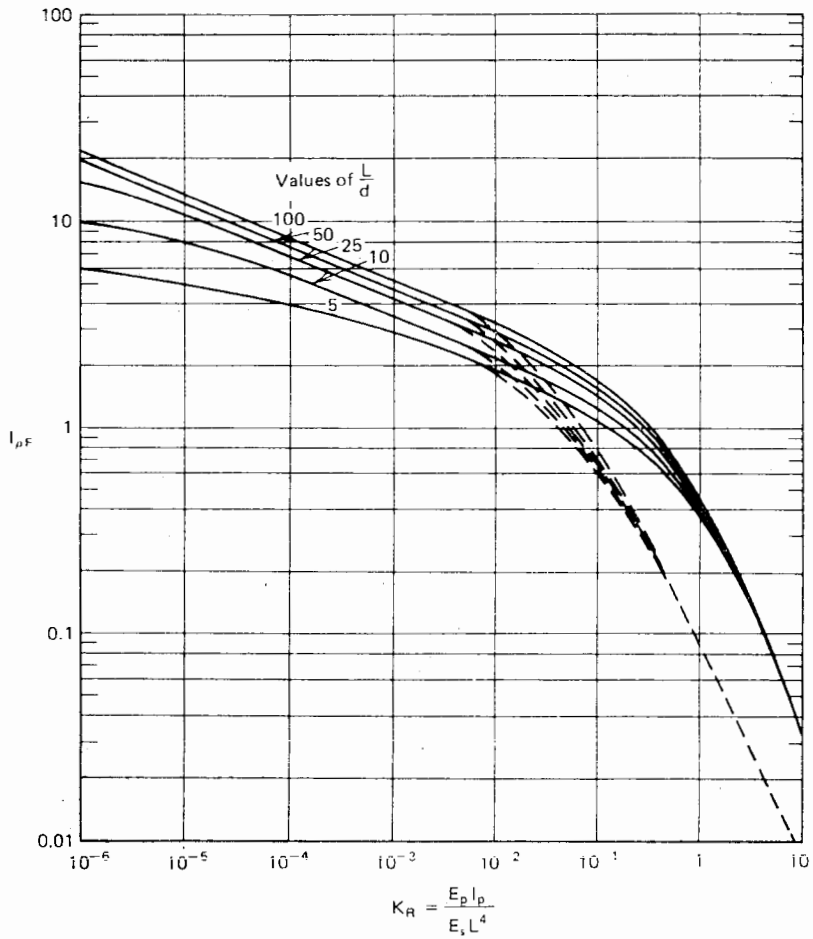

FIGURE 8.46 Influence factor $I_{\rho F}$ for fixed-head socketed piles in uniform soil.

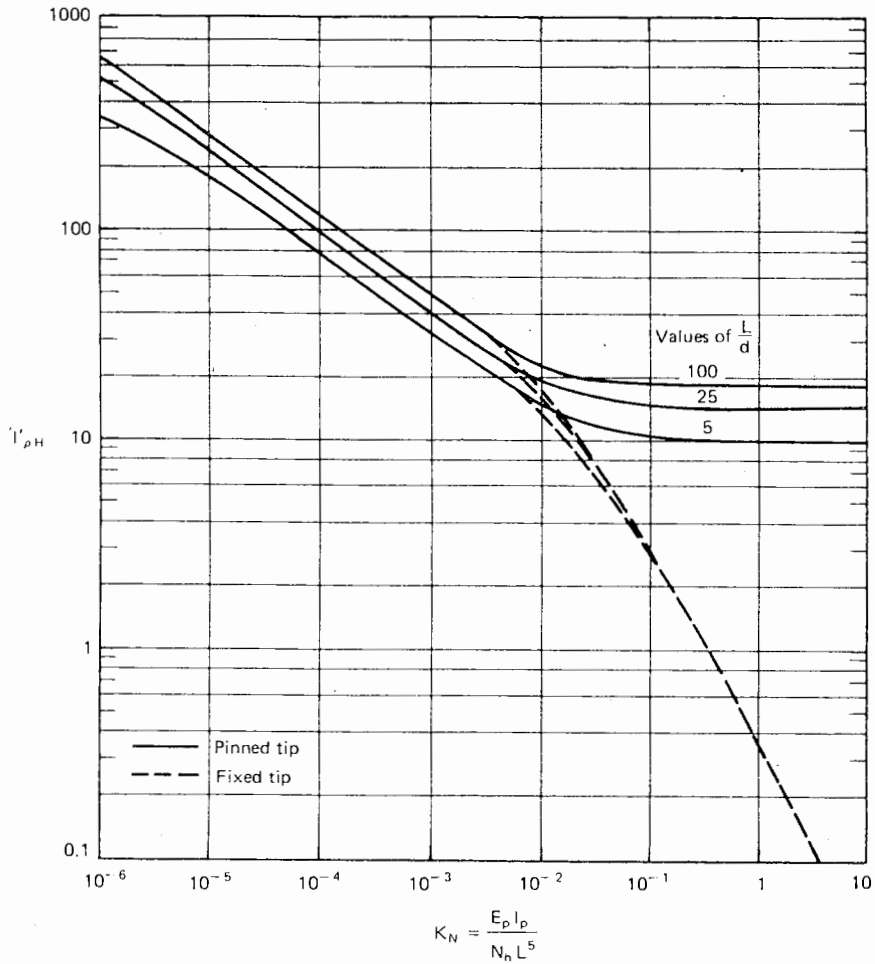

FIGURE 8.47 Values of $I'_{\rho H}$—free-head socketed pile, linearly varying E_s.

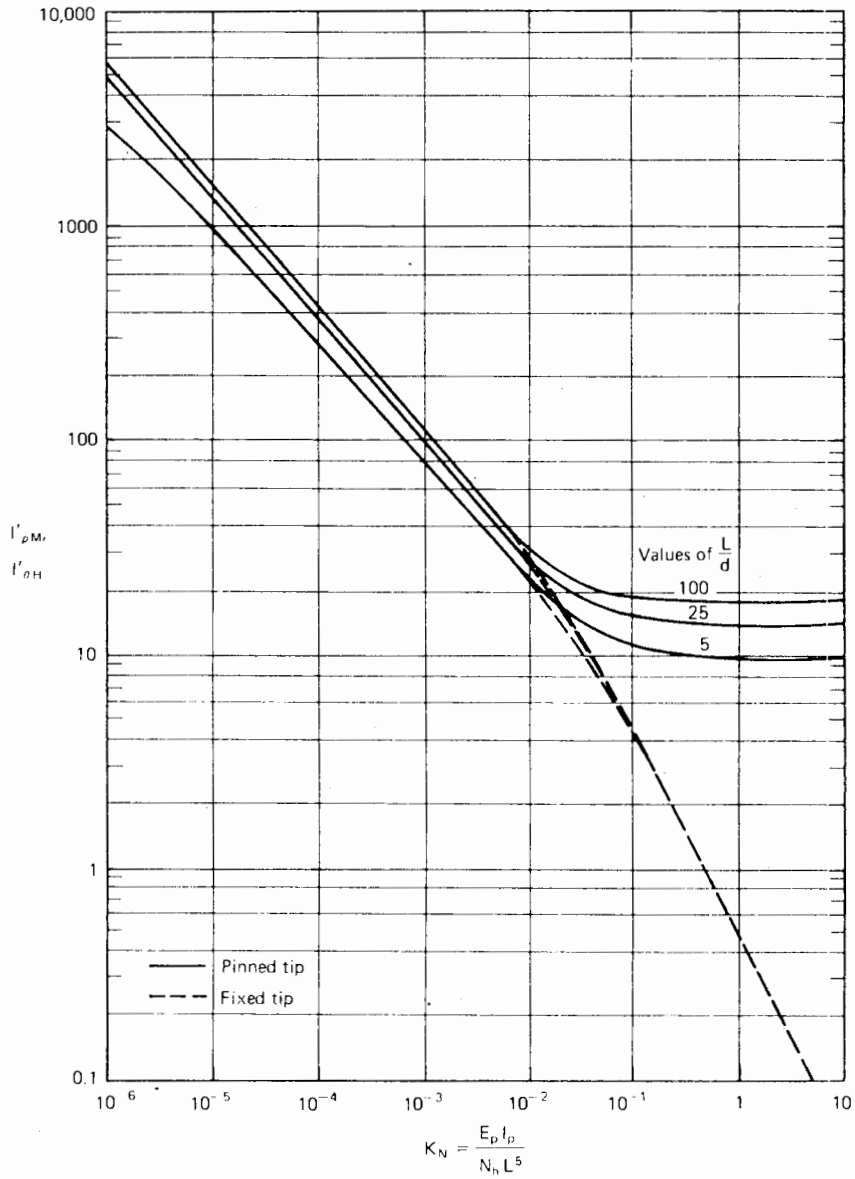

FIGURE 8.48 Values of $I'_{\rho M}$ and $I'_{\theta H}$–free-head socketed piles, linearly varying E_s.

For a fixed-head socketed pile, the groundline displacement is given by Eq. (8.68), and the elastic influence factor $I_{\rho F}$ is plotted in Fig. 8.46.

For the case of piles in a soil with a linearly increasing modulus with depth, the displacement and rotation is given by Eqs. (8.74), (8.75), and (8.76), as for floating piles. The elastic-influence factors ($I'_{\rho F}$, etc.) are plotted in Figs. 8.47 to 8.50. As with the case of a soil with uniform modulus, the yield factors F'_ρ, F'_θ, and $F'_{\rho F}$ for floating piles may be applied to socketed piles at the same load H, provided that the flexibility factor K_N is less than about 10^{-2}.

An example of the effect of pile length, end conditions, and soil modulus on pile-head movement is shown in Fig. 8.51 for a 1-ft-diameter concrete pile. The soil is elastic and has a uniform modulus E_s with depth. As the soil modulus decreases, the pile movement increases until the limiting displacement for an unsupported pile is reached; this limiting value is finite for all cases except the free-head, pinned-tip case. For the pile considered, the tip boundary condition only affects movement if the soil has a modulus less than about 40 lb/in.^{2}–that is, an extremely soft soil. The increase in the effective length of the pile with decreasing modulus is shown in Fig. 8.51*b*.

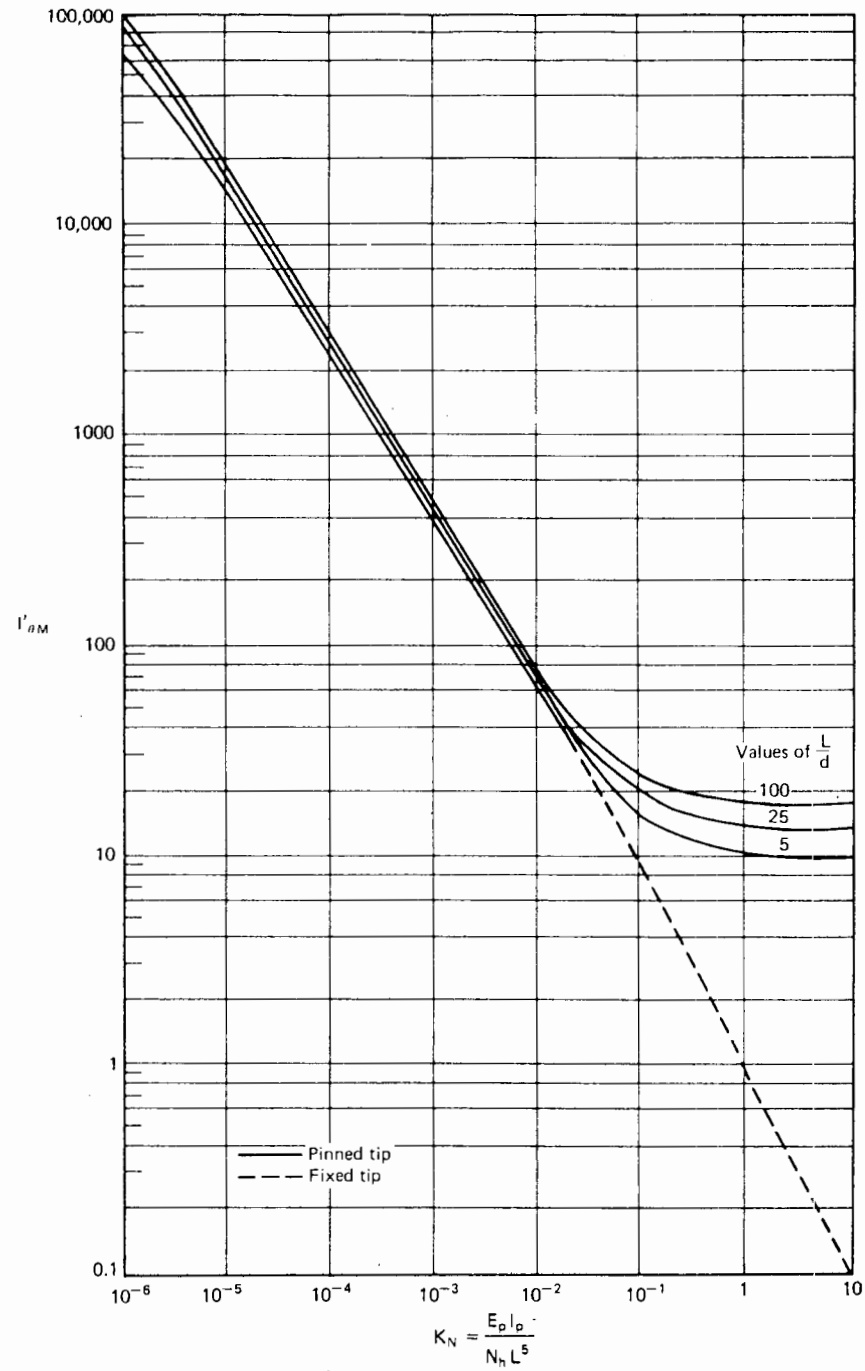

FIGURE 8.49 Values of $I'_{\theta M}$—free-head socketed pile, linearly varying E_s.

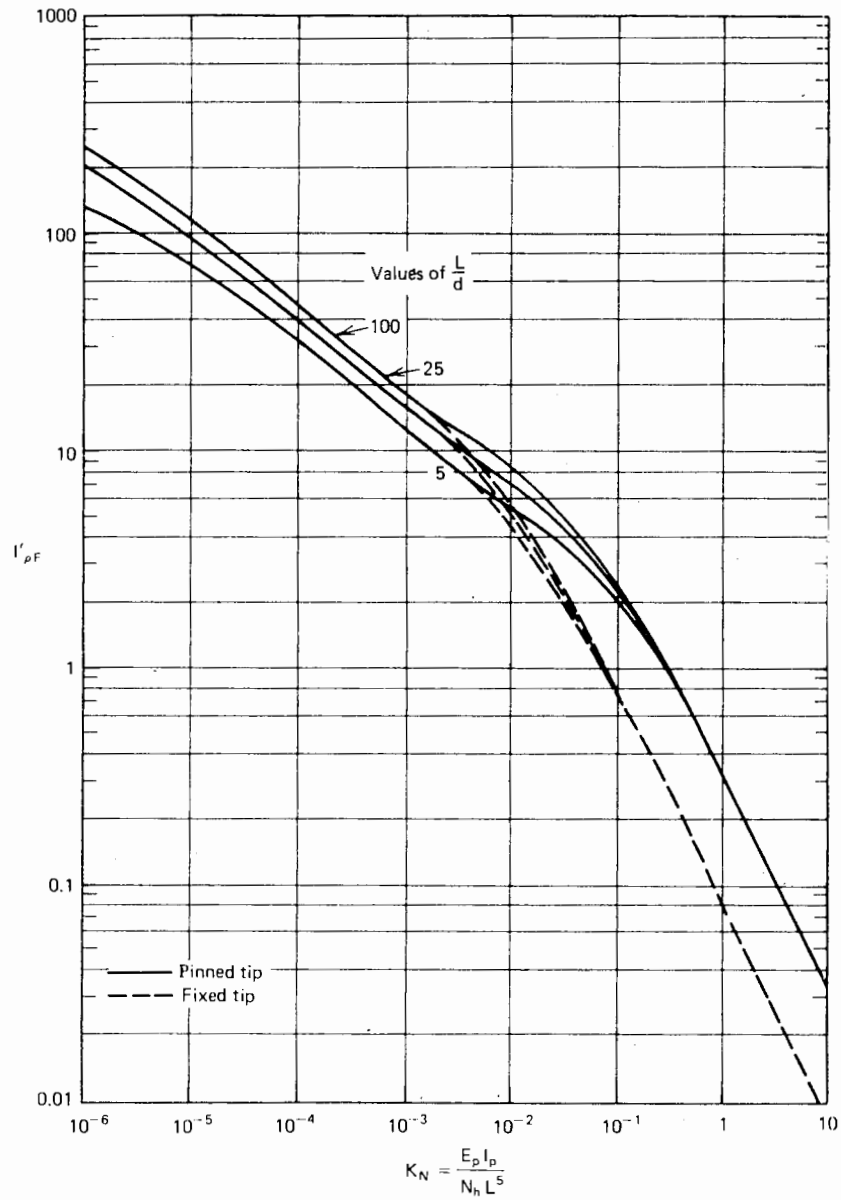

FIGURE 8.50 Values of $I'_{\rho F}$—fixed-head socketed pile, linearly varying E_s.

8.3.4.2 MOMENTS IN PILE

A summary of the moments developed in a socketed pile in a uniform elastic soil is given in Figs. 8.52, 8.53, and 8.54 for $L/d = 10$ and $L/d = 100$. These figures show, as a function of K_R, the moment at the head of a fixed-head pile, at the tip of a fixed-tip pile, and the maximum moment in a free-head pile subjected to horizontal load only. As with displacements, the tip boundary condition only influences the moment if K_R is greater than about 10^{-2}.

8.3.4.3 HORIZONTAL FORCE AT PILE TIP

For $L/d = 10$ and $L/d = 100$, and an elastic soil having uniform E_s with depth, the horizontal force developed at the pile tip is shown in Fig. 8.55 for free-head piles and in Fig. 8.56 for fixed-head piles. This force is generally very small for $K_R < 10^{-3}$, but increases rapidly in the range $K_R = 10^{-3}$ to 10^{-1}, and generally is a maximum value for a stiff pile ($K_R \geq 1$)—the exception is moment-loading on free-head, fixed-tip piles.

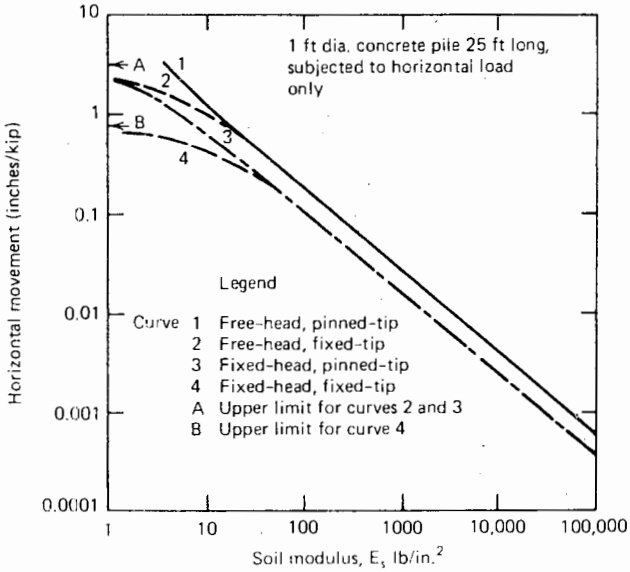

(a) Effect of soil modulus and end conditions

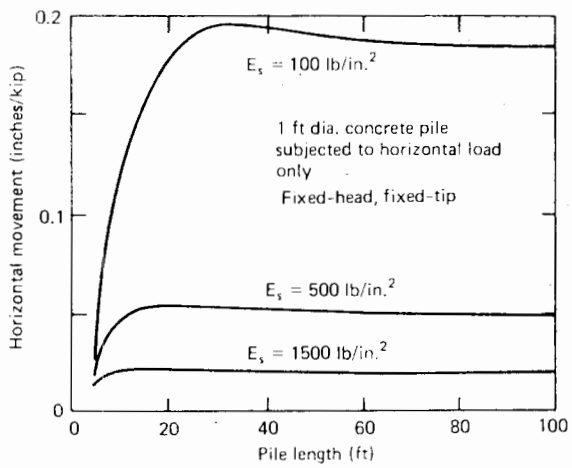

(b) Effect of pile length

FIGURE 8.51 Influence of soil modulus, pile length, and end conditions on horizontal movement of socketed pile in uniform soil.

8.3.4.4 TIP ROTATION OF PINNED TIP PILES

It is of interest to consider the tip rotation of pinned-tip piles, especially in relation to assessing the effectiveness of nominally fixed-tip piles. For a uniform elastic soil, influence factors $T_{\theta H}$, $T_{\theta M}$, and $T_{\theta F}$ for the tip rotation, θ_t, are given in Figs. 8.57, 8.58, and 8.59, where θ_t for free-head piles is given, as

$$\theta_t = \frac{H}{E_s L^2} \cdot T_{\theta H} + \frac{M}{E_s L^3} \cdot T_{\theta M} \qquad (8.78)$$

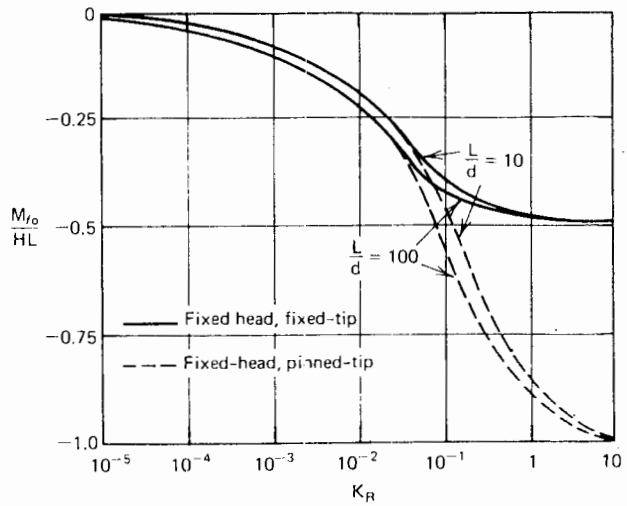

FIGURE 8.52 Fixing moment at pile head–socketed pile in uniform soil.

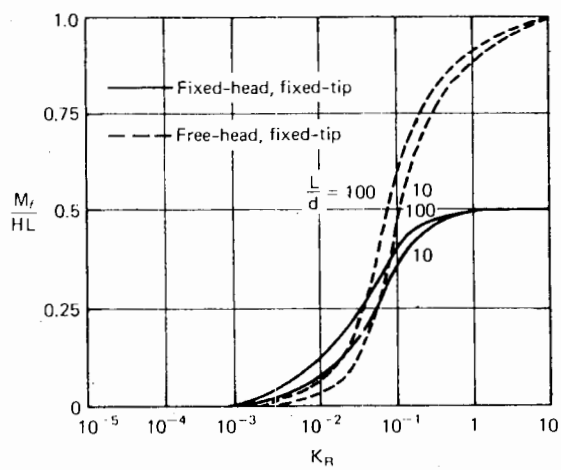

(a) Resulting from applied horizontal load

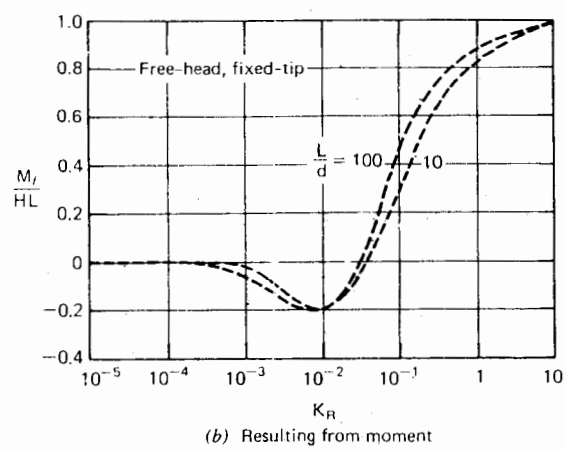

(b) Resulting from moment

FIGURE 8.53 Fixing moment at pile tip–socketed pile in uniform soil.

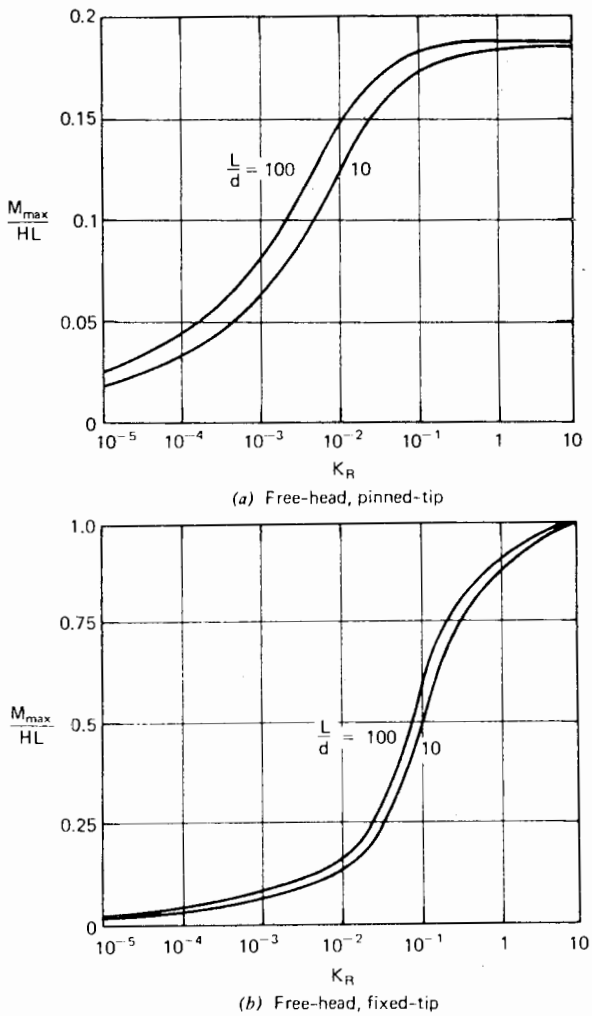

FIGURE 8.54 Maximum moment in free-head socketed piles (horizontal load only)–uniform soil.

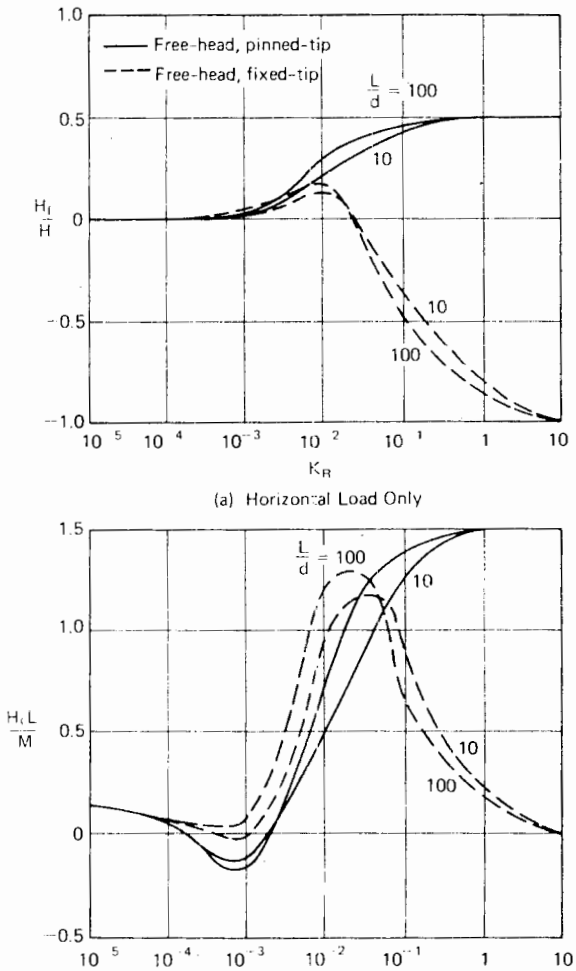

FIGURE 8.55 Tip force–free-head socketed piles in uniform soil.

or for fixed-head piles,

$$\theta_t = \frac{H}{E_s L^2} \cdot T_{\theta F} \tag{8.79}$$

For the free-head piles, the rapid changes in tip-rotation factor with increasing K_R reflect the change in deflected shape of the lower portion of the pile. For relatively stiff piles, the tip-rotation factors are identical with the corresponding values for head rotation. For fixed-head piles, the maximum value of $T_{\theta F}$ occurs for $K_R \simeq 0.02$; $T_{\theta F}$ tends to zero for a stiff pile.

8.3.4.5 EFFECTIVENESS OF A "FIXED-TIP" PILE

Because the bearing stratum has a finite modulus, some rotation of a nominally fixed-tip pile will inevitably occur.

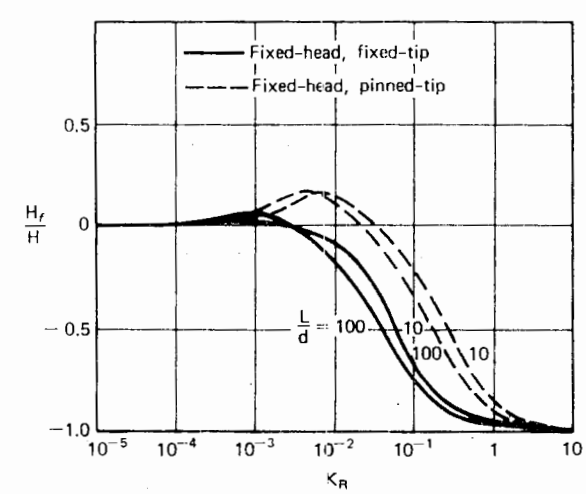

FIGURE 8.56 Tip force–fixed-head socketed piles in uniform soil.

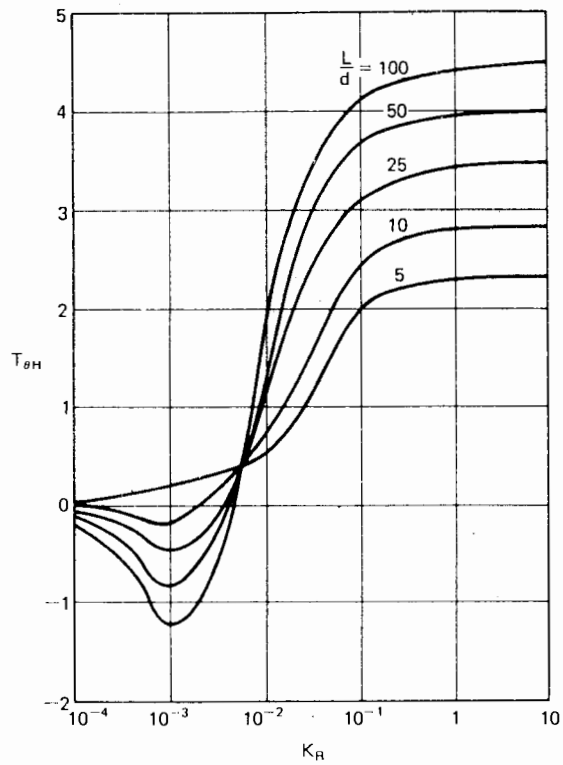

FIGURE 8.57 Influence factor $T_{\theta H}$ for tip rotation of free-head, pinned-tip socketed pile in uniform soil.

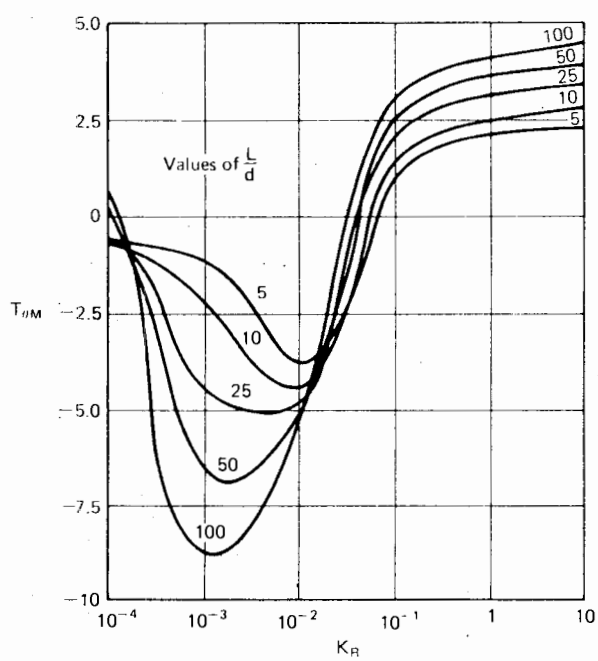

FIGURE 8.58 Influence factor $T_{\theta M}$ for tip rotation of free-head, pinned-tip socketed pile in uniform soil.

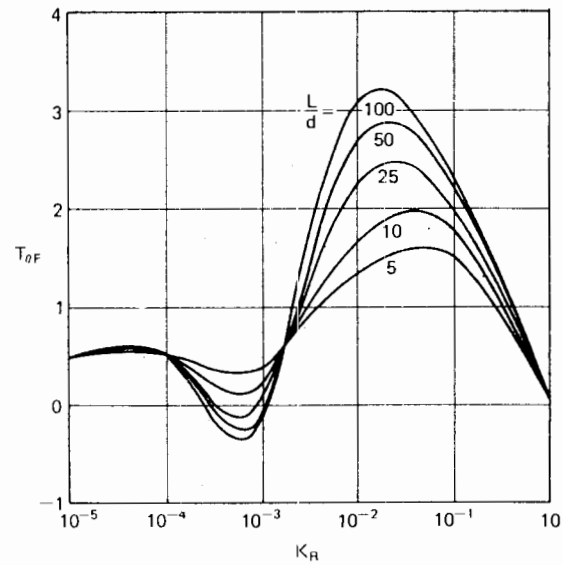

FIGURE 8.59 Influence factor $T_{\theta F}$ for laterally-loaded fixed-head, pinned-tip socketed pile in uniform soil.

For a given depth of embedment, L_e, of the tip in the bearing stratum, this rotation may be estimated by assuming the tip to be a floating pile of length L_e and diameter d, situated in a uniform semi-infinite elastic mass of the bearing-stratum material having moduli E_b and ν_b. The tip is acted upon by a horizontal force H_f and a moment M_f, which may be determined from Figs. 8.52 to 8.56. From Eq. (8.67), for a uniform elastic soil, the actual tip rotation, θ_f, is

$$\theta_f = \frac{H_f}{E_b L_e^2} \cdot I_{\theta H} + \frac{M_f}{E_b L_e^3} \cdot I_{\theta M} \qquad (8.80)$$

where

$I_{\theta H}$, $I_{\theta M}$ are obtained from Figs. 8.14 and 8.15

for

$$K_R = \frac{E_p I_p}{E_b L_e^4}$$

Alternatively, the solutions of Douglas and Davis (1964) may be used (Fig. 8.23) if K_R of the tip is greater than about 0.5. This procedure will tend to be conservative, overestimating the tip rotation, as no account is taken of the resistance of the pile base to rotation. A further approximation is involved in the above procedure, since any rotation of the tip will influence the load and moment there. While an iterative procedure could be devised to take this into account, this appears unnecessary, as only the order of the tip rotation is required.

A reasonable criterion for judging whether or not the tip rotation θ_f is satisfactorily small, is to compare it with the tip rotation θ_t of the corresponding pinned-tip pile (Eq. 8.78 or Eq. 8.79). For satisfactory performance as a fixed tip, θ_f should be only a small fraction of θ_t (e.g., 5%, although this figure will generally depend on engineering judgement in relation to the case being examined). If θ_f is found to be unacceptably large, the embedment depth, L_e, should be increased until θ_f is acceptably small.

As mentioned previously, the above procedure will only be necessary for stiff piles ($K_R \geqslant 10^{-2}$) since only then does socketing the tip influence pile behavior. An example illustrating the above procedure is described below.

Illustrative Example

The case considered is that of a 20-ft-long free-head concrete pier, 3 ft in diameter, loaded by a horizontal force of 50 kips applied at an eccentricity of 2 ft above the soil surface. The pier is situated in a 20-ft layer of soft alluvial silt, having an average c_u of 2.5 lb/in.^{2}, undrained Young's modulus, E_s, of 100 lb/in.^{2} (14.4 kip/ft^2), and underlain by sandstone. The average properties of the sandstone near the rock surface are $E_b = 1.5 \times 10^6$ lb/in.^{2}, $c_b = 5000$ lb/in.^{2}

In this example, an examination will be made of the relative merits of having a pinned tip to the pier and of having a fixed tip, socketed into the underlying sandstone.

Considering the pile-flexibility factor, K_R, it is found that $I_p = 82{,}700$ in.^{4}, and assuming $E_p = 3 \times 10^6$ lb/in.^{2},

$$K_R = \frac{3 \times 10^6 \times 82{,}700}{100 \times (240)^4} = 0.747$$

Also,

$$L/d = 20/3 = 6.67$$

The case of a pinned tip and a fixed tip will be considered in turn.

a) Pinned-Tip Pile

From Figs. 8.43 and 8.44, the displacement-influence factors may be determined. For the relevant values of L/d and K_R,

$$I_{\rho H} = 2.4$$

$$I_{\rho M} = 2.4$$

Because the value of K_R is so high, the yield factor, F_ρ, may be taken as unity. Therefore, under the working load (from Eq. 8.64),

$$\rho = \left(\frac{50}{14.4 \times 20}\right)(2.4 + \frac{2}{20} \times 2.4)/1.0$$

$$= 0.46 \text{ ft} = \mathbf{5.5 \text{ in.}}$$

From Fig. 8.55, the horizontal force, H_f, developed at the pile tip may be determined.

From Fig. 8.55*a*: $H_f/H = 0.50$
From Fig. 8.55*b*: $H_f L/M = 1.46$

$$\therefore H_f = 0.50 \times 50 + 1.46 \times \frac{100}{20}$$

$$= \mathbf{32.3 \text{ kips}}$$

$(M_f = 0)$

Now, assuming that this force has to be resisted by embedment of the pile into the rock (i.e., neglecting adhesion between the pile base and the rock), it is found that for a factor of safety of 3 and assuming the ultimate pressure of the rock near the surface to be $2c_b$, the required embeddment depth is only **0.5 in.**

Finally, considering the tip rotation of the pinned-tip pile (from Figs. 8.57 and 8.58),

$$T_{\theta H} = 2.4$$

$$T_{\theta M} = 2.4$$

Therefore, from Eq. (8.78),

$$\text{Tip rotation,} \quad \theta_t = \frac{50 \times 2.4}{14.4 \times 20^2} + \frac{2.4 \times 100}{14.4 \times 20^3}$$

$$= \mathbf{0.0229 \text{ radians}}$$

b) Fixed-Tip Pile

From Figs. 8.43 and 8.44, the displacement-influence factors are

$$I_{\rho H} = 0.44$$

$$I_{\rho M} = 0.68$$

$$\rho = \frac{50}{14.4 \times 20}(0.44 + \frac{2}{20} \times 0.68)/1.0$$

$$= 0.088 \text{ ft.} = \mathbf{1.05 \text{ in.}}$$

This is considerably less than the 5.5 in. for the pinned-tip case.

Considering now the horizontal force and the moment developed at the pile tip, from Fig. 8.55,

$$H_f/H = -0.75$$

$$H_f L/M = 0.80$$

From Figs. 8.53*a* and 8.53*b*,

$$M_f/HL = 0.80$$

$M_f/M = 0.75$

$\therefore$

$$H_f = -0.75 \times 50 + 0.30 \times \frac{100}{20} = -36.0 \text{ kips}$$

$$M_f = 0.80 \times 50 \times 20 + 0.75 \times 100 = 875 \text{ kip ft.}$$

Assuming again a factor of safety of 2 applied to the load and moment and an ultimate rock pressure of $2c$, it is found by statical considerations that the required embedded depth of the pile into the sandstone is 1.25 ft = 15 in.

An estimate must now be made for the actual rotation of this "fixed" tip to determine whether it is sufficiently small for the tip to be effectively fixed. For the embedded portion of the tip,

$$L_e/d = 1.25/3 = 0.42$$

$$K_R = \frac{3 \times 10^6 \times 82700}{1.5 \times 10^6 \times 15^4} = 3.28$$

For this value of K_R, the tip is rigid, and hence use may be made of the solutions of Douglas and Davis (1964) for the rotation of rigid plates. Using these solutions, it is found that

$$I_{\theta H} = 0.92$$

$$I_{\theta M} = 0.53$$

$$\therefore \text{ rotation of "fixed" tip} = \frac{-(36.0 \times 0.92)}{216{,}000 \times 1.25^2} + \frac{875 \times 1.53}{216{,}000 \times 1.25^3}$$

$$= 3.08 \times 10^{-3} \text{ radians}$$

This is about 14% of the tip rotation of the pinned-tip pile, so that the embedment of the tip 15 in. into the sandstone is unlikely to be sufficient for the fixed-tip condition to be achieved. Increasing the embedment depth to 24 in. reduces the rotation to 7.5×10^{-4} radians, or about 3.3% of the rotation of the pinned-tip pile, which should be satisfactory.

The above example indicates the advantage that may be gained by socketing the tip to obtain fixed-tip conditions, if the pile is relatively stiff. In socketing the pile 24 in. into rock rather than 0.5 in., a reduction in displacement at the ground line from 5.5 in. to 1.05 in. is obtained. However, it must be emphasized again that for piles that are more flexible and have a value of K_R of less than about 10^{-2}, no benefit is achieved at working loads by attempting to "fix" the pile tip.

8.4 ANALYSIS OF PILE GROUPS

8.4.1 Introduction

Many published methods of analyzing the behavior of pile groups subjected to horizontal load and moment make use of the theory of subgrade reaction, and have the advantage that groups containing battered piles and subjected to various types of loading can be readily considered. However, because the subgrade-reaction model is not continuous, the effects of interaction between piles cannot properly be considered. The consideration of the soil as an elastic material provides a convenient means of examining group effects for laterally loaded piles.

The following analysis has been described by Poulos (1971*b*). It parallels the analysis of axially-loaded piles, in that interaction between two identical piles is examined first, and the analysis is then extended to general pile groups. A simple approach is subsequently described for utilizing the solutions for single piles to obtain approximate load-deflection curves to failure for pile groups.

8.4.2 Elastic Analysis of Interaction between Two Piles

Two identical, equally-loaded piles are considered, each pile being divided into a number of elements, as for the single pile. The center-to-center pile-spacing is s, and the angle between the line joining the pile centers and the direction of loading is β, termed the departure angle (see Fig. 8.60). While elastic conditions prevail within the soil, the horizontal displacements of the soil and pile at each element may be equated, and together with the relevant equilibrium equations, solved for the unknown pressures. In the analysis that follows, the only interaction effect that is considered is the horizontal movement of one pile that results from loading on another pile, the loading and movement being in the same horizontal direction. A more general analysis along the lines of the present analysis would be possible but would not be of frequent practical importance.

The soil deflections along pile 1 may be expressed as

$$\{_s\rho\} = \frac{d}{E_s} [_1I + {}_2I] \{p\} \tag{8.81}$$

where

$[_1I + {}_2I]$ = the $(n + 1)$ by $(n + 1)$ matrix of influence factors I_{ij}, where $_1I_{ij}$ and $_2I_{ij}$ are the

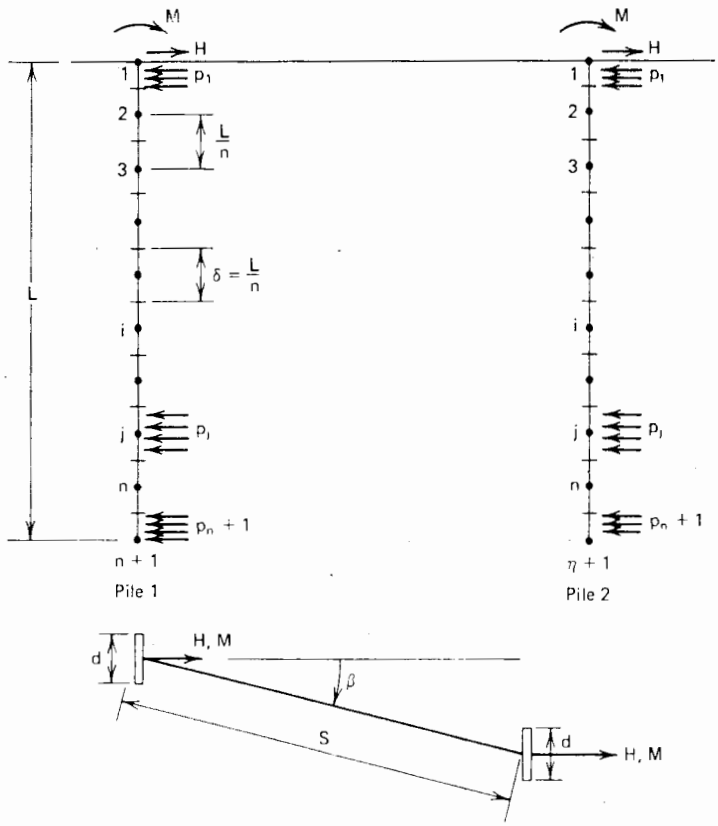

(a) Forces and pressures acting on piles

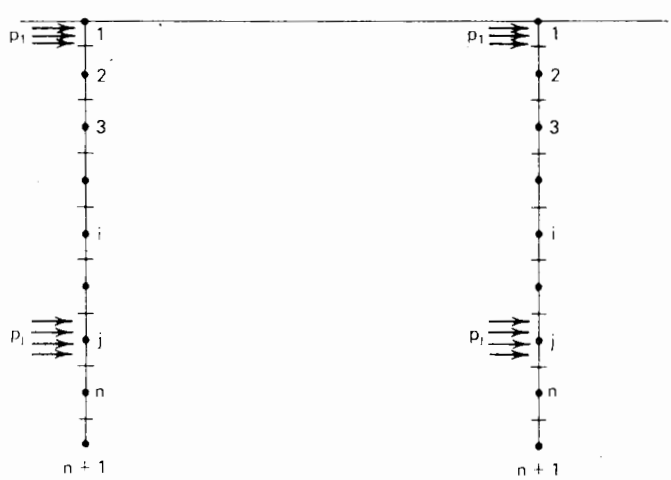

(b) Pressures acting on soil

FIGURE 8.60 Two laterally loaded piles.

influence factors for horizontal displacement at i caused by stress on element j of pile 1 and pile 2, respectively

The influence factors ${}_1I_{ij}$ are obtained as for the single pile (Section 8.3.1). Values of ${}_2I_{ij}$ are most conveniently obtained by assuming the uniform pressures on each element of pile 2 to be replaced by an equivalent point-load acting at the center of the element. This procedure is justified in view of the resulting simplification in evaluation of ${}_2I_{ij}$ and is unlikely to be seriously inaccurate except for extremely close spacings.

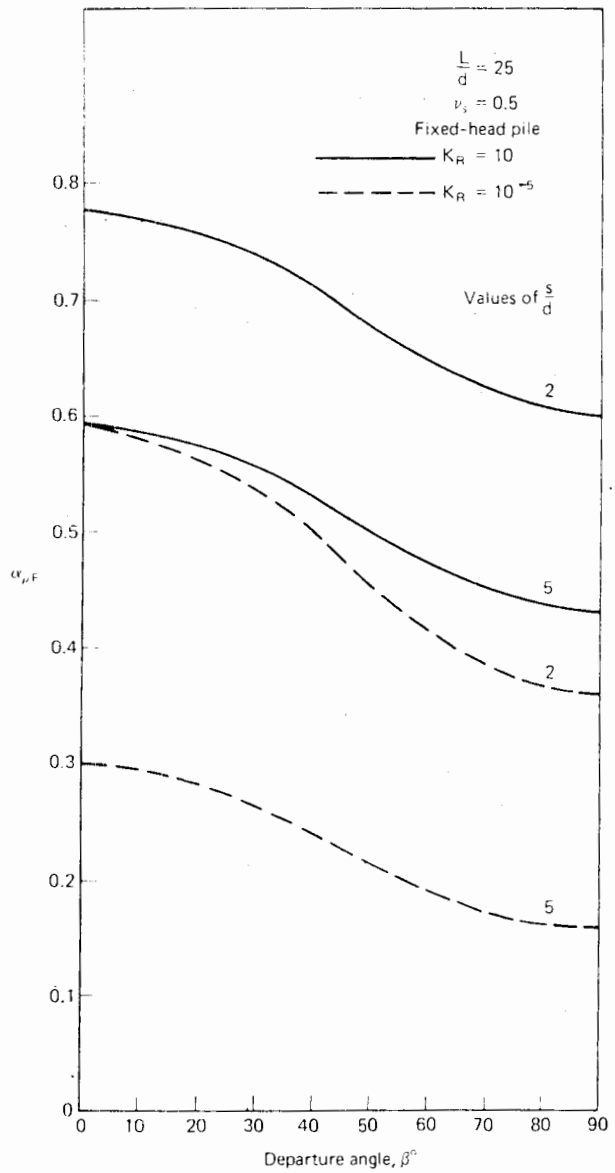

FIGURE 8.61 Typical variation of interaction factor with departure angle.

The displacements of the pile may be expressed in an identical manner to that for a single pile. For the free-head case, Eq. (8.56) is relevant, while for the fixed-head case, the relevant equation is (8.60).

Equating soil displacements from Eq. (8.81) and pile displacements from Eq. (8.56) or Eq. (8.60), solutions may be obtained for the influence of the second pile on the displacements and rotations of the first pile, for various spacings and values of the departure angle β.

It is convenient to express the additional displacement and rotation at the pile head in terms of interaction factors α_ρ and α_θ, where

$$\alpha_\rho = \frac{\text{Additional displacement caused by adjacent pile}}{\text{Displacement of pile caused by its own loading}} \tag{8.82}$$

$$\alpha_\theta = \frac{\text{Additional rotation caused by adjacent pile}}{\text{Rotation of pile due caused by own loading}} \tag{8.83}$$

The values of α_ρ and α_θ for various conditions of loading and head fixity are denoted as follows:

$\alpha_{\rho H}, \alpha_{\theta H}$: values of α_ρ and α_θ for a free-head pile subjected to horizontal load only.

$\alpha_{\rho M}, \alpha_{\theta M}$: values of α_ρ and α_θ for a free-head pile subjected to moment only (from the reciprocal theorem, $\alpha_{\rho M} = \alpha_{\theta H}$).

$\alpha_{\rho F}$: value of α_ρ for fixed-head pile.

In the solutions described, the piles have been divided into 21 elements, and purely elastic conditions are assumed to exist within the soil.

8.4.3 Solutions for Two-Pile Interaction

An example of the variation of the interaction factors with departure angle β is shown in Fig. 8.61, where $\alpha_{\rho F}$ is plotted against β for two particular spacings for both a stiff pile ($K_R = 10$) and a flexible pile ($K_R = 10^{-5}$). It will be

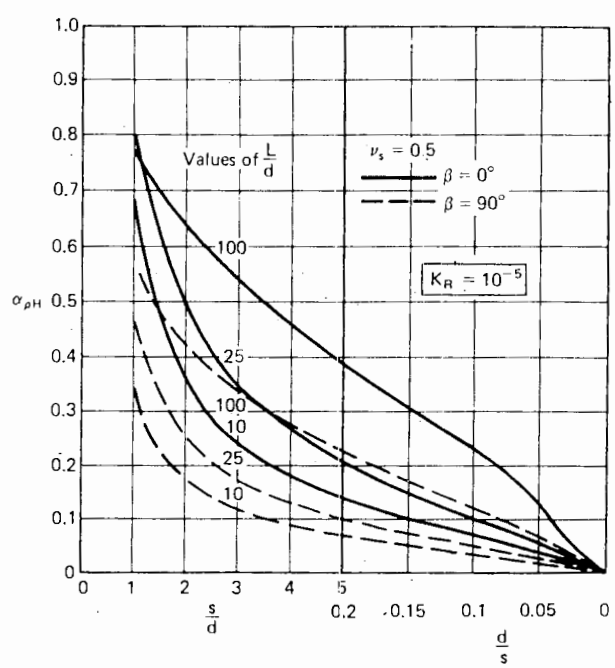

FIGURE 8.62 $\alpha_{\rho H}$ for $K_R = 10^{-5}$.

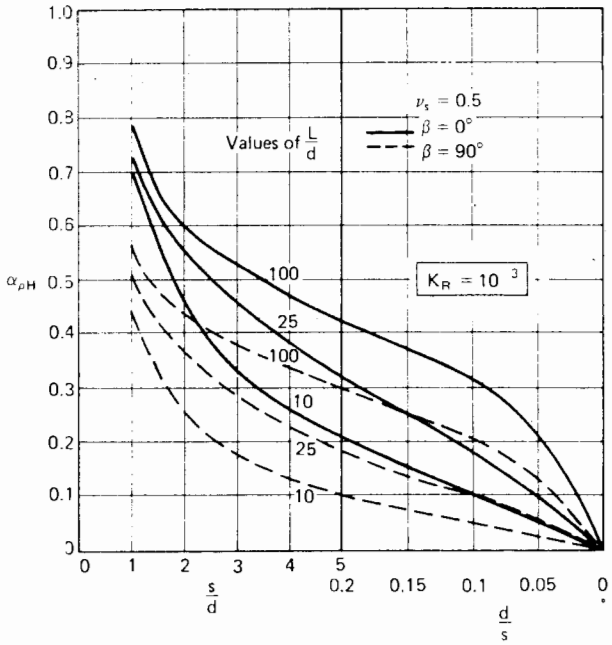

FIGURE 8.63 $\alpha_{\rho H}$ for $K_R = 10^{-3}$.

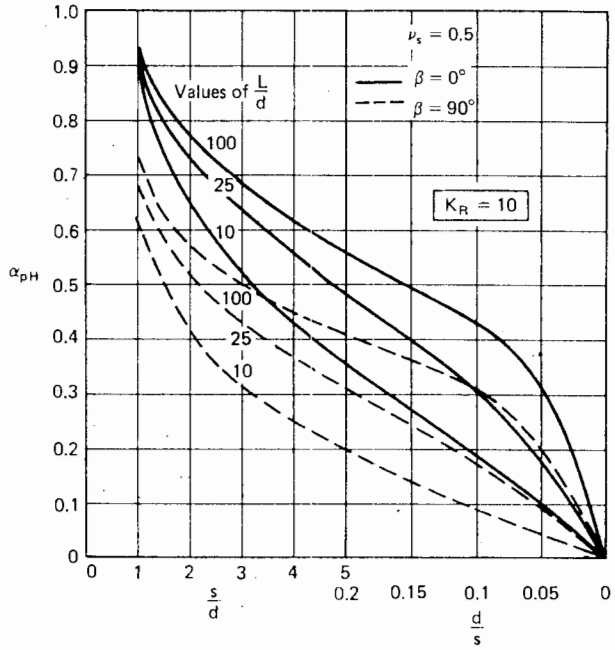

FIGURE 8.65 $\alpha_{\rho H}$ for $K_R = 10$.

seen that the variation of $\alpha_{\rho F}$ with β is sufficiently close to linear to be considered as such for practical problems, (a more accurate assumption is that $\alpha_{\rho F}$ varies linearly with $\sin^2 \beta$; however, this refinement is probably unwarranted for practical problems). The variation of other interaction factors is similarly close to linear. For convenience, a linear variation of all values of α with β will be subsequently assumed, so that only values of α for $\beta = 0°$ and $90°$ then need be computed.

Interaction factors for displacement and rotation of

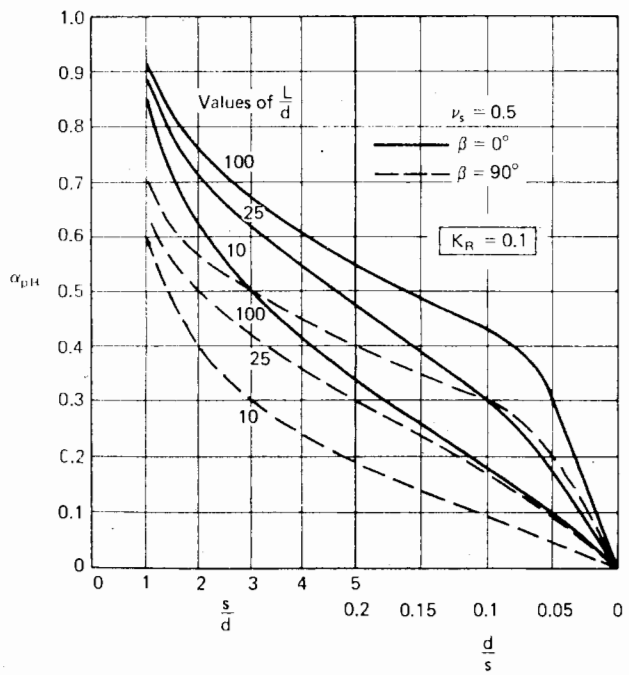

FIGURE 8.64 $\alpha_{\rho H}$ for $K_R = 10^{-1}$

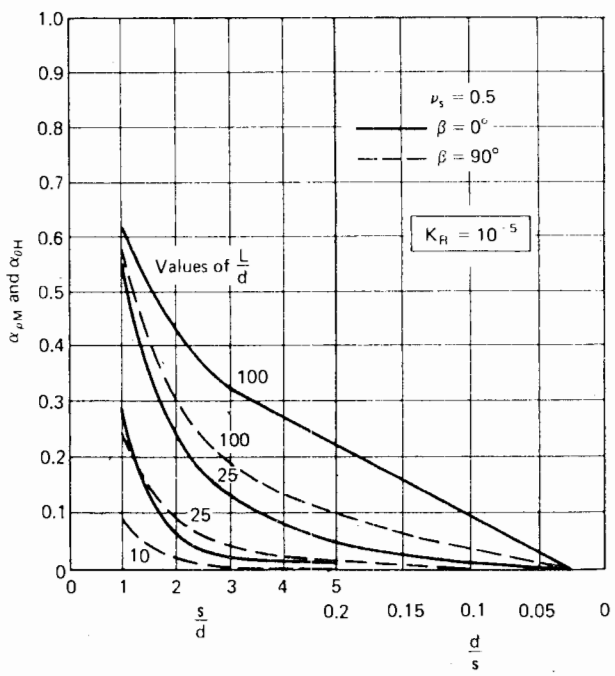

FIGURE 8.66 $\alpha_{\rho M}$ and $\alpha_{\theta H}$ for $K_R = 10^{-5}$.

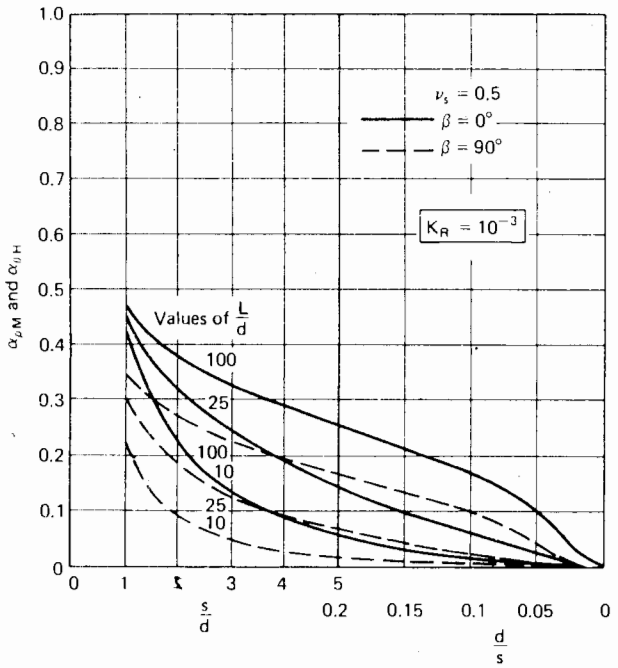

FIGURE 8.67 $\alpha_{\rho M}$ and $\alpha_{\theta H}$ for $K_R = 10^{-3}$.

the pile at the ground surface are shown in Figs. 8.62 to 8.77, for values of L/d of 10, 25, and 100. Four values of K_R ranging between 10^{-5} and 10 are considered. In all cases, $\nu_s = 0.5$, but since ν_s has relatively little influence on the interaction factors, the values for $\nu_s = 0.5$ can be used with little error for all values of ν_s.

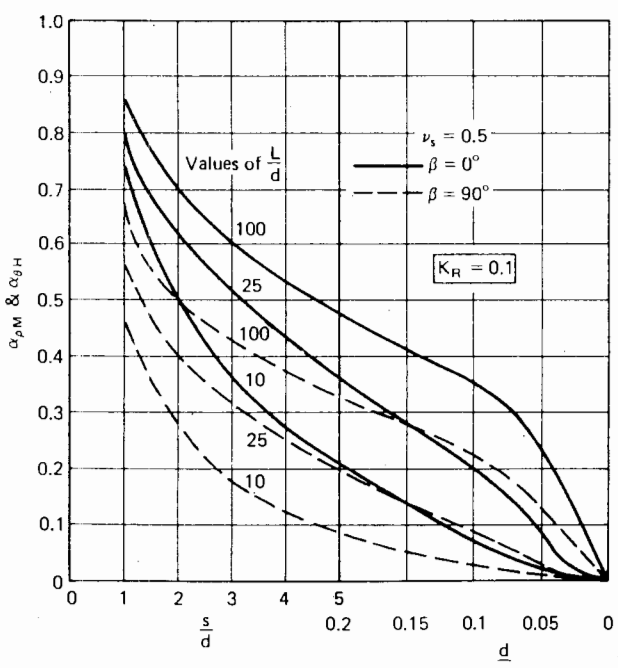

FIGURE 8.68 $\alpha_{\rho M}$ and $\alpha_{\theta H}$ for $K_R = 10^{-1}$.

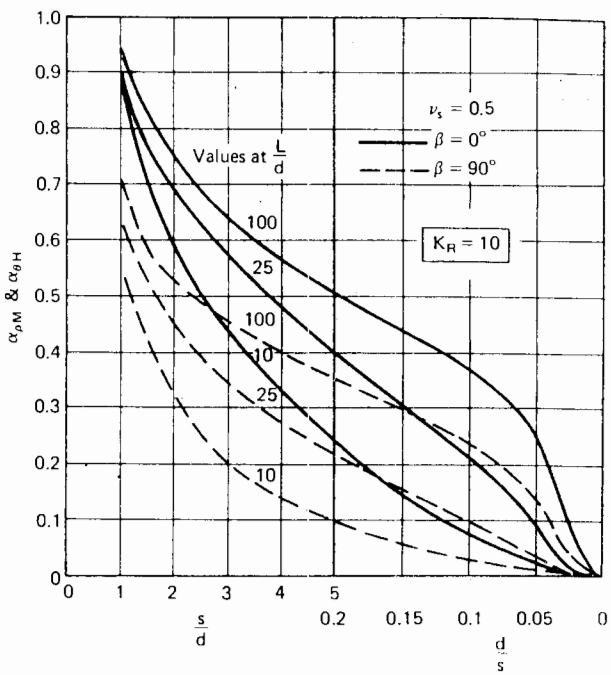

FIGURE 8.69 $\alpha_{\rho M}$ and $\alpha_{\theta H}$ for $K_R = 10$.

The following characteristics of behavior may be seen:

1. All α values decrease with increasing spacing and are greater for $\beta = 0°$ than for $\beta = 90°$.
2. All α values increase with increasing L/d.

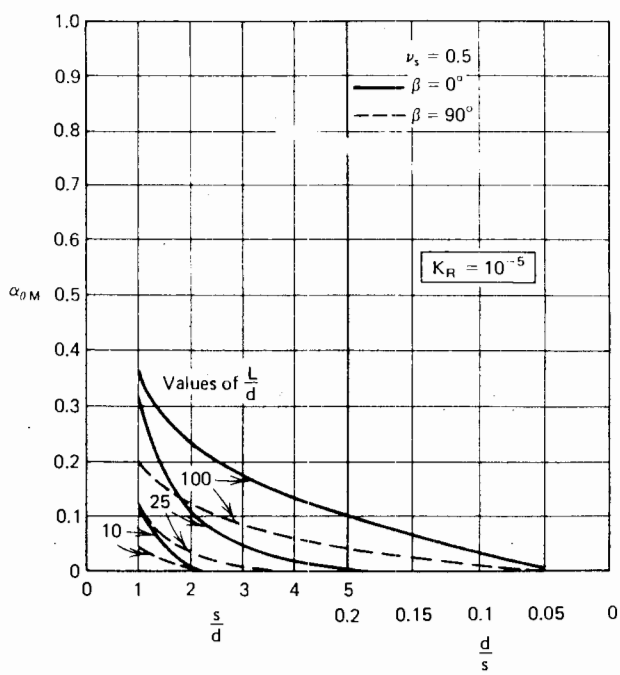

FIGURE 8.70 $\alpha_{\theta M}$ for $K_R = 10^{-5}$.

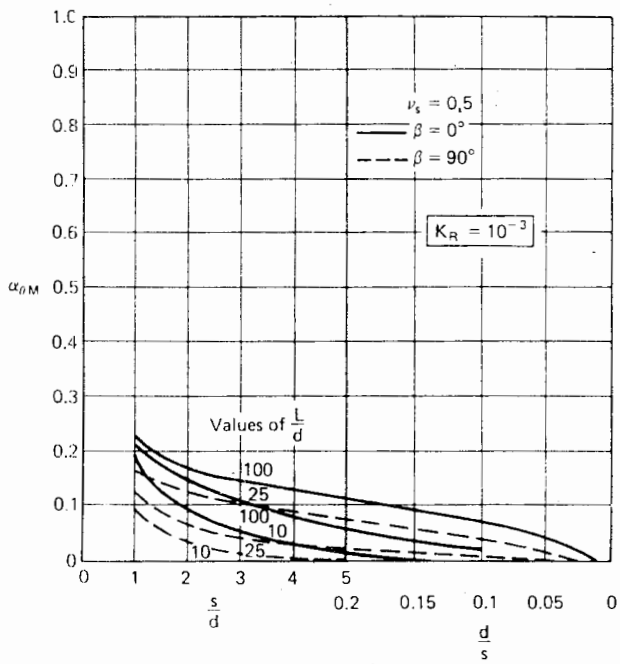

FIGURE 8.71 $\alpha_{\theta M}$ for $K_R = 10^{-3}$.

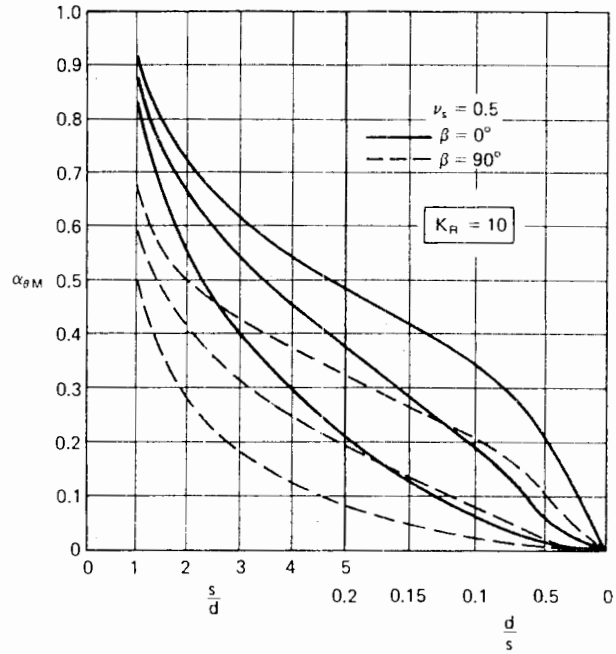

FIGURE 8.73 $\alpha_{\theta M}$ for $K_R = 10$.

3. All α values generally increase with increasing pile-stiffness factor K_R.
4. For a free-head pile, the interaction factors for moment are less than those for horizontal loading.
5. For a free-head pile, the deflection-interaction factors are greater than the corresponding rotation factors.
6. For horizontal loading only, values of $\alpha_{\rho F}$ are greater than the corresponding values for a free-head pile, $\alpha_{\rho H}$.

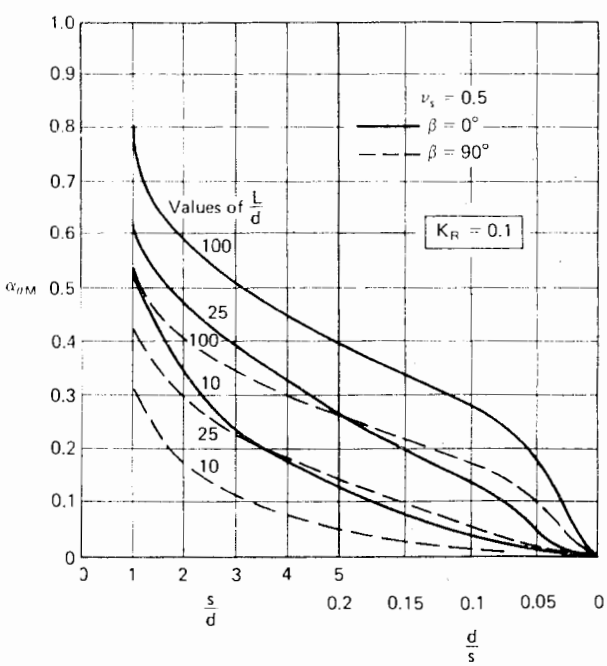

FIGURE 8.72 $\alpha_{\theta M}$ for $K_R = 10^{-1}$.

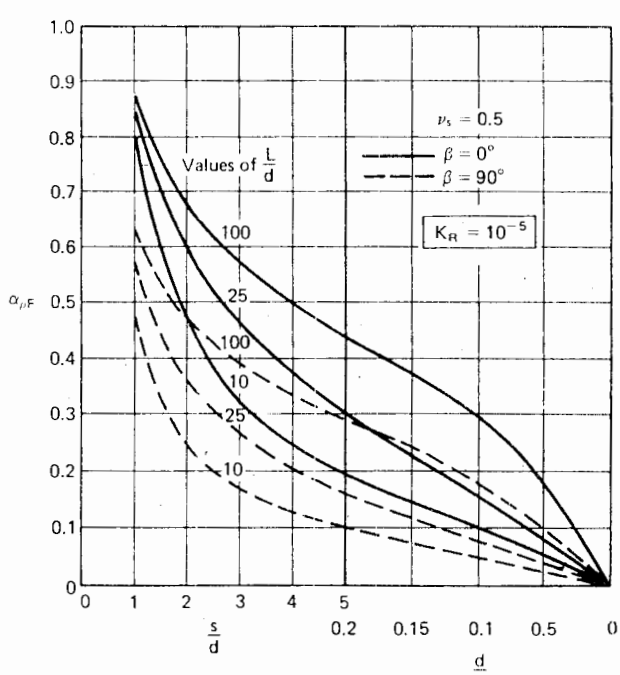

FIGURE 8.74 $\alpha_{\rho F}$ for $K_R = 10^{-5}$.

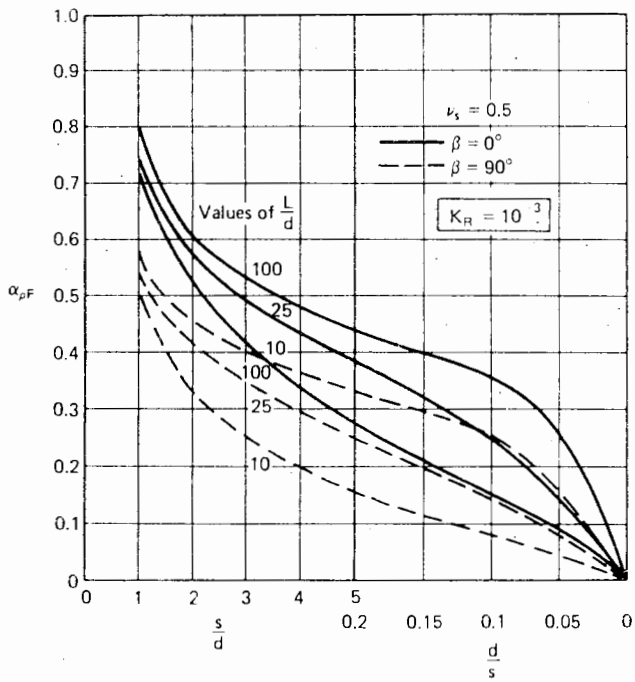

FIGURE 8.75 α_{pF} for $K_R = 10^{-3}$.

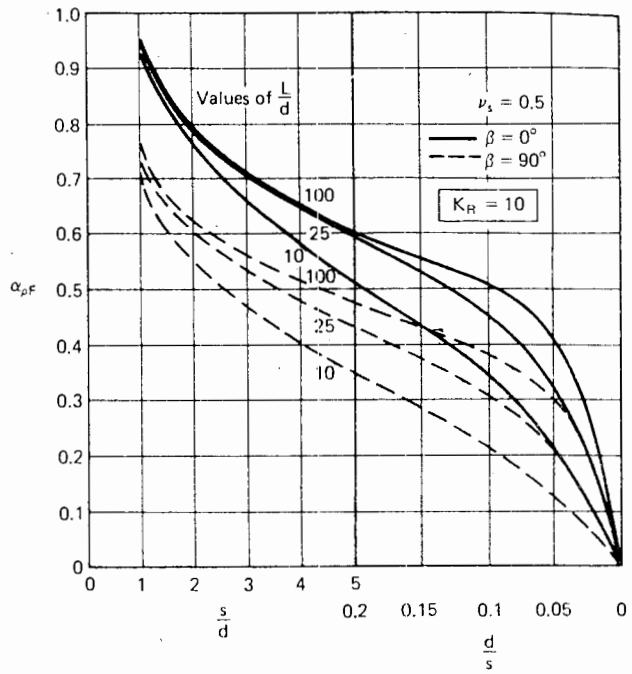

FIGURE 8.77 α_{pF} for $K_R = 10$.

The influence of a linearly increasing modulus with depth on the interaction between two piles in a typical case is shown in Fig. 8.78. The interaction factor tends to be less for the linearly increasing modulus than for the constant modulus, although the effect is small for $\beta = 90°$. For practical problems, the values of α for constant modulus in Figs. 8.62 to 8.77 may thus be used, assuming that $K_R = K_N$; their use will generally overestimate interaction and will thus be conservative.

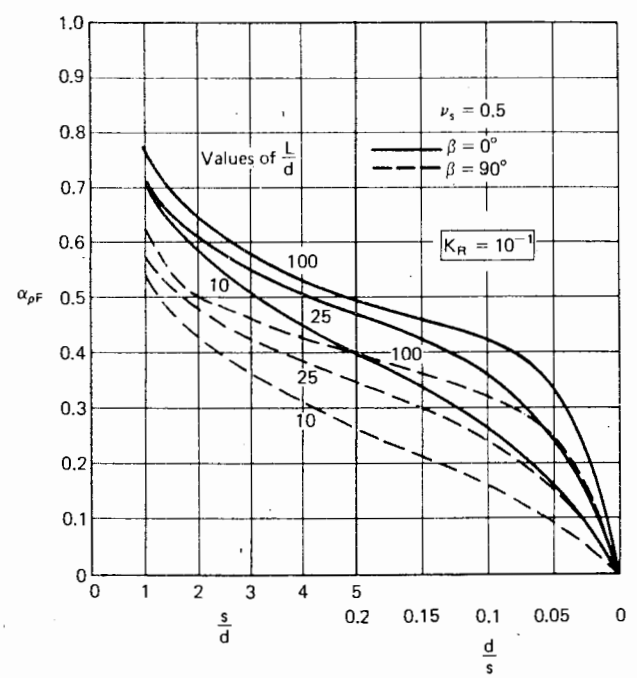

FIGURE 8.76 α_{pF} for $K_R = 10^{-1}$.

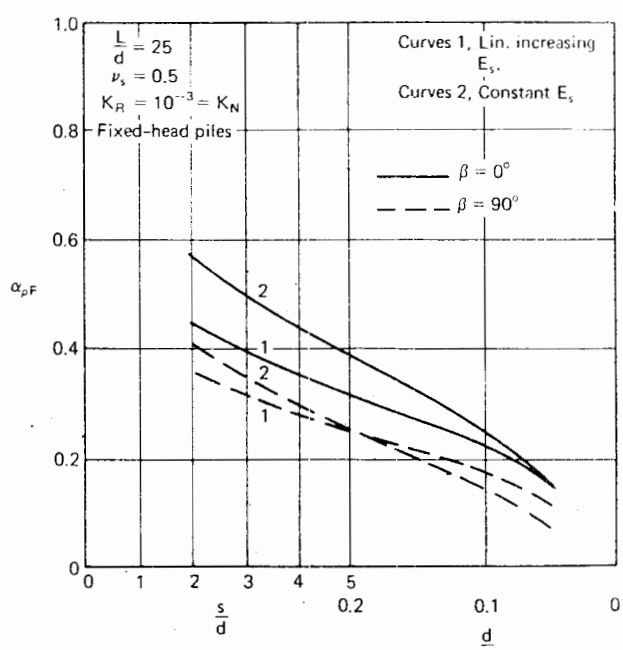

FIGURE 8.78 Influence of modulus distribution on interaction.

8.4.4 Elastic Analysis of General Pile Groups

An extension of the analysis for two piles to the case of a four-pile group has revealed that the principle of superposition, as described in Section 6.2.3 for axially-loaded groups, also applies to the laterally-loaded group. It therefore appears reasonable to extend the use of the superposition principle to the analysis of the displacement and rotation of any general pile group subjected to lateral load and moment.

Consideration may then be given to the calculation of lateral displacements and rotations at the ground surface for the following types of groups:

1. A free-head group in which each pile displaces equally.
2. A free-head group in which an equal (or known) horizontal load and/or moment acts on each pile of the group.
3. A fixed-head group in which each pile displaces equally.

For example, for a group of n free-head piles subjected to horizontal load only, the displacement of a pile k in the group is, by superposition,

$$\rho_k = \bar{\rho}_H \left[\sum_{\substack{j=1 \\ j \neq k}}^{n} \left(H_j \cdot \alpha_{\rho H k j} \right) + H_k \right] \tag{8.84}$$

where

$\bar{\rho}_H$ = the unit reference displacement, that is, the displacement of a single free-head pile under unit horizontal load
H_j = the load on pile j
$\alpha_{\rho H k j}$ = the value of $\alpha_{\rho H}$ for two piles, corresponding to the spacing between piles k and j and the angle β between the direction of loading and the line joining the centers of piles k and j.

If the total load on the group is H_G, then

$$H_G = \sum_{j=1}^{n} H_j \tag{8.85}$$

In the case of equal displacements, the n equations for pile displacements from Eq. (8.84) and the equilibrium equation (8.85) may be solved for the unknown loads and the group displacement.

In the case of equal loads in all piles, $H_j = H_G/n$, and the displacement of each pile may therefore be calculated directly from Eq. (8.84).

The analysis described above applies to cases involving horizontal loadings on a group of piles having their heads pinned to the pile cap. It may also be applied to fixed-head piles by using the appropriate unit-reference displacement and interaction factors. Where moment loading is applied to the group, axial forces will be developed in the piles and thus consideration of both axial and lateral interaction is necessary. This more general analysis is discussed in Chapter 9.

While direct consideration is given only to calculating the displacements at the ground surface, the movement at the top of a group loaded above the ground surface may readily be evaluated. To the calculated surface displacement is added the additional displacement caused by the rotation θ at the ground surface and the elastic deflection of the pile at the point of load application.

The group displacement may be conveniently expressed in terms of a displacement ratio R_ρ, which is the ratio of the group displacement to the displacement of a single pile carrying the same *average* load or moment as a pile in the group, and is analogous to the settlement ratio R_s for axially loaded groups. Alternatively, the displacement may be expressed as a group reduction factor R_R, defined as the ratio of the group displacement to the displacement of a single pile carrying the same *total* load or moment as the group, and is analogous to the group reduction factor R_G for axially loaded groups.

R_R is calculated as follows:

$$R_R = \frac{\rho_G}{H_G \bar{\rho}} \tag{8.86}$$

where $\bar{\rho}$ is the appropriate unit-reference displacement and ρ_G is the group displacement. While elastic conditions prevail in the soil, R_R and R_ρ are related simply as follows:

$$R_\rho = R_R n \tag{8.87}$$

where n is the number of piles in the group.

In practical problems, R_ρ is the more useful quantity; but in examining the behavior of various groups theoretically, the use of R_R has some advantage, since as with R_G, R_R always lies within the range 1 to $1/n$.

Various values of R_R may be determined, depending on the type of loading, pilehead condition, and whether deflection or rotation is considered. These values will be denoted as follows:

$R_{R\rho H}$ = group-reduction factor for deflection caused by horizontal load.

$R_{R\rho M}$ = group-reduction factor for deflection caused by applied moment.

$R_{R\theta H}$ = group-reduction factor for rotation caused by horizontal load ($= R_{R\rho M}$)

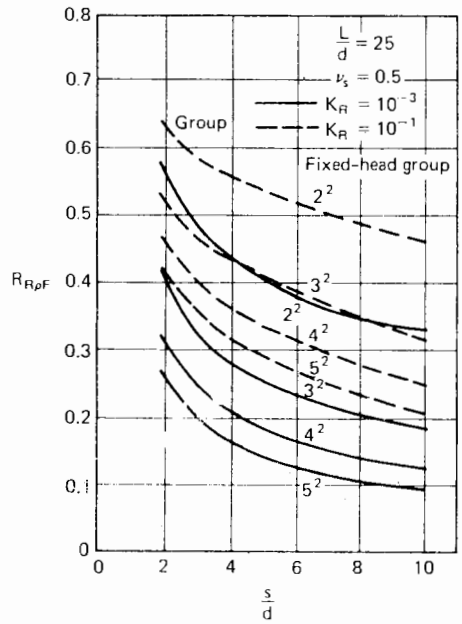

FIGURE 8.79 Influence of pile stiffness on $R_{R\rho F}$.

$R_{R\theta M}$ = group-reduction factor for rotation caused by applied moment.

$R_{R\rho F}$ = group-reduction factor for fixed-head pile.

8.4.5 Elastic Solutions for Square Groups

For 2^2, 3^2, 4^2, and 5^2 groups in a uniform soil, the variation of the group-reduction factor $R_{R\rho F}$ with pile spacing is shown in Fig. 8.79 for two values of K_R and for a fixed-head group. At any spacing, s, is considerably greater for the stiffer piles. For a group of free-head piles, $R_{R\rho H}$ is found to be smaller than $R_{R\rho F}$ for fixed-head piles (Fig. 8.80). Also, $R_{R\rho F}$ increases as L/d increases (Fig. 8.81).

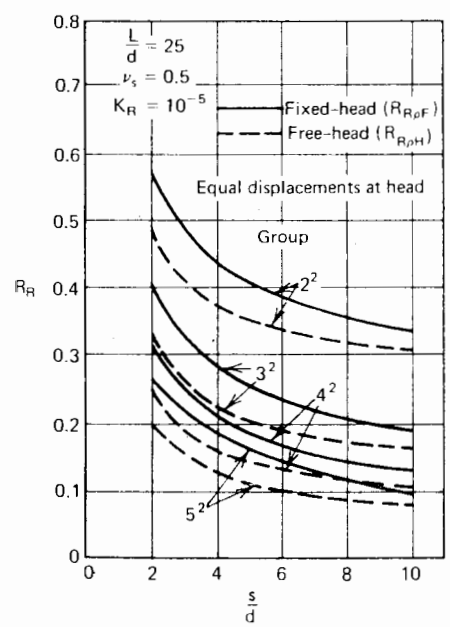

FIGURE 8.80 Influence of head fixity on R_R.

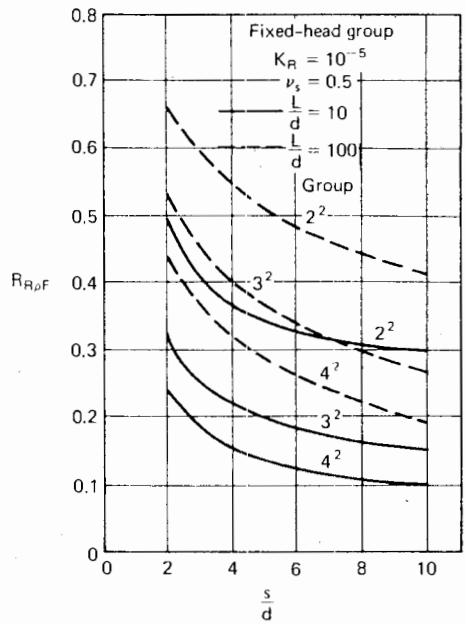

FIGURE 8.81 Influence of $\frac{L}{d}$ on R.

For a given total load, the displacement of a group decreases as the number of piles in the group increases. If, however, the displacement of the groups is plotted against the total group breadth, it is found that the value of the group reduction factor $R_{R\rho F}$ is almost independent of the number of piles in the group. Typical plots of $R_{R\rho F}$ versus group breadth are shown in Figs. 8.82 and 8.83. With the exception of the four-pile and nine-pile groups, for which $R_{R\rho F}$ tends to limiting values of 0.25 and 0.11, respectively, at relatively small breadths, the points lie closely on a single curve. Only for large breadths do the points for individual groups tend to diverge from the common curve, as $R_{R\rho F}$ tends to the limiting value of $1/n$, where n is the number of piles in the group. The dependence of $R_{R\rho F}$ on breadth rather than number of piles in the group parallels the similar dependence on breadth-only of axially-loaded groups.

Figure 8.84 shows the ratio ρ_i/ρ_{TF} of immediate to total-final movement for piles with $L/d = 25$ in an ideal elastic two-phase soil. This ratio depends primarily on the drained Poisson's ratio, ν'_s and is almost independent of factors such as the number of piles in the group, K_R, and the pile spacing. Even for the extreme case of $\nu'_s = 0$, $\rho_i/\rho_{TF} = 0.72$, and, for more practical values of ν'_s, is of the order of 0.8 to 0.9: in other words, the major part of

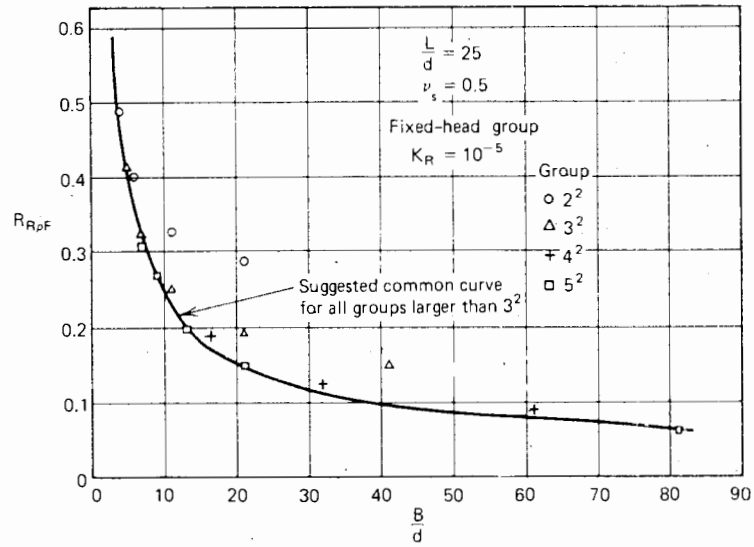

FIGURE 8.82 $R_{R\rho F}$ vs. group breadth – $K_R = 10^{-5}$

the movement (excluding creep) of a laterally-loaded pile group occurs immediately on loading.

For groups situated in a uniform soil and in which all piles displace equally, typical distributions of horizontal load within 3^2 and 4^2 groups are shown in Figs. 8.85 to 8.88. These figures show that:

1. The outer piles carry the greatest load and the center piles the least.
2. The load distribution becomes more uniform as spacing increases.
3. The relative maximum load in the group increases as the number of piles in the group increases.
4. The nonuniformity of load distribution generally becomes more pronounced as K_R and L/d increase.

Illustrative Example

The problem shown in Fig. 8.89 involves the calculation of the distribution of horizontal load and the horizontal displacement at the ground line of a six-pile group of 1-ft-diameter concrete piles situated in a uniform medium clay. It is assumed that the top of each pile is rigidly attached to a massive pile cap, so that the top of each pile is fixed and each displaces equally. The value of E_s shown in Fig. 8.90 is the value (assumed constant with

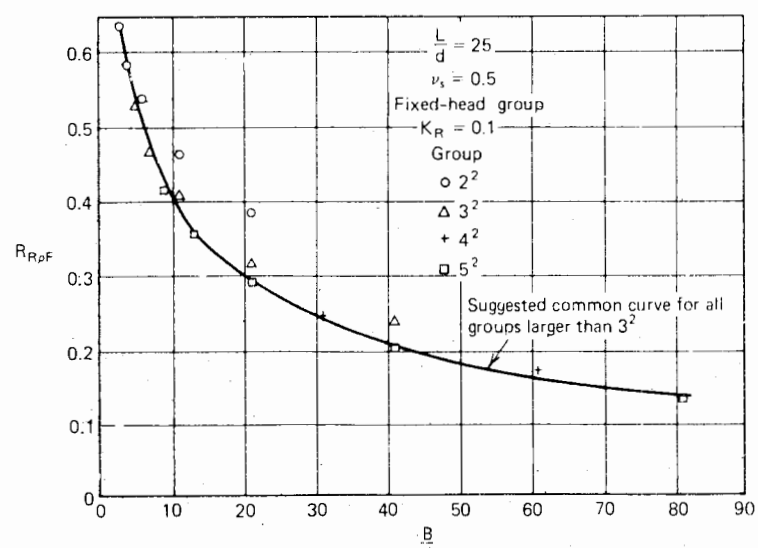

FIGURE 8.83 $R_{R\rho F}$ vs. group breadth – $K_R = 0.1$.

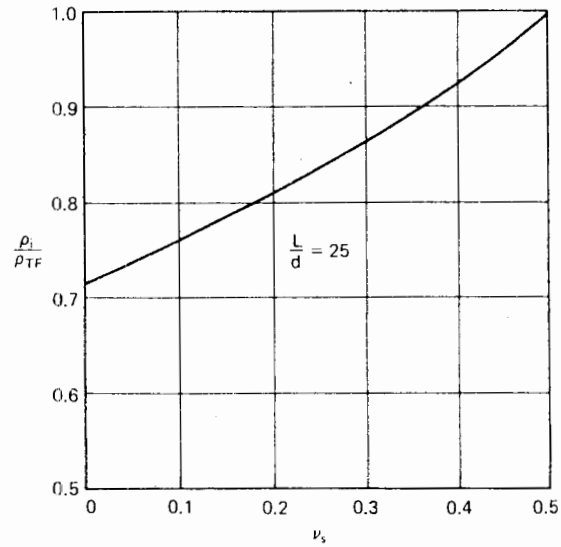

FIGURE 8.84 Ratio of immediate to total-final displacement for fixed-head groups.

depth) for the soil skeleton, so that the displacement calculated will be the total final displacement. The soil will be assumed to remain elastic.

Because of symmetry, there are only two unknown horizontal loads in the group. The load in piles 1, 3, 4, and

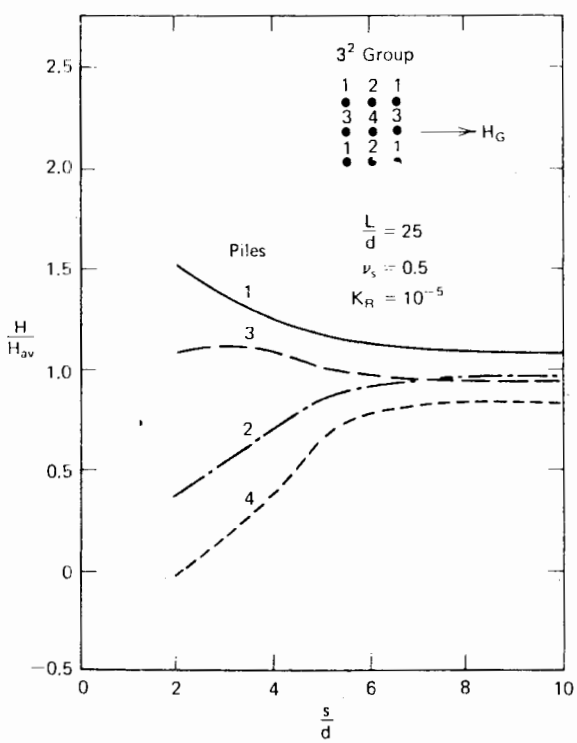

FIGURE 8.85 Typical horizontal load distributions in fixed-head pile group.

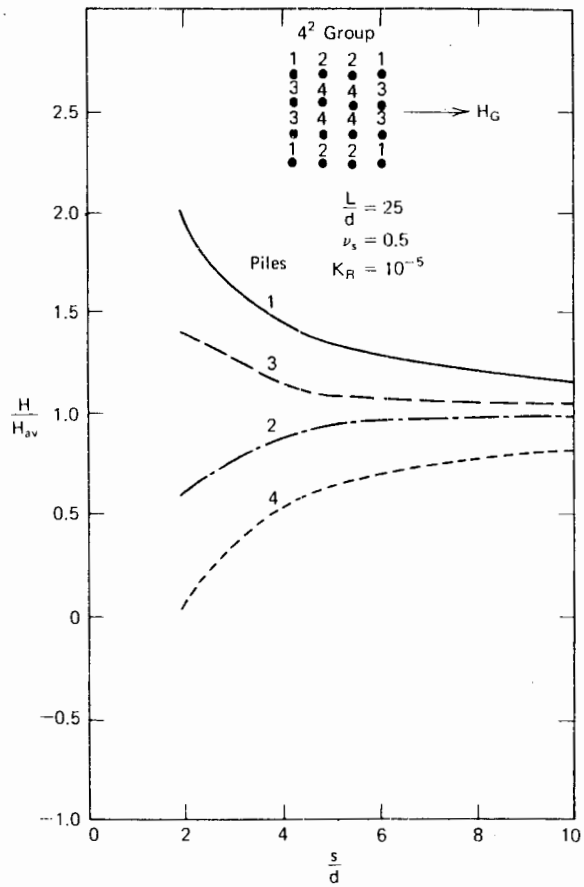

FIGURE 8.86 Typical horizontal load distributions in fixed-head pile group.

6 is H_1, and that in piles 2 and 5 is H_2. For piles 1, 3, 4, and 6, the displacement at the ground line is given by

$$\rho_1 = [H_1(1 + \alpha_{\rho F13} + \alpha_{\rho F14} + \alpha_{\rho F16}) + H_2(\alpha_{\rho F12} + \alpha_{\rho F15})]\bar{\rho}_F$$

where

$\alpha_{\rho F13}$ = interaction factor for deflection at pile 1 caused by load on pile 3, and similarly for other α values.

$\bar{\rho}_F$ = displacement of a single fixed-head pile under unit load

A similar expression may be written for the displacement ρ_2 at piles 2 and 5.

For the condition of equal displacement of all piles, $\rho_1 = \rho_2 = \rho$. Also, from equilibrium,

$$H_G = 4H_1 + 2H_2$$

where H_G is the total applied load.

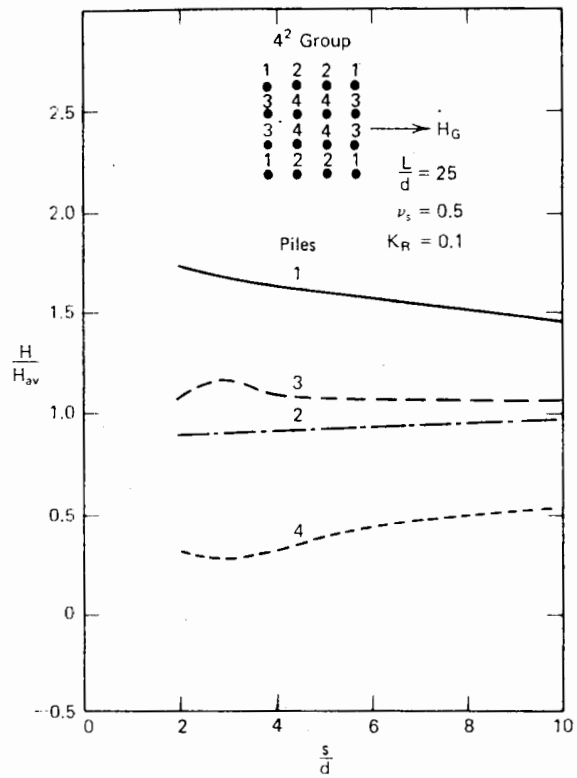

FIGURE 8.87 Typical horizontal load distributions in fixed-head pile group.

Thus, three equations are obtained for the unknowns H_1, H_2, and ρ.

From the given data,

$$K_R = \frac{E_p I_p}{E_s L^4} = 7.4 \times 10^{-4}$$

From Fig. 8.19, the unit displacement $\bar{\rho}_F$ for a single pile may be calculated. For $L/d = 25$ and $K_R = 7.4 \times 10^{-4}$,

$$I_{\rho F} = 4.7$$

Hence,

$$\bar{\rho}_F = \frac{4.7}{300 \times 0.500} = 31.4 \times 10^{-3} \text{ in./kip}$$

It is sufficiently accurate to use the interaction factors for $K_R = 10^{-3}$; and the relevant interaction factors, tabulated in Table 8.8, are obtained for the appropriate values of β and s/d and for $L/d = 25$, from Fig. 8.75.

Substituting the appropriate interaction factors for the displacement of piles 1, 3, 4, and 6,

$$\rho = [H_1(1 + 0.36 + 0.35 + 0.28) + H_2(0.50 + 0.38)] \times 31.4 \times 10^{-3}$$

that is,

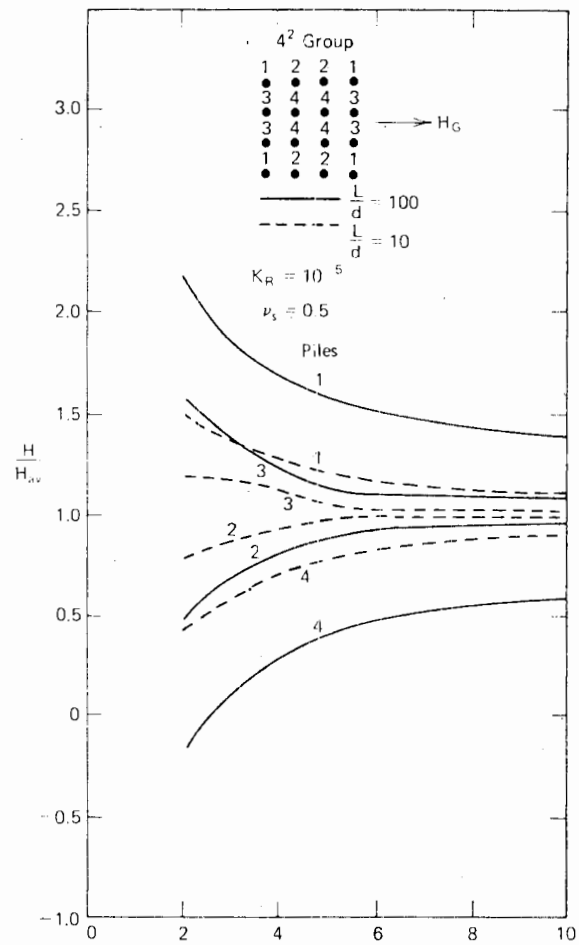

FIGURE 8.88 Typical horizontal load distributions in fixed-head pile group.

$$10^3\rho = 62.5 H_1 + 27.6 H_2.$$

Similarly, for piles 2 and 5, it may be shown that

$$10^3\rho = 55.2H_1 + 42.4H_2$$

TABLE 8.8

Pile No.	Influence on Pile 1 (Also Piles 3, 4, and 6)			Influence on Pile 2 (Also Pile 5)		
(j)	s/d	β°	$\alpha_{\rho Hij}$	s/d	β°	$\alpha_{\rho H2j}$
1	–	–	–	3	0	0.50
2	3	0	0.50	–	–	–
3	6	0	0.36	3	0	0.50
4	3	90	0.35	4.24	45	0.38
5	4.24	45	0.38	3	90	0.35
6	6.71	26.3	0.28	4.24	45	0.38

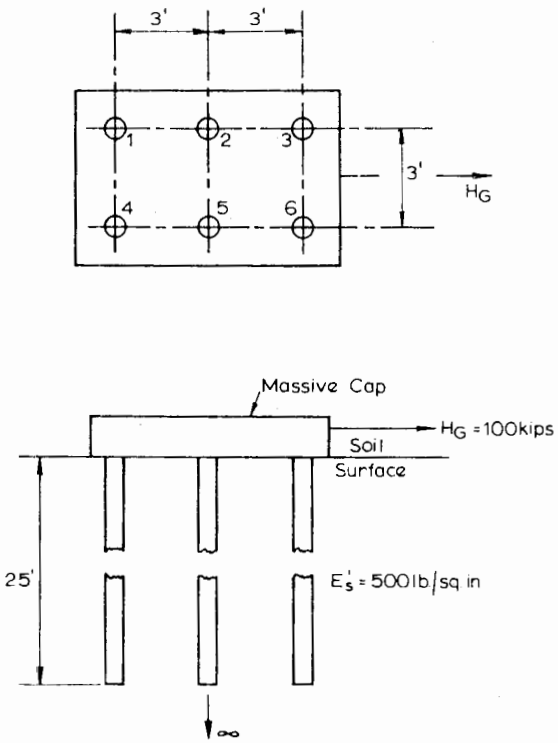

FIGURE 8.89 Illustrative example.

The equilibrium equation is

$$4H_1 + 2H_2 = 100$$

Solution of the above equations gives

H_1 = **20.1 kips**
H_2 = **9.8 kips**
ρ = **1.53 in.**

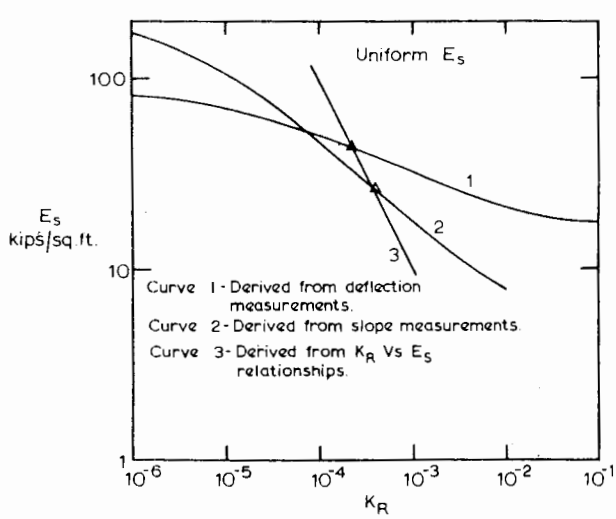

FIGURE 8.90*a* Method of backfiguring modulus from load test.

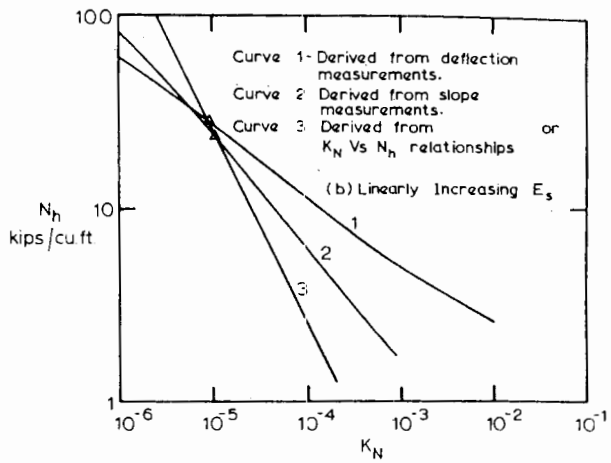

FIGURE 8.90*b* Method of backfiguring modulus from load test.

Under the average pile load of 16.67 kips, a single pile would deflect $16.67 \times 31.4 \times 10^{-3} = 0.52$ in. Thus, the group-displacement ratio $R_\rho = 1.53/0.52 = 2.94$. The group-reduction factor $R_{R\rho F} = R_\rho/6 = 0.49$.

8.4.6 Approximate Prediction of Load-Deflection Curve for a Group

In developing a simple practical procedure for load-deflection prediction of pile groups, the following assumptions are made:

1. The group reduction factors R_R remain constant for all loads up to the failure, although they are calculated from elastic theory.
2. The reduction in ultimate lateral-load capacity of the piles resulting from group effects is calculated by applying a lateral efficiency factor, η_L, to the ultimate lateral load capacity, H_u, of a single pile, and η_L applies equally to all piles in the group, so that the reduced ultimate lateral-load capacity, H_{ur}, of each pile is

$$H_{ur} = \eta_L H_u \tag{8.88}$$

3. All piles in the group deflect equally, so that the load-deflection curve for the group is obtained by computing the curve for a single pile having an ultimate load H_{ur}, and then multiplying the ordinates of this curve by the number of piles in the group.

With these assumptions the following expression may be derived for the ground-line deflection, ρ_G, of a free-head pile group in a soil with constant E_s:

$$\rho_G = \frac{H_G}{LE_s}(R_{R\rho H}I_{\rho H} + \frac{e}{L}R_{R\rho M}I_{\rho M})/F_\rho \qquad (8.89)$$

where

H_G = total load on group
$R_{R\rho H}$ = group-reduction factor for deflection caused by horizontal load
$R_{R\rho M}$ = group-reduction factor for deflection caused by moment
F_ρ = yield-displacement factor for a single pile, for $\frac{H}{H_u} = \frac{H_G}{nH_{ur}}$, H_{ur} being given by Eq. (8.88).
$I_{\rho H}, I_{\rho M}$ = single-pile elastic-influence factors (see Eq. 8.64).

Similar expressions may be derived for the rotation and deflection of a pile with varying E_s and for fixed-head piles.

If the deflection of the group at the point of load application, ρ_{Ga}, is required, the additional deflection caused by rotation is added to the ground-line deflection. Neglecting the deflection of the piles caused by bending of the freestanding portion, ρ_{Ga} is given by

$$\rho_{Ga} = \frac{H_G}{L^3E_s}[L^2R_{R\rho H}I_{\rho H} + eLR_{R\rho M}I_{\rho M})/F_\rho \qquad (8.90)$$

$$+ (eLR_{R\theta H}I_{\theta H} + e^2R_{R\theta M}I_{\theta M})/F_\theta]$$

where

$R_{R\theta M}$ = group-reduction factor for rotation caused by moment,
$I_{\theta H}, I_{\theta M}$ = single-pile elastic influence factors

and the symbols are as defined for Eq. (8.89).

A similar expression is obtained for soil with linearly varying E_s, and in Eq. (8.90), E_s is replaced by N_hL; $I_{\rho H}$, $I_{\rho M}$, and $I_{\theta M}$ are replaced by $I'_{\rho H}$, $I'_{\rho M}$, and $I'_{\theta M}$; and F_ρ, F_θ are replaced by F'_ρ, F'_θ.

The use of Eq. (8.89) or Eq. (8.90) enables the overall load-deflection behavior of the group to be calculated, and an example illustrating the application of this method is given below.

Focht and Koch (1973) developed a similar type of approach to the calculation of load-deflection behavior of groups, by combining a nonlinear subgrade-reaction analysis for a single pile with the elastic analysis for pile interaction. This approach also enables nonlinear load-deflection relationships to be obtained and has been applied to the prediction of deflections of offshore pile groups.

Illustrative Example

The problem considered will be one of the model tests reported by Oteo (1972), which is discussed in Section 8.6. Aluminium piles 8 mm in diameter with an embedded length of 220 mm were tested, with an eccentricity of loading of 55 mm above the ground surface. The group considered was a nine-pile square group with a center-to-center spacing of four diameters, in sand having an initial density of 1.80 t/m^3. The deflection of the group at the point of load application will be calculated for various loads.

From a single-pile test, the value of N_h was found to be 4.0 kg/cm^3 (39.23 MN/m^3), and hence the dimensionless pile-flexibility factor, $K_N = E_pI_p/N_hL^5$, is found to be 6.8×10^{-4}.

The deflection of the group at the point of load application is given by Eq. (8.90), modified for linearly varying E_s:

$$\rho_{Ga} = \frac{H_G}{L^4N_h}[(L^2R_{R\rho H}I'_{\rho H} + eLR_{R\rho M}I'_{\rho M})/F'_\rho$$

$$+ (eLR_{R\theta H}I'_{\theta H} + e^2R_{R\theta M}I'_{\theta M})/F'_\theta]$$

Values of the interaction factors $\alpha_{\rho H}$, and so on, for a soil with constant modulus are now used to calculate $R_{R\rho H}$, and so on (see Section 8.4.3). Assuming K_R equal to K_N, the following values are obtained:

$R_{R\rho H} = 0.322$
$R_{R\rho M} = R_{R\theta H} = 0.203$
$R_{R\theta M} = 0.149$

For $K_N = 6.83 \times 10^{-4}$, $I'_{\rho H} = 49$, $I'_{\rho M} = I'_{\theta H} = 128$, $I'_{\theta M} = 570$.

Substitution of the above values into the above equation gives

$$\rho_{Ga} = H_G\left[\left(\frac{0.115}{F'_\rho}\right) + \left(\frac{0.061}{F'_\theta}\right)\right]$$

where ρ_{Ga} is in mm and H_G is in kgf.

From the single-pile test, the ultimate lateral load is 2.7 kgf (at a deflection of 0.5 pile-diameters). Referring to Fig. 7.22, the group lateral-efficiency factor η_L is 0.60. The estimated reduced ultimate lateral-load of a pile in the group H_{ur} is therefore $0.60 \times 2.7 = 1.62$ kgf, and the group ultimate lateral-load capacity is $9 \times 1.62 = 14.58$ kgf. Values of F'_ρ and F'_θ may now be determined from Figs. 8.36 and 8.37 for $e/L = 55/220 = 0.25$ and $K_N = 6.8 \times 10^{-4}$. The calculations are tabulated in Table 8.9, and the load-deflection curve thus derived is plotted in Fig. 8.100, together with the measured curve.

TABLE 8.9 CALCULATION OF LOAD-DEFLECTION CURVE FOR GROUP

H_G (kgf)	$\frac{H_G}{nH_w}$	F'_ρ	F'_θ	ρ_{Ga} (mm)
1.46	0.1	1.0	1.0	0.26
2.92	0.2	0.90	1.0	0.55
5.84	0.4	0.68	0.88	1.39
8.76	0.6	0.55	0.72	2.57
11.66	0.8	0.40	0.56	4.63
13.14	0.9	0.36	0.52	5.74

8.5 DETERMINATION OF SOIL MODULUS

A number of methods may be employed to estimate the Young's modulus of the soil for use in the theoretical solutions given in the preceding sections. Among these are:

1. Laboratory tests in which the stress path of typical elements of soil along the pile are simulated.
2. Plate-bearing tests, preferably on vertical plates, at various depths.
3. Pressuremeter tests.
4. The use of full-scale loading tests to backfigure the modulus.
5. Empirical correlations with other properties.

Little evidence is available at present to indicate whether the first approach yields satisfactory values of modulus, although the simulation of the correct stress path caused by loading of the pile is easier in this case than for an axially-loaded pile. Nevertheless, the problems associated with the simulation of the effects of installation of the pile remain.

Similarly, little information is available on whether the use of values of modulus determined from plate-loading tests at various depths gives satisfactory load-deflection predictions for piles, although the use of such data gave reasonable predictions in one series of full-scale tests, as described in Section 8.6.

The use of pressuremeter tests by Frydman et al. (1975) and Baguelin et al (1978) has already been mentioned in Section 8.2.4, in relation to the determination of p-ρ curves, and such tests can also be interpreted, in terms of elastic theory, to give values of Young's modulus at various depths. The pile-soil yield pressure, p_y, may also be estimated from the limit pressure measured by the pressuremeter. This procedure has been applied to the pile test reported by Frydman et al. and has produced very promising agreement between the calculated and measured behavior.

Full-scale loading tests are probably the most satisfactory means of determining the soil modulus, since such factors as the effects of installation and pile-soil separation are taken into account automatically and reflected in the backfigured moduli. There appears to be two possible means of interpreting pile-load results:

1. To use the ground-line deflection at the working load to backfigure a *secant* value of soil modulus, which may be used with elastic theory to predict deflections at the working load (ignoring the effects of local yield and soil-pile separation).
2. To use the linear portion of the load-deflection curve to backfigure a *tangent* value of soil modulus, which may then be used with the theory (including the effects of local yield) to predict the load-deflection curve to failure.

The latter procedure would appear to be preferable, as a more relevant value of the pile-flexibility factor may be obtained. However, in some cases, the use of the first procedure may be more expedient if piles similar to the test pile are to be used in the foundation, and as shown in Section 8.3.2, the use of a secant modulus with purely elastic theory should give results of adequate accuracy at normal working loads. In either case, the principle of interpretation of the load test is the same. Considering first the case of E_s constant with depth and a free-head pile, the ground-line deflection for an elastic soil is, from Eq. (8.66)

$$\rho = \frac{H}{E_s L} \cdot I_{\rho H} + \frac{M}{E_s L^2} \cdot I_{\rho M} \tag{8.91}$$

By substituting the measured values of ρ, H, and M in this equation, E_s may be expressed as a function of $I_{\rho H}$ and $I_{\rho M}$. For various values of K_R, $I_{\rho H}$ and $I_{\rho M}$ may be obtained from the theoretical curves in Figs. 8.13 and 8.14, and hence a relationship between E_s and K_R is obtained from the definition $K_R = E_p I_p / E_s L^4$. Simultaneous solution (e.g., by graphical means) of these two relationships gives the values of E_s and K_R for the pile. Because the theoretical-influence factors are insensitive to the value of Poisson's ratio of soil, ν_s, the value chosen for this quantity is of secondary importance. The above procedure may similarly be applied to fixed-head piles or to the case of a linearly increasing modulus with depth, for which relationships between N_h and K_N would be derived.

A more complete definition of the soil modulus can be obtained if tests on piles of different proportions are made or if the ground-line rotation as well as the

deflection of a pile is measured. The case that best fits the data (constant E_s or linearly-increasing E_s) may then be determined. This procedure is analogous to the procedure for determining the subgrade-reaction modulus described by Reese and Cox (1969).

As an example of the application of the above procedure, the results of the test on Pile 1-*B* described by Alizadeh (1969) are analyzed. This pile was a Class *B* timber pile, of embedded length about 37 ft and situated in a soil profile consisting of 4 ft of sand and gravel underlain by clay and silt strata. The consistency of the clays ranged from soft to medium, with an average shear-strength of about 600 lb/ft^2. The pile was loaded at the ground line by jacking against an adjacent pile (Pile 1-*A*). At a load of 10 kips, for the first load cycle, a deflection of 0.80 in. and a slope of 0.012 radians were measured at the ground line.

Considering, first, the case of a soil modulus assumed to be constant with depth. The deflection and rotation θ may be expressed as in Eqs. (8.66) and (8.67). Substituting the appropriate values in these expressions, one obtains

$$E_s = 4.05\, I_{\rho H} \quad \text{kips/ft}^2\text{, from the deflection measurements}$$

and

$$E_s = 0.608 I_{\theta H} \quad \text{kips/ft}^2\text{, from the slope measurements}$$

From Figs. 8.13 and 8.14, values of $I_{\rho H}$ and $I_{\theta H}$ may be obtained for various values of pile-stiffness factor K_R. Hence, two plots of E_s versus K_R may be obtained (shown as curves 1 and 2 in Fig. 8.90*a*). A further relationship may be obtained from the definition of $K_R = E_p I_p / E_s L^4$, which upon substitution of the appropriate quantities, gives

$$E_s = 0.00949/K_R$$

This relationship is plotted as curve 3 in Fig. 8.90*a*. The backfigured E_s from the deflection measurement is given by the intersection of curves 1 and 3, while from the slope measurement, it is given by the intersection of curves 2 and 3. These values are, respectively, 44 kips/ft^2 and 26 kips/ft^2. If the assumption of constant soil modulus was valid, these two values should have been the same.

Now considering the case of a linearly varying modulus with depth, the deflection and slope may be expressed from Eqs. (8.74) and (8.75). As in the case of constant modulus, two relationships between N_h and K_N may be plotted; these are shown as curves 1 and 2 in Fig. 8.90*b*. Also, $K_N = E_p I_p / N_h L^5$, so that another N_h-versus-K_N relationship may be plotted; this is shown as curve 3 in Fig. 8.90*b*. The intersection of curves 1 and 3, giving the backfigured modulus from the deflection measurement, gives N_h = 28 kips/ft^3, while the value backfigured from the slope measurement (intersection of curves 2 and 3), gives N_h = 23 kips/ft^3. The closer agreement between these two values of N_h indicates that the assumption of a linearly varying modulus is a better approximation than a constant modulus. It is interesting to note that the value of the modulus of subgrade-reaction n_h backfigured by Alizadeh from subgrade-reaction theory is about 30 kips/ft^3, which is in reasonable correspondence with the backfigured values of N_h.

Empirical Correlations

From a number of published load-deflection measurements on full-scale piles, Poulos (1971*a*) backfigured *secant* values of E_s at working-load levels on the assumption that E_s is constant with depth. For cohesive soils, the values of E_s so deduced varied widely, lying within the range

$$\text{(secant) } E_s = 15c_u \text{ to } 95c_u \qquad (8.92)$$

with an average value of 40 c_u, where c_u = undrained shear-strength of clay. The lower values tended to be associated with very soft clays and the higher values with stiff clays. Banerjee and Davies (1978) backfigured values of E_s of between $100c_u$ and $180c_u$. All these values are lower than values normally associated with surface foundations or axially loaded piles, and this can be attributed to the effects of local yielding of the soil and pile-soil separation near the top of the pile (soil anisotropy may also have contributed slightly.) The scatter of the backfigured results also reflects the effects of local yielding, since more local yield may have occurred in the softer soils at working loads than in stiffer clays.

In order to obtain more-satisfactory correlations, values of the *tangent* modulus should be determined from the initial linear portions of the measured load-deflection curves. Although only a limited number of tangent values of modulus have been determined and related to c_u, the correlation appears to be more consistent and to suggest values of E_s in the range

$$\text{(tangent) } E_s = 250c_u \text{ to } 400c_u \qquad (8.93)$$

These values are about one half of those normally associated with surface foundations (D'Appolonia et al., 1971) and may reflect the effects of soil anisotropy and pile-soil separation, as described in Section 8.3.2.

The use of the correlation given by Eq. (8.93) rather than Eq. (8.92) enables a more logical prediction of the load-deflection relationship, since the effects of local yield

may be taken into account by determining the appropriate value of the yield-deflection factor, F_ρ (Eq. 8.64).

As indicated in the discussion of subgrade-reaction theory and from the example of pile-loading test interpretation described earlier, the assumption of a linearly varying modulus with depth may often by more satisfactory than a constant modulus, especially for soft clays and cohesionless soils. In these cases, it is reasonable to assume that the rate of modulus increase, N_h, is approximately equal to the modulus of subgrade reaction, n_h. Approximate ranges of values of n_h are discussed in Section 8.2.3. Banerjee and Davies (1978) found that a value of N_h of about 40 lb/in^3 fitted a number of experimental results.

At the present time, it has not been possible to distinguish between values of undrained moduli and drained moduli; however, most tests were probably carried out relatively rapidly so that the correlations quoted are best considered as being applicable to the undrained modulus. Also there is insufficient data for any distinction to be made between values of soil modulus for various installation methods.

Repeated-Loading and Cyclic-Loading Effects

The increased movement associated with repeated or cyclic loading can be taken into account in a crude manner by adopting a reduced modulus, as discussed in Sections 8.2.3 and 8.2.4 in relation to the subgrade-reaction approach. The apparent reduction in modulus found experimentally may arise from the cumulative effects of soil-pile separation as well as a genuine change in the soil properties with repeated loading. The analysis for a single-load application, outlined in Section 8.3.1, could be extended to take into account repeated loading, but as pointed out by Matlock (1970), the most feasible approach appears to be to seek a quasi-static approximation to the response of a pile to cyclic loading. Most of the current design procedures for this approach have been developed by Reese, Matlock and their co-workers on the basis of field and model tests, and are presented in terms of p-ρ ("p-y") curves (see Section 8.2.4). It is also possible to interpret some of their design recommendations in terms of the elastic-based theory. Cyclic or repeated loading influences both the soil modulus E_s and the pile-soil yield pressure p_y. For piles in soft clay, E_s appears to be unaffected by cyclic loading, but p_y is reduced as follows:

(a) for depth $z < z_r$ where z_r = transition depth (Eq. 8.53), the static value of p_y is multiplied by $0.72\, z/z_r$
(b) for depth $z > z_r$, the static value of p_y is multiplied by 0.72.

For stiff clays, the static value of E_s is multiplied by 0.4, while the static value of p_y is multiplied by 0.24.

For sand, no reduction tc the static value of E_s appears to be necessary, but the static value of p_y is multiplied by a factor which increases from about 0.25 at the surface to 1.0 or so at a depth of 3 diameters or greater.

The reduction in modulus and lateral resistance is likely to arise from one or both of two main causes:

(1) Build-up of excess pore pressure (mainly with clays).
(2) Actual degradation of particles at their contacts (mainly with granular materials, particularly calcareous sands).

It should be recognized that, in predicting the behavior of a prototype from small-scale tests, the significance of the first cause will be affected by the dependence of pore pressure dissipation on scale and period of cyclic loading.

8.6 COMPARISONS BETWEEN OBSERVED AND THEORETICAL LOAD-DEFLECTION BEHAVIOR

Tests of Mohan and Shrivastava (1971)

A series of field tests on steel pile piles was reported by Mohan and Shrivastava (1971). The load-deflection behavior was measured for seven piles, one of which was instrumented to record bending moments. A summary of the piles tested is given in Table 8.10. The soil profile, the results of standard penetration, and static and dynamic cone tests are shown in Fig. 8.91. In addition, plate-bearing tests were carried out at three depths, and the results of these tests were used to calculate values of E_s and c_u, on the assumption that the soil was purely cohesive. The values obtained are shown in Table 8.11.

Comparisons between the measured load-deflection curves and those predicted from the nonlinear analysis are shown in Fig. 8.92. The values of p_y input into the analysis were obtained from the values of c_u calculated from the plate-bearing tests, assuming $p_y = 9c_u$. Below 200-cm depth, a constant value of p_y of 1.3 kg/cm^2 was assumed. A uniform value of E_s of 35 kg/cm^2 was assumed for all piles except the shorter piles *N1* and *N2*, for which a constant value of 50 kg/cm^2 was used.

The agreement between predicted and observed load-deflection curves is reasonable for piles *N*2, *N*3, *N*6, and *IN*1, but the theory underpredicts movements for *N*1 and overpredicts for *N*4 and *N*5. Better agreement could have been obtained for these cases by varying the input parameters. Nevertheless, the comparisons generally suggest that the theory, together with values of E_s and p_y obtained from plate-loading tests, may be capable of giving fair load-deflection predictions for piles.

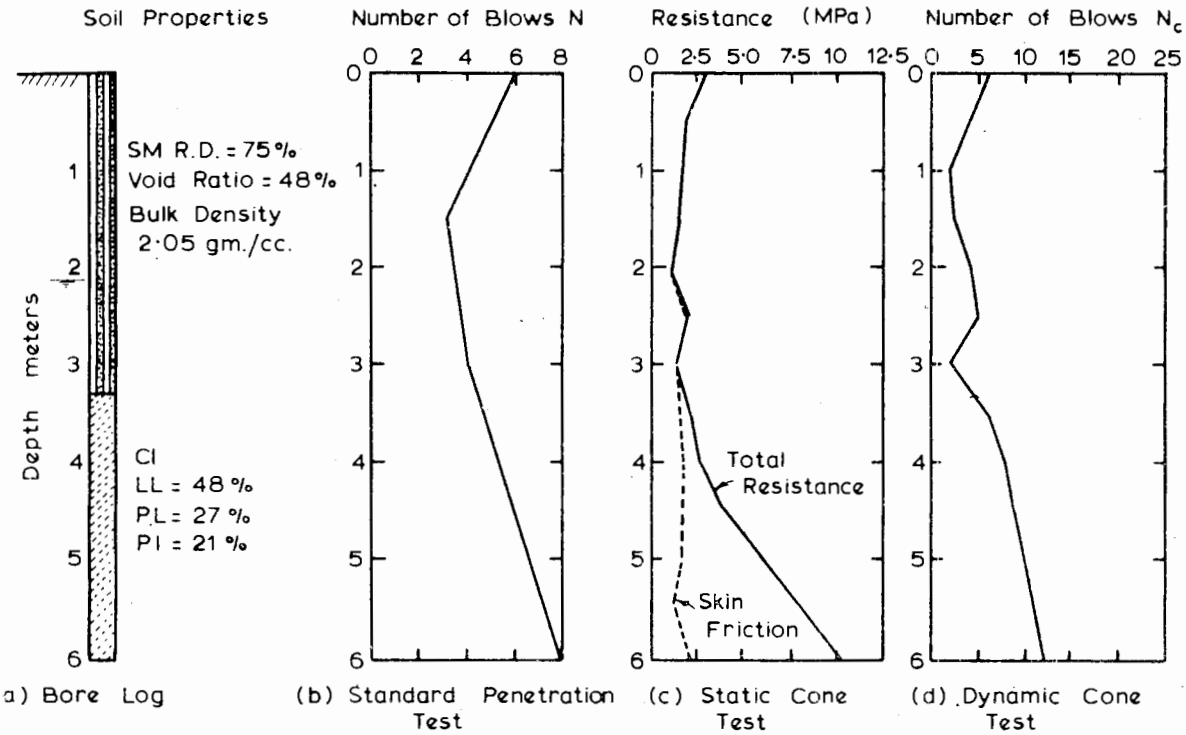

FIGURE 8.91 Soil data (tests of Mohan and Shrivastava, 1971).

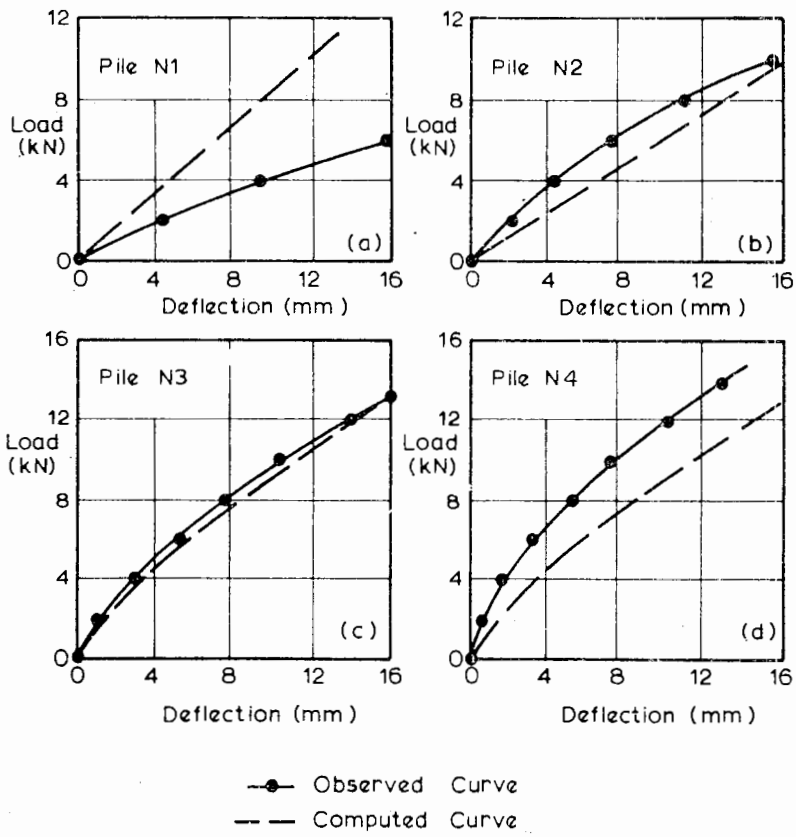

FIGURE 8.92*a* Comparison between observed and computed load deflection curves (tests of Mohan and Shrivastava, 1971).

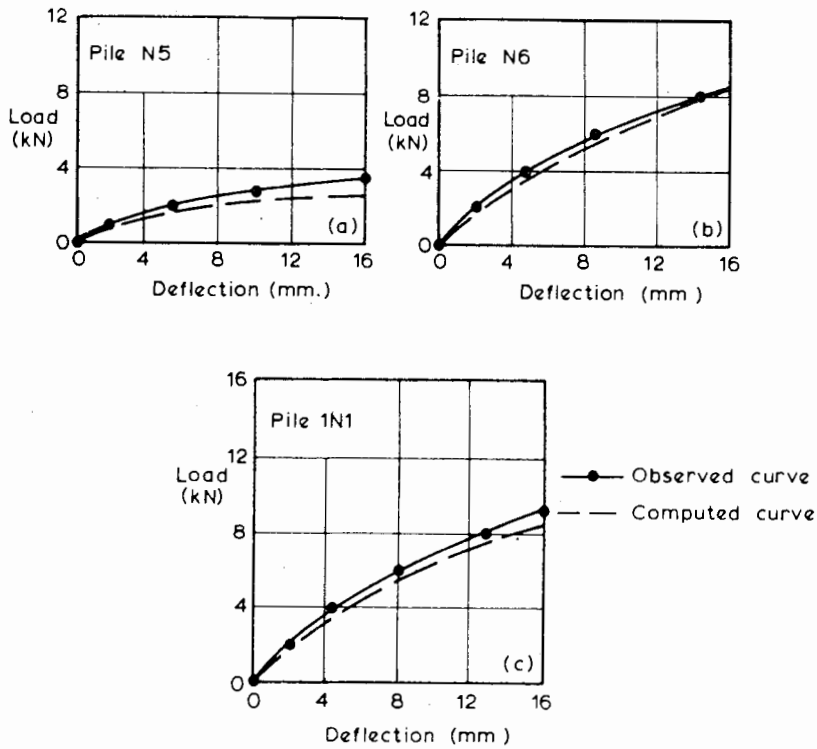

FIGURE 8.92*b* Comparison between observed and computed load- deflection curves (tests of Mohan and Shrivastava, 1971).

TABLE 8.10 SUMMARY OF PILES[a] TESTED BY MOHAN AND SHRIVASTAVA (1971).

Test	Pile Dia. (cm)	Embedded Length (cm)	Pile Stiffness, E_pI_p(kg cm²)
*N*1	10	200	6.22×10^8
*N*2	10	300	6.22×10^8
*N*3	10	400	6.22×10^8
*N*4	10	500	6.22×10^8
*N*5	3.8	525	0.316×10^8
*N*6	7.6	525	2.46×10^8
*IN*1[b]	10	525	3.20×10^8

[a] All piles are steel pipe.
[b] Instrumented pile.

TABLE 8.11 CALCULATED VALUES OF p_y AND E_s FROM PLATE-BEARING TESTS[a] BY MOHAN AND SHRIVASTAVA (1971)

Depth Below Surface (cm)	Dirn. of Loading	E_s (kg/cm²)	p_y (kg/cm²)
50	Vertical	121	4.2
50	Horizontal	82	3.1
100	Vertical	220	8.0
150	Vertical	35	1.8

[a] All tests on 30-cm square plate.

For the instrumented pile *IN*1, comparisons between the observed and theoretical distributions of deflection, slope, and moment with depth are given in Fig. 8.93. Again, the agreement is reasonable, and is at least as good as that reported by Mohan and Shrivastava, using Kubo's (1965) modified subgrade-reaction approach.

Similar agreement has been found by Poulos (1971*a*) between theoretical behavior and that reported by Kerisel and Adam (1967) from full-scale pile tests in clay.

Tests of Gleser (1953)

Gleser (1953) reported measurements of deflection and moment along a fixed-head pile in sand. In order to compare the measured distributions with the theory, the theoretical and measured pile-head deflections were equated and the soil modulus backfigured. The test was interpreted in two ways: first, as the case of a pile in a soil having constant soil-modulus E_s with depth; and second, as a pile in a soil whose modulus increases with depth. The calculated deflection and moment profiles are compared with the measured values in Fig. 8.94. As might be expected for a pile in sand, the calculated profiles for linearly varying E_s are in much closer agreement with the measurements than are the profiles for constant E_s.

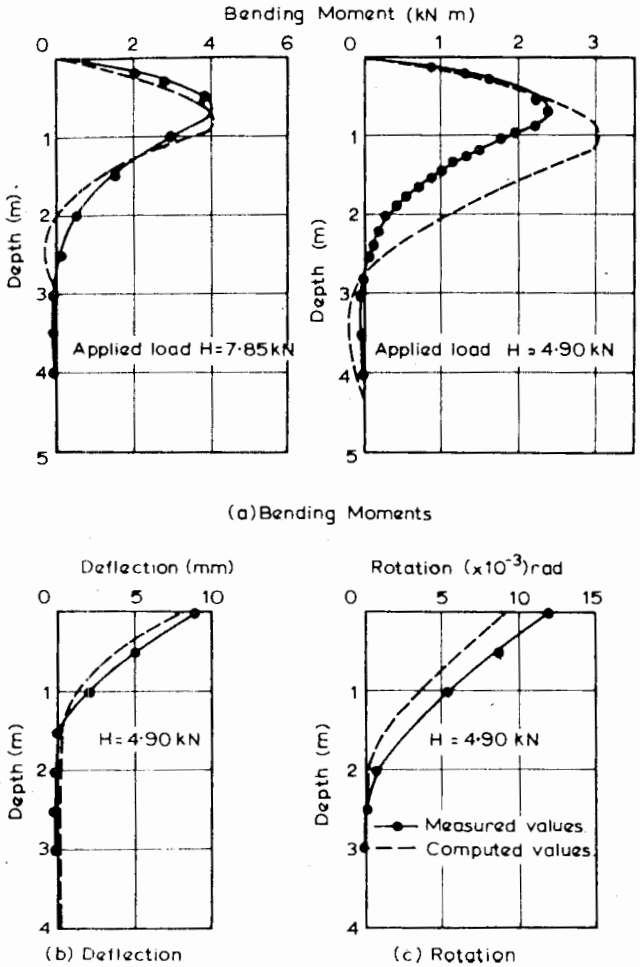

FIGURE 8.93 Comparisons between measured and computed behavior, pile 1N1 (Mohan and Shrivastava, 1971).

Model Tests of Prakash and Saran (1967)

A series of tests on groups of model piles in clay was reported by Prakash and Saran (1967). Tests, involving horizontal load near ground level, were carried out on free-head single piles and groups of four and nine piles, which may be considered as effectively free-headed, since significant rotations occurred at the pile caps. Comparisons between the measured and theoretical ratio of group displacement to single-pile displacement, for a load equal to the average load in the groups, are shown in Fig. 8.95. The average pile-load considered is well below the ultimate value for the single pile. Figure 8.95 shows reasonable agreement between theory and observation, although the theoretical displacement ratio is smaller at close spacings and larger at greater spacings.

Comparisons between the observed and predicted load-deflection behavior of two of the tests are shown in Fig. 8.96. In obtaining the predictions, values of E_s and p_y were backfigured from the reported single-pile test, and the group-efficiency factor was taken to be the value observed in the tests. In both cases, the agreement between the theoretical and predicted load-deflection curves is good.

Model Pile Tests of Druery and Ferguson (1969)

A series of free head tests on model brass piles in kaolin was carried out to obtain load-deflection curves to failure. A typical deflection-time relationship for a load increment is shown in Fig. 8.97. It is interesting to note that a considerable amount of the deflection occurs immediately on application of the load, as the theory predicts for an ideal two-phase elastic soil (Poulos, 1971*a*). For the case shown, the measured ratio of immediate to final deflection is 0.56, whereas the theory predicts a somewhat higher ratio of 0.73.

Load-deflection predictions were made assuming a uniform E_s and a constant value of p_y of 9 c_u along the pile. Two values of E_s were considered, 2500 lb/in.^{2} (175 kg/cm^2) and 1000 lb/in.^{2} (70 kg/cm^2), corresponding to values of E_s/c_u of approximately 450 and 180.

Comparisons between the two predicted load-deflection curves and the observed curves are shown in Fig. 8.98 for four of the tests. Final deflections (measured values after 90 min) are considered. The agreement is generally satisfactory, and with the exception of test 1, the predicted curve for E_s = 2500 lb/in.^{2} agrees more closely with the observed curve. This value of E_s is of the same order as the value of about 500 to 1000 c_u generally applicable to surface foundations (D'Appolonia et al., 1971)—allowing for reduction resulting from the effects of pile-soil separation, as previously mentioned—and is much higher than the average secant value of $40c_u$ backfigured from reported field tests (see previous section). It is interesting to observe that the difference between the predictions for E_s = 1000 lb/in.^{2} and E_s = 2500 lb/in.^{2} is much less than the factor of 2.5 between the E_s values themselves. In fact, it is found that the predictions are as sensitive to the value of p_y as to the value of E_s.

Comparisons between measured and predicted values of ultimate load H_u are shown in Fig. 8.99. Predicted values are given for both the simple statical theory, assuming a constant value of p_y of $9c_u$ along the whole length of the pile, and the modified approach of Broms (1964*a*) who assumes the same p_y distribution, except that p_y is taken as zero from the surface to a depth of $1.5d$ (see Section 7.2). The predicted values from both methods lie within 25% of the measured values, but the simple statical theory tends to overestimate H_u, whereas Broms's approach tends to underestimate H_u and therefore is more conservative.

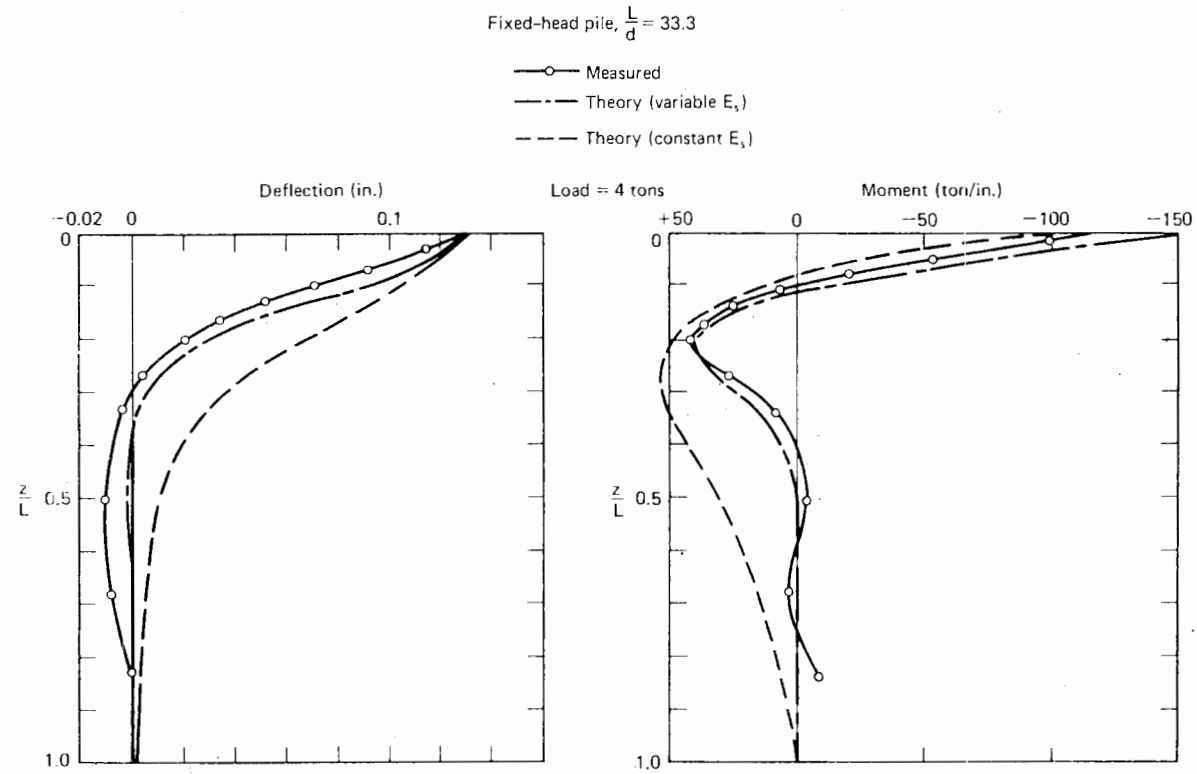

FIGURE 8.94 Comparisons between measured and theoretical deflections and rotations. Tests of Gleser (1953).

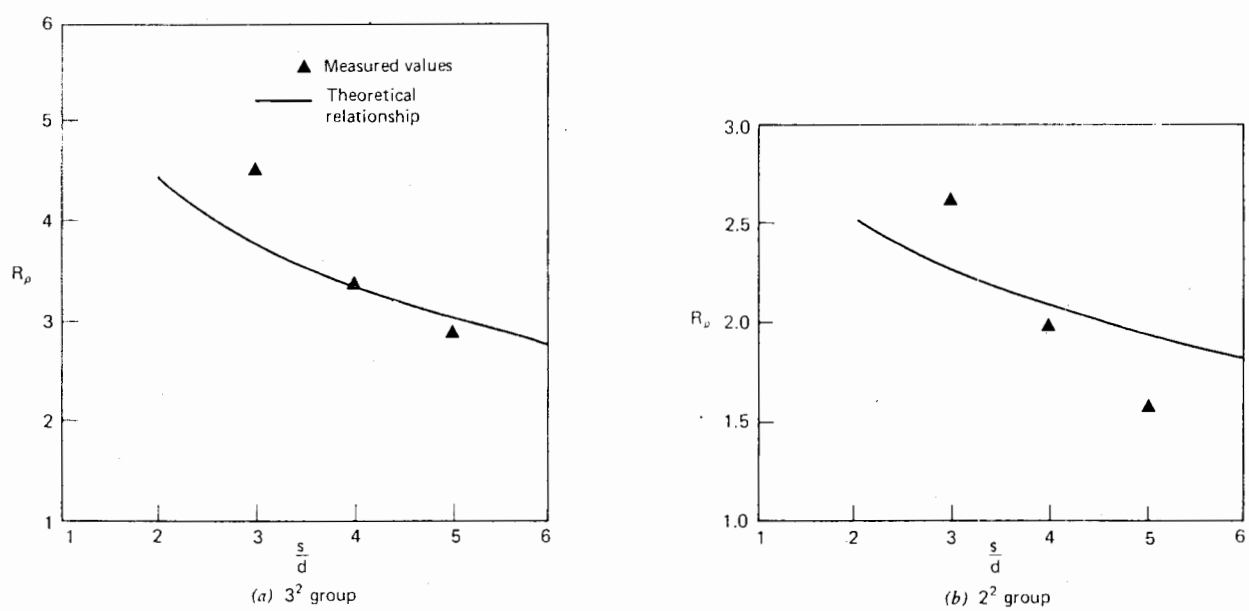

FIGURE 8.95 Comparison between theory and Prakash and Saran's results.

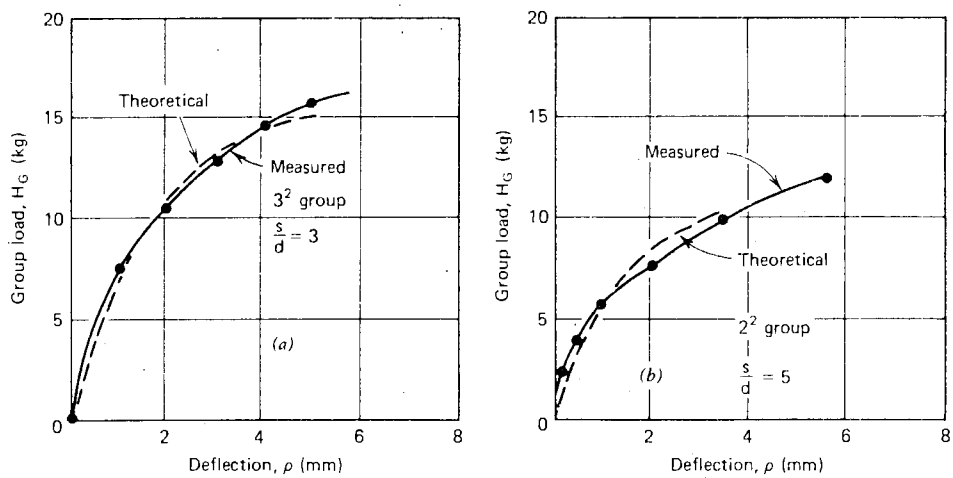

FIGURE 8.96 Comparisons between measured and predicted group load-deflection curves (tests of Prakash and Saran, 1967).

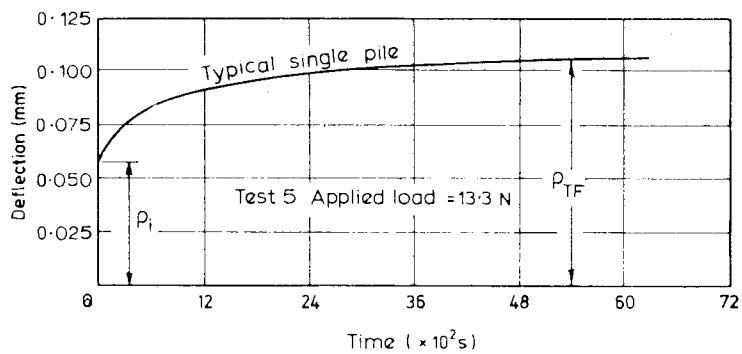

FIGURE 8.97 Typical time-deflection curve for pile (Druery and Ferguson, 1969).

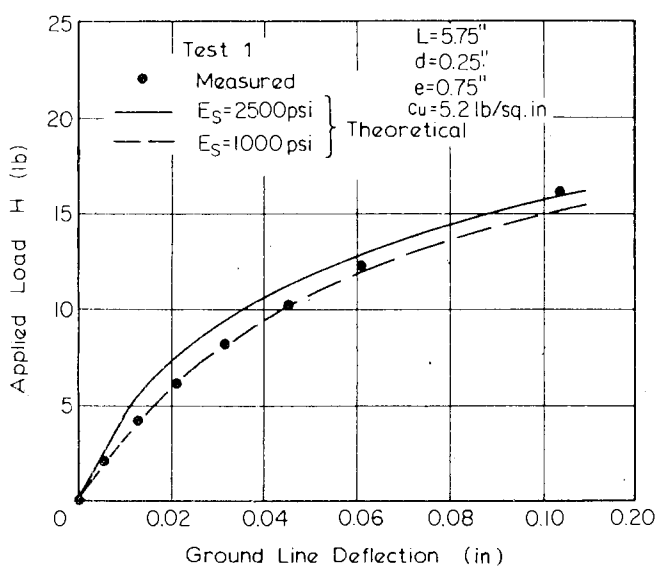

FIGURE 8.98*a* Comparisons between measured and theoretical load-deflection curves (tests of Druery and Ferguson, 1969).

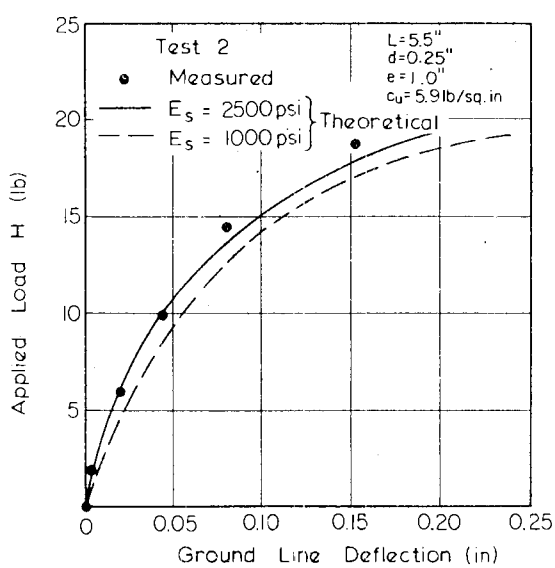

FIGURE 8.98*b* Comparisons between measured and theoretical load-deflection curves (tests of Druery and Ferguson, 1969).

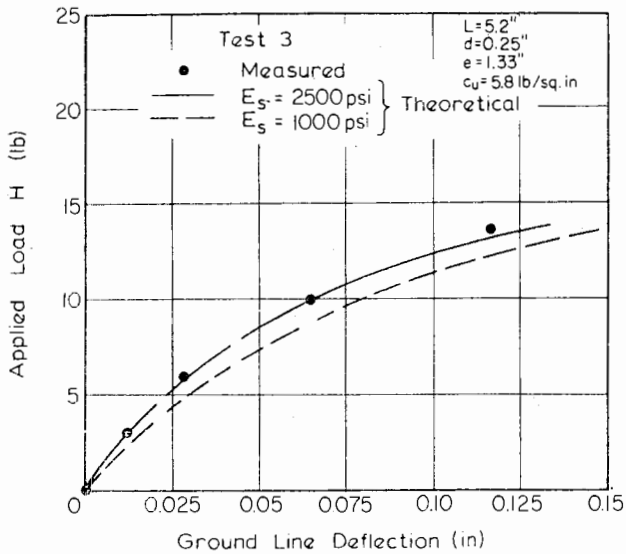

FIGURE 8.98*c* Comparisons between measured and theoretical load-deflection curves (Tests of Druery and Ferguson, 1969).

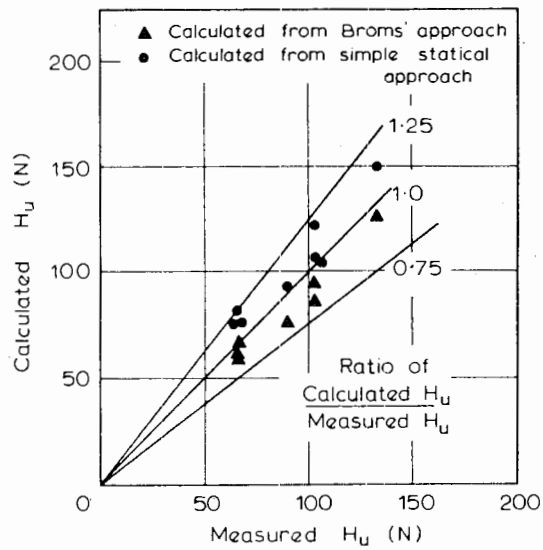

FIGURE 8.99 Comparisons between measured and calculated ultimate loads in model pile tests (tests of Druery and Ferguson, 1969).

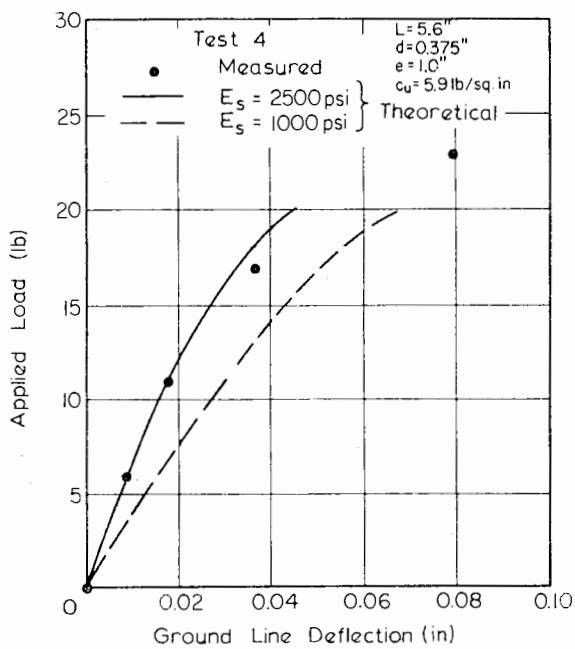

FIGURE 8.98*d* Comparisons between measured and theoretical load-deflection curves (tests of Druery and Ferguson, 1969).

Model Pile Tests of Oteo (1972)

Oteo (1972) carried out tests on aluminium-tube piles in sand. The piles were 8 mm in diameter, with an embedded length of 220 mm, and various initial densities of the sand were used. Both single piles and pile groups were tested. For nine-pile groups tested in sand with an initial density of 1.8 t/m^3, comparisons between the measured and predicted load-deflection curves, shown in Fig. 8.100, reveal close agreement. The basis of the prediction is discussed in the example given in Section 8.4.6. The results of a single-pile test were used to backfigure the rate of increase of Young's modulus with depth, N_h.

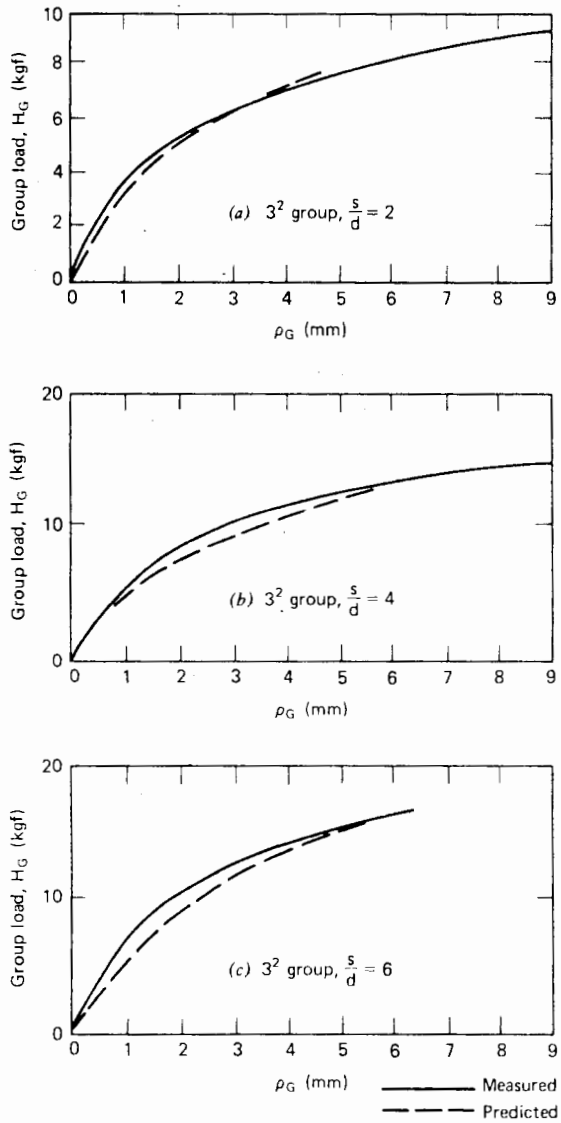

FIGURE 8.100 Comparisons between measured and predicted group load-deflection curves (tests of Oteo, 1972).

9

GENERAL ANALYSIS OF PILE GROUPS

9.1 INTRODUCTION

In previous chapters, the behavior of vertical pile groups under axial loading or lateral loading has been considered. In general, a pile group may contain battered piles and may be subjected to simultaneous axial load, lateral load, moment, and possibly, torsional load. Methods of analyzing this general problem may be broken down into three categories:

1. Simple statical methods that ignore the presence of the soil and consider the pile group as a purely structural system.
2. Methods that reduce the pile group to a structural system but that take some account of the effect of the soil by determining equivalent free-standing lengths of the piles. The theory of subgrade reaction is generally used to determine these equivalent lengths. Typical of these methods are those described by Hrennikoff (1950), Priddle (1963), Francis (1964), Kocsis (1968) and Nair et al. (1969). This type of approach will be termed the "equivalent bent method," following Kocsis (1968).
3. A method in which the soil is assumed to be an elastic continuum and interaction between piles can be fully considered.

The first two methods can only consider interaction between the piles through the pile cap and not interaction through the soil as well. Therefore, they assume that once the loads on any pile are known, the deflections of that pile may be calculated from these loads alone. The third method removes this limitation and allows consideration of pile interaction through the soil; the deflections of a pile are therefore not only a function of the load in that pile but also of the loads in all the piles in the group.

In this chapter, the three approaches mentioned above will be described, with emphasis being placed on the third method, that employing elastic theory. An example will be presented to compare the solutions from each approach.

9.2 SIMPLE STATICAL ANALYSIS

Traditional design methods have relied on the consideration of the pile group as a simple statically-determinate system, ignoring the effect of the soil. One such method, which may be employed either graphically or analytically, is illustrated in Fig. 9.1. Considering, for simplicity, loads and batter in the x, z plane only and piles having a pinned head, the steps in this method are as follows:

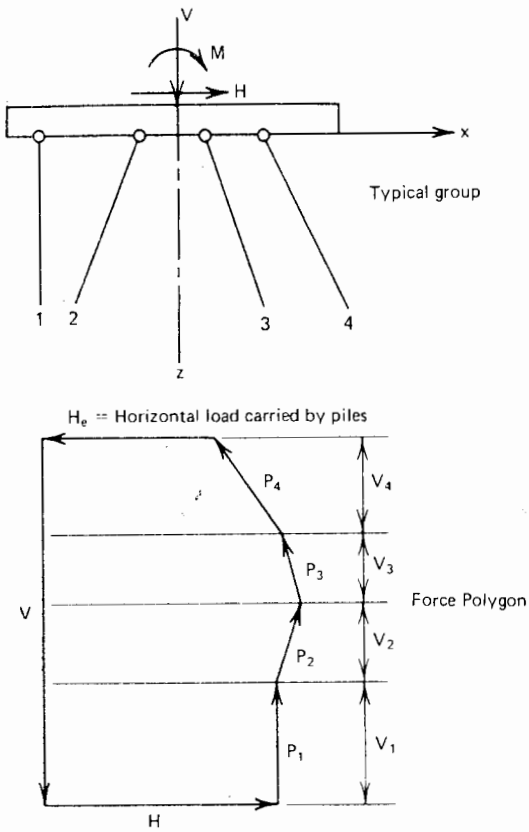

FIGURE 9.1 Simple statical method for determination of group load distribution.

1. Assuming each pile to take an equal share of the vertical load on the cap and assuming the vertical load in a pile, caused by moment in the cap, to be proportional to the distance x, the vertical pile loads are calculated as

$$V_i = \frac{V}{n} + \frac{Mx_i}{\sum_{j=1}^{n}(x_j^2)} \tag{9.1}$$

2. If the solution is done graphically, the forces V and H are plotted on a force polygon. The vertical pile forces, V_i, from Eq. (9.1) are then set off.
3. The force polygon is then completed by drawing lines parallel to the pile directions. The axial force, P_i, in each pile may thus be obtained. There is then a residual horizontal force, H_e, which is assumed to be equally distributed between each pile in the group.
4. If desired, the design of the group may be amended and the pile batters adjusted to give $H_e = 0$—that is no horizontal load in the piles, so that each pile is axially loaded.

It should be noted that this method cannot take into account different conditions of fixity at the pile head, and always assumes zero moment at the head of each pile. Although methods such as that described above are widely used in design, little is known as to their reliability, although it cannot be expected to be high in view of the simplicity of the assumptions. A comparison between this method and other methods will be given in Section 9.4.4.

9.3 EQUIVALENT-BENT METHOD

9.3.1 Principle of Method

The principle of this method is illustrated in Fig. 9.2 for a planar group. The actual group, shown in Fig. 9.2*a*, is acted upon by vertical and horizontal forces and a moment. The equivalent bent, shown in Fig. 9.2*a*, consists of the pile cap supported by fixed-end freestanding columns or cantilevers of equivalent lengths L_{e1}, L_{e2} and L_{e3}, and equivalent cross-sectional areas A_{e1}, A_{e2} and A_{e3}. There are a number of ways of converting the actual lengths and cross-sectional areas of the piles to equivalent values for the columns and these are discussed in 9.3.2 below. Once the equivalent lengths and areas have been determined, the equivalent bent may be analyzed by standard structural analysis techniques to determine the deflections, rotations, and pile loads in the system.

In order to simplify the structural analysis, the pile cap is frequently assumed to be rigid and the piles assumed to behave elastically. Saul (1968) and Reese et al. (1970) have presented matrix analyses in which the above assumptions are made, and in the former paper, torsional loading and dynamic forces may also be incorporated. However, if hand computation is contemplated, the method described by Nair et al. (1969) is more convenient. Their analytical procedure is as follows:

1. Through the rigid pile cap, arbitrary horizontal and vertical displacements, η and δ, and an arbitrary rotation, θ, are imposed. Thus, axial and lateral forces and moments will be introduced in the pile heads—these being a function of η, δ, and θ and of the arrangement and characteristics of the equivalent cantilevers, which reflect pile and soil properties. Expressions for these forces and moments can be determined from standard structural analysis, and are given in the original paper.
2. The moments and forces in the pile heads are added together in the various coordinate directions and equated to the external applied forces and moments. This will give three equations in three unknowns, δ, η, and θ.

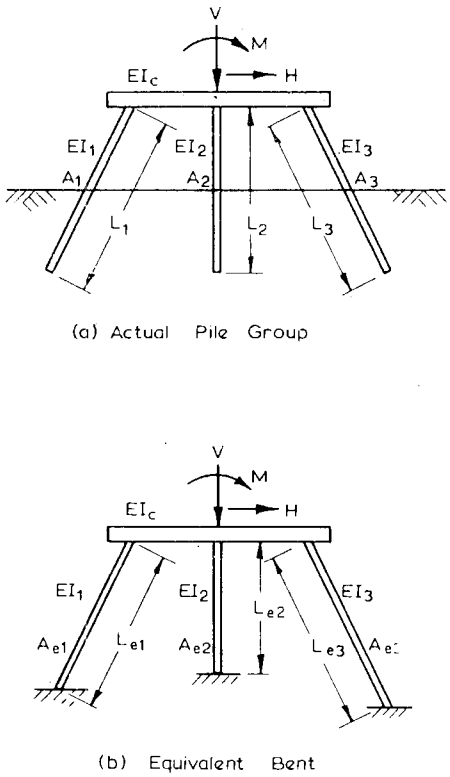

FIGURE 9.2 Principle of equivalent-bent approach.

3. These equations are solved for δ, η, and θ.
4. The moments and forces at each pile head are then determined using the expressions derived in step 1. The necessary information for the design of the group is thus obtained.

9.3.2 Determination of Equivalent Bent

In published methods using the above approach, the equivalent lengths of the piles are almost invariably determined from a subgrade-reaction analysis. The normal deflection (or rotation) of a pile subjected to normal load (or moment) is calculated and equated to the normal deflection (or rotation) of a cantilever under the same load (or moment), the cantilever having the same moment of inertia as the pile. The required equivalent length can then be determined (e.g., Francis, 1964; Kocsis, 1968; Nair et al., 1969). The equivalent area of each cantilever is commonly assumed to be that which gives the same axial deformation as the actual pile when considered as a column, the effect of side shear from the soil thus being neglected.

The equivalent lengths and areas of the cantilevers in the equivalent-bent method may also be determined by use of the solutions given in previous chapters for vertical and lateral loading of piles. Using this approach, some allowance can be made for side shear and for group effects as described below.

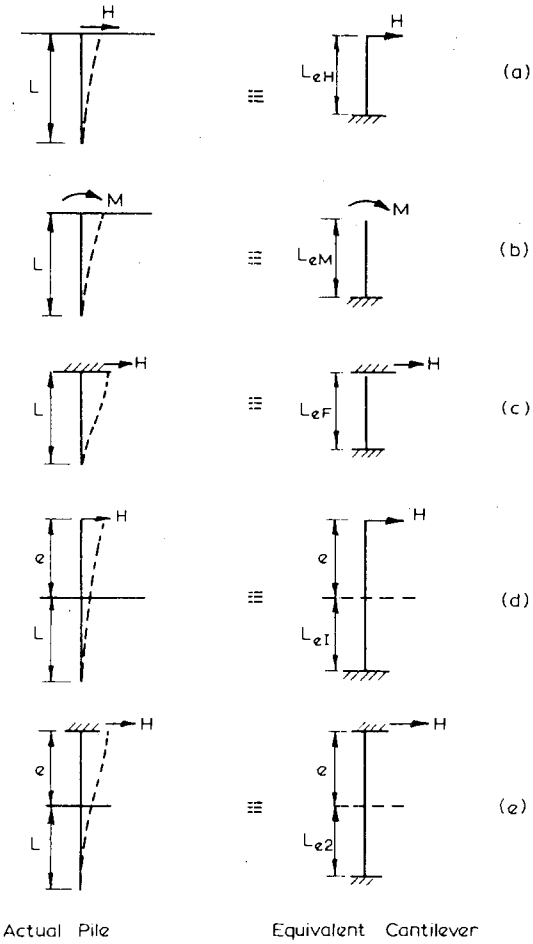

FIGURE 9.3 Equivalent cantilevers for laterally loaded piles.

a) Equivalent Length of Piles

The equivalent length will depend on the boundary condition at the pile head and on the type of loading assumed to act. A number of cases have been considered, as illustrated in Fig. 9.3, and the solutions derived for the equivalent cantilever lengths are summarized in Table 9.1. The group effect has again been taken into account approximately by applying the group displacement and rotation ratios to the single-pile movement (see Section 8.4).

The various ratios referred to in Table 9.1 are as follows:

$R_{\rho H}$ = group-displacement ratio for free-head piles subjected to horizontal load, obtained by superposition of values of $\alpha_{\rho H}$.

$R_{\rho M}$ = group-displacement ratio for free-head piles sub-

jected to moment, obtained by superposition of values of $\alpha_{\rho M}$.

$R_{\theta H}$ = group-rotation ratio for free-head piles subjected to horizontal load, obtained by superposition of $\alpha_{\theta H}$ values ($R_{\theta H} = R_{\rho M}$)

$R_{\theta M}$ = group-rotation ratio for free-head piles subjected to moment, obtained by superposition of $\alpha_{\theta M}$ values.

$R_{\rho F}$ = group-displacement ratio for fixed-head piles subjected to horizontal load, obtained by superposition of $\alpha_{\rho F}$ values.

Table 9.1 gives directly the equivalent lengths for constant Young's modulus, E_s, with depth; corresponding solutions for linearly increasing E_s may be obtained by replacing K_R by K_N (Eq. 8.73), and the influence factors $I_{\rho H}$, and so on, by $I'_{\rho H}$, and so on.

TABLE 9.1 EXPRESSIONS FOR EQUIVALENT CANTILEVER LENGTHS[a]

Case	Equivalent Length
a	$L_{eH} = L\sqrt[3]{3I_{\rho H}K_R R_{\rho H}}$
b	$L_{eM} = L\sqrt{2I_{\rho M}K_R R_{\rho M}}$
c	$L_{eF} = L\sqrt[3]{12I_{\rho F}K_R R_{\rho F}}$
d & *e*	L_e is the solution to the equation. $\left(\frac{L_e}{L}\right)^3 + 1.5\,\frac{M}{HL}\left(\frac{L_e}{L}\right)^2 = 3K_R\left(R_{\rho H}I_{\rho H} + \frac{M}{HL}I_{\rho M}R_{\rho M}\right)$ For case *d*, ($L_e = L_{e1}$) $M = He$ For case *e*, ($L_e = L_{e2}$) $M = -HL\left[\frac{I_{\theta H}K_R R_{\theta H} + 1/6(e/L)^2}{I_{\theta M}K_R R_{\theta M} + 1}\right] + He$

[a]The cantilever is assumed to have the same elastic modulus and moment of interia as the pile it replaces.

It should be noted that for case *e*, the first term of the expression for M represents the fixing moment developed at the pile head. If fixity is not considered to be fully effective, a reduction factor, ranging between 1 and 0, can be applied to this first term. In the limit, if no fixity is developed, case *e* then reduces to case *d*.

Table 9.2 gives an example of the difference between the equivalent lengths L_{eH} and L_{eM} obtained, assuming lateral load only and moment only to act, respectively. A single free-head pile only is considered so that $R_{\rho H} = R_{\rho M} = 1$. For flexible piles, the equivalent length, L_{eH}, is greater, but for rigid piles ($K_R > 10^{-1}$), L_{eM} becomes slightly greater. For most calculations, it would appear reasonable to take either the average of L_{eH} and L_{eM} as the equivalent length, or, conservatively, adopt L_{eH}.

TABLE 9.2 EQUIVALENT LENGTHS L_{eH} AND L_{eM} ($L/d = 50$, $\nu_s = 0.5$, single pile, constant E_s)

K_R	10^{-6}	10^{-5}	10^{-4}	10^{-3}	10^{-2}	10^{-1}
L_{eH}/L	0.0406	0.0818	0.157	0.293	0.551	1.123
L_{eM}/L	0.0251	0.0614	0.127	0.224	0.446	1.154

The derivation of the equivalent bent, as described above, assumes linear elastic soil response. As shown in Chapter 8, this may not be a good assumption for lateral loading. If desired, an iterative approach can be adopted, in which a nonlinear load-deflection curve is specified for each pile and the solution from the analysis of the equivalent bent is recycled, using successively corrected values of the equivalent cantilever length, until the load and deflection of each pile are compatible.

b) Equivalent Area

For a fully-embedded pile, the axial movement is given by Eq. (5.33). In order to make some allowance, albeit approximate, for the interaction of the piles through the soil, the single-pile axial movement should be multiplied by the settlement ratio R_s (Eq. 6.15) for the group. In other words, the settlement of a pile in the group is given (approximately) by

$$\rho = \left(\frac{P}{E_s d}\right)(IR_s) \tag{9.2}$$

where I is defined in Eq. (5.33*a*) and (5.34*a*).

The value of settlement ratio R_s may be estimated from the solutions presented in Section 6.3. For estimating R_s when the group contains battered piles, the battered piles can as a first approximation be considered as vertical piles located at the midpoint of the embedded part of the pile.

The equivalent cantilever will have a length L_e, which will be determined as described above (Table 9.1) for lateral-deflection equivalence. The axial deflection of this equivalent cantilever is

$$\rho = \frac{PL_e}{E_p A_e} \tag{9.3}$$

where

E_p = Young's modulus of pile and cantilever
A_e = equivalent area of cantilever

From Eqs. (9.2) and (9.3),

$$A_e = \left(\frac{L_e d}{IR_s}\right)\left(\frac{E_s}{E_p}\right) \tag{9.4}$$

For a pile having an unsupported length e above the ground surface, the axial deflection of this length must be added to that for the embedded portion. The corresponding expression for A_e is then

$$A_e = \frac{L_e + e}{\left(\frac{IR_s}{d}\right)\left(\frac{E_p}{E_s}\right) + \frac{e}{A}} \tag{9.5}$$

If an equivalent length L'_e is required, rather than A_e,

$$L'_e = \frac{L_e A}{A_e} \tag{9.6}$$

The above expressions for A_e and L'_e should apply for battered piles as well as vertical piles since, as shown in Table 9.3, the axial movement of a pile due to axial load is not significantly influenced by its inclination.

9.3.3 Torsional Response of Piles

In the preceding sections, only axial, lateral, and moment loading have been considered, but in some cases, a further component of loading, torsional moment, may be present (e.g., because of eccentric lateral loading). Relatively little work has been carried out on the torsional response of piles, but Poulos (1975*b*) has obtained elastic solutions for the rotation of a single pile subjected to torsion. The cases of a soil with uniform shear-modulus with depth and linearly varying shear-modulus have been considered. The principle of the analysis is similar to that of the settlement or lateral-load analyses in that expressions are derived for the rotation of the pile at various points along the pile, and of the rotation of the adjacent soil, using Mindlin's equations to evaluate the latter rotations. Imposition of rotational compatibility yields a series of equations that together with the equilibrium equation, can be solved for the shear stresses and rotations along the pile.

The solutions for single-pile rotation are shown in Figs. 9.4 and 9.5 as a function of a dimensionless torsional stiffness of the pile, K_T. In Fig. 9.4, for the case of constant soil modulus with depth, $K_T = G_P J_P / G_S d^4$, where G_P = shear modulus of pile, J_P = polar moment of inertia of pile section, G_S = shear modulus of soil, and d = pile diameter. For the case of a linearly-increasing soil modulus with depth (Fig. 9.5), $K_T = G_P J_P / N_G d^5$, where N_G = rate of increase of soil shear modulus with depth. Rotation increases as torsional stiffness decreases and as length-to-diameter ratio (L/d) decreases. The effect of L/d becomes less as the pile becomes less stiff, and for very flexible piles (small values of K_T), the rotation is independent of L/d.

Although no solutions have yet been obtained for torsional interaction of piles, it is likely that such interaction is small. Figures 9.4 and 9.5 provide a basis for evaluating the response of a pile in a group to torsion. They can also be used to evaluate the results of torsional pile-load tests (see Chapter 16). When incorporating torsional movements into an equivalent-bent analysis, it appears most convenient to determine an equivalent torsional stiffness, $G_P J_P$, of the cantilever such that the actual pile and the cantilever of equivalent length and area, deduced from Section 9.3.2, will have the same rotation. The structural analysis of the equivalent bent may then proceed.

9.4 ELASTIC CONTINUUM ANALYSIS OF PILE BEHAVIOR

The elastic analyses described in previous chapters for pile movements under axial and lateral loads may be extended to cover piles and pile groups subjected to combined loads.

9.4.1 Analysis of Single Battered Pile

In order to take account of groups containing battered piles, the behavior of a single battered pile is considered first, and the analysis is then extended to pile groups. The analyses described in the following sections have been presented by Poulos and Madhav (1971). The effect of torsional loading is not considered.

The analysis is considered in two stages:

1. A battered pile subjected to an axial load.
2. A battered pile subjected to a normal load and a moment.

In both cases, the soil is assumed to be an ideal elastic material with parameters E_s and ν_s that are constant throughout the mass.

9.4.1.1 BATTERED PILE SUBJECTED TO AXIAL LOAD

The analysis follows directly from that of a vertical pile (see Section 5.2). The pile is of diameter d and length L, and the

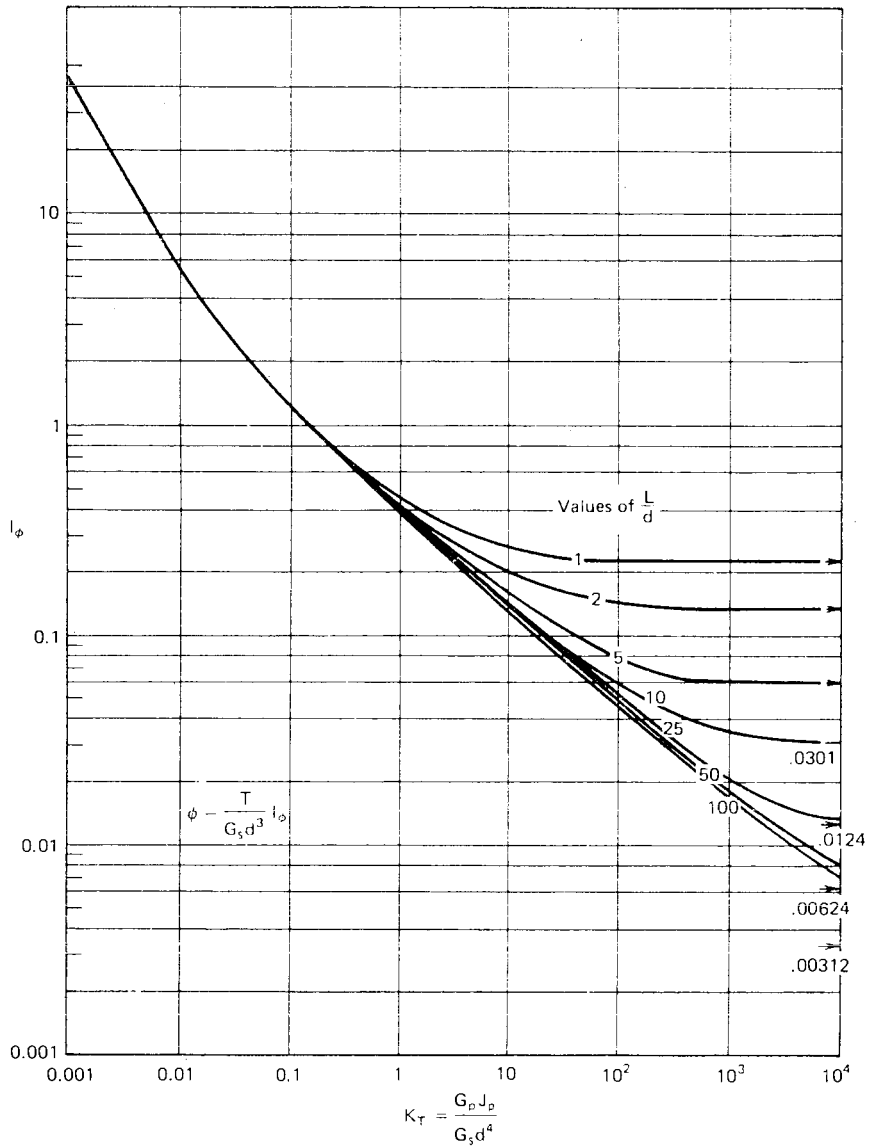

FIGURE 9.4 Influence factor for torsional rotation of pile head– constant G_S.

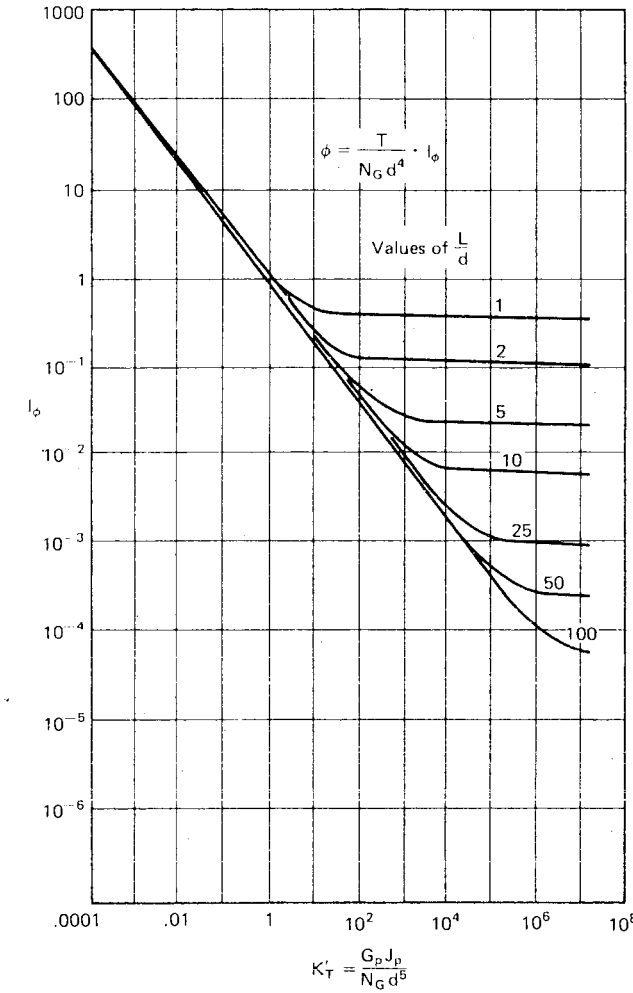

FIGURE 9.5 Influence factor for torsional rotation of pile head– linearly increasing G_S.

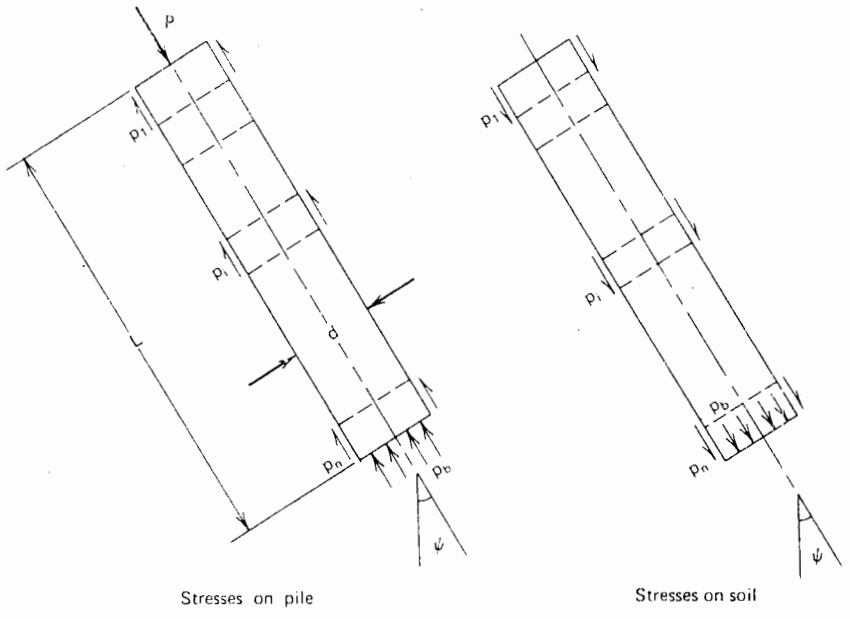

(a) Axially loaded pile

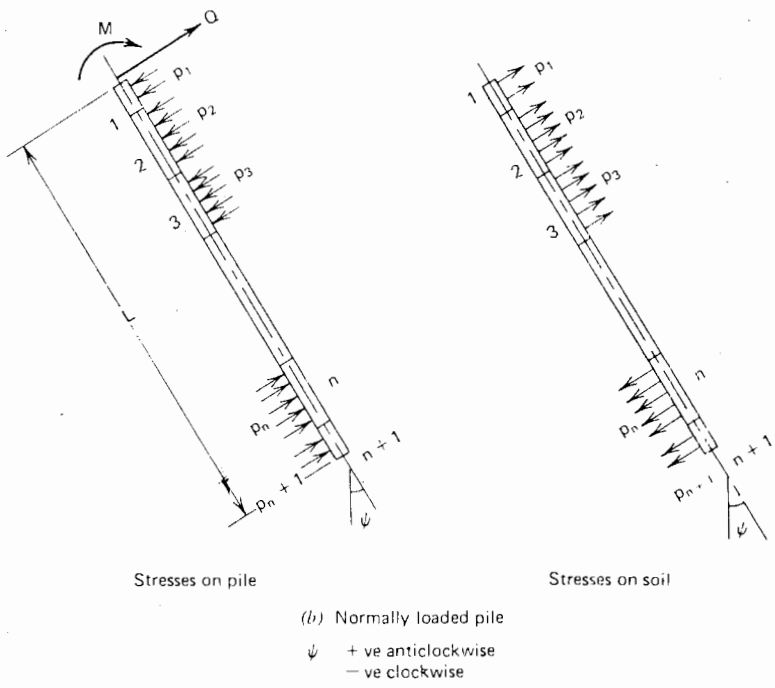

(b) Normally loaded pile

ψ + ve anticlockwise
− ve clockwise

FIGURE 9.6 Analysis of battered pile.

axial force is considered to mobilize only shear stresses on the periphery and a uniform normal stress on the base of the pile. The pile (Fig. 9.6*a*) is divided into n elements of equal length and the axial displacements of the soil at the center of each element are evaluated and equated, the resulting equations being solved to obtain the unknown stresses and displacements. In evaluating the soil displacements, the unknown force on each element is resolved into vertical and horizontal components, and vertical and horizontal displacements caused by each of these components are calculated using Mindlin's equations. These displacements are then combined to give the axial displacements.

9.4.1.2 BATTERED PILE SUBJECTED TO NORMAL LOAD AND MOMENT

The analysis in this case follows closely that described in Section 8.3. It is assumed that only stresses normal to the pile are mobilized in the soil by the applied load and moment, and that the plane of the batter and of the loading are identical. The pile is divided into elements, as shown in Fig. 9.6*b*, and the soil and pile displacements are evaluated at each element and equated, the resulting equations being solved for the unknown normal stresses and displacements. The soil displacements are evaluated in a similar manner to the axially-loaded pile.

Typical results for battered pile-displacements are given in Table 9.3*a* for axial load and in Table 9.3*b* for normal load and moment. In each case, the appropriate displacement-coefficient is given for piles with a batter angle, ψ, of 0^0 (a vertical pile) and 30°. It should be noted that the solutions for positive and negative batter-angles are identical.

It is significant that both the axial and normal displacements are almost unaffected by the batter of the pile; the maximum effect for a batter angle of 30° is approximately only 4%. The virtual independence of the normal displacement on batter angle appears to be unaffected by the pile-flexibility factor, K_R, and the boundary condition at the pile head.

9.4.1.3 BATTERED PILE SUBJECTED TO VERTICAL AND HORIZONTAL LOADS

The fact that the axial and normal displacements of a pile are almost independent of the pile batter means that solutions previously obtained for vertical and horizontal displacements of vertical piles may be applied to calculate the axial and normal displacements of battered piles. This, in turn, leads to a relatively simple method of calculating the horizontal and vertical displacements of a battered pile subjected to vertical and horizontal loads and moments. The vertical and horizontal loads V and H are first resolved into axial and normal components P and Q, as follows:

$$P = V \cos \psi + H \sin \psi \tag{9.7}$$

$$Q = H \cos \psi - V \sin \psi \tag{9.8}$$

The axial and normal displacements, ρ_a and ρ_N, may then be calculated and resolved into vertical and horizontal com-

TABLE 9.3 SOLUTIONS FOR DISPLACEMENTS OF BATTERED PILE

(a) Axial Displacement due to Axial Load Incompressible Pile

$\nu_s = 0.5$

	$I_{\rho a}$	
L/d	$\psi = 0$	$\psi = \pm 30$
10	1.415	1.382
25	1.860	1.859
100	2.542	2.538

$$\rho_a = I_{\rho a} \cdot \frac{P}{LE_s}$$

(b) Normal Displacement Caused by Normal Load and Moment

$\nu_s = 0.5$

	$I_{\rho N}$				$I_{\rho M}$				$I_{\rho F}$			
K_R	0.0001		10		0.0001		10		0.0001		10	
L/d ψ°	0	±30	0	±30	0	±30	0	±30	0	±30	0	±30
10	7.29	7.35	3.22	3.37	39.89	39.78	3.90	4.05	5.81	5.92	1.04	1.09
25	9.75	9.84	3.98	4.13	54.68	54.65	4.99	5.15	7.27	7.40	1.23	1.28
100	12.21	12.33	4.79	4.95	68.28	68.32	6.16	6.33	8.67	8.82	1.44	1.49

Free-head pile: $\rho_N = \frac{1}{E_s L}\left(I_{\rho N} \cdot Q + I_{\rho M} \cdot \frac{M}{L}\right)$

Fixed-head pile: $\rho_F = \frac{1}{E_s L}(I_{\rho F} \cdot Q)$

ponents. To simplify the analysis, it is assumed that lateral loads do not influence axial displacements and that axial loads do not affect lateral displacements. Tests reported by Evans (1954) show that this assumption is conservative in that the lateral deflection of a pile subjected to axial and lateral loads is less than that of the pile subjected to lateral load only. The following expressions are then obtained for the battered pile, for the case of constant E_s with depth:

Vertical displacement:

$$\rho_v = \frac{1}{E_s L}\left(V \cdot I_{vV} + H \cdot I_{vH} + \frac{M}{L} \cdot I_{vM}\right) \qquad (9.9)$$

where

$I_{vV} = I_{\rho a} \cos^2 \psi + I_{\rho N} \sin^2 \psi$
$I_{vH} = (I_{\rho a} - I_{\rho N}) \sin \psi \cos \psi$
$I_{vM} = -I_{\rho M} \sin \psi$
$I_{\rho a}$ = axial displacement-influence factor for axial load
$I_{\rho N}$ = normal displacement-influence factor for normal load
$I_{\rho M}$ = normal displacement-influence factor for moment loading

Horizontal displacement of free-head pile:

$$\rho_h = \frac{1}{E_s L}\left(V \cdot I_{hV} + H \cdot I_{hH} + \frac{M}{L} \cdot I_{hM}\right) \qquad (9.10)$$

where

$I_{hV} = (I_{\rho a} - I_{\rho N}) \sin \psi \cos \psi = I_{vH}$
$I_{hH} = I_{\rho a} \sin^2 \psi + I_{\rho N} \cos^2 \psi$
$I_{hM} = I_{\rho M} \cos \psi$

Rotation of free-head pile:

$$\theta = \frac{1}{E_s L^2}\left(V \cdot I_{\theta V} + H \cdot I_{\theta H} + \frac{M}{L} \cdot I_{\theta M}\right) \qquad (9.11)$$

where

$I_{\theta V} = -I_{\theta N} \sin \psi$
$I_{\theta H} = I_{\theta N} \cos \psi = I_{hM}$
$I_{\theta N}$ = rotation-influence factor for normal load
$I_{\theta M}$ = rotation-influence factor for moment loading

Horizontal displacement of fixed-head pile:

$$\rho_{hF} = \frac{1}{E_s L}(V \cdot I_{hFV} + H \cdot I_{hFH}) \qquad (9.12a)$$

where

$I_{hFV} = (I_{\rho a} - I_{\rho F}) \sin \psi \cos \psi$
$I_{hFH} = I_{\rho a} \sin^2 \psi + I_{\rho F} \cos^2 \psi$
$I_{\rho F}$ = normal displacement-influence factor for fixed-head pile

Vertical displacement of fixed-head pile:

$$\rho_{vF} = \frac{1}{E_s L}(V \cdot I_{vFV} + H \cdot I_{vFH}) \qquad (9.12b)$$

where

$I_{vFV} = I_{\rho a} \cos^2 \psi + I_{\rho F} \sin^2 \psi$
$I_{vFH} = (I_{\rho a} - I_{\rho F}) \sin \psi \cos \psi = I_{hFV}$

Since, as found above, the influence factors for axial and normal displacement and rotation of a battered pile are almost identical with those for the vertical and horizontal displacement and rotation of a vertical pile, $I_{\rho a}$ may be taken as IL/d, where I is evaluated as described in Section 5.3, while $I_{\rho N}$, $I_{\rho M}$, $I_{\rho F}$, $I_{\theta N}$, and $I_{\theta M}$ may be obtained from Figs. 8.13, 8.14, 8.15 and 8.19 as $I_{\rho H}$, $I_{\rho M}$, $I_{\rho F}$, $I_{\theta H}$, and $I_{\theta M}$, respectively.

For a soil with E_s increasingly linearly with depth from zero at the surface, the above theory can be employed by substituting $N_h L \cos \psi$ for E_s and using the I values in Figs. 8.33, 8.34, 8.35, and 8.38.

Although the above analysis is limited strictly to a pile in which the plane of the batter coincides with the plane of the horizontal loading, the general case of horizontal loading out of the batter plane could be analyzed approximately by resolving the horizontal load into an in-plane component and a component normal to this. If the horizontal load H is inclined at an angle ω to the plane of batter, the horizontal displacement caused by the in-plane component $H \cos \omega$ may then be calculated as described above, while the displacement in the direction normal to this may be calculated as the horizontal displacement of a vertical pile of length equal to the projected length of the pile, $L \cos \psi$, and subjected to a load $H \sin \omega$. The resultant magnitude and direction of the horizontal displacement may thus be calculated from these two components.

Illustrative Example

To illustrate the effect of batter on pile displacements, the numerical example shown in Fig. 9.7 has been evaluated. The case considered corresponds to a concrete pile in a medium-stiff soil. The vertical and horizontal displacement, ρ_v and ρ_h, and the rotation θ of the pile head are plotted against batter angle ψ for $-30^\circ \geqslant \psi \geqslant +30^\circ$. The effect of a positive batter in reducing ρ_h and θ is clearly shown. All displacements are significantly larger if a negative batter is

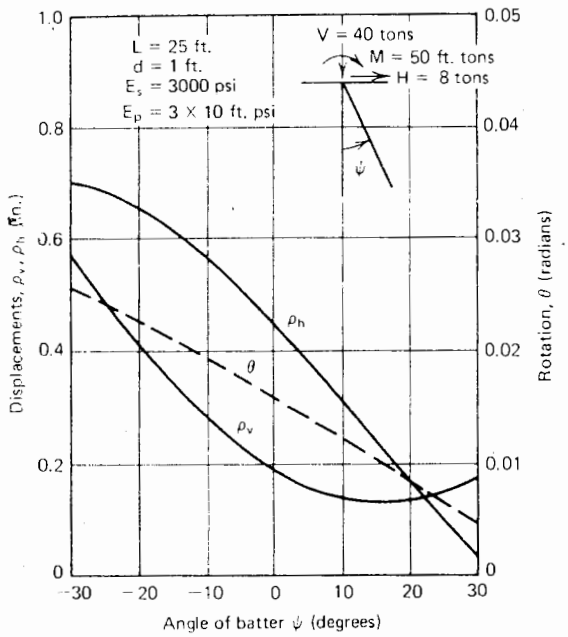

FIGURE 9.7 Typical example of effect of batter on pile movements and rotation.

employed. The vertical displacement, ρ_v, is a minimum for a batter angle of about +15°, and this characteristic is also somewhat similar to that found from experiments on model piles in sand reported by Awad and Petrasovits (1968).

9.4.2 Analysis of Pile Groups

Analyses of groups of vertical piles given in Chapters 6 and 8 were based on the use of "interaction factors," which express the increase in movement of a pile caused by an adjacent loaded pile, and which are functions of the pile spacing, relative stiffness, and geometry; and for horizontal loads, of the direction of loading. By summation of the interaction factors for each pile in a group resulting from all the other piles in the group, the displacement of each pile may be written in terms of the loads on each pile in the group.

A similar approach can be adopted for groups containing battered piles. The first case considered will be that of a group in which all the piles are battered in the same plane and on which the horizontal load acts in the same plane. In the interaction analysis for vertical piles, it is implicit that normal forces produce only normal deflections and that axial forces produce only axial deflections. Thus, considering two battered piles i and j in a group, it is assumed that an axial load on pile j will cause a deflection of pile i that is in the axial direction of pile i, and equal to the axial deflection of pile j under this axial load, multiplied by an interaction factor for axial loading. Similarly, it is assumed that a normal load on pile j will cause a deflection of pile i that is in the normal direction of pile i and equal to the normal deflection of pile j under this normal load, multiplied by an interaction factor for normal loading. Poulos (1974) has made the alternative assumptions that axial load on pile j causes a deflection of pile i that is in the axial direction of pile j; and similarly, that normal load on pile j causes a deflection of pile i that is in the normal direction of pile j. These assumptions, although apparently more logical, lead to solutions that do not satisfy the reciprocal theorem unless all piles are vertical or battered at equal angles. It will be assumed for simplicity that the interaction factors for two battered piles are identical with those for vertical piles at some equivalent spacing s_e. Calculations suggest that for practical ranges of pile flexibility, s_e is approximately the center-to-center distance between the piles one third of the vertical depth of the pile for lateral loading, and somewhat greater for axial loading. However, for convenience, the same equivalent spacing will be assumed for both axial and lateral loading (see Fig. 9.8). It is further assumed that the interaction factor for axial displacement caused by axial loads equals that for vertical displacement caused by vertical load on a vertical pile, and the rotation and normal-displacement interaction factors caused by normal load and moment are identical with those for rotation and horizontal displacement caused by horizontal load and moment on a vertical pile.

On the basis of the above assumptions, the resulting equations for vertical and horizontal displacement and rotation may be written conveniently in matrix form, as follows:

$$\begin{bmatrix} A_v & B_v & C_v \\ A_h & B_h & C_h \\ A_\theta & B_\theta & C_\theta \end{bmatrix} \begin{Bmatrix} V \\ H \\ M \end{Bmatrix} = \begin{Bmatrix} \rho_v \\ \rho_h \\ \theta \end{Bmatrix} \tag{9.13}$$

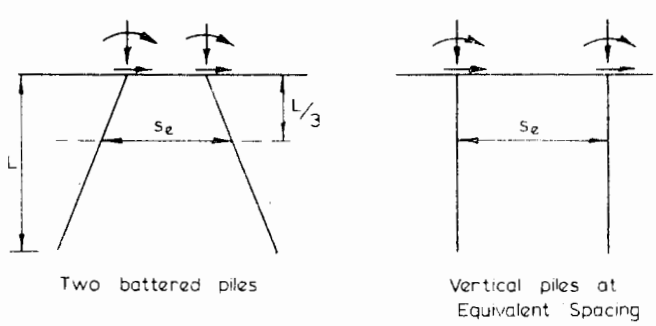

FIGURE 9.8 Equivalent spacing of battered piles.

where the coefficients of the sub-matrices are as follows:

$$A_{v\ddot{y}} = \rho_{a1}\alpha_{\ddot{y}} \cos\psi_j \cos\psi_i + \rho_{NQ1}\alpha_{\rho H\ddot{y}} \sin\psi_j \sin\psi_i$$
$$B_{v\ddot{y}} = \rho_{a1}\alpha_{\ddot{y}} \cos\psi_i \sin\psi_j - \rho_{NQ1}\alpha_{\rho H\ddot{y}} \sin\psi_i \cos\psi_j$$
$$C_{v\ddot{y}} = \rho_{NM1}\alpha_{\rho M\ddot{y}} \sin\psi_i$$
$$A_{h\ddot{y}} = \rho_{a1}\alpha_{\ddot{y}} \sin\psi_i \cos\psi_j - \rho_{NQ1}\alpha_{\rho H\ddot{y}} \cos\psi_i \sin\psi_j$$
$$B_{h\ddot{y}} = \rho_{a1}\alpha_{\ddot{y}} \sin\psi_j \sin\psi_i + \rho_{NQ1}\alpha_{\rho H\ddot{y}} \cos\psi_j \cos\psi_i$$
$$C_{h\ddot{y}} = \rho_{NM1}\alpha_{\rho M\ddot{y}} \cos\psi_i$$
$$A_{\theta\ddot{y}} = -\theta_{N1}\alpha_{\theta H\ddot{y}} \sin\psi_j$$
$$B_{\theta\ddot{y}} = \theta_{N1}\alpha_{\theta H\ddot{y}} \cos\psi_j$$
$$C_{\theta\ddot{y}} = \theta_{M1}\alpha\theta_{M\ddot{y}}$$

ρ_{a1} = axial deflection of single pile caused by unit axial load

ρ_{NQ1} = normal deflection of single pile caused by unit normal load

ρ_{NM1} = normal deflection of single pile caused by unit moment

θ_{N1} = rotation of single pile caused by unit normal load

θ_{M1} = rotation of single pile caused by unit moment

The above-mentioned unit deflections and rotations may be calculated from the theoretical relationships in Chapters 5 and 8 if values of the soil moduli can be estimated, or if pile-load test data are available, from the pile deflections at the working loads. The interaction factors α may be found in Figs. 6.2 to 6.5 while values of the interaction factors $\alpha_{\rho H}$, $\alpha_{\rho M}$, and $\alpha_{\theta M}$ are given in Figs. 8.62 to 8.77.

The submatrices A_v, B_v, and so on, are of order $n \times n$, while the vectors V, ρ_v, and so on are of order n. Equation (9.13) together with the three equations expressing vertical and horizontal load-equilibrium and moment-equilibrium, may be solved to obtain the $3n + 3$ unknown vertical and horizontal loads, moments, displacements, and rotations, for the desired boundary conditions at the pile heads.

A number of cases may be considered, including

1. A rigid pile-cap rigidly attached to the piles, so that the rotation and horizontal displacement of all piles are equal and the vertical displacement of a pile is related to its position in the group and the rotation.
2. Piles pinned to a rigid pile-cap, which is similar to case 1 except that the pile head moments are zero.
3. Piles attached to a massive cap, in which case horizontal and vertical displacements are equal but all pile-head rotations are zero.
4. Piles attached to a relatively flexible pile cap, so that each pile is subjected to known loads and moments.

No account is taken in the above analysis of the horizontal shear and rotational resistance of the cap, although the analysis could be extended to take these into account. For example, the influence of the cap on vertical movements may be allowed for as described in Chapter 10.

Groups in which piles are battered in different directions can be treated approximately by resolving the horizontal load into two components and calculating the in-line horizontal displacements caused by each component, using as the length of a pile its projected length in the plane of loading. The resultant horizontal displacement can then be calculated from these displacement components.

A more complete analysis which avoids many of the assumptions made above has been described by Banerjee and Driscoll (1976). However, because it does not employ interaction factors, a complete re-analysis is necessary for each group configuration, whereas the present analysis allows any group configuration to be rapidly analyzed once values of the interaction factors and single-pile responses have been evaluated.

9.4.3 Parametric Studies of Pile Groups

9.4.3.1 EFFECT OF PILE STIFFNESS AND BATTER ANGLE

The effects of pile stiffness and batter angle on the deflection and load distribution within a pile group are illustrated in Figs. 9.10 to 9.14 for a typical case of a group of six piles, as shown in Fig. 9.9. The pile cap is assumed to be rigid, and rigidly attached to piles in an elastic soil whose modulus is constant with depth. Three values of pile-stiffness factor K are considered: K = 100 (corresponding to concrete piles in a stiff soil), K = 1000 (corresponding to

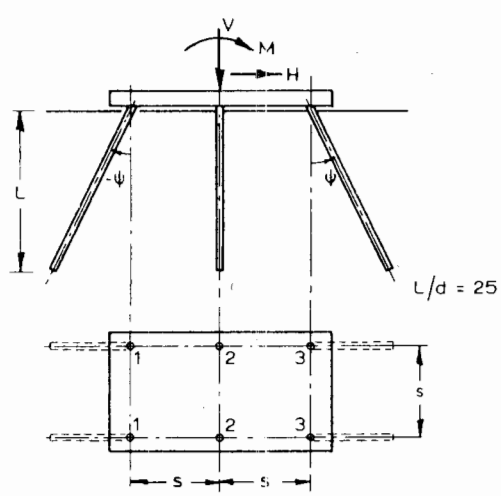

FIGURE 9.9 Pile group considered in parametric study of spacing and batter angle.

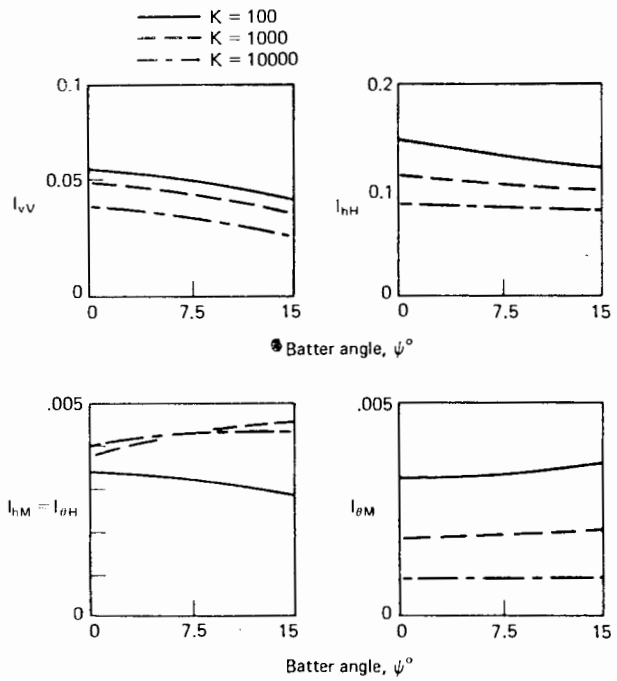

FIGURE 9.10 Effect of batter angle and relative stiffness on deflection and rotation coefficients: six-pile group, $L/d = 25$; $\nu_s = 0.5$; $s/d = 3$.

concrete piles in a medium-stiff soil), and $K = 10{,}000$ (corresponding to concrete piles in a soft soil). For each value of K, the value of pile-flexibility factor K_R is related as follows:

$$K_R = \frac{KI}{R_A L^4} \tag{9.14}$$

where

I = moment of inertia of pile section
R_A = area ratio, defined in Eq. (5.17)
L = pile length

The vertical deflection of the center of the pile cap, ρ_v, the horizontal deflection, ρ_h, and the rotation, θ, for a general loading system are given as follows:

$$\rho_v = \frac{V}{E_s d} \cdot I_{vV} + \frac{H}{E_s d} \cdot I_{vH} + \frac{M}{E_s d^2} \cdot I_{vM} \tag{9.15}$$

$$\rho_h = \frac{V}{E_s d} \cdot I_{hV} + \frac{H}{E_s d} \cdot I_{hH} + \frac{M}{E_s d^2} \cdot I_{hM} \tag{9.16}$$

$$\theta = \frac{V}{E_s d^2} \cdot I_{\theta V} + \frac{H}{E_s d^2} \cdot I_{\theta H} + \frac{M}{E_s d^3} \cdot I_{\theta M} \tag{9.17}$$

where

V = vertical load on group
H = horizontal load on group
M = moment on group
I_{vV}, I_{vH}, etc. = dimensionless deflection and rotation influence coefficients evaluated from the analysis

For the symmetrical group considered here, $I_{hV} = I_{\theta V} = I_{vH} = I_{vM} = 0$, or in other words, the horizontal deflection and rotation caused by unit vertical load are zero. Since ρ_v, ρ_h and θ define the rigid body displacement of the cap, to which the piles are assumed to rigidly attached, the displacements and rotation of any individual pile are readily calculated.

For a center-to-center spacing of $3d$ at the pile cap, Fig. 9.10 shows the effect on the deflection and rotation coefficients of the relative pile stiffness and the angle of batter of the outer piles. The coefficients are not greatly affected by pile batter, but the pile-stiffness factor, K, has a significant effect.

Corresponding solutions for the loads and moment on the front piles (type 3) of the group are given in Figs. 9.11 and 9.12. The actual vertical load V_3, horizontal load H_3, and moment M_3 in each pile are given by:

$$V_3 = VC_{VV} + HC_{VH} + MC_{VM}/d \tag{9.18}$$

$$H_3 = VC_{HV} + HC_{HH} + MC_{HM}/d \tag{9.19}$$

$$M_3 = VdC_{MV} + HdC_{MH} + MC_{MM} \tag{9.20}$$

where

V, H, M = the applied loads and moment on the group, as before
C_{VV}, C_{VH}, etc. = load and moment coefficients

Figure 9.11 shows that most load and moment coefficients are markedly influenced by pile batter and pile-stiffness factor K. However, the vertical pile load caused by vertical load on the group and the horizontal pile load caused by horizontal load on the group (coefficients C_{VV} and C_{HH}) are almost independent of both factors.

9.4.3.2 EFFECT OF PILE SPACING

The influence of pile spacing on the load and moment coefficients is shown in Fig. 9.12. Again, an increase in the spacing generally reduces the coefficients.

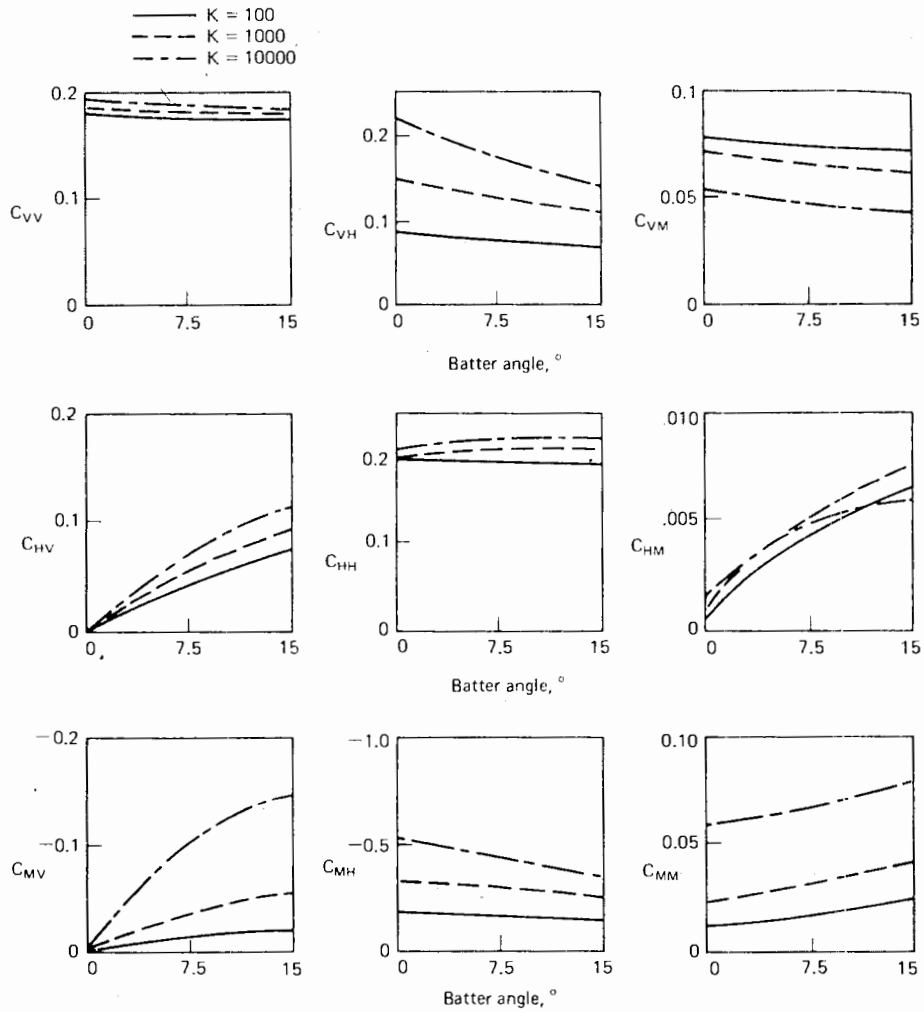

FIGURE 9.11 Effect of batter angle and relative pile stiffness on load and moment coefficient for pile No. 3: six-pile group; $L/d = 25$; $\nu_s = 0.5$; $s/d = 3$.

The effect of pile spacing on the deflection and rotation coefficients for the center of the cap of a six-pile group (Fig. 9.9) is shown in Fig. 9.13 for a batter angle of 15°. Almost all coefficients decrease with increasing spacing, as would be anticipated.

9.4.3.3 EFFECT OF NUMBER OF PILES IN GROUP

The effect of the number of piles in the group on the deflection and rotation coefficients for the center of the pile cap is shown in Fig. 9.14. A four-pile group and a six-pile group are compared for $K = 1000$ and a pile spacing of three diameters. As would be expected, deflection and rotation coefficients are greater for the four-pile group, and the rotation coefficients are most affected because of the closer spacing between the outer piles. The pile loads and moments are correspondingly greater in the four-pile group.

9.4.3.4 EFFECT OF PILE CONFIGURATION

In order to examine the effect of pile configuration on group rotation and deflections, the six groups shown in Fig. 9.15 have been analyzed. Group *A* is the one shown in Fig. 9.9, while group *B* is the same group except that the center two piles are removed. The other four groups have different piles battered. In all cases, the batter angle of any battered piles is 15°.

The deflection coefficients for the leading piles of each group are shown in Table 9.4. The following observations may be made:

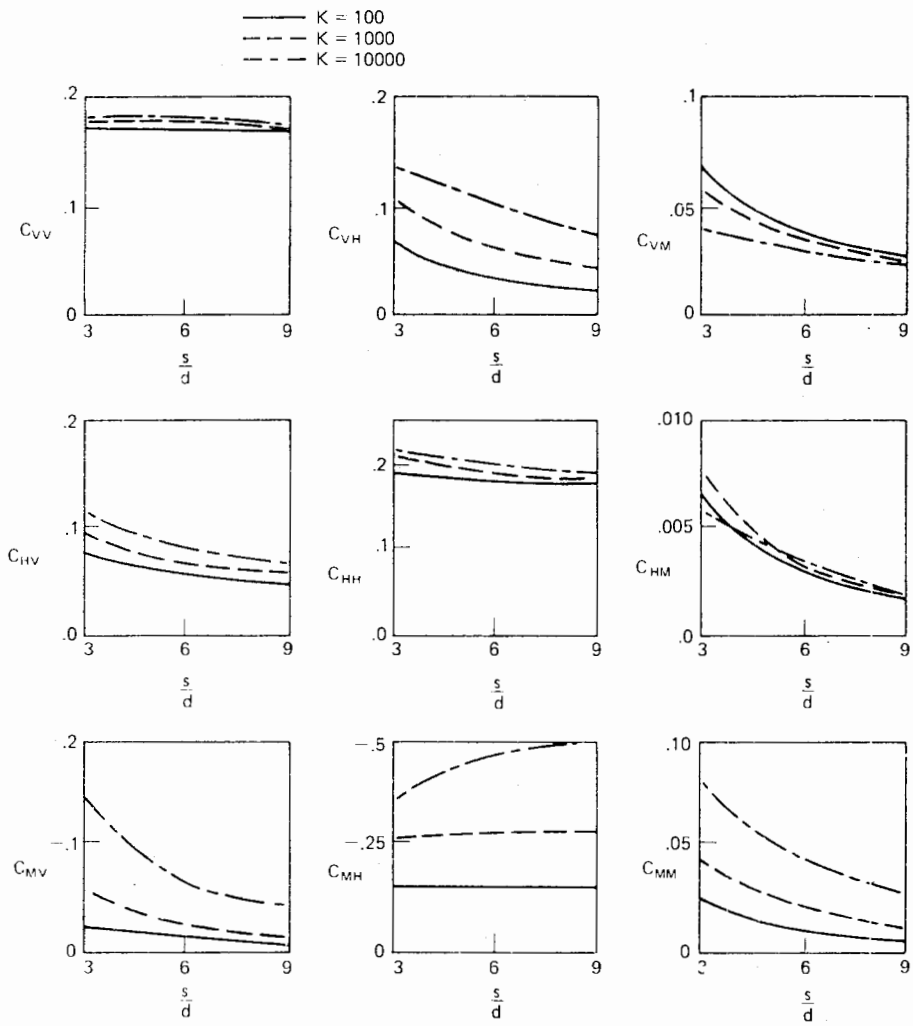

FIGURE 9.12 Effect of pile spacing on load and moment coefficients for pile No. 3: six-pile group; $L/d = 25$; $\nu_s = 0.5$; $s/d = 3$; batter angle $\psi = 15°$.

TABLE 9.4 EFFECT OF PILE CONFIGURATION ON DEFLECTION AND ROTATION COEFFICIENTS[a]

Coefficient[b] \ Group	*A*	*B*	*C*	*D*	*E*	*F*
I_{vV}	0.0391	0.0432	0.0609	0.0548	0.0451	0.0476
I_{vH}	0.0136	0.0121	0.0262	−0.00346	0.00495	0.00569
I_{vM}	0.00615	0.00671	0.00666	0.00463	0.00486	0.00571
I_{hV}	0	0	0.0148	−0.0148	−0.00733	−0.00677
I_{hH}	0.1006	0.1010	0.1093	0.1093	0.1026	0.1025
I_{hM}	0.00453	0.00403	0.00380	0.00380	0.00409	0.00416
$I_{\theta V}$	0	0	0.00102	−0.00102	−0.000818	0.000011
$I_{\theta H}$	0.00453	0.00403	0.00380	0.00380	0.00409	0.00416
$I_{\theta M}$	0.00205	0.00224	0.00188	0.00188	0.00189	0.00190

[a] See Fig. 9.15 for details of pile groups.
[b] Coefficients are for the leading piles of the group.

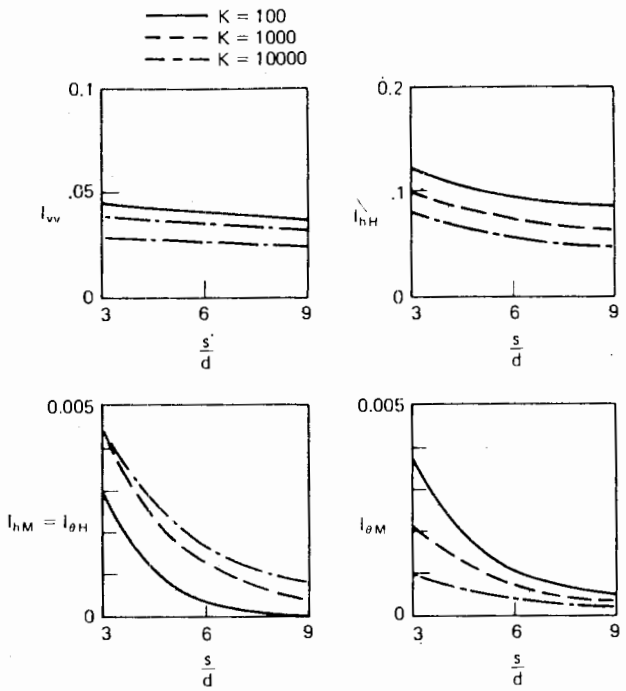

FIGURE 9.13 Effect of pile spacing on deflection and rotation coefficients: six-pile group; $L/d = 25$; $\nu_s = 0.5$; batter angle $\psi = 15°$.

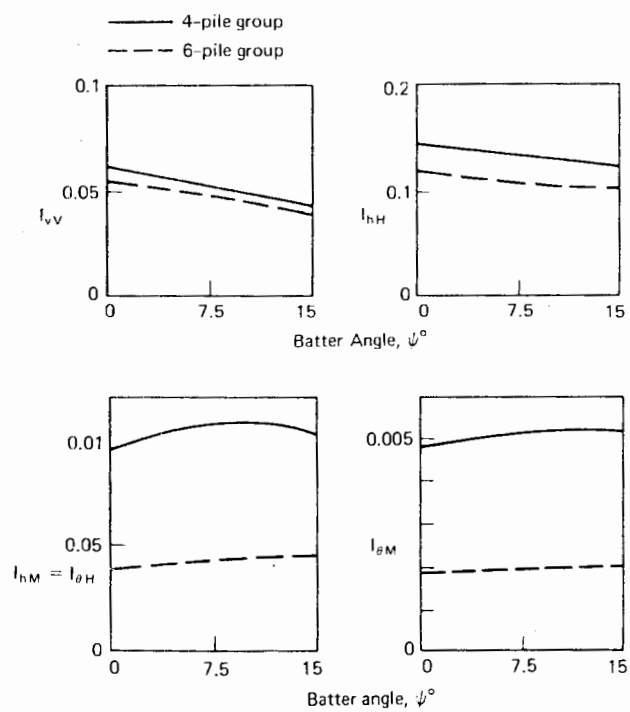

FIGURE 9.14 Effect of number of piles on deflection and rotation coefficients: $L/d = 25$; $\nu_s = 0.5$; $K = 1000$; $s/d = 3$.

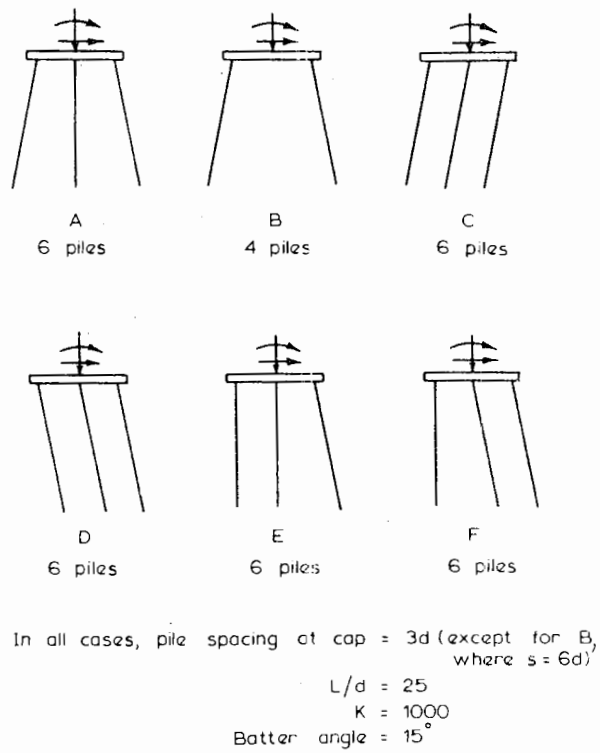

FIGURE 9.15 Groups considered in parametric study of effect of pile configuration.

1. The behavior of group *A* is very similar to that of group *B*—that is, the center piles in group *A* have little influence on the deflection and rotation coefficients.
2. The advantages of group *D* over group *C* arise primarily from the negative horizontal-deflection and rotation developed under vertical load.
3. Groups *E* and *F* behave similarly—that is, battering the center piles has a relatively small influence on the group deflection.

In order to gain a better appreciation of the relative merits of the six groups considered, a numerical example has been taken in which $L = 10$ m, $d = 0.4$ m, $E_s = 7000$ kN/m^2, $V = 1200$ kN, $H = 400$ kN, and $M = 600$ kNm. The resulting deflections and rotations for the center of the pile cap, calculated from Eqs. (9.15), (9.16), and (9.17) and the coefficients in Table 9.4, are shown in Table 9.5. As might be expected intuitively, group *C* is the least satisfactory. Groups *A* and *B* behave quite similarly, and from an economical viewpoint, group *B* would give satisfactory performance, provided that vertical and lateral stability are adequate.

TABLE 9.5 COMPARISON OF GROUP PERFORMANCE
V = 1200 kN, H = 400 kN, M = 600 kN m
L = 10 m d = 0.4 m E_s = 7000 kN/m²

Quantity \ Group	A	B	C	D	E	F
ρ_v (mm)[a]	16.8	18.5	27.4	22.1	18.9	19.4
ρ_h (mm)	16.8	16.6	24.0	11.3	13.7	14.0
θ	0.00436	0.00444	0.00497	0.00278	0.00312	0.00404

[a]For center of rigid pile cap.

TABLE 9.6 EFFECT OF BOUNDARY CONDITIONS AT TOP OF PILE: GROUP A IN FIG. 9.15

Coefficient	Piles Rigidly Attached but Cap Can Rotate	Piles Pinned to Cap	Piles Rigidly Attached to Massive Cap–No Top Rotation
I_{vV}	0.0391	0.0396	0.0391
I_{hH}	0.1006	0.1338	0.0906
$I_{hM} = I_{\theta H}$	0.00453	-0.00220	0
$I_{\theta M}$	0.00205	0.00345	0

TABLE 9.7 COMPARISON OF GROUP WITH VARIOUS BOUNDARY CONDITIONS
V = 1200 kN, H = 400 kN, M = 600 kN/m
L = 10 m, d = 0.4 m, E_s = 7000 kN/m²

Quantity	Piles Rigidly Attached but Cap Can Rotate	Piles Pinned to Cap	Piles Rigidly Attached to Massive Cap–No Top Rotation
ρ_v (mm)[a]	16.8	17.0	16.8
ρ_h (mm)	16.8	18.0	13.0
θ	0.00437	0.00384	0

[a]For center of cap.

9.4.3.5 EFFECT OF BOUNDARY CONDITIONS AT TOP OF PILE

For group A in Fig. 9.15, the deflection and rotation coefficients for the center of the pile cap for various boundary conditions at the junction of the pile top and pile cap are shown in Table 9.6. A larger horizontal deflection occurs if the piles are pinned, but the presence of a massive cap appears to have relatively little influence. The vertical movement caused by vertical load is unaffected by the boundary conditions. Considering the same numerical values as used in Table 9.5, the resulting deflections and rotation are shown in Table 9.7. Under this loading system, the lateral deflection of the group with pinned piles is larger than in the first, but the rotation is less. The group with a massive cap sustains the smallest movements.

9.5 COMPARISON OF METHODS OF PILE-GROUP ANALYSIS

To compare the three methods of analysis described in this chapter, two simple planar pile-groups have been analyzed. As shown in Fig. 9.16, each group has three piles. In the first, all piles are vertical, while in the second, the outer piles are battered. In applying the equivalent-bent method, the equivalent length of each member has been taken as the mean of L_{eH} and L_{eM} (Table 9.1). A computer program (Harrison, 1973) was used to evaluate the solution. For the elastic continuum analysis, the single-pile vertical and horizontal responses have been obtained from the theoretical solutions in Chapters 5 and 8, while the corresponding group effects have been determined from Chapters 6 and 8.

The piles are assumed to be rigidly attached to a rigid cap in both cases. The loads, moments, and deflections from each method of analysis are summarized in Table 9.8.

The main points of interest from this table are:

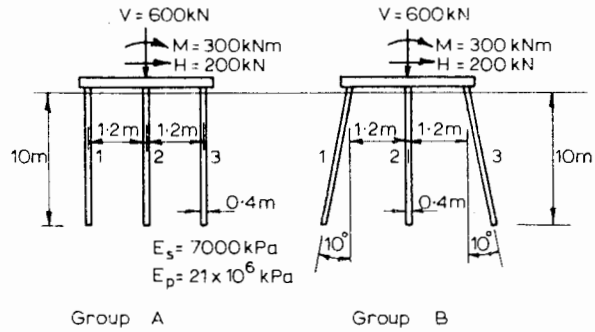

FIGURE 9.16 Pile groups considered in comparison of methods.

TABLE 9.8 COMPARISON OF METHODS OF GROUP ANALYSIS

	Quantity	Simple Statical Analysis	Equivalent-Bent Analysis	Elastic Continuum Analysis
Group *A*	V_1 (kN)	75	67.2	50.5
	V_2 (kN)	200	200.0	163.4
	V_3 (kN)	325	332.8	386.1
	H_1 (kN)	66.7	66.6	75.9
	H_2 (kN)	66.7	66.7	48.2
	H_3 (kN)	66.7	66.6	75.9
	M_1 (kN m)	0	−6.2	−39.6
	M_2 (kN m)	0	−6.2	−23.5
	M_3 (kN m)	0	−6.2	−39.6
	ρ_{v_3} (mm)		17.5	14.8
	ρ_h (mm)		8.9	11.8
	θ		0.00581	0.00248
Group *B*	V_1 (kN)	75	59.3	65.4
	V_2 (kN)	200	200.3	174.8
	V_3 (kN)	325	329.6	359.8
	H_1 (kN)	52.0	76.7	20.3
	H_2 (kN)	52.0	75.5	26.3
	H_3 (kN)	52.0	47.8	153.3
	M_1 (kN m)	0	−43.3	−6.4
	M_2 (kN m)	0	−26.9	−5.1
	M_3 (kN m)	0	66.9	−41.8
	ρ_{v_3} (mm)		16.4	12.9
	ρ_h (mm)		8.2	10.4
	θ		0.00490	0.00233

1. The vertical pile loads from the three methods are of the same order, although the elastic continuum analysis tends to predict a higher maximum load.
2. There is a considerable discrepancy between the computed pile moments from the equivalent bent and elastic continuum analysis. The simple statical analysis assumes zero moment in all piles.
3. The equivalent-bent approach predicts a considerably larger rotation than the elastic continuum analysis and a slightly larger vertical deflection of the leading pile, but a smaller horizontal deflection.

It should be noted that the computed rotation and horizontal deflection in the equivalent-bent method are sensitive to the equivalent length of the piles. For example, for Group *A*, if the equivalent length was taken as L_{eM} (= 1.96 m) instead of the mean of L_{eM} and L_{eH} (= 2.24 m), the vertical and horizontal deflections and rotation would be 16.8 mm, 6.7 mm, and 0.00521, compared with 17.5 mm, 8.9 mm; and 0.00581 in Table 9.8. On the other hand, if L_{eH} (=2.52 m) is used, the corresponding values are 18.2 mm, 11.4 mm, and 0.00639. The latter value of horizontal deflection corresponds more closely to that from the elastic continuum analysis in this case.

A more detailed comparison of the computed deflection and rotation under the individual components of load reveals that the vertical movements caused by vertical load as given by the equivalent-bent method and the elastic continuum method agree closely, but that the computed rotation caused by both horizontal load and moment is considerably greater in the equivalent-bent method. The equivalent-bent method also gives a larger horizontal deflection caused by moment, but a smaller horizontal deflection caused by horizontal load.

The above comparisons, therefore, highlight the difficulty of attempting to characterize a complex pile-soil system by a structural frame. Because it is of a more rational nature, the elastic continuum analysis should give more reliable deflection predictions.

10

PILE-RAFT SYSTEMS

10.1 INTRODUCTION

In the design of the foundation for a large building on a deep deposit of clay, it may be found that a raft foundation would have an adequate factor of safety against ultimate bearing-capacity failure, but that the settlements would be excessive. Traditional practice (assuming the addition of basements to produce a floating foundation is unacceptable) would then be to pile the foundation, and to choose the number of piles to give an adequate factor of safety against individual pile failure, assuming the piles take all the load. However, it is clearly illogical to design the piles on an ultimate-load basis when they have only been introduced in order to reduce the settlement of an otherwise satisfactory raft.

Pile-raft foundations have been successfully used in Mexico City (Zeevaert, 1957) and more recently in London (Hooper, 1973). In the latter case, the finite-element method has been employed to analyze the behavior of the foundation and compare it with the measured behavior. In a method of designing a pile-raft system proposed by Davis and Poulos (1972*b*), the number of piles required to reduce the settlement to the desired amount is determined without the need to resort to computer analysis. The Davis and Poulos method of analysis and design will be described in this chapter. Some alternative approaches to pile-raft analysis will also be mentioned.

10.2 ANALYSIS

The basis of the analysis is similar to that employed for freestanding groups (Chapter 6), except now the basic unit to be considered is a single pile with an attached circular cap resting on the soil surface, instead of the previous unit of a single freestanding pile. The interaction of pile-cap units can be considered in a fashion similar to that described in Section 6.2 for freestanding piles. The settlement interaction between two identical, equally-loaded units can again be expressed in terms of an interaction factor, α_r, where

$$\alpha_r = \frac{\text{Additional settlement caused by adjacent unit}}{\text{Settlement of single unit}} \tag{10.1}$$

Curves relating α_r to dimensionless pile spacing s/d are

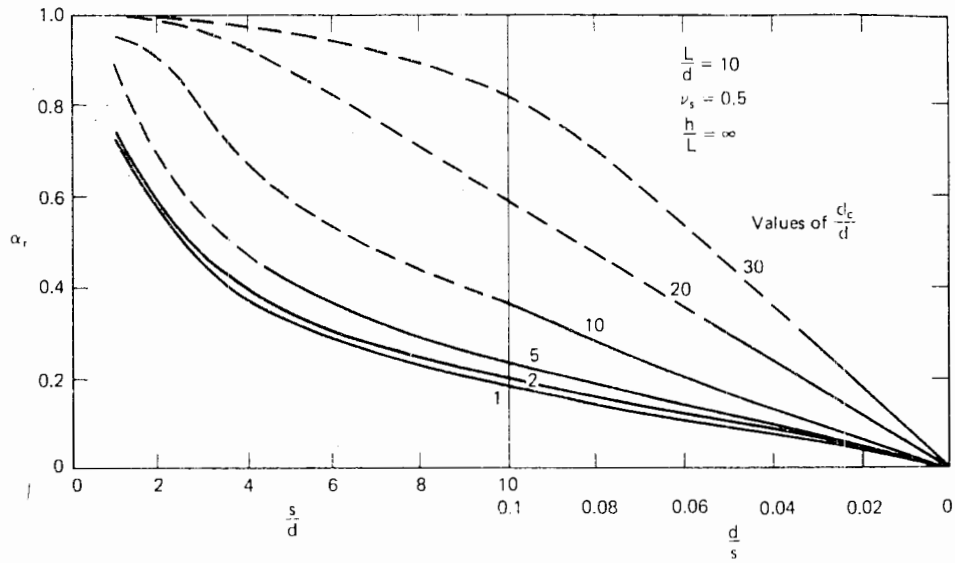

FIGURE 10.1 Interaction factors for pile-raft units, $\frac{L}{d} = 10$.

shown for various values of d_c/d (d_c = cap diameter) in Figs. 10.1, 10.2, and 10.3 for three values of L/d. In all cases, $\nu_s = 0.5$, the piles are incompressible ($K = \infty$), the pile cap is rigid, and the units are situated in a semi-infinite mass. Interaction increases as d_c/d increases, but the effect of d_c/d becomes smaller for larger L/d.

Corresponding curves for $\nu_s = 0$ are shown in Fig. 10.4 for $L/d = 25$. A comparison between these curves and those for $\nu_s = 0.5$ shows that for $d_c/d \leqslant 10$, greater interaction occurs for $\nu_s = 0$ than for $\nu_s = 0.5$, but that for $d_c/d > 10$, ν_s has little influence on interaction.

The curves in Figs. 10.1 to 10.4 may be used to analyze piled foundations or pile-raft systems by considering them to consist of several pile-cap units, each having an equivalent value of d_c/d such that the area occupied by the unit is the same as that occupied by a typical portion of the cap in the group. For example, for a square arrangement of piles in the group,

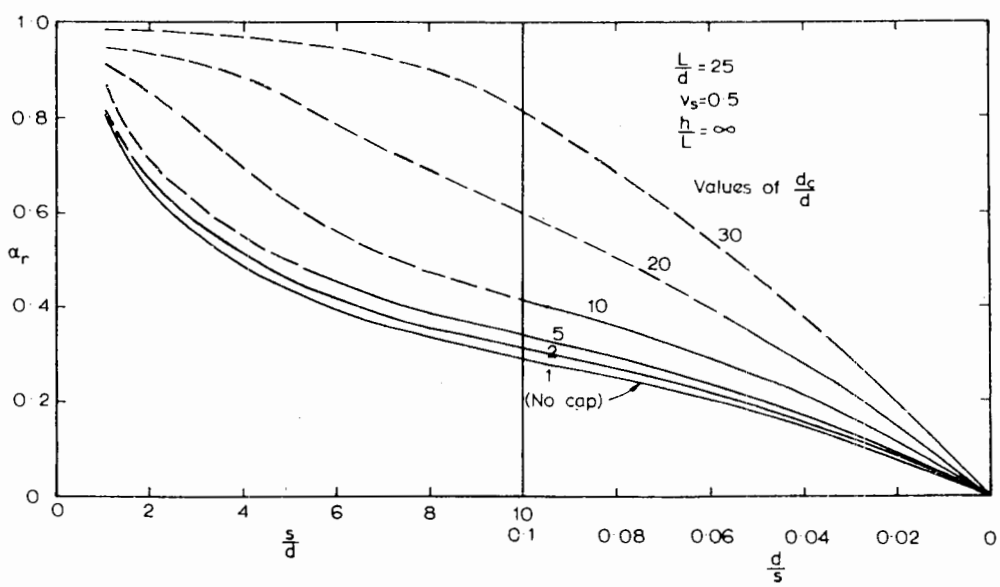

FIGURE 10.2 Interaction factors for pile-raft units, $\frac{L}{d} = 25$.

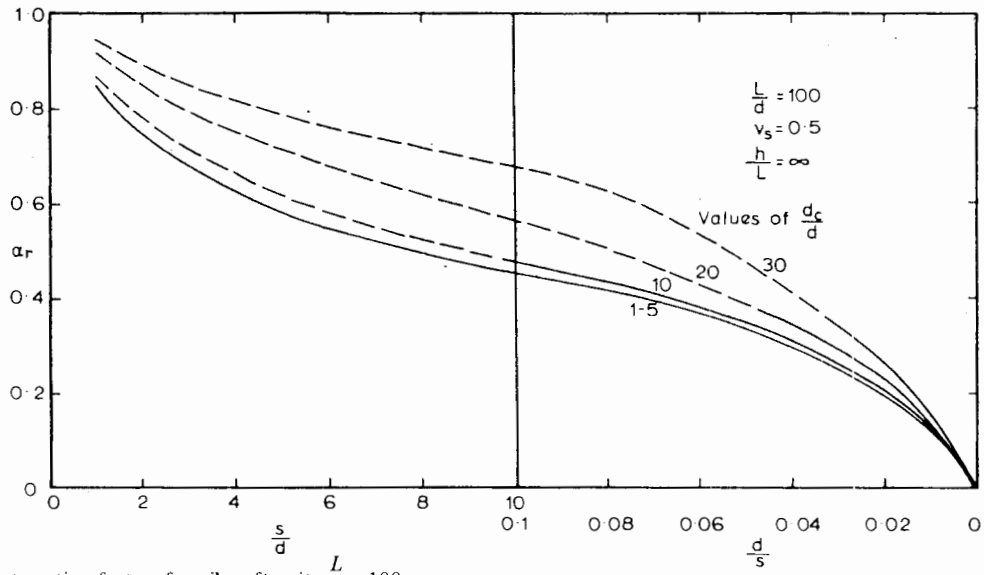

FIGURE 10.3 Interaction factors for pile-raft units, $\frac{L}{d} = 100$.

$$\text{equivalent } d_c/d = \sqrt{\frac{4}{\pi}} \cdot s/d \qquad (10.2)$$

It has been found that superposition can be applied to symmetrical arrangements of pile-cap units in a similar fashion to the freestanding piles in Section 6.2. Therefore, it is again reasonable to extend the use of superposition to the analysis of any general configuration of pile-cap units comprising a pile-raft system.

If a system consists of a total of n units, the settlement of a typical unit i is then given as

$$\rho_i = \bar{\rho}_1 \left[\sum_{\substack{j=1 \\ j \neq i}}^{n} (\bar{P}_j \alpha_{rij}) + \bar{P}_i \right] \qquad (10.3)$$

where

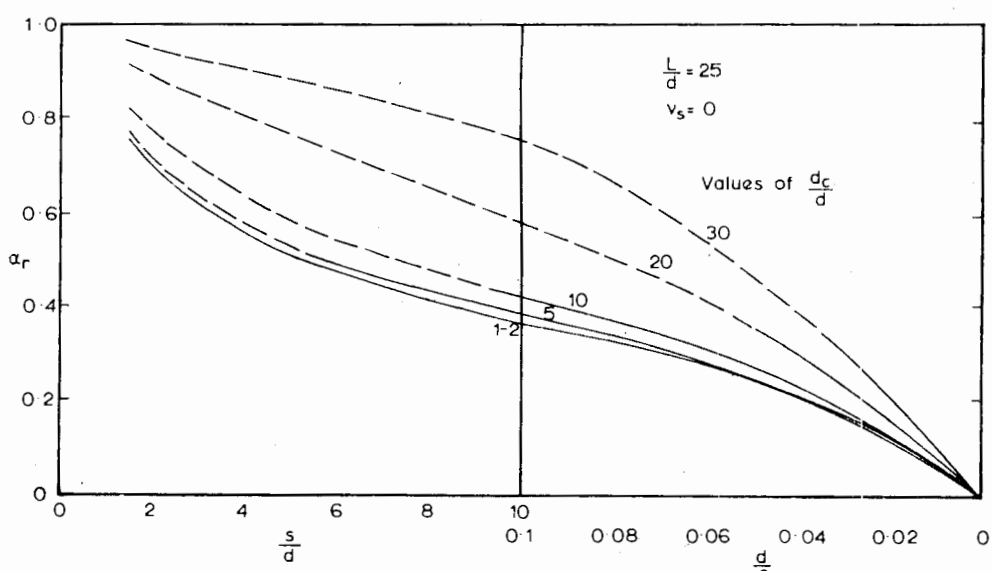

FIGURE 10.4 Interaction factors for pile-raft units, $\nu_s = 0$.

α_{rij} = the value of α_r, for the equivalent value of d_c/d of unit j, corresponding to the spacing between units i and j
$\bar{P}_j$ = load on unit j
$\bar{\rho}_1$ = the settlement of a single pile-cap unit under unit load

From Section 5.3.2, $\bar{\rho}_1$ can be expressed as

$$\bar{\rho}_1 = R_c \cdot \rho_1 \tag{10.4}$$

where

ρ_1 = settlement of freestanding pile under unit load
R_c = ratio of settlement of pile-cap unit to settlement of freestanding pile (Fig. 5.31)

As before, n equations may be obtained from Eq. (10.3) for the n piles in the group; together with the equilibrium equation

$$P_G = \sum_{j=1}^{n} \bar{P}_j \tag{10.5}$$

they may be solved for two limiting cases:

1. Equal displacement of each unit (corresponding to a rigid raft).
2. Equal load (or known loads) on each unit.

This latter case approximates the case of a uniformly-loaded, perfectly-flexible raft. However, it must be borne in mind that each pile-cap unit displaces vertically as a rigid unit, so the displacement of adjacent units will not in general be compatible. Thus, instead of continuously varying, the displacement varies in "steps" from one unit to the next. Hence, the use of the case of equal load in each unit can at best only be an approximation. This approximation will become more satisfactory as the pile spacing decreases.

The results of such an analysis may then be expressed either in terms of a settlement ratio $\bar{R}_S$, where

$$\bar{R}_S = \frac{\text{Average settlement of system}}{\text{Settlement of single unit carrying same } \textit{average load}} \tag{10.6}$$

or

$$\bar{R}_G = \frac{\text{Average settlement of system}}{\text{Settlement of single unit carrying same } \textit{total} \text{ load}} \tag{10.7}$$

These are related as

$$\bar{R}_S = n\bar{R}_G \tag{10.8}$$

For practical use, since pile tests are normally carried out on a single freestanding pile, it may be more convenient to express the settlements in terms of the settlement of a single freestanding pile—that is, in terms of R_S and R_G (Section 6.2). Thus,

$$R_S = R_c \cdot \bar{R}_S \tag{10.9}$$

and

$$R_G = R_c \cdot \bar{R}_G \tag{10.10}$$

The settlement, ρ, of the system is thus given by

$$\rho = R_S \cdot \frac{P_G}{n} \cdot \rho_1 \tag{10.11}$$

or

$$\rho = R_G \cdot P_G \cdot \rho_1 \tag{10.12}$$

For immediate settlements, ρ_1 is the immediate settlement, per unit load, of a single pile at the average load of a pile in the group; and for total final settlements, ρ_1 is the corresponding total final settlement per unit load.

10.3 ELASTIC SOLUTIONS FOR SQUARE GROUPS

Values of the group reduction factor R_G are plotted against dimensionless group breadth B/d in Figs. 10.5, 10.6, and to 10.7 for 2^2, 3^2, 4^2, and 5^2 groups for a rigid raft and for $\nu_s = 0.50$. The piles are incompressible and are embedded in a semi-infinite mass. Also shown are the values of R_G for the rigid raft only and for a rigid block (corresponding to an infinite number of piles).

For a given group breadth, R_G decreases as the number of piles increases. For large breadths, the effect of the number of piles becomes small, especially for piles having small L/d. As L/d increases, the influence of the number of piles becomes more marked and extends over a wider range of breadth.

A comparison between the values of R_G for a 3^2 freestanding group and for a 3^2 pile-raft system is shown in Fig. 10.8. At relatively close spacings, R_G is almost the same for both cases, indicating that the pile cap or raft

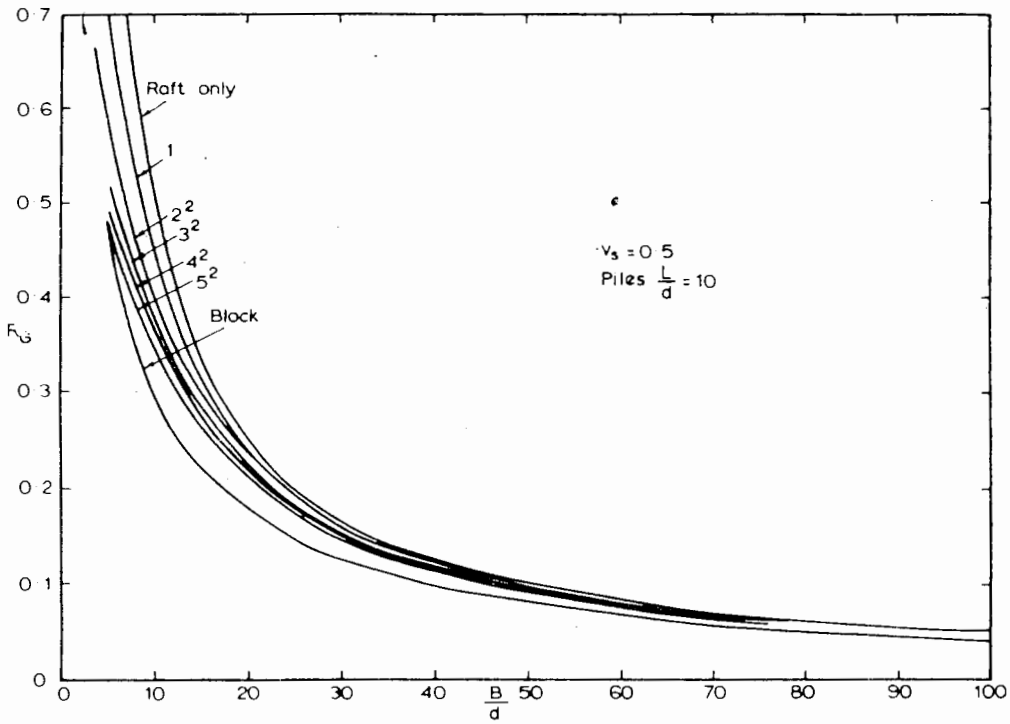

FIGURE 10.5 R_G vs. breadth, rigid raft, $\frac{L}{d} = 10$.

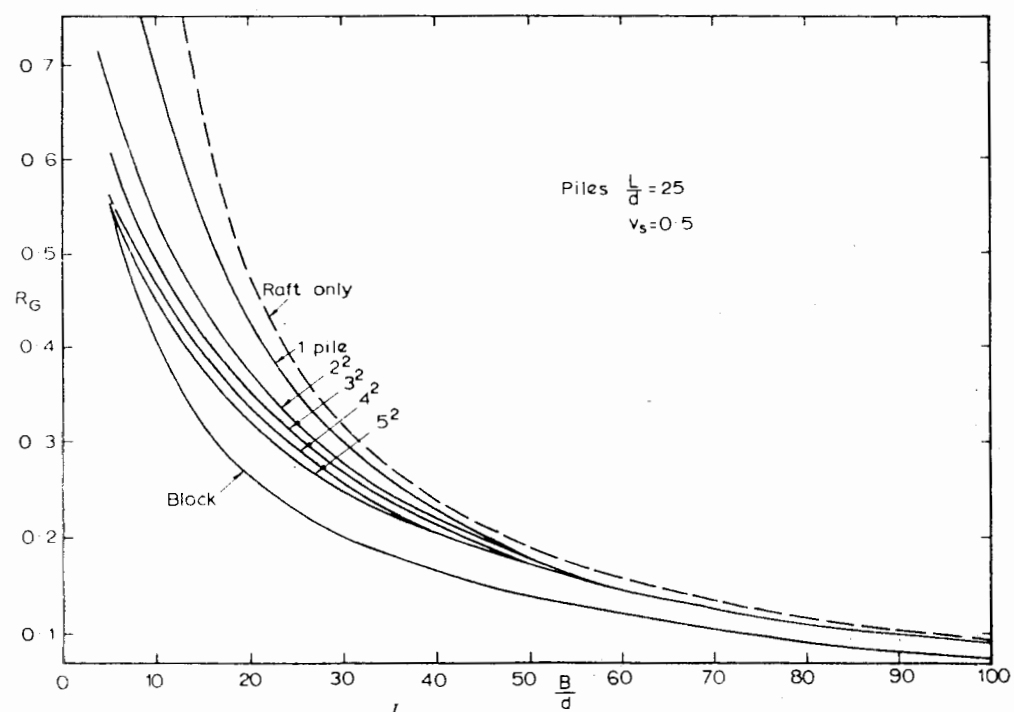

FIGURE 10.6 R_G vs. breadth, rigid raft, $\frac{L}{d} = 25$.

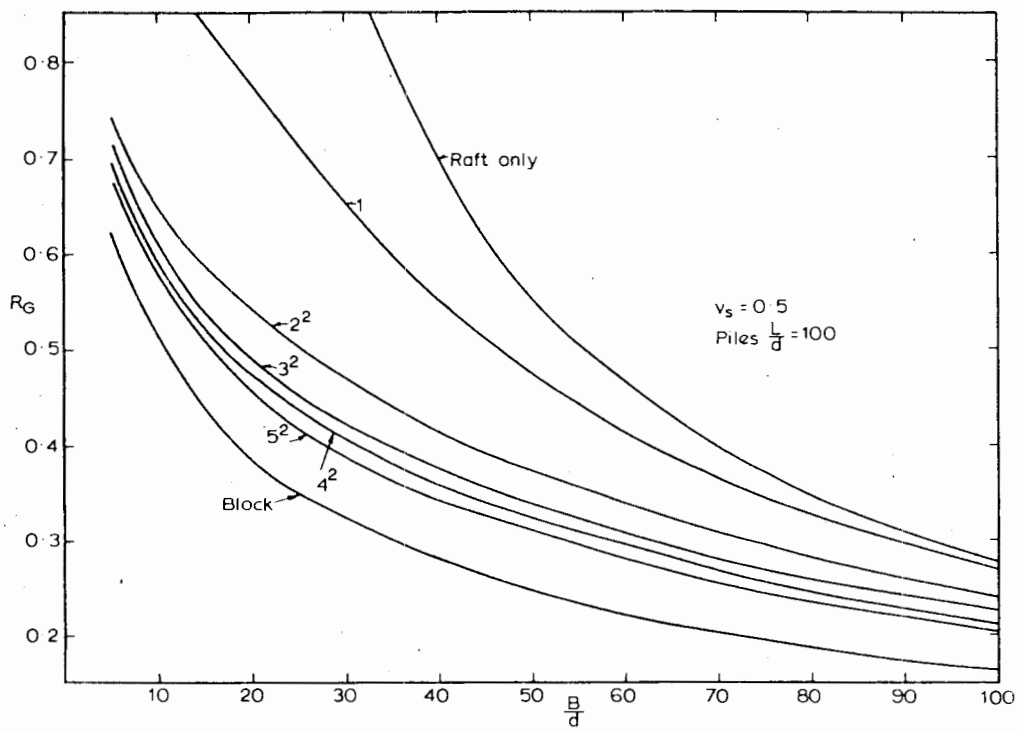

FIGURE 10.7 R_G vs. breadth, rigid raft, $\frac{L}{d} = 100$.

has virtually no influence on the settlement of the piles. As the spacing increases, the effect of the raft becomes more pronounced. The spacing, s/d, at which the raft begins to influence the settlement, increases as L/d increases and also as the number of piles in the group increases.

Typical curves of R_G versus B/d for the case of uniform loading are shown in Fig. 10.9 for the center of the system and in Fig. 10.10 for the corner. For the center, there appears to be a single mean curve for all groups between 2^2 and 6^2. For the corner, R_G decreases as the number of piles increases, up to a 6^2 group. Thus, at least up to a 6^2 group, the differential settlement will tend to increase as the number of piles increases.

As previously mentioned, the curves in Figs. 10.9 and 10.10 provide an approximate means of considering a perfectly flexible raft only for systems in which the pile spacing is not excessive or the number of piles too small. The general case of a raft of any flexibility could also be considered approximately by means of the interaction analysis described herein, but a more satisfactory analysis requires a new approach involving consideration of the overall action of the raft (see Section 10.5).

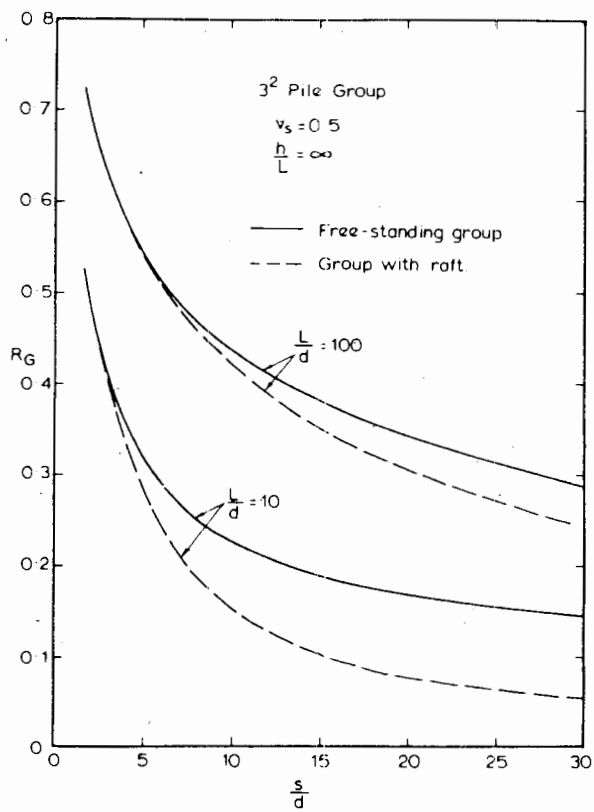

FIGURE 10.8 Comparisons between settlement of freestanding group and pile-raft system.

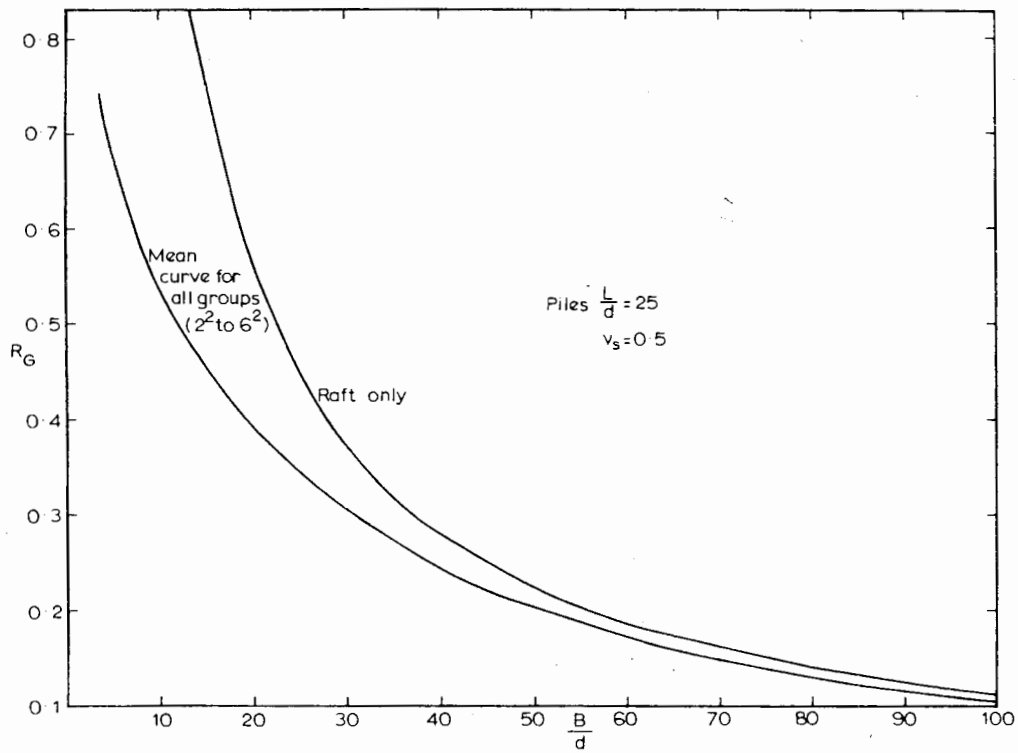

FIGURE 10.9 R_G vs. breadth, center of uniformly loaded system.

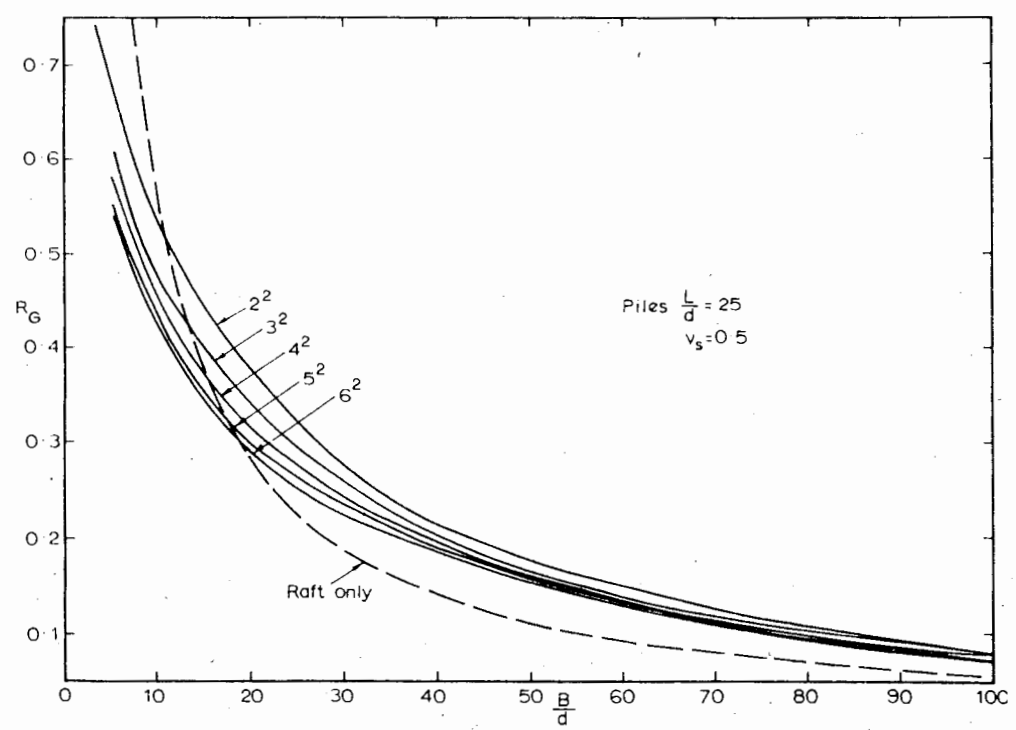

FIGURE 10.10 R_G vs. breadth, corner of uniformly loaded system.

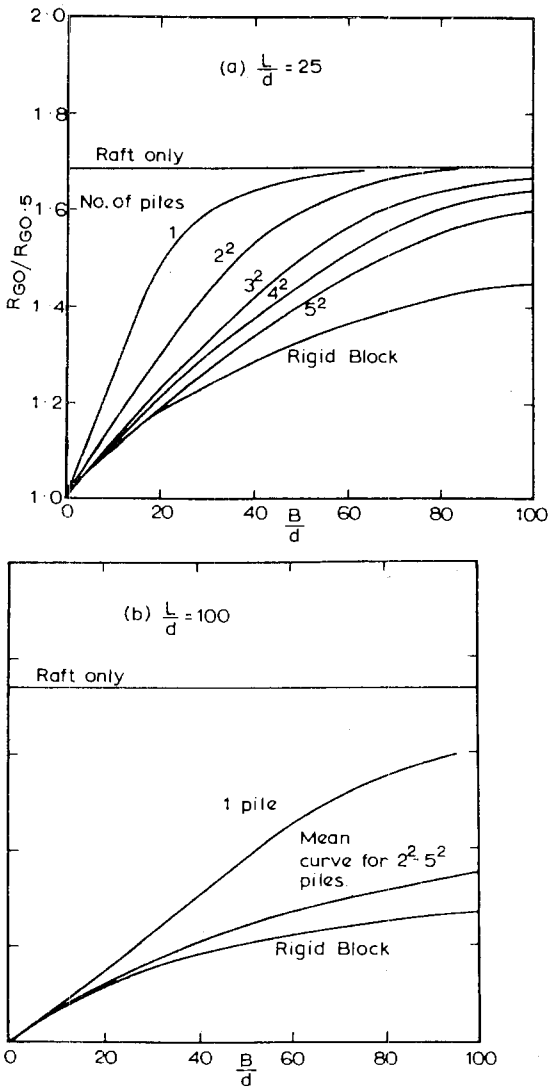

FIGURE 10.11 Influence of ν_s on R_G.

10.3.1 Influence of Poisson's ratio, ν_s.

The influence of ν_s on R_G is shown in Fig. 10.11, in which for $L/d = 25$ and 100, the ratio of R_G for $\nu_s = 0$ (R_{G0}) to R_G for $\nu_s = 0.5$ ($R_{G0.5}$) is plotted against group breadth for various rigid square systems. R_{G0} is generally greater than $R_{G0.5}$, the difference being greatest for the raft only and least for the rigid block. It has been found that the variation of R_G with ν_s is reasonably linear, so that the values of $R_{G0}/R_{G0.5}$ in Fig. 10.11 may be used to interpolate linearly for other values of ν_s. Thus, for any value of ν_s, the values of $R_{G\nu}$ may be estimated as

$$\frac{R_{G\nu}}{R_{G0.5}} = 1 + \left(\frac{R_{G0}}{R_{G0.5}} - 1\right)\left(1 - \frac{\nu_s}{0.5}\right) \qquad (10.13)$$

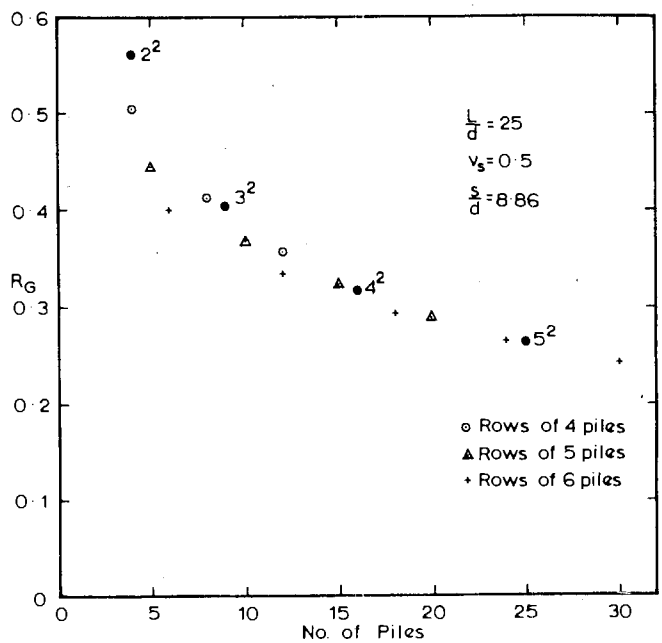

FIGURE 10.12 Influence of pile arrangement on settlement.

For the given group breadth and value of L/d, the value of $R_{G0}/R_{G0.5}$ may be interpolated from Fig. 10.11, and Eq. (10.13) then used to estimate the required value of $R_{G\nu}$.

The use of the above approximation will be described subsequently in relation to the calculation of consolidation settlements of the system.

10.3.2 Influence of Pile Arrangement

The foregoing solutions have only applied to square groups of piles. Solutions have also been obtained for rectangular groups having different numbers of piles in the two directions. It has been found that the settlement of a system depends primarily on the number of piles in the group, and not on the arrangement of the piles. A typical example showing the group-reduction factor R_G for $\nu_s = 0.5$ plotted against the number of piles is shown in Fig. 10.12 for a spacing of $8.86d$. It will be seen that, apart from groups containing small numbers of piles, R_G is almost independent of the arrangement of the piles. For small numbers of piles (e.g., four), less settlement occurs if the piles are placed in a row (i.e., 4×1) than if a square group (2^2) is used.

10.3.3 Systems Containing Large Numbers of Piles

For large systems containing a considerable number of piles, the value of B/d may be very large and that of R_G

very small, so that the use of the curves in Figs. 10.5, 10.6, and 10.7 may lead to inaccurate answers. It is then convenient to consider the piles as a number of small groups of piles within the system and to replace each small group by an equivalent single pile or pier. This equivalent pile should have the same area as the gross plan area of the small group and an equivalent length L_e/L (see Fig. 6.31). The system is thus replaced by a smaller number of shorter, larger-diameter piles. As an example, a system 40-ft square comprising an 8 X 8 group of 1-ft-diameter, 100-ft-long piles, each spaced at 5 ft, may be replaced by a system of 4 X 4 piles, each of equivalent diameter $d_e = 5\sqrt{\frac{4}{\pi}} = 5.65$ ft, and now at a spacing of 10 ft. From Fig. 6.31, the equivalent length of each pile is (for L/d = 100 and s/d = 5), L_e = $0.92L$ = 92 ft. Thus, the reference pile for the equivalent system is one having L_e = 92 ft and d_e = 5.65 ft, or L_e/d_e = 16.3. In terms of this reference pile, the group breadth is now 40/5.65 = 7.1 diameters, rather than the original group breadth of 40 diameters.

It has been found that the settlement of the system calculated for this equivalent system agrees with that of the original system to within about 2%.

10.3.4 Effect of Pile Compressibility and Raft Flexibility

It is obvious that finite compressibility of the piles in a pile-raft system will lead to increased settlement as compared with the case of rigid piles.

For a rigid raft, the previous solutions for a rigid pile may be utilized approximately for piles of finite compressibility by considering the compressible piles to be rigid piles of an equivalent length such that the settlement of the pile heads are equal. This equivalent length may be determined from the parametric solutions for a single pile given in Chapter 5.

No extensive parametric studies of the effects of raft flexibility or pile compressibility have yet been made. However, some indication of these effects may be inferred from results of elastic solutions for a piled strip obtained by Wiesner and Brown (1975) and Brown and Wiesner (1975). In the case of a long strip with a single pile, the width of the strip being 5 pile-diameters and the pile length 50 diameters, solutions for the ratio of the settlement of pile and strip to settlement of strip only are given in Fig. 10.13. These solutions depend on the pile-stiffness factor, $K = E_p R_A/E_s$, and a dimensionless strip-flexibility factor, $F_r = E_r I_r/E_s d^4$, where $E_r I_r$ is the raft stiffness, E_s is Young's modulus of soil, and d is pile diameter. Figure 10.13 shows that the effect of pile compressibility becomes more pronounced as the raft stiffness (i.e., the factor F_r) decreases.

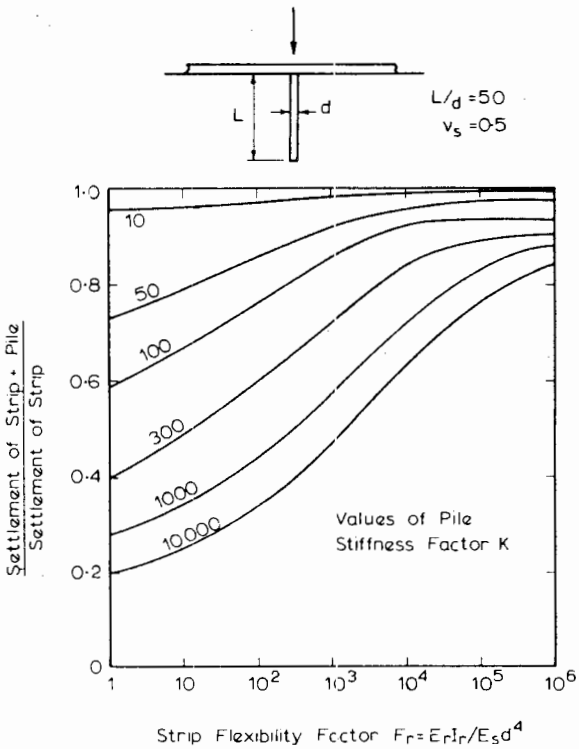

FIGURE 10.13 Effect of strip flexibility and pile compressibilit on settlement (Wiesner and Brown, 1975).

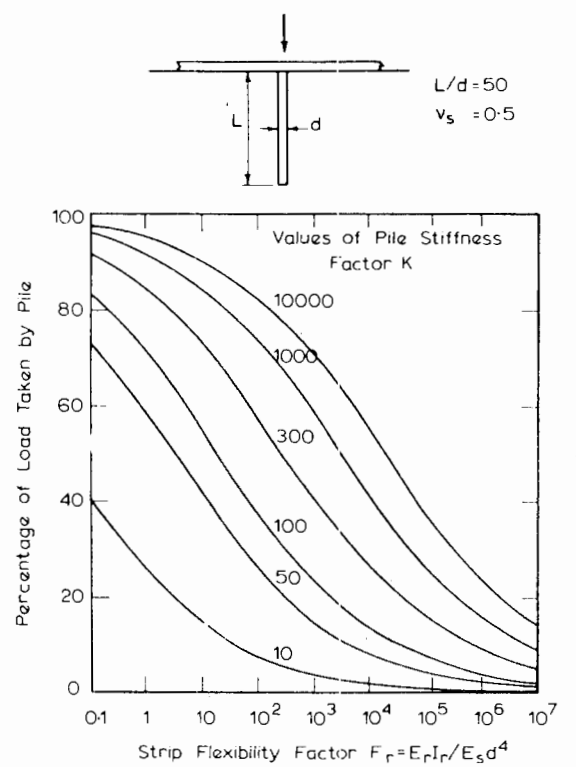

FIGURE 10.14 Effect of strip flexibility and pile compressibility on load taken by pile (Wiesner and Brown, 1975).

The use of even a very compressible pile beneath the very flexible strip ($F_r = 10$) causes a significant settlement-reduction as compared with the case of a strip only, and the use of an almost rigid pile reduces the settlement by almost 75%.

However, for a stiff strip ($F_r = 10^6$), compressible piles have virtually no influence on settlement, and even a rigid pile only reduces settlement by less than 20%.

The percentage ξ_s of the applied load taken by the pile beneath the strip of 5-diameter width is plotted in Fig. 10.14. This percentage decreases as the piles become more compressible or the strip becomes more rigid. For other values of strip width b, the percentage of load ξ_b is given approximately by

$$\xi_b = \xi_s - 2.3 \log_{10} (b/5d) \qquad (10.14)$$

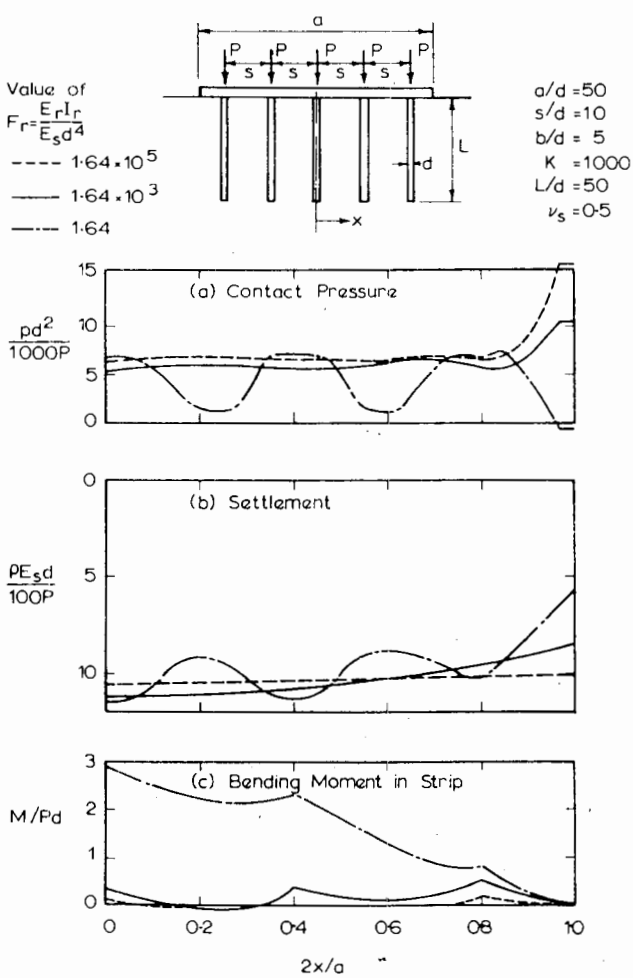

FIGURE 10.15 Typical solutions for strip with five piles (Wiesner and Brown, 1975).

A further example of the effect of strip flexibility is shown in Fig. 10.15 for a strip with five piles, and equal concentrated loads above each pile. Distributions of dimensionless contact pressure, settlement, and bending moment in the strip are given for three values of strip stiffness. The strip and pile lengths are 50 pile diameters, and the strip width is 5 diameters. Figure 10.15 shows that as the strip flexibility decreases, the contact pressures near the piles decrease while the settlements near the piles increase, The magnitude of the bending moments increases as the strip becomes stiffer.

Although the results presented in Figs. 10.13, 10.14, and to 10.15 are only indicative, they may be useful in suggesting orders of correction to be applied to the solutions for a rigid raft and rigid piles.

10.4 SIMPLIFIED ANALYSIS FOR LOAD-SETTLEMENT CURVE TO FAILURE

A simplified method of obtaining the load-settlement curve to failure for a piled foundation or pile-raft system has been described by Davis and Poulos (1972*b*). The method is similar in principle to that employed for large-diameter piles in Section 5.4, and assumes that for loading under undrained conditions, purely elastic conditions prevail up to the load at which the piles would fail if no cap were present. Thereafter, it is assumed that any additional load is taken entirely by the raft or cap and that the additional settlement of the system is then given by the settlement of the raft only. Thus, referring to Fig. 10.16, the undrained load-settlement curve of the pile-raft system consists of two linear sections:

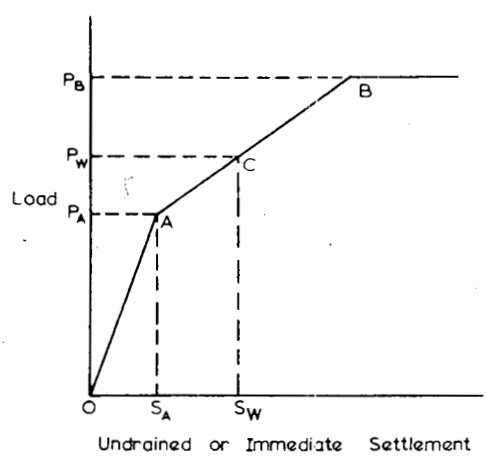

FIGURE 10.16 Simplified approach for calculation of undrained load-settlement curves.

1. The line $0A$, from zero load to the ultimate load P_A of the piles alone, the settlement being calculated from Eq. (10.11) or Eq. (10.12).
2. The line AB, from the load P_A to the ultimate load P_B of the whole system (piles plus raft), the settlement being calculated from the equation for the settlement of the raft acting alone without the piles. For example, for a square rigid raft $B \times B$ with m piles, the overall undrained settlement at a working load P_w is given by

$$\rho_w = P_A R_{G0.5} \rho_1 + \frac{0.947\,(P_w - P_A)(1-\nu_s^2)}{BE_u} \qquad (10.15)$$

where the first term represents the settlement of the pile-raft system, calculated on an elastic basis for $\nu_s = 0.5$, and the second term represents the settlement of the raft acting alone. This second term will only be operative if $P_w > P_A$, that is, if the failure load of the piles is exceeded.

It should be emphasized that the above basis of calculating the ultimate load P_B of the system as the sum of the capacities of the piles and the raft is only valid where relatively few piles are added to the cap or raft (i.e., where the pile-cap units are sufficiently widely-spaced to act individually). If the pile spacing is sufficiently close for block failure to occur rather than individual-unit failure, the ultimate load of the group should be calculated on this basis. It should also be mentioned that the simplified approach discussed above does not consider the effects of local slip along the piles or of local yield of the cap as the load increases toward failure.

In calculating consolidation settlements, it is again assumed that the consolidation process is not affected by any local yielding occurring under undrained conditions, so that the consolidation settlement, ρ_{CF}, is

$$\rho_{CF} = \rho_{TFe} - \rho_{ie} \qquad (10.16)$$

where ρ_{TFe}, ρ_{ie} are the total-final and immediate settlements of the system from a purely elastic analysis. The above procedure will yield the correct value of ρ_{CF} for the limiting cases of the raft only and of the rigid block and for those systems in which the failure load of the piles is not reached. It is therefore reasonable to assume that it will give satisfactory results for other cases involving piles that have slipped.

At the working load P_w,

$$\rho_{TFe} = P_w R_{G\nu'} \rho_{1TF} \qquad (10.17)$$

and

$$\rho_{ie} = P_w R_{G0.5} \rho_{1i} \qquad (10.18)$$

where

$R_{G0.5}$ = the elastic value of R_G for the pile-raft system for $\nu_s = \nu_u = 0.5$
$R_{G\nu'}$ = the elastic value of R_G for $\nu_s = \nu_s'$
ρ_{1TF} = total final settlement of a single pile under unit load
ρ_{1i} = immediate settlement of a single pile under unit load

$$\therefore \rho_{CF} = P_w(R_{G\nu'}\rho_{1TF} - R_{G0.5}\rho_{1i}) \qquad (10.19)$$

Both ρ_{1TF} and ρ_{1i} may be obtained either from a pile-loading test (the settlement per unit-load, at the working load) or from the theoretical relationships described in Chapter 5.

The total final settlement of the system is then the sum of the immediate settlement (taking account of possible pile slip) and ρ_{CF}, or

$$\rho_{TF} = P_A R_{G0.5}\rho_{1i} + \frac{0.71(P_w - P_A)}{BE_u} + P_w(R_{G\nu'}\rho_{1TF} - R_{G0.5}\rho_{1i}) \qquad (10.20)$$

The value of $R_{G\nu'}$ may be estimated from Eq. (10.13).

If only a few piles are added to the raft or cap, the failure load of these piles may well be far exceeded at the

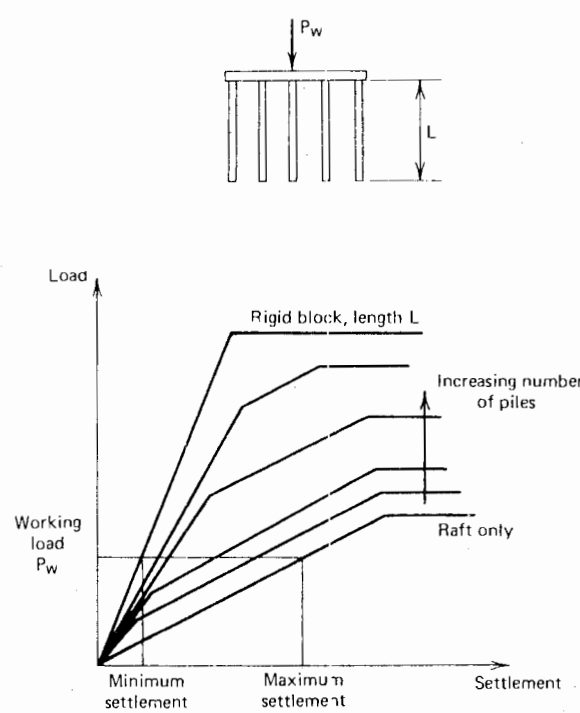

FIGURE 10.17 Concept of pile-raft system.

working load of the whole system. Despite the fact that these piles may have failed, they are nevertheless effective in reducing the settlement of the system, as is shown diagrammatically in Fig. 10.17. The validity of the above approach is dependent on, among other factors, the raft maintaining contact with the underlying soil. It is conceivable that with a relatively large number of piles, and with relatively soft clay directly beneath the raft, the raft could be "held up" by the piles because of the effects of negative friction and lose contact with the soil, thus effectively reducing the system to a freestanding group. This situation will probably only occur when the piles are sufficiently closely-spaced to act as a block, in which case the raft would be ineffective, even if contact were maintained. However, where only a small number of piles are present in the system, and these piles are overloaded at the working load of the system, continuous contact between the raft and soil should be maintained. This latter case is the one being primarily considered here.

The use of the simplified approach described above is demonstrated in the example of the design of a pile-raft system, given below.

Illustrative Example

The case of a square, rigid raft 50 ft on a side, resting on a deep deposit of soft clay, will be considered. The total working load on the raft is 3500 tons. The relevant average parameters of the clay are as follows:

$$c_u = 0.69 \text{ tons/ft}^2$$
$$\phi_u = 0$$
$$E_u = 70 \text{ tons/ft}^2$$
$$E' = 63 \text{ tons/ft}^2$$
$$\nu' = 0.35$$

It is specified that the maximum total final settlement of the raft must not exceed 6 in.

The problem is to investigate the adequacy of the raft alone, both in regard to ultimate bearing-capacity and settlement; and if the raft alone is found to be inadequate, to determine the number of piles that must be added to the raft to satisfy design requirements.

Considering first the ultimate bearing-capacity of the raft alone, and considering undrained conditions: the average ultimate pressure is $q_u = 5.69c_u$ (Cox, Eason, and Hopkins; 1961). Therefore,

$$P_u = B^2 q_u = 2500 \times 5.69 \times 0.69 = 9830 \text{ tons}$$

This gives a factor of safety against undrained bearing-capacity failure of $\frac{9830}{3500} = 2.81$, which is adequate.

Considering now the settlement of the raft alone. For a rigid, square raft on a semi-infinite mass,

$$\rho = .947 \frac{P}{B}\left[\frac{(1-\nu_s^2)}{E_s}\right]$$

Considering the total final settlement under the working load of 3500 tons,

$$\rho_{TF} = .947 \times \frac{3500}{50} \times \frac{(1 - 0.35^2)}{63} = 0.925 \text{ ft}$$

This settlement is excessive, and hence piles must be added to the raft to reduce the settlement.

Calculations will be detailed for 1-ft diameter, 100-ft-long piles. Results for other types of piles will be summarized.

Immediate Settlements

Considering undrained conditions first: The bearing capacity of a single pile, assuming (possibly rather conservatively) that $c_a/c_u = 2/3$, is found to be **145.5. tons.** The undrained settlement of a single pile under unit load is (from Eq. 5.33)

$$\rho_{1i} = \frac{I}{dE_u}$$

For this case, $L/d = 100$ and $I = 0.0254$ for $\nu_s = 0.5$. Therefore,

$$\rho_{1i} = 0.000354 \text{ ft/ton}$$

Thus, from Eq. (10.15), the immediate settlement of the pile-raft system may be written as

$$\rho_i = 0.000354 R_{G0.5} P_A + [0.000203 (3500 - P_A)] \text{ ft}$$

The calculation of ρ_i for various numbers of piles is shown in Table 10.1. The values of $R_{G0.5}$ are obtained from Fig. 10.7 for $L/d = 100$ and for $B/d = 50/1 = 50$.

Consolidation Settlements

These are calculated as the difference between the *elastic* values of ρ_i and ρ_{TF} for the system. The total final settlement of a single pile under unit load is

$$\rho_{1TF} = \frac{I}{dE_s'}$$

For $L/d = 100$ and for $\nu_s' = 0.35$, I is found to be 0.0242. Hence,

$$\rho_{1TF} = 0.000384 \text{ ft/ton}$$

From the previous calculations,

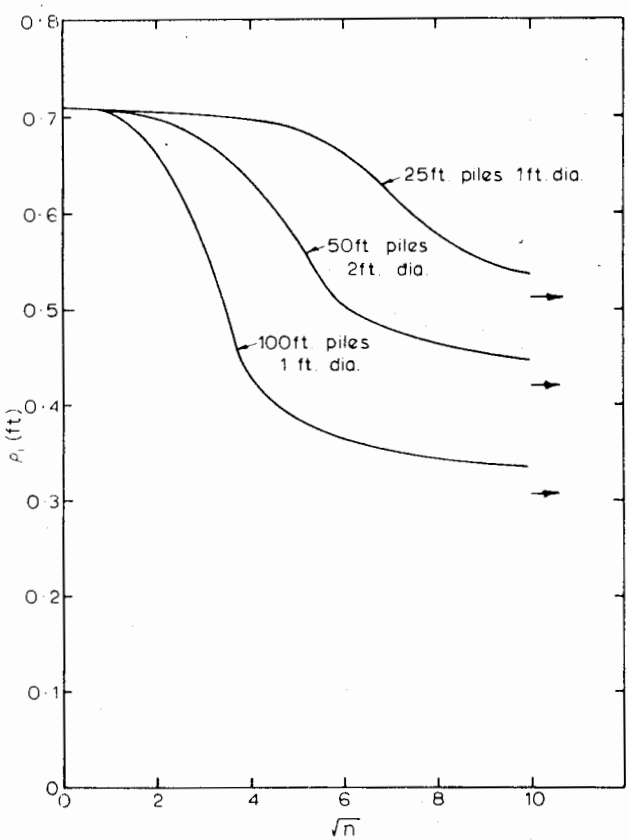

FIGURE 10.18 Immediate settlement vs. number of piles—illustrative example.

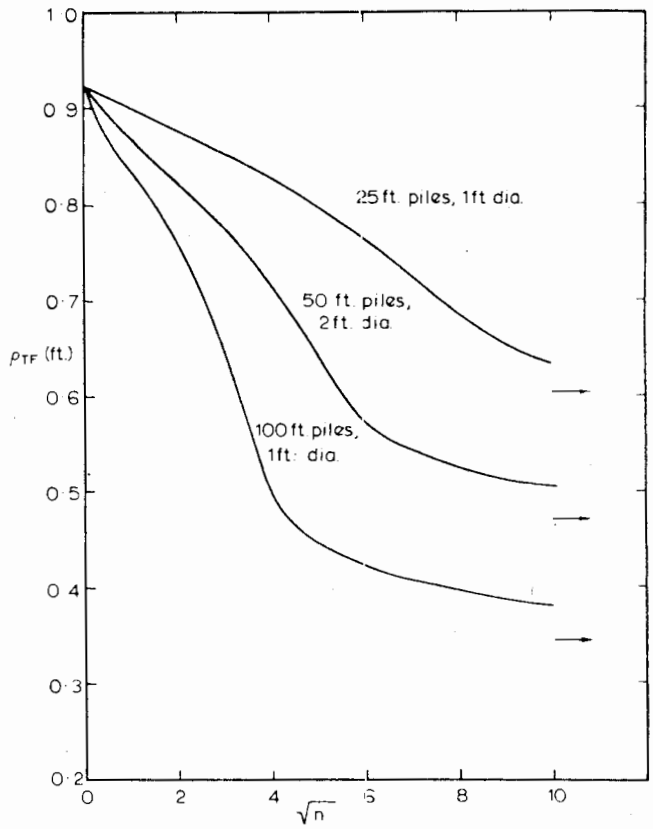

FIGURE 10.19 Total-final settlement vs. number of piles—illustrative example.

$$\rho_{ii} = .000354 \text{ ft/ton}$$

Therefore, from Eq. (10.19),

$$\rho_{CF} = 3500 \times (R_{Gv}0.000384 - R_{G0.5}0.000354)$$
$$= 1.343\, R_{Gv} - 1.240 R_{G0.5} \text{ ft}$$

Values of ρ_{CF} are shown in Table 10.1, together with the total settlement ($\rho_i + \rho_{CF}$).

The variation of ρ_i and ρ_{TF} with the number of piles in the system is shown in Figs. 10.18 and 10.19. It will be seen that in order to satisfy the specified settlement criterion, only 16 of the 1-ft-diameter, 100-ft-long piles are required. The undrained bearing-capacity of this system is 12,100 tons. The traditional design procedure, which determines the number of piles solely on the basis of ultimate bearing-capacity with no allowance made for the raft, gives the required number of piles as 68 (to give the same load capacity as the raft, i.e., 9830 tons). Thus, a very considerable economy in design is effected. Furthermore, the use of 68 piles rather than 16 leads to a further reduction in settlement of only 0.1 ft.

Also shown in Figs. 10.18 and 10.19 are the relationships between settlement and number of piles for two other, different types of piles. It is notable that the shorter 50-ft piles, even though they are of larger diameter, are not as efficient in reducing settlement as the 1-ft-diameter, 100-ft-long piles. The settlement criterion cannot be satisfied by using 1-ft-diameter, 25-ft-long piles, regardless of the number used. It is interesting to note that for such piles, the normal design procedure would require the use of 246 such piles to satisfy bearing-capacity requirements.

10.5 OTHER ANALYTICAL APPROACHES

In addition to the method described in detail in this chapter, a number of alternative approaches to analyzing pile-raft systems can be contemplated. Those described by Brown et al. (1975) are listed below:

1. Strip-superposition method, in which solutions for pile-strip footings (Brown and Wiesner, 1975) are super-

TABLE 10.1

No. of Piles	Load Capacity of Piles P_A (Tons)	$R_{G0.5}$ (from Fig. 10.7)	ρ_I (ft)	$\frac{R_{G0}}{R_{G0.5}}$ (from Fig. 10.11)	$\frac{R_{G0.35}}{R_{G0.5}}$ (Eq. 10.13)	$R_{G0.35}$	ρ_{CF} (Eq. 10.19) (ft)	ρ_{TF} (ft)
0	0		0.710				0.215	0.925
1	145.5	0.474	0.704	1.39	1.12	0.530	0.126	0.830
4	291	0.373	0.689	1.24	1.07	0.399	0.074	0.763
9	1310	0.338	0.602	1.24	1.07	0.362	0.067	0.669
16	2330	0.325	0.429	1.24	1.07	0.348	0.065	0.494
25	3640	0.310	0.384	1.24	1.07	0.332	0.062	0.446
36	5240	0.295	0.366	1.24	1.07	0.316	0.059	0.425
49	7130	0.285	0.353	1.23	1.07	0.305	0.057	0.410
64	9310	0.275	0.341	1.23	1.07	0.294	0.054	0.395
∞ (block)	28,400	0.247	0.306	1.20	1.06	0.262	0.049	0.355

posed to obtain the settlement of the raft. This method does not require the use of a computer but is limited to giving settlements only.

2. "Plate on springs" analysis, in which the raft is analyzed as a plate using the finite-element method, with the piles being replaced by springs located at appropriate nodes. The stiffness of these springs can be estimated from the elastic solutions for a pile (allowing for interaction effects) or from the pile-raft analysis described earlier in this chapter.

3. "Plate on springs and continuum" method. Here the raft is again treated as a plate and the piles are replaced by springs, as in the method above; but in addition, the soil is treated as an elastic continuum as far as support to the raft itself is concerned.

4. "Plate on piles and continum" method. This approach has been described by Hain (1975). It gives a closer representation of the real problem by treating the pile as in the normal pile-settlement analysis (Chapter 5), the raft as a plate, and the soil as an elastic continuum. Interaction among the piles, raft, and soil is then taken into account in a logical manner. Hain and Lee (1978) have used this analysis to successfully predict the load and settlement distribution for two pile-raft systems, one in Mexico City (the La Azteca building) and the other in London (Hyde Park Cavalry Barracks).

5. Simplified finite-element analyses; Hooper (1973) and Desai, Johnson, and Hargett (1974) have described finite-element analyses of piled-foundation problems in which the foundation, the piles, and the soil are represented by finite elements, without performing a full three-dimensional analysis. The case Hooper described was approximately axially-symmetric, and each concentric ring of piles was simulted by a continuous annulus with an overall stiffness equal to the sum of the stiffnesses of the individual piles. The treatment used by Desai et al. was similar, except that rows of piles were simulated by a continuous strip. While such approaches offer flexibility in being capable of taking into account such factors as soil inhomogeneity, they suffer from the fact that a considerable volume of data is required, and there will be difficulties in choosing an appropriate stiffness for the ring or strip simulating the piles, and in dealing with pile slip.

These last four approaches require the use of a computer but have the advantage that distributions of settlement, pile load, and raft-bending moment can be obtained.

The results of analyses based on five methods (the first four approaches, 1 to 4, above, plus the method described in detail in this chapter) were compared by Brown et al. (1975). They analyzed two relatively simple problems, one involving concentrated loads acting at the location of the piles, and the other being a raft-pile system subjected to uniform loading over the whole area; in each case, both a stiff raft and a relatively flexible raft were considered. The plate-on-piles and continuum method (4 above) was assumed to give the reference solutions, as it involved the least approximation. From the point of view of settlement, the most satisfactory of the other four methods was found to be the elastic-based analysis described in this chapter. The method of strip superposition overestimated settlements, while the plate-on-springs and continuum method consistently underestimated settlement, presumably because it ignores the downward movement of the continuum arising from the settlement of the piles. The settlements given by the plate-on-springs method were generally too

large, although the error depended on the basis adopted for the selection of spring stiffnesses.

From the point of view of bending moments in the raft, none of the simple methods gave accurate results when compared with the values from the plate-on-piles and continuum analysis. (It should be noted that the method of this chapter does not predict bending moments in the raft.)

In summary, if only the settlement of the pile-raft system is required, the elastic-based analysis is likely to be adequate if the raft is very stiff or very flexible. If bending moments in the raft are required, none of the simple methods are satisfactory and a proper analysis of plate on piles and continuum is desirable.

11

NEGATIVE FRICTION ON END-BEARING PILES

11.1 INTRODUCTION

It has long been recognized that when end-bearing piles are situated in a consolidating soil-mass, a downward force is induced in the pile because of the downward movement of the soil relative to the pile. This downdrag effect is commonly termed "negative friction," since downward shear-stresses are developed along the pile. Measurements on long steel end-bearing piles in soft clay by Johannessen and Bjerrum (1965) have revealed that the downdrag force may be sufficiently large to cause the design load to be exceeded. In consequence, additional settlement of the pile occurs, stemming partly from elastic pile-compression and partly from penetration of the pile tip into the bearing stratum, or even crushing of the pile.

Consolidation of the soil may arise from a number of causes: for example, surface loading of the soil, consolidation of a soil under its own weight, ground water withdrawal, the effect of pile driving in soft soils. Downdrag can also arise because of downward movement of a relatively incompressible layer—gravel or sand, for instance—caused by settlement of an underlying compressible layer.

The magnitude of the downdrag force developed in a pile will depend on a number of factors:

1. The pile characteristics—type, method of installation, length, shape of cross section, surface treatment (if any).
2. Soil characteristics—type, strength, compressibility, depth of layer, stiffness of bearing stratum.
3. Cause of soil movement.
4. Time since installation of the pile.

In this chapter, a number of field studies on instrumented piles are reviewed, and then various methods of estimating downdrag forces are described, with emphasis placed on the method based on an elastic analysis with allowance for slip between the pile and soil. Finally, a number of solutions from this analysis are presented, including solutions for the rate of development of downdrag force with time.

Only end-bearing piles (i.e., piles resting on a relatively stiff stratum) are considered. Friction or floating piles are also subjected to forces caused by consolidation of the embedding soil, but these are considered in Chapter 12.

TABLE 11.1 DOWNDRAG MEASUREMENTS ON PILES

Reference	Pile Const. Details	L (m)	d (cm)	Maximum Negative Friction Load (Tons)	τ_a/σ'_v	(1) ρ_s (2) ρ_p (3) $\Delta\rho_{sp}$ (cm)	Soil Condition	P.I.	c_u/σ'_v	L.I.	Sens-itivity	Observations
Johannessen, Bjerrum (1965)	Steel Pile pile, closed tip, driven to rock	53 I	47	~400	0.20	1) 200 2) 10 3) 190	Soft marine clay	25 ± 6	0.15 ± 0.05	0.5 ± 0.1	4 ± 2	Large negative-friction loads caused rock point to penetrate ~10 cm into rock, consolidation caused by a fill surcharge.
		57 II	50	300	0.18	1) 27 2) 5.3 3) 21.7	"	"	"	"	"	Piles II, III driven at different sites from I.
		41 III	50	250	0.23	1) 7 2) 3.2 3) 3.8	"	"	"	"	"	Driven in an area consolidating over the last 70 yr. Disturbance caused by pile driving increased settlement by 3-5 cm. $\Delta\rho_s$/time before driving = 0.1 cm/yr
Bjerrum, Johannessen (1969)	Pile *A*: closed tip steel pipe pile driven to end bearing on rock	~30	30	120	0.26	1) ~20 2) 3.3 3) 16.7	7-m fill, clayey silt, silty clay	15 ± 5	0.25 ± 0.05	0.7 ± 0.2	4 ± 2	Control pile, no special treatment, no enlarged point. (Piles *A-D* at Heröya Site)
	Pile *B*: similar to *A* but with enlarged point	27	30	10	~0.03		"	"	"	"	"	Enlarged point (diam. = 40 cm) used to protect asphalt-bitumen. (Bitumen 1-mm thick, 80/100 penetration) Bentonite slurry around bitumen.
	Pile *C*: similar to *A* but with enlarged point	28	30	57	~0.16		7-mm fill, clayey silt, silty clay	15 ± 5	0.25 ± 0.05	0.7 ± 0.2	"	Direct current used to reduct negative friction. ≈40-ton reduction caused by 4 amperes; 20-ton reduction caused by enlarged point.

	Pile *D*: identical to *B* but without bitumen	30	30	~100	~0.22			"	"	"	"	"	Enlarged point, bentonite slurry used to separate effect of bitumen–Pile *B*.
	Sørenga Site: Pile *C*, driven steel-pipe pile to end-bearing on rock	~57	50	300	0.18	1) 2) 3)	5 2.5 2.5	Soft marine clay	25 ± 6	0.15 ± 0.05	0.5 ± 0.1	4 ± 2	Control pile, no enlarged point, no treatment. Point penetrated 2.5 cm into rock.
	Pile *D*, same as Pile *C*	~57	50	15	~0.01	1)	5	"	"	"	"	"	Bitumen covered, bentonite stabilized, fill (20 m) separated from pile by casing. Negative friction reduced by 285 tons. Enlarged point (69 cm used).
	Pile *E*, same as pile *C*	~57	50	210	~0.13	1)	5	Soft marine clay	25 ± 6	0.15 ± 0.05	0.5 ± 0.1	4 ± 2	Bitumen covered, enlarged point, but no bentonite or casing; bitumen scraped off during driving.
	Heröya pile 85	32	50	300	0.25	1)	~30	7-m fill, clayey silt, silty clay	15 ± 5	0.25 ± 0.05	0.7 ± 0.2		Enlarged tip?
Fellenius, Broms (1969)	Precast reinforced piles driven to end-bearing in sand, silt	40	32	30 tons (metric)	0.05			Very soft, sensitive marine clay	45 ± 5	0.35 ± 0.05	1.0 (+0.5 −0.1)	18 ± 6	Negative friction caused by consolidation of soil remolded by pile driving.
Endo, Minou, Kawasaki, Shibata (1969)	(1) Steel-pipe piles, point closed, driven to end-bearing in alluvium	43	61	250 to 300 tons (U.S.)	~0.35	1) 2) 3)	5.4 12.5 7.1	Silty sand, soft silt	45 ± 3	0.55 ± 0.05	0.6 ± 0.1	low	Negative friction caused by consolidation of clay by pumping underlying layers. Settlements 672 days after driving.

TABLE 11.1 (Continued)

Reference	Pile Const. Details	L (m)	d (cm)	Maximum Negative Friction Load (Tons)	τ_a/σ'_v	(1) ρ_s (2) ρ_p (3) $\Delta\rho_{sp}$ (cm)	Soil Condition	P.I.	c_u/σ'_v	L.I.	Sens-itivity	Observations
	(2) Steel pipe, point open; driven as in (1)	43	61	180 metric tons	~0.20		Same as in (1)	45 ± 3	0.55 ± 0.05	0.6 ± 0.1	low	
	(3) Steel pipe, point closed; driven as a friction pile	31	61	160 tons	~0.30		"	"	"	"	"	
Bozozuk & Labrecque (1969)	Composite pile, concrete-filled steel tube: pile $B2$	82	99	920 tons (U.S.)	~0.18	1) 37 2) 1.5 3) 35.5	Gray, silty clay	40	0.25 ± 0.05	0.4 to 1.5	10 to 30	Negative friction caused by embankment loading—pile placed 18 months after embankment construction commenced. Early pile heave noted, caused by cement hydration, and electro-osmosis applied to pile.

11.2 FIELD STUDIES ON INSTRUMENTED PILES

In recent years, a number of tests on instrumented piles have been carried out to study the effects of negative friction. A summary of some of these tests is given in Table 11.1, and the results are discussed below in relation to a number of aspects of behavior.

11.2.1 Observed Downdrag Forces

Table 11.1 shows that extremely large downdrag loads can be developed in piles if the pile surface area is large. The soil consolidation causing these loads arises from several causes, as discussed above. Although the available data are not conclusive, it appears that downdrag loads induced by the effects of driving the pile are usually much less than those stemming from consolidation of the soil by loading or drainage.

In several cases where large soil settlements have occurred, the measured distribution of load along the pile indicates that slip between the pile and the soil has occurred along almost the entire shaft. Even in cases where the soil settlement is relatively small (e.g., pile *C*, Bjerrum et al., 1969), large downdrag forces can occur.

11.2.2 Development of Downdrag with Time

The measurements have shown that downdrag forces are time-dependent in that they are related to the pore water pressures. The dissipation of pore pressures has a two-fold effect: it leads to settlement of the soil, and at the same time, to an increase in the pile-soil adhesion because of the increase in effective stress. An example of the variation with time of soil and pile settlement, pore pressure and downdrag force, is shown in Fig. 11.1 for a test reported by Johannessen and Bjerrum (1965). A theoretical method for estimating the variation of downdrag load with time is described in Section 11.3.3.

11.2.3 Effect of Pile Driving on Negative Friction

The tests of Fellenius and Broms (1969) have shown that the dissipation of high excess pore pressures, caused by pile driving in sensitive clays, may develop appreciable downdrag loads in the pile, even though relative pile-soil movements may only be a few millimeters. Thus, downdrag forces may frequently occur in driven end-bearing piles, although they are not accounted for in design. A further case in which pile driving leads to additional load in the pile from consolidation caused by pile driving is reported by Resendiz et al. (1969).

The variation of downdrag load with time (logarithmic scale) for two piles tested by Fellenius and Broms, is shown in Fig. 11.2. It shows the same characteristic shape as a consolidation curve.

11.2.4 Methods of Reducing Negative Friction

11.2.4.1 SURFACE COATINGS

The reduction of negative friction by applying coatings to the pile has been investigated under several field conditions by Bjerrum et al. (1969) and Hutchinson and Jensen (1968). In tests on long steel-pile piles carried out by Bjerrum et al. (1969) at two different sites, control piles were established with rock points and no enlarged tip and measurements taken of the downdrag developed if no treatment was applied. Bitumen-covered piles were also driven with enlarged points and a bentonite slurry, in order to protect the bitumen coatings; downdrag loads in these piles were found to be reduced by more than 90%. In order to evaluate the effectiveness of the bentonite, piles with enlarged tips and a bentonite slurry but no bitumen coating were driven, and the reduction in downdrag in this case was about 15% compared with the control piles. Thus, the bitumen was responsible for a 75% reduction in downdrag; however, when no bentonite slurry was used to stabilize the enlarged hole caused by the passage of the enlarged tip, the bitumen was largely scraped off by the surface fill, resulting in a reduction in downdrag of only 30%. The advantages of different types of bitumen coatings were discussed by Hutchinson and Jensen (1968).

A series of laboratory model tests carried out by Koerner and Mukhopadhyay (1972) also confirmed that the use of asphalt coating on a pile can significantly reduce negative friction. The softer and thicker the asphalt coating, the greater the reduction.

Brons, Amesz, and Rinck (1969) report the use of a 1-cm-thick layer of bitumen on a vibrocasing pile, also with a resulting decrease in downdrag load greater than 90%. The effect of a bentonite slurry was also investigated, and if no piles were driven nearby, the downdrag reduction was about 85%, but if piles were driven 1.8 m apart, the corresponding reduction was only 50%.

Walker and Darvall (1973) have reported a 50-fold reduction in maximum downdrag-load by the use of a bitumen coating on a steel-tube pile. An average thickness of 1.5 mm of hand-sprayed commercial 60/70 penetration bitumen was used, and precautions were taken to avoid stripping of the coating in the upper layers of the soil.

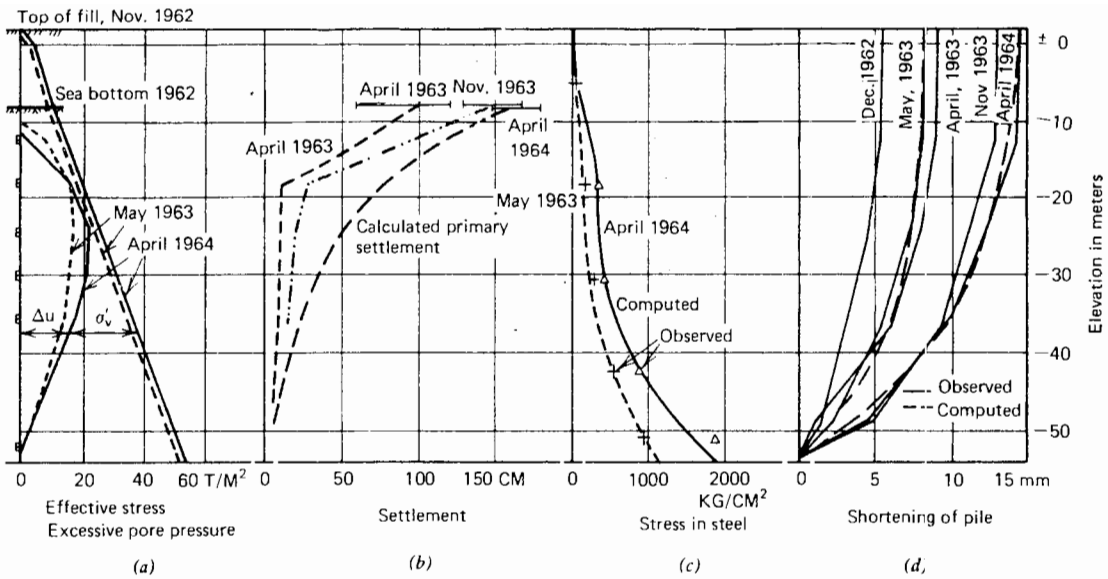

(a) Excess pore pressure and effective stresses in ton/m^2; *(b)* settlement in cm; *(c)* computed and observed steel stresses in kg/cm^2; *(d)* computed and observed shortening of pile in mm.

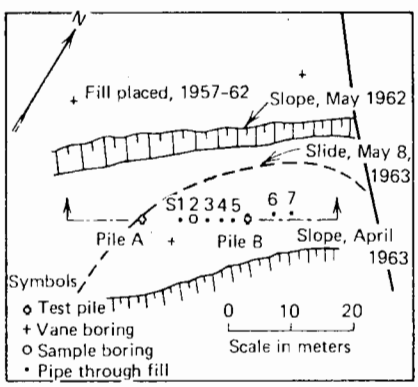

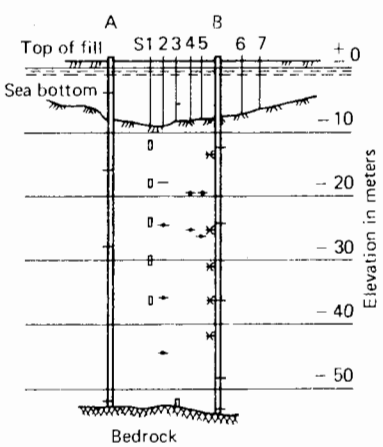

Symbols

- Measurement points in test piles
- Piezometer
- Settlement anchor
- Cobalt capsule

(c) Site plan and section

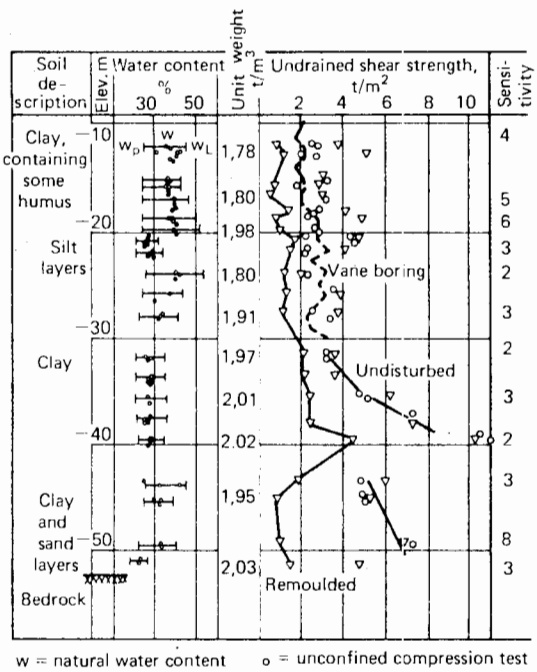

w = natural water content
w_L = liquid limit
w_p = plastic limit
○ = unconfined compression test
▽ = laboratory cone test

(f) Soil Properties

FIGURE 11.1 Measurements of downdrag on steel piles (after Johannessen and Bjerrum, 1965). (© Canada, 1965, by University of Toronto Press.)

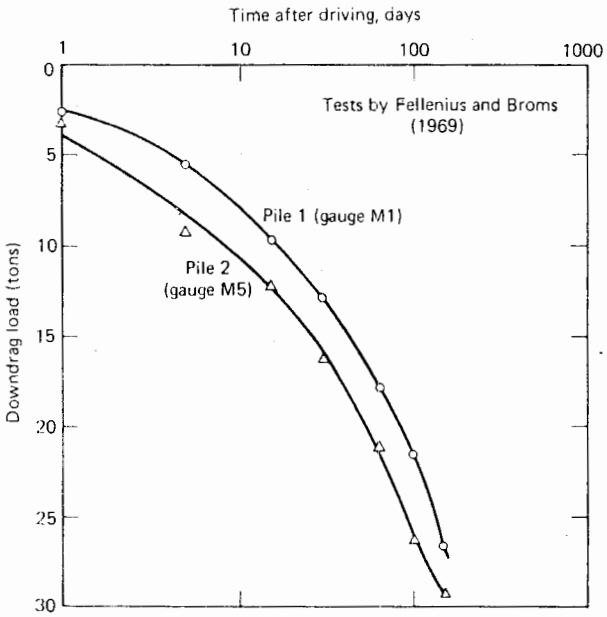

FIGURE 11.2 Variation of downdrag load with time.

Claessen and Horvat (1974) also found significant reductions in downdrag with the use of bitumen coatings. However, it was found that the point-bearing capacity of the pile was affected by the presence of the bitumen layer near the pile toe, and that the permissible base pressure was reduced to a value comparable with that for a corresponding surface plate. To avoid this problem, it was recommended that the lower part of the pile should remain uncoated over a length of about 10 times the diameter or width of the pile.

The effectiveness of bitumen or bentonite treatment therefore is probably highly-dependent on local soil conditions and pile-installation procedure, but in some circumstances, very significant reductions in downdrag may be achieved.

11.2.4.2 USE OF ELECTRO-OSMOSIS

Bjerrum et al. (1969) experimented with the use of electro-osmosis to reduce negative friction. A reduction of 50% in downdrag, as compared with an untreated pile, was achieved with currents of about 4 amp, although the current required to eliminate negative friction entirely was too high to be economical. The success achieved may have stemmed in part from the fact that the soil conditions (clayey silt and silty clay) were favorable for the application of electro-osmosis; in highly plastic soil, electro-osmosis may not be successful (Mitchell, 1970). Bozozuk and Labrecque (1969) also attempted to use electro-osmosis to relieve negative-friction forces in a long pile in silty clay, but the effectiveness of this treatment could not be accurately determined, although it did appear to be at best partially effective in the lower part of the pile.

In a further case in which electro-osmosis has been successfully used to relieve negative friction (M.I.T., 1973), treatment of a steel pile in Boston blue clay for only six hours was sufficient to eliminate virtually all drawdrag in the pile.

The theoretical analysis described in the following section may be adapted to predict the rate of reduction of downdrag in a pile as a result of electro-osmotic treatment, by using the theory of electro-osmotic flow in a soil to determine the rate of increase of pore pressures with time along the pile, and hence the rate of decrease of adhesion.

11.3 ANALYSIS OF DOWNDRAG FORCES

11.3.1 Introduction

Possibly the earliest-formulated and most widely used method of estimating downdrag forces is that described by Terzaghi and Peck (1967). The maximum downdrag force that can be transmitted to the pile is calculated as the sum of limiting shear-forces along the pile. For the typical case of a single pile, shown in Fig. 11.3, the downdrag force P at any depth z is

$$P = \int_0^z \tau_a C dz \tag{11.1}$$

where

τ_a = limiting soil-pile shear stress
C = pile perimeter

The maximum value of P occurs at the tip of the pile if the bearing stratum is rigid.

The relevant value of pile-soil adhesion τ_a will be the value for drained conditions if the final value of P stemming from consolidation settlement is required. τ_a may be obtained from the Coulomb expression

$$\tau_a = c'_a + K_s \sigma'_v \tan \phi'_a \tag{11.2}$$

where

c'_a = drained soil-pile adhesion
K_s = coefficient of lateral pressure

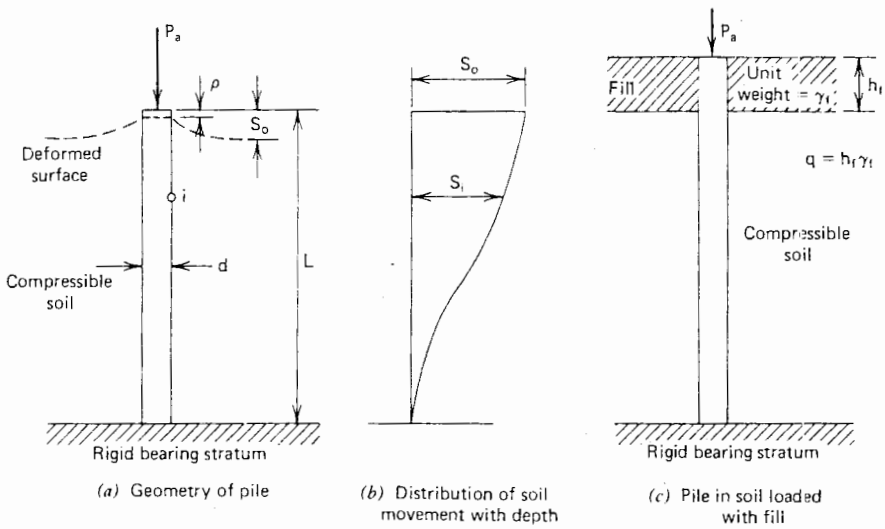

FIGURE 11.3 Negative friction problem.

σ'_v = vertical effective stress
ϕ'_a = drained angle of friction between pile and soil.

The values of these parameters are discussed below.

Zeevaert (1959) pointed out that the transfer of vertical stress to the pile through negative friction reduces the vertical overburden pressure on the bearing stratum. If this stratum consists of sand, the point-bearing capacity of the pile will be reduced, since it depends on the vertical stress. Thus, negative friction will have the dual effect of inducing downdrag load and reducing the point-bearing capacity. In his analysis accounting for this reduction in point capacity, Zeevaert showed that for soil conditions typical to Mexico City, the reduction in point capacity together with the induced downdrag force severely reduced the allowable load capacity of the pile. However, if the point resistance is not strongly dependent on the effective vertical stress (e.g., cemented or cohesive compacted strata), the correction for reduced tip resistance does not apply. Furthermore, for a sand bearing stratum, if the piles are driven well into the stratum, most of the pile load may be resisted by side shear, so that little load may reach the tip. Thus, the reduction in pile tip capacity only occurs under certain special conditions, and in most cases, it is probably sufficient to ignore the decrease in vertical effective stress with depth. This procedure may overestimate the base resistance, but this will be compensated for by the tendency to overestimate the downdrag force.

Locher (1965) compared the computed downdrag load in a pile from Terzaghi and Peck's approach, Zeevaert's approach, and an empirical approach developed by Elmasry (1963). There was relatively close agreement between computed downdrag loads, although Zeevaert's method gave the lowest value.

A number of methods have recently been developed that make use of the theory of elasticity to estimate downdrag forces (Salas and Belzunce, 1965; Begemann, 1969; Verruijt, 1969; Poulos and Mattes, 1969*b*; Poulos and Davis 1972). These methods have the advantage over previously described methods in that the dependence of downdrag on the settlement of the soil can be studied, rather than assuming that sufficient settlement occurs to mobilize the adhesion along the whole length of the pile. Walker and Darvall (1973) have described a finite-element analysis that can be used similarly to analyze the interrelationship between settlement and downdrag.

The analysis described below follows Poulos and Mattes (1969*b*) and Poulos and Davis (1972), and is an extension of the settlement analysis of a single pile (Chapter 5). The analysis is divided into two parts:

1. Analysis of final downdrag force.
2. The development of downdrag force with time during consolidation.

11.3.2 Analysis of Final Downdrag Force

The problem is illustrated in Fig. 11.3. The pile is divided into elements as for the axially-loaded end-bearing pile in Section 5.2.1. While elastic conditions prevail within the soil, soil and pile displacements at each element are equated to obtain the unknown shear stresses along the pile. It will be assumed that the bearing stratum is rigid.

The vertical displacement of the soil at any point arises from two sources: the shear stresses along the pile and the consolidation of the soil layer itself. The soil displacements caused by the shear stresses are given by Eq. (5.22) as (taking downward displacements as positive and $k = 1$)

$$\{_{s1}\rho\} = \frac{-d}{E_s}[I - I']\{p\} \tag{11.3}$$

where

$\{_{s1}\rho\}$ = vector of soil displacements caused by shear stress
$\{p\}$ = vector of shear stresses
$[I - I']$ = matrix of displacement-influence factor (including the effect of the "mirror image" elements, Fig. 5.5)

The net downward soil-displacements are then

$$\{_s\rho\} = \{S\} + \{_{s1}\rho\}$$
$$= \{S\} - \left(\frac{d}{E_s}\right)[I - I']\{p\} \tag{11.4}$$

where

$\{S\}$ = vector of consolidation settlements at the elements along the pile

For the determination of the final downdrag force, the elements of $\{S\}$ are the final consolidation settlements.

The displacements of the pile elements are determined as described in Chapter 5. For the particular case in which the bearing stratum is rigid and an axial load P_a applied to the pile head, the pile displacements are expressed as

$$\{_p\rho\} = \frac{1}{E_p R_A}[D]\{p\} + \frac{P_a}{A_p E_p}\{h\} \tag{11.5}$$

where

$\{_p\rho\}$ = pile-displacement vector
$\{p\}$ = shear-stress vector
$[D]$ = matrix of values of D defined in Eq. (5.23)
$\{h\}$ = vector of distances h_i of the center of element i above the base
E_p = pile modulus
A_p = area of pile section
R_A = area ratio (Eq. 5.10)

Equating soil and pile displacements from Eqs. (11.4) and (11.5), the following equation is derived:

$$\left[\frac{D}{Kd} + I - I'\right]\{p\} = \frac{E_s}{d}\{S\} - \left(\frac{p_a}{Kd}\right)(R_A)[h] \tag{11.6}$$

where

$K = \left(\frac{E_p}{E_s}\right)(R_A)$ = the pile-stiffness factor
p_a = applied axial stress = P_a/A_p

Equation (11.6) may be solved to obtain the n unknown shear stresses along the pile shaft. The load per unit area, p_b, transferred to the pile tip may then be obtained, from equilibrium considerations, as

$$p_b = \frac{4}{\pi d^2} p_a A_p + \frac{4L}{nd}\sum_{j=1}^{n} p_j \tag{11.7}$$

11.3.3 Development of Downdrag with Time

The above analysis for final downdrag force may be extended to consider the development of downdrag force with time, provided that certain simplifying assumptions are made. The main assumptions are:

1. The pile is impermeable. For a fully permeable pile, the final downdrag should develop relatively rapidly because of the rapid dissipation of pore pressures in the vicinity of the pile.
2. For the case in which the consolidation of the soil layer is caused by the placement of a surcharge on the soil surface, the presence of the pile does not influence the excess pore pressures in the soil near the pile. Some evidence to support this assumption has been given by Poorooshasb and Bozozuk (1967).

Under purely elastic conditions, the displacement-compatability equation is identical to Eq. (11.5), except that the vector $\{S\}$ of soil displacements is now a function of the pore pressure at each point. For each time considered, the vector $\{S\}$ is input into the analysis and Eqs. (11.6) and (11.7) are solved to determine the distribution of negative friction and downdrag force in the pile. The procedure is repeated for the required number of time steps.

For the simple case of constant surcharge applied to the clay, the rate of pore-pressure dissipation may readily be obtained from the classical Terzaghi solution and the settlement vector $\{S\}$ may be computed within the computer

program at each time step. The effect of delaying installation of the pile for some time after settlement of the clay has begun can also readily be handled by starting the computation of $\{S\}$ at the time of installation. For loading that varies with time, or cases involving pore pressures created by driving the pile or by the application of electro-osmosis, a numerical analysis may be necessary to determine the variation of pore pressure—and hence settlement—with time along the pile.

11.3.4 Modifications to Elastic Analysis

11.3.4.1 PILE-SOIL SLIP

The above elastic analysis may be modified to take account of local yield or slip between the pile and the soil in a manner similar to that described in Section 5.2.3. Such a modification is very desirable in considering negative friction, since, as mentioned in Section 11.2, the field evidence indicates that shaft-soil slip is very likely to occur when soils consolidate past a pile, especially with soft clays. At any given time, the shear stress p on an element, as given by the elastic analysis, is compared with the pile-soil shear strength τ_a at that element. If p is greater than τ_a, it is set equal to τ_a, displacement compatability now being considered only at the elastic elements. A new solution is obtained and the procedure repeated until all shear stresses are less than or equal to τ_a. The value of τ_a at any time t can be estimated from the Coulomb expression

$$\tau_a = c'_a + \sigma'_n \tan \phi'_a \tag{11.8}$$

where

c'_a, ϕ'_a = effective stress values of pile-soil adhesion and friction angle
σ'_n = effective normal stress at time t

For the case of a surcharge on the surface (see Fig. 11.3*c*), assuming the water table to be at or above the surface of the consolidating layer, Eq. (11.8) may be written in dimensionless form, for a point i at depth z below the surface, as

$$\frac{\tau_a}{q} = \frac{c'_a}{q} + K_s \tan \phi'_a \left[\left(\frac{\gamma L}{q}\right)\left(\frac{z}{L}\right) + \frac{q_t}{q} - \frac{u_i}{q}\right] \tag{11.9}$$

where

K_s = coefficient of lateral pressure, assumed to remain constant during consolidation
γ = submerged unit weight of soil
u_i = excess pore pressure at i at time t
q_t = effective applied surcharge pressure at time t
q = reference value of effective surcharge pressure (e.g., the maximum value)

(Values of $K_s \tan \phi'_a$ will be discussed in Section 11.4.7.)

If the consolidating soil layer is overlain by other layers and has an initial effective stress p_0 acting at the top of the layer, it can be treated as having an equivalent pile-soil adhesion c'_{ae}, where

$$c'_{ae} = c'_a + p_0 K_s \tan \phi'_a \tag{11.10}$$

11.3.4.2 PILE CRUSHING

If the downdrag force induced in a pile is sufficiently large, the crushing strength of the pile may be reached; if this occurs, the crushed portion of the pile can sustain no additional load and a redistribution of load in the remaining portion of the pile occurs. The additional displacement that accompanies the crushing of the pile now enters into the analysis as an additional variable. At each time, the maximum axial stress in the pile, from the analysis for an infinitely strong pile, is checked against the crushing strength, q_c, of the pile; if it exceeds q_c, the element can sustain no shear stress, as the load in this crushed portion remains constant (assuming ideal elastoplastic behavior of the pile material). Thus for the crushed elements, the displacement-compatability equations are replaced by equations stating that the shear stress is zero. A further equation is provided by the condition that the axial stress at the top of the crushed portion equals the crushing strength, q_c. Thus, for a surcharge pressure q, and crushing at the top of element k,

$$\sum_{i=1}^{k-1}\left(\frac{p_i}{q}\right) = \left(\frac{n}{4L/d}\right)\left(\frac{q_c}{q}\right) \tag{11.11}$$

A total of $(n + 1)$ equations is then obtained for the n shear stresses and the unknown displacement caused by crushing. These equations are solved and the procedure repeated until the axial stress does not exceed the crushing strength of the pile at any point. This solution is then the required solution for the time considered. The whole procedure can be repeated for a number of times after installation of the pile.

11.4 THEORETICAL SOLUTIONS FOR SINGLE PILE

There are a large number of parameters that may be investigated: the pile parameters L/d and K; the soil parameters

ν_s, c'_a/q, $\gamma L/q$, and $K_s \tan \phi'_a$; the drainage conditions of the soil layer; and two time parameters—the time t_0, between the commencement of consolidation of the soil and installation of the pile, and the time t, between the commencement of consolidation of the soil and the time being considered. The latter parameters may conveniently be expressed as dimensionless time factors,

$$T_{v0} = \frac{c_v t_0}{L^2} M \tag{11.12a}$$

and

$$T_v = \frac{c_v t}{L^2} M \tag{11.12b}$$

where

c_v = coefficient of consolidation of soil
M = 1 (one-way drainage) or 4 (two-way drainage)

For most of the numerical results given in this chapter, the effects of the parameters c'_a/q, $\gamma L/q$, and $K_s \tan \phi'_a$ are given, while the other parameters are kept constant at typical values $L/d = 50$, $K = 1000$, and $\nu_s = 0$; however, some indication of the effects of taking other values of L/d, K, and ν_s is also given.

Attention is concentrated on the maximum downdrag force in the pile and the settlement of the top of the pile, and the results are presented as in Poulos and Davis (1975). Some detailed distributions of force and stress along the pile have been presented previously (Poulos and Mattes, 1969*b*; Poulos and Davis, 1972).

An illustrative example outlining the use of the solutions is given in Section 11.4.8.

11.4.1 Final Maximum Downdrag Force

The final maximum force P_N in a pile, generally occurs at the pile tip and may be expressed conveniently in terms of the downdrag force for full slip, as follows:

$$P_N = P_{NFS} \cdot N_R \cdot N_T + P_a \tag{11.13}$$

where

P_{NFS} = final maximum downdrag force if full pile-soil slip occurs
N_R = correction factor for cases in which full slip does not occur
N_T = correction factor for effects of delayed installation
P_a = axial force in pile at top of consolidating layer

The first term in Eq. (11.13) represents the maximum downdrag force; the addition of the term P_a is correct if full slip occurs, but only approximate in other cases. However, the resulting overestimate of load at the pile tip is generally small in most practical cases. It should also be noted that P_a may include the axial force caused by negative friction of overlying soil layers, as well as applied axial force at the pile head. If such layers are noncohesive, it will generally be sufficiently accurate to assume for the calculation of P_a that full slip occurs between the pile and these layers.

P_{NFS} is expressed as

$$P_{NFS} = \pi d \int_0^L \tau_a dz \tag{11.14}$$

where

τ_a = final pile-soil adhesion (Eq. 11.2)

For a uniform soil layer,

$$P_{NFS} = \pi d L \left[c'_a + K_s \tan \phi'_a \left(\frac{\gamma L}{2} + q \right) \right] \tag{11.15}$$

Correction factor N_R represents the ratio of the actual maximum downdrag force to that for full slip along the pile, and is plotted in Figs. 11.4, 11.5, and 11.6 as a func-

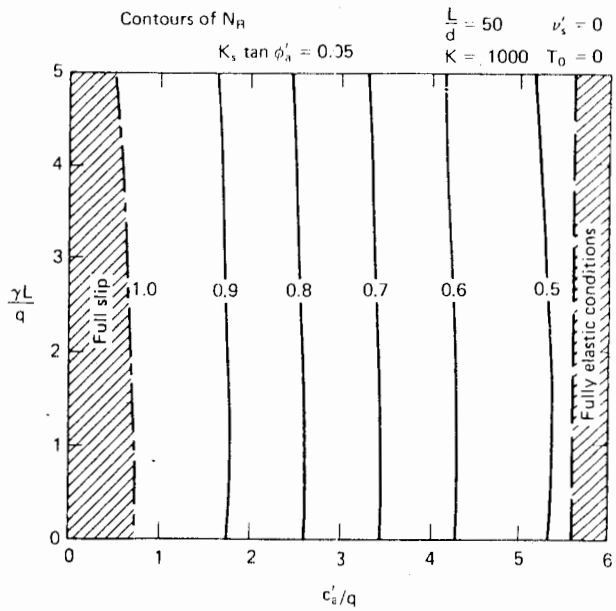

FIGURE 11.4 Values of downdrag reduction factor N_R. ($K_s \tan \phi'_a = 0.05$.)

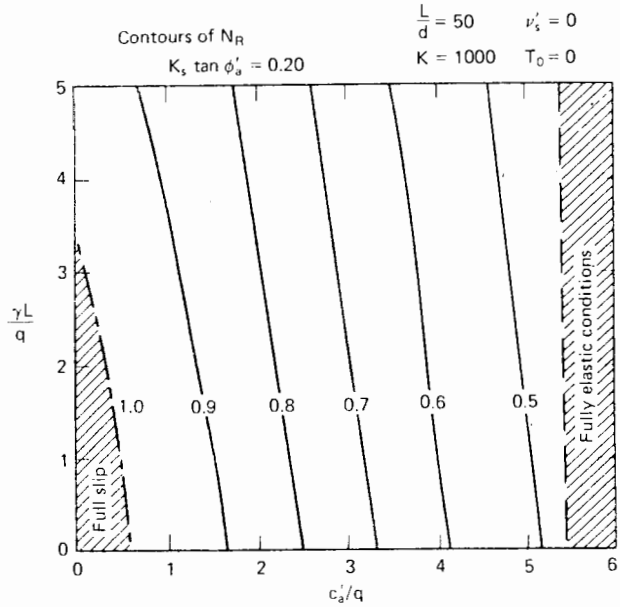

FIGURE 11.5 Values of downdrag reduction factor N_R. ($K_s \tan \phi'_a = 0.20$.)

tion of c'_a/q and $\gamma L/q$, for three values of $K_s \tan \phi'_a$. The curves in Figs. 11.4, 11.5, and 11.6 are for $L/d = 50$, $\nu_s = 0$, and $K = 1000$. A decrease in K or L/d tends to decrease N_R, but the effects are generally small and these figures may be applied to most cases involving full or partial slip. The regions in which N_R is unity represent cases in which

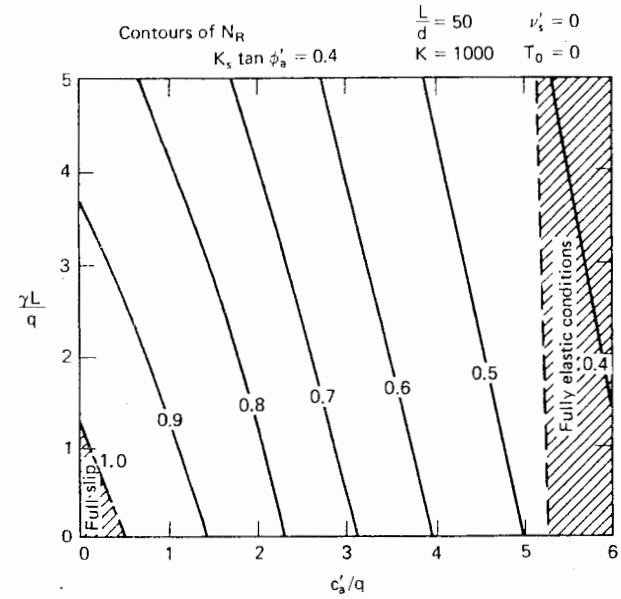

FIGURE 11.6 Values of downdrag reduction factor N_R. ($K_s \tan \phi'_a = 0.4$.)

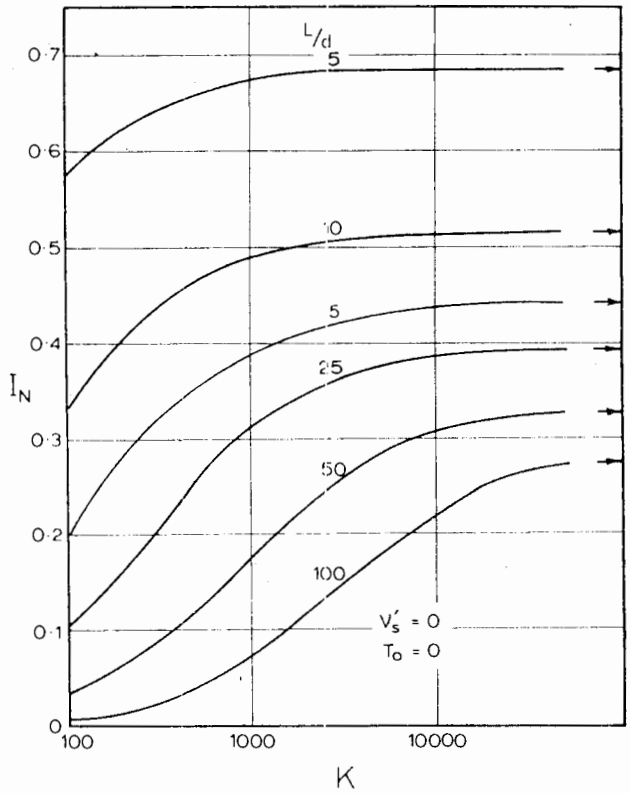

FIGURE 11.7 Influence factors for final downdrag at pile tip – elastic analysis.

full slip occurs along the pile. As c'_a/q and $\gamma L/q$ increase, N_R tends to decrease, but only for high values do fully-elastic conditions prevail (generally for $c'_a/q > 5$). Such cases arise if the soil is stiff, or the consolidating layer is situated beneath a deep overlying layer, or the applied pressure q causing consolidation of the layer is small.

If fully elastic conditions are indicated, a more satisfactory prediction may be made by using the elastic solutions, in which case the values of K and ν_s may become significant.

If the soil settlement is assumed to vary linearly from S_0 at the surface to zero at the base, the elastic maximum downdrag force may be expressed approximately as follows:

$$P_N = I_N E_s S_0 L R N_T + P_a \qquad (11.16)$$

where

I_N = elastic influence factor

$$R = \frac{(1 - 2\nu'_s)(1 + \nu'_s)}{(1 - \nu'_s)}$$

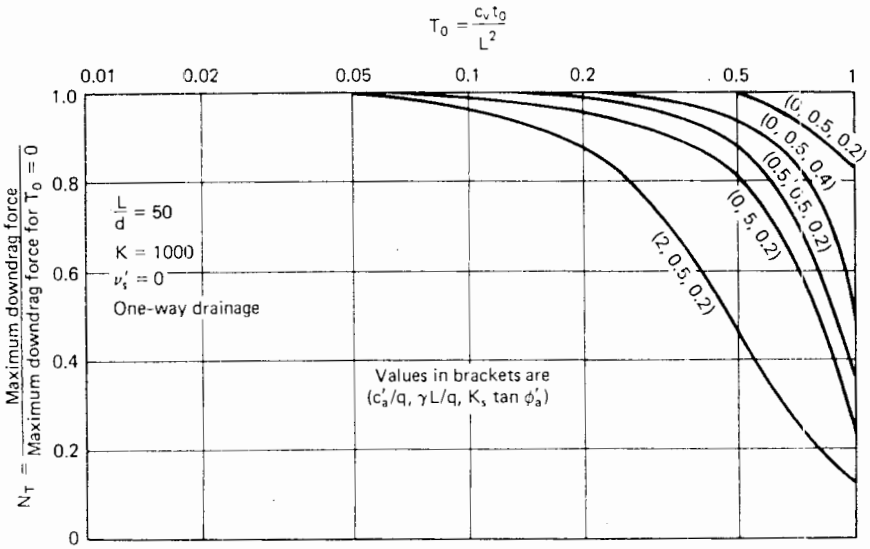

FIGURE 11.8 Downdrag reduction factor N_T—one-way drainage.

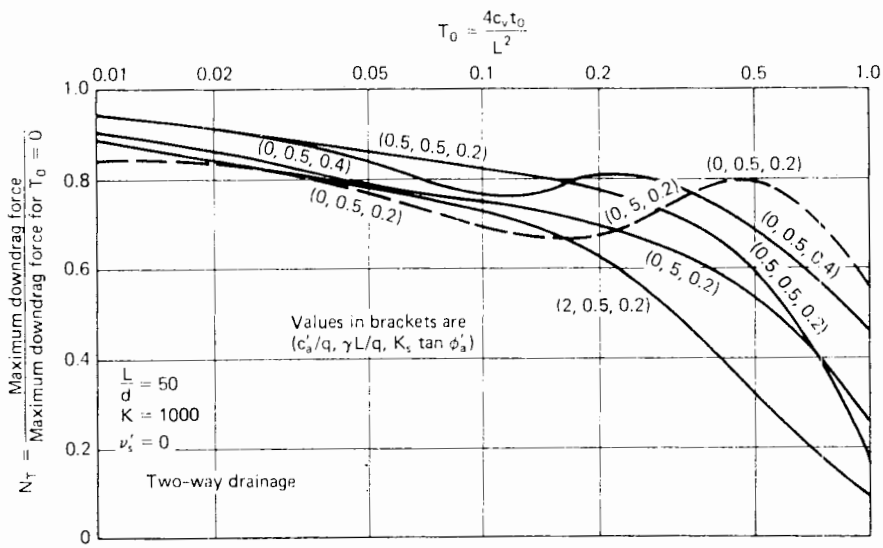

FIGURE 11.9 Downdrag reduction factor N_T—two-way drainage.

For a uniform layer subjected to a surcharge pressure q, Eq. 11.16 becomes

$$P_N = I_N q L^2 R N_T + P_a \tag{11.17}$$

Values of I_N are plotted in Fig. 11.7. L/d and K have a major influence on I_N, but the effect of soil Poisson's ratio, ν_s', is relatively small and may be approximately accommodated by use of the factor R.

The effect of having a linearly-varying soil modulus with depth rather than a constant value has been investigated. If the distributions of E_s are chosen so that the average value is the same in both cases, it is found that downdrag forces and pile movement are decreased (typically by 10 to 25%) as compared with the case of a linearly-varying E_s. Thus, the assumption of constant E_s with depth will be conservative when soil conditions are elastic. In all the ensuing solutions in this chapter, a constant E_s is assumed.

Values of N_T are shown in Figure 11.8 for one-way (top) drainage and in Fig. 11.9 for two-way drainage. N_T represents the ratio of maximum downdrag force for delayed installation at time T_0 to that for $T_0 = 0$. For one-way drainage, N_T decreases as T_0 increases, although only

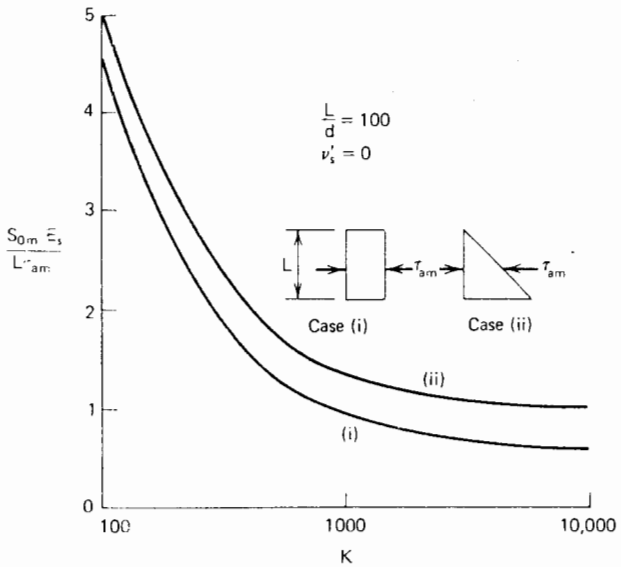

FIGURE 11.10 Surface settlement required to mobilize maximum downdrag force.

for $T_0 > 0.1$ is N_T significantly less than 1.0. At a given value of T_0, it appears that N_T tends to decrease as either c_a'/q, $K_s \tan \phi_a'$, or $\gamma L/q$ increase. Similar characteristics generally apply for two-day drainage, but the effects of delayed installation are much more pronounced than for one-way drainage. Also, for certain combinations of low values of the pile-soil parameters, N_T oscillates because positive friction is developed near the pile tip when installation is delayed, thus causing the location of the maximum downdrag force to move upward from the pile tip.

If the pile tip rests on or is embedded in an underlying layer that is not perfectly rigid, Eqs. (11.13), (11.16), and (11.17) will tend to overestimate P_N if full slip has not occurred along the pile. Positive friction will be developed in the embedded portion and the load transfer may be analyzed approximately by assuming the tip to be a pile acted upon by the maximum downdrag force. An estimate of the additional tip movement may also be made in this way.

For a pile in a soil layer in which the settlement away from the pile varies linearly with depth to zero at the base, the surface settlement S_{0m} required to mobilize full slip along the length of the pile is shown in Fig. 11.10 for two idealized distributions of pile-soil adhesion τ_a. S_{0m} is greater for a triangular distribution of τ_a than for constant τ_a with depth, and also increases as the pile-stiffness factor K decreases.

11.4.2 Rate of Development of Downdrag Force

The rate of development of the maximum downdrag force with time is shown for one-way and two-way drainage in Figs. 11.11 and 11.12 as a dimensionless plot of time factor T_v versus the degree of downdrag development U_N, where U_N is the ratio of the maximum downdrag caused by negative friction at any time, to the final maximum value at $T_v = \infty$. Curves are shown for the purely elastic case and for a case in which full slip occurs finally. The occurrence of slip increases the rate of downdrag development as compared with the case of no slip, but the difference is not great. As expected, the downdrag force develops more

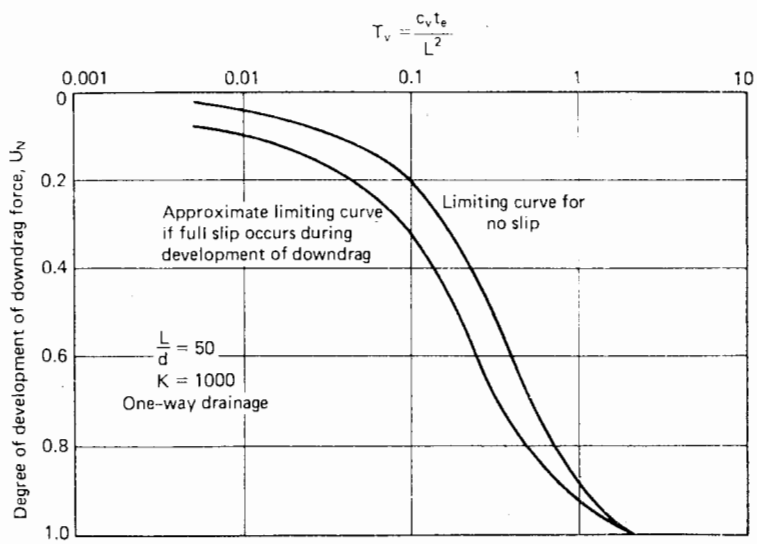

FIGURE 11.11 Development of downdrag force--one-way drainage.

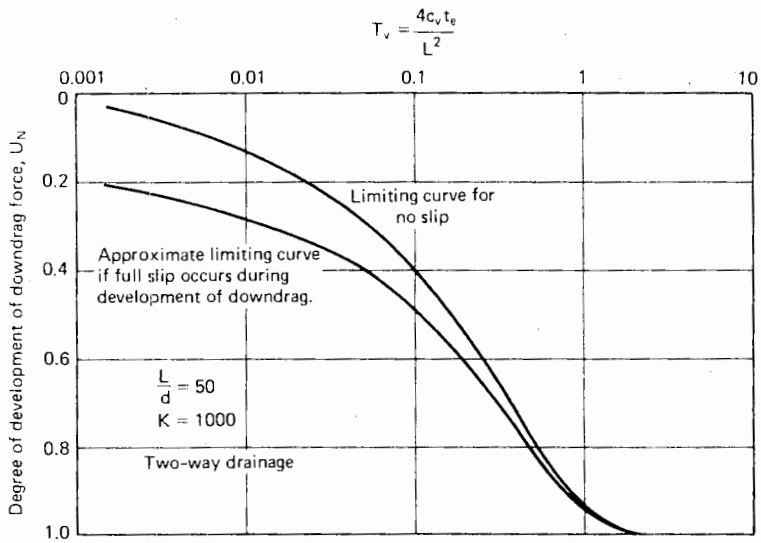

FIGURE 11.12 Rate of development of downdrag force–two-way drainage.

rapidly when two-way drainage conditions prevail. The curves are not greatly affected by L/d, ν_s, or K unless K is less than 100.

Although the curves shown are strictly applicable only for $T_0 = 0$, it has been found that the curves for $T_0 \neq 0$ are very similar, provided that the time factor T_v is defined in terms of the elapsed time $t_e = t - t_0$ since installation of the pile. Thus, Figs. 11.11 and 11.12 may be used approximately for all values of T_0.

Thus at any time t_e after installation of the pile, assuming the axial load P_a has been applied at zero time, the maximum downdrag force, P_t, can be calculated as

$$P_t = U_N \cdot (P_N - P_a) + P_a \tag{11.18}$$

where

P_N = final maximum downdrag force, calculated from Eq. (11.13) or Eq. (11.16), if more appropriate
U_N = degree of development of downdrag, for a time factor $T_v = Mc_v t_e/L^2$
P_a = axial force in pile at top of consolidating layer

11.4.3 Pile Settlement

In a manner similar to downdrag force, the axial movement ρ of the pile at the level of the top of the consolidating layer can be expressed as

$$\rho = \rho_{FS} Q_R Q_T + \frac{P_a L}{E_p A_p} \tag{11.19}$$

where

ρ_{FS} = axial movement of pile if full pile-soil slip occurs
Q_R = correction factor for cases in which full slip does not occur
Q_T = correction factor for effects of delayed installation
P_a = axial force in pile at top of consolidating layer

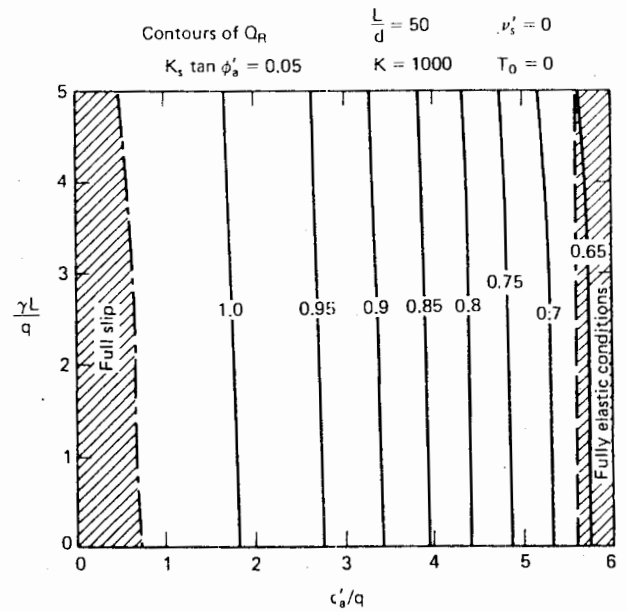

FIGURE 11.13 Values of deflection reduction factor Q_R. ($K_s \tan \phi_a' = 0.05$.)

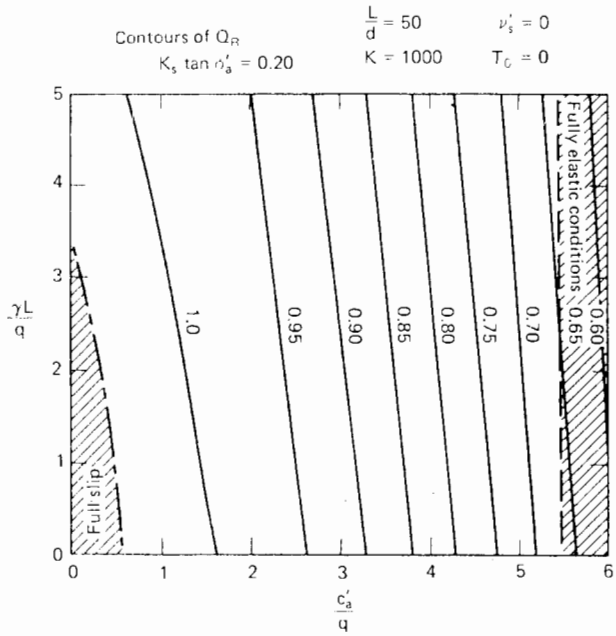

FIGURE 11.14 Values of deflection reduction factor Q_R. ($K_s \tan \phi'_a = 0.20$.)

By integration of the strains in the pile, it may be shown that ρ_{FS} in a uniform soil is

$$\rho_{FS} = \frac{2qL^2R_A}{E_p d}\left[\frac{c'_a}{q} + K_s \tan \phi'_a \left(\frac{\gamma L}{3q} + 1\right)\right] \quad (11.20)$$

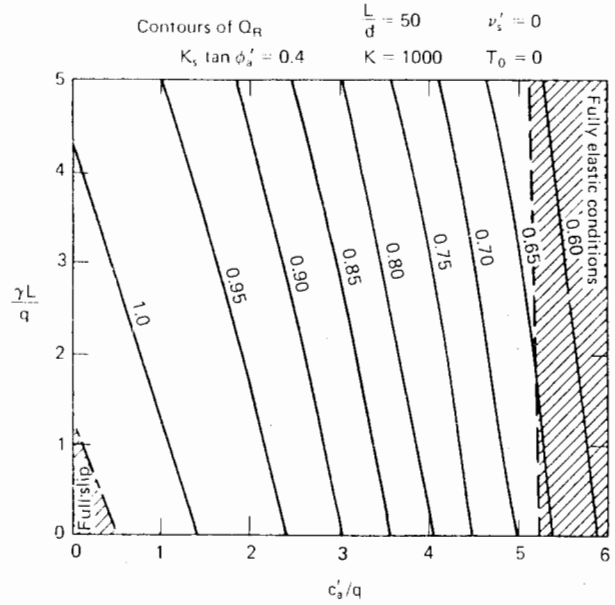

FIGURE 11.15 Values of deflection reduction factor Q_R. ($K_s \tan \phi'_a = 0.4$.)

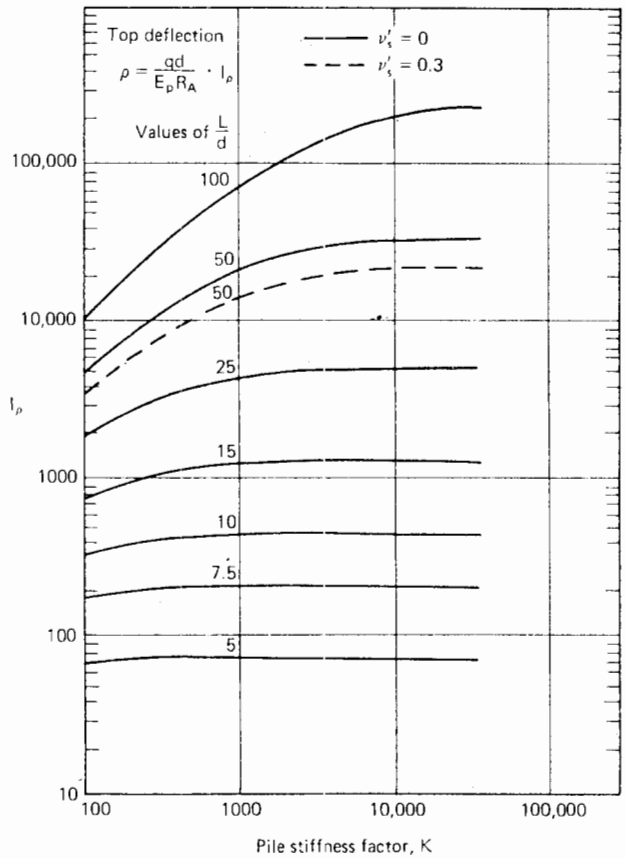

FIGURE 11.16 Elastic solutions for top deflection of pile.

Correction factor Q_R is plotted in Figs. 11.13, 11.14, and 11.15 as a function of c'_a/q and $\gamma L/q$ for three values of $K_s \tan \phi'_a$. A value of $Q_R = 1.0$ indicates that full slip occurs along the pile. Q_R tends to decrease with increasing c'_a/q and $\gamma L/q$, but at a slower rate than the downdrag-force correction factor N_R. Cases in which conditions remain entirely elastic are also indicated in Figs. 11.13, 11.14, and 11.15, and in such cases, the use of elastic solutions is preferable.

For elastic conditions, the axial movement of the pile may be expressed approximately as follows:

$$\rho = \frac{qd}{E_p R_A} \cdot I_\rho \cdot Q_T + \frac{P_a L}{E_p A_p} \quad (11.21)$$

where

q = applied surcharge on soil
R_A = area ratio of pile
I_ρ = settlement-influence factor

Values of I_ρ are plotted in Fig. 11.16 as a function of K

and L/d, for $\nu_s' = 0$. One curve for $\nu_s' = 0.3$ and $L/d = 50$ also gives some indication of the effect of ν_s'.

Q_T is plotted in Figs. 11.17 and 11.18 for one- and two-way drainage. Q_T generally decreases as T_0 increases, reflecting the corresponding reduction in axial force.

The second term in Eqs. (11.19) and (11.21) represents the settlement of the pile acting as a freestanding column under the axial load. The addition of this value to the settlement caused by downdrag will give the correct settlement if full slip occurs, or a slight overestimate in other cases. It should be noted that P_a includes the axial force caused by negative friction developed between the pile and any overlying layers.

If the bearing stratum is not rigid, the additional tip settlement may be estimated conservatively by treating the pile tip as resting on (or embedded in, if appropriate) the bearing stratum and being subjected to the maximum axial force in the pile.

When the consolidating soil layer is overlain by other layers, the settlement of the portion of the pile in these layers must be added to the calculated pile-settlement at the level of the top of the consolidating layer.

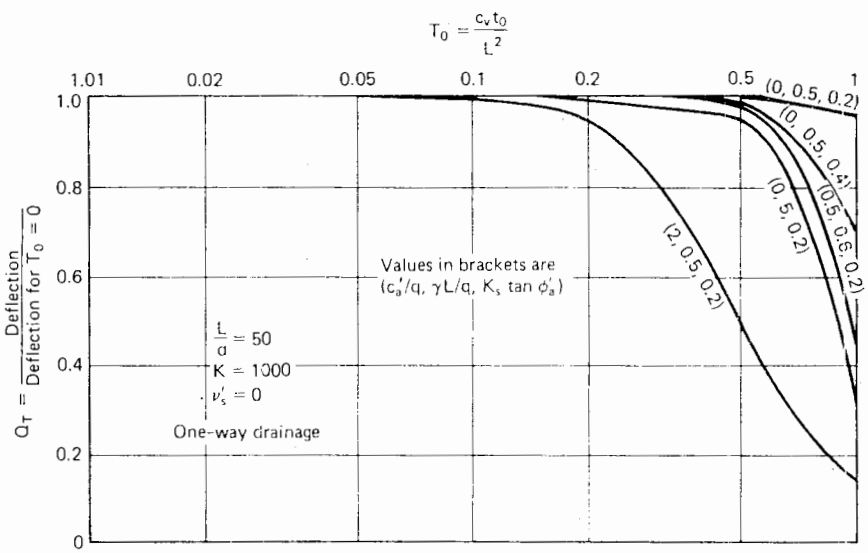

FIGURE 11.17 Deflection reduction factor Q_T—one-way drainage.

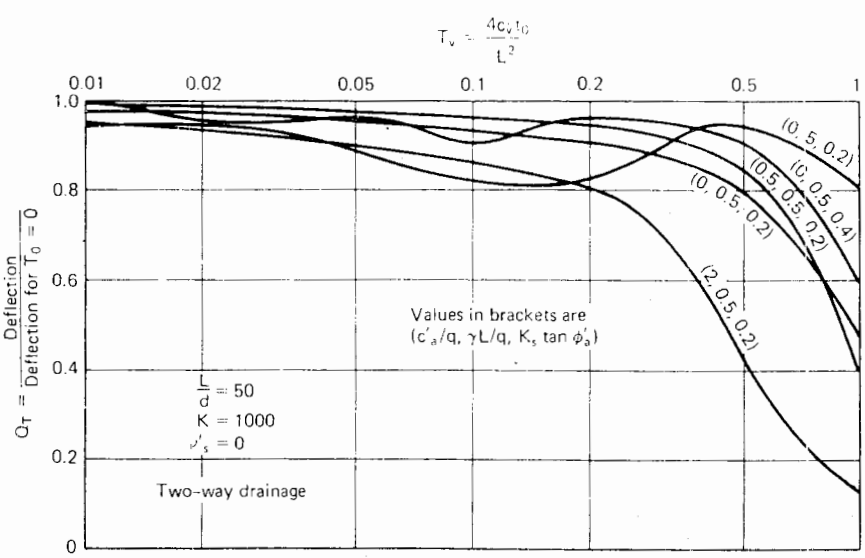

FIGURE 11.18 Deflection reduction factor Q_T—two-way drainage.

11.4.4 Rate of Development of Settlement

As with the maximum downdrag force, the settlement of the pile ρ_t at any time t_e after installation may be calculated as

$$\rho_t = U_\rho\left(\rho - \frac{P_a L}{E_p A_p}\right) + \frac{P_a L}{E_p A_p} \qquad (11.22)$$

where

ρ = final deflection of pile, from Eq. (11.19), or Eq. (11.21), if appropriate

U_ρ = degree of pile settlement, for a time factor $T_v = Mc_v t_e/L^2$

The first term represents the time-dependent component resulting from negative friction and the second the constant value resulting from applied load. U_ρ is plotted against time factor T_v in Figs. 11.19 and 11.20 both for a purely elastic soil and one in which pile-soil slip occurs and for one- and two-way drainage. As with the maximum downdrag force, the pile movement develops more rapidly if pile-soil slip occurs or if two-way drainage conditions exist. Also, L/d, K, and ν_s' have little influence on the U_ρ-versus-T_v curve,

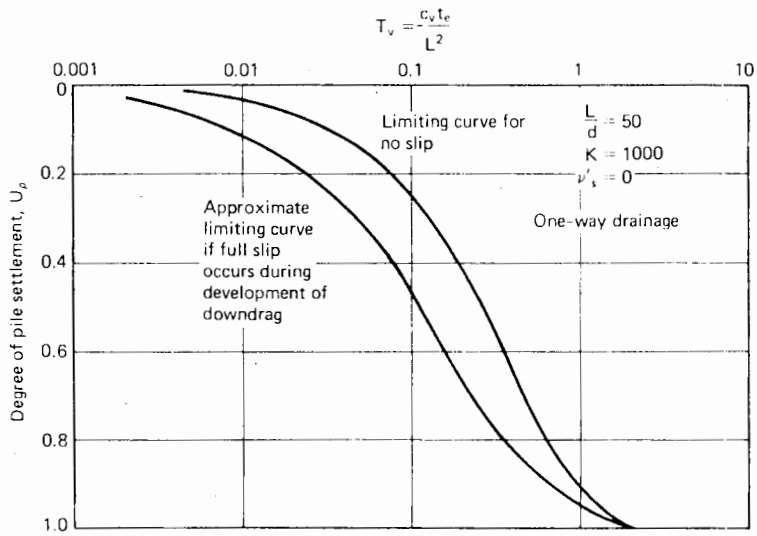

FIGURE 11.19 Degree of pile settlement vs. time factor—one-way drainage.

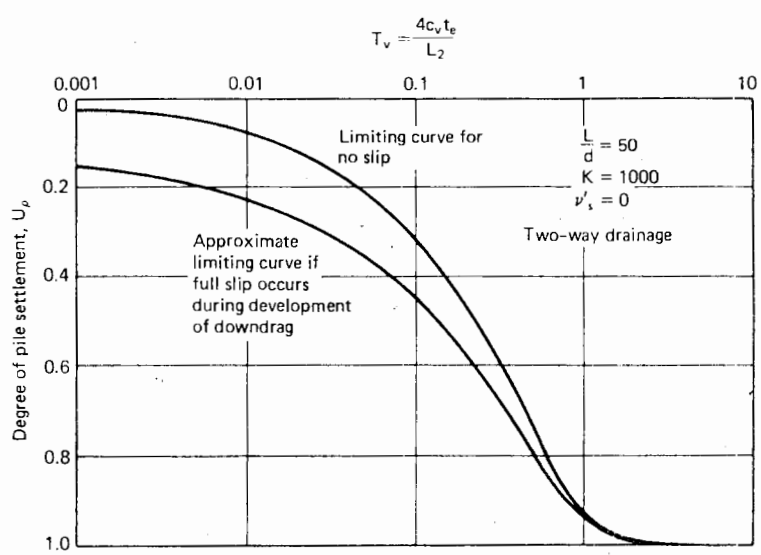

FIGURE 11.20 Degree of pile settlement vs. time factor—two-way drainage.

and this curve is also independent of T_0, provided that T_v is defined in terms of t_e.

11.4.5 Effect of Pile Crushing

The influence of pile crushing on the relationship between pile-head displacement and T_v is shown in Fig. 11.21 for a typical case in which the pile is installed in an elastic soil at the same time as placement of the surcharge ($T_0 = 0$). In this case no crushing occurs unless the relative crushing strength of the pile q_c/q is less than 246. As q_c/q decreases, the value of T_v at which crushing commences becomes less and the final downdrag load developed in the pile also decreases. The resulting displacement of the pile head increases markedly, however, and even for $q_c/q = 200$ (corresponding approximately to a concrete pile in a layer subjected to about 18 ft of fill), the displacement is about 30% greater than for the case of no crushing. Also shown in Fig. 11.21 is the displacement-versus-T_v curve for the limiting case of $q_c/q = 0$. This curve corresponds to the time-settlement curve of the soil layer. The final settlement in this case is more than five times that for the case of no crushing.

Typical distributions of downdrag load and shear stress at various values of T_v are shown in Fig. 11.22 for $q_c/q = 200$. The growth with time of the crushed region of the pile can be seen.

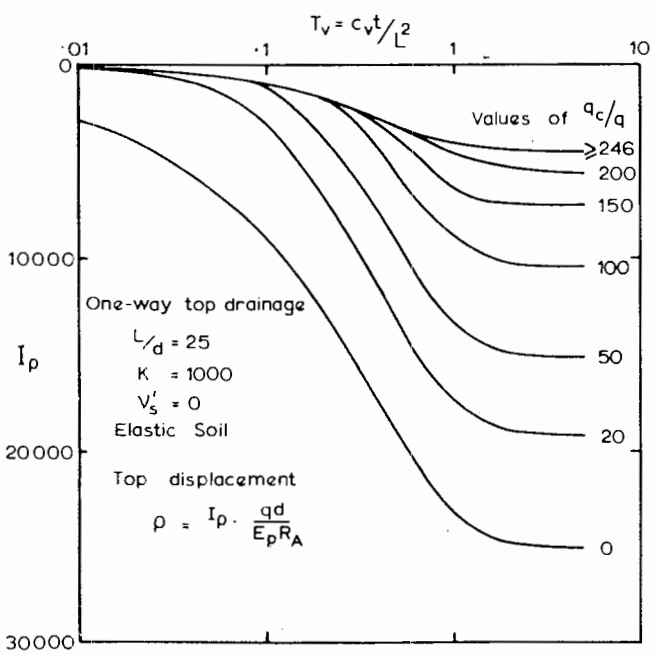

FIGURE 11.21 Influence of pile crushing on pile displacements.

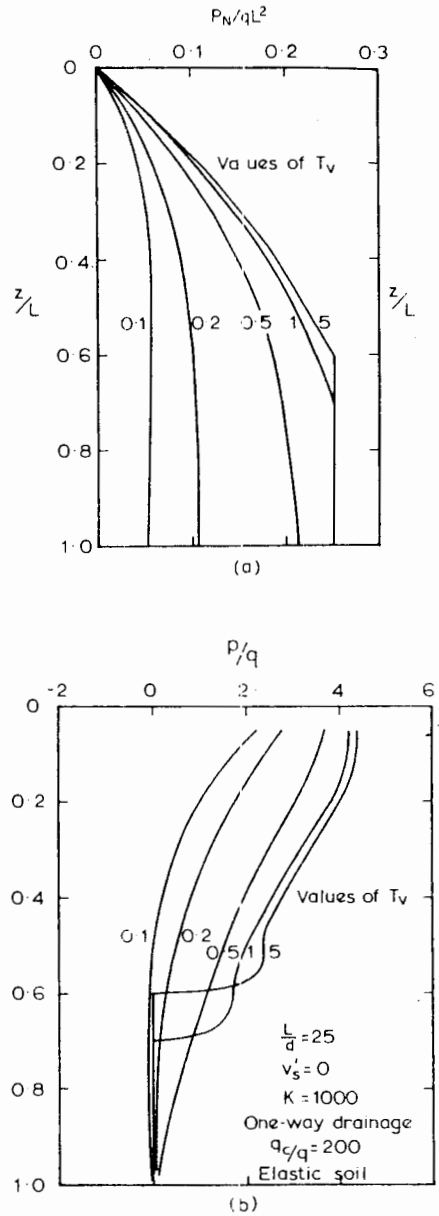

FIGURE 11.22 Stress and load distributions in a partially crushed pile.

If local yield occurs or if installation of the pile is delayed, crushing of the pile is less likely, since the loads developed may be considerably smaller than the elastic values.

If an axial load acts simultaneously, the possibility of crushing of the pile increases. This case can be considered approximately by assigning to the pile a reduced crushing strength equal to the actual crushing strength minus the applied axial stress.

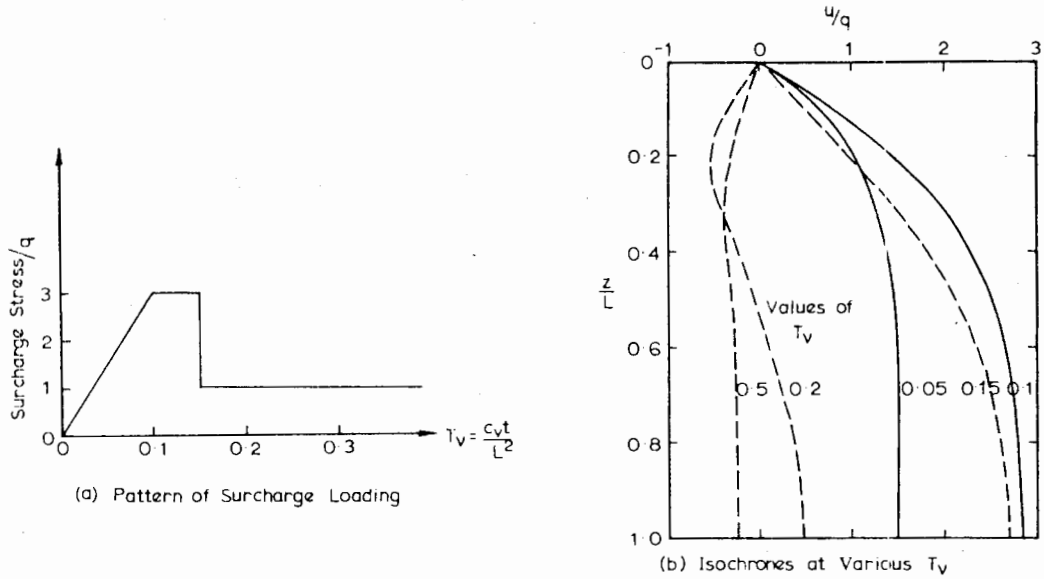

FIGURE 11.23 Surcharging sequence and isochrones for example.

11.4.6 Pile in Soil Subjected to Variable Loads

As an example of the further application of the analysis, Fig. 11.23 shows the case of a pile installed in a layer that is subjected to a variable surcharging loading. The development with time of downdrag force at the tip is examined for various times of installation T_0 after commencement of placement of the surcharge. The soil is assumed to have a constant permeability during the consolidation process, but to have a value of m_v for expansion or recompression of one fifth of the value for virgin compression. The distribution of pore pressure in the layer at various times has been obtained by a finite-difference analysis. The resulting isochrones are shown in Fig. 11.23.

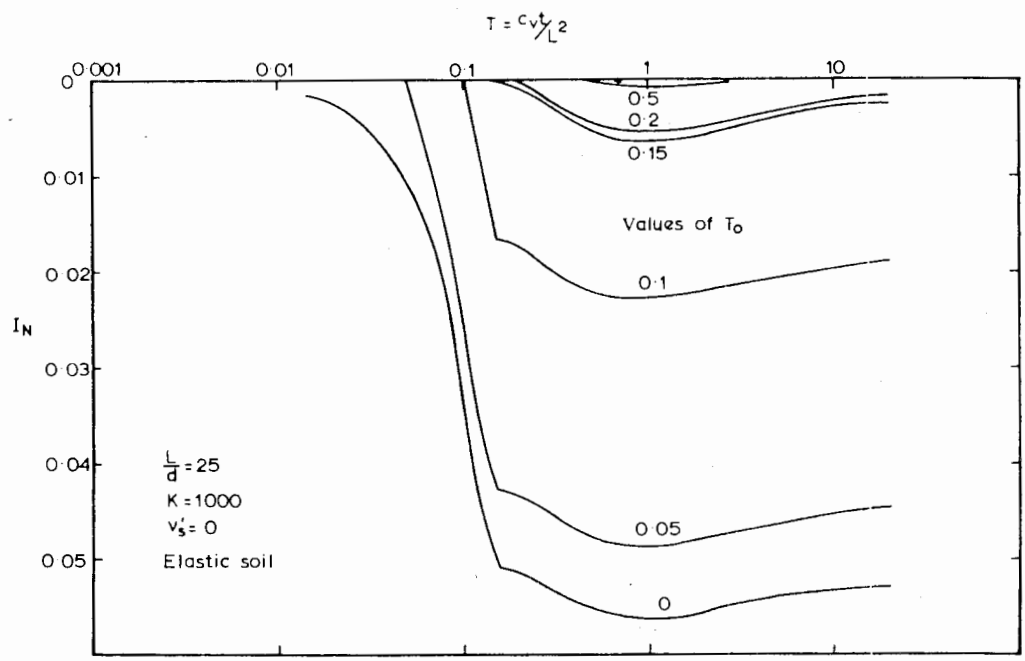

FIGURE 11.24 Downdrag load-time relationships for example.

The variation of maximum downdrag load ($P_N = I_N q L^2$) with time for various values of T_0 is shown in Fig. 11.24. It will be seen that when the pile is installed during the period of build-up of surcharge, the downdrag increases rapidly with time until removal of the excess surcharge. A further small increase in downdrag is followed by a decrease to a final value of load—which in this case, is very close to the load in the pile at the time of removal of excess surcharge. The later the time of installation, the less the ultimate downdrag load.

If the pile is installed after removal of the excess surcharge (i.e., $T_0 \geqslant 0.15$), only very small downdrag loads result. The downdrag reaches a maximum value at some considerable time after installation (in this case, about $T_v = 1$) and decreases thereafter. A pile installed after $T_v = 0.5$ experiences virtually no downdrag force. It is interesting to note that for $T_0 > 0.15$, a considerable portion of the pile may be subjected to upward stresses (positive friction) although downdrag forces always exist in some position of the pile, generally near the top.

11.4.7 Data on Pile-Soil Parameters

The most important parameters in the analysis are the pile-soil shear-strength parameters and Young's modulus, E_s and Poisson's ratio, ν_s, of the soil. The former parameters are of great importance if full or partial slip occurs, while E_s and ν_s only become important when conditions are elastic or nearly so. In many cases involving soft soils, estimates of the values of E_s and ν_s will not be necessary.

With normally-consolidated clays, it seems reasonable to assume that $c'_a/q = 0$ unless the clay is overlain by other layers, in which case an equivalent value, c'_{ae}/q, may be determined from Eq. 11.10. If $c'_a/q = 0$, $\tau_a/\sigma'_v = K_s \tan \phi'_a$. An examination of values of τ_a/σ'_v deduced from available field-test data was made by Dawson (1970). It was found that τ_a/σ'_v tended to increase with increasing plasticity index and increasing c_u/σ'_v, where c_u = undrained shear strength. Coating a pile with bitumen greatly reduced τ_a/σ'_v. The correlations obtained by Dawson are shown in Figs. 11.25 and 11.26 and may be useful for design purposes when no other data is available. Walker and Darvall (1970) also examined some of the same data as Dawson and found that, as previously noted by Endo et al. (1969), τ_a is frequently closely-approximated by the original undrained shear strength, c_u, of the soil (Fig. 11.27). This fact also emerges from an examination of Fig. 11.25, and may provide a useful approximate means of estimating τ_a in the absence of other information.

The estimation of drained Young's modulus E_s of the soil presents some difficulties. The value appropriate to the case of negative friction is likely to be different from the value appropriate to axial loading (see Chapter 5). The effects of pile installation in the case of axial loading are very important, but these effects are likely to be greatly modified by the consolidation of the soil. It appears likely that E_s will correspond more closely to the value for the soil layer subjected to surface loading, and in this case, E_s may be conveniently estimated from the results of oedometer tests via the following equation for an ideal elastic soil:

$$E_s = \frac{(1 - 2\nu'_s)(1 + \nu'_s)}{m_v(1 - \nu'_s)} \tag{11.23}$$

where

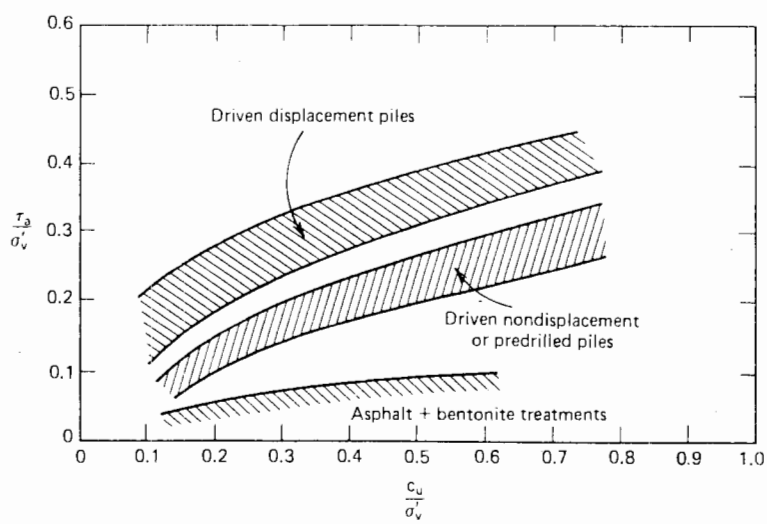

FIGURE 11.25 Suggested design values of pile-soil adhesion (after Dawson, 1970).

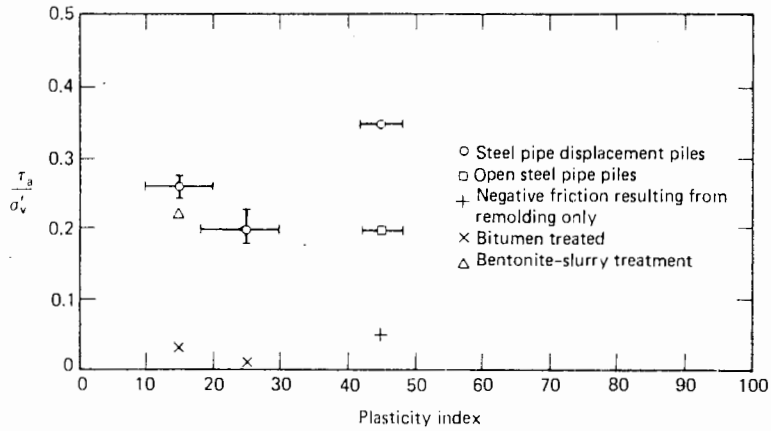

FIGURE 11.26 Pile-soil adhesion vs. plasticity index (after Dawson, 1970).

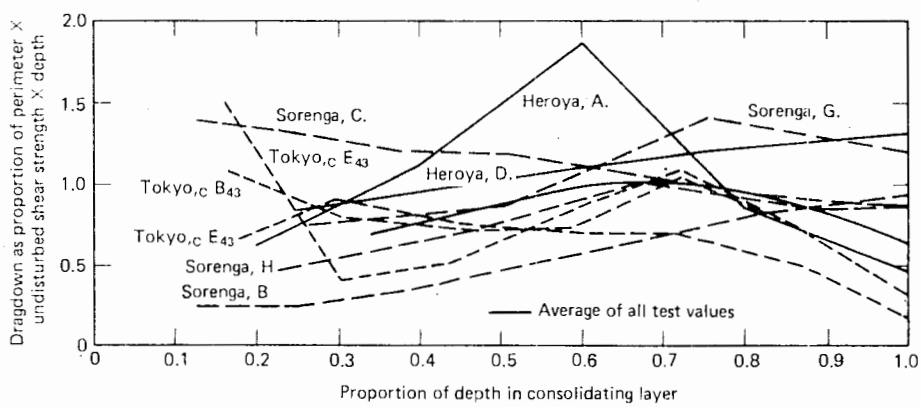

FIGURE 11.27 Summary of negative friction data in dimensionless form for steel-pipe piles in clay (Walker and Darvall, 1970).

m_v = coefficient of volume-decrease from oedometer test
ν'_s = drained Poisson's ratio of soil

For normally consolidated clays, ν'_s generally lies between 0.3 and 0.4, with values decreasing to 0.2 or less for overconsolidated clays.

Illustrative Example

To illustrate the use of the parametric solutions described above, the following example is considered.

A soil profile consists of 4 m of sand overlying 16 m of clay overlying impermeable shale. The water table is 1-m below the surface of the sand. Three meters of fill is to be placed over the site, and one year after placement of the fill, 0.4-m-diameter piles will be installed to rock. The working load on each pile is 500 kN. It is desired to calculate the final maximum force in the pile and the final movement of the pile head, and also the maximum force and movement six years after installation of the pile.

The following data will be assumed:

Fill and sand	γ	= 19.62 kN/m^3
	ϕ'	= 35°
Clay	γ	= 18.65 kN/m^3
	c_u/σ'_v	= 0.3
	m_v	= 5.4 × 10^{-5} m^2/kN
	c_v	= 18.5 m^2/yr
Pile	E_p	= 20 × 10^6 kN/m^2

The shale is assumed to be rigid.

a) Final Maximum Force in Pile

The force in the pile will arise from the applied axial load, the downdrag on the pile caused by the consolidating clay, and the downdrag on the pile caused by the fill and sand overlying the clay. The first two components are given by Eq. (11.13), and to apply this equation, P_{NFS} must be calculated after the pile-soil parameters are selected.

It will be assumed that $K_s \tan \phi'_a = c_u/\sigma'_v = 0.3$. The equivalent pile-soil adhesion c'_{ae} is calculated from Eq. (11.10), and assuming $c'_a = 0$,

$$c'_{ae} = c'_a + p_0 K_s \tan \phi'_a$$
$$= 0 + [(4 \times 19.62) - (3 \times 9.81)] \times 0.3$$
$$= \mathbf{14.7\ kN/m^2}$$

The applied stress caused by the fill is

$$q = 3 \times 19.62 = \mathbf{58.86\ kN/m^2}$$
$$\therefore c'_{ae}/q = 14.7/58.86 = \mathbf{0.25}$$
$$\gamma L/q = \frac{(19.62 - 9.81) \times 16}{58.86} = 2.67$$

Applying Eq. (11.15),

$$P_{NFS} = \pi \times 0.4 \times 16 \left[14.7 + 0.3 \left(\frac{9.81 \times 16}{2} + 58.86\right)\right]$$
$$= \mathbf{1125\ kN}$$

Since pile installation is delayed one year after fill placement, $T_0 = 18.5 \times 1/16^2 = \mathbf{0.072}$. Interpolating between Figs. 11.5 and 11.6 for $K_s \tan \phi'_a = 0.3$, $N_R = \mathbf{0.90}$. Because conditions at the pile-soil interface are not elastic, an estimate of E_s and ν'_s will not be required, as there will be no need to use the elastic solutions in this case.

Assuming one-way drainage of the clay layer and interpolating between the available curves from Fig. 11.8, $N_T = \mathbf{0.99}$.

From Eq. (11.13),

$$P_N = 1125 \times 0.90 \times 0.99 + 500$$
$$= \mathbf{1502\ kN}$$

The downdrag caused by the overlying sand layer and fill must now be added. It will be assumed that $c'_a = 0$, $\phi'_a = 0.71\phi' = 25°$, and $K_s = 0.5$, so that $K_s \tan \phi'_a = 0.23$. It will further be assumed that full slip occurs between the pile and these soil layers.

At the level of the water table,

$$\sigma'_v = 4 \times 19.62$$
$$= \mathbf{78.5\ kN/m^2}$$

At the level of the top of the clay,

$$\sigma'_v = 78.5 + 3 \times 9.81$$
$$= \mathbf{107.9\ kN/m^2}$$

The downdrag force caused by these layers is then

$$\pi \times 0.4\ [(0 + 78.5)/2 \times 4 + (78.5 + 107.9)/2 \times 3] \times 0.23$$
$$= \mathbf{126\ kN}$$

The final maximum axial force in the pile is therefore

$$1502 + 126 = \mathbf{1628\ kN}$$

The possibility of crushing of the pile should also be checked. The maximum axial stress is $1628/(\pi \times 0.2^2) = 12955\ \text{kN/m}^2$. This is less than the normal compressive strength of concrete and hence crushing should not occur.

b) Final Axial Movement of Pile

The axial movement of the portion of the pile in the clay is given by Eq. (11.19). From Eq. 11.20),

$$\rho_{FS} = \frac{2 \times 58.9 \times 16^2 \times 1.0}{20 \times 10^6 \times 0.14} [0.25 + 0.3(2.67/3 + 1)]$$
$$= 0.00308\ \text{m} = \mathbf{3.1\ mm}$$

From Figs. 11.14 and 11.15,

$$Q_R = \mathbf{1.0}$$

From Fig. 11.16,

$$Q_T = \mathbf{1.0}$$

Now the axial force in the pile at the top of the clay layer

$$= 500 + 126 = 626\ \text{kN}.$$

Substituting into Eq. (11.19),

$$\rho = \mathbf{7.1\ mm}$$

(The component resulting from the axial load of 626 kN is 4.0 mm.)

The compression of the pile above the top of the clay is given, to sufficient accuracy, as

$$\frac{(500 + 626)/2 \times 7}{20 \times 10^6 \times \pi \times 0.2^2} = .0016\ \text{m}$$
$$= \mathbf{1.6\ mm}$$

The total final axial movement of the pile head is therefore

$$7.1 + 1.6 = \mathbf{8.7\ mm}$$

c) Maximum Force and Deflection After Six Years

Six years after installation of the pile, $T_v = 18.5 \times 6/16^2 = 0.43$. It will be assumed that the downdrag force and deflection resulting from the fill and sand layers have been fully developed at this time and that only the downdrag force caused by the clay is time-dependent.

From Fig. 11.11, interpolating between the two curves, $U_N = 0.73$. Applying Eq. (11.18), the maximum pile load after six years is

$$P_t = 0.73(1528 - 626) + 626$$

$$= 1357 \text{ kN}$$

From Fig. 11.19, $U_\rho = 0.79$. From Eq. (11.22), the pile-head movement after six years is

$$\rho_t = 0.79(7.1 - 4.0) + 4.0 + 1.6$$

$$= 8.0 \text{ mm}$$

11.5 PILE GROUPS

In groups of end-bearing piles in consolidating soil, downdrag loads in individual piles are likely to be smaller than on an isolated pile, since the presence of additional piles tends to reduce the soil settlements within the groups. The inner piles of a group may thus have considerably smaller downdrag loads than the outer piles.

An analysis of the effects of negative friction on groups may be made by extending the elastic analysis for single piles, combining the single-pile analysis (Section 11.3.3) with the pile-group analysis (Chapter 6). A full analysis requires consideration of each pile in a group, the consideration of pile-soil displacement compatability at each element of each pile, and solution of the subsequent equations for the specified boundary conditions, for example, rigid pile cap (in this particular case, unknown axial forces at the pile heads will also need to be included in the set of equations). Such an analysis will give the stress and load distribution in each pile of the group. Allowance can also be made for pile-soil slip or partial crushing of the pile. However, for relatively large pile-groups, the number of equations to be solved may be large.

A simplified approach may be made by first considering the interaction between two piles in a consolidating layer. The results of this analysis may be expressed in terms of a downdrag interaction factor α_d, where

$$\alpha_d = \frac{\text{Reduction in downdrag load caused by adjacent pile}}{\text{Downdrag load in single pile}} \tag{11.24}$$

An example of the relationship between α_d and dimensionless spacing s/d is shown in Fig. 11.28 for $L/d = 25$. The larger the value of pile stiffness K, the larger the value of α_d (i.e., the greater the reduction in downdrag load). It is also found that at a given s/d, α_d increases as L/d decreases.

The two-pile analysis may be extended to symmetrical pile groups, and it is found that for such groups, the individual pile loads may be estimated approximately from the solutions for two-pile interaction, as follows:

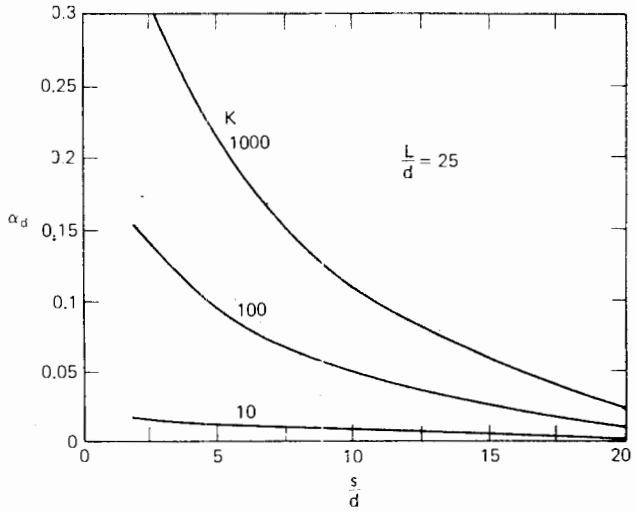

FIGURE 11.28 Interaction curves for two end-bearing piles subjected to negative friction.

$$P_i = P_1 \prod_{\substack{j=1 \\ j \neq i}}^{n} (1 - \alpha_{dij}) \tag{11.25}$$

where

P_i = downdrag load at pile i
P_1 = downdrag load in isolated single pile
α_{dij} = downdrag interaction factor for spacing between piles i and j
Π denotes a repeated product

The above superposition rule is approximate only and tends to underestimate the pile loads, especially for stiff piles at close spacings. It may be useful, however, as a guide to the load distribution within a group. For example, for a square group consisting of four corner piles and a center pile, with $L/d = 25$, $K = 1000$, and the corner piles spaced at five diameters, the downdrag load on the corner piles is found to be $0.38 P_1$, and on the center pile, $0.19 P_1$.

The above approximate analysis takes no account of pile-soil slip. For small groups in very soft clay, the consolidation settlements may be sufficiently large that slip will occur along all piles in the group, so that there will be no downdrag reduction from a group effect. On the other hand, for large groups of closely spaced piles, the presence of the piles will suppress the settlement of even very soft soils and it is likely that considerable reduction in downdrag loads will occur. However, as pointed out by Zeevaert (1959), group effects may result in a decrease in the point-bearing capacity of a pile.

Tests carried out on model piles by Koerner and Mukhopadhyay (1972) confirmed that the group effect de-

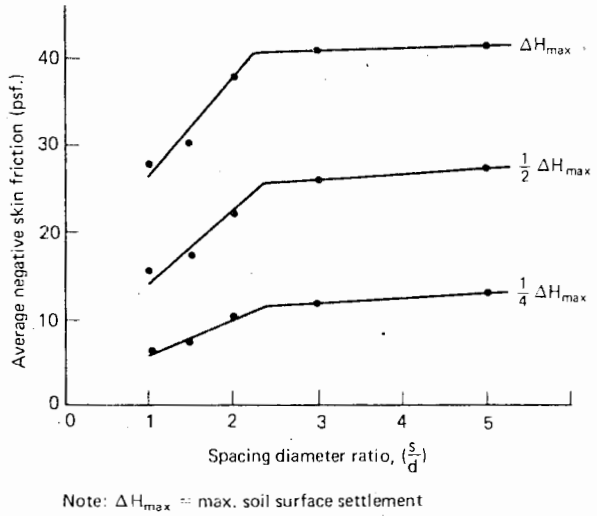

FIGURE 11.29 Effect of pile-group spacing on average negative skin friction. Model tests of Koerner and Mukhopadhyay (1972).

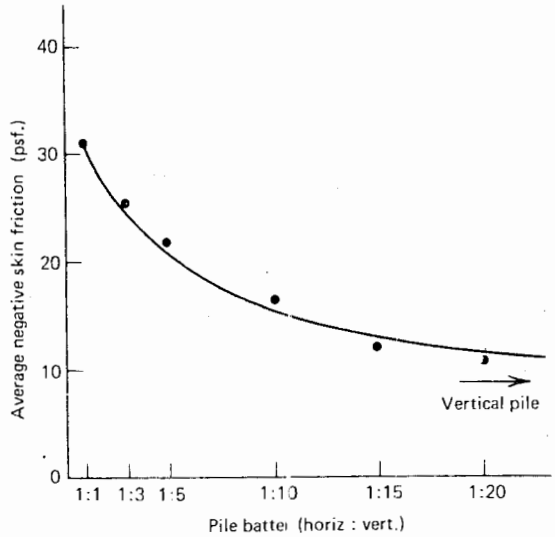

FIGURE 11.30 Effect of pile batter on average negative skin friction. Model tests of Koerner and Mukhopadhyay (1972).

creases negative skin friction. A 3 × 3 group of piles was tested for various pile spacings, and it was found that for spacings closer than about 2.5 diameters, a distinct reduction in negative skin friction occurred, as shown in Fig. 11.29. This reduction was apparent at all values of surface deflection of the soil up to the maximum value (not specified by the authors). The authors noted the similarity with the behavior of pile groups subjected to axial loading, in which positive skin friction is also decreased by group action. The extent of the reduction is, however, not as great as would be calculated on the basis of the elastic interaction curves in Fig. 11.28, probably because of the occurrence of considerable pile-soil slip in the model tests.

If a pile group in a consolidating layer contains batter piles, these piles will be subjected to normal stress as well as shear stress. The development of this additional normal stress will tend to increase the shear stress, and hence the axial force, in the piles. Bending of the pile will also occur. An analysis of this problem can be carried out by combining the analysis for a pile subjected to axial soil-movements with that for a pile subjected to soil movements in a normal direction (see Chapter 13).

A preliminary analysis carried out by M. R. Madhav (private communication) suggests that the vertical and lateral movements of a pile with an unrestrained head are dramatically increased as the batter angle increases. For example, for $K = 5000$, $L/d = 50$, and a batter angle of 15°, the vertical movement is increased by a factor of about 10, as compared with the case of a vertical pile. This additional movement arises primarily from the development of normal displacements for the battered pile. If the pile head is restrained or fixed, the pile head's force or moment will be correspondingly increased as the batter angle is increased.

Some measurements of the negative skin friction on battered model piles made by Koerner and Mukhopadhyay (1972) are shown in Fig. 11.30. For commonly-used batter angles, the negative skin friction may be twice that acting on a vertical pile.

A further indication of the large downdrag forces that can occur in batter piles was found in the case reported by M.I.T. (1973), in which at least one batter pile in a group of piles beneath a bridge abutment was found to have pulled out of the pile cap because of the effects of downdrag. The vertical piles were therefore subjected to increased axial forces, because the batter piles could carry none of the applied axial load.

11.6 COMPARISONS BETWEEN MEASURED AND PREDICTED PILE BEHAVIOR

For the purposes of comparing observations of pile behavior in the presence of negative friction with the behavior predicted from the theoretical analyses given in this chapter, two series of observations reported in the literature have been considered (Bjerrum et al. (1969); Walker and Darvall (1973)). In the series of tests described by Bjerrum et al. (1969), deflections and loads have been measured on a number of piles at two different sites and sufficient data is presented to allow theoretical predictions to be made.

The effects of delayed installation are also present in these cases.

Tests of Bjerrum et al–Heröya Site

At the first site (Heröya), 8 m of fill, sand, and gravel overlie a layer of silty clay of variable thickness (20 to 30 m) that overlies gravel and bedrock. The fill had been placed 2 to 4 years prior to installation of the test piles. The main object of the tests was to determine the effectiveness of various methods of reducing downdrag forces, as measurements on piles installed earlier had revealed that very large downdrag forces were developed because of reclamation filling. Two of the steel-tube test piles were chosen for analysis, pile A, an uncoated pile, and pile C, which was subjected to electro-osmosis. Both were driven to bedrock.

For the theoretical analysis, the following parameters were chosen or deduced from the published data:

Pile A $L = 30$ m, $d = 0.3$ m (7 mm wall thickness), $q = 98.1$ kN/m^2, $\gamma_{sub} = 9.81$ kN/m^3, $K_s \tan \phi'_a = 0.25$, $c'_a = 0$, $E_s = 9.81$ MN/m^2, $K = 1280$, $c_v = 70$ m^2/yr, $t_o = 3$ yrs, $t = 5$ yrs.

Pile C As for pile A, except that $L = 20$ m and $K_s \tan \phi'_a = 0.17$. Piezometer measurements indicated that one-way drainage conditions were present at this site. It was also assumed that full slip occurred between the fill and pile and that for the fill, $K_s \tan \phi'_a = 0.20$ and $\gamma = 19.6$ kN/m^3.

Because detailed distributions of downdrag force and deflection were required to compare with the corre-

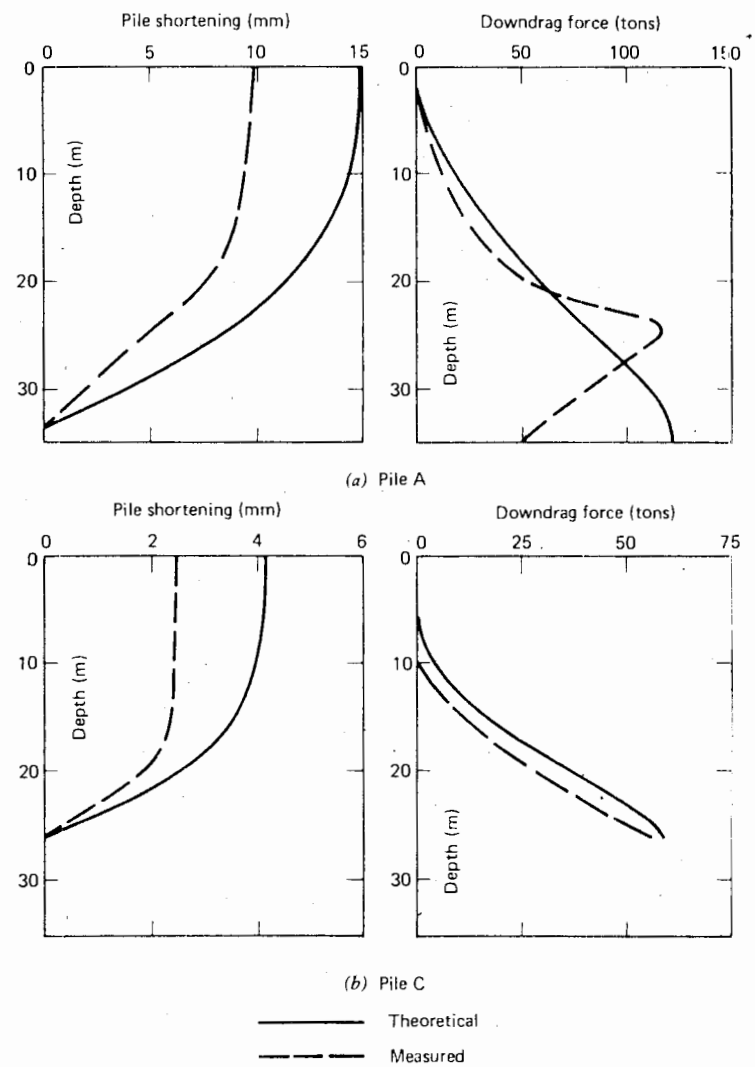

FIGURE 11.31 Comparisons with pile tests of Bjerrum et al. (1969) at Heröya.

sponding measured distributions, a computer program was used to obtain the theoretical solutions. The resulting comparisons are shown in Fig. 11.31. For both piles, the agreement between measured and predicted downdrag-force distributions is good but the measured pile-shortening is less than predicted. The irregularity in the measured force near the tip of pile A may be attributed to the fact that the lower part of the pile was resting against steeply sloping bedrock, thus causing load transfer to the rock by adhesion.

Tests of Bjerrum et al–Sörenga Site

At the second site (Sörenga), 10 to 15 m of fill overlay 30 to 40 m of clay overlying bedrock. At one end of the site, fill had been placed a few years before the piles were installed. At the other end, the fill had been in place for about 70 years and measurements showed that the consolidation under this fill was complete. Three test piles (C, D, E) were installed in the newly filled area, and two (G, H) in the older area. Piles C and G were analyzed, both being conventional uncoated steel-tube piles driven to bedrock.

For pile C, the following data were adopted after an examination of the available data given by Bjerrum et al.:

$L = 40$ m, $d = 0.5$ m (8-mm wall thickness),
$q = 147.1$ kN/m, $\gamma_{sub} = 9.81$ kN/m^3, $K_s \tan \phi'_a = 0.20$,
$E_s = 9.81$ MN/m^2, $K = 1280$, $c_v = 80$ m^2/yr,
$t_o = 2.5$ yr, $t = 4.5$ yr.

The characteristics of the fill were assumed to be the same as at the Heröya site. Piezometer measurements indicated two-way drainage conditions.

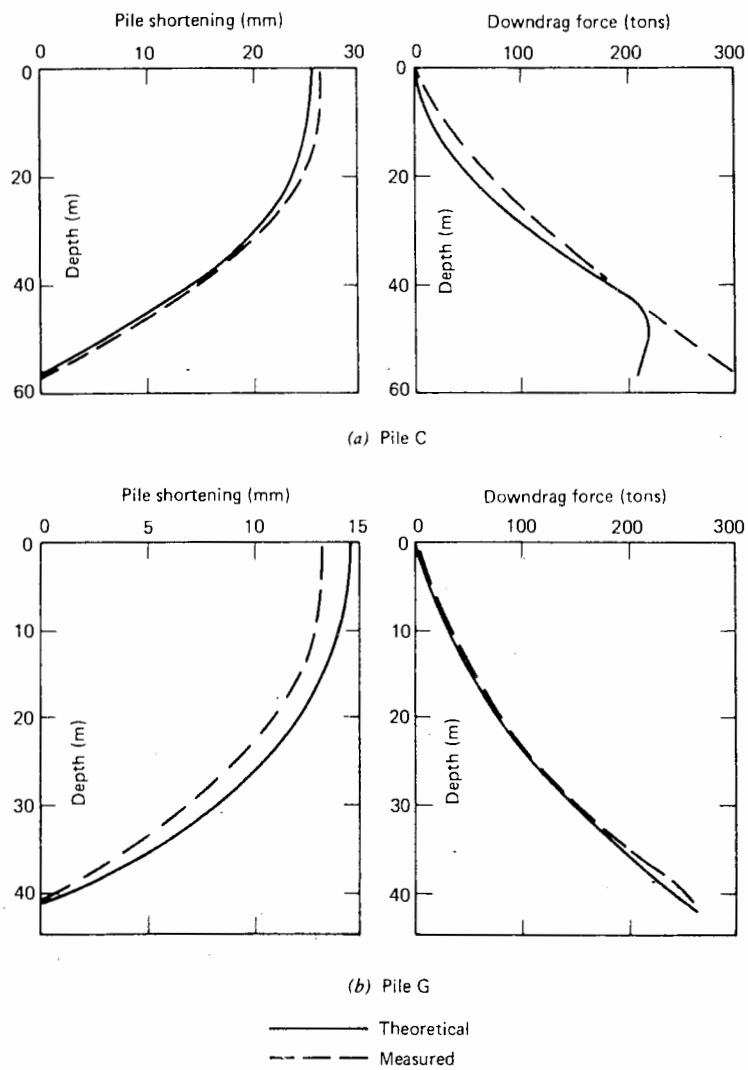

FIGURE 11.32 Comparisons with pile tests of Bjerrum et al. (1969) at Sorenga.

Comparisons between measured and theoretical distributions of pile shortening and downdrag force for pile C are shown in Fig. 11.32, which reveals a remarkable degree of agreement. The only point of disagreement is near the tip, where the theory predicts a smaller downdrag force. The theory suggests that slip does not occur in this region, and the bearing stratum is assumed rigid in the analysis, whereas in reality, the finite compressibility of the bearing stratum may allow sufficient movement of the pile to generate full slip near the tip.

At the location of pile G, fill had been placed 70 years previously and consolidation under this fill was almost certainly complete. Nevertheless, a soil movement of about 70 mm was measured in the vicinity of the pile in a two-year period. It is a reasonable conjecture that this settlement resulted from the three-dimensional effects of the recent filling at the other end of the site. Calculations were carried out for pile G, assuming that the settlement of the soil decreased linearly from 70 mm at the surface of the soil to zero at the pile tip. The pile and soil parameters were as for pile C, except that for pile G, L = 30 m. The resulting comparison between measured and theoretical downdrag force and pile shortening, shown in Fig. 11.32, reveals very close agreement. This case provides evidence that large downdrag forces may occur when soil movements are caused by three-dimensional effects arising from loading at some distance from the pile.

A further comparison was made with another pile (B), which was installed at the same time as the recent fill was placed. The pile and soil parameters were taken to be the same as for pile C, except that filling and pile installation were assumed to be simultaneous (i.e., t_0 = 0). Detailed measurements were not given for this pile, but the maximum downdrag force was reported to be about 400 tons (3.99) MN), while the theoretical calculations gave a value of 408 tons (4.07 MN), with full slip along the whole length of the pile. The values of pile shortening did not agree well (100 mm measured, 29 mm calculated); however, the average axial stress in the pile was on the order of 3200 kgf/cm^2 (314 MN/m^2), and it is therefore probable that yielding of the pile occurred, resulting in increased shortening of the pile.

Test of Walker and Darvall

A further documented case of downdrag measurement in an end-bearing pile has been presented by Walker and Darvall (1973). Two steel-shell piles of 0.76-m diameter and 11-mm wall thickness (one pile uncoated, one coated with bitumen) were driven into a soil profile consisting of 2 m of recent fill and 7 m of sand overlying firm silty clay, sandy silt, and dense sand and gravel, the piles being founded in the latter layers. Three meters of fill were placed over the site and measurements were made of downdrag force, soil settlement, and pore pressure in the soil.

In obtaining a theoretical solution for this case, the following parameters were selected for the clay and pile: L = 16.5 m (in clay), q = 3.9 t/m^2 (38.3 kN/m^2), γ_{sub} = 9.81 kN/m^3, $K_s \tan \phi'_a$ = 0.4, E_s = 170 kgf/cm^2 (16.7 MN/m^2). For the overlying sand, recent fill and fill material, full slip was assumed to occur at the pile-soil interface, with $K_s \tan \phi'_a$ = 0.45 and γ = 22.6 kN/m^3. Walker and Darvall were of the opinion that consolidation under the new fill had occurred very rapidly and that creep was in progress when the latest measurements were made (about 250 days after commencement of filling). Accordingly, in the theoretical analysis, the measured soil-surface settlement of 35 mm was input in the analysis and the soil settlement was assumed to vary linearly with depth to zero at the top of the sandy silt layer.

A comparison between measured and theoretical distribution of downdrag force in the uncoated pile, shown in Fig. 11.33, again reveals good agreement. There is also good agreement between the present theoretical solution and that of Walker and Darvall, which was based on a finite-element analysis using a nonlinear stress-strain relationship for the soil. It is significant to note that the present calculations indicate that slip occurs only near the top of the pile in the clay. Thus, an estimate of downdrag force assuming full slip along the whole length would give incorrect predic-

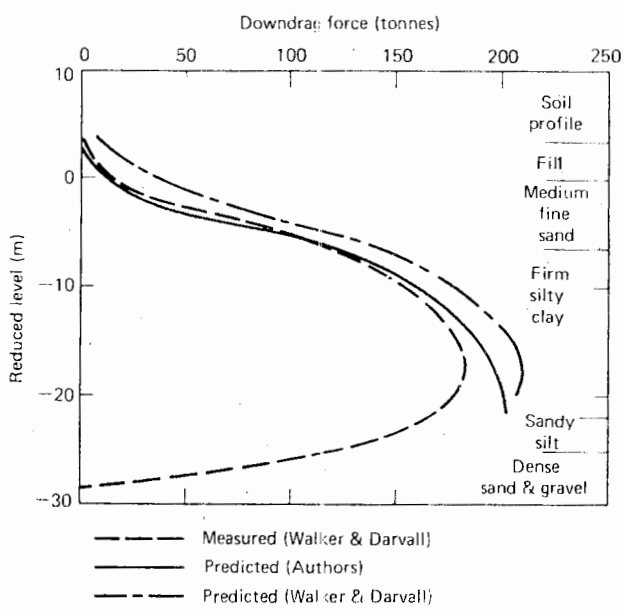

FIGURE 11.33 Comparison with pile tests of Walker and Darvall (1973).

tions of both the magnitude and distribution of downdrag; the use of the measured downdrag to infer $K_s \tan \phi'_a$ would give an erroneous value.

The measurements indicate the development of positive friction and consequent reduction in downdrag force in the sandy silt, sand, and gravel layers underlying the clay. In the theoretical analysis, the pile was assumed to be end-bearing on the sandy silt, and consequently the calculated downdrag force at this level is somewhat greater than the measured value.

12

PILES IN SWELLING AND SHRINKING SOILS

12.1 INTRODUCTION

Foundations in expansive clays are frequently subjected to severe movements arising from moisture changes within the clay, with consequent cracking and damage caused by distortion. Donaldson (1965) classifies the migration of moisture beneath structures into three phases:

1. A primary phase caused by the erection of the structure, resulting in a change in the moisture regime until an equilibrium state is reached under the new conditions.
2. The fluctuation caused by seasonal climatic changes.
3. The results of extraneous influences, such as broken drains, leaking water pipes, local concentrations of stormwater, and gardening operations.

Piles have been used extensively for foundations in swelling soils in order to anchor down the structure at a depth where changes in moisture content are negligible, so that movements of the structure are minimized. However, considerable uplift forces are induced in such piles because of the action of the swelling soil.

An analogous problem arises with piles in soils undergoing shrinking or consolidation, when downdrag forces are induced in the piles by negative friction. The effect of negative friction on end-bearing piles has been discussed in Chapter 11. In this chapter, the effect of soil movements on the behavior of floating piles will be considered. Because of the similarity in approach between a pile in a swelling soil and a pile in a consolidating or shrinking soil, attention will be concentrated on the case of a swelling soil, although some theoretical differences between the two cases will be considered.

In designing piles in swelling soils, there are three requirements:

1. The pile must be able to carry the structural load safely i.e. there must be adequate ultimate load capacity.
2. The pile must have sufficient tensile strength to withstand the tensions developed in the pile due to uplift forces.

3. The movement of the piles due to the uplift forces and the structural load must be less than the prescribed limit.

In this chapter, attention is focused on the latter two aspects, since few problems arise in obtaining adequate load-carrying capacity in expansive soils. Existing methods of determining pile-uplift forces and movements are reviewed and then an analysis based on elastic theory is described. Some results of this analysis are presented to indicate some of the theoretical trends and then a series of curves are presented for use in design. Finally, the relationship between theoretical and observed pile-behavior is examined for a number of case histories.

12.2 EXISTING METHODS OF ANALYSIS

A relatively simple approach for the calculation of the tensile forces in a pile in a swelling soil was outlined by Collins (1953). The approach was developed for an underreamed pile anchored in nonexpansive soil, and it was assumed that full slip occurred between the expansive soil and the shaft, so that the shear stress along the pile equals the pile-soil adhesion. Referring to Fig. 12.1*a*, the total tension T in the pile at any depth h is

$$T = \int_0^h \pi d \tau_a dz \tag{12.1}$$

where

τ_a = pile-soil adhesion

As in the case of piles in sand or piles in clay under drained conditions, τ_a may be expressed as

$$\tau_a = c'_a + K_s \sigma'_v \tan \phi'_a \tag{12.2}$$

where

c'_a = effective adhesion
K_s = coefficient of horizontal pressure
σ'_v = effective vertical stress
ϕ'_a = effective angle of friction between pile and soil

Thus,

$$T = \pi \int_0^h d(c'_a + K_s \sigma'_v \tan \phi'_a) dz \tag{12.3}$$

At the tip of the pile, there is zero tension ($T = 0$), so that there is a transition zone near the underreamed section. The probable variation of tension with depth is shown in Fig. 12.1*a*.

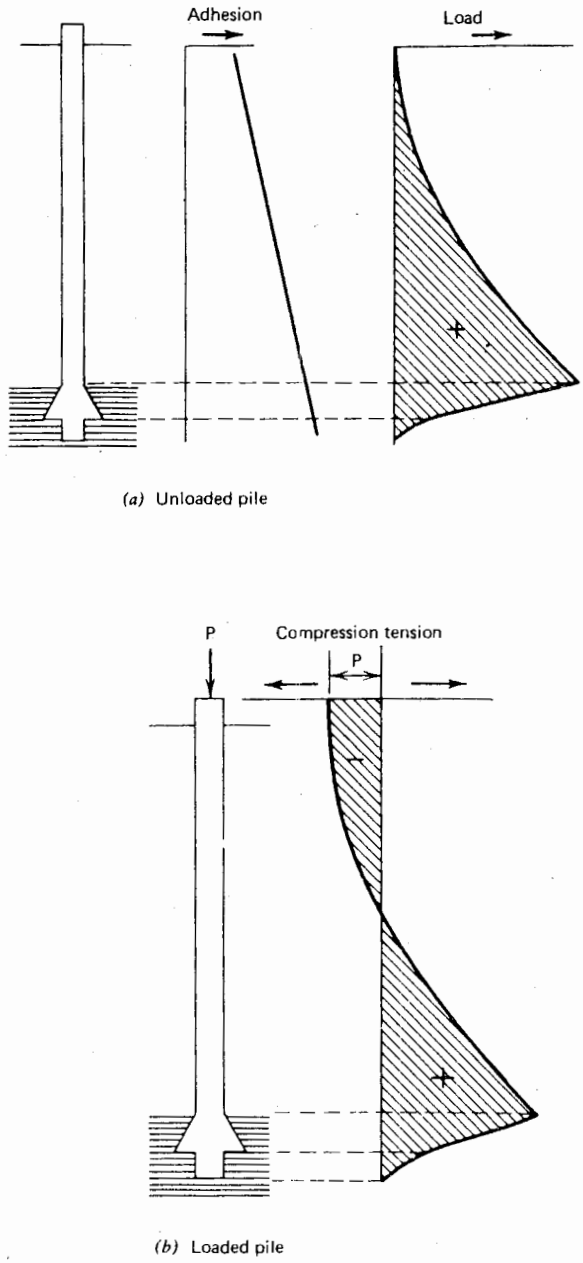

(*a*) Unloaded pile

(*b*) Loaded pile

FIGURE 12.1 Forces in underreamed pile in expansive soil (after Collins, 1953).

If a vertical load P is applied to the top of the pile, Eq. (12.3) is modified to

$$P + T = \pi \int_0^h d(c'_a + K_s \sigma'_v \tan \phi'_a) dz \tag{12.4}$$

The probable load-distribution is shown in Fig. 12.1*b*.

Collins originally suggested that c'_a and ϕ'_a should be taken as the values of c' and ϕ' from drained-strength tests and that K_s could be taken as 1.0. Subsequently, Donaldson (1967*b*) suggested that a reduction factor of between 0.3 and 0.7 should be applied to the measured drained shear-strength to obtain the pile-soil adhesion, τ_a. A summary of suggested methods of obtaining τ_a is given in Section 12.6.

Bozozuk (1972) described an analysis in which the location of the "neutral point" (i.e., the point at which the maximum load occurs) was computed, assuming full slip to occur along the pile. The maximum load on the pile could then be obtained. An extension to this analysis to allow for loads caused by horizontal stresses generated by an embankment was also described.

Sahzin (1968), in obtaining expressions for the movement of a pile in swelling soil, analyzed the work done by friction forces in the upper portion of the pile, which tend to lift the pile, and the applied load and the friction forces in the lower half, which tend to resist uplift. Sahzin found good agreement between pile movements and those predicted from his approach.

12.3 ANALYSIS BASED ON ELASTIC THEORY

The existing approaches described in the previous section depend on the assumption that slip occurs along the entire pile shaft. Also, the first two consider only the loads developed in the piles, and only the method described by Sahzin considers the pile movement. A more satisfactory analysis can be carried out by employing elastic theory in a fashion similar to that described in Chapters 5 and 6 for pile settlements and in Chapter 11 for negative friction on end-bearing piles.

12.3.1 Basic Analysis

The problem is illustrated in Fig. 12.2. A circular pile, length L, diameter d, and base diameter d_b, is situated in a soil mass in which occurs, away from the pile, a general specified distribution of movement, S (either swelling or shrinking), with depth. The pile is divided into n cylindrical elements, each with a uniform shear stress, p_j, acting on the periphery. In the basic analysis, the soil is assumed to be homogeneous and linearly elastic and it is assumed that no slip occurs at the pile-soil interface.

Defining downward soil displacements and shear stresses as positive, as shown in Fig. 12.2, the soil displacements along the pile can be expressed as

$$\{_s\rho\} = -\frac{d}{E_s}[I_s]\{p\} + \{S\} \qquad (12.5)$$

where

$[I_s]$ = the $(n+1)$ by $(n+1)$ matrix of displacement-influence factors
E_s = Young's modulus of soil
$\{S\}$ = the $(n+1)$ vector of soil movements, negative for swelling
$\{_s\rho\}$ = the $(n+1)$ vector of soil displacements
$\{p\}$ = the $(n+1)$ vector of shear stresses at the soil-pile interface and the base pressure—with positive directions as in Fig. 12.2

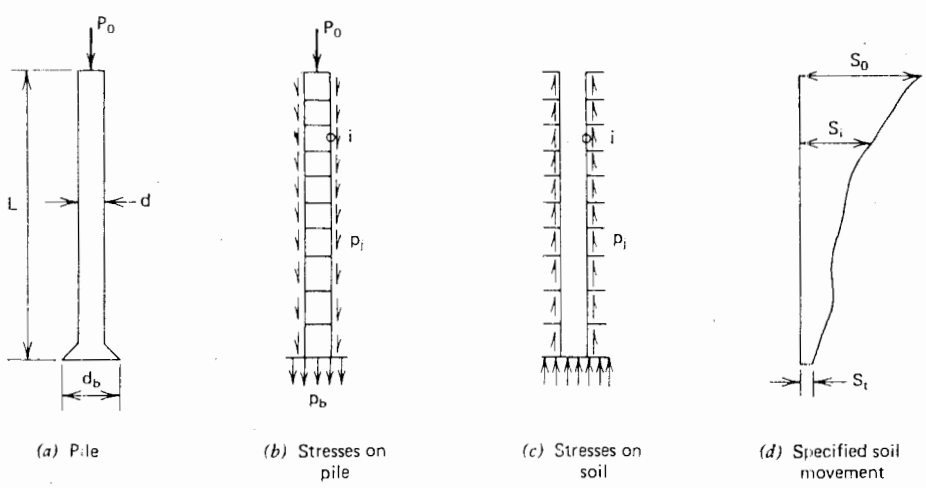

(*a*) Pile (*b*) Stresses on pile (*c*) Stresses on soil (*d*) Specified soil movement

FIGURE 12.2 Pile in swelling or consolidating soil.

The elements of $[I_s]$ are obtained by double integration of the Mindlin equations as described in Appendix A. Poissons' ratio of the soil, ν_s, is not a very important parameter of the values of I_s.

Without slip, the pile displacements ${}_p\rho = {}_s\rho$. For the more general case of a compressible pile, the pile displacements must be compatible with the elastic properties of the piles and the analysis could proceed along the lines described in Section 5.3. Here, only the single case of an incompressible pile is considered, and therefore ${}_p\rho = {}_s\rho = \rho$ = constant. It follows that

$$d\{p\} = E_s[I_s]^{-1}\{\rho - S\} \tag{12.6}$$

Also, from equilibrium of the pile,

$$P_0 + \sum_{j=1}^{n} p_j \pi d\, L/n + p_b \pi d_b^2/4 = 0 \tag{12.7}$$

where

P_0 = applied downward load on pile top

For a given distribution $[S]$, equations (12.6) and (12.7) may be solved to obtain the displacement, ρ, and the distribution of shear-stress, p, from which the load in the pile P at any depth can be calculated.

The above basic analysis fails to take account of several factors which are likely to be important in real situations. The modifications that can be made to allow for these factors are set out below.

12.3.2 Pile-Soil Slip

The effects of pile-soil slip along the shaft can be allowed for by specifying a limiting value of shear stress, τ_a, at each element along the pile, and a limiting base pressure equal to the bearing capacity of the base. The solution must be recycled until the shear stresses and the base pressure do not exceed the limiting values (see Chapter 5). τ_a will usually be expressed in terms of effective stress by the Coulomb expression. Second, the possibility of tension between the pile tip and the soil may be overcome by specifying in the computer program that the base pressure, p_b, cannot be positive—that is if the pile is of uniform diameter, the tip separates from the soil and hence carries no load. For an enlarged base pile, compressive stresses will, however, act on the top of the enlarged portion of the base if p_b is positive. It should be noted that if full slip occurs along a pile, the load distribution in the pile will remain constant and the movement of the pile subsequent to full slip will be that occurring at the point of shear reversal.

12.3.3 Compression Failure of Pile

Allowance can be made for compression failure (see Chapter 11). If the load at a point in the pile reaches the crushing load, it can increase no further, and hence shear stresses below that point will reduce to zero and the shear stresses above that point will redistribute, with a consequent increase in pile displacement. The solution is recycled until the load in the pile nowhere exceeds the crushing strength.

12.3.4 Tension Failure of Pile

When the tensile load reaches the tensile-load capacity of the pile, the pile is assumed to fracture and in effect becomes two piles. Two equilibrium equations now apply:

1. For the upper fractured portion:

$$P_0 + \sum_{j=1}^{m} p_j \frac{\pi dL}{n} = 0 \tag{12.8}$$

where

m = number of elements in fractured portion

2. For the lower portion:

$$\sum_{j=m+1}^{n} p_j \frac{\pi dL}{n} + p_b \frac{\pi d_b^2}{4} = 0 \tag{12.9}$$

A new variable, the displacement of the fractured portion of the pile, is now introduced, so that the $n+3$ equations may now be solved for the n unknown shear stresses, the base pressure, and the displacements of the upper and lower portions of the pile.

12.3.5 Nonuniform Soil

Approximate allowance for the effect of variation of the modulus of elasticity of the soil with depth can be made by substituting the matrix $[I_s/E_s]$ for $[I_s]/E_s$ in Eq. (12.3). By this procedure, the soil displacement at a particular depth will be calculated as if the modulus at that particular

depth was also the modulus at all other depths. This approximation will clearly be unsatisfactory when the variation of modulus from top to bottom is very large or there are sudden major changes. A more satisfactory solution can be obtained by using, for E_s, the mean of the values at the influencing and influenced elements (see Section 5-2-2).

12.3.6 Variation with Time

For cases in which the soil movements are time-dependent and the variation of pile loads and displacements with time is required, a consolidation analysis may be combined with the above analysis (see Chapter 11). Alternatively, appropriate values of soil displacement S may be input at each time considered, and the solution carried out as before.

12.4 TYPICAL SOLUTIONS FOR PILE MOVEMENT AND LOAD

12.4.1 Purely Elastic Soil-Pile Interface

On the assumptions that

1. The soil is a homogeneous elastic half-space,
2. The pile-soil interface does not slip,
3. The pile is incompressible and does not fail in tension or compression,

a series of solutions have been obtained for the pile movement and the maximum load in the pile for various length-to-diameter ratios, L/d, of the pile, and a number of soil-movement profiles. In all cases, the soil movement is assumed to decrease linearly with depth from S_0 at the surface to zero at a depth z_s. Both a uniform diameter pile ($d_b/d = 1$) and a pile with an enlarged base ($d_b/d = 2$) are considered. As long as elastic conditions are preserved, the solutions are applicable for swelling or shrinking soils, except for a change in sign. In all cases, 10 elements have been used to divide the pile, and ν_s is taken as 0.3.

Pile Movement

The variation of dimensionless pile movement, ρ_p/S_0, with L/d and z_s/L, is shown in Figs. 12.3 and 12.4 for $d_b/d = 1$ and 2, respectively. These figures show that

1. The pile movement increases as the depth of swelling increases.

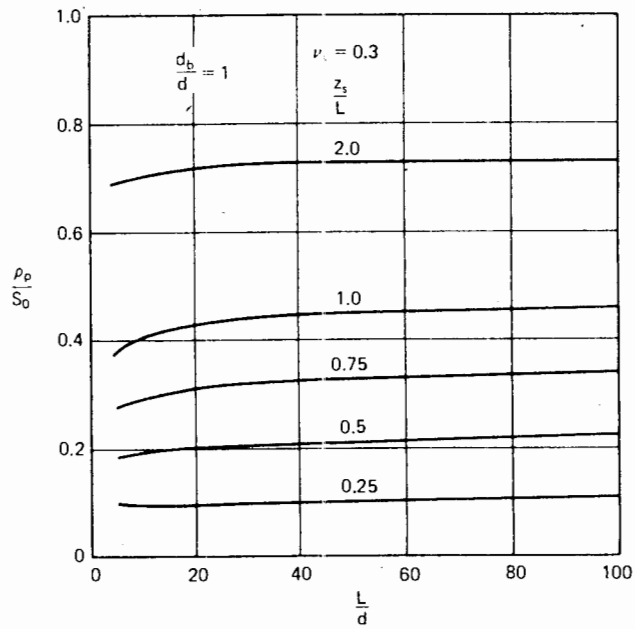

FIGURE 12.3 Elastic solutions for pile movement—uniform-diameter pile.

2. For a given movement profile, the value of L/d has relatively little effect on the pile movement, especially with uniform-diameter piles.
3. An enlarged base is only effective in reducing the pile movements when L/d is relatively small ($\leqslant 20$). The maxi-

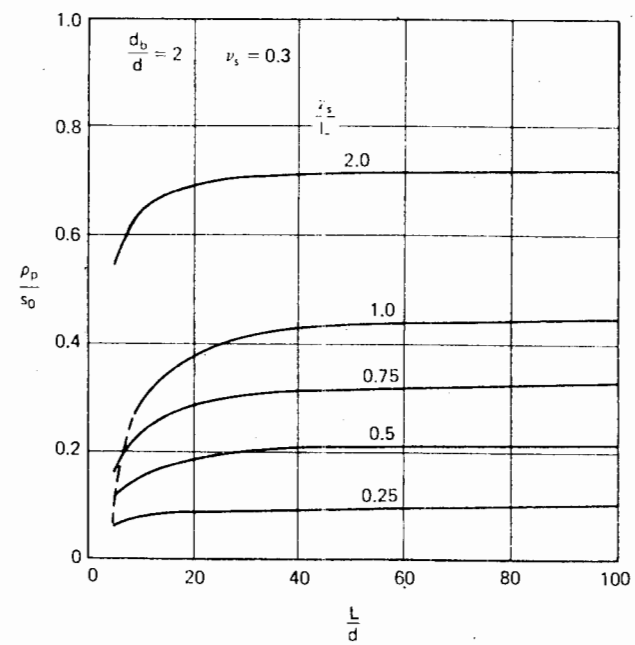

FIGURE 12.4 Elastic solutions for pile movement—pile with enlarged base.

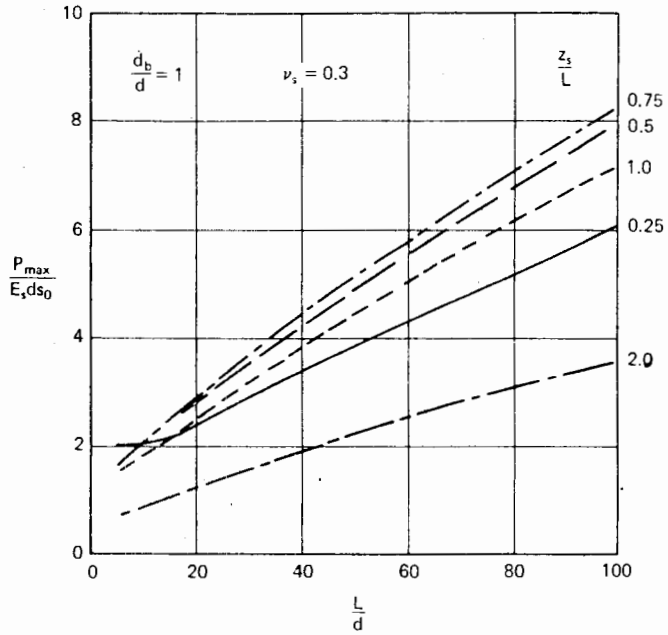

FIGURE 12.5 Elastic solutions for maximum pile load–uniform-diameter pile.

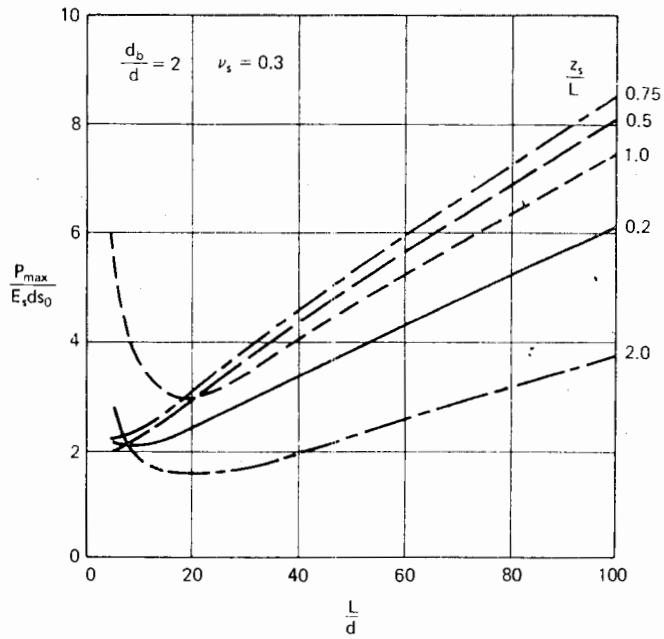

FIGURE 12.6 Elastic solutions for maximum pile load–pile with enlarged base.

mum effect is obtained when $z_s/L = 1$ that is, the pile is founded at the bottom of the zone of movement.

Maximum Pile Load

The variation of dimensionless pile load, $P_{max}/E_s d S_0$, with L/d and z_s/L, is shown in Fig. 12.5 and 12.6. An examination of these figures reveals that

1. In most cases, the largest pile load is developed when z_s/L is about 0.75.
2. The maximum pile load generally increases as L/d increases.
3. The presence of an enlarged base on relatively short piles ($L/d \leqslant 20$) results in significantly increased loads as compared with the case of a uniform-diameter pile.

12.4.2 Solutions Incorporating Pile-Soil Slip

The above elastic solutions are useful in giving an indication of the influence of pile slenderness, base diameter, and soil-movement profile on pile behavior. However, for real soils, these elastic solutions are of very limited validity, as it is found that slip between soil and pile commences at very small soil movements. In order to illustrate the influence of various factors on pile behavior, a number of solutions for relatively idealized cases are examined. When failure occurs between soil and pile or within the pile, the solutions for shrinking and swelling soils are no longer interchangeable. Attention will be focused on piles in swelling soils, although some comparisons are made between the behavior of a pile in a swelling and shrinking soil. Several of the solutions given have been presented by Poulos and Davis (1973). Negative values of pile force imply tension, while negative values of ρ_p indicate upward pile movement.

The Effect of Pile Length and Base Diameter

For a given soil profile with a linear distribution of soil swelling from S_0 at the surface to zero at a depth of $10d$, the variation of pile movement and maximum pile force with increasing soil movement is shown in Fig. 12.7 for three different pile lengths. For each length, both a uniform-diameter pile and a pile with a base diameter twice the shaft diameter are considered. The pile-soil interface shear-strength, τ_a, varies linearly from zero at the surface to $0.01E_s$ at a depth of $20d$, and the base bearing-capacity is assumed to vary from $0.36E_s$ for $L = 5d$, to $0.64E_s$ at $L = 20d$; these values correspond approximately to a soil having $\phi' = 30°$.

Figure 12.7 shows that, as would be expected, pile movement decreases as pile length increases. When the pile is entirely situated in the swelling zone ($L = 5d$), movement of the pile continues after full slip has occurred along the shaft. For piles founded below the zone of swelling, a limit-

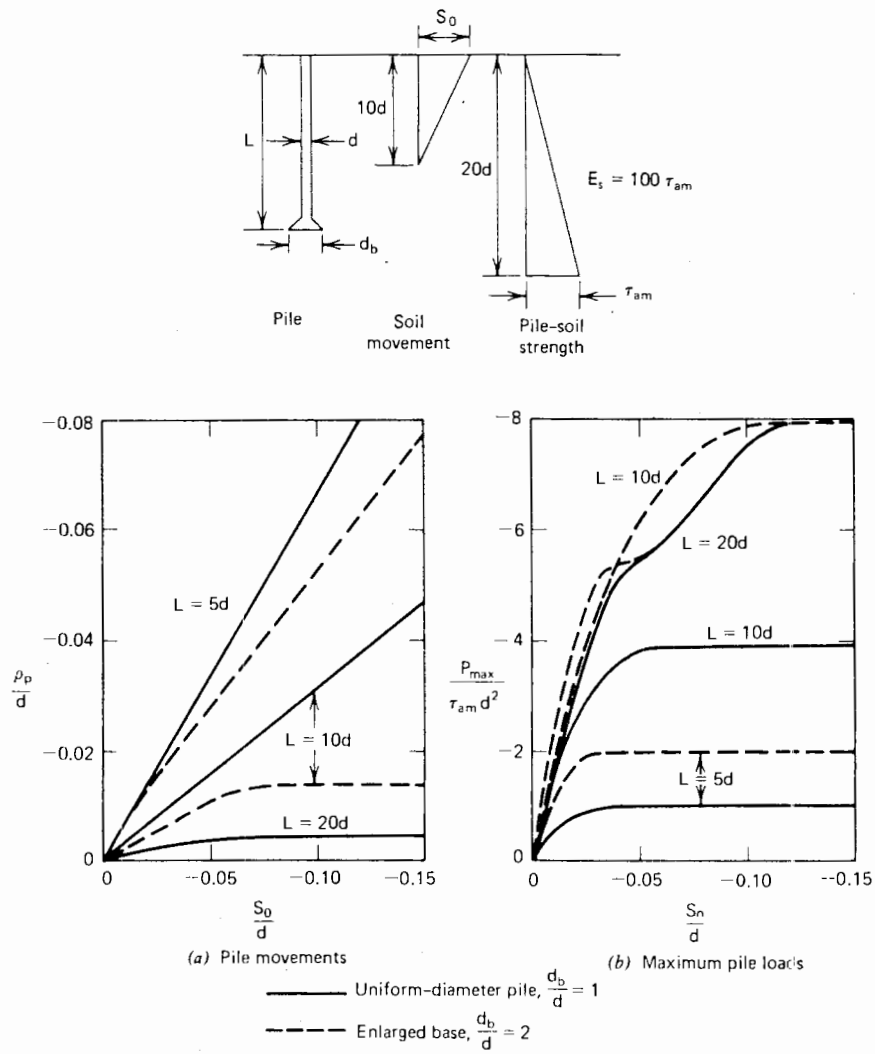

FIGURE 12.7 Effect of pile length and base diameter.

ing pile movement is reached after a certain soil movement occurs. The advantage of founding a pile below the swelling zone is obvious. The maximum tensile load in the pile generally increases markedly as the length increases; relatively small loads are developed when the pile is entirely within the swelling zone.

The presence of an enlarged base leads to a decrease in pile movement, although the effect is relatively small, especially for $L = 5d$ and $L = 20d$, or in other words, when the pile is entirely in the swelling zone, or anchored well below the swelling zone. In the latter case, the enlarged base has virtually no effect. The corresponding maximum loads are considerably greater for the enlarged base piles, except for the $L = 20d$ pile. It is therefore apparent that the enlarged base has the greatest influence when the pile is situated at or near the bottom of the swelling zone, and that the most efficient means of reducing pile movements is either to use a uniform-diameter pile founded well below the swelling zone (of length about twice the depth of this zone) or to use an underreamed pile founded at or just below the bottom of the swelling zone.

For the uniform-diameter piles considered in Fig. 12.7, the load distributions are shown in Fig. 12.8 for various values of dimensionless soil movement S_0/d. As the pile length increases, the load in the pile increases and the distribution of load also changes; the relative position of the maximum load moves toward the top of the pile. For the $L = 5d$ and $10d$ piles, slip occurs along the whole length

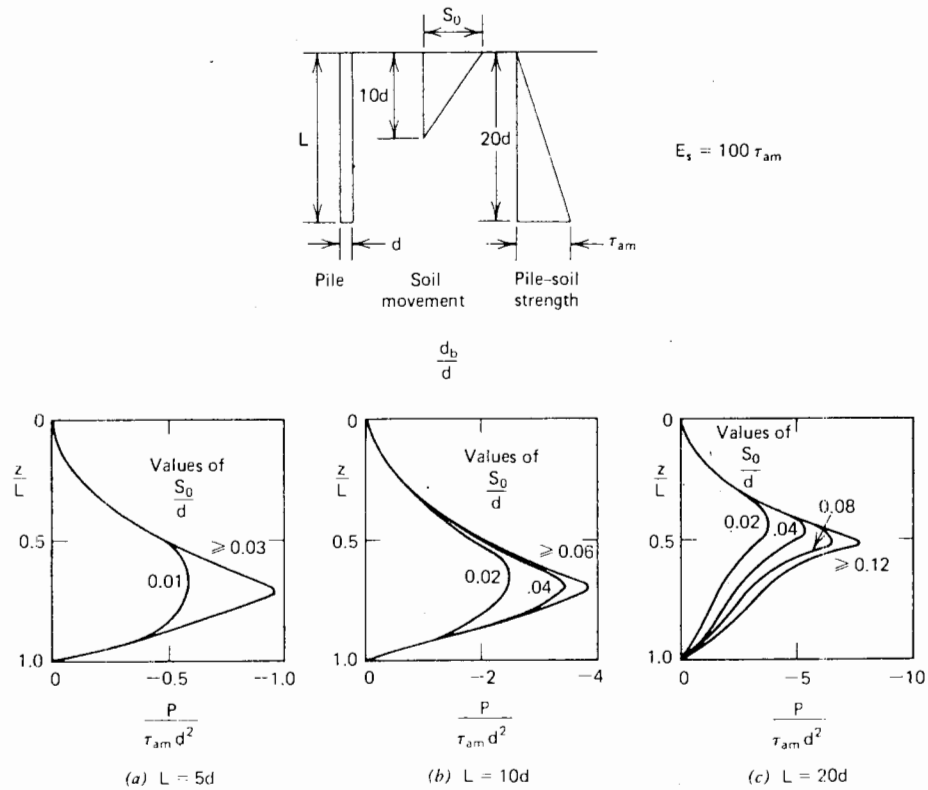

FIGURE 12.8 Typical load distributions.

of the pile at relatively small soil movements. For the $L = 20d$ pile, no change in load occurs after S_0/d reaches about 0.12, but slip only occurs along the upper half of the pile.

The Effect of Pile Shaft Diameter

For a given pile length and soil-swelling profile, the effect of pile diameter is shown in Fig. 12.9. As the diameter

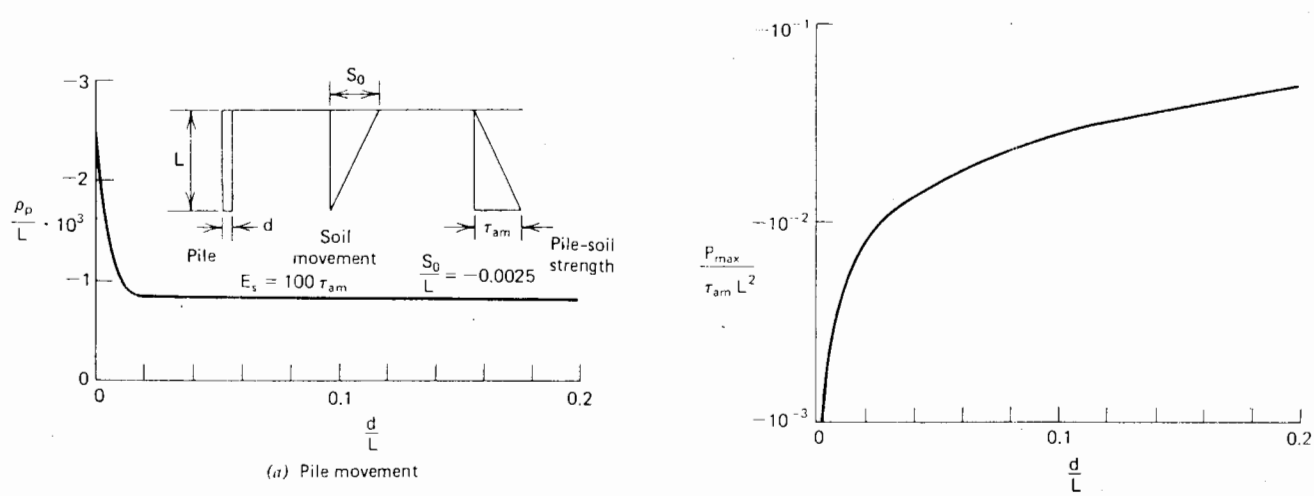

FIGURE 12.9 Influence of pile diameter.

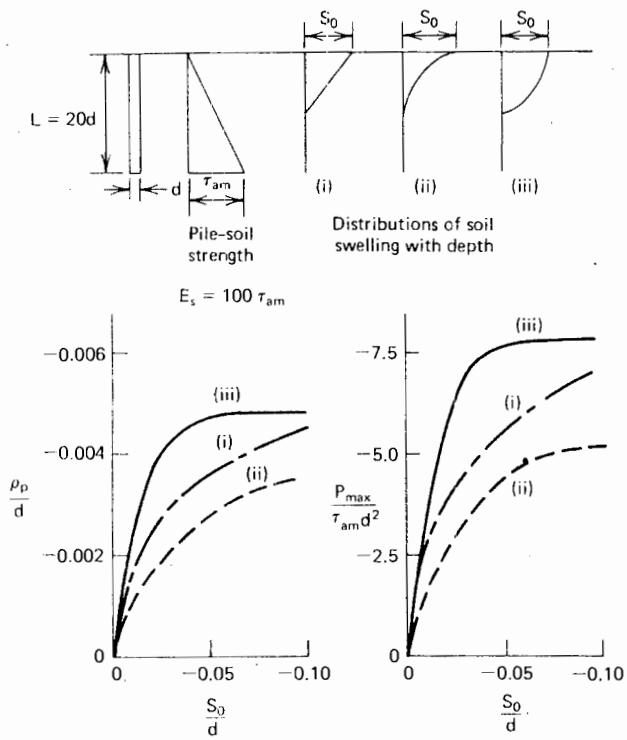

FIGURE 12.10 Influence of soil-swelling profile.

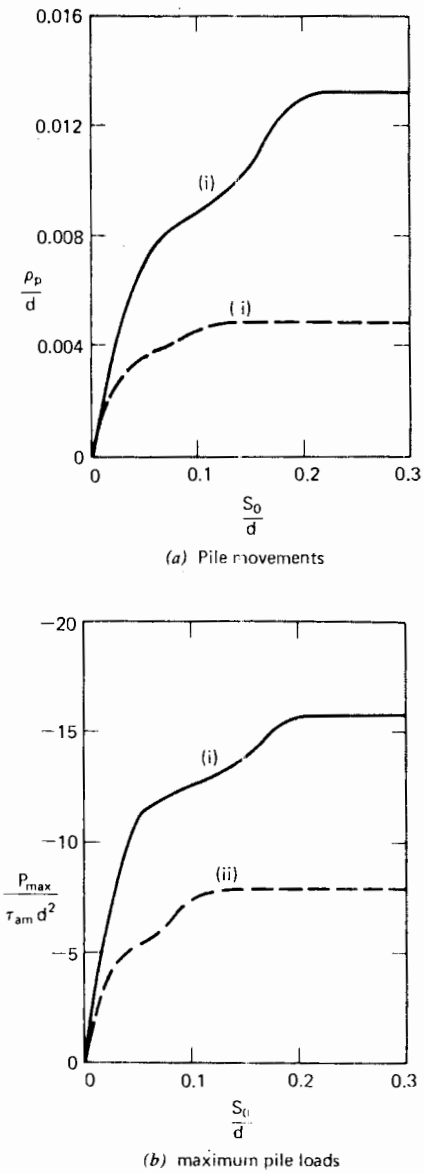

increases, pile movement decreases, but the maximum load increases. However, the rate of decrease of pile movement is almost negligible for diameters greater than about $0.03L$, and even a slender pile ($d = 0.01L$) moves only about 20% more than a relatively large-diameter pile ($d = 0.2L$). The theory therefore suggests that small-diameter piles founded well below the swelling zone can satisfactorily suppress upward movements in swelling soils. Donaldson (1967*a*), has described the successful use of small-diameter piles to support conventional brick buildings on expansive soils in South Africa.

The Effect of Distribution of Soil Movement

The effect of the shape of the soil-swelling profile for a given depth of movement is shown in Fig. 12.10. Both the pile movement and the maximum pile load are greatest when the soil movements decrease slowly with depth near the top of the pile (case 3) and least when the soil movements decrease rapidly (case 2).

The Effect of Pile-Soil Strength Distribution

The effect of the distribution of pile-soil adhesion is shown in Fig. 12.11. A 20-diameter pile with a linearly increasing

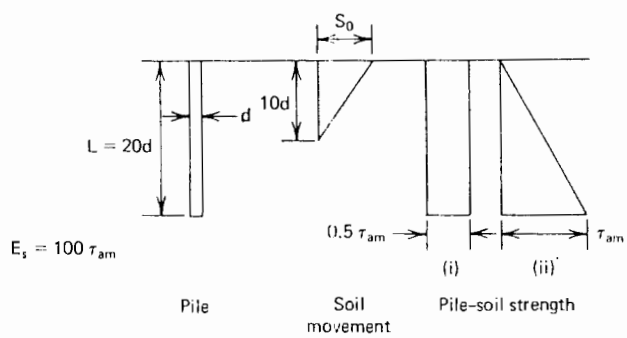

FIGURE 12.11 Effect of pile-soil strength distribution.

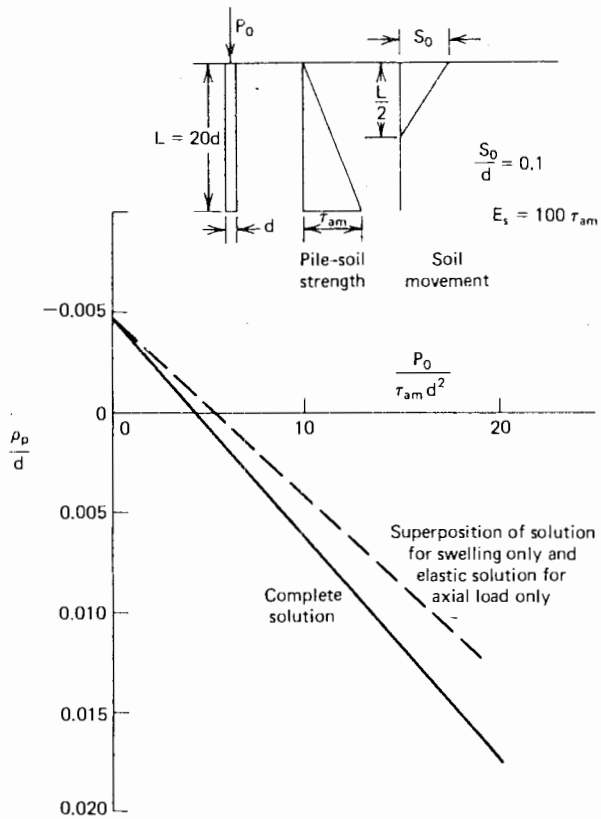

FIGURE 12.12 Effect of axial load on pile movement.

strength-distribution and a uniform strength distribution of the same average value is considered. For a given soil movement, the pile movement and maximum pile load are considerably greater for the uniform distribution.

The Effect of Axial Load

The effect of axial load on the pile movement is shown in Fig. 12.12. In the case considered, the downward movement increases almost linearly with increasing axial load. Comparison of Figs. 12.12 and 12.7 shows that the axial load required to prevent upward movement is only about half of the maximum tensile load developed in the unloaded pile. Also shown in Fig. 12.12 are the pile movements calculated on the assumption that the effects of axial load and soil swelling can be superposed. Although superposition is not strictly valid in this case, because slip occurs along part of the pile shaft, it nevertheless provides an approximate estimate of pile movement. Taking account of pile-soil slip in the solution for axial load would lead to increased movements and closer correlation with the complete solution.

12.4.3 Effect of Tensile Failure of the Pile

An example of the effect of tensile failure on pile movement is shown in Fig. 12.13, where pile movement is plotted against soil-surface movement for two tensile strengths. The pile and soil details are as shown in Fig. 12.12 except that the pile-soil interface remains elastic, that is, τ_a is large. When tensile failure occurs, the upper portion moves upward more rapidly than before failure, while the lower part, according to the analysis, suffers a small downward movement at failure and then an upward movement as the soil movement increases. As the tensile strength increases, the soil movement required to cause tensile failure also increases. Tensile failure will not occur if the tensile strength exceeds the maximum tensile load, which in this case, is $0.393E_sd^2$.

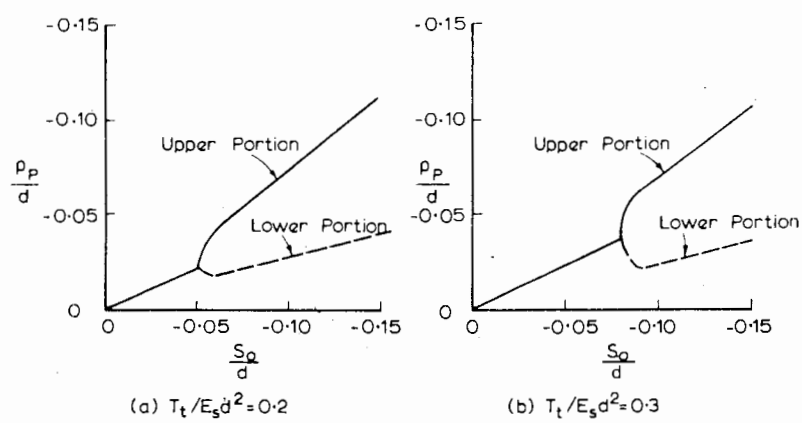

FIGURE 12.13 Effect of tensile failure of pile.

It should be noted that the accuracy of solutions in which tensile failure occurs depends to a large extent on the previous history of the pile, since once failure has occurred and the pile has separated, it remains separated. If too large an increment in soil movement is taken, the point of separation may be inaccurately computed; thus, small increments are desirable for accuracy.

12.4.4 Differences Between Piles in Swelling and Consolidating Soils

For piles in a given soil profile, the pile movement and maximum pile load are shown in Table 12.1 for both a swelling soil and a consolidating soil, for three different pile lengths. The pile movements tend to be smaller for the pile in consolidating soil, especially for the longer piles.

TABLE 12.1 DIFFERENCE BETWEEN PILE IN SWELLING AND CONSOLIDATING SOIL[a]

$S_0/d = 0.1$ $\quad \nu_S = 0.3$ $\quad \tau_a = .001E_S z/d$

L/d	d_b/d	$\frac{P_{max}}{E_S L^2}$		$\frac{\rho_p}{d}$	
		Swelling	Consolidation	Swelling	Consolidation
5	1	-0.0096	0.0173	-0.0556	0.0547
	2	-0.0196	0.0196	-0.0525	0.0509
10	1	-0.0385	0.0543	-0.0179	0.0164
	2	-0.0785	0.0785	-0.0139	0.0081
20	1	-0.0785	0.0503	-0.0048	0.0024
	2	-0.0785	0.0503	-0.0047	0.0023

[a] Soil movement decreases linearly from S_0 at surface to zero at depth $10d$.

The maximum pile load is greater for short piles in consolidating soils, but as the length is increased, the maximum load eventually becomes less than that for the same pile in a swelling soil. For uniform-diameter piles, the lower portion of the pile in a swelling soil is in tension so that no load is carried by the base, whereas in a consolidating soil, the base does carry load. The effect of the enlarged base is only significant for the $L = 10d$ pile, that is, when the pile only extends to the bottom of the zone of soil movement.

12.5 DESIGN CURVES

Dimensionless curves have been prepared to enable rapid estimates of the maximum pile load and movement for a pile in a swelling-soil profile. Both a uniform pile-soil shear strength, τ_a, and linearly increasing τ_a with depth, have been considered. These curves are shown in Figs. 12.14 and 12.15 for linearly increasing τ_a with depth, as functions of the dimensionless maximum soil-movement, $\frac{S_0 E_S}{d\tau_{am}}$ and the

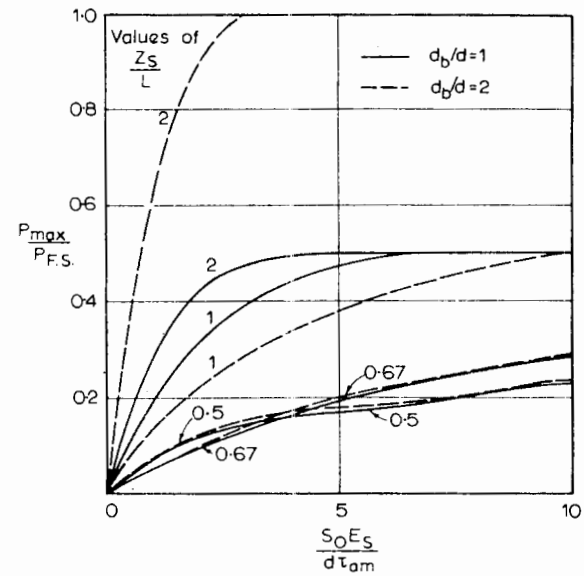

FIGURE 12.14 Maximum pile load in swelling soil. Linearly increasing pile-soil shear strength with depth.

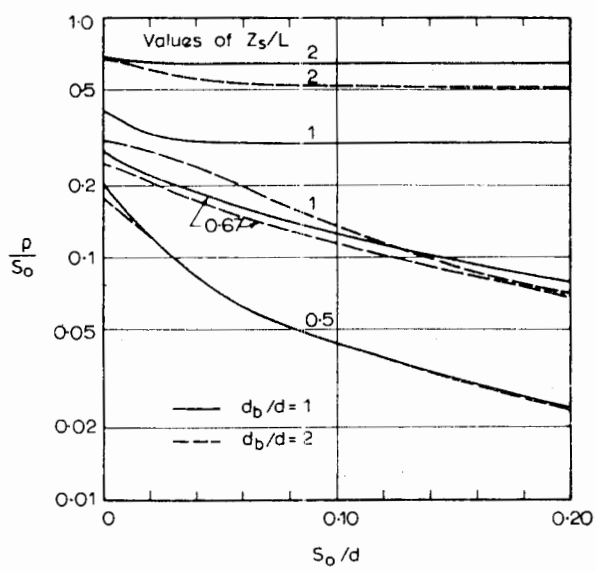

FIGURE 12.15 Pile movement in swelling soil. Linearly increasing pile-soil shear strength with depth

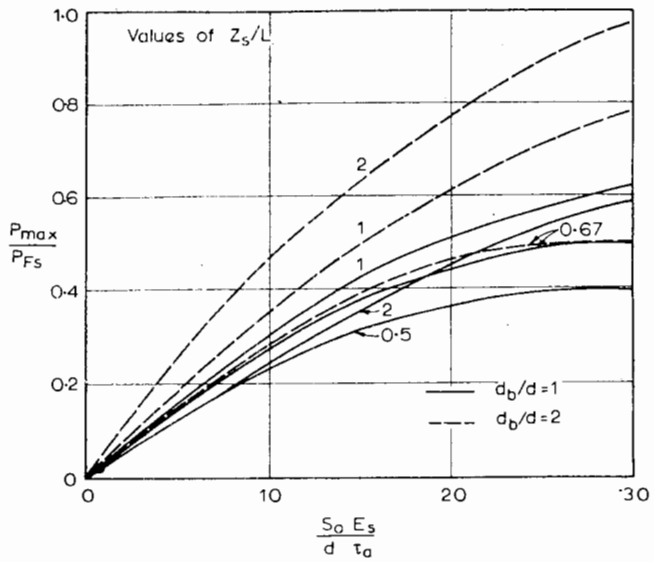

FIGURE 12.16 Maximum pile load in swelling soil. Constant pile-soil shear strength with depth.

dimensionless depth of swelling, z_s/L, and in Figs. 12.16 and 12.17 for a constant τ_a with depth. In Fig. 12.14, τ_{am} is the pile-soil adhesion at the level of the pile tip. The maximum pile load, P_{max}, is expressed as a ratio of the load P_{FS} that would occur if full adhesion was mobilized along the whole shaft, that is,

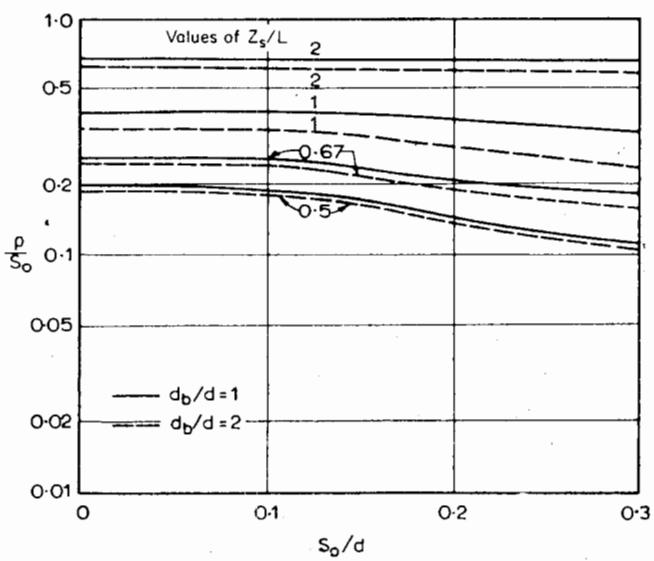

FIGURE 12.17 Pile movement in swelling soil. Constant pile soil shear strength with depth.

$$P_{FS} = \int_0^L \tau_a \pi d dz \qquad (12.10)$$

The following assumptions have been made in obtaining the curves in Figs. 12.14 to 12.17:

1. The depth of swelling is $10d$.
2. The soil movement decreases linearly with depth from S_0 at the surface to zero at a depth of z_S.

Figs. 12.3, 12.4, 12.5, 12.6, 12.10, and 12.11 provide a basis for estimating the effect of departures from the assumed conditions.

When an axial load acts simultaneously on the pile, Fig. 12.12 suggests that in the absence of a complete analysis, the effects of swelling and axial load may be superposed with sufficient accuracy, using the solutions for settlement and load distribution in an axially loaded pile given in Chapter 5. In estimating the maximum resulting load within the pile, the load distributions for axial load and swelling may be superposed. For swelling, Fig. 12.8 provides a guide to the shape of the load distribution. For axial load, Fig. 5.9 suggests that the load frequently decreases approximately linearly with depth. The proportion of load transferred to the pile base may be estimated from Eq. (5.31) or Eq. (5.32).

An example is given below to illustrate the application of the curves presented herein.

Illustrative Example

A 15-ft concrete pile, 1 ft in diameter, is situated in a soil in which the upper 10 ft is subjected to seasonal movement. The maximum soil heave is 3 in. The maximum force and the movement of the pile will be estimated for two conditions:

1. Zero axial load.
2. An axial load of 30 kips.

The following data is assumed:

E_s = 2000 lb/in.^{2} = 288 kips/ft^2 (constant with depth)
ν_s = 0.4
τ_a = 10 lb/in.^{2} = 1.44 kips/ft^2 (constant with depth)
E_p = 3 X 10^6 lb/in.^{2}

(a) Zero Axial Load

From Eq. (12.10),

$$P_{FS} = -\int_0^{15} \tau_a \pi d dz$$
$$= -1.44 \times \pi \times 1 \times 15$$
$$= -67.8 \text{ kips}$$

From Fig. 12.16, for $d_b/d = 1$, $z_s/L = 10/15 = 0.67$ and $\left(\frac{S_0}{d}\right)\left(\frac{E_s}{\tau_a}\right) = 50$,

$$\frac{P_{\max}}{P_{FS}} = 0.5$$

$$\therefore P_{\max} = -33.9 \text{ kips}$$

From Fig. 12.17, $\rho/S_0 = 0.19$; that is, $\rho = 0.57$ in. (upward)

(b) With Axial Load of 30 kips

From Eq. (5.31), proportion of applied axial load transferred to base is

$$\beta = \beta_0 C_K C_v$$

Here

$$K = \frac{3 \times 10^6}{2000} = 1500 \text{ and } L/d = 15.$$

From Figs. 5.9, 5.10, and 5.11,

$$\beta_0 = 0.085, C_K = 0.97, C_v = 0.95$$
$$\therefore \beta = 0.078$$

or,

$$\text{base load} = 0.078 \times 30 = 2.3 \text{ kips}$$

Assuming, for simplicity, a linear load distribution with depth, the load at any depth may be calculated.

By inspection of Fig. 12.8, the maximum tensile force caused by swelling occurs at a depth of about $0.6L$, or 9 ft. At this level, the axial force caused by the applied loading is about 13.6 kips. Thus, a net tensile force of (33.9 - 13.6) = 20.3 kips occurs at this point (the maximum tensile force does not necessarily occur at this point; however, in this case, within the limits of interpolation, the maximum tensile force occurs at or very near this point).

Considering now the axial movement caused by the applied loading, from Eq. (5.33),

$$\rho = \frac{P}{dE_s} I$$

For the parameters of this problem, from Figs. 5.18 to 5.21, $I = 0.107$ and

$$\rho = \frac{30{,}000}{12 \times 2000} \times 0.107$$
$$= 0.13 \text{ in. (downward)}$$

Thus, the net movement caused by axial load and swelling is 0.13 - 0.57 = -0.44 in. (i.e., net upward movement)

12.6 APPLICATION OF THEORETICAL ANALYSIS TO PRACTICAL PROBLEMS

In applying the theoretical analysis described in the previous section to practical problems, estimates are required of the following quantities:

1. The soil-movement profile.
2. The pile-soil interface strength.
3. The soil modulus.

12.6.1 Prediction of Soil-Movement Profile

Two cases may be considered:

1. Movements in saturated soils.
2. Movements in unsaturated soils.

The first case applies to many problems involving consolidating soils, and soil movements may be predicted at various depths by conventional methods of settlement analysis.

Unsaturated soils are frequently encountered in relatively arid regions and the prediction of movements caused by seasonal moisture changes is often necessary. Methods for prediction of such movements are however not as well established as for saturated soils. Existing methods may be divided into five categories:

1. Methods based on free swell. In cases where it can be assumed that the soil has free access to water, the magnitude of heave may be estimated from experimental data relating swelling pressure to volume change and applied surcharge loading. If the initial water content is known, and the distribution of vertical pressure with depth is known, the amount of heave may be determined for various depths in the soil.
2. Methods based on effective-stress concepts. One such method, described by Blight (1965), relies on the validity of the effective-stress law for unsaturated soils and the χ factor; some dispute about this validity exists. Variations of

pore suction resulting from moisture changes can be estimated by finite-difference solution of the diffusion equation for moisture movement in unsaturated soils (Richards, 1965). Alternatively, an approximate solution may be obtained from the solution for classical one-dimensional consolidation, using a value of the coefficient of swell appropriate to the average suction in the soil profile during the heave process (Blight, 1965).

3. Methods based on the specific-volume versus moisture-content relationship. This approach has been developed by De Bruijn (1961) and relates the specific volume, v, of a soil element (the volume per unit mass of grains) to the moisture content, m. From such a relationship, the volume strain at depth for a given moisture content change may be calculated, whereby the resulting soil movement may be determined.

4. Methods based on a laboratory simulation of the anticipated moisture history of elements of soil and the measurement of the consequent strains (Aitchison and Woodburn, 1969).

5. Empirical methods. Because of the difficulties in application of some of the above methods, some empirical methods have been developed to estimate soil heave in swelling soils. One such method is suggested by Van der Merwe (1964), in which the total heave of a soil profile extending to a depth of h feet is given by:

$$S = \int_{z_2}^{z_1} F \cdot (PE) dz \qquad (12.11)$$

where

F = factor indicating the relative decrease in heave at depth z to that at surface
PE = potential expansiveness
z_1, z_2 = depth to bottom and top of expansive layer ($h = z_1 - z_2$)

TABLE 12.2 VALUES OF POTENTIAL EXPANSIVENESS (VAN DER MERWE, 1964)

Degree of Expansiveness	*PE* in./ft of soil
Very high	1
High	0.5
Medium	0.25
Low	0

F is given by

$$F = e^{z/k} \qquad (12.12)$$

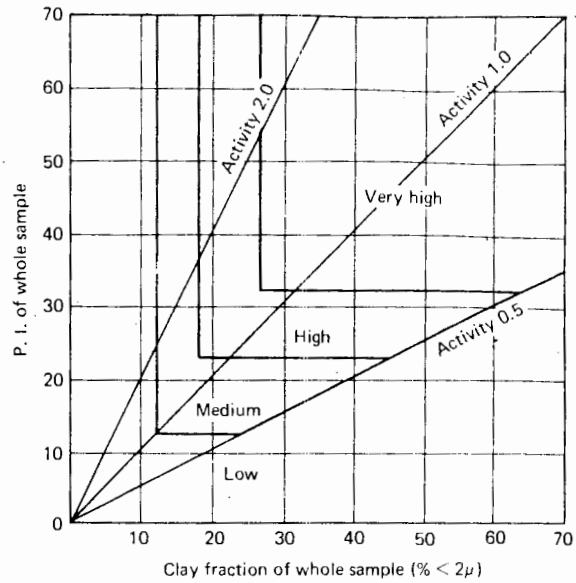

FIGURE 12.18 Determination of potential expansiveness of soils (after Van der Merwe, 1964).

where k is a reference depth indicating the virtual end of the swelling zone; a value of 20 ft for two sites in South Africa was suggested by Van der Merwe.

The potential expansiveness, PE, was related to the clay fraction and the plasticity index of the soil, and a classification into very high, high, medium, and low degrees of expansiveness is shown in Fig. 12.18. Van der Merwe suggests the values of PE shown in Table 12.2.

12.6.2 Pile-Soil Interface Strength

It is commonly assumed that the shear strength between soil and pile increases with depth, approximately in proportion to the overburden pressure. In situations where the soil is normally consolidated and is going to remain saturated (zero air voids but not necessarily positive pore water pressure), the limited experience from measurement of negative friction on piles in soft, normally consolidated clays (see Chapter 11, Fig. 11.25) may be taken to be reasonably applicable to the case when the pile is affected by shrinking or consolidation of the soil. This experience suggests that, in the equation

$$\tau_a = c'_a + K_s \sigma'_v \tan \phi'_a \qquad (12.13)$$

where

c'_a = adhesion

ϕ'_a = effective pile-soil friction angle
σ'_v = effective overburden stress
K_s = a coefficient of horizontal earth pressure

the combined term $K_s \tan \phi'_a$ usually lies within the range 0.2 to 0.3, and that c'_a can be neglected. For $\phi'_a \approx 20$, this corresponds to a range in K_s of 0.5 to 0.8, or somewhat greater than the coefficient of earth pressure at rest, K_0.

For swelling situations, especially when swelling occurs under relatively arid conditions, the soil must be in an overconsolidated state, and corresponding to the higher values of K_0 for overconsolidated soils, a higher value of K_s may be expected. South African experience (Collins, 1953; Baikoff and Burke, 1965; Donaldson, 1967*b*) appears to suggest in such situations a range in K_s of 1.0 to 1.5. The cohesion term also is not necessarily negligible. For soils swelling from an initially unsaturated condition, the effective-stress concept is of doubtful validity, and as a practical approach, it may be better to use the total instead of the effective overburden stress in Eq. (12.13) and appropriately determined values of adhesion and pile-soil friction angle. For example, Collins (1953) recommends the use of a value

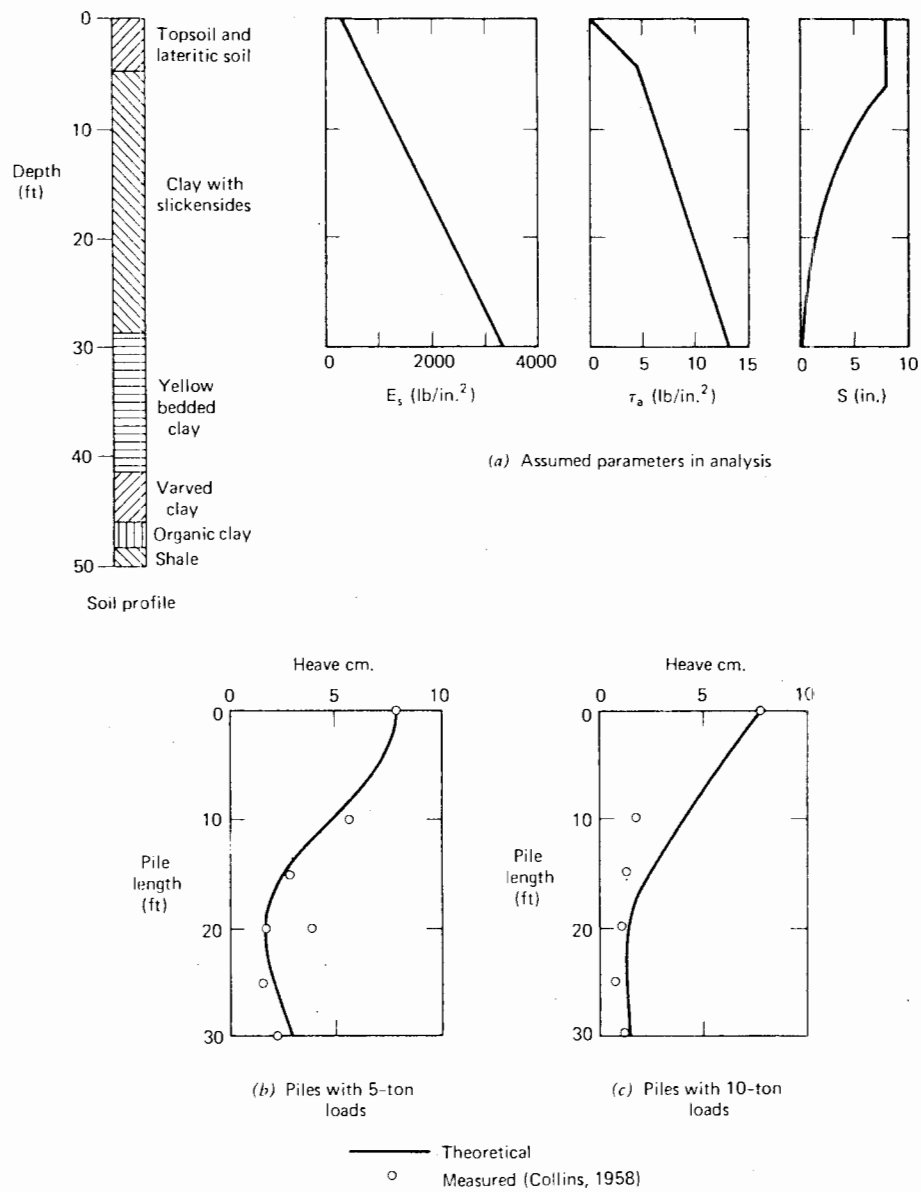

FIGURE 12.19 Comparisons between measured and predicted pile movements.

of K_s = 1 with the drained shear-strength parameters of the soil, while Donaldson (1967*b*) suggests the use of the drained shear-strength multiplied by a factor ranging from 0.3 to 0.7. If the soil is severely cracked before swelling starts, the high values of K_s given above may not be attained in the earlier stages of swelling, but for design purposes, it would be unwise to rely on the reduction in upward force on the pile this implies.

12.6.3 Soil Modulus

The most satisfactory means of estimation is to backfigure E_s from a pile-load test in-situ, using the theoretical solutions for an axially loaded pile. If such a load test is not possible, a rough estimate may be made by using the correlations between E_s and the undrained cohesion, c_u, of the clay in Fig. 5.42. The value of c_u should be that appropriate to the final moisture content of the soil. Alternatively, a very rough estimate of E_s may be made from the value of m_v obtained from an oedometer over an appropriate range of stress and moisture content, using Eq. (11.23) and an estimated value of ν_s.

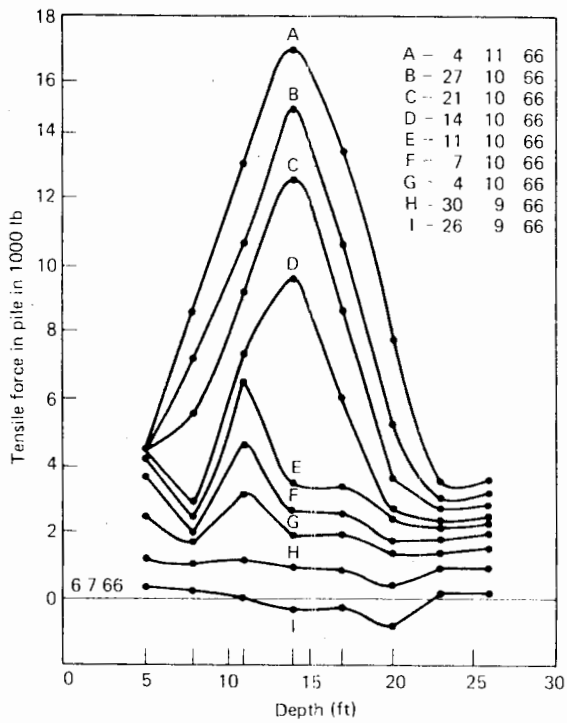

FIGURE 12.20 Tensile forces measured in a pile during accelerated heaving test (Donaldson, 1967).

12.7 OBSERVATIONS OF PILE BEHAVIOR AND COMPARISONS WITH THEORY

Collins (1958) presented an extensive series of observations on the movements of 37 houses founded on expansive soils, with 24 of these houses being founded on underreamed piles. The houses were on two sites, Leeuhof in the Transvaal, and Odendaalrus in the Orange Free State. A typical soil-profile for the Leeuhof site is shown in Fig. 12.19. Undrained and drained strengths of this profile have been reported by Collins (1953). The measured soil-heave at various depths, to June 1956, is given in Table 12.3.

TABLE 12.3 SOIL HEAVE VS. DEPTH (COLLINS, 1958)

Depth of point (ft)	Heave (cm)	Soil Layer (ft)	Expansion of Soil Layer	
			cm	Percent of 7.9 cm
6	7.9	6–12	4.0	51
12	3.9	12–18	2.6	33
18	1.3	18–24	0.4	5
24	0.9	Below 24	0.9	11

The houses were divided into two groups—one in which the average load per pile was 5 tons, and the other in which the average load was 10 tons—and each house was founded on piles taken to a specific depth. It is interesting to note that the houses on piles founded at a 30-ft depth showed a greater movement than those at a 20- or 25-ft depth. It was subsequently found that the 30-ft piles had failed in tension. Considerably smaller movements were experienced with the piles carrying 10-ton loads.

The measurements at the Odendaalrus site were more variable, although they showed a tendecy for movements to decrease with increasing pile depth.

Theoretical predictions of the behavior of the piles at Leeuhof were made using the measured soil-profile, and as previously described, using the drained strengths to estimate the pile-soil adhesion and the undrained strength to estimate the soil modulus. A summary of the measured and predicted pile movements is shown in Fig. 12.19, together with the chosen parameters for the analysis. The agreement is good for the piles with 5 tons, but for the 10 ton loads, the theory somewhat overestimates the heave. It is significant to note that the theory predicts that tensile failure occurs for the 30-ft piles, resulting in larger pile movements. This prediction is substantiated by the observations.

Donaldson (1967b)

An instrumented test pile was installed at Leeuhof, South Africa, and the development of tensile force with time was measured. The pile was a 9-in-diameter concrete pile, 34 ft long, with a central steel-pipe core containing strain gauges and acting also as tensile reinforcement. Heave of the soil around the pile was accelerated by filling, with water, four holes of 4-in diameter, drilled to depths of 15 ft at a 3-ft radius from the pile—hence flooding the site.

The measured tensile forces at various dates are shown in Fig. 12.20. The increase in tensile force with time as the heave increases is clearly seen. At the latest date shown in Fig. 12.20, the average heave of points at 1-ft radius was 9 mm, and at 5-ft radius, 5.5 mm.

A theoretical calculation was carried out for the latest load distribution in the test pile, using soil data similar to that used for Collin's tests. The soil-surface movement remote from the pile was assumed to be 9 mm. A comparison between the theoretical and measured load distribution is shown in Fig. 12.21. Within the obvious limitations imposed by the uncertain soil data, the agreement is satisfactory.

Other measurements of pile behavior in swelling soils have been reported by Doroshkevich and Boim (1967), who examined the effect of axial load on pile uplift, and Newland (1968), who reported movements of a building founded on piers in expansive clay. However, in neither case are sufficient data reported for theoretical calculations to be made and compared with measurements.

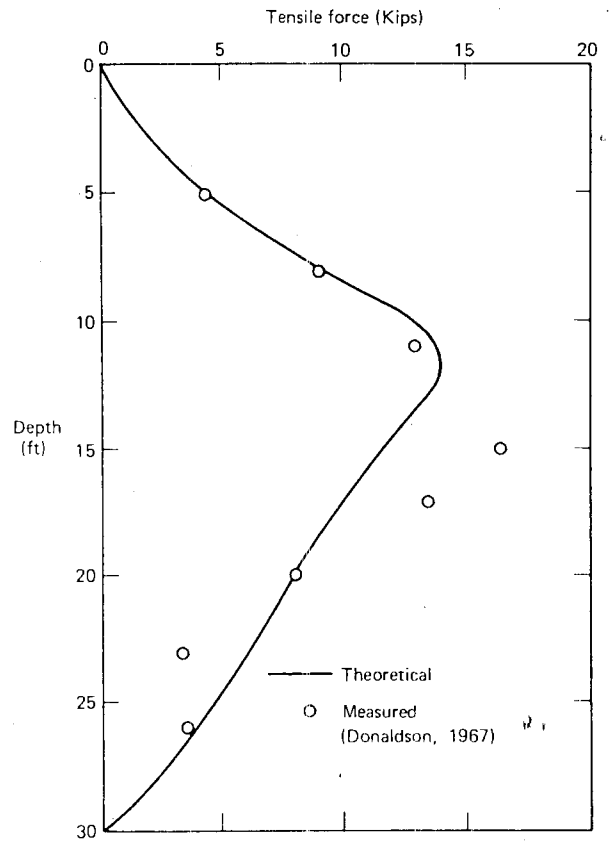

FIGURE 12.21 Comparison between measured and predicted force in pile.

13

PILES IN SOIL UNDERGOING LATERAL MOVEMENT

13.1 INTRODUCTION

When piles are situated in a soft soil layer that is subjected to horizontal movement, horizontal pressures are developed between the pile and the soil, with a consequent development of bending moments and deflections in the piles This phenomenon is the lateral-load analogue of the phenomenon of "negative friction" developed in piles by vertical movement of the surrounding soil. A number of instrumented field cases has been reported–for example, Franx and Boonstra (1948), Heyman and Boersma (1961), Heyman (1965), Leussink and Wenz (1969) and Nicu et al. (1971) (a summary of these and other cases was made by Marche and Lacroix, 1972). In most of the above-mentioned cases, the piles have been in bridge abutments where the horizontal displacements of the soil arose from the construction of an embankment at the soil surface. Leussink and Wenz (1969) have described a test on a pile near an ore-storage embankment in which horizontal movements were sufficiently large to cause structural failure of the pile.

From an examination of case records, Marche and Lacroix (1972) attempted to relate the ratio of the horizontal displacement of a pile to the embankment settlement with the relative flexibility of the pile (Fig. 13.1), and found that this ratio increases with increasing pile-flexibility. De Beer and Wallays (1972) have described a relatively simple method of determining bending moments and forces in a pile when an unsymmetrical surcharge is placed around the pile. Ito and Matsui (1975) have developed a theoretical analysis for the forces in a row of piles in soil undergoing plastic deformation.

A theoretical analysis of the problem of a single pile in a soil subjected to lateral soil movement has been given by Poulos (1973*b*) and is described below. This analysis is an extension of analyses previously described for laterally loaded piles in Chapter 8, in which both elastic behavior and lateral yield of the soil at the soil-pile interface are taken into account. It should be emphasized, however, that the principle of the analysis described herein may equally well be applied to other representations of soil behavior–for example, the subgrade-reaction model. A quantitative

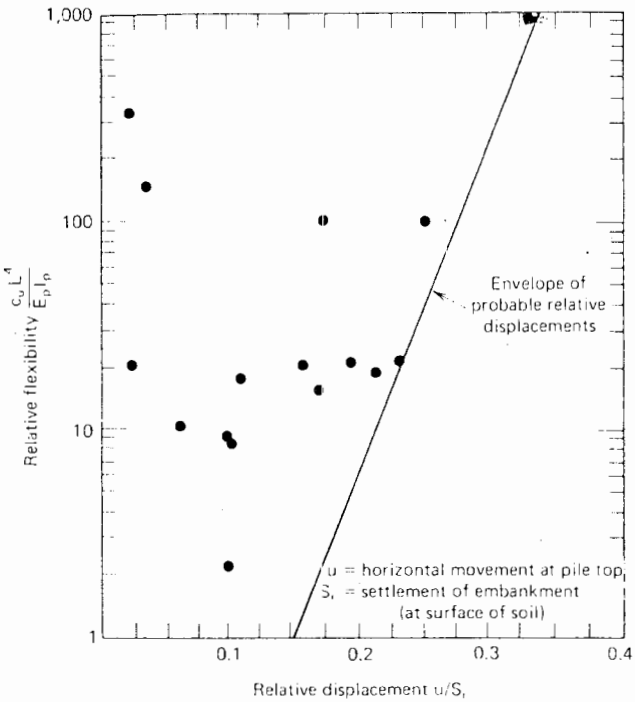

FIGURE 13.1 Relative displacement as a function of relative flexibility (after Marche and Lacroix, 1972). (Reproduced by permission of the National Research Council of Canada, from the *Canadian Geotechnical Journal*, vol. 9, 1972, pp. 1–24.)

examination will be made of some of the factors influencing the development of pile moments and displacements, and some comments are made regarding values of soil parameters required as input for practical problems. A number of comparisons are then described between observed pile behavior and that given by the theory.

13.2 ANALYSIS

The pile is assumed to be a thin vertical strip of width d, length L, and constant flexibility $E_p I_p$, and divided into $n + 1$ elements, all elements being of equal length δ, except those at the top and tip, which are of length $\delta/2$ (Fig. 13.2). The soil in the basic analysis is assumed to be an ideal, isotropic, elastic material, having a Young's modulus (E_s) and Poisson's ratio (ν_s) that are unaffected by the presence of the pile. The stresses developed between the pile and the soil are assumed to act normal to the face of the pile, and no account is taken of possible shear stresses developed between the soil and the sides of the pile.

In order to better approximate real soil behavior, it is assumed that the Young's modulus, E_s, may vary along the pile and that the horizontal pressure between pile and soil (i.e., the difference between the soil pressures on the opposite faces of the pile) has a limiting value, p_y, that may also vary along the pile.

A solution to the problem is obtained by imposing displacement compatibility between the pile and the adjacent soil. The pile displacements are obtained from the equation of flexure of a thin strip. By writing this equation in finite-difference form for each node point along the pile, the pile displacements may be expressed as

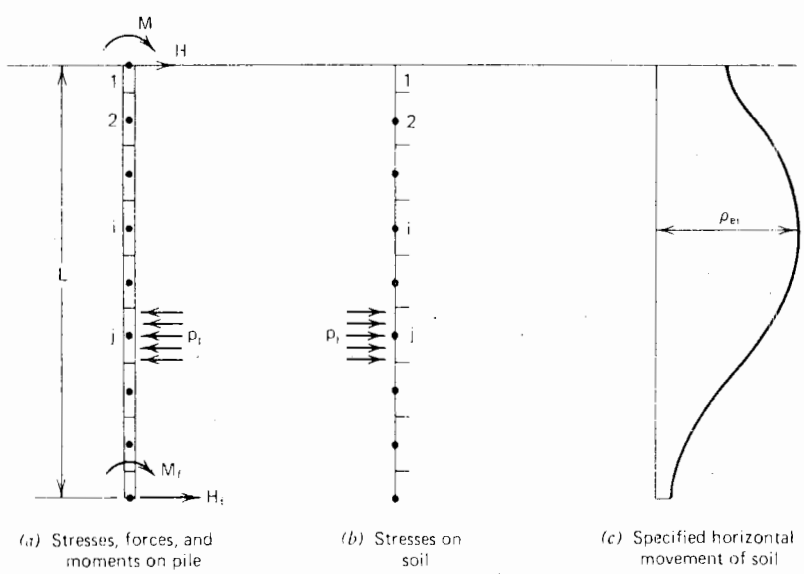

FIGURE 13.2 Piles in soil undergoing lateral movement. The problem.

$$[D]\{\rho\} = -\frac{dL^4}{E_p I_p}\{p\} \tag{13.1}$$

where

$\{\rho\}$ = pile-displacement vector
$\{p\}$ = horizontal-pressure vector
$[D]$ = matrix of finite-difference coefficients

The soil displacements arise both from the external source of movement (e.g., an embankment) and the pressures caused by pile-soil interaction, and may be expressed as

$$\{\rho\} = \frac{d}{E_{sr}}\left\{\frac{E_{sr}}{E_s}\right\}[I]\{p\} + \{\rho_e\} \tag{13.2}$$

where

E_{sr} = a reference value of soil modulus
E_s = soil modulus at a node point
$\left\{\frac{E_{sr}}{E_s}\right\}$ = vector of values of $\frac{E_{sr}}{E_s}$
$[I]$ = matrix of soil-displacement factors
$\{\rho_e\}$ = vector of external soil displacements

The elements of $[I]$ may be evaluated from the Mindlin equation for horizontal displacement caused by horizontal load within a semi-infinite mass. If the soil is underlain by a rigid base, approximate allowance for the reduction in displacement may be made by the approach described in Chapter 8. The consideration of a nonuniform soil modulus by introduction of the $\{E_{sr}/E_s\}$ vector is only approximate, as the Mindlin equation is strictly only applicable to a homogeneous soil (in effect, it is assumed that the stress distribution in a nonhomogeneous mass is the same as that in a homogeneous soil).

While the soil remains elastic, Eqs. (13.1) and (13.2) yield the following equation when soil and pile displacements are equated:

$$\left[D + \frac{II}{K_R n^4}\right]\{\rho\} = \frac{[II]}{K_R n^4}\{\rho_e\} \tag{13.3}$$

where

$[II] = [I]^{-1}$, the inverted soil-displacement-factor matrix
$K_R = \frac{E_p I_p}{E_s L^4}$ = pile-flexibility factor

In addition to the above equations, the horizontal-load and moment-equilibrium equations may be written in terms of displacements together with the appropriate boundary conditions at the head and tip of the pile. To allow for the possibility of restraint or external loading at the top and tip of the pile, top and tip horizontal forces are introduced as unknowns in the system of equations. Moments at the top and tip, however, may be readily expressed in terms of the displacements.

By solving the complete system of equations, the displacements may be determined whereby the horizontal pressures may be evaluated from Eq. (13.1) or Eq. (13.2). These pressures may now be compared with the specified soil-yield pressures along the pile. At elements where the computed pressure exceeds the yield pressure, the displacement-compatibility equation for that element, from Eq. (13.3), is replaced by the beam equation for that element, from Eq. (13.1), with the pressure, p, set to the yield pressure, p_y. The solution is recycled until the computed pressures do not exceed the yield values. From the displacements and pressures thus computed, the slope, moment, and shear-force distribution along the pile may be calculated. If desired, the above analysis may further be modified to allow for possible pile-soil separation along the upper portion of the shaft, and for plastic bending of the pile.

Extension to the case of a pile group is also possible with the soil-displacement influence matrix I including the contributions of surrounding piles. However, a major problem with such an analysis at present is in determining how group effects influence the value of yield pressure, p_y. (This subject has been discussed in Chapter 7.).

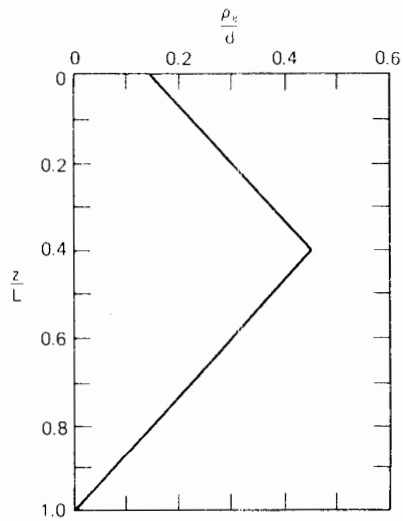

FIGURE 13.3 "Standard" soil-movement profile for theoretical solutions.

13.3 TYPICAL RESULTS

In order to examine the effect of various factors on pile behavior, a number of solutions have been obtained for idealized cases. Simple distributions of horizontal movements with depth in the soil mass in the vicinity of the pile are assumed (Figs. 13.3 and 13.7). Actual distributions can usually be approximated in this way. The distributions of E_s and p_y along the pile are taken to be either constant or linearly increasing with depth. Twenty-one elements have been used to divide the pile.

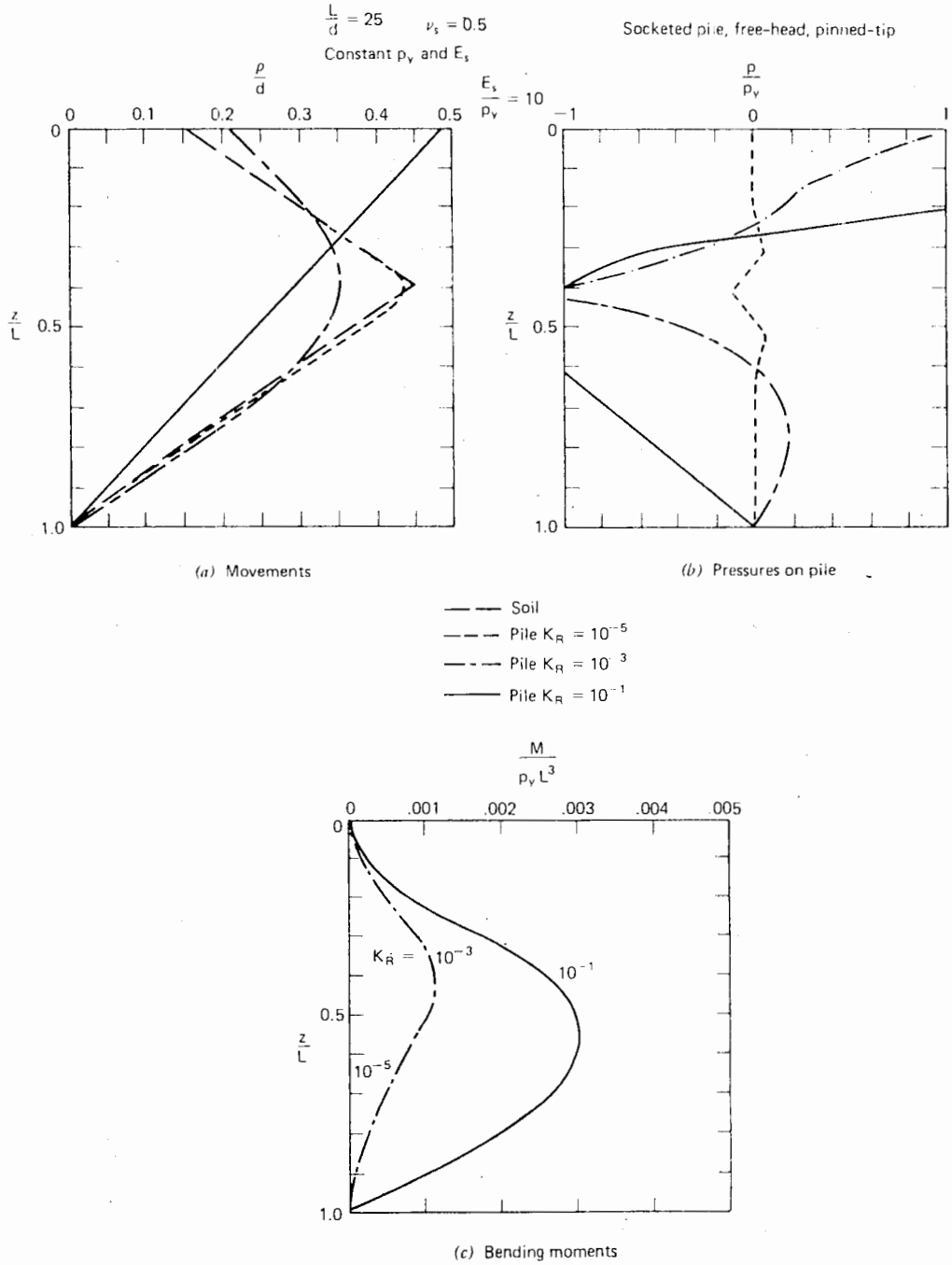

FIGURE 13.4 Effect of relative pile stiffness–free-head pile.

13.3.1 Effect of Relative Pile Flexibility

For a free-head, pinned-tip socketed pile in a soil having constant modulus E_s and yield pressure p_y, and subjected to the "standard" external soil movements (Fig. 13.3), the distributions of pile movement, pressure, and bending-moment are shown in Fig. 13.4 for three values of K_R, 10^{-5} (a very flexible pile), 10^{-3} (a pile of medium flexibility), and 10^{-1} (a relatively stiff pile). For the very flexible pile, the pile displacement follows the soil displacement almost exactly, and in consequence, small pressures and moments are developed. As the pile becomes stiffer, pressures and moments increase and the pile-movement distribution changes. It is interesting to note

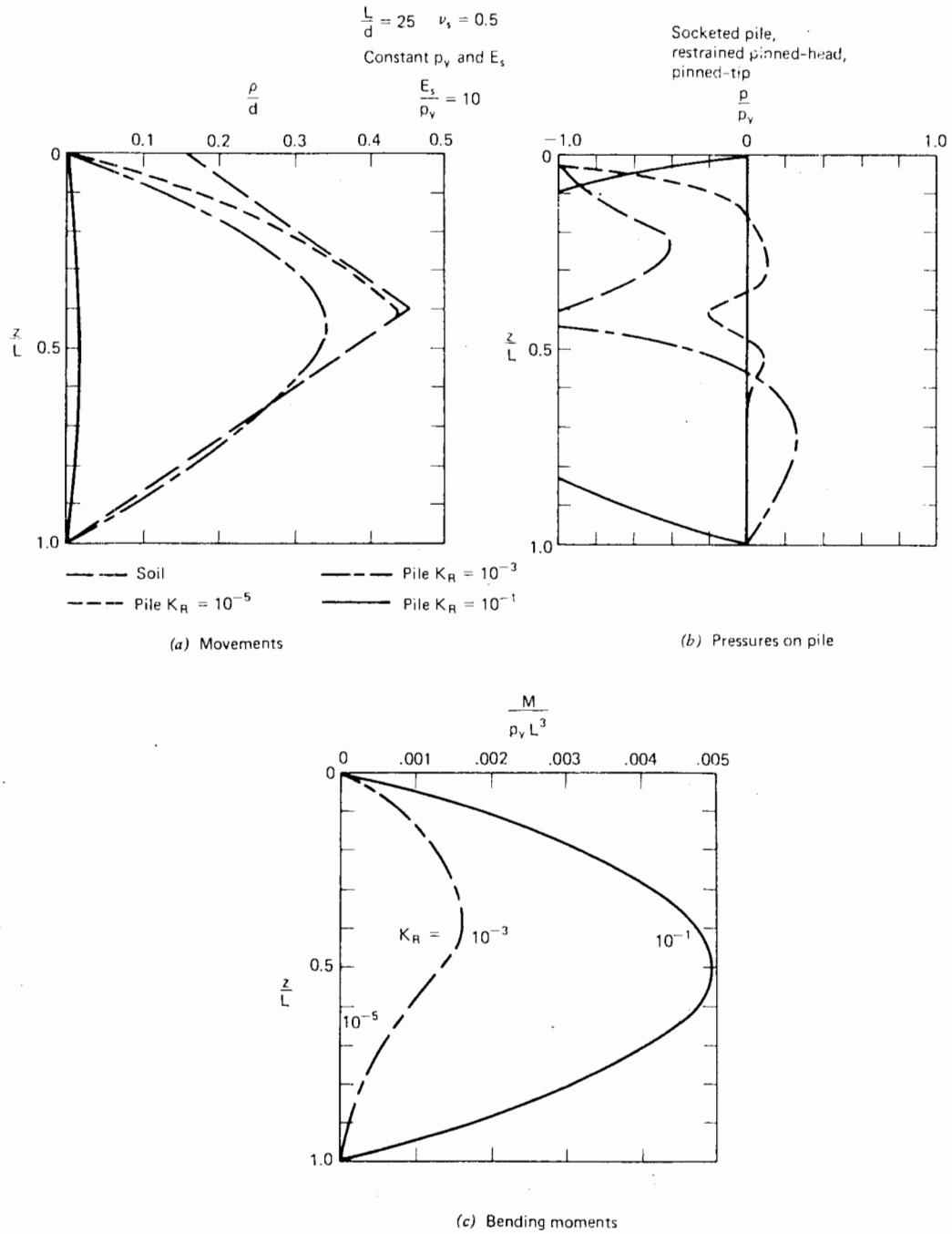

FIGURE 13.5 Effect of relative pile stiffness—restrained-head pile.

that in this case, where no head restraint is provided, the movement of the top of a stiff pile is substantially greater than the surface soil movement, so that it is an advantage in this case to have a more flexible pile.

Corresponding distributions of movement, pressure, and moment for a pile with a fully-restrained pinned head are shown in Fig. 13.5. In this case, increasing the pile stiffness reduces the subsurface movements of the pile, but leads to generally greater pressures and moments than in an unrestrained pile, as well as to a relatively large restraining force at the head.

13.3.2 Effect of Boundary Conditions

An example of the effect of head and tip boundary-counditions is shown in Fig. 13.6 for a pile of medium flexibility ($K_R = 10^{-3}$) subjected to the standard soil-movement profile. As previously indicated, the provision of head restraint reduces the pile movements near the surface, but also increases the moment. The provision of tip fixity, in this case, has virtually no effect on pile movements except near the tip, where a relatively large moment is developed.

13.3.3 Effect of Soil-Movement Distribution

For the same pile as that considered in Fig. 13.6, with an unrestrained pinned head and a inned tip, movement and moment distributions for three soil-movement profiles are shown in Fig. 13.7. In all three cases, the maximum movement is the same. For relatively flexible piles, such as those considered here, the head movement is largely dependent on the magnitude of the soil surface movement. The maximum moment in the pile is greatest for the uniform soil-movement profile. The moments tend to decrease as the soil-movement profile tends to a triangular distribution with zero movement at the base of the layer and maximum movement at the top of the layer; in the latter case, the pile and soil movements are identical, if the pile is pinned at the tip and unrestrained at top, and no moments are developed in the pile.

13.3.4 Effect of Magnitude of Soil Movement

Fig. 13.8 shows the variation in displacement and moment distributions along a free-head socketed pile with increasing magnitude of soil movement. In this case, conditions re-

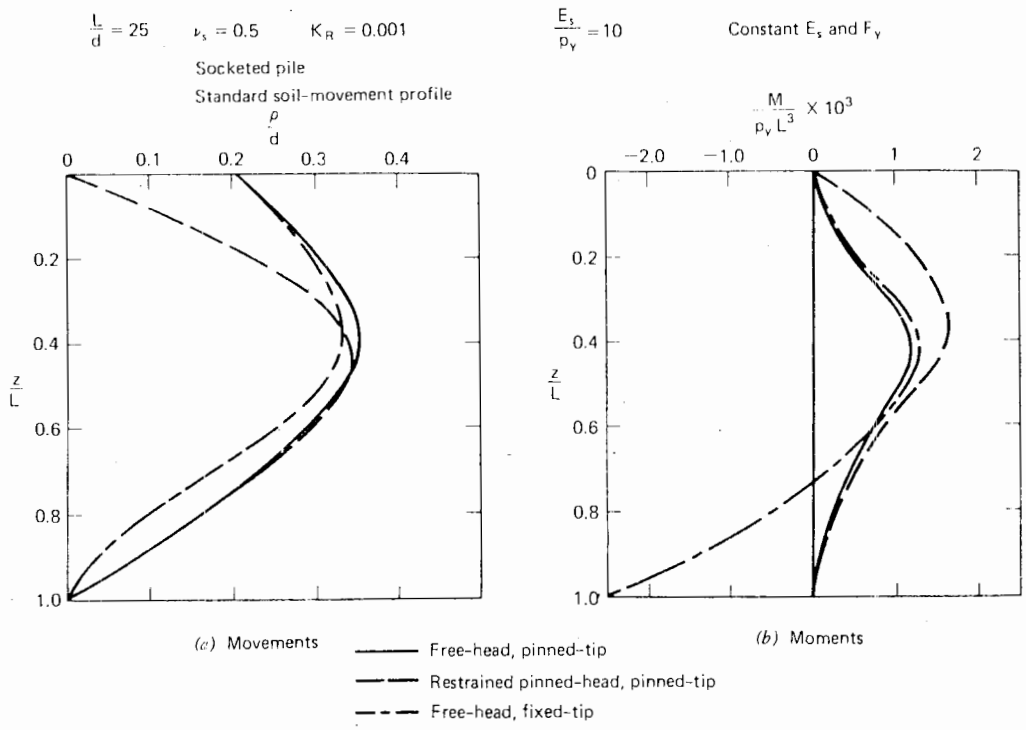

FIGURE 13.6 Effect of boundary conditions.

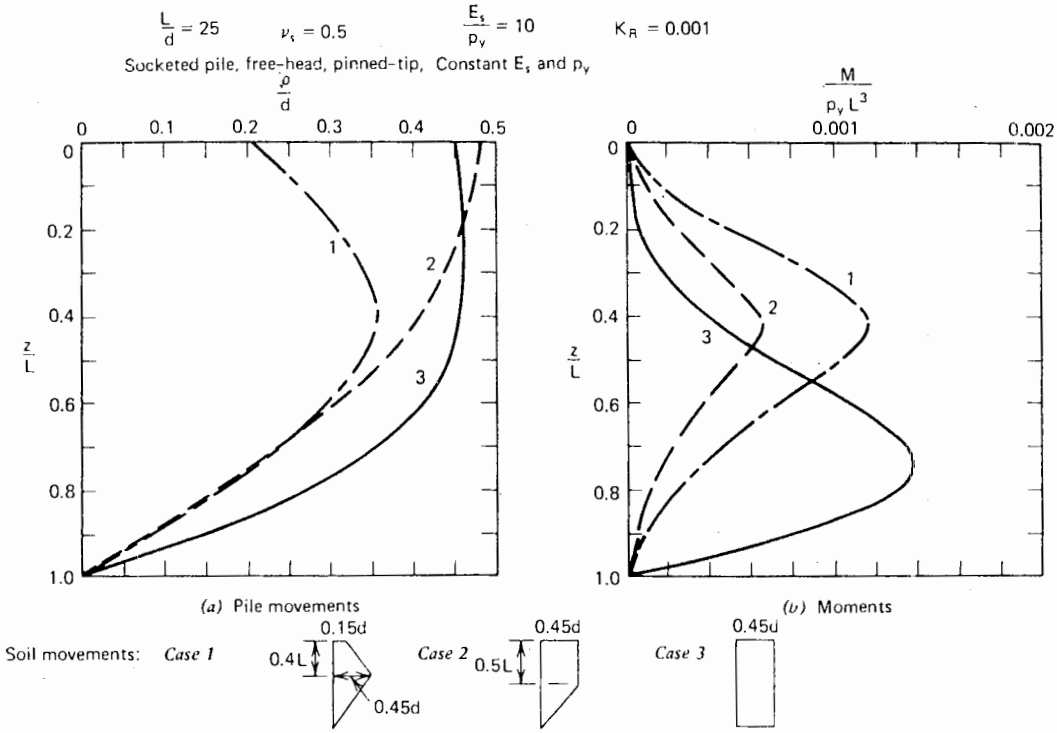

FIGURE 13.7 Effect of distribution of soil movement.

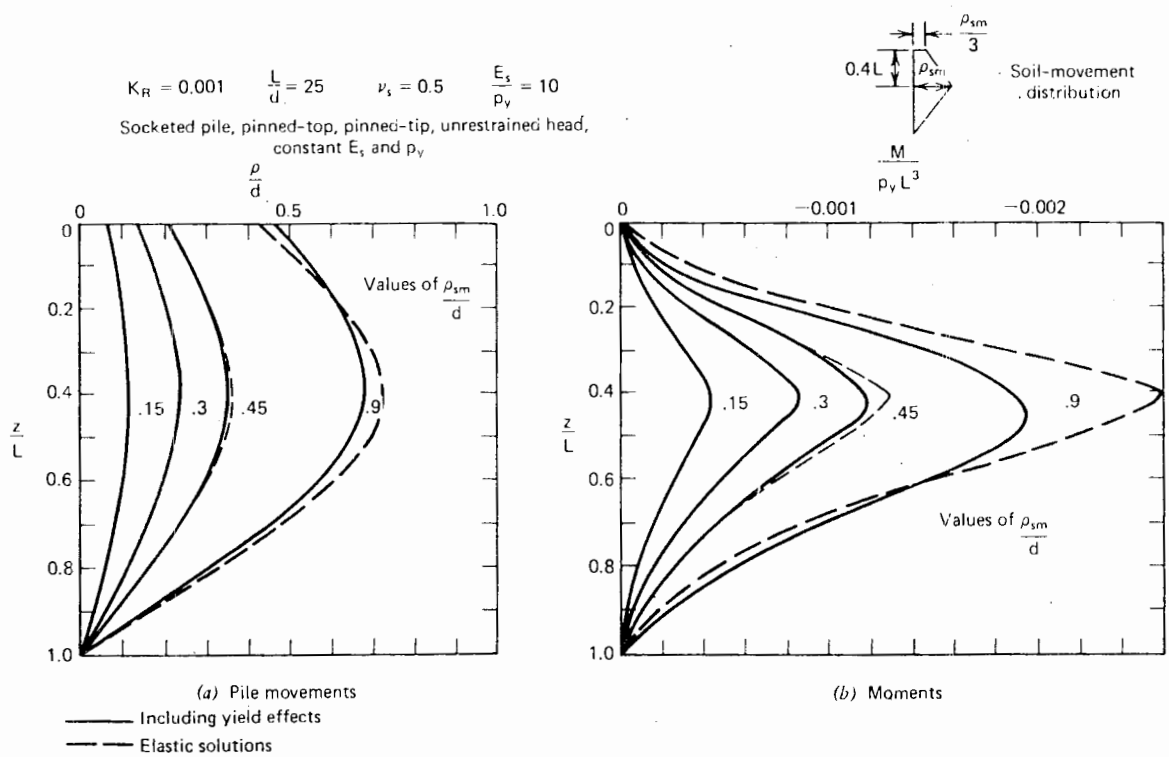

FIGURE 13.8 Effect of magnitude of movement and local yield.

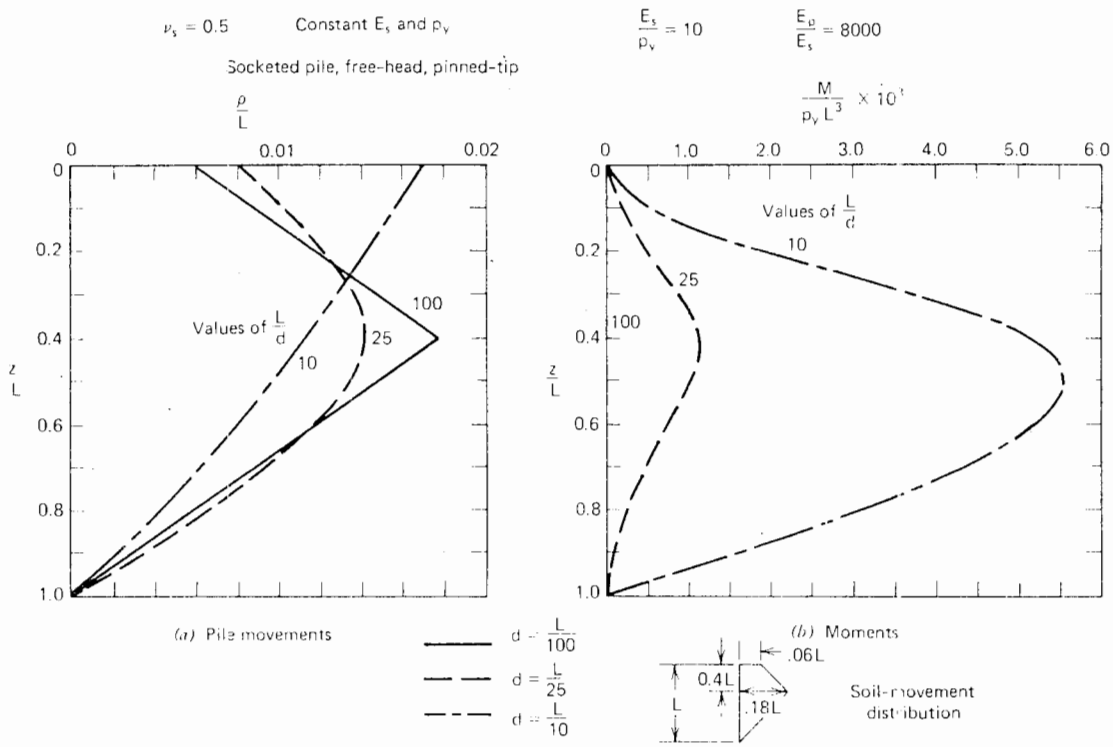

FIGURE 13.9 Effect of pile diameter.

main elastic until the maximum soil movement reaches about $0.4d$. For greater soil movements, the elastic solution tends to overestimate both pile deflection and moment, although the differences between the purely elastic solutions and those including yield are not great, even for relatively large magnitudes of soil movement (e.g., $\rho_{sm}/d = 0.9$). Thus, Fig. 13.8 indicates that in some cases, especially those involving relatively flexible piles and small soil movements, an elastic analysis may be adequate or at worst, should provide an overestimate of pile deflection and moment.

13.3.5 Effect of Pile Diameter

If the diameter of a pile is changed but the length remains constant, the L/d ratio changes and the pile-flexibility factor, K_R, also changes. A typical example of the effects of changing the diameter of a socketed pile is shown in Fig. 13.9. Comparison with Fig. 13.4 shows that the principal effect of changing diameter is to decrease K_R. The effect of changing the value of L/d is of secondary importance.

13.3.6 Effect of E_s and p_y Distributions

The foregoing solutions have been for the case of constant soil modulus E_s and yield pressure p_y in the soil layer. Typical solutions for a socketed pile in a soil with E_s and p_y varying linearly with depth from zero at the surface, are shown in Fig. 13.10. In this case, the pile-flexibility factor is defined as $K_N = E_p I_p / N_h L^5$, where N_h is the rate of increase of Young's modulus with depth (see Chapter 8). For a given value of K_N, the pile-movement profile appears to be similar to that for the case of uniform E_s, but for a pile with a larger K_R value. For example, the displacement profile for $K_N = 10^{-3}$ (in a linearly varying E_s) is very similar to that for $K_R = 10^{-1}$ (uniform E_s, see Fig. 13.4). The moments are expressed in dimensionless form as $M/p_{yb}L^3$, where p_{yb} is the soil-yield pressure at the level of the pile tip. A comparison between the moments in Fig. 13.9*b* and those for a uniform soil in Fig. 13.4*c* reveals that for comparable values of p_y in each case, considerably larger moments are developed when p_y is uniform. These larger moments arise because the values of p_y along the upper portion of the pile are considerably larger, and in

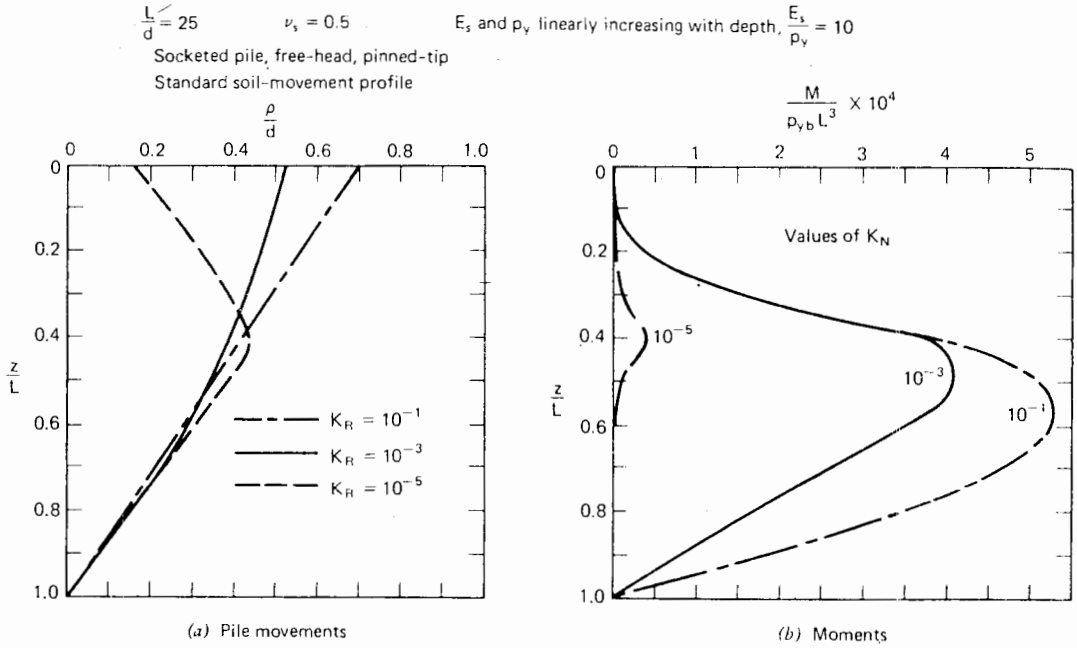

FIGURE 13.10 Pile in soil with linearly varying modulus and yield pressure.

general, the distribution of p_y has a greater influence on pile behavior than does the distribution of E_s.

13.4 APPLICATION OF ANALYSIS TO PRACTICAL PROBLEMS

In addition to data on pile geometry and boundary conditions, the analysis requires the following data as input:

1. The distribution of horizontal soil movement ρ_e with depth.
2. The distribution of soil modulus E_s with depth.
3. The distribution of soil yield pressure p_y with depth.

The estimation of E_s and p_y has been discussed previously, in Chapters 7 and 8. However, some comments on horizontal soil movements are necessary.

Ideally, the horizontal soil movements resulting from an embankment or foundation can be estimated either from the appropriate elastic theory if the soil profile is reasonably uniform (see, for example, Davis and Taylor, 1962), or from a finite-element analysis in more complicated cases. However, a number of comparisons between measured and theoretical horizontal movements (Poulos, 1972*c*) revealed that the predicted values were often very much smaller than the observed, despite the fact that reasonable agreement was obtained between predicted and observed settlements. Because predicted horizontal movements are much more sensitive than settlements to such factors as soil anisotropy and nonhomogeneity, it appears unlikely that horizontal movements can be predicted with confidence at the present time. Thus, it is desirable, if possible, to use field measurements of horizontal movements as input data. Such measurements should be for the surface at least, but preferably should include values at depth obtained with inclinometers or slope indicators.

13.5 COMPARISONS WITH FIELD MEASUREMENTS

There are only a few reported measurements of pile behavior in the presence of lateral soil movements in which sufficient data is available to enable comparisons between observed and predicted behavior to be made. Three such series of measurements are considered herein.

Heyman and Boersma (1961)

Heyman and Boersma (1961) have described tests on three instrumented steel-box piles, 30 cm square and 12.5 m long, founded in sand, peat, and clay layers underlain by

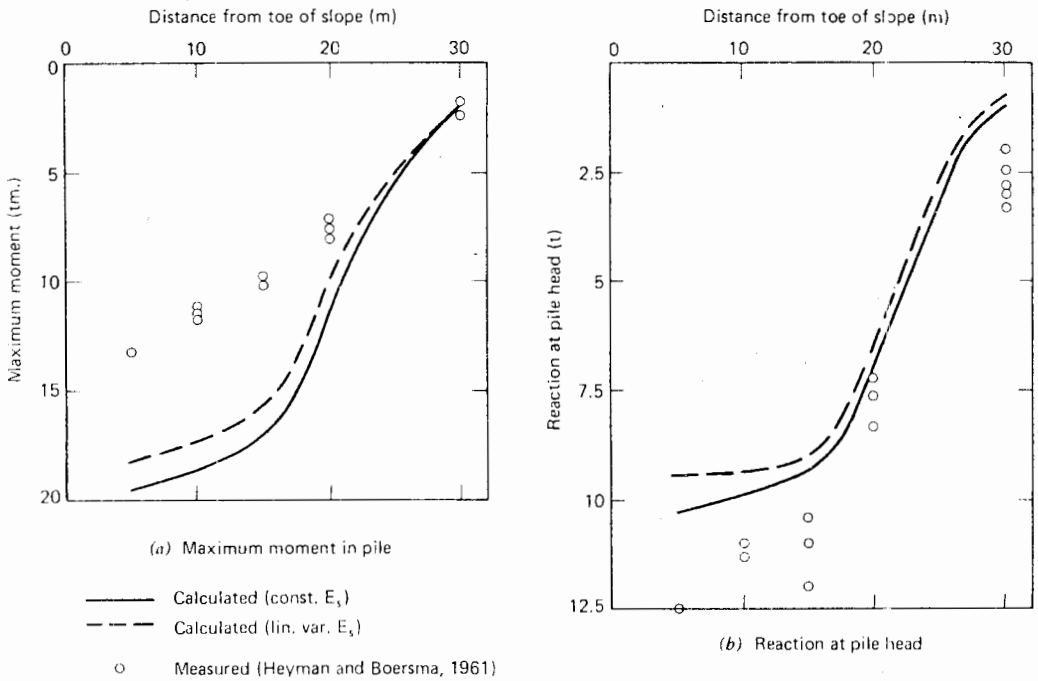

FIGURE 13.11 Comparison between measured and theoretical pile moment and reaction.

sand at about 11 m. The pile heads were propped against a heavy concrete beam founded on an eight-pile bent to restrain head movement. A 7-m-high road embankment of hydraulic fill was constructed in stages, with the embankment toe originally 30 m from the piles. The distribution of lateral soil movement with depth was measured by an inclinometer, while readings of the moment distribution and the head reaction in the pile were also recorded. The embankment was progressively extended in the direction of the piles in steps of 5 m, with readings being taken at each step. A period of two to three weeks rest was allowed at each step, but relatively little time-dependency of moment or head reaction was noted.

In obtaining theoretical solutions, the measured soil movements were used as input and the following assumptions were made:

1. Both the pile tip and the pile head were pinned but restrained from moving horizontally.
2. The values of yield pressure p_y were assumed to be 9 c_u for cohesive soils and three times the Rankine passive pressure for cohesionless soils, as recommended by Broms, 1964*a,b* (see Chapter 7).
3. Two distributions of E_s were used:
   (a) Constant E_s with depth of 500 t/m^2.
   (b) E_s varying linearly from zero at the surface to 1500 t/m^2 at the level of the pile tip.

Comparisons between theoretical and measured maximum-moment, M_{max}, and pile-head reaction, H, are shown in Fig. 13.11. The theory tends to overestimate M_{max} and underestimate H, although the variation with distance of the pile from the toe is reasonably well-predicted. The assumed E_s distribution has relatively little influence on the solutions. For constant E_s, the value of E_s also has relatively little influence on the solutions; a larger E_s leads to a smaller H and M_{max}, but even a four-fold increase in E_s only gives a decrease of about 12% in M_{max} and about 8% in H.

Heyman (1965)

The test piles and soil profile described by Heyman (1965) are very similar to those described by Heyman and Boersma (1961). Two test piles 12.5 m long were instrumented, one situated at the toe of the embankment and the other at 12 m from the toe. The embankment was constructed in three stages to a maximum height of 4 m. The measured horizontal soil movements were not described in detail, but it was stated that for the full embankment height, the movements were almost constant with depth, varying from 1.5 cm at 12 m from the toe to 3 cm at the toe.

In the theoretical analysis, the above soil movements were used as input and the same assumptions were made regarding soil and pile parameters as in the Heyman and

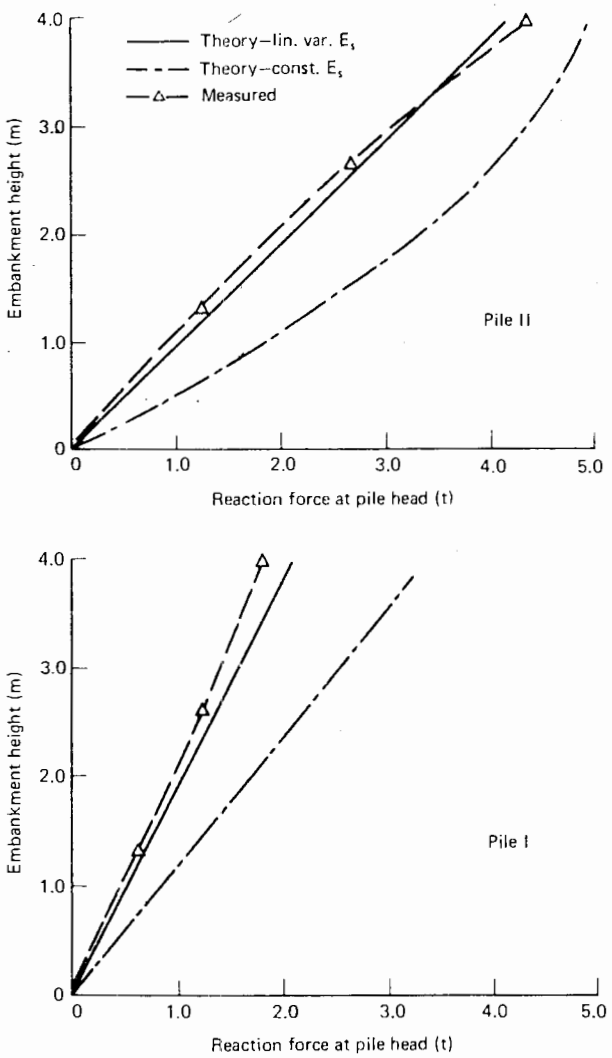

FIGURE 13.12 Theoretical and measured reaction force–tests of Heyman (1965).

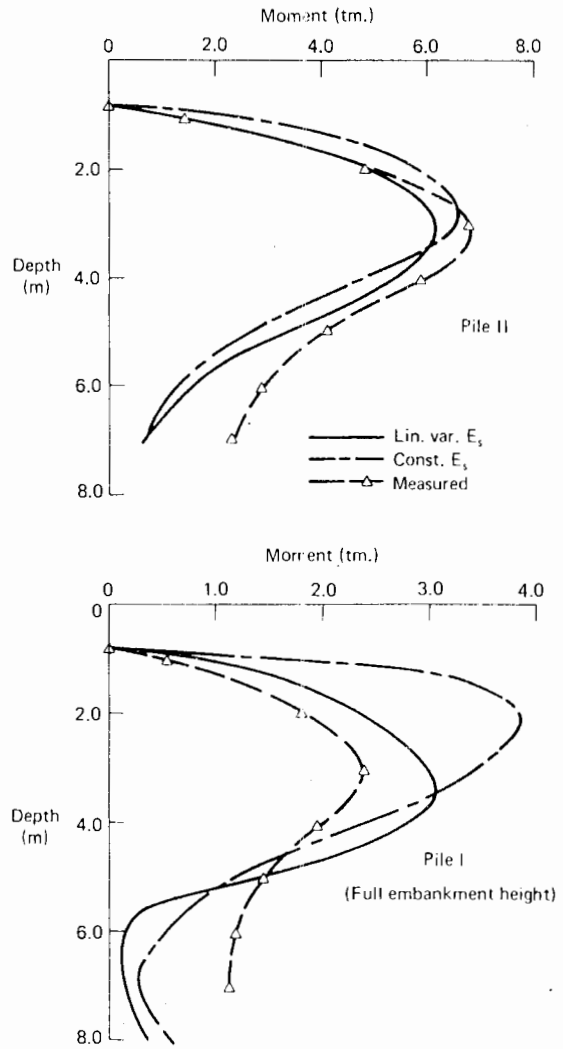

FIGURE 13.13 Theoretical and measured moments–tests of Heyman (1965).

Boersma tests. It was further assumed that the horizontal soil movements increased linearly with embankment height.

Comparisons between theoretical and measured head-reaction are shown in Fig. 13.12, while the moment distributions for the maximum embankment height are shown in Fig. 13.13. The theoretical solutions for head reaction, assuming a linearly varying E_s with depth, are in excellent agreement with the measured values, while the solutions for constant E_s overestimate H. Reasonable agreement is also found between the moments when a linearly varying E_s is assumed in the theory, although there is a tendency for the theory to underestimate the moment in the lower portion of each pile.

Leussink and Wenz (1969)

A test pile was built up of four channel sections to form a box 0.85 m wide and 30 m long and installed in a soil profile of sand and organic clay and peat overlying sand at 20 m depth. The pile head was hinged to an almost rigid support. A rectangular test-embankment of ore was constructed to a maximum height of about 6 m and measurements taken of the horizontal soil movements at various locations beneath the embankment and of the test pile situated adjacent to the embankment. It was found that the soil movements were sufficiently large (maximum of about 80 cm) to cause failure of the test pile. Soil movements taken just prior to failure enabled a comparison to

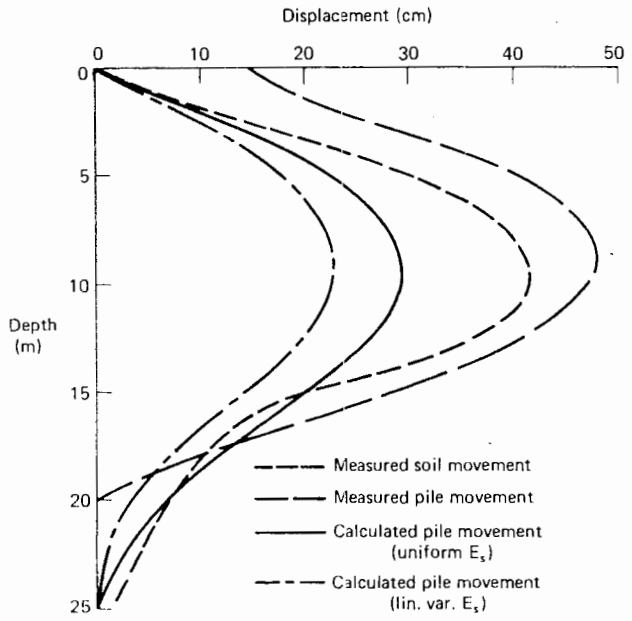

FIGURE 13.14 Measured and theoretical pile movements—tests of Leussink and Wenz (1969).

be made between the theoretical and measured displacement-profile of the pile.

In the analysis, the following assumptions were made:

1. The pile was pinned at the pile head and restrained from moving, while the tip was effectively pinned and restrained from movement at a depth of about 5 m in the sand beneath the organic clay.
2. The yield pressures, p_y, were given by 9 c_u for cohesive soils and three times the Rankine passive pressure for cohesionless soils.
3. Two distributions of E_s were used:
   (a) Constant E_s with depth of 350 t/m^2.
   (b) E_s linearly varying from zero at the surface to 1050 t/m^2 at the level of the pile tip.

A comparison between the measured and theoretical pile displacements is shown in Fig. 13.14. Because some movement of the pile head did in fact occur, the "measured" pile movements in Fig. 13.14 are the values relative to the pile head.

The shapes of the measured and theoretical movements are similar, but the theoretical values for both distributions of E_s are less than those measured. Part of the discrepancy may be attributed to the choice of parameters in the analysis, but the additional pile movements caused by the impending failure of the pile may also have contributed significantly. Such nonelastic pile movements were not considered in the theoretical analysis. In addition, it appears that the reported measured pile-movements correspond to a slightly larger embankment load (20 t/m^2) than the measured soil movements (which are for an embankment load of 18 t/m^2), so that the agreement in Fig. 13.14 may be regarded as fair.

14

BUCKLING OF SLENDER PILES

14.1 INTRODUCTION

Early investigations of the buckling of piles (Granholm, 1929) showed that for piles of normal dimensions driven through soft soil, buckling should not take place except in extremely soft soil. However, with the increasing use of very slender piles (e.g., Bjerrum, 1957; Brandtzaeg and Harboe, 1957) and long piles that extend for a considerable distance above the ground line, the possibility of buckling has had to be reconsidered, and a considerable amount of research has been carried out in recent years in an attempt to obtain more accurate estimates of pile-buckling loads. The majority of analytical methods proposed have employed subgrade-reaction theory, although elastic-continuum theory has also been used more recently.

In this chapter, the subgrade-reaction analysis is described and available solutions for the elastic buckling load of fully-embedded and partially-embedded piles are presented. The effects of various practical complications such as pile imperfections, inelastic buckling, and group effects are also discussed. A brief discussion of the elastic approach to the problem is given and some comparisons between solutions from this approach and the subgrade-reaction analysis are described.

14.2 FULLY EMBEDDED PILES

14.2.1 Basic Subgrade-Reaction Theory

For an elastic pile embedded in a "Winkler" medium and subjected to an axial load P at the head, the governing differential equation for the horizontal deflection ρ along the pile is (e.g., Hetenyi, 1946):

$$E_p I_p \left(\frac{d^4\rho}{dz^4}\right) + \frac{Pd^2\rho}{dz^2} + k_h d\rho = 0 \qquad (14.1)$$

where

$E_p I_p$ = flexural stiffness of pile
k_h = modulus of subgrade reaction
d = pile diameter or width

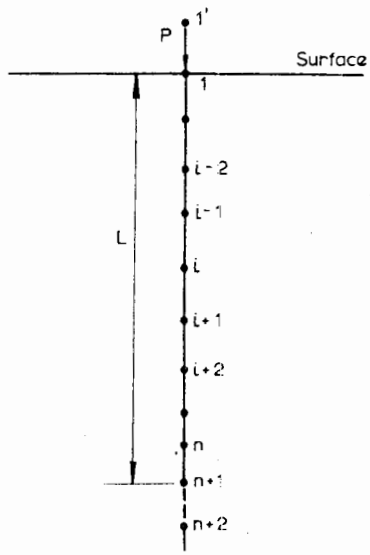

FIGURE 14.1 Finite-difference representation of pile.

The solution to the above equation involves the determination of the characteristic values of P for instability of the pile.

Analytical solutions can be obtained using variational methods (Timoshenko, 1936; Toakley, 1965; Reddy and Valsangkar, 1970). Alternatively, finite-difference methods can be used to determine the eigenvalues. For a typical point i on the pile (Fig. 14.1), Eq. (14.1) can be written as

$$\rho_{i-2} + \left[\bar{P}_0\left(\frac{P_i}{P_0}\right) - 4\right]\rho_{i-1} + \left[6 - 2\bar{P}_0\left(\frac{P_i}{P_0}\right) + \frac{k_{hi}/k_{hr}}{n^4 R^4}\right]\rho_i + \left[\bar{P}_0\left(\frac{P_i}{P_0}\right) - 4\right]\rho_{i+1} + \rho_{i+2} = 0 \tag{14.2}$$

where

$$\bar{P}_0 = \frac{P_0 L^2}{n^2 E_p I_p}$$

P_0 = axial load at pile head
P_i = axial load at point i
k_{hi} = modulus of subgrade reaction at i
k_{hr} = a reference value of k_h
$R^4 = E_p I_p / L^4 k_{hr} d$
n = number of elements in pile

Equation (14.2) may be written for points 2 to n along the pile, and four further equations may be derived, expressing the boundary conditions at the two ends. A system of $n + 2$ equations is thus obtained:

$$[D]\{\rho\} = 0 \tag{14.3}$$

where

$[D]$ = matrix of finite difference coefficients
$\{\rho\}$ = vector of horizontal pile displacements

By equating the determinant of $[D]$ to zero and solving, the eigenvalues of $\bar{P}_0$ may be obtained. The required buckling load is the lowest value. Use of the numerical approach enables any distribution of axial load and modulus of subgrade reaction along the pile to be considered.

A number of solutions have been obtained for various combinations of head and tip boundary conditions and for the cases of constant k_h with depth and linearly increasing k_h with depth. These solutions are described below. The influence of various practical complications is considered in Section 14.4.

14.2.2 Solutions for Constant k_h

One of the earliest solutions was obtained by Timoshenko (1936) for a pin-ended pile along which no load-transfer occurs. The critical load, P_{cr}, is given by

$$\frac{P_{cr}}{P_E} = m^2 + \frac{\beta^2}{m^2} \tag{14.4}$$

where

$P_E = \dfrac{\pi^2 E_p I_p}{L^2}$ = Euler load of a strut in air

$\beta^2 = \dfrac{k_h d L^4}{\pi^4 E_p I_p}$

L = pile length
m = number of buckled half-waves

The value of m is obtained from the condition that P_{cr} is a minimum. Thus, when $\beta = 0$, P_{cr} is a minimum for $m = 1$ and $P_{cr} = P_E$. As β increases—that is, k_h increases—the number of buckled half-waves, and hence P_{cr}, increases. For an infinitely long pile, buckling occurs in half-wavelengths of

$$L/\sqrt{\beta} = \sqrt[4]{\frac{\pi^4 E_p I_p}{k_h d}}$$

and

$$P_{cr} = P_{cr\infty} = 2\sqrt{E_p I_p k_h d} = 2\beta P_E \tag{14.5}$$

Bjerrum (1957) has used the above expression to calculate buckling values for initially straight piles, and has shown that buckling need only be considered if

$$I_p/A^2 \leqslant \frac{\sigma^2_{\max}}{4k_h d E_p} \tag{14.6}$$

where

$\sigma_{\max}$ = yield stress of pile material
A = cross-sectional area of pile

For steel piles, with

$\sigma_{\max} = 52{,}000$ lb/in.^{2},
$E_p = 30 \times 10^6$ lb/in.^{2}
$k_h d = 75$ lb/in.^{2} (typical value for soft clay)

buckling is only likely if $I_p/A^2 < 0.30$. This only occurs for shapes such as round and square steel-bars and tram-rails such as are used in underpinning operations.

Solutions for various boundary conditions have been presented by Davisson (1963). The axial load is again assumed to be constant in the pile—that is, no load transfer occurs and the pile initially is perfectly straight. The solutions are shown in Fig. 14.2 in dimensionless form, as a plot of U_{cr} versus $l_{\max}$, where

$$U_{cr} = \frac{P_{cr}R^2}{E_p I_p} \tag{14.7}$$

$$R = \sqrt[4]{E_p I_p / k_h d} \tag{14.8}$$

$$l_{\max} = L/R \tag{14.9}$$

Figure 14.2 shows that the boundary conditions exert a controlling influence on U_{cr}, with the lowest buckling loads occurring for piles with free (unrestrained) ends.

An alternative presentation of solutions has been given by Francis et al. (1965) and Toakley (1965), in which the pile is considered as a pin-ended strut in air of equivalent length, l_e, so that the buckling load is

$$P_{cr} = \frac{\pi^2 E_p I_p}{l_e^2} \tag{14.10}$$

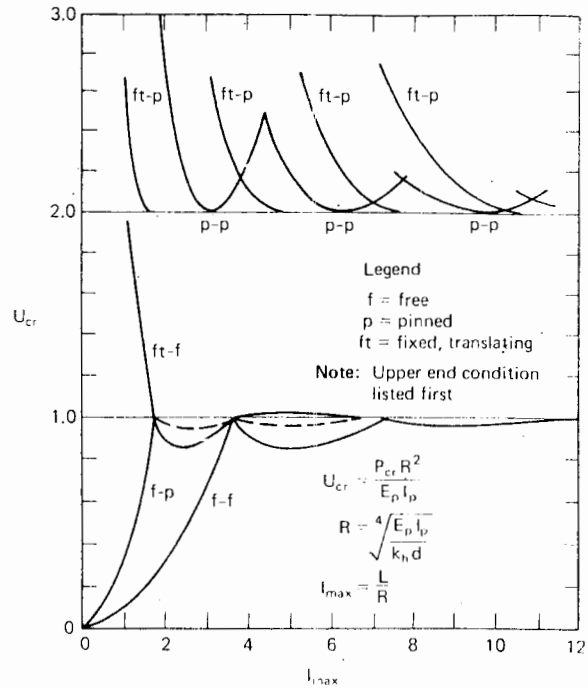

FIGURE 14.2 Buckling load vs. length for k_h = constant (Davisson, 1963).

Equivalent length, l_e, is a function of the boundary conditions at the pile top and tip, and of the distribution of k_h along the pile. Solutions for l_e/l' are shown in Fig. 14.3 for various boundary conditions, where

$$l' = \sqrt[4]{\frac{\pi^4 E_p I_p}{k_h d}} \tag{14.11}$$

that is,

$$l' = \pi R$$

where R is defined in Eq. (14.8).

Buckling loads calculated from the use of Fig. 14.3 are identical with those from Fig. 14.2.

Methods of determining k_h and typical values for various soil types are discussed in Section 8.2.

14.2.3 Solutions for Linearly Varying k_h

A number of solutions have been obtained by Davisson (1963) for the case $k_h = n_h z/d$, and these solutions are shown in Fig. 14.4 for the case of an initially straight pile

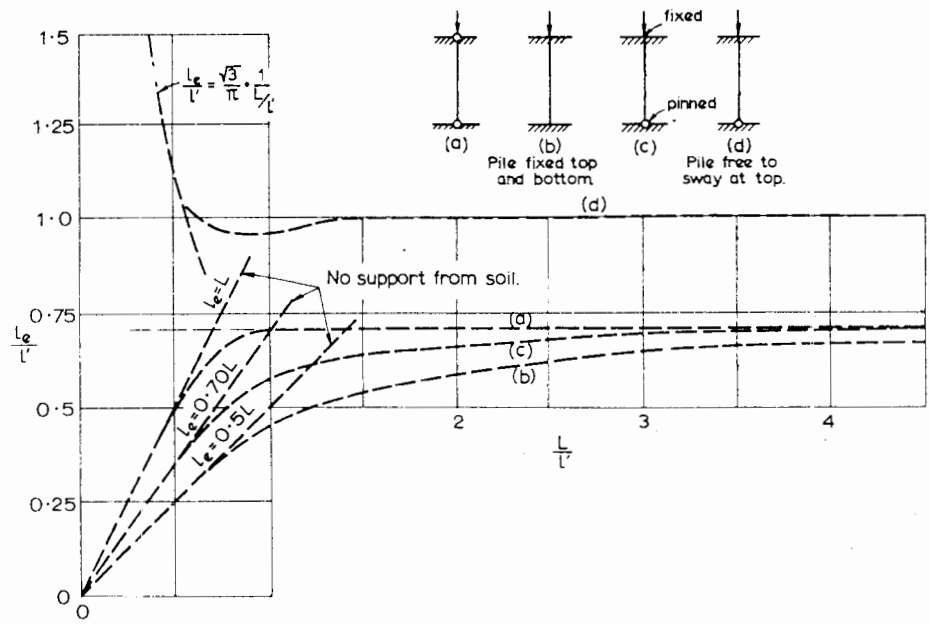

FIGURE 14.3 Piles in uniform medium; various end conditions; plot of l_e/l' vs. L/l' (Francis et al., 1965).

and no axial load transfer along the pile. The dimensionless buckling load, V_{cr}, is defined as

$$V_{cr} = \frac{P_{cr}T}{E_pI_p} \tag{14.12}$$

where

P_{cr} = critical buckling load

$$T = \sqrt[5]{\frac{E_pI_p}{n_h}} \tag{14.13}$$

and the dimensionless length, $Z_{\max}$, is

$$Z_{\max} = \frac{L}{T} \tag{14.14}$$

Figure 14.4 shows that the boundary condition at the top of the pile is of considerable importance. In cases where buckling is likely to be a problem, great benefit can be obtained by ensuring that the pile head is restrained from translation and, preferably, fixed against rotation.

The determination of n_h is discussed in Section 8.2.

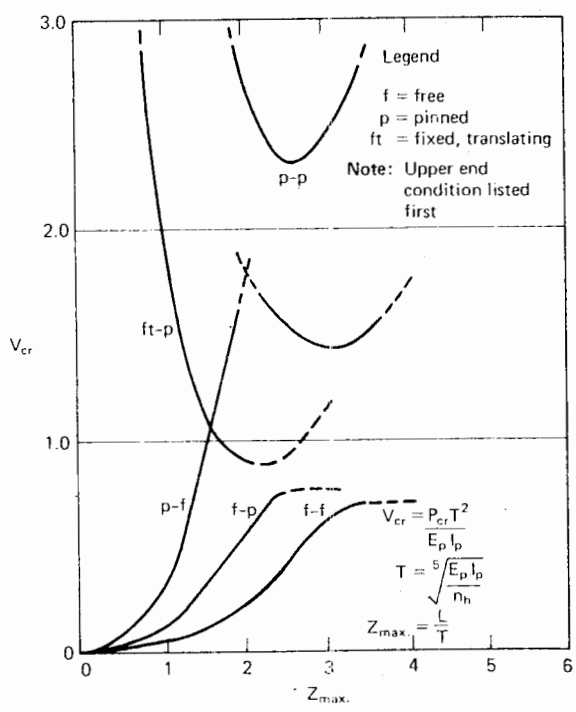

FIGURE 14.4 Buckling load vs. length for $k_h = n_h z/d$ (Davisson, 1963).

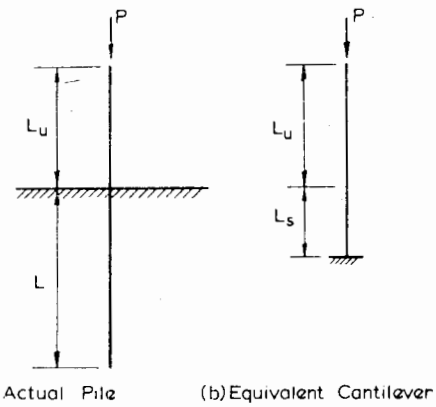

FIGURE 14.5 Partially embedded piles.

14.3 PARTIALLY EMBEDDED PILES

14.3.1 Theoretical Approach

The basic equation (14.1) again applies and solutions may be obtained either by analytical means (e.g., Reddy and Valsangkar, 1970) or numerical means. In the case of the numerical analysis, the modulus of subgrade reaction at points above the ground line can simply be made very small and the solution obtained as before.

14.3.2 Solutions for Constant k_h

For two sets of boundary conditions, constant axial load in the pile and a relatively long pile ($l_{max} > 4$; see Eq. 14.9 for l_{max}), Davisson and Robinson (1965) have presented solutions for the buckling load of a partially embedded piles, in terms of an equivalent freestanding length of the embedded portion of the piles (this form of presentation parallels that given in Fig. 14.3 for fully embedded piles).

The solutions are given in Fig. 14.6, in which

$$S_R = \frac{L_s}{R} \tag{14.15}$$

$$J_R = \frac{L_u}{R} \tag{14.16}$$

L_s = equivalent free length of embedded portion of pile (see Fig. 14.5)
L_u = unsupported pile length

and R is defined in Eq. (14.8), with L = embedded length.

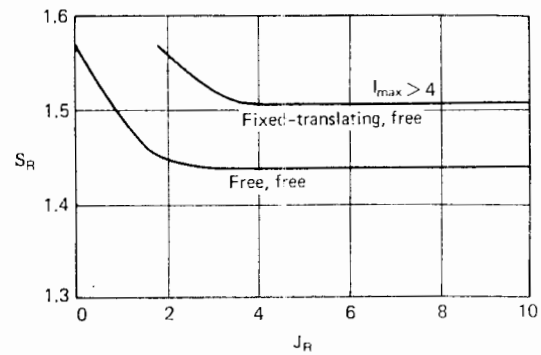

FIGURE 14.6 Dimensionless depth of fixity for buckling. Constant k_h (after Davisson and Robinson, 1965). (© Canada, 1965, by University of Toronto Press.)

The critical load is then

$$P_{cr} = \frac{\pi^2 E_p I_p}{4(S_R + J_R)^2 R^2} \tag{14.17}$$

14.3.3 Solutions for Linearly Varying k_h

Solutions for a long pile ($Z_{max} > 4$; defined in Eq. (14.14), with L = embedded length) for the case $k_h = n_h z/d$ are shown in Fig. 14.7 (Davisson and Robinson, 1965), again in terms of an equivalent length of embedded portion of pile. In this case,

$$S_T = \frac{L_s}{T} \tag{14.18}$$

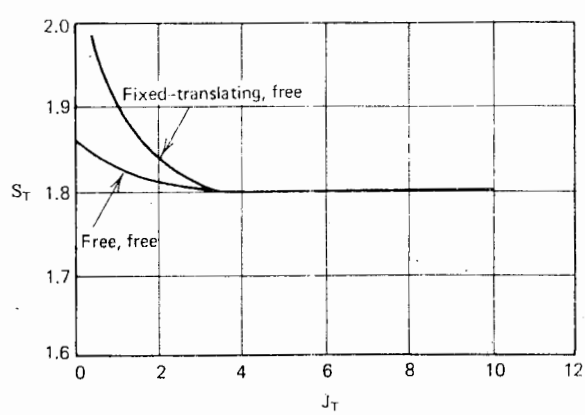

FIGURE 14.7 Dimensionless depth of fixity for buckling. Linearly varying k_h (after Davisson and Robinson, 1965). (© Canada, 1965, by University of Toronto Press.)

$$J_T = \frac{L_u}{T} \tag{14.19}$$

and T is defined in Eq. (14.13).

The buckling load is

$$P_{cr} = \frac{\pi^2 E_p I_p}{4\,(S_\tau + J_T)^2 T^2} \tag{14.20}$$

Lee (1968) carried out model tests on ¼-in.–to–½-in.–diameter piles in dry sand and found good agreement between the measured buckling loads and those predicted by Davisson and Robinson's solutions.

14.4 EFFECT OF PRACTICAL COMPLICATIONS

14.4.1 Axial Load Transfer Along Pile

The theoretical solutions given in the preceding sections are for piles in which the axial load is constant along the pile, that is, no load transfer occurs along the pile. This condition is satisfied for relatively short or stiff end-bearing piles, but for floating piles and compressible end-bearing piles, considerable load transfer occurs (see Chapter 5). The effect of axial load transfer on the critical buckling load has been investigated by Francis et al. (1965), Toakley (1965), and Reddy and Valsangkar (1970). The latter have considered the following idealized axial load distributions:

Fully embedded piles:

$$P = P_0\,(1 - \psi\, z/L) \tag{14.21a}$$

and

$$P = P_0\,(1 - \psi\, z^2/L^2) \tag{14.21b}$$

where

P_0 = load at pile head
z = depth below surface
L = pile length
ψ = parameter ($0 \leqslant \psi \leqslant 1$)

Partially embedded piles:

$$P = P_0\,[1 - \psi\,(\frac{x}{L_t} - n)] \tag{14.22}$$

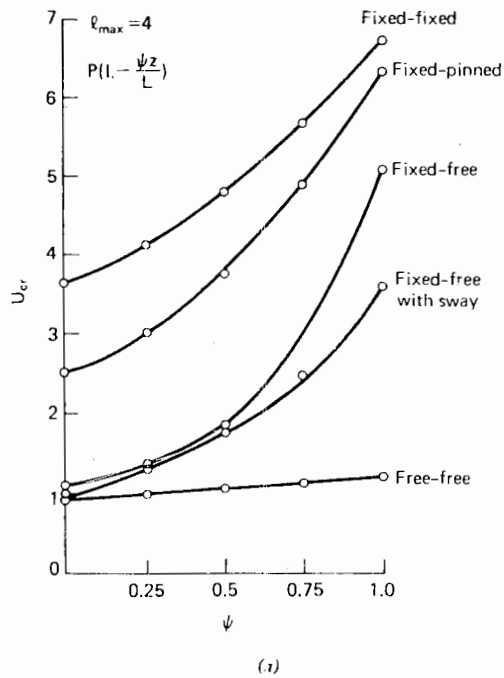

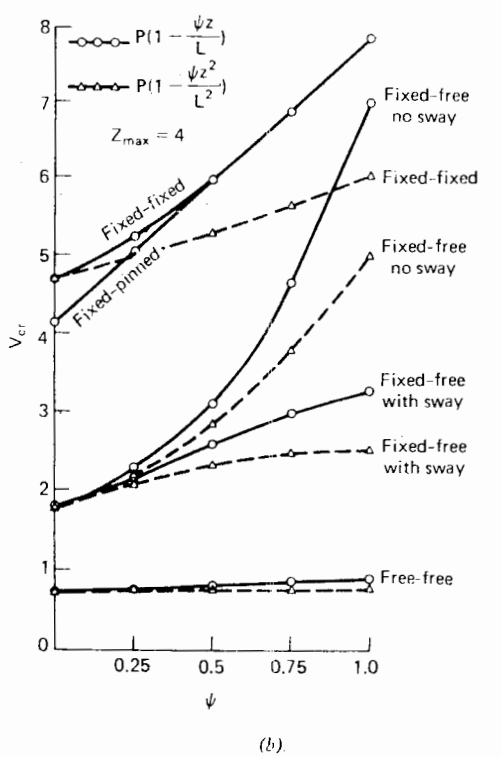

FIGURE 14.8 Effect of skin friction on buckling loads for (a) constant soil modulus; (b) linear soil modulus (Reddy and Valsangkar 1970).

where

L_t = total length of pile $(L + L_u)$
n = ratio of unsupported length to total length, $L_u/(L + L_u)$

In the latter case, the dimensionless length is defined as

$$Z'_{\max} = L_t/T \tag{14.23}$$

Also, ψ can be greater than one.

For both cases, the value of ψ could be estimated from the elastic solutions for base load given in Chapter 5.

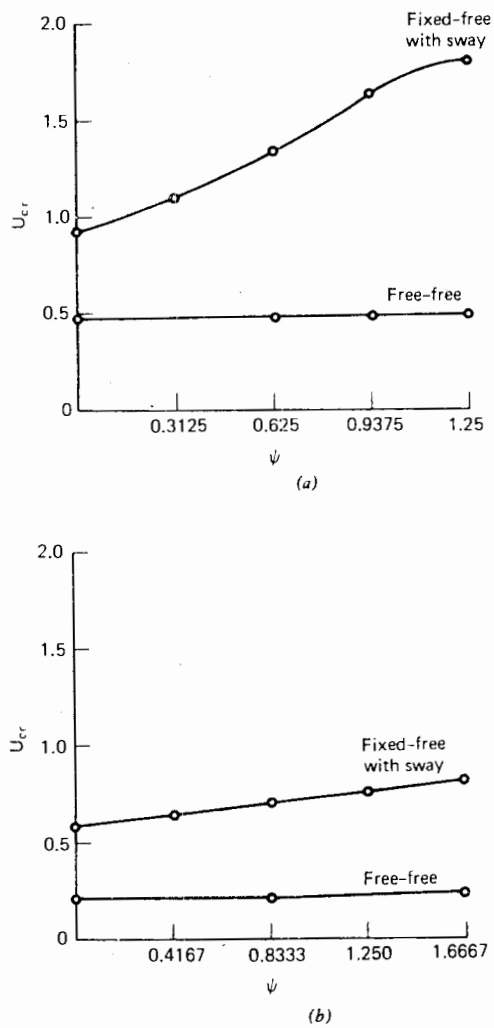

FIGURE 14.9 Effect of skin friction for partially supported pile for constant soil modulus: (a) $n = 0.2$, $l_{\max} = 0.4$; (b) $n = 0.4$, $l_{\max} = 4$ (Reddy and Valsangkar, 1970).

The variation with ψ of the dimensionless buckling loads, $U_{cr} = P_{cr} R^2/E_p I_p$ and $V_{cr} = P_{cr} T^2/E_p I_p$, is shown in Fig. 14.8 for fully embedded, relatively long piles. Considerable increase in the buckling load occurs because of load transfer, this increase being most marked for the fixed-free-with-sway case—piles with a free tip and a head that can translate but not rotate. Corresponding curves for typical partially-embedded piles are shown in Figs. 14.9 and 14.10.

14.4.2 Initial Imperfections

This aspect has been investigated by Francis et al. (1965). If the soil is assumed to have a constant modulus of subgrade reaction, k_h, that is independent of lateral deflection, a pile free of imperfections remains straight until the critical load, P_{cr}, is reached. A pile with imperfections deflects laterally from the onset of loading into a form governed by the imperfections but gradually moves into the theoretical buckling mode as P_{cr} is approached.

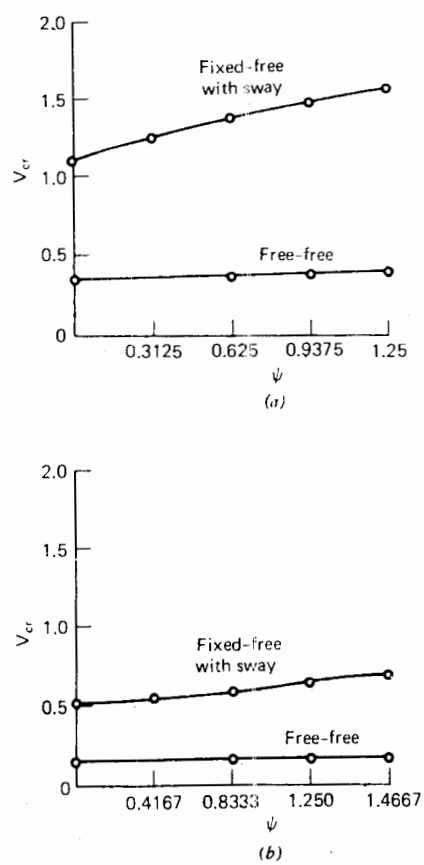

FIGURE 14.10 Effect of skin friction for partially supported pile for linear soil modulus: (a) $n = 0.2$, $Z_{\max} = 4$; (b) $n = 0.4$, $Z_{\max} = 4$ (Reddy and Valsangkar, 1970).

In real soils, k_h decreases with increasing lateral deflection, and ultimately the soil becomes plastic, that is, k_h becomes zero for further increase in pile deflection. For a fully embedded pin-ended pile, the buckling load in a uniform plastic medium is equal to the Euler load of the pin-ended strut in air. This is one half the value for the pile in a uniform mass with constant k_h, providing the half-wave length of the pile does not alter.

An eccentricity is a general representation of an imperfection in a pile. A series of model pile tests on fully embedded pin-ended piles, carried out by Hoadley (1964), confirmed that loading eccentricity decreases P_{cr}. These tests also revealed that on the average, the post-buckling load capacity of the pile (after elastic buckling had commenced) was 0.53 times the elastic buckling load. Assuming that the soil along the pile has become fully plastic subsequent to elastic buckling, the above relationship between post-buckling and elastic critical loads is in excellent agreement with the theoretical prediction that the critical load in a plastic medium is one half that in an elastic mass.

14.4.3 Inelastic Buckling

For piles that fail inelastically, Granholm (1929) suggested the following interaction equation:

$$\frac{1}{P_{\text{ult}}} = \frac{1}{P_s} + \frac{1}{P_{cr}} \tag{14.24}$$

where

P_{ult} = collapse load of pile
P_{cr} = elastic buckling load
P_s = short-column load capacity of pile section

Golder and Skipp (1957) carried out model pile tests that showed that the above expression overestimated P_{ult} for very soft soils ($c_u < 115$ lb/ft^2) but underestimated P_{ult} for $c_u > 115$ lb/ft^2. Hoadley, Francis, and Stevens (1969) found that P_{ult} is overestimated for a soil with an average c_u of about 500 lb/ft^2. Francis et al. (1965), however, found good agreement between measured and predicted ultimate load for a full-scale hollow steel pile in soft silty clay, but in another case, involving a prestressed concrete pile in silty clay, the measured load was about 20% higher than the predicted value. In both the latter cases, the soil was stiffer than the very soft soil in Golder and Skipp's tests, so that Eq. (14.24) may be expected to usually give a conservative estimate of P_{ult}, except for very soft soils.

14.4.4 Group Effects

Model tests carried out by Toakley (1964) with groups of two and three steel-strip piles in soft silt showed that the critical load is reduced by grouping when the piles are closely spaced. The test results are summarized in Table 14.1, together with tests on isolated piles. Full-scale tests reported by Hoadley, Francis, and Stevens (1969), however, show little interaction between closely-spaced piles. As an approximate means of estimating group effects, the value of k_h may be reduced arbitrarily, as suggested in Section 8.2. Alternatively, an elastic analysis of group interaction under lateral loading (Section 8.4) may provide a more rational reduction factor for k_h.

TABLE 14.1 EXPERIMENTAL RESULTS ON PILE GROUPS (TOAKLEY, 1964)

No. of Piles	Spacing (in.)	Av. Pile Load at Failure (lb)	Group Efficiency (%)
1/8-inch Piles			
1		1475	100
2	1	900	61.0
2	2	992	67.2
2	3	1012	68.6
2	4	1226	83.1
2	6	1025	69.5
3	2	928	62.9
3	4	1156	78.3
24-Gauge Piles			
1		128	100
2	3	83	64.9
2	6	101	79.0

14.5 ANALYSIS USING ELASTIC THEORY

The elastic analyses of pile behavior under axial and lateral loads have been extended by Madhav and Davis (1974) to examine the problem of buckling of a pile in an ideal elastic soil medium. As previously discussed, this representation of

a soil should be more realistic than the simpler Winkler spring model.

14.5.1 Analysis

For the basic analysis, the same assumptions are made as in the analysis of a laterally-loaded socketed pile (Chapter 8): that the soil is a homogeneous, isotropic, elastic layer underlain by a rigid base, and that the pile is of length L, diameter (or width) d, with the tip resting on the rigid base, and is divided into $n + 1$ elements (see Fig. 14.11).

The lateral displacements of the soil adjacent to the pile elements are given in Chapter 8:

$$\{{}_s\rho\} = \frac{d}{E_s}[{}_sI]\{p\} \tag{14.25}$$

where

$\{{}_s\rho\}$ = vector of soil displacements
$[{}_sI]$ = $(n+1) \times (n+1)$ matrix of soil-displacement-influence factors
$\{p\}$ = vector of soil pressures
E_s = Young's modulus of soil

The elements of $[{}_sI]$ are obtained as described in Chapter 8. Inverting Eq. (14.25),

$$\{p\} = \frac{E_s}{d}[{}_sI]^{-1}\{{}_s\rho\} \tag{14.26}$$

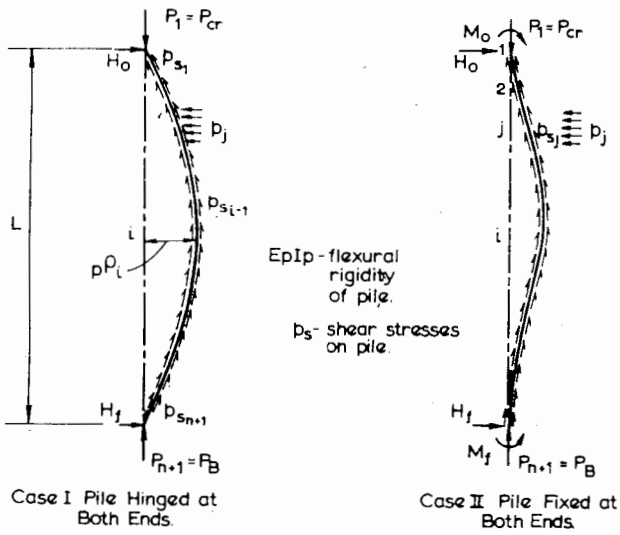

FIGURE 14.11 Pile loading and boundary conditions for elastic analysis.

Assuming the pile to be a thin beam, the basic equation of bending is

$$(E_pI_p)\left(\frac{d^2{}_p\rho}{dz^2}\right) = M \tag{14.27}$$

where

E_pI_p = flexural rigidity of pile
${}_p\rho$ = lateral deflection of pile axis
M = bending moment

At any point i, the moment M_i can be expressed as

$$\begin{aligned} M_i = {} & \frac{-dL^2}{n^2}\{C_i\}\{p\} + H_0z_i + M_0 - P_{1p}\rho_i \\ & + (P_1 - P_2)\,[{}_p\rho_i - ({}_p\rho_1 + {}_p\rho_2)/2] \\ & + (P_2 - P_3)\,[{}_p\rho_i - ({}_p\rho_2 + {}_p\rho_3)/2] + \cdots\cdots \\ & + (P_{i-1} - P_i)\,[{}_p\rho_i - ({}_p\rho_{i-1} + {}_p\rho_i)/2] \end{aligned} \tag{14.28}$$

where

P_i = axial load at the level of point i
$\{C_i\}$ = vector of coefficients for the moment of the pressures p at point i
H_0 = horizontal load at top of pile
M_0 = moment at top of pile
z_i = depth of point i below surface

Expressing Eq. (14.27) in finite-difference form, and applying it to all points on the pile, the following matrix equation is obtained:

$$\begin{aligned} \frac{E_pI_p}{L^2}n^2\,[B]\{{}_p\rho\} = \Big\{ & \frac{-dL^2}{n^2}[C]\{\rho\} + H\{G\} \\ & + M_0\{1\} - P_0[\alpha]\{{}_p\rho\}\Big\} \end{aligned} \tag{14.29}$$

where

$[B]$ = matrix of finite-difference coefficients with the only nonzero elements being $B(i, i) = -2$, $B(i, i-1) = B(i, i+1) = 1$

$[C]$ = matrix of coefficients for the moment of the pressures p at various points on the pile
$\{G\}$ = column vector, with $G_i = z_i$
$\{1\}$ = column vector of values of unity

$[\alpha]$ = matrix of coefficients for the moment at various points on the pile caused by the axial loads

with

$$\alpha(i,j) = \frac{\beta_{i-1} - \beta_{i+1}}{2} \text{ for } j < i$$

$$\alpha(i,j) = \frac{\beta_{i-1} + \beta_i}{2} \text{ for } j = 1$$

$$\alpha(i,j) = 0 \text{ for } j > i$$

$\beta_i = P_i/P_0$
= proportion of axial load at point i

For horizontal force equilibrium,

$$H_0 + H_f = \frac{dL}{n}\{E\}\{p\} \tag{14.30}$$

where

H_f = load at tip
$\{E\}$ = vector, with $E(j) = 1$ for $j = 2$ to n; $E(1) = E(n+1) = 0.5$

For moment equilibrium,

$$H_f L = M_0 - M_f + \frac{dL^2}{n^2}\{F\}\{p\} - P_0\{\alpha^1\}\{{}_\rho\rho\} \tag{14.31}$$

where

$\{F\}$ = row vector

with

$$F(j) = (j-1) \text{ for } j = 2 \text{ to } n$$
$$F(1) = 0.125$$
$$F(n+1) = 0.5n - 0.125$$

and

$\{\alpha^1\}$ = row vector

with

$$\alpha^1(j) = (\beta_j - \beta_{j+2})/2$$

The appropriate boundary conditions are now invoked. For example, for a pile restrained from translation at top and tip, but free to rotate, the boundary conditions are

$$\rho_1 = \rho_{n+1} = 0$$
$$M_1 = M_{n+1} = 0$$

These conditions may be incorporated into the equations previously derived to reduce the order of the problem from $n+1$ to $n-1$ unknowns. Then, by equating soil and pile displacements—that is, $\{{}_s\rho\} = \{{}_p\rho\} = \{\rho\}$—Eq. (14.29) reduces to the following form:

$$[[A] + P^*[\xi]]\{\rho\} = 0 \tag{14.32}$$

where

$$[A] = K_R n^2 [B] + \frac{1}{n^2}\left[[C] - \frac{1}{L}\left\{n\{E\} - \{F\}\right\} \cdot \{G\}\right][{}_sI]^{-1}$$

$$[\xi] = [\alpha] - \frac{1}{L}\{\alpha^1\}\{G\}$$

$$P^* = \frac{P_0}{E_s L^2}$$

$$K_R = \frac{E_p I_p}{E_s L^4} = \text{pile-stiffness factor}$$

Multiplying Eq. (14.32) by $-[\xi]^{-1}$,

$$[-[\xi]^{-1}[A] - P^*[1]]\{\rho\} = 0 \tag{14.33}$$

where $[I]$ is the unit matrix.

Equation (14.33) is of standard form and may be solved to obtain the smallest eigenvalue:

$$P^*_{cr} = P_{cr}/E_s L^2$$

where

P_{cr} = buckling load of the pile

In employing the above analysis, the most satisfactory means of determining the matrix $[\alpha]$, involving the axial load distribution in the pile, is to use the distribution obtained from a single-pile analysis for axial load only (Chapter 5). This distribution will be dependent on the value of the pile-stiffness factor $K = E_p/E_s \cdot R_A$, where R_A = area ratio of pile.

14.5.2 Typical Solutions

Typical solutions for the buckling load of an end-bearing pile pinned and restrained from translation at top and

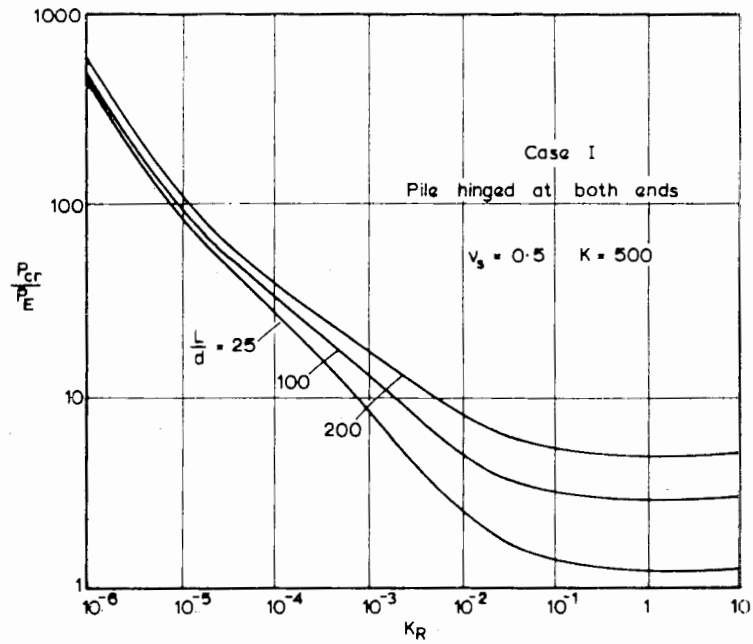

FIGURE 14.12 Effect of L/d ratio on buckling loads.

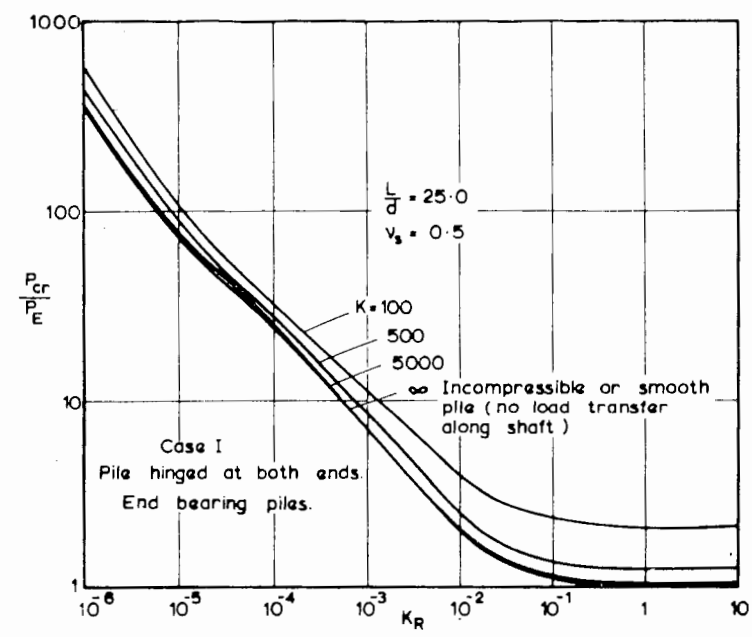

FIGURE 14.13 Effect of pile-stiffness factor K_R on buckling loads.

bottom, are shown in Figs. 14.12 and 14.13. In all cases, 10 elements have been used to divide the pile. The buckling load, P_{cr}, is expressed in dimensionless form as a ratio of the Euler load $P_E = \pi^2 E_p I_p / L^2$ (i.e., the buckling load of a column without soil support). P_{cr}/P_E increases with increasing pile-flexibility (i.e., decreasing K_R), and with increasing slenderness, L/d. The effect of the axial load distribution is shown in Fig. 14.13, where values of P_{cr}/P_E are plotted for various values of pile-stiffness factor K. The lower the value of K, the greater is the load transfer to the soil along the pile shaft. P_{cr}/P_E increases as K decreases, thus confirming the conclusion reached from subgrade-reac-

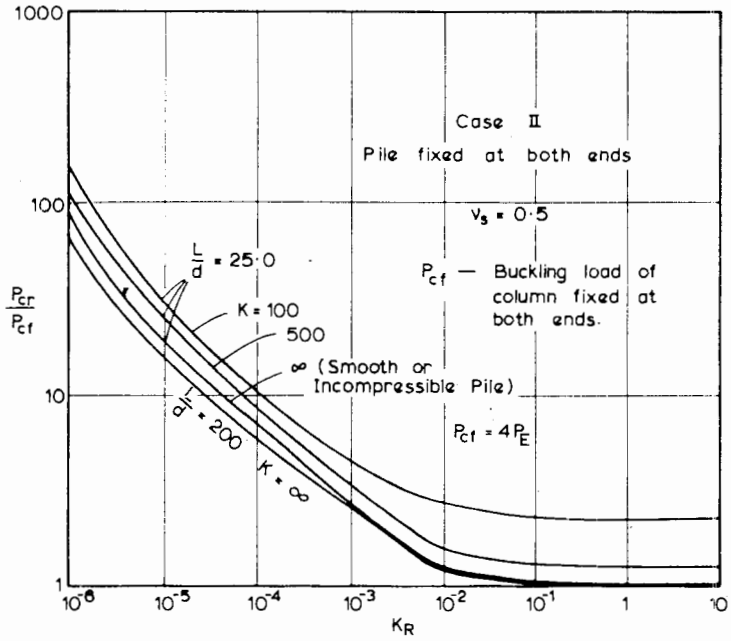

FIGURE 14.14 Buckling loads for a fixed ended pile.

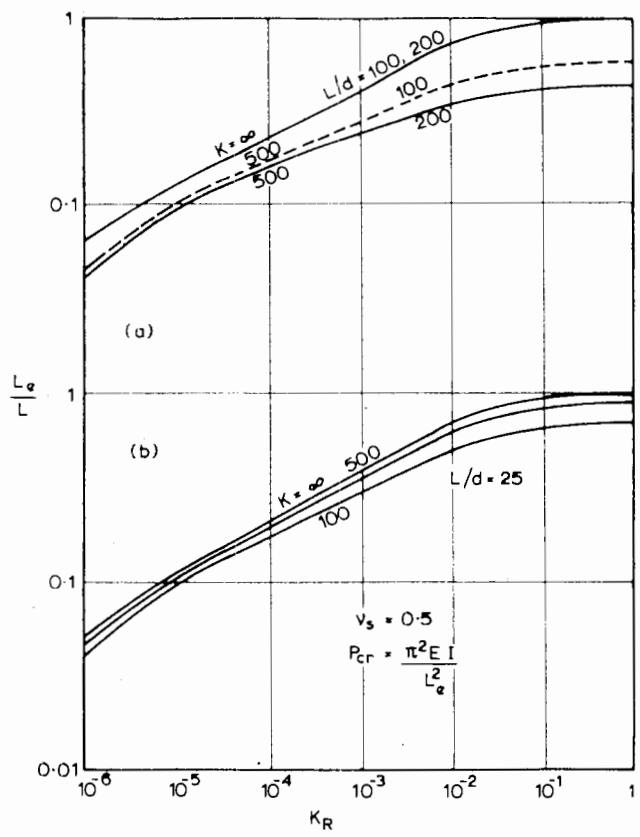

FIGURE 14.15 Equivalent column lengths of fully embedded pin-pin piles.

tion analyses, that the buckling load increases as the amount of load transfer increases (Section 14.4.1).

Solutions for a pile fixed at both ends are shown in Fig. 14.14. In this case, P_{cr} is expressed as a ratio of the buckling load, $P_{cf} = 4P_E$, of a column without soil surrounding

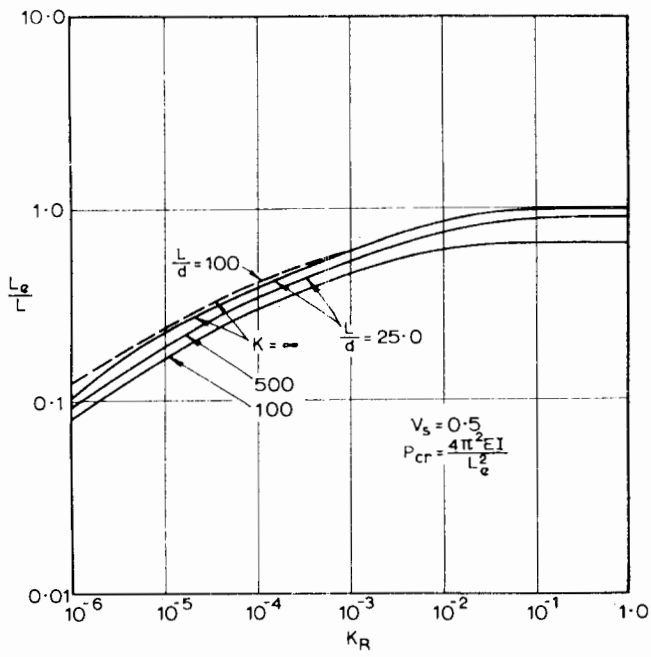

FIGURE 14.16 Equivalent column lengths of fully embedded fixed piles.

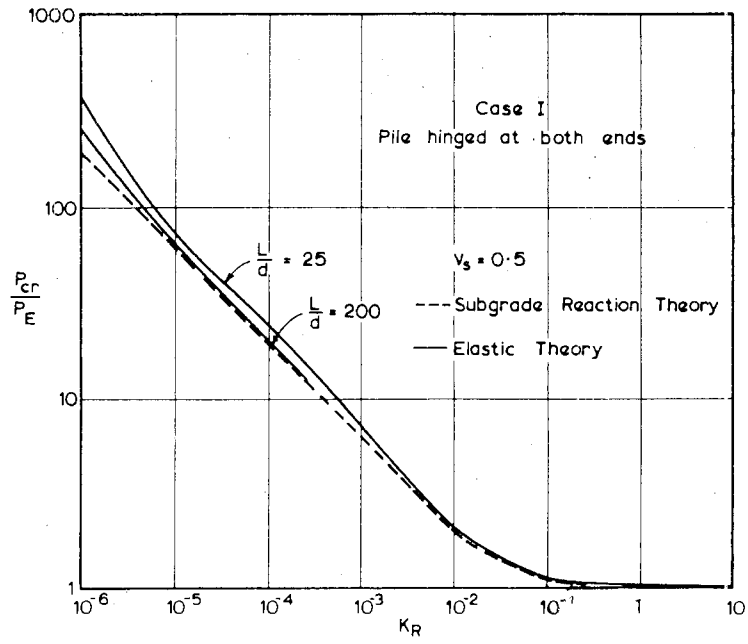

FIGURE 14.17 Comparison of elastic and subgrade-reaction theories.

it. The effect of the soil in increasing the buckling load is less for this case than for the pile pinned at both ends.

Alternative presentations of solutions from the elastic analysis are shown in Figs. 14.15 and 14.16, where the equivalent length of the pile L_e, as a ratio of L, is plotted against K_R for various values of L/d.

It should be noted that for a particular pile section, K_R and K are not independent quantities, and it may readily be shown that

$$\frac{K_R}{K} = \frac{I_p}{R_A L^4} \tag{14.34}$$

For a solid circular pile, Eq. (14.34) reduces to

$$\frac{K_R}{K} = \left(\frac{\pi}{64}\right)\left(\frac{d}{L}\right)^4 \tag{14.35}$$

14.5.3 Comparison with Subgrade-Reaction Solutions

A comparison between elastic and subgrade-reaction solutions for the buckling load of a pile pinned at the top and tip is shown in Fig. 14.17. In order to make this comparison, the modulus of subgrade reaction, k_h, and Young's modulus of the soil, E_s, have been related by equating the solutions for a rigid pile, free at the top and pinned at the tip. For $L/d = 25$, this gives $k_h d \simeq 0.8\ E_s$. Figure 14.17 shows that the elastic theory gives larger buckling loads than the subgrade-reaction theory for relatively flexible piles ($K_R < 10^{-3}$), but for stiffer piles, the solutions are almost identical. The difference between the solutions becomes more marked as L/d decreases.

Figure 14.17 indicates that the estimation of the buckling load from the simpler subgrade-reaction theory will generally give a conservative value, but unless the pile is extremely flexible, the error will not be serious.

15

DYNAMIC LOADS ON PILES

15.1 INTRODUCTION

The design of a foundation subjected to dynamic loading must satisfy the usual requirements of safety and stability, and in addition, must satisfy certain design criteria relating to the prevention of excessive dynamic movements of the foundation and structure. The design criteria most often encountered relate to the dynamic response of the foundation. These are expressed in terms of the limiting amplitude of vibration at a particular frequency or a limiting value of peak velocity or peak acceleration. A summary of the displacement-amplitude–versus–frequency relationships for various sensitivities of response by persons has been given by Richart (1962) and is shown in Fig. 15.1. The envelope described by the shaded line in this figure as "limit for machines and machine foundations" relates to persons standing and being subjected to vertical vibrations and indicates a limit for safety, not a limit for satisfactory operation of machines. It should be noted that the magnitudes of vibration involved in the criteria in Fig. 15.1 are much smaller than the displacements usually considered for foundations subjected to static loads.

In the design of foundations subjected to dynamic loads the response of the foundation, in the form of stress, strain, deflection, and so on, must be determined and compared with the design criterion adopted. In the estimation of this response, three important steps that among others must be considered, are

1. Definition of the loads.
2. Use of an appropriate method of analysis.
3. Selection of soil and foundation parameters for use in the analysis.

In this chapter, consideration will be given first to the estimation of various types of dynamic loads to which the foundation may be subjected. Analyses for the determination of foundation response under vertical and horizontal loading are then described and information regarding the required soil parameters is given, where possible. Torsional loading on piles has been considered by Richart et al. (1970) and Novak and Howell (1977), but will not be discussed here.

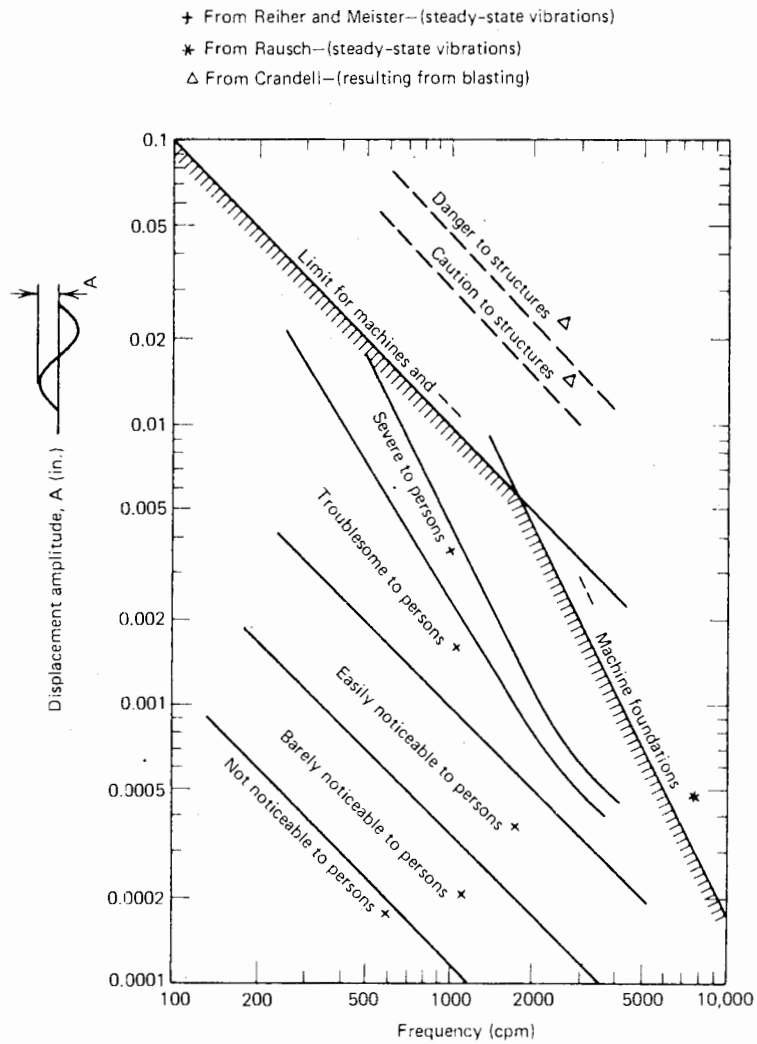

FIGURE 15.1 General limits of displacement amplitude for a particular frequency of vibration (from Richart, 1962).

15.2 ESTIMATION OF DYNAMIC LOADS

In general, a foundation has six degrees of freedom, and there are, correspondingly, six modes of vibration (Fig. 15.2). In many cases, the principal unbalanced forces are predominantly vertical or horizontal, so that the corresponding vibration modes are vertical, horizontal, and pitching.

Dynamic loads may broadly be divided into two main categories (Nair, 1969):

1. Loads applied directly to the foundation–for example, machine loads, wave forces, pile driving.

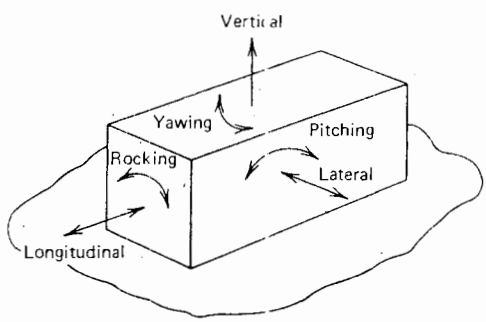

FIGURE 15.2 Six modes of vibration.

2. Loads applied to the foundation through the soil—for example, earthquake loads, ' ist effects, distant vibrating sources.

In this section, attention will be confined to machine loads, wave forces, and earthquake forces. Forces in a pile caused by pile driving have been considered in detail in Chapter 4.

15.2.1 Machine Loads

These are primarily steady-state vibrations developed by machines having rotating or reciprocating parts. The frequency of the steady-state vibrations is the same as the operating frequency of the machine.

Multimass Vibrators
The simplest case of unbalanced forces is that associated with oscillators used for deteriming the vibration response of soils. A typical type of oscillator has counter-rotating shafts, each carrying an eccentric circular weight W_1, mounted on a base. The horizontal unbalanced forces cancel, and the unbalanced vertical force has a magnitude of

$$Q = m_0 r\omega^2 \sin \omega t \tag{15.1}$$

where

Q = vertical force
m_0 = total unbalanced rotating mass = $2W_1/g$
r = eccentric radius of each mass
ω = angular velocity
t = time

The output is thus a sinusoidally varying force of period $2\pi/\omega$ and maximum value $m_0 r\omega^2$.

Rotating Machinery
Rotating machinery designed to operate at a constant speed for long periods of time includes turbines, axial compressors, centrifugal pumps, and fans. In such cases, some unbalance of forces always exists in practice, although it is theoretically possible to balance the moving parts. In certain types of machinery, unbalanced forces are developed on purpose (e.g., compaction machinery, vibratory rollers, vibroflotation equipment). In such cases, the maximum dynamic force is given by

$$Q = m_e e\omega^2 \tag{15.2}$$

where

m_e = total unbalanced mass
e = eccentric radius to the center of gravity of this mass
ω = angular velocity

Reciprocating Engines
In a reciprocating engine, unbalanced periodic forces arise as a result of the need to decelerate and accelerate the moving parts. In multicylinder engines and compressors, it is possible to arrange the cylinders in a manner that minimizes the unbalanced forces. The forces developed by both single and multicylinder machines for different crank arrangements and numbers of cylinders have been summarized by Richart, Hall, and Woods (1970). In general, multicylinder engines have smaller unbalanced forces than do one- and two-cylinder engines and compressors.

15.2.2 Wave Forces

The forces introduced into piles by waves have received considerable attention in recent years because of the increased activity in offshore construction. The methods that form the basis for most design work were proposed by Morison et al. (1950) and Crooke (1955), and both depend on a knowledge of water-particle motion and empirically determined coefficients. In the Morison formula, the force is taken to be composed of two parts, one depending on friction or drag effects and the other on inertia effects. As pointed out by Nair (1969), this formula is only approximate, as the existence of drag forces is a violation of the assumption in the simple theory on which the inertia force term is based. However, more-refined analyses do not appear to have produced any better agreement with measured forces than the Morison equation.

For large-diameter piles in which the diameter is not negligible in comparison to the wavelength, the waves interact with the piling, causing wave deformation, reflection, and diffraction. In this case, Morison's theory is not reliable, and an analysis based on diffraction theory is preferable.

More-detailed information on wave forces, and also wind forces on exposed structures, is summarized by Myers et al. (1969).

15.2.3 Earthquake Forces

An element of soil in the ground during an earthquake is subject to time-dependent stresses, displacements, and

strains that will vary with location and soil type. Nair (1969) classifies three methods of accounting for earthquake forces:

1. Equivalent static load at surface, taking either this load as a certain percentage (e.g., 10%) of the vertical static load, or as the base shear utilized in the seismic analysis of the structure, or as a force based on an average ground acceleration (a seismic coefficient times gravitational acceleration).
2. Equivalent dynamic load applied at the surface, often assumed to be sinusoidal; that is, $F(t) = F_0 \sin \omega t$, where F_0 is the equivalent static load and ω is a frequency corresponding to the predominant frequency of the earthquake.
3. One component of earthquake acceleration at bedrock. Earthquakes introduce two components of motion in the horizontal and one in the vertical plane, the amplitude of the latter usually being considerably less. Since the two horizontal components are usually similar, the earthquake motion is usually applied in the form of a prescribed horizontal acceleration.

The use of equivalent static or dynamic loads, though convenient, does not have a rational basis. For example, Seed and Martin (1966) have suggested that in relation to embankment design, the equivalent seismic coefficient is between 0.4 and 0.25, depending on the position of the potential failure circles. However, the seismic coefficient varies with depth, so the use of a single value may be inaccurate, especially for pile foundations.

The use of one component of the earthquake acceleration applied at bedrock has the most rational basis. The soil mass and the embedded piles overlying the bedrock are assumed to be set in motion by the imposed acceleration, which is usually taken to vary only with time, not spatially. Analyses given in soil-mechanics literature have generally been based on using old earthquake records, although accelerograms can be generated artificially by stochastic processes.

Because the deformations produced in the soil by a horizontal base excitation are primarily shear deformations, the real system may be considered as discrete system based on a column of soil having a unit cross-sectional area and a height equal to the depth of the soil layer (Idriss and Seed, 1968; Penzien et al., 1964). The response of the entire soil mass may then be analyzed by assuming the mass to be lumped at discrete points down the depth of the layer and the linkages connecting adjacent masses to consist of a system of springs and dashpots. This system may be nonlinear and can be adapted to any desired representation of dynamic soil behavior. The use of such models to analyze the response of a pile-foundation system is discussed briefly in Section 15.6. However, it should be emphasized here that although such analyses may give useful qualitative information, it may be unwise to place too great a reliance on the quantitative results, since the random nature of earthquake motion makes the satisfactory prediction of earthquake performance an extremely difficult task.

15.3 PILE RESPONSE TO AXIAL LOADS

15.3.1 End-Bearing Piles

The problem of a pile bearing on a rigid stratum with no tip deformation and no load transfer to the soil along the shaft can be analyzed by solving the wave equation on the assumption that lateral deformations of the pile can be neglected. The solution to this equation may be written as follows:

$$\frac{AL\rho}{m} = \frac{AL\gamma}{W} = \frac{2\pi f_n L}{\mathrm{v}} \tan\left(\frac{2\pi f_n L}{\mathrm{v}}\right) \tag{15.3}$$

where

A = cross-sectional area of pile
L = length of pile
ρ = mass density of pile material
m = added mass at top of pile
γ = unit weight of pile material = ρg
W = weight of added mass at top of pile = mg
f_n = natural frequency of pile
v = longitudinal wave velocity in pile

From Eq. (15.3), solutions may be recovered for both the natural frequency, f_n, and the maximum dynamic pile force, P_m (which can be shown to occur always at the pile tip). For the limiting cases of a weightless pile or the pile only with no added mass, these solutions reduce to very simple forms, while the solutions for the general case may be expressed in terms of these limiting solutions. The solutions may be summarized as follows:

1. Weightless pile ($\gamma = 0$):

$$f_n(\gamma=0) = \frac{1}{2\pi}\sqrt{\frac{AE_p g}{WL}} \tag{15.4a}$$

$$P_m(\gamma=0) = \frac{aAE_p}{L} \tag{15.4b}$$

2. Pile only with no added mass ($W = 0$):

$$f_n(W=0) = \frac{1}{4L}\sqrt{\frac{E_p g}{\gamma}} \tag{15.5a}$$

$$P_m(W=0) = \frac{\pi}{2}\left(\frac{aAE_p}{L}\right) \tag{15.5b}$$

3. General case:

$$f_n = \left(\frac{2\lambda}{\pi}\right) f_{n(W=0)} = \sqrt{\frac{\lambda}{\tan\lambda}}\,[f_{n(\gamma=0)}] \tag{15.6a}$$

$$P_m = \left(\frac{2\lambda}{\pi \sin\lambda}\right) P_{m(W=0)} = \left(\frac{\lambda}{\sin\lambda}\right) P_{m(\gamma=0)} \tag{15.6b}$$

where

a = amplitude of movement at top of pile
E_p = Young's modulus of pile
λ = solution of the equation

$$\lambda \tan\lambda = \gamma AL/W \tag{15.7}$$

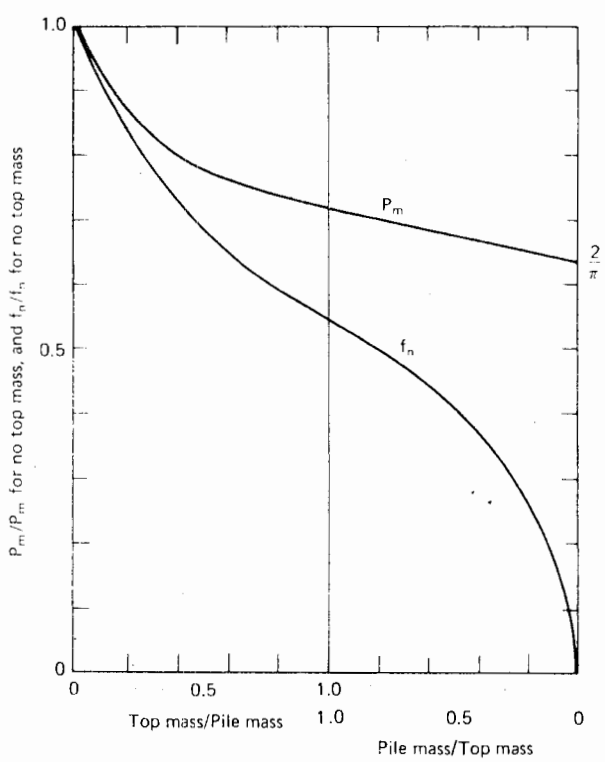

FIGURE 15.3 Solutions for natural frequency and maximum force in an end-bearing pile with no load transfer.

For the general case, solutions are plotted in Fig. 15.3 in terms of the values for zero top mass.

For a number of typical cases, the influence of axial loading on the resonant frequency of end-bearing piles to rock is shown in Fig. 15.4 (Richart, 1962). The top three curves illustrate the resonant frequencies of unloaded steel, concrete, and wooden piles (Eq. 15.3). As the axial load is increased on a pile of given length, the resonant frequency is reduced.

The above solutions are applicable only to point-bearing piles along which no load transfer occurs so that the properties of the embedding soil have no influence on response of the pile to dynamic axial load. The more general case of

Material	E(lb/in.^{2})	γ(lb/ft^3)
Steel	29.4×10^6	480
Concrete	3.0×10^6	150
Wood	1.2×10^6	40

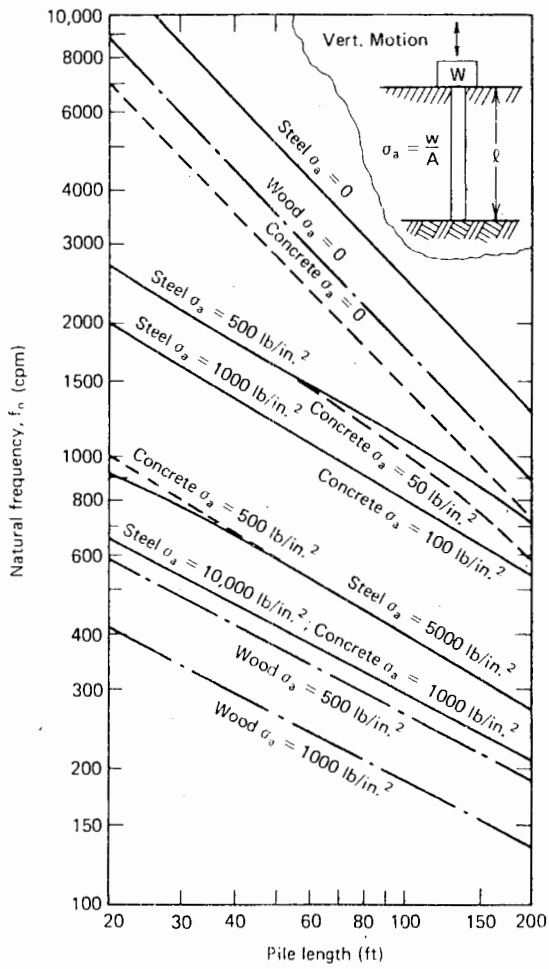

FIGURE 15.4 Resonant frequency of vertical oscillation for a point-bearing pile carrying a static load W—loaded stratum is rigid (from Richart, 1962).

floating piles, or end-bearing piles with some load transfer, is discussed below.

15.3.2 Floating Piles or End-Bearing Piles with Load Transfer

For floating piles, it would clearly be absurd to attempt an analysis on the assumption that no load transfer from the shaft to the soil occurs. There would appear to be at least four methods that could be employed to examine the response of floating piles to vertical loads, and these are listed below in descending order of sophistication:

1. A three-dimensional analysis (e.g., using the finite element method) in which the propagation of waves through the pile and soil is considered.
2. An approximate elastic analysis in which the problem is simplified to one of plane strain and it is assumed that the elastic waves only propagate horizontally.
3. Solution of the one-dimensional wave equation, for example, in a similar manner to the solution of this equation to analyze the pile-driving process.
4. An analysis of the response of a lumped-parameter mass-spring-dashpot system representing the pile and soil.

The first approach, although possible, involves certain problems in the numerical analysis–for example, the treatment of the boundaries of the problem, and doe not appear to have been extensively used as yet for pile foundations. It is probably too expensive in computer time to be economically feasible for practical design purposes. The second approach has been used by Novak (1974; 1977) to obtain an approximate solution for pile response to vertical loading. He assumed the soil to be composed of a set of independent infinitesimally-thin horizontal layers of infinite extent. This model could be thought of as a generalized Winkler material that possesses inertia and dissipates energy. By applying small harmonic excitations, Novak derived solutions for the equivalent stiffness and damping constants of the pile-soil system. The third method, involving extension of the numerical method of analysis used for pile driving (Chapter 4), does not appear to have been used. The fourth approach, the use of a lumped-parameter model, has been successfully applied to shallow foundations (e.g., Richart et al., 1970) and has been applied to pile foundations by Barkan (1962) and Maxwell et al. (1969), who used a single-degree-of-freedom model; and Madhav and Rao (1971), who used a two degree-of-freedom model. Because of its simplicity and usefulness for design purposes, attention here will be concentrated on the single-degree-of-freedom model.

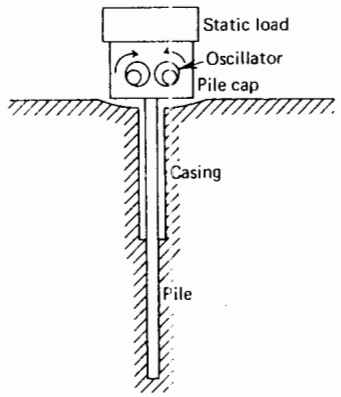

(a) Pile and soil system

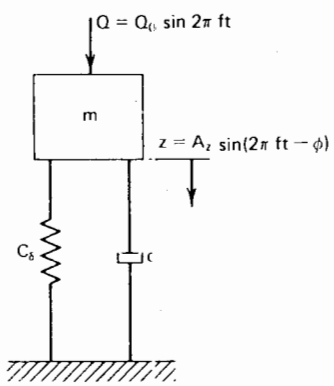

c = Damping coefficient
C_δ = Effective spring constant
m = Equivalent mass of system
Q = Periodic exciting force
Q_0 = Magnitude of exciting force
t = Time
z = Periodic displacement
A_z = Amplitude of displacement
ϕ = Phase angle between Q_0 and z
f = Frequency (Hz)

(b) Mechanical model system

FIGURE 15.5 Analytical model for floating pile (Maxwell et al., 1969). (Reprinted by permission of the American Society for Testing and Materials, © 1969.)

The single-degree-of-freedom model of the lumped-parameter system is illustrated in Fig. 15.5. Provided that appropriate values of the mass, damping, and spring constant can be selected for the system, use can be made of the solutions from elementary dynamics to determine the foundation response. For convenience, a summary of some of the more useful relationships is given in Table 15.1, while the response curves for a so-called constant-force excitation ($Q=Q_0\sin 2\pi ft$) is shown in Fig. 15.6, and those for a rotating mass excitation ($Q = m_e e\omega^2 \sin\omega t$) are shown in Fig. 15.7.

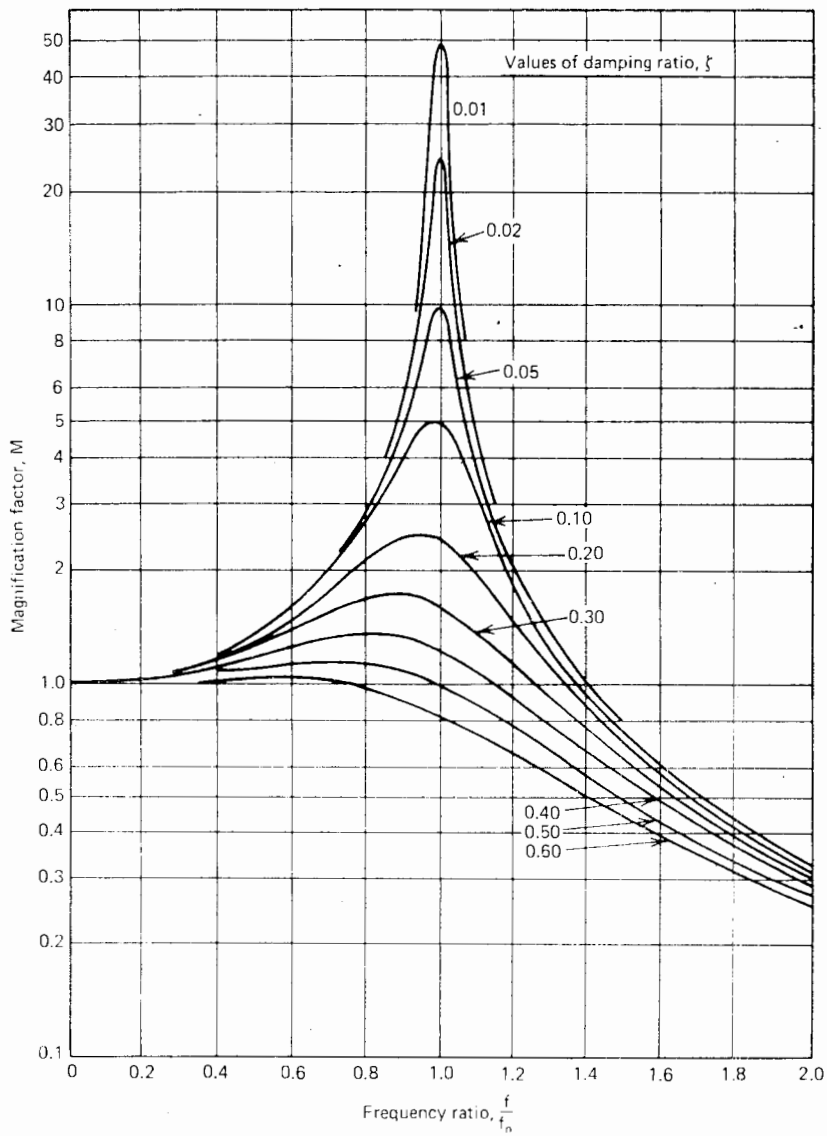

FIGURE 15.6 Response curves for constant force excitation.

In using the lumped-parameter approach, Barkan (1962) has ignored damping (i.e., assumed $c = 0$) and assumed the equivalent mass m to be the mass of the structure (or machine) and the supporting piles. The equivalent spring constant C_δ (termed the "coefficient of elastic resistance" by Barkan) used in Barkan's analysis is plotted in Fig. 15.8 as a function of pile length, but it is not specified whether these values are relevant to truly floating or predominantly end-bearing piles. In terms of the pile-settlement theory in Chapter 5, C_δ is the ratio of load P to settlement ρ and can be evaluated from Eq. (5.33) or Eq. (5.34).

As mentioned previously, Novak (1974) obtained analytical solutions for the stiffness and damping constants. His solutions demonstrated that these constants are not highly frequency-dependent, and that the most important parameters governing the response are the slenderness ratio and the ratio of shear-wave velocities in the pile and the soil. Ignoring the frequency dependence, Novak's solutions for the stiffness and damping constants of a pile with no tip movement (i.e., end-bearing pile) are shown in Table 15.2 for concrete and timber piles. His subsequent investigations (Novak, 1977) indicated that the damping of floating piles

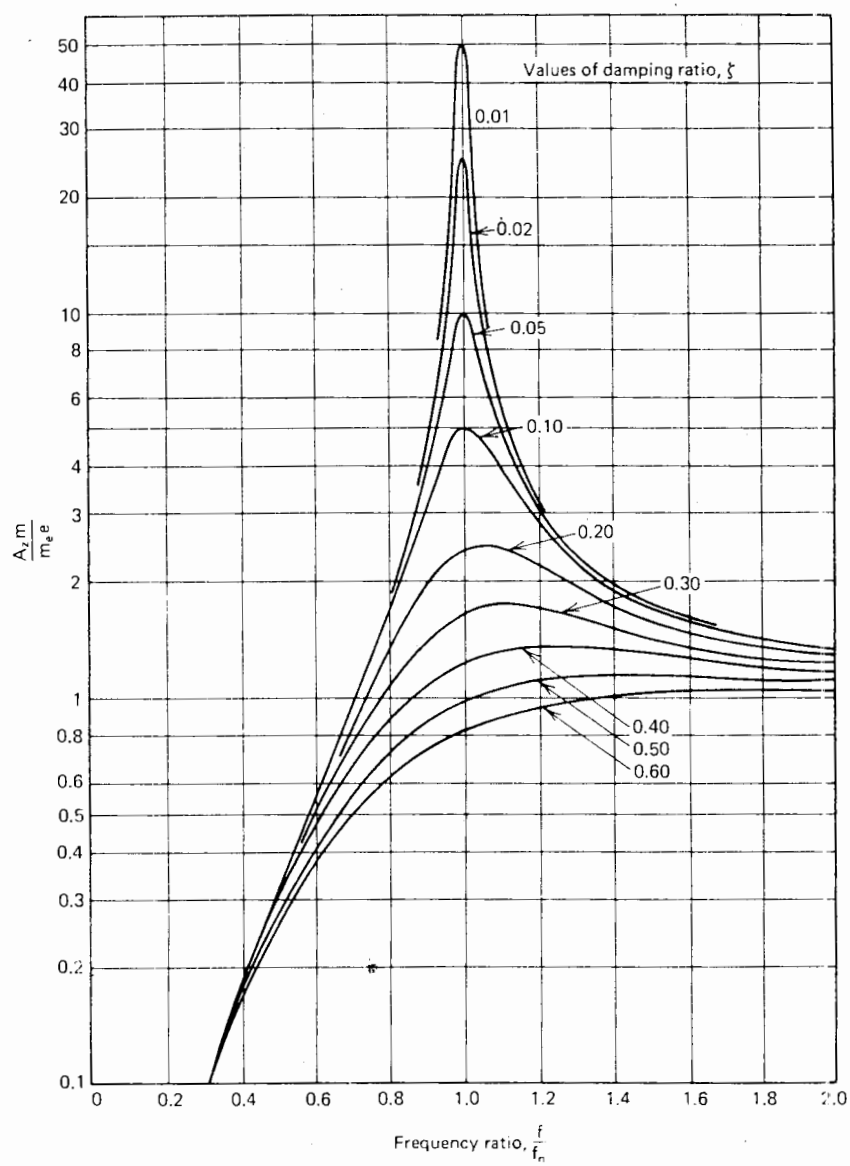

FIGURE 15.7 Response curves for rotating mass excitation.

is larger than that of end-bearing piles, and that the vertical dynamic response of a footing supported by floating piles can be much smaller than if it is supported by end-bearing piles. Some typical solutions for stiffness and damping constants of floating piles are given in the latter reference. In using Novak's solutions to evaluate the response of a footing or structure supported by the piles, the mass in the equivalent lumped-parameter system is taken to be that of the footing or the structure itself.

Maxwell et al. (1969) have also employed the lumped-parameter model in Fig. 15.5, but have considered the equivalent mass m to be only the above-ground mass of the oscillator, pile cap, and static load. They carried out a series of tests on steel H-piles and concrete-filled pipe piles, in silty sand and clay overlying sand, to determine the relationship between frequency and displacement. From the test results, values of equivalent stiffness C_δ and damping ratio ζ were backfigured. At resonance, the dynamic value of C_δ was found to be greater than the static stiffness for comparable piles, but it was suggested that the use of the static stiffness would be adequate for practical purposes. Damping was found to be slight, the computed damping

TABLE 15.1 SUMMARY OF RELATIONS FOR SINGLE-DEGREE-OF-FREEDOM VIBRATION

Critical damping	$c_c = 2\sqrt{C_\delta m}$
Damping ratio	$\zeta = \frac{c}{c_c}$
Undamped natural frequency	$f_n = \left(\frac{1}{2\pi}\right)\sqrt{\frac{C_\delta}{m}}$
Static displacement	$\rho_s = \frac{Q_0}{C_\delta}$
Amplitude-magnification factor during vibration	$M = \left[\left(1-\frac{f^2}{f_n^2}\right)^2 + \left(2\zeta\frac{f}{f_n}\right)^2\right]^{-1/2}$

For Constant-Force Excitation $Q = Q_0 \sin 2\pi ft$	For Rotating-Mass Excitation $Q = m_e e\omega^2 \sin\omega t \quad (\omega = 2\pi f)$
Amplitude at frequency f	
$A_z = \frac{Q_0}{C_\delta}(M)$	$A_z = \frac{m_e e}{m}\left(\frac{f}{f_n}\right)^2 M$
Maximum amplitude of vibration	
$A_{zm} = \frac{Q_0}{C_\delta}\frac{1}{2\zeta\sqrt{1-\zeta^2}}$	$A_{zm} = \left(\frac{m_e e}{m}\right)\left(\frac{1}{2\zeta\sqrt{1-\zeta^2}}\right)$
Frequency for maximum amplitude	
$f_m = f_n\sqrt{1-2\zeta^2}$	$f_m = f_n\left(\frac{1}{\sqrt{1-2\zeta^2}}\right)$

Note: For rotational motion,

$$f_n = \frac{1}{2\pi}\sqrt{\frac{C_\delta}{I}}$$

where

I = mass moment of inertia about appropriate axis.

TABLE 15.2[a] STIFFNESS AND DAMPING CONSTANTS FOR A SINGLE VERTICALLY LOADED END-BEARING PILE[b]

L/d	$\frac{V_s}{v_c}$	Concrete Piles $f_{18,1}$	Concrete Piles $f_{18,2}$	Timber Piles $f_{18,1}$	Timber Piles $f_{18,2}$
10	0.01	0.050	0.001	0.050	0.003
	0.02	0.051	0.005	0.054	0.013
	0.03	0.052	0.010	0.059	0.029
	0.04	0.055	0.018	0.066	0.050
	0.05	0.057	0.029	0.075	0.073
25	0.01	0.021	0.002	0.022	0.008
	0.02	0.023	0.011	0.030	0.029
	0.03	0.027	0.024	0.040	0.054
	0.04	0.032	0.032	0.053	0.077
	0.05	0.038	0.038	0.067	0.098
50	0.01	0.011	0.005	0.015	0.015
	0.02	0.016	0.020	0.027	0.039
	0.03	0.023	0.035	0.040	0.060
	0.04	0.030	0.048	0.053	0.079
	0.05	0.038	0.061	0.067	0.099

[a] Reproduced by permission of the National Research Council of Canada, from the *Canadian Geotechnical Journal*, Vol 11, 1974, pp. 574–598.

[b] After Novak (1974).

V_s = shear-wave velocity in soil = $[E_s g/(2(1+\nu_s)\gamma_s)]^{1/2}$

v_c = longitudinal-wave velocity in pile = $[E_p g/\gamma_p]^{1/2}$

Stiffness $C_\delta = \frac{2E_p A}{d} \cdot f_{18,1} = k_{zz}$ in Novak's terminology

Damping constant (coefficient of equivalent viscous damping)

$$c = \frac{2E_p A}{V_s} \cdot f_{18,2} = c_{zz} \text{ in Novak's terminology}$$

where

A = area of pile cross section
E_p = Young's modulus of pile
γ_s = soil unit weight
γ_p = pile unit weight

Note: for solid pile,

$$\frac{V_s}{v_c} = \left(\frac{1}{K}\frac{\gamma_p}{\gamma_s}\frac{1}{2(1+\nu_s)}\right)^{1/2}$$

where K = pile stiffness factor.

ratio ζ for single piles being on the order of 0.04 to 0.05. However, it was also found that both the stiffness and the damping ratio varied with frequency, so that the use of a single frequency-independent value of each of these parameters would not lead to an accurate prediction of pile response for all frequencies. In particular, the response at resonance cannot be reliably predicted from data on stiffness and damping generated at a nonresonant frequency. The variation of stiffness, expressed in terms of a stiffness ratio $C_\delta/C_{\delta n}$ (where $C_{\delta n}$ = stiffness at resonant frequency) and damping ratio ζ with frequency ratio f/f_n, is shown in Fig. 15.9.

Maxwell et al. also carried out tests to determine the effect of a pile cap, by performing a test with the cap (typically of a diameter about twice the equivalent diameter of the pile) in contact with the soil, and then excavating beneath the cap and carrying out another test. Typical test results, shown in Figs. 15.10 and 15.11, illustrate the importance in reducing dynamic displacements of the pile cap being in contact with the soil.

It should be noted that because the stiffness of a pile foundation is generally greater than that of a corresponding surface foundation, the natural frequency of the foundation-soil system will be increased by the use of piles. On the

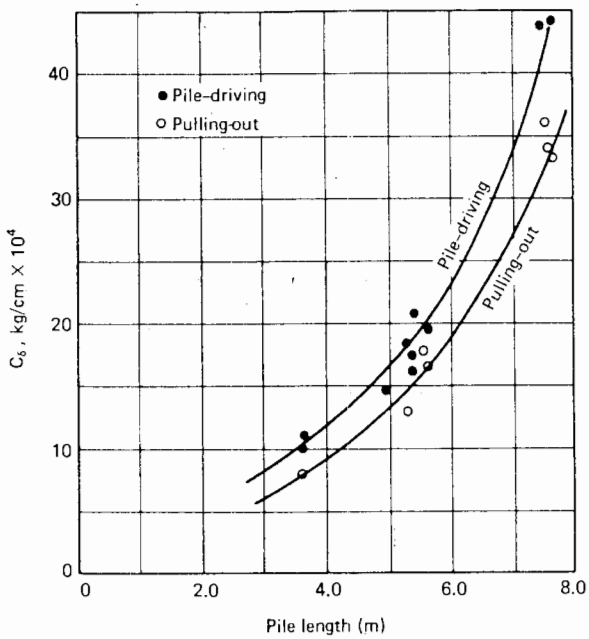

FIGURE 15.8 Variation of the coefficient C_δ of a pile (Barkan, 1962). (From *Dynamics of Bases and Foundations*, by D. D. Barkan, © 1962, McGraw-Hill Book Company Inc. Used with permission of McGraw-Hill Book Company.)

other hand, because of the much lower damping, the amplitude of dynamic movement of the pile foundation near resonance may well exceed that of the surface foundation (Novak, 1974)—that is, the use of piles may have an detrimental effect on the dynamic response.

15.3.3 Pile Groups

The approaches described above for single piles may be applied to pile groups, provided appropriate values of the spring stiffness and damping ratio can be determined. Barkan applied a correction factor μ to the single-pile value of C_δ, as shown in Table 15.3. However μ corresponds to the inverse of the settlement ratio R_s (see Chapter 6), and the use of the elastic theory given in that chapter would appear to provide a better method of estimating μ. Nevertheless, Barkan found, from tests on pile groups in saturated sand, that the measured natural frequency was in quite good agreement with that calculated from the appropriate expression in Table 15.1, although being consistently 5 to 15% higher.

Maxwell et al. (1969) carried out a field test on a four-pile group and found that as with the single piles tested, the stiffness and damping were frequency-dependent, (see

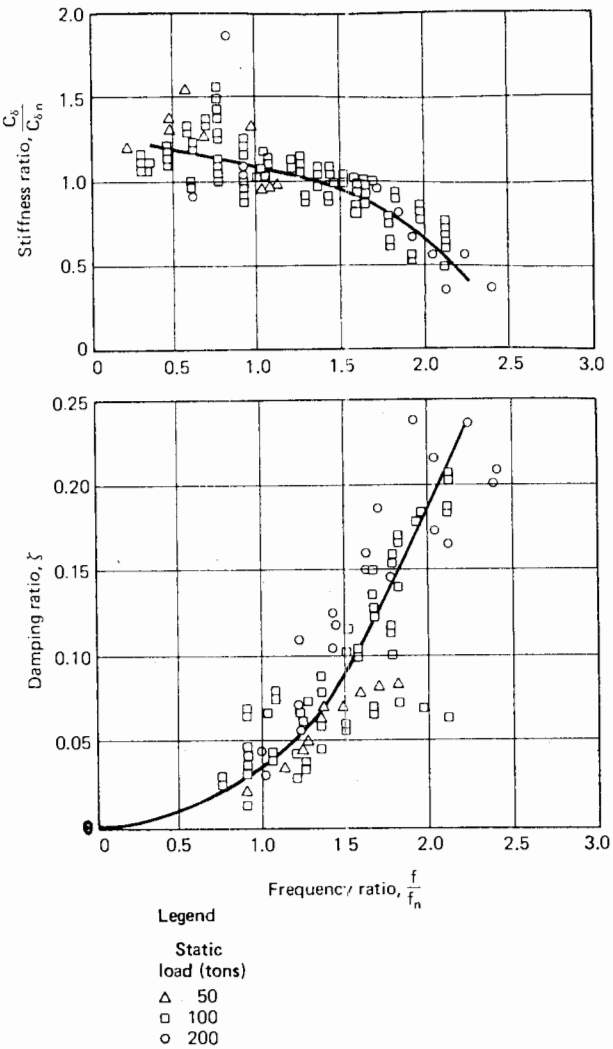

FIGURE 15.9 Stiffness and damping ratio vs. frequency ratio, pipe pile *D*-1 (Maxwell et al., 1969). (Reprinted by permission of the American Society for Testing and Materials, © 1969.)

TABLE 15.3 CORRECTION FACTOR μ FOR PILE GROUPS[a] (Barkan, 1962)

Spacing/Diameter	μ
6	0.65
4.5	0.64
3	0.41

[a] From Dynamics of Bases and Foundations, by D. D. Barkan, © 1962, McGraw-Hill Book Company Inc. Used with permission of McGraw-Hill Book Company.

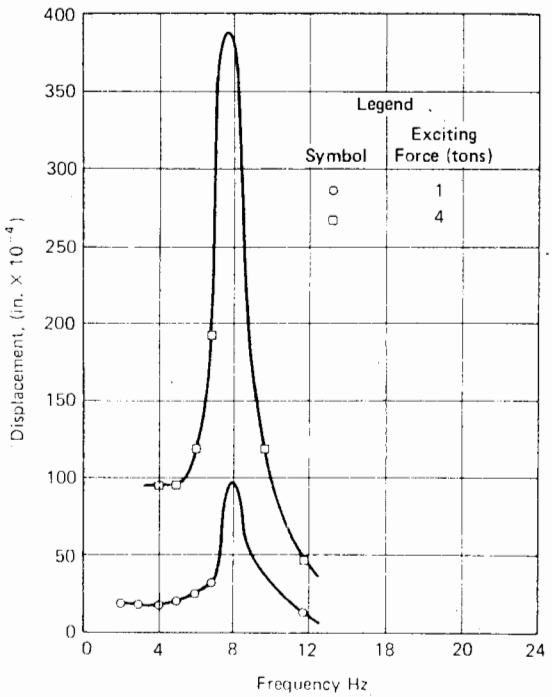

FIGURE 15.10 Results of constant-force test on uncased H-pile *D*-4 before excavation of soil under cap (Maxwell et al. 1969). (Reprinted by permission of the American Society for Testing and Materials, © 1969.)

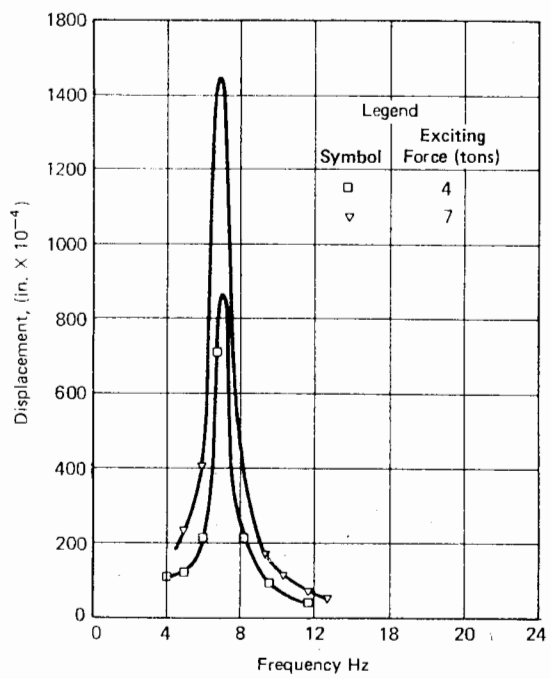

FIGURE 15.11 Results of constant-force test on uncased H-pile *D*-4 after excavation of soil under cap (Maxwell et al. 1969). (Reprinted by permission of the American Society for Testing and Materials, © 1969.)

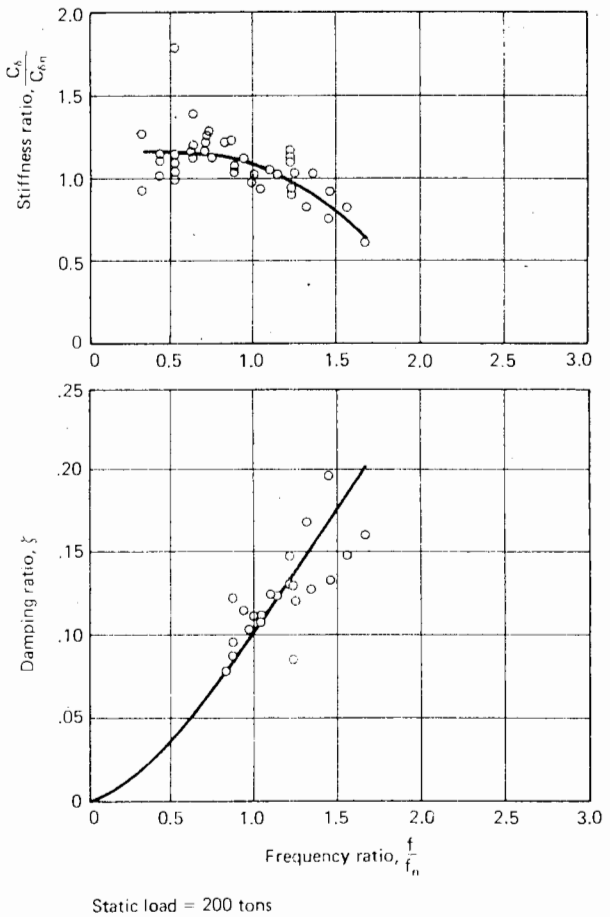

FIGURE 15.12 Stiffness and damping ratio vs. frequency ratio; four H-pile cluster *D*-3 (Maxwell et al. 1969). (Reprinted by permission of the American Society for Testing and Materials, © 1969.)

Fig. 15.12). Comparison between Figs. 15.9 and 15.12 shows that the damping for the pile group is greater than for the single pile, the value of ζ being about 0.1 at the resonant frequency as compared with about 0.04 for the single pile.

Novak and Grigg (1976) carried out tests on model piles and pile groups subjected to both vertical and horizontal excitation. Group effects were allowed for by the modification of the single-pile analyses through the use of interaction factors (see Chapters 6 and 8). The theory was found to predict all the qualitative features of response of the pile groups. The use of the soil modulus derived from a static single-pile test was found to yield reasonable predictions of natural frequency and resonant amplitude.

For relatively large groups of piles or groups having a breadth larger than the pile length, a simple approach may be employed for determining the amplitude of vibration, by

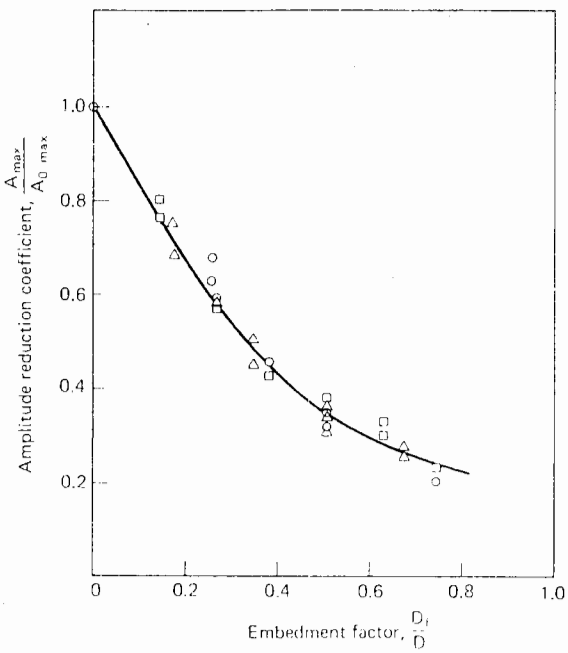

FIGURE 15.13 Amplitude reduction factor versus embedment factor for circular footings on sand (Chae, 1970).

considering the groups as a buried foundation and applying a correction factor to the calculated amplitude of the corresponding surface foundation. Chae (1970) has presented values of this correction factor as a function of relative embedment depth D_f/D (D_f = embedment depth; D = circle diameter) from tests on model circular footings on sand, and these are shown in Fig. 15.13. Values of D_f/D up to 0.8 only are considered. The maximum amplitude A_{omax} of the surface foundation may be calculated as

$$A_{omax} = \left(\frac{Q_0}{C_\delta}\right) \frac{B}{0.85\,(B - 0.18)^{1/2}} \tag{15.8}$$

where

Q_0 = amplitude of disturbing force
C_δ = equivalent spring stiffness
B = mass ratio $= \dfrac{m_0(1 - \nu_s)}{\rho D^2}$
m_0 = mass of foundation
ρ = mass density of soil
ν_s = Poisson's ratio of soil

For foundation shapes other than circular, the mass ratio of a circle of equal area may be used to compute A_{omax}. C_δ can probably be determined with sufficient accuracy from a calculation of immediate settlement under static conditions. Normally, ν_s would be taken as 0.5.

Chae's tests showed that although embedment significantly decreases the amplitude of vibrations, the resonant frequency is not appreciably affected, so that the value for a surface foundation may be used. On the basis of the theory for the soil as an elastic half-space, the resonant frequency, f_n, can be calculated as

$$f_n = \left[\frac{(G_s/\rho)^{1/2}}{\pi D}\right]\left[\frac{(B - 0.36)^{1/2}}{B}\right] \tag{15.9}$$

where

G_s = shear modulus of soil, preferably determined from a dynamic test

The equivalent dimensions of a pile group may be estimated as described in Section 6.3. If the embedded depth, D_f/D, is greater than 0.8, the above simple approach cannot validly be used, and resort must be made to the method described in the previous section.

15.4 PILE RESPONSE TO LATERAL LOADING

In examining the response of a single pile subjected to a time-dependent horizontal force and moment, at least three approaches may be employed

1. The pile is reduced to an equivalent cantilever. The resonant frequency and the amplitude of vibration of the cantilever may than be determined by standard methods. However, no information can be obtained on the moments, stresses, and displacements along the length of the pile for dynamic loads.
2. The pile is considered as a beam on an elastic foundation subjected to time-dependent loading and analyzed by finite differences. Moments, stresses, and displacements along the length of the pile may be analyzed, and impact loads as well as harmonic loads can be considered.
3. The approximate analytical technique developed by Novak (1974) and described previously for vertical response can be used. This approach derives stiffness and damping constants for piles and pile groups, and thus enables use of the simple "lumped-parameter" approach to determine the lateral response.

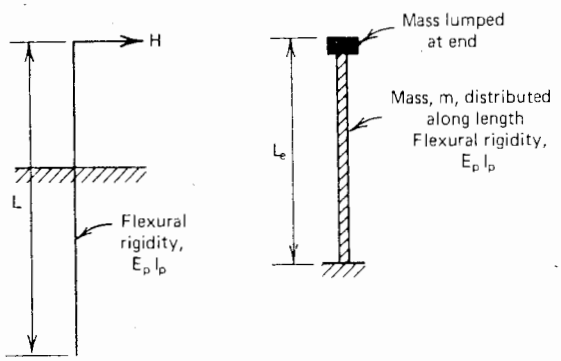

(a) Actual pile (b) Equivalent cantilever

FIGURE 15.14 Pile as equivalent cantilever.

15.4.1 Equivalent Cantilever Systems

The problem is illustrated in Fig. 15.14*a*, and a general representation of the equivalent cantilever is shown in Fig. 15.14*b*. The mass of the pile may be considered to be uniformly distributed along its length with a mass lumped at the end. The length L_e of the equivalent cantilever may be estimated from the consideration of the beam on an elastic foundation subjected to a horizontal static load, as used by Davisson and Robinson (1965) and Nair et al. (1969) (See Chapter 14.).

For the case of a cantilever of uniform cross-section with no concentrated static mass at the top, the natural frequencies, f_n, are given by

$$f_n = \left(\frac{C_\omega}{2\pi}\right)\sqrt{\frac{E_p I_p}{m L_e^3}} \tag{15.10}$$

where

$E_p I_p$ = stiffness of cantilever in bending
m = mass of cantilever
L_e = equivalent length of cantilever
C_ω = coefficient
= 3.52, 22.03, and 61.70 for the first three modes of vibration

The above solution may be used for cases in which the static lateral load is negligible in relation to the weight of the pile.

For the case of a weightless cantilever having a static load at the top, the solution for the lowest natural frequency, f_n, is approximate by the Southwell-Dunkerley expression (Richart et al., 1970):

$$f_n \simeq \frac{3.13}{\sqrt{\rho_1}}\ Hz \tag{15.11}$$

where

ρ_1 = static deflection of top under the static load, in *in.*

The above solution may be applied in cases where the static lateral load is large in relation to the weight of the pile.

For the simple case of a floating pile in a uniform Winkler medium, Warburton (1964) derived the following expression for natural frequency:

$$f_n = \left(\frac{1}{2\pi}\right)\sqrt{\frac{k_h d}{\rho A}} \tag{15.12}$$

where

k_h = horizontal modulus of subgrade reaction (see Section 8.2)
d = pile diameter or width
ρ = mass density of pile
A = cross-sectional area of pile

For more-complicated problems, the frequency-displacement relationship and resonant frequency of the cantilever may be obtained by solving the appropriate equation of motion. If the forced vibration has a frequency very different from the resonant frequency of the system or any of its harmonics, the amplitude of motion under the forced vibration is unlikely to be much greater than that given by a static analysis using the maximum and minimum values of applied load.

In an alternative approach described by Hayashi et al. (1965), nonlinear and viscous behavior of the soil is considered. Results presented by them indicate that the nonlinear effects introduced by the soil have a significant effect on the pile response.

15.4.2 Finite-Difference Analysis

This analysis, presented by Tucker (1964), is an extension of the static analysis described in Section 8.2. The representation of the pile is shown in Fig. 15.15. In the general case, the width or diameter of the pile, and hence the bending stiffness $E_p I_p$—denoted here as F—may vary along the pile. In the static case, lateral and axial loads H and P may act. The soil is assumed to be a Winkler material and provides a lateral resistance, S_i, per unit length at any point i. To

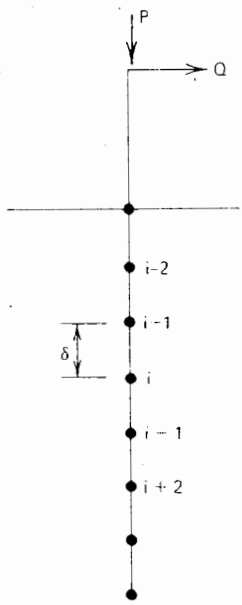

FIGURE 15.15 Finite-difference representation of pile.

allow for rotational restraints along the pile (e.g., at the pile head), a rotational elastic restraint, R_i, is assumed at the point i ($R_i = 0$ if no restraint is provided at i).

The finite-difference expression for the static behavior of the pile at a point i may be expressed as follows (Matlock and Ingram, 1963):

$$a_i\rho_{i-2} + b_i\rho_{i-1} + c_i\rho_i + d_i\rho_{i+1} + e_i\rho_{i+2} = f_i \qquad (15.13)$$

where

$$a_i = F_{i-1} - \frac{\delta}{4}(R_{i-1} + \delta P_{i-1})$$

$$b_i = -2(F_{i-1} + F_i)$$

$$c_i = F_{i-1} + 4F_i + F_{i+1} + \delta^3 S_i + \frac{\delta}{4}(R_{i-1} + \delta P_{i-1}) + \frac{\delta}{4}(R_{i+1} + \delta P_{i+1})$$

$$d_i = -2(F_i + F_{i+1})$$

$$e_i = F_{i+1} - \frac{\delta}{4}(R_{i+1} + \delta P_{i+1})$$

$$f_i = \delta^3 H_i$$

δ = distance between adjacent node points
$F_i = E_p I_p$ at i
P_i = axial load at i
R_i = rotational restraint at i
S_i = spring factor for lateral soil resistance at $i = k_{hi} d\delta$
H_i = applied lateral load at i
d = pile diameter

The inclusion of dynamic effects involves the addition of terms to the above equation, representing inertial and damping characteristics of the pile-soil system. Inertial properties of the soil medium are assumed to be included in the elastic restraints, S. Inertial properties of the pile and soil damping are then represented as additional forces on the pile at each point i. Thus the resulting lateral load at i is

$$H_i = H_i' - H_{ai} - H_{vi} \qquad (15.14)$$

where

H_i' = applied lateral load
H_{ai} = inertial force
H_{vi} = damping force

H_{ai} is related to the acceleration at i, and H_{vi} to the velocity at i, as follows:

$$H_{ai} = \left(\frac{W_i}{g}\right)\left(\frac{\partial^2 \rho_i}{\partial t^2}\right) \qquad (15.15)$$

$$H_{vi} = J_i\left(\frac{\partial \rho_i}{\partial t}\right) \qquad (15.16)$$

where

W_i = weight of pile element at point i
g = gravitational acceleration
J_i = damping factor at i

The acceleration, $\frac{\partial^2 \rho_i}{\partial t^2}$, and the velocity, $\frac{\partial \rho_i}{\partial t}$, may be written in terms of higher-order backward differences so that Eqs. (15.15) and (15.16), for a time t, and a time increment δt, become

$$H_{ai,t} = \frac{W_i}{g(\delta t)^2}(2\rho_{i,t} - 5\rho_{i,t-1} + 4\rho_{i,t-2} - \rho_{i,t-3}) \qquad (15.17)$$

$$H_{vi,t} = \frac{J_i}{6\delta t}(11\rho_{i,t} - 18\rho_{i,t-1} + 9\rho_{i,t-2} - 2\rho_{i,t-3}) \qquad (15.18)$$

Equations (15.14), (15.17), and (15.18) may now be incorporated into Eq. (15.13). If the coefficients for all unknown deflection values for any time t are placed on the

left-hand side and all known values on the right-hand side, the resulting expression is

$$A_i\rho_{i-2,t} + B_i\rho_{i-1,t} + C_i\rho_{i,t} + D_i\rho_{i+1,t} + E_i\rho_{i+2,t} = G_i \tag{15.19}$$

where

$$A_i = F_{i-1} - \frac{\delta}{4}(R_{i-1,t} + \delta P_{i-1,t})$$

$$B_i = -2(F_{i-1} + F_i)$$

$$C_i = F_{i-1} + 4F_i + F_{i+1} + \delta^3 S_{i,t} + \frac{\delta}{4}(R_{i-1,t} + \delta P_{i-1,t}) + \frac{\delta}{4}(R_{i+1,t} + \delta P_{i+1,t}) + \delta^3(2W_i/(\delta t)^2 + J_i/6\delta t)$$

$$D_i = -2(F_i + F_{i+1})$$

$$E_i = F_{i+1} - \frac{\delta}{4}(R_{i+1,t} + \delta P_{i+1,t})$$

$$G_i = \delta^3 H_{i,t} + W_i(5\rho_{i,t-1} - 4\rho_{i,t-2} + \rho_{i,t-3})\frac{\delta^3}{(\delta t)^2} + \frac{J_i\delta^3}{6\delta t}(18\rho_{i,t-1} - 9\rho_{i,t-2} + 2\rho_{i,t-3})$$

The above equation can be applied to all interior-node points of the pile, and these, together with the equations describing the top and tip boundary conditions and the horizontal-load and moment-equilibrium equations, describe the behavior of the pile at a time t.

To solve a particular problem, an initial set of conditions (deflection, velocity and acceleration) must be specified and Eq. (15.19) and the associated boundary-condition and equilibrium equations must be solved for each time increment δt.

Tucker (1964) presented two examples illustrating the use of the above approach. The first involved impact loading of a 70-ft-long pile with two section changes and its lower 55 ft embedded in a material having a linearly increasing modulus of subgrade reaction with depth. Time increments of 0.02 seconds were used in the solution. The problem is shown in Fig. 15.16, together with the solutions for displacement versus time and moment-distribution at two times. The second example, one of forced vibrations on a free-head pile, simulates the model pile tests of Gaul (1958). A sinusoidally varying load was applied at the mud line, and 10 elements were used for the pile. Each load cycle was represented by 20 time-increments, and several frequencies of load application were considered, varying from 1 to 200 cycles per second. Calculations at each frequency were continued until the oscillation of the pile had stabilized into a pattern. The problem and the solutions for amplitude versus frequency and peak moment versus depth for three frequencies, are shown in Fig. 15.17. The latter curves show that pile bending moments increase significantly as the vibration frequency approaches the natural frequency of the system (about 80 to 85 cps here). The

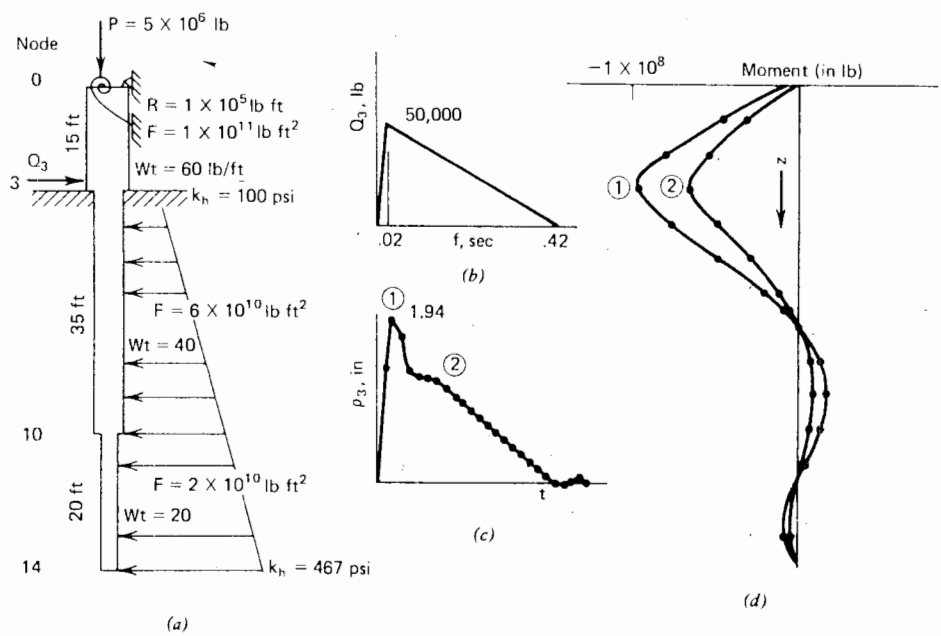

FIGURE 15.16 Example of impact loading on a restrained-head pile (Tucker, 1964).

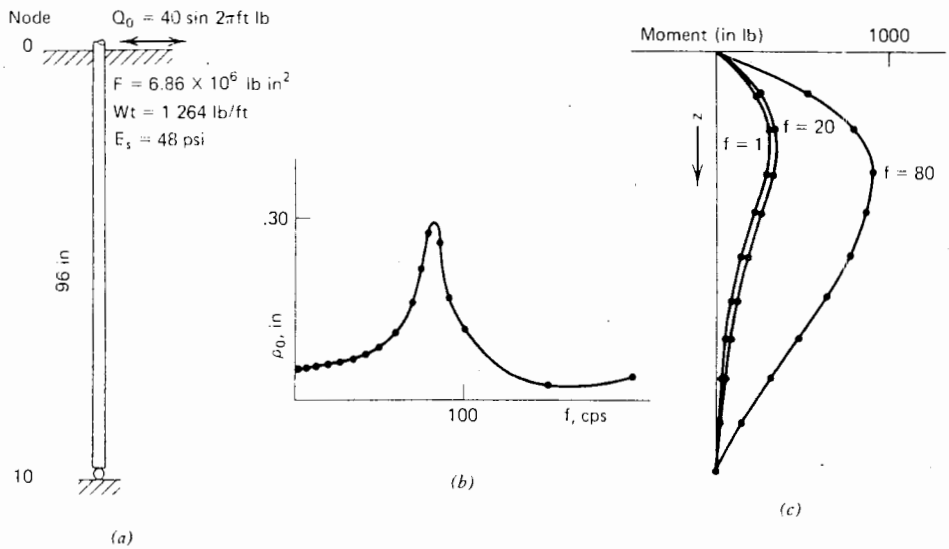

FIGURE 15.17 Example of forced vibration of a model free-head pile (Tucker, 1964).

peak moment curve for a frequency of 1 cps agrees well with that obtained experimentally by Gaul.

Further developments of the above method of analysis, and also a number of test results, have been described by Chan and Matlock (1973), Agarwal (1973), and Prakash and Chandrasekaran (1973).

An alternative analysis for pile response to dynamic lateral loads, employing a finite-element formulation for the pile, has been described by Ross (1971). Nonlinear soil-resistance properties and geometrical nonlinearity of the piles were taken into account, and a study of a pile subjected to wave forces was made. It was found that maximum displacements based on the dynamic analysis were considerably greater than maximum displacements by static analysis, especially along the upper portion of the pile. It was also found that the magnitude and distribution with depth of the subgrade-reaction modulus of the soil influenced the dynamic response considerably.

All the above analyses are based on subgrade-reaction theory, with the soil being represented as a Winkler material. It is also possible to extend the static-elastic analysis described in Chapter 8 by incorporating inertia and damping terms in the basic pile-bending equation. Such an approach, while allowing for continuity of the soil mass, is, however, still approximate, as it relies on static-elastic theory to give the dynamic response of the pile-soil system. Preliminary calculations indicate that the natural frequency of a pile in a uniform soil given by such an analysis is quite similar to that given by a subgrade-reaction analysis.

15.4.3 Novak's Analysis

Novak (1974) has derived lateral stiffness and damping constants for single piles, including values for coupled rotation and translation; Table 15.4 reproduces some of these solutions. It is again found that the frequency dependence of stiffness and damping can generally be ignored, and that the important parameters are the ratio of shear-wave velocities in the pile and soil, and the slenderness ratio L/d. The effect of static load was investigated and found to be significant only with extremely poor soils. Most stiffness and damping parameters were reduced by the presence of axial load, but the damping caused by rotation was increased.

15.4.4 Pile Groups

The methods currently available for the analysis of pile groups for dynamic surface loads are usually extensions of methods of structural analysis in which the piles are reduced to equivalent cantilevers. Such analyses, described by Shubinski et al. (1967), Nath and Harleman (1967), and Saul (1968), can take account of vertical and torsional loading as well as lateral loads. However, some uncertainty may arise in some of these analyses regarding the structural approximation of the group. An approximate estimate of the behavior of a group under dynamic lateral loading may be obtained by analyzing a single pile under such loading and then allowing for group effects on the basis of a static

TABLE 15.4[a] STIFFNESS AND DAMPING CONSTANTS FOR LATERAL RESPONSE OF PILES HAVING $L/d > 12.5$[b]

Pile Material	$\frac{V_s}{v_c}$	Stiffness Parameters			Damping Parameters		
		$f_{7,1}$	$f_{9,1}$	$f_{11,1}$	$f_{7,2}$	$f_{9,2}$	$f_{11,2}$
Concrete ν_s=0.4	0.01	0.202	−0.0194	0.0036	0.139	−0.0280	0.0084
	0.02	0.285	−0.0388	0.0100	0.200	−0.0566	0.0238
	0.03	0.349	−0.0582	0.0185	0.243	−0.0848	0.0438
	0.04	0.403	−0.0776	0.0284	0.281	−0.1130	0.0674
	0.05	0.450	−0.0970	0.0397	0.314	−0.1410	0.0942
Wood ν_s=0.4	0.01	0.265	−0.0336	0.0082	0.176	−0.0466	0.0183
	0.02	0.374	−0.0673	0.0231	0.249	−0.0932	0.0516
	0.03	0.459	−0.1010	0.0425	0.305	−0.1400	0.0949
	0.04	0.529	−0.1350	0.0654	0.352	−0.1860	0.1460
	0.05	0.592	−0.1680	0.0914	0.394	−0.2330	0.2040
Concrete ν_s=0.25	0.01	0.195	−0.0181	0.0032	0.135	−0.0262	0.0076
	0.02	0.275	−0.0362	0.0090	0.192	−0.0529	0.0215
	0.03	0.337	−0.0543	0.0166	0.235	−0.0793	0.0395
	0.04	0.389	−0.0724	0.0256	0.272	−0.1057	0.0608
	0.05	0.435	−0.0905	0.0358	0.304	−0.1321	0.0850
Wood ν_s=0.25	0.01	0.256	−0.0315	0.0074	0.169	−0.0434	0.0165
	0.02	0.362	−0.0630	0.0209	0.240	−0.0868	0.0465
	0.03	0.444	−0.0945	0.0385	0.293	−0.1301	0.0854
	0.04	0.512	−0.1260	0.0593	0.339	−0.1735	0.1315
	0.05	0.573	−0.1575	0.0828	0.379	−0.2168	0.1838

[a] Reproduced by permission of the National Research Council of Canada, from the *Canadian Geotechnical Journal*, vol. 11, 1974, pp. 574-590.

[b] After Novak (1974).

Translation stiffness constant, $k_{xx} = \frac{8E_pI_p}{d^3}(f_{11,1})$

Translation damping constant, $c_{xx} = \frac{4E_pI_p}{d^2V_s}(f_{11,2})$

Rotation stiffness constant, $k_{\psi\psi} = \frac{2E_pI_p}{d}(f_{7,1})$

Rotation damping constant, $c_{\psi\psi} = \frac{E_pI_p}{V_s}(f_{7,2})$

Cross-stiffness constant, $k_{x\psi} = \frac{4E_pI_p}{d^2}(f_{9,1})$

Cross-damping constant, $c_{x\psi} = \frac{2E_pI_p}{dV_s}(f_{9,2})$

where

I_p = moment of inertia of pile cross-section
E_p = Young's modulus of pile
V_s = shear wave velocity in soil
v_c = longitudinal wave velocity in pile
d = pile diameter

analysis of pile interaction (see Chapter 8). Novak and Grigg (1976) have used this approach to modify Novak's single-pile solutions and have obtained good agreement between the response so calculated and the response of groups of model piles.

15.5 PILE RESPONSE TO EARTHQUAKE FORCES

An analysis of this problem has been described by Penzien et al. (1964). The analysis is divided into two parts:

1. The determination of the dynamic response of the soil medium alone when excited through its lower boundary by a prescribed horizontal seismic motion.
2. The determination of the interaction of the entire structural system (structure and piles) with the moving soil medium.

Dynamic Response of Soil Alone

The soil is assumed to be of infinite horizontal extent and of constant depth, and is idealized as a discrete-mass system based on a column of soil having a unit cross-sectional area and a height equal to the soil-layer depth. The mass is lumped at discrete points along the depth of the layer, the number of points being dependent on the accuracy required. Use of this idealization permits the consideration of a layered-soil profile and nonlinear and hysteretic soil properties. The idealization used by Penzien et al. (1964) consists of masses linked by a bilinear hysteretic spring and nonlinear dashpot connected in parallel, which are then connected in series to a second nonlinear dashpot. Suggestions for determining the parameters of this model are given.

Alternative models of soil behavior may be used, and for the simple case of a linear homogeneous isotropic elastic model, an exact analysis can be performed (Idriss and Seed, 1968).

Interaction of Structural System and Soil

The consideration of interaction of the soil and structural system within the soil is similar to that for static analyses, in that each discrete point along the system is subjected to an acceleration–time history that is equivalent to that of the soil medium at that point when acting alone. The behavior of the structural system may be readily obtained from structural analysis. Hence, soil and system displacements, velocities and accelerations may be equated at each discrete point and the resulting equations solved for each time-step considered.

Penzien et al. (1964) consider a relatively complicated structural system comprising a bridge deck supported on piles, but for the simple case of a single pile, the pile behavior may be obtained from the beam equation. The pile response may then be analyzed by the method described in Section 15.4, using the calculated soil acceleration at each point at each time for calculating the applied lateral force, or alternatively, using the calculated soil deflections as an input into the analysis.

A study by Penzien (1970) has shown that during the critical time-periods of the earthquake, the piles move essentially with the soil, interaction effects being small. Hence, the pile curvatures are essentially controlled by the motion of the surrounding soil. In a layered soil in which considerable differences in strain may develop between layers, large curvatures could be introduced in the pile (e.g., piles driven through a soft-clay layer into a dense-sand layer). The curvatures and deformations so introduced could well exceed the capacity of the pile section if it were designed for vertical loads only, and it would appear desirable to allow for moments and lateral deformations in the design of piles in earthquake areas.

It is possible that greater pile-soil interaction could occur with shorter, stiffer piles or a stiffer, heavier superstructure than that considered by Penzien. It must also be emphasized that this analysis was based on a particular earthquake record (El Centro 1940, N-S component). Somewhat different conclusions might be reached for different acceleration-time inputs.

For a single pile, an indication of the bending moments, reactions and deflections caused by earthquake loading may be obtained from a static analysis of piles subjected to horizontal soil movements (Chapter 13), if the vertical distribution of maximum horizontal movements caused by an earthquake can be estimated. In fact, in many practical cases, the natural frequency of the piles may be considerably higher than the predominant frequency of the lateral soil movements, so that a static analysis as described above will give a quite reasonable estimate of the pile response.

16

PILE LOAD TESTS

16.1 INTRODUCTION

Pile load tests are usually carried out for one or more of the following reasons:

1. To serve as a proof test to ensure that failure does not occur before a selected proof load is reached, this proof load being the minimum required factor times the working load.
2. To determine the ultimate bearing capacity as a check on the value calculated from dynamic or static approaches, or to obtain backfigured soil data that will enable other piles to be designed.
3. To determine the load-settlement behavior of a pile, especially in the region of the anticipated working load. This data can be used to predict group settlements and settlements of other piles.
4. To indicate the structural soundness of the pile.

The most common type of test is a compression test, although uplift, lateral-load, and even torsion-load tests are also performed. A variety of test procedures have been developed for carrying out pile load tests; among the most common procedures for compression tests are

1. Maintained loading tests.
2. Constant-rate-of-penetration (C.R.P.) tests.
3. Method of equilibrium.

In this chapter, these procedures and their interpretation are reviewed, and the possible effects of the loading system on the measured settlement of the pile are examined theoretically. Lateral and torsional testing are also described briefly.

It must be emphasized that in many cases, the results of a test on a single pile cannot be extrapolated directly to predict the behavior of pile groups or other piles. As pointed out by Chellis (1962), the volume of soil influenced by a single pile is much less than that of a large group, so the influence of deep-seated compressible layers may not be apparent in a pile load test, although such layers may critically affect the behavior of a group. Pile load tests should therefore be accompanied by detailed site investigation to define accurately the entire soil profile.

16.2 MAINTAINED LOADING TEST

16.2.1 Procedure

This is the usual method of carrying out a test, especially if the load-settlement relationship is required. The procedure is to apply the load in stages, the load at each stage being maintained constant until the resulting settlement of the pile virtually ceases before applying the next increment. The Civil Engineering Code of Practice No. 4 (1954) takes a rate of movement of 0.012 in./hr (0.305 mm/hr) as the limiting rate before addition of the next increment. Cooling and Packshaw (1950) recommend 0.0033 in./hr (0.084 mm/hr), while A.S.T.M. D1143-57T requires a rate of settlement less than 0.012 in./hr (0.305 mm/hr) or until 2 hr has elapsed, whichever occurs first. It is perhaps doubtful whether a time interval of 2 hr is always adequate to ensure completion of consolidation settlement. However, as is shown theoretically in Chapter 5, the major proportion of the settlement of a pile occurs as immediate settlement, so relatively short intervals between load increments should be acceptable—at least at load levels not approaching failure.

The usual procedure is to increase the load in stages until the proposed working load is reached, and then to unload and to leave the load off until the rise or rebound substantially ceases. The pile is then reloaded to the working load or to the next higher stage, and the test continued to the maximum load. The unloading of the pile from the maximum load is often carried out in stages, with a pause at each stage until rebound virtually ceases before unloading to the next stage. The precise loading and unloading procedure may often be specified by building codes or established practice in a particular organization.

The following methods are commonly used to apply the load or downward force on the pile:

1. A platform is constructed on the head of the pile, on which a mass of heavy material, termed "kentledge," is placed.
2. A bridge, carried on temporary supports, is constructed over the test pile and loaded with kentledge. The ram of a hydraulic jack, placed on the pile head, bears on a crosshead beneath the bridge beams, so that a total reaction equal to the weight of the bridge and its load may be obtained. Whitaker (1970) recommends that the supports be more than 1.25 m (4 ft) away from the test pile, to minimize the effect of the supports on pile settlement.
3. Anchor piles capable of withstanding an upward force are constructed on each side of the test pile, with a beam tied down to the heads of the anchor piles and spanning the test pile. In testing piles installed for the actual structure rather than for special test piles, it is often convenient to test an interior member of a group in this manner. A hydraulic jack on the head of the test pile applies the load and obtains a reaction against the underside of the beam. This method is sometimes called the "bootstrap" method. Whitaker (1970) recommends that any anchor pile should be at least three test-pile diameters from the test pile, center to center, and in no case less than 1.5 m (5 ft). For piles with enlarged bases, the spacing should be the greater of twice the base diameter or four times the shaft diameter of the test pile. However, even with these spacings, considerable interaction between the anchor piles and the test pile may occur, resulting in an inaccurate indication of the settlement of the pile (the measured value will be less than the correct value).
4. Ground anchors that usually transfer the reaction to stiffer strata below the level of the pile tip. Because the upper portion of an anchor cable does not usually transfer load to the soil, ground anchors can be placed closer to the test pile than can reaction piles.

The last three methods may affect the measured settlement of the test pile, in some cases significantly, and if load-settlement is required, steps should be taken to minimize the effects of the test-load reactions or to correct for them. A theoretical examination of possible errors arising from methods 3 and 4 is described in Section 16.5, and the approach could be adapted for method 2.

The settlement of the pile head may be measured by direct leveling with reference to a fixed datum, or by a wire held under constant tension between two supports and passing across a scale attached to the test pile, or by dial gauges attached to a beam supported on two foundations sufficiently far from the test pile for the reaction system to be unaffected by the ground movement. In order to measure pile movements and loads at various points along the pile, displacement rods (sometimes termed "tell-tales") or strain gauges may be installed. This type of instrumentation can be installed in almost all types of conventional piles, but more readily in cast in-situ concrete piles. In general, tell-tales are simple to install, read, and maintain, and Vijayvergiya (1969) and Tomlinson (1977) give details of the tell-tale system and its interpretation. As pointed out by Fuller and Hay (1970), the installation of tell-tales or strain gauges results in a physical change in the cross section of the pile, and thus its elastic properties; thus, it may sometimes be advisable not to install too much instrumentation along the pile. In many cases, a tell-tale at the pile tip may give sufficient information.

16.2.2 Interpretation of Load Tests

16.2.2.1 EMPIRICAL METHODS FOR WORKING LOADS

A considerable number of arbitrary or empirical rules have been used or are contained in codes to serve as criteria for determining the allowable working load from load-test results. A number of these rules have been summarized by Chellis (1961), and a few are quoted below.

1. The test load shall be twice the design load and shall be maintained constant for at least 24 hr, and until settlement or rebound does not exceed 0.22 in. in 24 hr. The design load shall not exceed one half the maximum applied load, provided the load-settlement curve shows no signs of failure and the permanent settlement of the top of the pile, after completion of the test, does not exceed ½ in. (Boston Building Code).
2. Tests shall be made with 200% of the proposed load, and considered unsatisfactory if after standing 24 hr, the total settlement after rebound is more than 0.01 in. per ton of total test load (building laws of the City of New York).
3. Observe the point at which the gross settlement begins to exceed 0.03 in. per ton of additional load, and divide by a factor of safety of 2 for static loads, or 3 for vibratory loads (W. H. Rabe).
4. Observe the point at which the gross settlement begins to exceed 0.05 in. per ton of additional load, or at which the plastic settlement begins to exceed 0.03 in. per ton of additional load, and divide by a factor of safety of 2 for static loads, and 3 for vibratory loads (R. L. Nordlund).
5. Take two thirds of the maximum test load in a case where settlement is not excessive and where load and settlement were proportional and the curve remained a straight line. Where the test load was carried to failure, take two thirds of the greatest load at which settlement was not excessive and at which loads and settlement were proportionate (United States Steel Co.).

Chellis considers rules 3 and 4 the most reasonable, although 3 may be too conservative. Rules such as 5 are unreliable, as various impressions of the steepness of the load-settlement curves may be obtained by varying the scale of the graph, so that a finite limit of the change-of-load to change-of-settlement ratio is desirable.

16.2.2.2 ULTIMATE LOAD

In carrying out a maintained load test to determine the load capacity of a pile, Whitaker (1970) suggests that it is necessary first to estimate the load capacity so that a suitable loading and reaction system may be provided, and then to define some physical event by which "failure," and hence the ultimate load capacity of the pile, may be recognized. Among the commonly-used definitions of the ultimate load capacity are:

1. The load that causes a settlement equal to 10% of the pile diameter (Terzaghi, 1942).
2. The load at which the rate of settlement continues undiminished without further increment of load, unless this rate is so slow as to indicate that settlement may be a result of consolidation of the soil (Civil Engineering Code of Practice No. 4, 1954).

Whitaker (1970) considers the latter definition inadequate to define failure, especially with piles in cohesive soil.

Van Weele (1957) has suggested a method of cyclic loading to provide some indication of the distribution of load between adhesion and end-bearing. A plot of the elastic recovery at each unloading cycle versus load applied at that cycle is used to separate the two components. The curve usually becomes a straight line soon after the early load increments. The distance between this curve and a line drawn through the origin and parallel to the straight part of the curve, represents the portion of load carried by adhesion. This procedure is approximate only. An alternative method is outlined by Woodward et al. (1972).

The importance of residual stresses in driven piles on pile-test interpretation has been stressed by Holloway et al. (1975). Compressive residual loads are likely to exist in the lower part of the pile, and these appear to depend on the pile-soil system only, independent of the impact pile-driving apparatus used. When a residual point-load remains after driving, a portion of the point-bearing capacity has already been mobilized; however, if load distribution measurements are made, the gauges are generally zeroed at the start of the test, and the residual loads are ignored in the test interpretation. In compression load tests to failure, the measured point-bearing value in such cases is only that mobilized from the start of the load test. The actual point capacity is the measured value plus the residual point load. Conversely, in the tensile load tests, the effect of residual compressive loads is to cause an apparent tensile resistance at the point. While the effects of residual loads are not readily taken into account, recognition of their effects may at least resolve apparent anomalies in some load tests.

16.2.2.3 SETTLEMENT BEHAVIOR

The load-settlement relationship may be used directly to determine the single-pile settlement at the working load. In estimating the settlement of a group or the settlement of a pile of different proportions, the average soil modulus along the pile may be determined by fitting the measured load-

settlement behavior to the theoretical behavior. Knowing the soil modulus, the stiffness of the pile relative to the soil may be determined, whereby the appropriate theoretical settlement-influence factor may be determined for a single pile (Chapter 5), or the appropriate theoretical group-settlement ratio (ratio of group settlement to single pile settlement at the average pile load) may be determined for a pile group (Chapter 6). In the latter case especially, the additional effects of any deep-seated compressible strata must be carefully considered in the settlement estimate.

An example illustrating the use of the theoretical solutions to backfigure the average soil modulus from a pile load test is given below.

Example of Interpretation of Pile Load Test to Backfigure Soil Modulus

As a simple example, the case of 0.3-m-diam., 15-m-long floating concrete test pile in a 30-m-thick layer of clay will be considered. It will be assumed that at a load of 50 metric ton, an immediate settlement of 10 mm and a final settlement of 13 mm is recorded. In order to backfigure the average undrained and drained values of E_s of the clay, use is made of Eq. (5.33).

Considering first the undrained modulus, from Fig. 5.18,

$$I_0 = .044 \text{ for } L/d = 15/0.3 = 50 \text{ and } d_b/d = 1$$

and

$$R_h = 0.87 \text{ from Fig. 5.20, for } L/d = 50 \text{ and } h/L = \frac{30}{15} = 2$$

Assuming the undrained Poisson's ratio of the soil is 0.5, $R_\nu = 1$, from Fig. 5.21. Substituting for ρ (= 10 mm), P, d, I_0, R_ν, and R_h into Eq. (5.33), it is found that

$$E_s = 63.8\, R_K \text{ kgf/cm}^2 \tag{16.1}$$

R_K is a function of a pile-stiffness factor K, and hence E_s, and is plotted in Fig. 5.19. Thus Eq. (16.1) must be solved together with the equation defining K, that is,

$$K = \frac{E_p R_A}{E_s} \tag{16.2}$$

For a solid pile, $R_A = 1$, and assuming $E_p = 2 \times 10^5$ kgf/cm^2,

$$E_s = 2 \times 10^5 / K \text{ kgf/cm}^2 \tag{16.3}$$

Solution of Eqs. (16.1) and (16.3) is most easily carried out graphically, using a tabulation such as is given in Table 16.1. The graphical solution is shown in Fig. 16.1, from which the required undrained value of E_s is found to be 73 kgf/cm^2.

Considering now the determination of the drained value of Young's modulus, it will be assumed that the drained Poisson's ratio of the soil is 0.3. From Fig. 5.21, $R_\nu = 0.93$. The other factors in Eq. (5.33) remain unchanged, so that substitution into this equation, using now the final value of ρ of 13 mm, gives

$$E_s = 45.6\, R_K \text{ kgf/cm}^2 \tag{16.4}$$

Equation (16.3) remains valid, and graphical solution of Eqs. (16.3) and (16.4) in Fig. 16.1 gives the drained value of E_s as about 50 kgf/cm^2.

As an alternative to the above procedure, the theoretical relationship between settlement and E_s can be plotted

TABLE 16.1

K	R_K (Fig. 5.19)	Undrained E_s (kg/cm^2) (Eq. 16.1)	E_s (kg/cm^2) (Eq. 16.3)	Drained E_s (kg/cm^2) (Eq. 16.4)
10000	1.02	65.0	20	46.5
5000	1.08	68.9	40	49.2
2000	1.19	76.0	100	54.3
1000	1.37	87.5	200	62.5
500	1.68	107.2	400	76.6

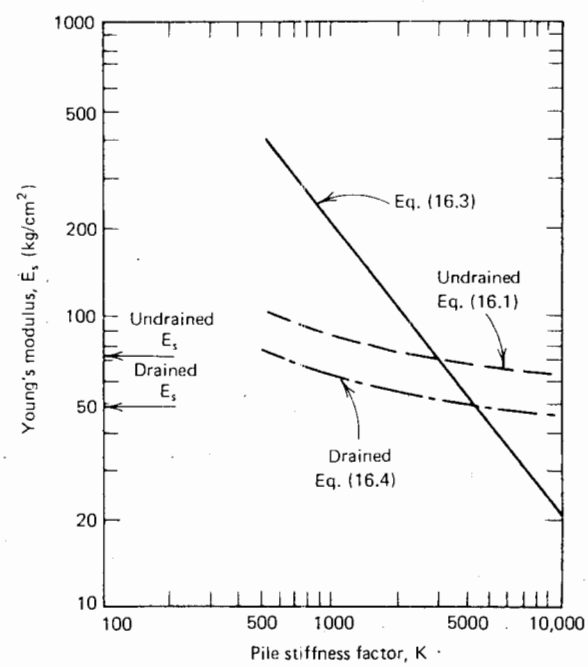

FIGURE 16.1 Graphical solution for soil moduli from pile load test.

for any given load, and the value of E_s corresponding to the measured settlement may be read off this plot. For the problem above, this latter procedure would require one curve to be drawn for each value of ν_s, from which the undrained and drained values of E_s could be determined.

16.3 CONSTANT-RATE-OF-PENETRATION TEST

This test, frequently termed the C.R.P. test, was developed by Whitaker (1957) for model piles and was subsequently used for full-scale pile tests (Whitaker and Cooke, 1961; Whitaker, 1963). In carrying out the C.R.P. test, the pile is made to penetrate the soil at a constant speed from its position as installed, and the force applied at the top of the pile to maintain the rate of penetration is continuously measured. The force is usually applied by a hydraulic jack and the settlement of the pile head measured by means of a dial gauge supported on a beam. The test is usually arranged to take about the same time as a laboratory undrained test of a sample of the soil, in an attempt to ensure that the undrained load capacity and the load-undrained settlement relationship are obtained.

The prime object of the test is usually to determine the ultimate load capacity. The data resulting from the test are plotted as a graph of force versus penetration. The curve in the case of a floating pile will be similar to one of those shown in Fig. 16.2*a*. The values of force reached at the points marked A represent the ultimate load in each case. The force-penetration curve for an end-bearing pile is similar to that shown in Fig. 16.2*b*. The upper part of the curve is straight, or substantially straight, and shows a steady increase in force with increasing penetration; the ultimate load is taken as the point A, which represents the beginning of this straight portion. This line is found to be a continuation of the force-settlement relationship for installation of the pile from the surface of the bearing stratum entirely by a C.R.P. technique. Identification of the point A is often difficult in practice, and Whitaker (1970) suggests that it is usually satisfactory to take the ultimate load as the force required to cause a penetration of 10% of the pile diameter.

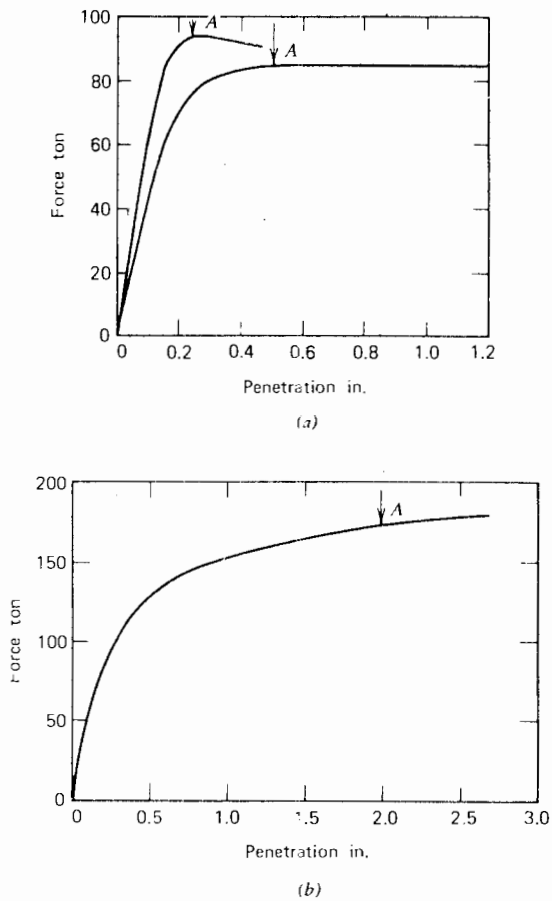

FIGURE 16.2 C.R.P. test (after Whitaker, 1970).

16.4 METHOD OF EQUILIBRIUM

This procedure, which has been described by Mohan, Jain, and Jain (1967), is primarily designed to determine the ultimate load capacity, although it also appears to provide reasonable settlement data. The principle is to apply to the pile, at each stage of the test, a load slightly higher than the required load and then to decrease the load to the desired value. By this means, the rate of settlement diminishes much more rapidly than with the maintained load procedure and equilibrium is reached in a matter of minutes rather than hours. The procedure suggested by Mohan, Jain, and Jain is first to apply about one tenth of the estimated ultimate load by hydraulic jack in a period of three to five minutes. It is maintained for about 5 min and then allowed to reduce itself via downward movement of the pile. Within a few minutes, a state of equilibrium is generally reached. The next increment of load is then applied and the process is repeated. For higher loads, it is desirable to maintain the initial load for a period of 10 to 15 min before it is allowed to relax. The total time required by this method is generally reduced to about one third of that required in a maintained-load test. At each stage, a cycle of loading and unloading may also be adopted and the elastic rebound of the pile top measured, in order to separate the side adhesion

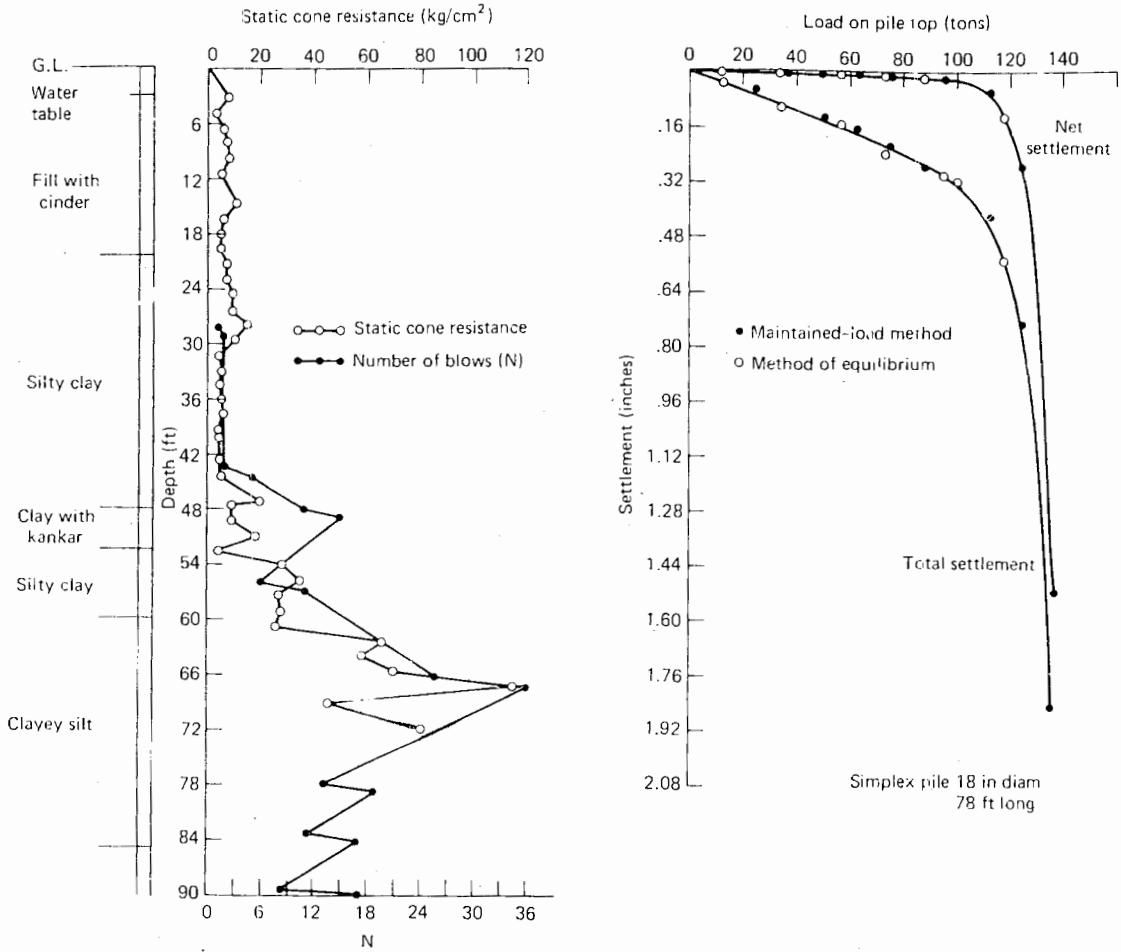

FIGURE 16.3 Load-settlement curves from maintained load test and method of equilibrium (after Mohan et al., 1967).

and point-bearing capacities (Van Weele, 1957; Jain and Kumar, 1963).

A number of tests were carried out by Mohan, Jain, and Jain (1967) to compare this method with the maintained-load procedure. A typical comparison, shown in Fig. 16.3, reveals excellent agreement, in regard to both ultimate load capacity and load-settlement behavior.

16.5 SOURCES OF ERROR IN SETTLEMENT MEASUREMENTS IN PILE LOAD TESTS

Some of the loading and settlement procedures commonly used in pile load tests may lead to inaccuracies in the measurement of the settlement of a test pile. A theoretical examination of such inaccuracies caused by the following procedures (see Fig. 16.4) has been made by Poulos and Mattes (1975):

1. The use of a reference beam to measure the settlement (Fig. 16.4*a*).
2. The use of anchor piles to provide reaction for the test load (Fig. 16.4*b*).
3. The use of ground anchors to provide reaction for the test load (Fig. 16.4*c*).

16.5.1 Errors Resulting from Use of Reference Beam

With this system of settlement measurement, the beam supports settle because of the loaded pile. A theoretical assessment of the resulting errors involved in settlement measured may be made by using the solutions for the settlement of a point on the surface of the soil caused by a loaded pile (Section 5.3.3). From Eq. (5.40), this settlement, ρ_s, is given by

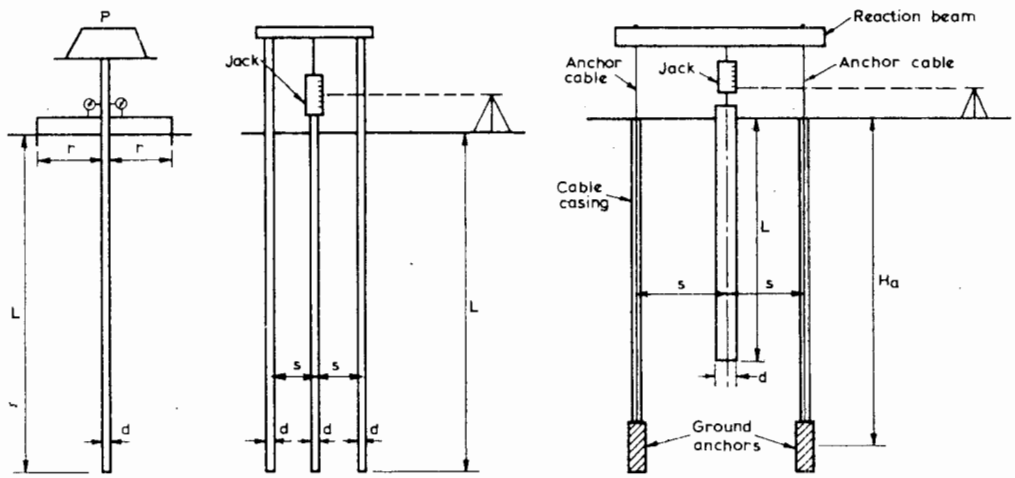

(a) Settlement Measurement Using Reference Beam. (b) Test Pile Jacked Against Reaction Piles. (c) Test Pile Jacked Against Ground Anchors

FIGURE 16.4 Pile load test arrangements.

$$\rho_s = \left(\frac{P}{LE_s}\right)(I_\rho) \tag{16.5}$$

where I_ρ is plotted in Figs. 5.32, 5.33, and 5.34. The true settlement of the pile itself, ρ, resulting from the applied load, is given from Eq. (5.33) as

$$\rho = \frac{PI}{E_s d} \tag{16.6}$$

where

I = settlement-influence factor

The measured settlement, ρ_m, is therefore

$$\rho_m = \rho - \rho_s$$

$$= \frac{P}{LE_s}\left[I - I_\rho\left(\frac{L}{d}\right)\right] \tag{16.7}$$

It is convenient now to define a correction factor, F_c, to be applied to the measured settlement, ρ_m, to obtain the true settlement ρ—that is,

$$\rho = F_c \rho_m \tag{16.8}$$

or, the correction factor F_c is defined as

$$F_c = \frac{\text{True settlement of loaded pile}}{\text{Measured settlement}} \tag{16.9}$$

From Eqs. (16.6), (16.7), and (16.8),

$$F_c = \frac{I}{I - \left(\frac{d}{L}\right)(I_\rho)} \tag{16.10}$$

The correction factor F_c evaluated for a floating pile is plotted in Figs. 16.5 and 16.6 for the cases of a pile in a deep layer and a pile in a finite layer. Figure 16.5 indicates that serious errors (i.e., large values of F_c) can arise in settlement measurements on a test pile in a deep soil layer unless each support of the reference beam is placed about 0.5 to 1 pile-length away from the pile. In terms of the dimensionless distance r/L, the effect is more severe for shorter piles. Figure 16.6 shows how the effect of the support-beam movement diminishes with decreasing soil-layer thickness. However, even for an end-bearing pile (H/L = 1), it is desirable to have the supports 0.3 to 0.5 pile-lengths away from the test pile.

16.5.2 Errors Resulting from Jacking Against Anchor Piles

With this method of load application, the upward loads on the anchor piles cause an upward movement of the test pile because of interaction. As a result, if the settlement of the test pile is measured with reference to a remote benchmark, the measured settlement will be less than the true settlement. A theoretical examination of the magnitude of this under-registration may be made by using the pile-settlement interaction solutions described in Section 6.2.

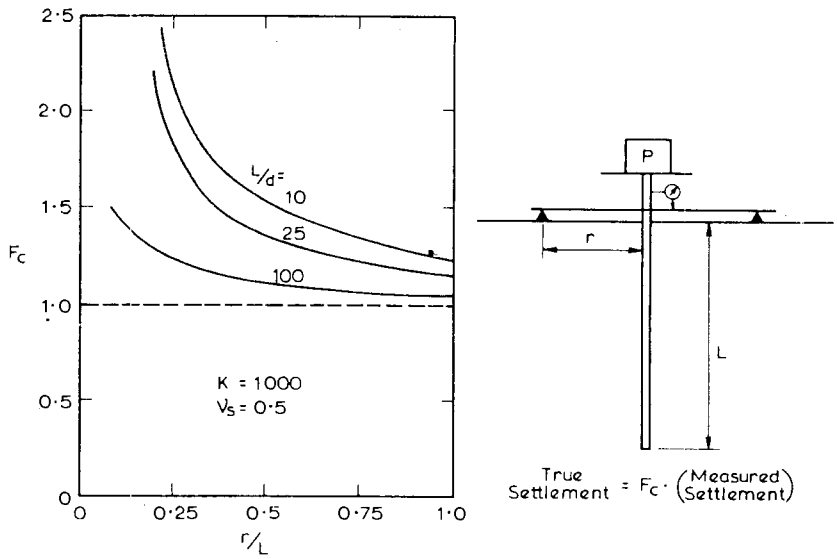

FIGURE 16.5 Correction factor F_c for floating pile in deep layer of soil.

The true settlement of the test pile resulting from the applied load is again given by Eq. (16.6). The upward movement of the test pile because of the reaction on the anchor piles is given (using Eq. 6.12) as

$$\Delta\rho = \frac{PI}{dE_s} \cdot \alpha_1 \tag{16.11}$$

where

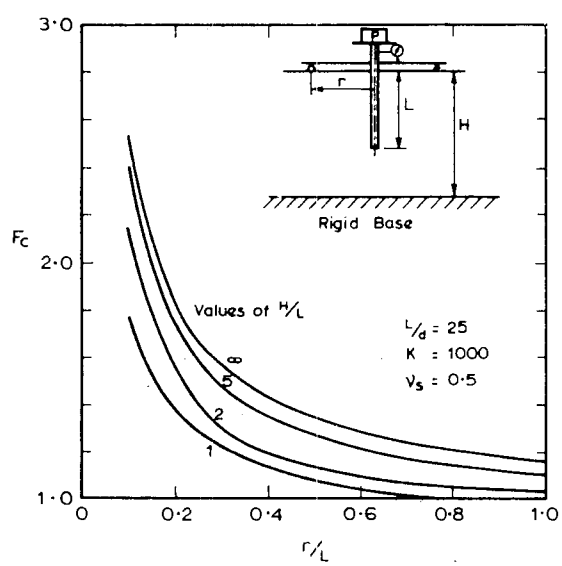

FIGURE 16.6 Effect of layer depth on settlement correction factor F_c.

α_1 = interaction factor for two piles at a spacing of s, where s is the distance between the test pile and each reaction pile (Fig. 16.4*b*).

The measured settlement, ρ_m, relative to a remote benchmark, is therefore

$$\rho_m = \rho - \Delta\rho = \left(\frac{PI}{dE_s}\right)(1 - \alpha_1) \tag{16.12}$$

Defining again the correction factor F_c as in Eq. (16.9), it is found that

$$F_c = \frac{1}{(1 - \alpha_1)} \tag{16.13}$$

Values of F_c for various cases are plotted in Figs. 16.7, 16.8, and 16.9. The case of a floating pile in a deep soil layer is considered in Fig. 16.7. It may be seen that in the range of spacings between the test and reaction piles commonly used (2.5 to 4 diameters), F_c may be 2 or even greater, or in other words, the measured settlement may be one half or less of the true settlement. The error becomes more severe for stiffer, more slender piles. Unfortunately, it is for such cases (i.e., long piles in very soft soils), that accurate settlement measurements may be most necessary.

Figure 16.8 shows values of F_c for end-bearing piles resting on a rigid stratum. In this case, the interaction is generally much less, and consequently, large values of F_c do

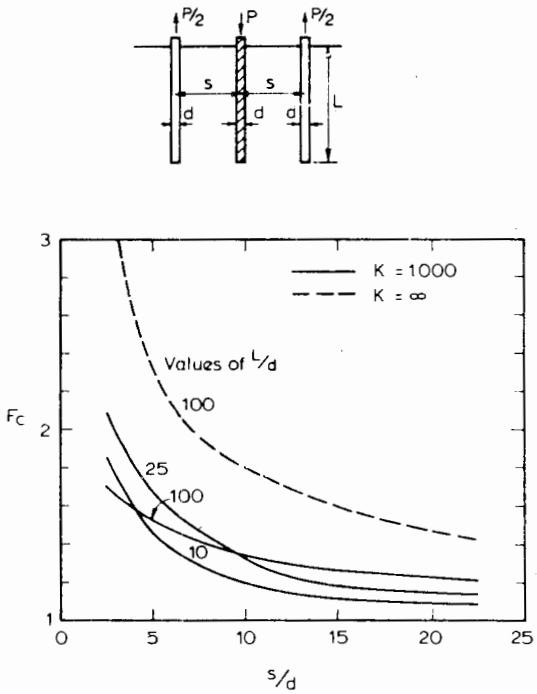

FIGURE 16.7 Correction factor F_c for floating pile in a deep layer jacked against two reaction piles.

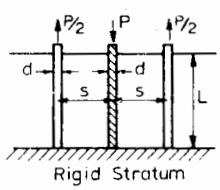

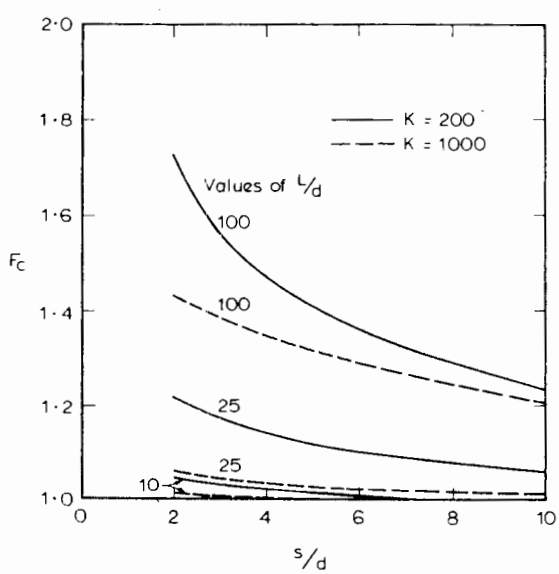

FIGURE 16.8 Correction factor F_c for end-bearing pile on rigid stratum jacked against two reaction piles.

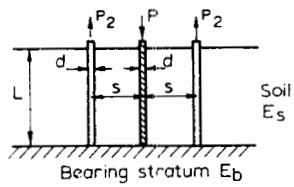

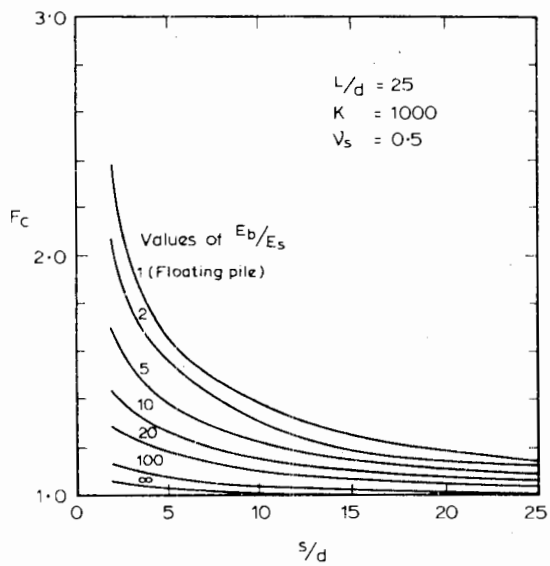

FIGURE 16.9 Correction factor F_c. Effect of bearing stratum for end-bearing pile jacked against two reaction piles.

not occur at normal spacings unless the piles are relatively slender and compressible.

The effect of the relative stiffness of the bearing stratum on F_c is shown in Fig. 16.9. As the bearing stratum becomes stiffer, interaction decreases and hence F_c decreases for a given pile spacing. However, significant errors in settlement measurement may still occur at normal pile spacings unless the bearing stratum has a stiffness about 10 times (or more) greater than the overlying soil.

Figures 16.7, 16.8 and 16.9 suggest that if settlement measurements are made with reference to a remote benchmark, the usual spacing of about three diameters may result in significant undermeasurement of the settlement of the test pile. Increasing the spacing to at least five diameters would appear most desirable, especially for long piles in deep, soft deposits.

An alternative means of settlement measurement is possible with the anchor-pile system by measuring the settlement of the test pile with reference to the reaction piles, that is, by fixing a dial gauge to the cross beam joining the reaction piles. The consequences of this procedure may again be examined using pile-interaction

theory. The upward movement of each reaction pile, ρ_a, is given by Eq. (16.12) as

$$\rho_a = \frac{0.5P}{dE_s} I - \frac{PI\alpha_1}{dE_s} + \frac{0.5PI\alpha_2}{dE_s}$$

$$= \frac{PI}{dE_s}(0.5 - \alpha_1 + 0.5\alpha_2) \qquad (16.14)$$

where

I = single-pile settlement influence factor
α_1 = interaction factor for two piles at a spacing of s
α_2 = interaction factor for two piles at a spacing of $2s$

The settlement of the test pile relative to the reaction piles, ρ'_m, is then

$$\rho'_m = \rho_m + \rho_a$$

$$= \frac{PI}{dE_s}(1.5 - 2\alpha_1 + 0.5\alpha_2) \qquad (16.15)$$

Defining a correction factor F'_c as

$$F'_c = \frac{\text{True settlement of loaded pile}}{\text{Measured settlement relative to reaction piles}} \qquad (16.16)$$

it may be shown from Eqs. (16.15) and (16.16) that

$$F'_c = \frac{1}{(1.5 - 2\alpha_1 + 0.5\alpha_2)} \qquad (16.17)$$

Values of F'_c are plotted against dimensionless spacing s/d in Fig. 16.10 for a floating pile in a deep soil layer. Comparison with Fig. 16.7 shows that F'_c is generally less than F_c, in other words, less correction of the measured settlement is required if measurement is made with respect to the anchor piles. For piles of medium compressibility (K = 1000), Fig. 16.10 shows that F'_c is above unity at a spacing of about five diameters. It must be pointed out, however, that at larger spacings or in cases where little interaction is likely to occur between the test pile and the reaction piles, F'_c will be less than one—that is, the measured settlement will be *greater* than the true settlement. In such cases, the soil modulus backfigured from the uncorrected measured settlement would be too small in contrast to the value that would be obtained from the settlement measured with reference to a remote point, which would be too large. Thus, measurement of the test-pile settlement relative to the reaction piles would appear to have advantages over other means of settlement measurement, in that it gives a settlement either closer to or larger than the real settlement. However, in any such pile test, measurement of the settlement by both the alternative methods is desirable so that a better assessment of the true settlement may be made.

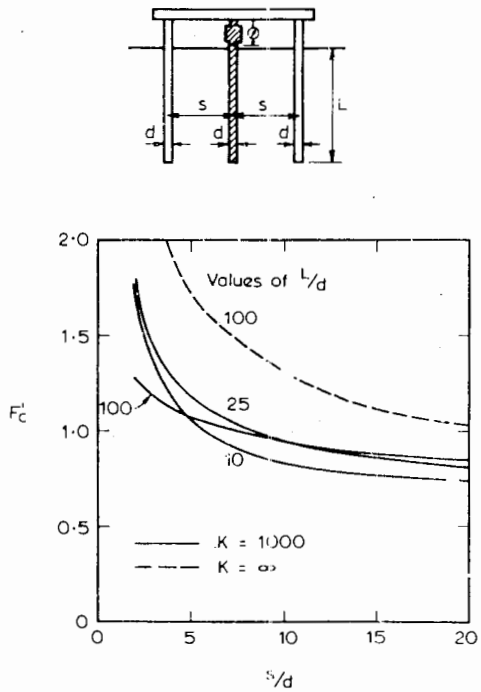

FIGURE 16.10 Correction factor F'_c for floating pile in a deep layer jacked against two reaction piles—settlement measured in relation to anchor piles.

All the above solutions apply for a homogeneous soil stratum. The expressions in Eq. 16.13 and Eq. 16.17 also apply for non-homogeneous soils, provided that appropriate values of the interaction factors are used. Since these factors tend to be smaller for non-homogeneous soils than for homogeneous soils, the errors involved in the test procedure will be correspondingly smaller; however, the general characteristics of behaviour and variation of F_c and F'_c with spacing remain similar.

16.5.3 Errors Resulting from Jacking Against Ground Anchors

The upward reaction on each ground anchor will tend to reduce the settlement of the test pile. Because the cables for the ground anchors are generally cased and the anchors themselves are small in relation to the test pile, it is reasonable to approximate each anchor as an upward point load acting at the center of the anchor. To simplify calculations, it is then assumed that the effect of the ground anchor on

the test pile is the same as its effect on a point located half way along the pile. With the above approximations, the upward movement, $\Delta\rho$, of the test pile caused by the ground anchors can be written as

$$\Delta\rho = \left(\frac{2P/2}{E_s L}\right) I_M \tag{16.18}$$

where I_M is the vertical displacement factor for a buried point load. I_M may be evaluated most readily from Mindlin's equation for a point load within a semi-infinite elastic mass.

The true pile settlement, ρ_t, is again given by Eq. (16.6), so the measured settlement ρ_m of the test pile is

$$\rho_m = \frac{P}{E_s d}\left(I - I_M \frac{d}{L}\right) \tag{16.19}$$

Defining the correction factor F_c as in Eq. (16.9),

$$F_c = \frac{1}{\left(1 - \frac{I_M}{I}\frac{d}{L}\right)} \tag{16.20}$$

F_c is plotted against dimensionless anchor spacing in Fig. 16.11 for various values of embedment of the anchors. The test pile and the anchors are assumed to be in a deep layer. Figure 16.11 shows that if the anchors are located 1.5 pile-lengths or more below the surface, F_c is less than 1.2, in other words, the error in the measured settlement is less than 20%. Beyond an anchor depth of about $2L$, the radial distance of the anchors from the piles has little effect on the measured settlement.

The case considered in Fig. 16.11 is not likely to occur frequently in practice, since to obtain adequate load capacity, the anchors are usually secured into a stiffer layer at or below the level of the pile tip. In such a case, the upward movements caused by the anchors would be less than given by Eq. (16.18), so that F_c will be less than indicated in Fig. 16.11.

Figure 16.11 will also generally give an overestimate of F_c for an end-bearing test-pile bearing on a stiff layer. The extreme case of a pile through very soft soil and bearing on a stiff layer may be examined by considering the pile tip as a rigid circular area carrying the total applied load, and the anchors as point loads acting on the surface of a semi-infinite mass of modulus E_b (the bearing stratum). For this case, F_c is plotted in Fig. 16.12 together with the other limiting case of a pile in a homogeneous deep layer, with anchors at the level of the pile tip (the curve for $H_a/L = 1.0$

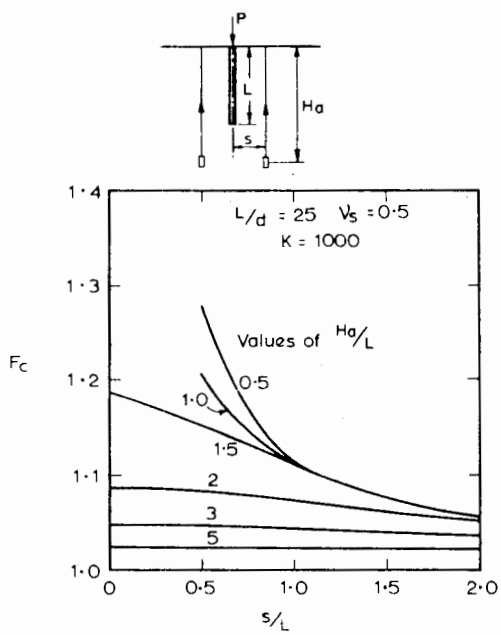

FIGURE 16.11 Correction factor F_c for floating pile in a deep layer jacked against ground anchors.

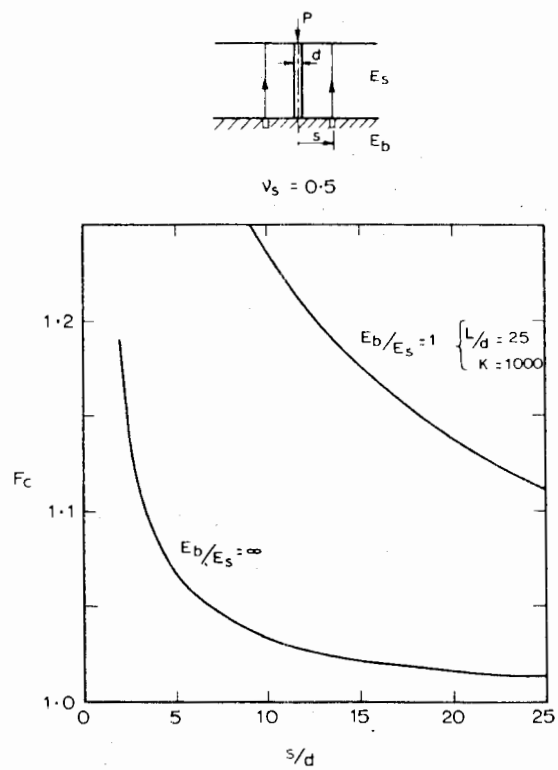

FIGURE 16.12 Correction factor F_c for end-bearing pile jacked against ground anchors.

in Fig. 16.11). It may be seen that when the pile bears on to very stiff rock through very soft soil, $(E_b/E_s \rightarrow \infty)$, F_c is extremely small even for very closely-spaced anchors, whereas the corresponding value for the homogeneous layer $(E_b/E_s = 1)$ is considerably greater. In practice, the value of F_c would lie between these two limiting values.

Figure 16.12 indicates that when anchors are to be fixed at the level of the pile tip, the spacing between the test pile and the anchors should be as great as possible, and preferably 10 diameters or greater. Greater spacings may be achieved most readily by installing inclined anchors.

Comparison with the other two test systems shows that F_c for the anchor system is generally much less, that is, less error is involved in settlement measurements when anchors are used.

16.6 LATERAL LOAD TESTS

The usual method of carrying out lateral load tests is to install a pair of piles and jack their heads apart. A description of the method is given by Wagner (1953). The piles should be placed sufficiently far apart so as not to obtain significant interaction between the movements of each pile, and hence a horizontal beam is frequently inserted between the piles and the jack reacts against one of the pile heads and the beam to the other pile head. If necessary, the effects of interaction with less than ideal spacing between the piles can be estimated, as explained for vertical tests in Section 16.5, using the theory given in Chapter 8, Section 8.4. Examples of loading arrangements for both vertical and battered piles have been described by Alizadeh and Davisson (1970) and Tomlinson (1977).

The procedure employed for the test varies, but typically the load is applied in a number of increments and each increment is left on until a specified rate of movement is reached. Alizadeh and Davisson (1970) used for each increment a minimum period of one hour, or until the pile head movement was less than 0.01 in per hr. Tests were carried to lateral deflections approaching 2 in.

Lateral deflection of the pile head is usually measured with a dial gauge. Strain gauges are also frequently installed along the embedded portion of the pile to measure flexural stresses whereby the bending moments may be obtained. With steel piles, inclinometers may also be installed with the pile to measure the variation of lateral deflection with depth along the pile. Hanna (1967) has also employed inclinometer readings along steel H-piles to indicate the bending of piles during driving.

Lateral load tests are usually used to indicate the load-deflection behavior of a pile. The allowable design load is often taken as the load required to produce a specified deflection (e.g., 0.25 in) divided by the required factor of safety (McNulty, 1956). The values of the subgrade-reaction modulus of the soil or the elastic modulus of the soil may also be backfigured from a test by fitting the observed behavior to the theoretical, as described in Section 8.5. This procedure enables predictions to be made of movements of piles of other dimensions or of groups of laterally loaded piles. In such cases, the influence of any soft layers underlying the pile tips is of much less significance than in the case of vertical loading.

16.7 TORSIONAL TESTING

Axial load tests presently represent the only certain method of determining the ultimate axial load capacity of individual piles, but conventional procedures and equipment are relatively costly and inconvenient, especially if high load capacities are anticipated.

The possibility of carrying out torsional loading tests on piles has been examined by Stoll (1972), who devised a simple field torque-shear-load test that could be applied to cylindrical piles. The piles must, of course, be capable of carrying the required torque without failure of the pile material itself, so that in stiffer soils, relatively short or stiff piles may be necessary. The key feature of the test apparatus is that torque is applied by small-capacity hydraulic jacks reacting horizontally against adjoining job piles, utilizing the large mechanical advantage available at the usual spacing (i.e., 3 to 5 ft or wider).

Stoll was of the opinion that the pile-soil shear strength from torsional tests would not exceed the value for axial loading. Model tests reported by Poulos (1975*b*) showed that in clay, the values deduced from axial and torsional tests were in fact very similar. It was also found possible in these tests to backfigure the shear modulus of the soil from the measured torque-rotation relationship, using the elastic theory described in Section 9.3.3, and to use this value to predict the settlement of a pile loaded axially. Thus, there is some evidence that torsional load tests may be useful for predicting the behavior of axially loaded piles in clay. For sands, however, because of the dependence of the pile-soil shear strength on the stress state, torsional tests may give misleading results; for example, for model piles in sand, Broms and Silberman (1964) obtained considerably lower values from torsional tests than from axial tests.

APPENDIX A

INTEGRATION OF MINDLIN'S EQUATIONS FOR PILE SETTLEMENT ANALYSIS

The geometry of a typical cylindrical pile element is shown in Fig. A1. For a general point i in the soil mass, the value of I_{ij} is

$$I_{ij} = 2 \int_{(j-1)\delta}^{j\delta} \int_{0}^{\pi/2} {}_pI \, d\theta \, dc \qquad \text{(A1)}$$

where

${}_pI$ = influence factor for vertical displacement due to a vertical point load
δ = length of element = L/n.

From Mindlin's equation, ${}_pI$ is given by

$${}_pI = \frac{(1+\nu)}{8\pi(1-\nu)} \left\{ \frac{z_1^2}{R_1^3} + \frac{(3-4\nu)}{R_1} + \frac{(5-12\nu+8\nu^2)}{R_2} + \frac{[(3-4\nu)z^2 - 2cz + 2c^2]}{R_2^3} + \frac{[6cz^2(z-c)]}{R_2^5} \right\} \qquad \text{(A2)}$$

where

$$z = h + c$$
$$z_1 = h - c$$
$$R_2^2 = \frac{d^2}{4} + x^2 - xd\cos\theta + z^2$$
$$R_1^2 = \frac{d^2}{4} + x^2 - xd\cos\theta + z_1^2$$

The integral with respect to c in Eq. (A1) can be evaluated analytically to give

$$\int {}_pI \, dc = \frac{1+\nu}{8\pi(1-\nu)} \left\{ \frac{z_1}{D_1} - 4(1-\nu)\ln(z_1 + D_1) + 8(1-2\nu+\nu^2)\ln(z+D) + \frac{[2h^2z/r^2 - 4h - (3-4\nu)z]}{D} + \frac{2(hr^2 - h^2z^3/r^2)}{D^3} \right\} \qquad \text{(A3)}$$

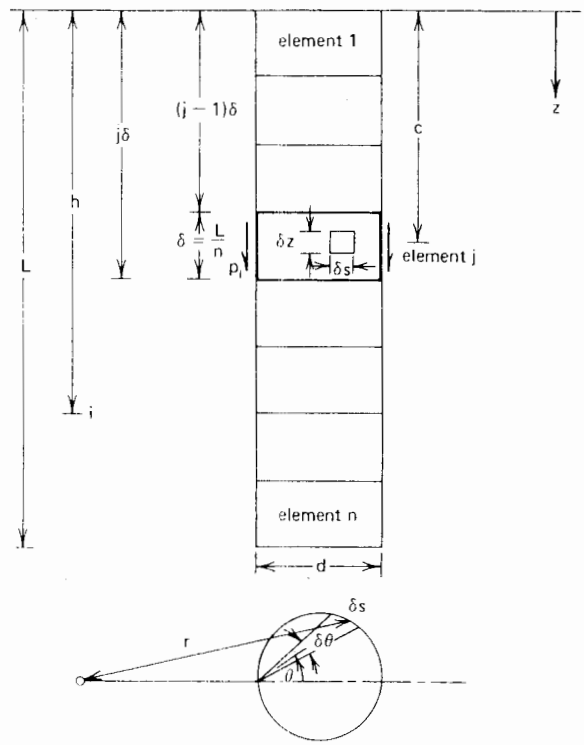

Figure A1 Single pile–basic geometry.

where

h and r are defined in Fig. A1,

$$D_1 = (r^2 + z_1^2)^{1/2}$$
$$D = (r^2 + z^2)^{1/2}$$

and the limits of integration in Eq. (A3) are

z_1 from $h-(j-1)\delta$ to $h-j\delta$

and

z from $h+(j-1)\delta$ to $h+j\delta$

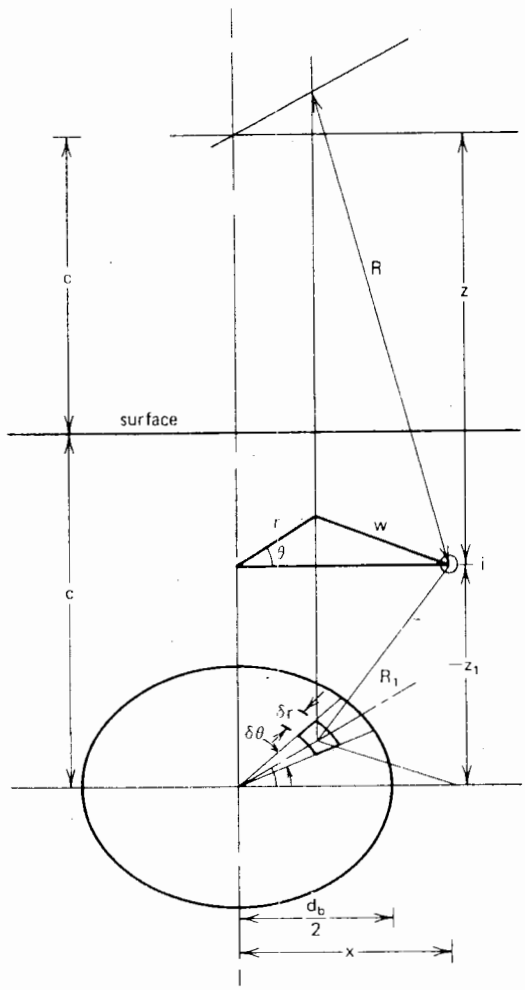

Figure A2 Geometry for integration over circular area.

The integral with respect to θ is, however, only conveniently evaluated numerically.

The geometry of the pile base is shown in Fig. A2. To allow for an enlarged base, a base radius r_b ($=d_b/2$) different from the pile shaft radius is considered. For a general point i in the soil mass,

$$I_{ib} = \frac{1}{d} \int_0^{2\pi} \int_0^{r_b} {}_pI\, r\, dr\, d\theta \qquad \text{(A4)}$$

where

${}_pI$ is given in Eq. (A2), and for this case,

$$\begin{aligned} c &= n\delta = L \\ R_2^2 &= z^2 + x^2 + r^2 - 2rx\cos\theta \\ R_1^2 &= z_1^2 + x^2 + r^2 - 2rx\cos\theta \\ z &= z_1 + 2c \end{aligned}$$

The integration with respect to r can be done analytically and yields

$$\begin{aligned} \int_p I dr = \frac{(1+\nu)}{8\pi(1-\nu)} \Bigg| & \frac{z_1^2(rA - R_0^2)}{(R_0^2 - A^2)\sqrt{X_0}} \\ & + (3 - 4\nu)[\sqrt{X_0} + A \ln(2\sqrt{X_0} + 2r - 2A)] \\ & + (5 - 12\nu + 8\nu^2)[\sqrt{X_1} + A \ln(2\sqrt{X_1} + 2r - 2A)] \\ & + [(3 - 4\nu)z^2 - 2cz + 2c^2] \frac{(Ar - B)}{(B - A^2)\sqrt{X_1}} \\ & + 6cz^2(z - c)\left\{\frac{-1}{3\sqrt{X_1}^3} + A\left[\frac{r - A}{3(B - A^2)\sqrt{X_1}}\right.\right. \\ & \left.\left. \times \left(\frac{1}{X_1} + \frac{2}{B - A^2}\right)\right]\right\} \Bigg| \end{aligned}$$

where

$$\begin{aligned} R_0^2 &= z_1^2 + x^2 \\ A &= x\cos\theta \\ X_0 &= r^2 - 2Ar + R_0^2 \\ X_1 &= r^2 - 2Ar + B \\ B &= R_0^2 + 4c^2 + 4cz_1 \\ z &= z_1 + 2c \end{aligned} \qquad \text{(A5)}$$

The integration with respect to θ is again evaluated most readily by numerical means.

In evaluating the integrals with respect to θ in Eqs. (A1) and (A4), intervals of $\pi/50$ are usually adequate. To avoid the singularity which occurs when calculating displacements on the pile shaft for $i=j$, it is most expedient to calculate ordinates at the mid-point of each interval and then apply the simple rectangular rule for integration to evaluate the complete double integral. The value of the integral converges to a constant value as the number of intervals in θ is increased, and as mentioned above, intervals of $\pi/50$ are generally sufficient to ensure convergence.

For the center of the base resulting from shear stress on element j,

$$I_{bj} = \pi \int_{(j-1)\,\delta}^{j\delta} {}_pI\, dc \qquad \text{(A6)}$$

The integral in Eq. (A6) is given in Eq. (A3), with $h = L$, $D^2 = z^2 + d^2/4$ and $D_1^2 = z_1^2 + d^2/4$.

For the vertical displacement of the base resulting from the base itself, it is desirable to make an approximate allowance for the effect of the rigidity of the base by multiplying the displacement of the center of the uniformly-loaded circular base by a factor of $\frac{\pi}{4}$; this is the ratio of the surface displacement of a rigid circle on the surface of a half-space

to the center displacement of a corresponding uniformly loaded circle, and may be assumed to apply approximately to embedded areas. Thus,

$$I_{bb} = \frac{\pi}{4} \cdot 2\frac{\pi}{d} \int_0^{r_b} {}_pI\, r\, dr \tag{A7}$$

where

${}_pI$ is given in Eq. (A2), and now

$$\begin{aligned} c &= n\delta = L \\ R_2{}^2 &= 4c^2 + r^2 \\ R_1 &= r \\ z_1 &= 0 \end{aligned}$$

The integral in Eq. (A7) can readily be evaluated analytically, and gives

$$I_{bb} = \frac{\pi(1+\nu)}{16(1-\nu)d}\left[(3-4\nu)\frac{d_b}{2} + (5-12\nu+8\nu^2)(R-z) + \frac{(5-8\nu)}{2}z^2\left(\frac{1}{z}-\frac{1}{R}\right) + \frac{z}{2} - \frac{z^4}{2R^3}\right] \tag{A8}$$

where

$$R = \left(z^2 + \frac{d_b{}^2}{4}\right)^{1/2}$$

$$z = z_1 + 2c = 2L$$

APPENDIX B

ELASTIC EQUATIONS USED FOR LATERALLY-LOADED PILE ANALYSIS

The basic equation from which the required solution is derived is that obtained by Mindlin (1936), for the horizontal displacements caused by a horizontal point load within the interior of a semi-infinite elastic-isotropic homogeneous mass. Referring to Fig. B1, this solution is as follows:

$$\rho_x = \frac{Q}{16\pi G(1-\nu)}\left[\frac{(3-4\nu)}{R_1} + \frac{1}{R_2} + \frac{x^2}{R_1^3} + \frac{(3-4\nu)x^2}{R_2^3} + \frac{2cz}{R_2^3}\left(1 - \frac{3x^2}{R_2^2}\right) + \frac{4(1-\nu)(1-2\nu)}{R_2+z+c} \times \left(1 - \frac{x^2}{R_2(R_2+z+c)}\right)\right] \quad \text{(B1)}$$

Douglas and Davis (1964) integrated this equation over a rectangular area, and obtained the following solution.

At the upper corners A and B (see Fig. B2), for a uniform horizontal pressure p,

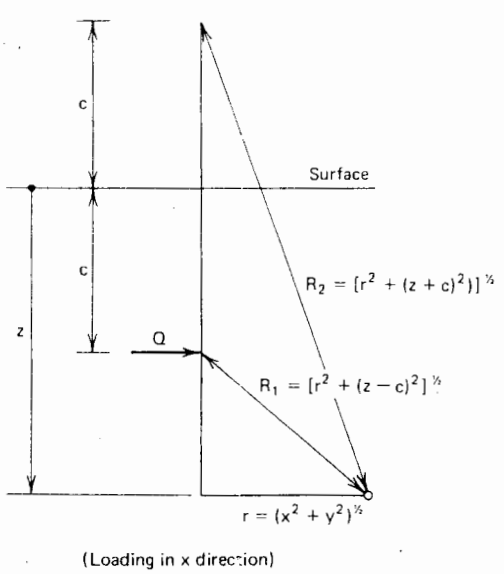

Figure B1 Definition of point-load problem.

$$\rho_x = \frac{pb}{32\pi G(1-\nu)}[(3-4\nu)F_1 + F_4 + 4(1-2\nu) \times (1-\nu)F_5] \quad \text{(B2)}$$

At the lower corners D and C,

$$\rho_x = \frac{pb}{32\pi G(1-\nu)}[(3-4\nu)F_1 + F_2 + 4(1-2\nu) \times (1-\nu)F_3] \quad \text{(B3)}$$

where

$$K_1 = \frac{2c_1}{b}$$

$$K_2 = \frac{2c_2}{b}$$

$$F_1 = -(K_1-K_2)\ln\left[\frac{(K_1-K_2)}{2+\sqrt{4+(K_1-K_2)^2}}\right] - 2\ln\left[\frac{2}{(K_1-K_2)+\sqrt{4+(K_1-K_2)^2}}\right]$$

$$F_2 = 2\ln\left[\frac{2(K_1+\sqrt{1+K_1^2})}{(K_1+K_2)+\sqrt{4+(K_1+K_2)^2}}\right] + (K_1-K_2) \times$$

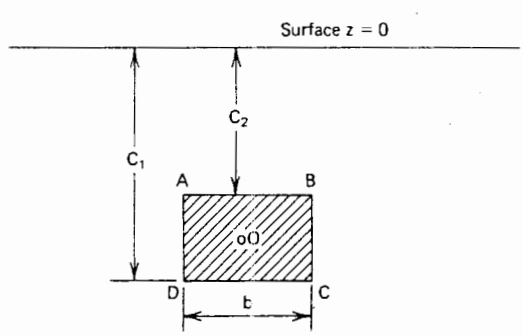

Figure B2 Definition of rectangular area.

$$\ln\left[2+\frac{\sqrt{4+(K_1+K_2)^2}}{(K_1+K_2)}\right]-K_1^2$$

$$\times\left[\frac{\sqrt{4+(K_1+K_2)^2}}{(K_1+K_2)}-\frac{\sqrt{1+K_1^2}}{K_1}\right]$$

$$F_3 = -2K_1\ln\left(\frac{K_1}{1+\sqrt{1+K_1^2}}\right)+(K_1+K_2)\times$$

$$\ln\left[\frac{(K_1+K_2)}{2+\sqrt{4+(K_1+K_2)^2}}\right]-$$

$$\ln\left[\frac{(K_1+K_2)+\sqrt{4+(K_1+K_2)^2}}{2(K_1+\sqrt{1+K_1^2})}\right]+\frac{(K_1+K_2)}{4}\times$$

$$[\sqrt{4+(K_1+K_2)^2}-(K_1+K_2)]-$$

$$K_1(\sqrt{1+K_1^2}-K_1)$$

$$F_4 = -2\ln\left[\frac{2(K_2+\sqrt{1+K_2^2})}{(K_1+K_2)+\sqrt{4+(K_1+K_2)^2}}\right]+$$

$$(K_1-K_2)\ln\left[\frac{2+\sqrt{4+(K_1+K_2)^2}}{(K_1+K_2)}\right]+$$

$$K_2{}^2\left[\frac{\sqrt{4+(K_1+K_2)^2}}{(K_1+K_2)}-\frac{\sqrt{1+K_2^2}}{K_2}\right]$$

$$F_5 = 2K_2\ln\left(\frac{K_2}{1+\sqrt{1+K_2^2}}\right)-(K_1+K_2)\times$$

$$\ln\left[\frac{K_1+K_2}{2+\sqrt{4+(K_1+K_2)^2}}\right]+$$

$$\ln\left[\frac{(K_1+K_2)+\sqrt{4+(K_1+K_2)^2}}{2(K_2+\sqrt{1+K_2^2})}\right]-\left(\frac{K_1+K_2}{4}\right)\times$$

$$[\sqrt{4+(K_1+K_2)^2}-(K_1+K_2)]-K_2(K_2-\sqrt{1+K_2^2})$$

For the displacement at other points in the same plane, the principle of superposition may be employed.

REFERENCES

Adams, J. I. & Hanna, T. H. 1970. "Ground Movements Due to Pile Driving." Conf. on Behavior of Piles, Inst. Civ. Engrs., London.

Agarwal, S. L. 1973. "Discrete Element Analysis and Its Experimental Verification for Vertical Piles Under Dynamic Lateral Loads." Proc. 8th Int. Conf. S.M. & F.E., Moscow, vol. 2.1, paper 3/2: 9–12.

Agerschou, H. A. 1962. "Analysis of the *Engineering News* Pile Formula." J.S.M.F.D., ASCE, 88, SM5: 1–11.

Airhart, T. P., Coyle, H. M., Hirsch, T. J. & Buchanan, S. J. 1969. "Pile-Soil System Response in a Cohesive Soil." *ASTM, STP* 444: 264–294.

Aitchison, G. D. & Woodburn, J. A. 1969. "Soil Suction in Foundation Design." Proc. 7th Int. Conf. S.M. & F.E., vol. 2: 1–8.

Alizadeh, M. 1969. "Lateral Load Tests on Instrumented Timber Piles." *ASTM, STP* 444: 379–394.

Alizadeh, M. & Davisson, M. T. 1970. "Lateral Load Tests on Piles–Arkansas River Project." *J.S.M.F.D., ASCE*, vol. 96, SM5: 1583–1604.

Avery, S. B. & Wilson, S. D. 1950. Discussion to Paper by Cummings, Kerkhoff, & Peck. Proc. ASCE, vol. 75, 1190–1199.

Awad, A. & Petrasovits, G. 1968. "Considerations on the Bearing Capacity of Vertical and Batter Piles Subjected to Forces Acting in Different Directions." Proc. 3rd Budapest Conf. S.M. & F.E., Budapest: 484–497.

Baguelin, F., Jézéquel, J. F., & Shields, D. H. 1978. "The Pressuremeter and Foundation Engineering." Clausthal: Trans Tech Publications.

Baguelin, F., & Frank, R. 1979. "Theoretical Studies of Piles Using the Finite Element Method." Proc. Conf. Num. Methods in Offshore Piling, London. Inst. Civ. Engrs., Paper no. 11.

Baikoff, E. M. A. & Burke, T. J. 1965. "Determination of Foundations for Heaving Soils." Trans. So. African Instn. Civ. Engrs., vol. 7, no. 8.

Balaam, N. P., Poulos, H. G., & Booker, J. R. 1975. "Finite Element Analysis of the Effects of Installation on Pile Load-Settlement Behavior." *Geot. Eng.*, vol. 6, no. 1: 33–48.

Balaam, N. P., Booker, J. R., & Poulos, H. G. 1976. "Analysis of Granular Pile Behavior Using Finite Elements." Univ. of Sydney Civ. Eng. Res. Rep. R290, Aust.

Balla, A. 1961. "The Resistance to Breaking Out of Mushroom Foundations for Pylons." Proc. 5th Int. Conf. S.M. & F. E., vol. 1: 569–576.

Banerjee, P. K. and Davies, T. G. 1977. "Analysis of Pile Groups Embedded in Gibson Soil." Proc. 9th Int. Conf. S. M. & F. E., Tokyo, vol. 1: 381–386.

Banerjee, P. K., & Driscoll, P. M. 1976. "Three-Dimensional Analysis of Raked Pile Groups." Proc. Instn. Civ. Engrs, Part 2, vol. 61: 653–671.

Banerjee, P. K., & Davies, T. G. 1978. "The Behaviour of Axially and Laterally Loaded Single Piles Embedded in Non-Homogeneous Soils." Geot., vol. 28, no. 3; 309–326.

Banerjee, P. K. 1978. "Analysis of Axially and Laterally Loaded Pile Groups," in Developments in Soil Mechanics, Ed. C. R. Scott, Ch. 9. London, Applied Science Publishers.

Barber, E. S. 1953. Discussion to Paper by S. M. Gleser. *ASTM, STP* 154: 96–99.

Barden, L. & Monckton, M. F. 1970. "Tests on Model Pile Groups in Soft and Stiff Clay." *Geot.*, vol. 20: 94–96.

Barkan, D. D. 1962. *Dynamics of Bases and Foundations*. New York: McGraw-Hill.

Barker, W. R. & Reese, L. C. 1970. "Load-Carrying Characteristics of Drilled Shafts Constructed with the Aid of Drilling Fluids." Res. Rep. 89–9, Center for High. Res., Univ. of Texas, Austin.

B.C.P. Committee 1971. "Field Tests on Piles in Sand." *Soils and Fndns.*, vol. 11, no. 2: 29.

Begemann, H. K. S. 1953. "Improved Method of Determining Resistance to Adhesion by Sounding Through a Loose Sleeve Placed Behind the Cone." Proc. 3rd Int. Conf. S.M. & F.E., vol. 1: 213–217.

Begemann, H. K. S. 1965. "The Maximum Pulling Force on a Single Tension Pile Calculated on the Basis of Results of the Adhesion Jacket Cone." Proc. 6th Int. Conf. S.M. & F.E., vol. 2: 229–233.

Begemann, H. K. S. 1969. "Negative Skin Friction of a Single Pile." Spec. Session no. 8, 7th Int. Conf. S.M. & F.E., paper no. 1.

Bender, C. H., Lyons, C. G., & Lowery, L. L. 1969. "Applications of Wave-Equation Analysis to Offshore Pile Foundations." 1st Offshore Tech. Conf., Texas, paper OTC 1055.

Beredugo, Y. O. 1966. "An Experimental Study of the Load Distribution in Pile Groups in Sand." *an. Geot. Jnl.*, vol. 3, no. 3: 145–166.

Berezantzev, V. G., Khristoforov, V., & Golubko , V. 1961. "Load Bearing Capacity and Deformation of Piled Foundations." Proc. 5th Int. Conf. S.M. & F.E., vol. 2: 11–15.

Bishop, R. F., Hill, R. & Mott, N. F. 1945. "The Theory of Indentation and Hardness Test." Proc. Phys. Soc., 57: 147–159.

Bjerrum, L. 1957. "Norwegian Experiences with Steel Piles to Rock." *Geot.*, vol. 7: 73–96.

Bjerrum, L., Johnson, W., & Ostenfeld, C. 1957. "The Settlement of a Bridge Abutment on Friction Piles." Proc. 4th Int. Conf. S.M. & F.E., vol. 2: 14–19.

Bjerrum, L., Brinch Hansen, J., & Sevaldson, R. 1958. "Geotechnical Investigations for a Quay Structure in Horten." N.G.I., pub. no. 28: 1–17.

Bjerrum, L. & Johannessen, I. J. 1960. "Pore Pressures Resulting from Driving Piles in Soft Clay." Conf. on Pore Press. & Suction in Soil, Butterworths, Sydney, Aust.: 14–17.

Bjerrum, L. & Simons, N. E. 1960. "Comparison of Shear Strength Characteristics of Normally Consolidated Clays." Proc. ASCE Res. Conf. on Shear Strength of Cohesive Soils: 711–726.

Bjerrum, L., Johannesson, I. J., & Eide, O. 1969. "Reduction of Skin Friction on Steel Piles to Rock." Proc. 7th Int. Conf. S.M. & F.E., vol. 2: 27–34.

Blight, G. E. 1965. "The Time-Rate of Heave of Structures on Expansive Clays." *Moisture Equilibria and Moisture Changes in Soils Beneath Covered Areas*, Butterworths, Sydney, Aust.: 78.

Blight, G. E. 1967. "Observations on the Shear Testing of Indurated Fissured Clays." Proc. Geot. Conf., Oslo: 97.

Bogdanovic, L. J. 1961. "The Use of Penetration Tests for Determining the Bearing Capacity of Piles." Proc. 5th Int. Conf. S.M. & F.E., vol. 2: 17–22.

Booker, J. R. & Poulos, H. G. 1976*a*. "Analysis of Creep Settlement of Pile Foundations." *Jnl. Geot. Eng. Divn., ASCE*, vol. 102, no. GT1: 1–14.

Booker, J. R. & Poulos, H. G. 1976*b*. "Finite Element Analysis of Piles in Viscoelastic Soil." Proc. 2nd Int. Conf. on Numerical Methods in Geomechanics, Blacksburg, vol. 1: 425–437.

Bowles, J. E. 1977. *Foundation Analysis and Design*. 2nd Ed. New York: McGraw-Hill.

Bozozuk, M. & Labrecque, A. 1969. "Downdrag Measurements on 270-Ft Composite Piles." *ASTM, STP* 444: 15–40.

Bozozuk, M. 1972. "Downdrag Measurements on a 160-Ft Floating Pipe Test Pile in Marine Clay." *Can. Geot. Jnl.*, vol. 9, no. 2: 127–136.

Brandtzaeg, A. & Harboe, E. 1957. "Buckling Tests of Slender Steel Piles in Soft, Quick Clay." Proc. 4th Int. Conf. S.M. & F.E., vol. 2: 19–23.

Brinch Hansen, J. 1961. "The Ultimate Resistance of Rigid Piles Against Transversal Forces." *Geoteknisk Institut. Bull. No. 12*, Copenhagen.

Bromham, S. B. & Styles, J. R. 1971. "An Analysis of Pile Loading Tests in a Stiff Clay." Proc. 1st Aust.-N.Z. Conf. Geomechs., Melbourne, vol. 1: 246–253.

Broms, B. B. 1963. "Allowable Bearing Capacity of Initially Bent Piles." *J.S.M.F.D., ASCE*, vol. 89, SM5: 73–90.

Broms, B. B. & Silberman, J. O. 1964. "Skin Friction Resistance for Piles in Cohesionless Soils." *Sols Soils*, no. 10: 33.

Broms, B. B. 1964*a*. "Lateral Resistance of Piles in Cohesive Soils." *J.S.M.F.D., ASCE*, vol. 90, SM2: 27–63.

Broms, B. B. 1964*b*. "Lateral Resistance of Piles in Cohesionless Soils." *J.S.M.F.D., ASCE*, vol. 90, SM3: 123–156.

Broms, B. B. 1965. Discussion to paper by Y. Yoshimi. *J.S.M.F.D., ASCE*, vol. 91, SM4: 199–205.

Broms, B. B. 1966. "Methods of Calculating the Ultimate Bearing Capacity of Piles–A Summary." *Sols-Soils* no. 18–19: 21–32.

Broms, B. B. 1972. "Stability of Flexible Structures (Piles and Pile Groups)." Proc. 5th Eur. Conf. Soil Mech. Fndn. Eng., Madrid, vol. 2: 239–269.

Brons, K. F., Amesz, A. W., & Rinck, J. 1969. "The Negative Skin Friction Along the Shaft of a Foundation Pile." Spec. Sess. No. 8, 7th Int. Conf. S.M. & F.E., paper no. 2.

Brown, P. T., Poulos, H. G., & Wiesner, T. J. 1975. "Piled Raft Foundation Design." Proc. of Symp. on Raft Foundations, CSIRO, Aust.

Brown, P. T. & Wiesner, T. J. 1975. "The Behavior of Uniformly Loaded Piled Strip Footings." *Soils and Fndns*, vol. 15, no. 4: 13–21.

Burland, J. B. (1973). "Shaft Friction of Piles in Clay–A Simple Fundamental Approach." *Ground Eng.*, vol. 6, no. 3, May: 30–42.

Burland, J. B., Butler, F. G., & Dunican, P. 1966. "The Behaviour and Design of Large-Diameter Bored Piles in Stiff Clay." Proc. Symp. on Large Bored Piles, Inst. Civ. Engrs, London: 51–71.

Butterfield, R. and Banerjee, P. K. 1970. "A Note on the Problem of a Pile-Reinforced Half Space." *Geot.*, vol. 20, no. 1: 100–103.

Butterfield, R. and Banerjee, P. K. 1971*a*. "The Elastic Analysis of Compressible Piles and Pile Groups." *Geot.*, vol. 21, no. 1: 43–60.

Butterfield, R. and Banerjee, P. K. 1971*b*. "The Problem of Pile Group and Pile Cap Interaction." *Geot.*, vol. 21, no. 2: 135–142.

Cambefort, H. 1953. "La Force Portante des Groupes de Pieux." Proc. 3rd Int. Conf. S.M. & F.E., vol. 2: 22–29.

Cambefort, H. and Chadeisson, R. 1961. "Critere pour l'Evaluation de la Force Portante d'un Pieu." Proc. 5th Int. Conf. S.M. & F.E., vol. 2: 23–31.

Chae, Y. S. 1970. "Dynamic Behaviour of Embedded Foundation-Soil Systems." *High. Res. Rec.* no. 323: 49–59.

Chan, J. H. C. & Matlock, H. 1973. "A Discrete-Element Method for Transverse Vibrations of Beam Columns Resting on Linearly Elastic or Inelastic Supports." Proc. 5th Offshore Tech. Conf., Houston, Vol. 2: 205–218.

Chandler, R. J. 1966. Discussion to paper by Whitaker and Cooke. Proc. Symp. on Large Bored Piles: 95–97.

Chandler, R. J. 1968. "The Shaft Friction of Piles in Cohesive Soils in Terms of Effective Stress." *Civ. Eng. and Pub. Wks. Rev.*, Jan.: 48–51.

Chellis, R. D. 1961. *Pile Foundations*. New York: McGraw-Hill.

Chellis, R. D. 1962. "Pile Foundations," ch. 7 in *Foundations Engineering*, ed. by G. A. Leonards. New York: McGraw-Hill.

Chellis, R. D. 1969. "Piles and Pile Structures," in *Handbook of Ocean and Underwater Engineering*, ed. by Myers, Holm, & McAllister. McGraw-Hill, New York: 8.56–8.98.

Claessen, A. I. M. & Horvat, E. 1974. "Reducing Negative Friction with Bitumen Slip Layers." *Jnl. Geot. Eng. Divn., ASCE*, vol. 100, no. GT8: 925–944.

Clemence, S. P. & Brumund, W. F. 1975. "Large-Scale Model Test of Drilled Pier in Sand." *Jnl. Geot. Eng.*

Div., ASCE, vol. 101, No. GT6, 537–550.
Coates, D. F. & Gyenge, M. 1956. "Plate-Load Testing on Rock for Deformation and Strength Properties." *Testing Tech. for Rock Mechs., ASTM*: 19–25.
Coates, D. F. 1967. *Rock Mechanics Principles*. Can. Mines Branch Monograph 874, Ottawa.
Collins, L. E. 1953. "A Preliminary Theory for the Design of Underreamed Piles." Trans. So. African Instn. Civ. Engrs., vol. 3, no. 11.
Collins, L. E. 1958. "Some Observations on the Movement of Buildings on Expansive Soil in Vereeniging and Odendaalrus." Trans. So. African Instn. Civ. Engrs., vol. 7, no. 9.
Cooke, R. W. & Whitaker, R. 1961. "Experiments on Model Piles with Enlarged Bases." *Geot.*, vol. 11: 1–13.
Cooke, R. W. 1966. Discussion to paper by Burland et al. Proc. Symp. on Large Bored Piles: 92.
Cooling, L. C. & Packshaw, S. 1950. "Notes of Pile-Loading Tests." *Chart. Civ. Engr.*, May: 16–20.
Cox, A. D. 1962. "Axially Symmetric Plastic Deformation in Soils–II. Indentation of Ponderable Soils." *Int. J. Mech. Sci.*, vol. 4: 371.
Cox, A. D., Eason, G., & Hopkins, H. G., 1961. "Axially Symmetric Plastic Deformation in Soils." *Phil. Trans. Roy. Soc. London*, series A, 254: 1–45.
Coyle, H. M. & Reese, L. C. 1966. "Load Transfer for Axially Loaded Piles in Clay." *J.S.M.F.D., ASCE*, vol. 92, SM2: 1–26.
Coyle, H. M. & Sulaiman, I. H. 1967. "Skin Friction for Steel Piles in Sand." *J.S.M.F.D., ASCE*, vol. 93, SM6: 261–278.
Coyle, H. M., Bartoskewitz, R. E., & Lowery, L. L. 1970. "Prediction of Static Bearing Capacity from Wave Equation Analysis." 2nd Offshore Tech. Conf., Texas, paper OTC 1202.
Coyle, H. M. & Gibson, G. C. 1970. "Empirical Damping Constants for Sands and Clays." *J.S.M.F.D., ASCE*, vol. 96, SM3: 949–965.
Crooke, R. C. 1955. "Re-Analysis of Existing Wave Force Data on Model Piles." U.S. Army Corps Engrs., Beach Erosion Board Tech. Memo 71.
Cumming, D. A. & Gerrard, C. M. 1964. "Computation of Stresses in Pavements." Proc. 2nd Conf. Aust. Rd. Res. Bd., 2, pt 2: 729.
Cummings, A. E., Kerkhoff, G. O., & Peck, R. B. 1950. "Effect of Driving Piles in Soft Clay." *Trans. ASCE*, vol. 115: 275–286.
D'Appolonia, E. & Romualdi, J. P. 1963. "Load Transfer in End-Bearing Steel H-Piles." *J.S.M.F.D., ASCE*, vol. 89, SM2: 1–25.
D'Appolonia, E. & Hribar, J. A. 1963. "Load Transfer in a Step-Taper Pile." *J.S.M.F.D., ASCE*, vol. 89, SM6: 57–77.
D'Appolonia, D. J. & Lambe, T. W. 1971. "Performance of Four Foundations on End-Bearing Piles." *J.S.M.F.D., ASCE*, vol. 97, SM1: 77–93.
D'Appolonia, D. J., Poulos, H. G., & Ladd, C. C. 1971. "Initial Settlement of Structures on Clay." *J.S.M.F.D., ASCE*, vol. 97, SM10: 1359–1377.
Darragh, R. D. & Bell, R. A. 1969. "Load Tests on Long Bearing Piles." *ASTM STP* 444: 41–67.
Davis, E. H. 1961. "The Application of the Theory of Plasticity to Foundation Problems–Limit Analysis." Post-Grad. Course on Fndn. Eng., Univ. of Sydney, Aust.
Davis, E. H. & Booker, J. R. 1971. "The Bearing Capacity of Strip Footings from the Standpoint of Plasticity Theory." Proc. 1st Aust.-New Zeal. Conf. on Geomechs., Melbourne, Vol. 1: 276–282.
Davis, E. H. & Poulos, H. G. 1963. "Triaxial Testing and Three-Dimensional Settlement Analysis." Proc. 4th Aust.-N.Z. Conf. S.M. & F.E.: 233–246.
Davis, E. H. & Poulos, H. G. 1968. "The Use of Elastic Theory for Settlement Prediction Under Three-Dimensional Conditions." *Geot.*, vol. 18: 67–91.
Davis, E. H. & Poulos, H. G. 1972. "Rate of Settlement Under Two- and Three-Dimensional Conditions." *Geot.*, vol. 22: 95–114.
Davis, E. H. & Poulos, H. G. 1972. "The Analysis of Pile-Raft Systems." *Aust. Geomechs. Jnl.*, vol G2, no. 1: 21–27.
Davis, E. H. & Taylor, H. 1962. "The Movement of Bridge Approaches and Abutments on Soft Foundation Soils." Proc. 1st Aust. Road Res. Bd. Conf, Canberra, p. 740.
Davisson, M. T. & Gill, H. L. 1963. "Laterally Loaded Piles in a Layered Soil System." *J.S.M.F.D., ASCE*, vol. 89, SM3: 63–94.
Davisson, M. T. 1963. "Estimating Buckling Loads for Piles." Proc. 2nd Pan-Amer. Conf. on S.M. & F.E., Brazil, vol. 1: 351–371.
Davisson, M. T. & Prakash, S. 1963. "A Review of Soil-Pile Behavior." *High Res. Rec.*, No. 39: 25–48.
Davisson, M. T. & Robinson, K. E. 1965. "Bending and Buckling of Partially Embedded Piles." Proc. 6th Int Conf. S.M. & F.E., vol. 2: 253–246.
Davisson, M. T. 1970. "Lateral Load Capacity of Piles." *High. Res. Rec.*, No. 333: 104–112.
Dawson, A. W. 1970. "Downdrag on Pile Foundations." M. Sc. Eng. project, Dept. Civ. Eng., M.I.T.
De Beer, E. E. & Wallays, M. 1972. "Forces Induced in Piles by Unsymmetrical Surcharges on the Soil Around the Pile." Proc. 5th Eur. Conf. S.M. & F.E., Madrid, vol. 1: 325–332.
De Bruijn, C. M. A. 1961. "Swelling Characteristics of a Transported Soil Profile at Leeuhof, Vereeniging (Transvaal)." Proc. 5th Int. Conf. Soil Mechs. Fndn. Eng., vol. 1: 43.
de Mello, V. F. B. 1969. "Foundations of Buildings on Clay." *State of the Art Report*: 49–136. Proc. 7th Int. Conf. S.M. & F.E., Mexico City.
de Mello, V. F. B. 1971. "The Standard Penetration Test." Proc. 4th Pan-Amer. Conf. S.M. & F.E., Puerto Rico, vol. 1: 1–86.
Desai, C. S. 1974. "Numerical Design–Analysis for Piles in Sands." *Jnl. Geot. Eng. Divn., ASCE*, vol. 100, no. GT6: 613–635.
Desai, C., & Abel, J. F. 1972. *Introduction to the Finite Element Method*. New York: Van Nostrand Reinhold.
Desai, C. S., Johnson, L. D., & Hargett, C. M. 1974. "Analysis of Pile Supported Gravity Lock." *Jnl. Geot. Eng. Divn., ASCE*, vol. 100, no. GT9: 1009–1029.
Desai, C. S., & Appel, G. C. 1976. "3-D Analysis of Laterally Loaded Structures." 2nd Int. Conf. Num. Methods in Geomechs, Blacksburg. ASCE, vol. 1: 405–418.

Desai, C. S. & Christian, J. T. 1977. *Numerical Methods in Geotechnical Engineering*. New York: McGraw-Hill.

Donaldson, G. W. 1965. "A Study of Level Observations on Buildings as Indications of Moisture Movements in the Underlying Soil" in *Moisture Equilibria and Moisture Changes in Soils Beneath Covered Areas*. Butterworths, Sydney, Aust.: 156–164.

Donaldson, G. W. 1967*a* "The Use of Small-Diameter Piles in Expansive Soil." Proc. 4th Reg. Conf. for Africa on Soil Mechs. & Fndn. Eng., vol. 1: 249.

Donaldson, G. W. 1967*b*. "The Measurement of Stresses in Anchor Piles." Proc. 4th Reg. Conf. for Africa on Soil Mechs. & Fndn. Eng., vol. 1: 253.

Doroshkevich, N. M. & Boim, V. P. 1967. "In-situ Study of the Bearing Capacity of Driven Piles in Expansive Soil." Proc. 3rd Asian Conf. S.M. & F.E.: 81–83.

Douglas, D. J. & Davis, E. H. 1964. "The Movement of Buried Footings Due to Moment and Horizontal Load and the Movement of Anchor Plates." *Geot.*, vol. 14: 115–132.

Downs, D. I. & Chieurzzi, R. 1966. "Transmission Tower Foundations." *J. Power Divn., ASCE*, vol. 92, PO2: 91–114.

Druery, B. M. & Ferguson, R. A. 1969. "An Experimental Investigation of the Behaviour of Laterally Loaded Piles." B. E. thesis, Dept. Civil Eng., Univ. of Sydney, Aust.

Duncan, N. & Hancock, K. E. 1966. "The Concept of Contact Stress in the Assessment of the Behaviour of Rock Masses as Structural Foundations." Proc. 1st Conf. Int. Soc. of Rock Mechs., Lisbon, vol. 2: 487–492.

Dvorak, A. 1966. "Tests of Anisotropic Shale for Foundations of Large Bridges." Proc. 1st Cong. Int. Soc. of Rock Mechs., Lisbon, vol. 2: 537.

Egorov, K. E., Kuzmin, P. G., & Popov, G. P. 1957. "The Observed Settlements of Buildings as Compared with Preliminary Calculations." Proc. 4th Int. Conf. S.M. & F.E., vol. 1: 291–296.

Eide, O., Bjerrum, L., & Landva, A. 1961. "Short- and Long-Term Test Loading of a Friction Pile in Clay." Proc. 5th Int. Conf. S.M. & F.E., vol. 2: 45.

Ellison, R. D., D'Appolonia, E., & Thiers, G. R. 1971. "Load-Deformation Mechanism for Bored Piles." *J.S.M. F.D., ASCE*, vol. 97, SM4: 661–678.

Elmasry, M. A. 1963. "The Negative Skin Friction of Bearing Piles." Thesis presented to Swiss Fed. Inst. of Tech., Zurich.

Endo, M., Minou, A., Kawasaki, K., & Shibata, T. 1969. "Negative Skin Friction Acting on Steel Pipe Piles in Clay." Proc. 7th Int. Conf. S.M. & F.E., vol. 2: 93–98.

Esu, F. & Ottaviani, M. 1975. Discussion to paper by C. S. Desai. Proc. Geot. Eng. Divn., A.S.C.E., vol. 101, no. GT7: 693–695.

Evangelista, A. and Viggiani, C. 1976. "Accuracy of Numerical Solutions for Laterally Loaded Piles in Elastic Half-Space." Proc. 2nd Int. Conf. Numerical Methods in Geomechanics, Blacksburg, vol. 3: 1367–1370.

Evans, L. T. 1953. "Bearing Piles Subjected to Horizontal Loads." *ASTM, STP* 154.

Feagin, L. B. 1937. "Lateral Pile Loading Tests." *Trans. ASCE*, vol. 102: 236–254.

Fellenius, B. 1955. "Results of Tests on Piles at Gothenburg Railway Station." *Bull. No. 5*, Geot. Dept., Sw. State R.

Fellenius, B. H. & Broms, B. B. 1969. "Negative Skin Friction for Long Piles Driven in Clay." Proc. 7th Int. Conf. S.M. & F.E., vol. 2: 93–98.

Fellenius, B. H. & Broms, B. B. 1969. "Negative Skin Friction for Long Piles Driven in Clay." Spec. Sess. No. 8, 7th Int. Conf. S.M. & F.E., paper no. 12 (see also vol. 2 of Conf. Proc.).

Flaate, K. S. 1964. "An Investigation of the Validity of Three Pile Driving Formulae in Cohesionless Material." *Pub. No. 56*, N.G.I., Oslo, Norway.

Focht, J. A. 1967. Discussion to paper by Coyle and Reese. *J.S.M.F.D., ASCE*, Vol. 93, SM1: 133–138.

Focht, J. A. & Koch, K. J. 1973. "Rational Analysis of the Lateral Performance of Offshore Pile Groups." Proc. 5th Offshore Tech. Conf., Houston, Vol. 2, paper OTC 1896: 701–708.

Forehand, P. W. & Reese, J. L. 1964. "Prediction of Pile Capacity by the Wave Equation." *J.S.M.F.D., ASCE*, vol. 90, SM2: 1–25.

Francis, A. J. 1964. "Analysis of Pile Groups with Flexural Resistance." *J.S.M.F.D., ASCE*, vol. 90, SM3: 1–32.

Francis, A. J., Stevens, L. K., & Hoadley, P. J. 1965. Paper to Symp. Soft Ground Eng., Brisbane. Inst. Engrs., Aust.

Franx, C. & Boonstra, G. C. 1948. "Horizontal Pressures on Pile Foundations." Proc. 2nd Int. Conf. S.M. & F.E., vol. 1: 131–135.

Freeman, C. F., Klajnerman, D., & Prasad, G. D. 1972. "Design of Deep Socketed Caissons into Shale Rock." *Can. Geot. Jnl.*, vol. 9, no. 1: 105–114.

Frydman, S., Sha'al, B., and Mazurik, A. 1975. "Analysis of an Instrumented Laterally Loaded Pile." Proc. 5th Asian Reg. Conf. Soil Mechs. Fndn. Eng., Bangalore, India.

Fukuoka, M. 1977. "The Effects of Horizontal Loads on Piles Due to Landslides." Proc. 10th Spec. Session, 9th Int. Conf. Soil Mechs. Fndn. Eng., Tokyo.

Fuller, F. M. & Hay, H. E. 1970. "Pile Load Tests Including Quick-Load Test Method, Conventional Methods and Interpretations." *High Res. Rec.*, No. 333: 74–86.

Gaul, R. D. 1958. "Model Study of a Dynamically Laterally Loaded Pile." *J.S.M.F.D., ASCE*, Feb. 1958, paper 1535.

Gibson, R. E. & Lumb, P. 1953. "Numerical Solution of Some Problems in the Consolidation of Clay." Proc. Inst. Civ. Engrs., London: 182.

Glanville, W. H., Grime, G., Fox, E. N., & Davies, W. W. 1938. "An Investigation of the Stresses in Reinforced Concrete Piles During Driving." Br. Bldg. Res. Bd., tech. paper no. 20, D.S.I.R.

Gleser, S. M. 1953. "Lateral Load Tests on Vertical Fixed-Head and Free-Head Piles," *ASTM, STP* 154: 75–93.

Goble, G. G., Scanlan, R. H., & Tomko, J. J. 1967. "Dynamic Studies on the Bearing Capacity of Piles." *High Res. Rec.*, no. 67.

Golder, H. Q., & Leonard, M. W. 1954. "Some Tests on Bored Piles in London Clay." *Geot.*, vol. 4: 32–41.

Golder, H. Q. 1957. "A Note on Piles in Sensitive Clays." *Geot.*, vol. 7: 192–195.

Golder, H. Q. & Skipp, B. O. 1957. "The Buckling of Piles in Soft Clay." Proc. 4th Int. Conf. S.M. & F.E., vol. 2: 35–39.

Golder, H. Q. & Osler, J. C. 1968. "Settlement of a Furnace Foundation, Sorel, Quebec." *Can. Geot. Jnl.*, vol. 5, no. 1: 46–56.

Granholm. H. 1929. "On the Elastic Stability of Piles Surrounded by a Supporting Medium." *Ingen. Vetenk. Akad. Handl.*, no. 89, Stockholm.

Griffel, W. 1966. *Handbook of Formulas for Stress and Strain.* New York: Ungar.

Hagerty, D. J. & Peck. R. B. 1971. "Heave and Lateral Movements Due to Pile Driving." *J.S.M.F.D., ASCE,* vol. 97, SM11: 1513–1532.

Hain, S. J. 1975. "Analysis of Rafts and Raft Pile Foundations," in *Soil Mechs: Recent Developments.* Proc. Symp., Univ. N.S.W., Aust.: 213–254.

Hain, S. J. & Lee, I. K. 1978. "The Analysis of Flexible Pile-Raft Systems." Geot., vol. 28, no. 1: 65–83.

Hanna, T. H. 1963. "Model Studies of Foundations Groups in Sand." *Geot.*, vol. 13, no. 4: 334.

Hanna, T. H. 1967. "The Measurement of Pore Water Pressures Adjacent to a Driven Pile." *Can. Geot. Jnl.*, vol. 4, no. 3: 313.

Hanna, T. H. 1968. "The Bending of Long H-Section Piles." *Can. Geot. Jnl.*, vol. 5, no. 3: 150–172.

Hanna, T. H., & Tan, R. H. S. 1973. "The Behavior of Long Piles Under Compressive Loads in Sand." *Can. Geot. Jnl.*, vol. 10, no. 3: 311–340.

Harrison, H. B. 1973. *Computer Methods in Structural Analysis.* Englewood Cliffs, N.J.: Prentice-Hall.

Hayashi, S., Miyazawa, N., & Yamashita, I. 1965. "Lateral Resistance of Steel Piles Against Statical and Dynamical Loads." Proc. 3rd World Conf. on Earthquake Eng., vol. 2.

Hetenyi, M. 1946. "Beams on Elastic Foundations." Ann Arbor, Mich.: Univ. of Mich. Press.

Heyman, L. & Boersma, L. 1961. "Bending Moments in Piles Due to Lateral Earth Pressures." Proc. 5th Int. Conf. S.M. & F.E., vol. 2: 425–429.

Heyman, L. 1965. "Measurement of the Influence of Lateral Earth Pressure on Pile Foundations." Proc. 6th Int. Conf. S.M. & F.E., vol. 2: 257–260.

Hirsch, T. J., Lowery, L. L., Coyle, H. M., & Samson, C. H. 1970. "Pile-Driving Analysis by One-Dimensional Wave Theory: State of the Art." *High Res. Rec.*, no. 333: 33–54.

Hoadley, P. J. 1964. M. Eng. Sc. thesis, Univ. of Melbourne, Aust.

Hoadley, P. J., Francis, A. J., & Stevens, L. J. 1969. "Load Testing of Slender Steel Piles in Soft Clays." Proc. 7th Int. Conf. S.M. & F.E., Mexico, vol. 2: 123–130.

Holloway, P. M., Clough, G. W., & Vesic, A. S. 1975. "The Mechanics of Pile-Soil Interaction in Cohesionless Soils." Duke Univ. School of Eng., *Soil Mechs.* series, no. 39.

Hooper, J. A. 1973. "Observations on the Behavior of a Piled Raft Foundation on London Clay." Proc. Instn. Civ. Engrs., pt. 2, vol. 55: 855.

Housel, W. S. & Burkey, J. R. 1948. "Investigation to Determine the Driving Characteristics of Piles in Soft Clay." Proc. 2nd Int. Conf. S.M. & F.E., vol. 5: 146–154.

Housel, W. S. 1966. "Pile Load Capacity–Estimates and Test Results." *J.S.M.F.D., ASCE,* vol. 92, SM4: 1–29.

Hrennikoff, A. 1950. "Analysis of Pile Foundations with Batter Piles." *Trans. ASCE,* vol. 115: 351.

Hutchinson, J. N. & Jensen, E. V. 1968. "Loading Tests on Piles Driven into Estuarine Clays at Port Kharramashahr, Iran, and Observations of the Effect of Bitumen Coatings on Shaft Bearing Capacity." *N.G.I.*, pub. no. 78: 1–12.

Idriss, I. M. & Seed, H. B. 1968. "Seismic Response of Horizontal Soil Layers." *J.S.M.F.D., ASCE,* vol. 94, SM4: 1003–1031.

Ireland, H.O. 1957. "Pulling Tests on Piles in Sand." Proc. 4th Int. Conf. S.M. & F.E., vol. 2: 43–54.

Isaacs, D.V. 1931. "Reinforced Concrete Pile Formulae." *Trans. Instn. Engrs. Aust.*, 12: 313–323.

Ito, T. & Matsui, T. 1975. "Methods to Estimate Lateral Force Acting on Stabilizing Piles." *Soils and Foundns,* vol. 15, no. 4: 43–59.

Jain, G. S. & Kumar, V. 1963. "Calculations for Separating Skin Friction and Point Bearing in Piles." *ASTM Jn. Materials, Research & Standards,* vol. 3, no. 4: 290–293.

Jampel. S. 1949. "An Analysis of Groups of Piles, I & II." *Concrete and Constructional Eng.*, vol. 44, 7: 201–208 and 8: 253–257.

Jaspar, J. L. & Shtenko, V. W. 1969. "Foundation Anchor Piles in Clay-Shales." *Can. Geot. Jnl.*, vol. 6: 159–174.

Johannessen, I. J. & Bjerrum, L. 1965. "Measurement of the Compression of a Steel Pile to Rock Due to Settlement of the Surrounding Clay." Proc. 6th Int. Conf. S.M. & F.E., vol. 2: 261–264.

Johnson, S. M., 1962. "Determining the Capacity of Bent Piles." *J.S.M.F.D., ASCE,* vol 88, SM6: 65–79.

Kerisel, J. 1961. "Fondations Profondes en Milieu Sableux." Proc. 5th Int. Conf. S.M. & F.E., vol. 2: 73–83.

Kerisel, J. 1965. "Vertical and Horizontal Bearing Capacity of Deep Foundations in Clay." Symp. on Brg. Cap. and Settl. of Fndns., Duke Univ.: 45–52.

Kerisel, J. & Adam, M. 1967. "Calcul des Forces Horizontales Applicables aux Fondations Profondes dans les Argiles et Limons." Annales I.T.B.T.P., No. 239: 1653.

Kerisel, J. & Quatre, J. M. 1966. "Tassements sous les Fondations." *Annales des Ponts et Chaussees,* 3: 143–164.

Kezdi, A. 1957. "The Bearing Capacity of Piles and Pile Groups." Proc. 4th Int. Conf. S. M. & F.E., vol. 2: 46–51.

Kishida, H. & Meyerhof, G. G. 1965. "Bearing Capacity of Pile Groups Under Eccentric Loads in Sand." Proc 5th Int. Conf. S.M. & F.E., vol. 2: 270–274.

Kishida, H. 1967. "Ultimate Bearing Capacity of Piles Driven into Loose Sand." *Soil and Fndns.*, vol. 7, no. 3: 20–29.

Klohn, E. J. & Hughes, G. T., 1964. "Buckling of Long Unsupported Timber Piles." *J.S.M.F.D., ASCE,* vol. 90, SM6: 107–123.

Kocsis, P. 1968. *Lateral Loads on Piles.* Chicago: Bureau of Eng.

Koerner, R. M. & Mukhopadhyay, C. 1972. "Behavior of Negative Skin Friction on Model Piles in Medium-Plasticity Silt." *High. Res. Rec.*, no. 405: 34–44.

Koerner, R. M. & Partos, A. 1974. "Settlement of Building on Pile Foundation in Sand." *Jnl. Geot., Eng. Divn., ASCE,* vol. 100, no. GT3: 265.

Koizumi, Y. & Ito, K. 1967. "Field Tests with Regard to Pile Driving and Bearing Capacity of Piled Foundations." *Soils and Fndns.*, no. 3: 30.

Kubo, J. 1965. "Experimental Study of the Behaviour of Laterally Loaded Piles." Proc. 6th Int. Conf. S.M. & F.E., vol. 2: 275–279.

Ladanyi, B. 1963. "Expansion of a Cavity in a Saturated Clay Medium." *J.S.M.F.D., ASCE,* vol. 89, SM4: 127–161.

Ladanyi, B. 1977. Discussion. *Can. Geot. Jnl.*, vol. 14, no. 1: 153–155.

Ladd, C. C. 1965. "Stress-Strain Behavior of Anisotropically Consolidated Clays during Undrained Shear." Proc. 6th Int. Conf. S.M. & F.E., vol. 1: 282.

Lambe, T. W. 1964. "Methods of Estimating Settlements." *J.S.M.F.D., ASCE,* vol. 90, SM5: 43.

Lambe, T. W. & Horn, H. M. 1965. "The Influence on an Adjacent Building of Pile Driving for the M.I.T. Materials Center." Proc. 6th Int. Conf. S.M. & F.E., vol. 2: 280.

Lee, I. K. 1973. "Application of Finite Element Method in Geot. Engg., Part I–Linear Analysis" Ch. 17 in *Finite Element Techniques–A Short Course of Fundamentals and Application,* Univ. of N.S.W., Aust.

Lee, K. L. 1968. "Buckling of Partially Embedded Piles in Sand." *J.S.M.F.D., ASCE,* vol. 94, SM1: 255–270.

Lenci, C., Maurice, J., & Madignier, F. 1968. "Pieu Vertical Sollicité Horizontalement." *Annales des Ponts et Chaussees,* VI, Nov-Dec.: 337–383.

Leussink, H. & Wenz, K. P. 1969. "Storage Yard Foundations on Soft Cohesive Soils." Proc. 7th Int. Conf. S.M. & F.E., vol. 2: 149–155.

Lo, K. Y. & Stermac, A. G. 1965. "Induced Pore Pressures During Pile Driving Operations." Proc. 6th Int. Conf. S.M. & F.E., vol. 2: 285.

Lo, K. Y. 1968. Discussion to Paper by Orrje and Broms, *J.S.M.F.D., ASCE,* vol. 94, SM2: 606–608.

Lo, M. B. 1967. Discussion to Paper by Y. O. Beredugo. *Can. Geot. Jnl.*, vol. 4: 353–354.

Locher. H. G. 1965. "Combined Cast-in-Place and Precast Piles for Reduction of Negative Friction Caused by Embankment Fill." Proc. 6th Int. Conf. S.M. & F.E., vol. 2: 290–294.

Lowery, L. L., Hirsch, T. J., Edwards, T. C., Coyle, H. M., & Samson, C. H., 1969. "Use of the Wave Equation to Predict Soil Resistance on a Pile During Driving." Spec. Session No. 8, 7th Int. Conf. S. M. & F.E., Mexico.

Lundgren, H. & Mortensen, K. 1953. "Determination by the Theory of Plasticity of the Bearing Capacity of Continuous Footings on Sand." Proc. 3rd Int. Conf. Soil Mech. Fndn. Eng., vol. 1: 409–412.

MacDonald, H. F. 1963. "Uplift Resistance of Caisson Piles in Sand." M. Sc. thesis, Nova Scotia Tech. College, Can.

Madhav, M. R. & Rao, N. S. V. K. 1971. "Model for Machine-Pile Foundation-Soil System." *J.S.M.F.D., ASCE,* vol. 97, SM1: 295–299.

Madhav, M. R., Rao, N. S. V. K., & Madhavan, K. 1971. "Laterally Loaded Pile in Elasto-Plastic Soil." *Soils and Fndns.*, vol. 11, no. 2: 1–15.

Madhav, M. R. & Davis, E. H. 1974. "Buckling of Finite Beams in Elastic Continuum." *Jnl. Eng. Mechs. Div., ASCE,* vol. 100, no. EM6: 1227–1236.

Madhav, M. R. & Rao, K. K. 1975. "Analysis of Initially Bent Piles" in *Anal. of Soil Beh. and Its App. to Geot. Structs.* Proc Symp., Univ. N.S.W., Aust.: 145–155.

Mansur, C. I. & Kaufman, R. I. 1956. "Pile Tests, Low-Sill Structure, Old River La." *J.S.M.F.D. ASCE,* vol. 82, SM4, proc. paper 1079.

Marche, R. & Lacroix, Y. 1972. "Stabilite des Culées de Ponts Establies sur des Pieux Traversant une Couche Molle." *Can. Geot. Jnl.*, vol. 9, no. 1: 1–24.

Matlock, H. & Ripperberger, E. A. 1958. "Measurement of Soil Pressure on a Laterally Loaded Pile." Proc ASTM, vol. 58: 1245–1259.

Matlock, H. & Reese, L. C. 1960. "Generalized Solutions for Laterally Loaded Piles." *J.S.M.F.D. ASCE,* vol 86, SM5: 63–91.

Matlock, H. & Reese, L. C. 1961. "Foundation Analysis of Offshore Pile Supported Structures." Proc. 5th Int. Conf. S.M. and F.E., vol 2: 91–97.

Matlock, H. & Ingram, W. B. 1963. "Bending and Buckling of Soil-Supported Structural Elements." Proc. 2nd Pan-Amer. Conf. S.M. & F.E., Brazil.

Matlock, H. 1970. "Correlations for Design of Laterally Loaded Piles in Soft Clay." Proc. 2nd Offshore Tech. Conf., Houston, vol. 1: 577–594.

Mattes, N. S. and Poulos, H. G. 1969. "Settlement of Single Compressible Pile." *J.S.M.F.D. ASCE,* vol. 95, SM1: 189–207.

Mattes, N.S. 1969. "The Influence of Radial Displacement Compatability on Pile Settlements." *Geot.*, vol. 19: 157–159.

Mattes, N. S. & Poulos. H. G. 1971. "Model Tests on Piles in Clay." Proc. 1st Aust.-N.Z. Conf. on Geomechs., Melbourne: 254–259.

Mattes, N. S. 1972. "The Analysis of Settlement of Piles And Pile Groups in Clay Soils." Ph.D. thesis, Univ. of Sydney, Aust.

Matthewson, C. D. 1969. "The Elastic Behavior of a Laterally Loaded Pile." Ph.D. thesis, Univ. of Canterbury, Christchurch, N.Z.

Maxwell, A. A., Fry, Z. B., & Poplin. J. K. 1969. "Vibratory Loading of Pile Foundations." *ASTM, STP* 444: 338–361.

McCammon, N. R. & Golder, H. Q. 1970. "Some Loading Tests on Long Pipe Piles." *Geot.*, vol 20: 171–184.

McClelland, B. & Focht, J. A. 1958. "Soil Modulus for Laterally Loaded Piles." *Trans. ASCE,* vol. 123: 1049.

McClelland, B., Focht, J. A., & Emrich, W. J. 1969. "Problems in Design and Installation of Offshore Piles." *J.S.M.F.D., ASCE,* vol. 95, SM6: 1419–1514.

McClelland, B. 1972. "Design and Performance of Deep Foundations." Proc. Spec. Conf. on Perf. of Earth and Earth-supp. Structs., ASCE, vol. 2: 111.

McClelland, B. 1974. 'Design of Deep Penetration Piles for Ocean Structures." *Jnl. Geot. Eng. Div., ASCE,* vol. 100, no. GT7: 705–747.

McKenzie, I. M. 1969. "Foundation Load Tests on Sydney

Sandstone." Roch Mechs. Symp., Inst. Engrs. Aust., Sydney, Aust.: 132–134.
McNulty, J. F. 1956. "Thrust Loading on Piles." *J.S.M.F.D., ASCE,* vol. 82, no. SM4, paper 1081.
Meyerhof, G. G. 1953*a*. "The Bearing Capacity of Foundations Under Eccentric and Inclined Loads." Proc. 3rd Int. Conf. S.M. & F.E., vol. 1: 440.
Meyerhof, G. G. 1953*b*. "The Bearing Capacity of Concrete and Rock." *Mag. of Concrete Research,* April: 107–116.
Meyerhof, G. G. & Murdock. L. J. 1953. "An Investigation of the Bearing Capacity of Some Bored and Driven Piles in London Clay." *Geot.,* vol. 3: 267.
Meyerhof, G. G. 1956. "Penetration Tests and Bearing Capacity of Cohesionless Soils." *J.S.M.F.D., ASCE,* vol. 82, SM1: 1–19.
Meyerhof, G.G. 1959. "Compaction of Sands and Bearing Capacity of Piles." *J.S.M.F.D., ASCE,* vol. 85: SM6: 1–29.
Meyerhof, G. G. 1963. "Some Recent Research on the Bearing Capacity of Foundations." *Can. Geot. Jnl.,* vol. 1, no. 1: 16.
Meyerhof, G. G. & Adams, J. I. 1968. "The Ultimate Uplift Capacity of Foundations." *Can. Geot. Jnl.,* vol. 5, no. 4: 225–244.
Meyerhof, G. G. 1976. "Bearing Capacity and Settlement of Pile Foundations." *Jnl. Geot. Eng. Div., ASCE,* vol. 102, no. GT3: 195–228.
Milligan, V., Soderman, L., & Rutka. A. 1962. "Experience with Canadian Varved Clays." *J.S.M.F.D., ASCE,* vol. 88, SM4: 32–67.
Mindlin, R. D. 1936. "Force at a point in the Interior of a Semi-Infinite Solid." *Physics* 7: 195.
M.I.T. 1973. "Proceedings of a Symposium on Downdrag of Piles," ed. by J. E. Garlanger and T. W. Lambe. M.I.T. Soils Pub. no. 331.
Mitchell, J. K. 1970. "In-Place Treatment of Foundation Soils." *J.S.M.F.D., ASCE,* vol. 96, SM1: 73–110.
Mohan, D. & Chandra, S. 1961. "Frictional Resistance of Bored Piles in Expansive Clays." *Geot.,* vol. 11: 291.
Mohan, D. & Jain, G. S. 1961. "Bearing Capacity of Piles in Expansive Clays." Proc 5th Int. Conf. S.M. & F.E., vol. 2: 117.
Mohan, D., Jain, G. S., & Kumar, V. 1963. "Load Bearing Capacity of Piles." *Geot.,* vol. 13, no. 1: 76–86.
Mohan, D., Jain, G. S., & Jain, M. P. 1967. "A New Approach to Load Tests." *Geot.,* vol. 17: 274–283.
Mohan, D., Jain, G. S., & Sharma, D. 1967. "Bearing Capacity of Multiple Under-Reamed Bored Piles." Proc. 3rd Asian Conf. S.M. & F.E., Haifa, vol. 1: 103–106.
Mohan, D., Murthy, V. N. S., & Jain, G. S. 1969. "Design and Construction of Multi-Under Reamed Piles." Proc. 7th Int. Conf. S.M. & F.E., vol. 2: 183–186.
Mohan, D. and Shrivastava, S. P. 1971. "Nonlinear Behaviour of Single Vertical Pile Under Lateral Loads." 3rd Annual Offshore Tech. Conf., Houston, vol. 2, paper OTC 1485: 677–684.
Mohr, H. A. 1963. Discussion on Paper by S. M. Johnson. *J.S.M.F.D., ASCE,* vol. 89, SM4: 213.
Moore, P. J. & Spencer, G. K. 1969. "Settlement of Building on Deep Compressible Soil." J.S.M.F.D., ASCE, vol. 95, SM3: 769.
Morgan, J. R. & Poulos, H. G. 1968. "Settlement and Stability of Deep Foundations" in *Soil Mechanics–Selected Topics,* ed. by I. K. Lee. Sydney, Aust.: Butterworths: 528–609.
Morison, J. R. O'Brien, M. P., Johnson, J. W., & Schaff, S. A. 1950. "The Force Exerted by Surface Waves on Piles." *Petroleum Trans. Amer. Inst. Min. Met. & Pet. Engrs,* vol. 189: 149–154.
Moser, M. A. 1973. Discussion. Proc. 8th Int. Conf. Soil Mechs. Fndn. Eng., Moscow, vol. 4.3: 252–253.
Mosley, E. T. & Raamot, T. 1970. "Pile-Driving Formulas." *High. Res. Rec.,* no. 333: 23–32.
Murayama, S. & Shibata, T. 1960. "The Bearing Capacity of a Pile Driven into Soil and Its New Measuring Methods." *Soils and Fndns.,* vol. 1, no. 2: 2–11.
Myers, J. J., Holm, C. H., & McAllister, R. F. 1969. *Handbook of Ocean and Underwater Engineering.* New York: McGraw-Hill.
Nair, K. 1967. "Load-Settlement and Load Transfer Characteristics of a Friction Pile Subject to a Vertical Load." Proc. 3rd Pan-Amer. Conf. S.M. & F.E., 1: 565–590.
Nair, K., Gray, H., & Donovan, N. 1969. "Analysis of Pile Group Behavior," *ASTM, STP* 444: 118–159.
Nair, K. 1969. "Dynamic and Earthquake Forces on Deep Foundations." *ASTM, STP* 444: 229–261.
Nat. Swedish Council. 1964. "Driving and Test Loading of Long Concrete Piles, Tests at Gubbero, Gothenburg." IVA Subcomm. on Piles. Rep. 99.
Nath, J. H. & Harleman, D. R. F. 1967. "The Dynamics of Fixed Towers in Deep Water Random Waves." Proc. Civil Eng. in the Oceans, ASCE Conf., San Francisco.
Newland, P. L. 1968. "The Behavior of a Pier Foundation in Swelling Clay." Proc. 4th Aust. Road Res. Conf., Melbourne, paper no. 499S.
Nicu, N. D., Antes, D. R., & Kessler, R. S. 1971. "Field Measurements on Instrumented Piles Under an Overpass Abutment." *High Res. Rec.,* no. 345.
Nishida, Y. 1963. "Pore Pressure in Clay Induced by Pile Friction." Proc. 2nd Pan-Amer. Conf. S.M. & F.E., Brazil, vol. 2: 225–233.
Nordlund, R. L. 1963. "Bearing Capacity of Piles in Cohesionless Soils." *J.S.M.F.D., ASCE,* vol. 89, SM3: 1–35.
Novak, M. & Beredugo, Y. O. 1972. "Vertical Vibration of Embedded Footings." *J.S.M.F.D., ASCE,* vol. 98, SM12: 1291–1310.
Novak, M. 1974. "Dynamic Stiffness and Damping of Piles." *Can. Geot. Jnl.,* vol. 11, no. 4: 574–598.
Novak, M. & Grigg, R. F. 1976. "Dynamic Experiments with Small Pile Foundations." *Can. Geot. Jnl.,* vol. 13, no. 4: 372–395.
Novak, M. and Howell, J. F. 1977. Torsional Vibrations of Pile Foundations." *Jnl. Geot. Eng. Divn., ASCE,* vol. 103, no. GT4: 271–285.
Novak, M. 1977. "Vertical Vibration of Floating Piles." *Jnl. Eng. Mechs. Div., ASCE,* vol. 103, no. EM1: 153–168.
Olsen, R. E. & Flaate, K. S. 1967 "Pile-Driving Formulas for Friction Piles in Sands." *J.S.M.F.D., ASCE,* vol. 93, SM6: 279–296.
Orrje, O. & Broms, B. B. 1967. "Effects of Pile Driving on Soil Properties." *J.S.M.F.D., ASCE,* vol. 93, SM5: 59–73.

Oteo, C. S. 1972. "Displacements of a Vertical Pile Group Subjected to Lateral Loads." Proc. 5th Eur. Conf. S.M. & F.E., Madrid, vol. 1:397–405.

Palmer, L. A. and Thompson, J. B. 1948. "The Earth Pressure and Deflection Along the Embedded Lengths of Piles Subjected to Lateral Thrusts." Proc. 2nd Int. Conf. S.M. and F.E., Rotterdam, vol. 5: 156–161.

Palmer, D. J. & Holland, G. R. 1966. "The Construction of Large Diameter Bored Piles with Particular Reference to London Clay." Symp. on Large Bored Piles, Inst. Civ. Engrs: 105–120.

Pandey, V. J. 1967. "Some Experiences with Bored Piling." *J.S.M.F.D., ASCE*, vol. 93, SM5: 75–87.

Parola, J. F. 1970. "Mechanics of Impact Pile Driving." Ph.D. dissertation, Univ. of Illinois, Urbana, Ill.

Parr, R. G. & Varner, M. J. 1962. "Strength Tests on Overhead Line Tower Foundations." Elec. Res. Assoc. Rep. 0/T28.

Parsons, J. D. & Wilson, S. D. 1954. "Safe Loads on Dog-Leg Piles." Proc. Sep. No. 475, ASCE, vol. 80.

Peck, R. B. 1958. "A Study of the Comparative Behavior of Friction Piles." High. Res. Bd. Spec. Rep. 36.

Peck, R. B. & Davisson, M. T. 1962. Discussion. Trans. ASCE, vol. 127, pt. 4: 413.

Peck, R. B., Hansen, W. E., & Thorburn, T. H. 1974. *Foundation Engineering*, 2nd ed. New York: Wiley.

Peck, G. M. 1969 "The Rational Design of Large Diameter Bored Piles Founded on Rock." Rock Mechs. Symp., Inst. Engrs. Aust., Sydney: 48–51.

Pells, P. J. N. 1977. "Theoretical and Model Studies Related to the Bearing Capacity of Rock." Paper presented to Sydney Group of Aust. Geomechs. Soc., Inst. Engrs. Aust.

Penzien, J., Schaffey, C. F., & Parmelee, R. A. 1964. "Seismic Analysis of Bridges on Long Piles." *J. Eng. Mechs. Div. ASCE*, EM3: 223–254.

Penzien, J. 1970. "Soil-Pile Foundation Interaction" in *Earthquake Engineering*, ed. by R. L. Wiegel, Englewood Cliffs, N. J.: Prentice-Hall.

Philcox, K. T. 1962. "Some Recent Developments in the Design of High Buildings in Hong Kong." *Struct. Eng.*, vol. 40, Oct.: 303–323.

Pichumani, R. & D'Appolonia, E. 1967. "Theoretical Distribution of Loads Among the Piles in a Group." Proc. 3rd Pan-Amer. Conf. S.M. & F.E., Caracas, Venezuela.

Plantema, I. G. 1957. "Influence of Density of Sounding Results in Dry, Moist and Saturated Sands." Proc. 4th Int. Conf. S.M. & F.E., vol. 1: 237–240.

Poorooshasb, H. B. & Bozozuk, M. 1967. "Skin Friction on a Single Pile to Bedrock." Proc. 3rd Pan-Amer. Conf. S.M. & F.E., vol. 1: 613–621.

Poulos, H. G. & Davis, E. H. 1968. "The Settlement Behavious of Single Axially-Loaded Incompressible Piles and Piers." *Geot.* vol. 18: 351–371.

Poulos, H. G. 1968. "The Influence of a Rigid Pile Cap on the Settlement Behaviour of an Axially-Loaded Pile." *Civ. Eng. Trans.*, Inst. Engrs. Aust., vol. CE10, no. 2: 206–208.

Poulos, H. G. 1968. "Analysis of the Settlement of Pile Groups." *Geot.* vol. 18: 449–471.

Poulos, H. G. 1969. "The Settlement of Under-Reamed and Step-Taper Piles." *Civ. Eng. Trans.*, Inst. Engrs. Aust., vol. CE11: 83–87.

Poulos, H. G. & Mattes, N. S. 1969*a*. "The Behaviour of Axially-Loaded End-Bearing Piles." *Geot.*, vol. 19: 285–300.

Poulos, H. G. & Mattes, N. S. 1969*b*. "The Analysis of Downdrag in Eng-Bearing Piles Due to Negative Friction." Proc. 7th Int. Conf. S.M. & F.E., vol. 2: 204–209.

Poulos, H. G. 1971*a*. "Behaviour of Laterally Loaded Piles: I–Single Piles." *J.S.M.F.D., ASCE*, vol. 97, no. SM5: 711–731.

Poulos, H. G. 1971*b*. "Behaviour of Laterally-Loaded Piles: II–Pile Groups." *J.S.M.F.D., ASCE*, vol. 97, no. SM5: 733–751.

Poulos, H. G. 1971*c*. Discussion to "Load-Deformation Mechanism for Bored Piles," by R. D. Ellison, E. D'Appolonia, & G. R. Thiers. *Jnl. Soil Mechs. & Fndns. Div., ASCE*, vol 97, no. SM12: 1716.

Poulos, H. G. & Mattes, N. S. 1971*a*. "Displacements in a Soil Mass Due to Pile Groups." *Aust. Geomechs. Jnl*, vol. G1, no. 1: 29–35.

Poulos, H. G. & Mattes, N. S. 1971*b*. "Settlement and Load Distribution Analysis of Pile Groups." *Aust. Geomechs. Jnl.*, vol. G1, no. 1: 18–28.

Poulos, H. G. & Madhav, M. R. 1971. "Analysis of the Movement of Battered Piles." Proc. 1st Aust.-N.Z. Conf. on Geomechs., Melbourne: 268–275.

Poulos, H. G. & Davis, E. H. 1972. "The Development of Negative Friction with Time in End-Bearing Piles." *Aust. Geomechs. Jnl.*, vol. G2, no. 1: 11–20.

Poulos, H. G. 1972*a*. "Behaviour of Laterally Loaded Piles: III–Socketed Piles." *J.S.M.F.D., ASCE*, vol. 98, no. SM4: 341–360.

Poulos, H. G. 1972*b*. "Settlement Analysis of Two Buildings on End-Bearing Piles." Proc. 3rd SE Asian Conf. Soil. Eng., Hong Kong: 129–134.

Poulos, H. G. 1972*c*. "Difficulties in Prediction of Horizontal Deformations of Foundations." *J.S.M.F.D., ASCE*, vol. 98, SM8: 843–848.

Poulos, H. G. 1972*d*. "Load-Settlement Prediction for Piles and Piers." *J.S.M.F.D., ASCE*, vol. 98, SM9: 879–897.

Poulos, H. G. 1973*a*. "Load-Deflection Prediction for Laterally Loaded Piles." *Aust. Geomechs. Jnl.*, vol. G3, no. 1: 1–8.

Poulos, H. G. 1973*b*. "Analysis of Piles in Soil Undergoing Lateral Movement." *J.S.M.F.D., ASCE*, vol. 99, SM5: 391–406.

Poulos, H. G. & Davis, E. H. 1973. "Theory of Piles in Swelling and Shrinking Soils." Proc. 8th Int. Conf. S.M. & F.E., Moscow, vol. 2.2: 169–176.

Poulos, H. G. 1974. "Analysis of Pile Groups Subjected to Vertical and Horizontal Loads." *Aust. Geomechs. Jnl.*, vol. G4, no. 1: 26–32.

Poulos, H. G. & Davis, E. H. 1974. *Elastic Solutions for Soil and Rock Mechanics*. New York: Wiley.

Poulos, H. G. & Mattes, N. S. 1974. "Settlement of Pile Groups Bearing on Stiffer Strata." *Jnl. Geot. Eng. Div., ASCE*, vol. 100, no. GT2: 185–190.

Poulos, H. G. 1975*a*. "Lateral Load-Deflection Prediction for Pile Groups." *Jnl. Geot. Eng. Div., ASCE*, vol. 101, no. GT1: 19–34.

Poulos, H. G. 1975*b*. "Torsional Response of Piles." *Jnl. Geot. Eng. Div., ASCE*, vol. 101, no. GT10: 1019–1035.

Poulos, H. G. & Davis, E. H. 1975. "Prediction of Downdrag Forces in End-Bearing Piles." *Jnl. Geot. Eng. Div., ASCE*, vol. 101, no. GT2: 189–204.

Poulos, H. G. & Mattes, N. S. 1975. "A Theoretical Examination of Errors in Measured Settlements of Test Piles." Proc. 2nd Aust.-N.Z. Conf. on Geomechs: 174–178.

Poulos, H. G. 1976. "Behaviour of Laterally Loaded Piles Near a Cut or Slope." *Aust. Geomechs. Jnl.*, vol. G6, no. 1: 6–12.

Poulos, H. G., & Adler, M. A. 1978. "Analysis of Lateral Response of Non-Uniform Section Piles." Civ. Eng. Res. Rep. R330, Univ. of Sydney, Australia.

Poulos, H. G. 1979. "Settlement of Single Piles in Non-homogeneous Soil." Jnl. Geot. Eng. Div., ASCE, Vol. 105, no. GT5: 627–641.

Prakash, S. 1962. "Behaviour of Pile Groups Subjected to Lateral Loads." Ph.D. thesis, Univ. of Illinois, Urbana.

Prakash, S. & Saran, D. 1967. "Behaviour of Laterally-Loaded Piles in Cohesive Soils." Proc. 3rd Asian Conf. S.M.: 235–238.

Prakash, S. & Chandrasekaran, V. 1973. "Pile Foundation under Lateral Dynamic Loads." Proc. 8th Int. Conf. S.M. & F.E., Moscow, vol. 2.1, paper 3/31: 199–202.

Prandtl, L. 1923. "Anwendungsbeispiele zu Einem Henchyschen Satz Ueber das Plastische Gleichgewicht." *Z. Angew. Math. Mech.*, vol. 3: 468.

Press, H. 1933. "Die Tragfahigkeit von Pfallgnippen in Beziehund zu der des Einzelpfahles." *Bautechnik*, vol. 11: 625–627.

Priddle, R. A. 1963. "Load Distribution in Piled Bents." Trans., Inst. Engrs. Aust., vol. CE5, no. 2: 43–54.

Radugin, A. E. 1969. "Increase of Bearing Capacity of Short Piles with Time." *Soil Mechs. & Fndn. Eng.*, March-April: 103–107.

Randolph, M. F. 1977. "A Theoretical Study of the Performance of Piles." Ph.D. Thesis, Cambridge Univ., U.K.

Randolph, M. F. & Wroth, C. P. 1978. "Analysis of Deformation of Vertically Loaded Piles." *Jnl. Geot. Eng. Div, ASCE*, vol. 104, no. GT12: 1465–1488.

Reddy, A. S. & Valsangkar, A. J. 1968. "An Analytical Solution for Laterally Loaded Piles in Layered Soils." *Sols-Soils*, no. 21: 23–28.

Reddy, A. S. & Valsangkar, A. J. 1970. "Buckling of Fully and Partially Embedded Piles." *J.S.M.F.D., ASCE*, vol. 96, SM6: 1951–1965.

Reese, L. C. & Cox, W. R. 1969. "Soil Behaviour from Analysis of Tests on Uninstrumented Piles Under Lateral Loading." *ASTM, STP* 444: 160–176.

Reese, L. C. & Matlock, H. 1956. "Non-Dimensional Solutions for Laterally Loaded Piles with Soil Modulus Assumed Proportional To Depth." Proc. 8th Texas Conf. S.M. and F.E., Spec. Pub. 29, Bureau of Eng. Res., Univ. of Texas, Austin.

Reese, L. C., Hudson, B. S. & Vijayvergija, B. S. 1969. "An Investigation of the Interaction Between Bored Piles and Soil." Proc. 7th Int. Conf. S.M. & F.E., vol. 2: 211–215.

Reese, L. C., O'Neill, M. W., and Smith, R. E. 1970. "Generalized Analysis of Pile Foundations." *J.S.M.F.D., ASCE*, vol. 96, SM1: 235.

Reese, L. C., Cox, W. R., & Koop, F. D. 1974. "Analysis of Laterally Loaded Piles in Sand." Proc. 6th Offshore Tech. Conf., Houston, paper OTC 2080: 473–483.

Reese, L. C., Cox, W. R., & Koop, F. D. 1975. "Field Testing and Analysis of Laterally Loaded Piles in Stiff Clay." Proc. 7th Offshore Tech. Conf., Houston, paper OTC 2312: 671–690.

Reese, L. C. & Welch, R. C. 1975. "Lateral Loadings of Deep Foundations in Stiff Clay." *Jnl. Geot. Eng. Div., ASCE*, vol. 101, no. GT7: 633–649.

Reese, L. C. 1975. "Laterally Loaded Piles." Proc. of the Seminar Series, Design, Construction and Performance of Deep Foundations; Geot. Group and Continuing Education Committee, San Francisco section, ASCE; Univ. of Calif., Berkeley.

Reese, L. C., Touma, F. T. & O'Neill, M. W. 1976. "Behavior of Drilled Piers Under Axial Loading." *Jnl. Geot. Eng. Div., ASCE*, vol. 102, GT5: 493–510.

Reese, L. C. 1977. "Laterally Loaded Piles: Program Documentation." *Jnl. Geot. Eng. Div., ASCE*, vol. 103, no. GT4: 287–305.

Rehnman, S. E. & Broms, B. B. 1970. "Bearing Capacity of End-Bearing Piles Driven to Rock." Proc. 2nd Cong. of Int. Soc. of Rock Mechs, Beograd, vol 2: 15–22.

Resendiz, D., Auvinet, G., and Silva, C. 1969. "Conception et Comportement des Fondations des Palais des Sports de la Ville de Mexico en Presence de Frottenment Negatif." Spec. Sess. No. 8, 7th Int. Conf. S.M. & F.E., paper 18.

Richards, B. G. 1965. "An Analysis of Subgrade Conditions at the Horsham Experimental Road Site Using the Two-Dimensional Diffusion Equation on a High-Speed Digital Computer," in *Moisture Equilibria and Moisture Changes in Soils Beneath Covered Areas.* Sydney: Butterworths, 243.

Richart, F. E. 1962. "Foundation Vibrations." Trans. ASCE, vol. 127, pt. 1: 863–898.

Richart, F. E., Hall, J. R., & Woods, R. D. 1970. *Vibrations of Soils and Foundations*. Englewood Cliffs, N. J.: Prentice-Hall.

Robinsky, E. I. & Morrison, C. E. 1964. "Sand Displacement and Compaction Around Model Friction Piles." *Can. Geot. Jnl.*, vol. 1, no. 2: 81.

Roscoe, K. H. 1957. "Comparison of Tied and Free Pier Foundations." Proc. 4th Int. Conf. S.M. & F.E., vol. 2: 419.

Ross, H. E. 1971. "Dynamic Response of Offshore Piling." 3rd Offshore Tech. Conf., Texas, paper OTC 1480.

Rowe, P. W. 1956. "The Single Pile Subject to Horizontal Force." *Geot.*, vol. 6: 70–85.

Rowe, R. K. & Poulos, H. G. 1979. "A Method for Predicting the Effect of Piles on Slope Behaviour." Proc. 3rd Int. Conf. Num. Methods in Geomechs, Aachen. Balkema. vol. 3: 1073–1085.

Rowe, R. K., Booker, J. R. & Balaam, N. P. 1978. "Application of the Initial Stress Method to Soil-Structure Interaction." *Int. Jnl. for Num. Meth. in Eng., vol. 12:* 873–880.

Rutledge, P. C. 1950. Discussion on Paper by Cummings, Kerkhoff, and Peck. Trans. ASCE, vol. 115.

Saffery, M. R. & Tate, A. P. K. 1961. "Model Tests on Pile Groups in a Clay Soil with Particular Reference to the Behaviour of the Group When It Is Loaded Eccentrically." Proc. 5th Int. Conf. S.M. & F.E., vol. 2: 129–134.

Sahzin, V. S. 1968. "Method of Determining the Magnitude of Rise of Piles Following Flooding of Swelling Soils." *Soil Mechs. & Fndn. Eng.*, No. 1: 149.

Salas, J. A. J. & Belzunce, J. A. 1965. "Resolution Theorique de la Distribution des Forces dans les Pieux." Proc. 6th Int. Conf. S.M. & F.E., vol. 2: 309–313.

Salas, J. A. J. 1965. Discussion on Div. 4, Proc. 6th Int. Conf. S.M. & F.E., vol. 3: 489–492.

Samson, C. H., Hirsch, T. J., & Lowery, L. L. 1963. "Computer Study of Dynamic Behaviour of Piling." *J. Struct. Divn, ASCE*, vol. 89, ST4: 413–449.

Saul, W. E. 1968. "Static and Dynamic Analysis of Pile Foundations." *J. Struct. Div., ASCE*, vol. 94, ST5: 1077–1100.

Sawko, F. 1968. "A Simplified Approach to the Analysis of Piling Systems." *Struct. Eng.*, vol. 46, no. 3: 83–86.

Scanlan, R. H. & Tomko, J. J. 1969. "Dynamic Prediction of Pile Static Bearing Capacity." *J.S.M.F.D., ASCE*, vol. 95, SM2: 583–604.

Schmertmann, J. H. 1969. Discussion. Proc. 7th Int. Conf. S.M. & F.E., vol. 3: 250–251.

Seed, H. B. & Reese, L. C. 1957. "The Action of Soft Clay Along Friction Piles." Trans. ASCE, vol. 122: 731–754.

Seed, H. B. & Martin G. R. 1966. "The Seismic Coefficient in Earth Dam Design." *J.S.M.F.D., ASCE*, vol. 92, SM3: 25–58.

Sharman, F. A. 1961. "The Anticipated and Observed Penetration Resistance of Some Friction Piles Entirely in Clay." Proc. 5th Int. Conf. S.M. & F.E., vol. 2: 135–141.

Sherman, W. C. 1969. "Instrumented Pile Tests in a Stiff Clay." Proc. 7th Int. Conf. S.M. & F.E., vol. 2: 227–232.

Shubinski, R. P., Wilson, E. L., & Selna, L. G. 1967. "Dynamic Response of Deepwater Structures." Proc. Civil Engr. in the Oceans, ASCE Conf., San Francisco.

Shultze, E. & Mezler, K. J. 1965. "The Determination of the Density and the Modulus of Compressibility of Non-Cohesive Soils by Soundings." Proc. 6th Int. Conf. S.M. & F.E., vol. 1: 354–358.

Simek, J. 1966. "Resultats d'Observations de l'Influence d'une Force Horizontale sur des Groupes de Pieux." *Sols-Soils*, no. 18–19: 11–18.

Singh, A. & Verma, R. K. 1973. "Lateral Resistance of a Field Model of Pile Group in Sand and Its Comparison with a Laboratory Model." *Ind. Geot. Jnl.*, vol. 3, no. 2: 113–127.

Skempton, A. W. & Bishop, A. W. 1950. "The Measurement of the Shear Strength of Soils." Geot., vol. 1, no. 2: 90.

Skempton, A. W. 1950. Discussion to Paper by G. Wilson, *J. Inst. Civ. Engs.*, London, vol. 34, no. 5: 76–81.

Skempton, A. W. 1951. "The Bearing Capacity of Clays." Build. Res. Congress, London. Inst. Civ. Engrs., div. I: 180.

Skempton, A. W. 1953. Discussion: Piles and Pile Foundations, Settlement of Pile Foundations. Proc. 3rd Int. Conf. S.M. & F.E., vol. 3: 172.

Skempton, A. W. 1959. "Cast-In-Situ Bored Piles in London Clay." *Geot.*, vol. 9: 158.

Skempton, A. W. 1966. "Summing Up." Symp. on Large Bored Piles, London: 155.

Smith, E. A. L. 1960. "Pile Driving Analysis by the Wave Equation." *J.S.M.F.D., ASCE*, vol. 86, SM4: 35–61.

Soderberg, L. 1962*a*. "Consolidation Theory Applied to Foundation Pile Time Effects." *Geot.*, vol. 12: 217.

Soderberg, L. O. 1962*b*. Discussion to Paper by E. A. L. Smith. Trans. ASCE: 1171–1174.

Sokolovskii, V. V. 1965. *Statics of Soil Media*. London: Butterworths.

Sorensen, T. & Hansen, B. 1957. "Pile Driving Formulae, An Investigation Based on Dimensional Considerations and a Statistical Analysis." Proc. 4th Int. Conf. S.M. & F.E., vol. 2: 61–65.

Sowa, V. A. 1970. "Pulling Capacity of Concrete Cast in Situ Bored Piles." *Can. Geot. Jnl.*, vol. 7: 482–493.

Sowers, G. F., Martin, C. B., Wilson, L. L., & Fausold, M. 1961. "The Bearing Capacity of Friction Pile Groups in Homogeneous Clay from Model Studies." Proc. 5th Int. Conf. S.M. & F.E., vol. 2: 155–159.

Sowers, G. B. & Sowers, G. F. 1970. *Introductory Soil Mechanics and Foundations*, 3rd ed. New York: Macmillan.

Spence, B. E. 1965. "Uplift Resistance of Piles with Enlarged Bases in Clay." M.Sc. thesis, Nova Scotia Tech. College, Can.

Spillers, W. R. & Stoll, R. D. 1964. "Lateral Response of Piles." *J.S.M.F.D., ASCE*, vol. 90, SM6: 1–9.

Steinbrenner, W. 1934. "Tafeln zur Setzungberechnung." *Die Strasse*, 1: 221.

Stoll, U. W. 1972. "Torque Shear Test on Cylindrical Friction Piles." *Civ. Eng., ASCE*, vol. 42, no. 4: 63–64.

Sullivan, W. R., Reese, L. C., & Fenske, C. W. 1979. "Unified Method for Analysis of Laterally Loaded Piles in Clay." Conf. on Num. Methods in Offshore Piling, London. Inst. Civ. Engrs., Paper no. 17.

Tavenas, F. A. 1971. "Load Test Results on Friction Piles in Sand." *Can. Geot. Jnl.*, vol. 8: 7–22.

Taylor, D. W. 1948. *Fundamentals of Soil Mechanics*. New York: Wiley.

Terzaghi, K. 1942. "Discussion of the Progress Report of the Committee on the Bearing Value of Pile Foundations." Proc. ASCE, vol. 68: 311–323.

Terzaghi, K. 1943. *Theoretical Soil Mechanics*. New York: Wiley.

Terzaghi, K. 1955. "Evaluation of Coefficients of Sub-grade Reaction." *Geot.*, vol. 5: 297.

Terzaghi, K. & Peck, R. B. 1967. *Soil Mechanics in Engineering Practice*. New York: Wiley.

Thomas, D. 1965. "Static Penetration Tests in London Clay" *Geot.*, vol. 15: 174.

Thorne, C. P. & Burman, B. 1968. "The Use of the Static (Dutch) Cone Penetrometer for the In-Situ Testing of Soils." Proc. Symp. on Field Measurements, paper no. 498S, Aust. Road Res. Board, Melbourne.

Thorne, C. P. 1977 "The Allowable Loadings of Foundations on Shale and Sandstone in the Sydney Region. Part 3. Field Test Results." Paper presented to Sydney Group of Aust. Geomechs. Soc., Inst. Engrs. Aust.

Thurman, A. G. & D'Appolonia, E. 1965. "Computed Movement of Friction and End-Bearing Piles Embedded in Uniform and Stratified Soils." Proc. 6th Int. Conf. S.M. & F.E., vol. 2: 323–327.

Timoshenko, P. S. 1936. *Theory of Elastic Stability*. New York: McGraw-Hill.

Toakley, A. R. 1964. M.Eng.Sc. thesis, Univ. of Melbourne, Aust.

Toakley, A. R. 1965. "Buckling Loads for Elastically Supported Struts." *J. Eng. Mechs. Div. ASCE*, vol. 91, EM3: 205–231.

Tomlinson, M. J. 1957. "The Adhesion of Piles Driven in Clay Soils." Proc. 4th Int. Conf. S.M. & F.E. vol. 2: 66–71.

Tomlinson, M. J. 1970. "Some Effects of Pile Driving on Skin Friction." Conf. on Beh. of Piles, Inst. Civ. Engrs., London: 59–66.

Tomlinson, M. J. 1975. *Foundation Design and Construction*. 3rd Ed. London: Pitman.

Tomlinson, M. J. 1977. *Pile Design and Construction Practice*. London: Viewpoint Publications.

Touma, F. T. & Reese, L. C. 1974. "Behaviour of Bored Piles in Sand." *Jnl. Geot. Eng. Div., ASCE*, vol. 100, no. GT7: 749–761.

Trofimenkov, J. G. & Mariupolskii, L. G. 1965. "Screw Piles Used for Mast and Tower Foundations." Proc. 6th Int. Conf. S.M. & F.E., vol. 2: 328–332.

Tschebotarioff, G. P. 1951. *Soil Mechanics Foundations and Earth Structures*. New York: McGraw-Hill.

Tschebotarioff, G. P. 1953. "The Resistance to Lateral Forces of Single Piles and Pile Groups." *ASTM, STP* 154: 38.

Tucker, R. L. 1964. "Lateral Analysis of Piles with Dynamic Behaviour." Proc. Conf. on Deep Fndns., Mexico City, vol. 1: 157–171.

Turner, E. A. 1962. "Uplift Resistance of Transmission Tower Footings." *J. Power Div., ASCE*, vol. 88, paper 3187.

Valliappan, S., Lee, I. K., & Boonlualohr, P. 1974. "Settlement of Piles in Layered Soils." Proc. 7th Biennial Conf., Aust. Rd. Res. Bd., Adelaide, vol. 7, pt. 7: 144–153.

Van der Merwe, D. H. 1964. "The Prediction of Heave from the Plasticity Index and the Percentage Clay Fraction." *The Civil Engr. in So. Africa*, vol. 6, no. 6: 103.

Van der Veen, C. & Boersma, L. 1957. "The Bearing Capacity of a Pile Predetermined by a Cone Penetration Test." Proc. 4th Int. Conf. S.M. & F.E., vol. 2: 72–75.

Van der Veen, C. 1965. "Loading Test on an Unorthodox Concrete Cuff Pile." Proc. 6th Int. Conf. S.M. & F.E., vol. 2: 333–337.

Van Weele, A. F. 1957. "A Method of Separating the Bearing Capacity of a Test Pile into Skin Friction and Point Resistance." Proc. 4th Int. Conf. S.M. & F.E., vol. 2: 76.

Verruijt, A. 1969. "A Simplified Elastic Method for the Calculation of Negative Skin Friction of Piles." Spec. Sess. No. 8, 7th Int. Conf. S.M. & F.E., paper 5.

Vesic, A. S. 1961. "Bending of Beam Resting on Isotropic Elastic Solid." *Jnl. Eng. Mechs. Div., ASCE*, vol. 87, EM2: 35–53.

Vesic, A. S. 1964. "Investigations of Bearing Capacity of Piles in Sand." Proc. No. Amer. Conf. on Deep Fndns., Mexico City, vol. 1: 197–224.

Vesic, A. S. 1965. "Ultimate Loads and Settlements of Deep Foundations in Sand." Proc. Symp. on Bearing Capacity and Settlement of Foundations, Duke Univ. 53–68.

Vesic, A. S. 1967. "A Study of Bearing Capacity of Deep Foundations." Final Rep., Proj. B-189, School of Civil Eng., Georgia Inst. Tech., Atlanta, Ga.

Vesic, A. S. 1969. "Experiments with Instrumented Pile Groups in Sand." *ASTM, STP* 444: 177–222.

Vesic, A. S. 1969*b*. Discussion. Proc. 7th Int. Conf. S.M. & F.E., vol. 3: 242–244.

Vesic, A. S. 1972. "Expansion of Cavities in Infinite Soil Mass." *J.S.M.F.D., ASCE*, vol. 98: 265–290.

Vesic, A. S. 1975. "Principles of Pile Foundation Design." Duke Univ. School of Eng., Soil Mechs., series no. 38.

Vijayvergiya, V. N. 1969. "Load Distribution Along a Bored Pile Determined by Tell-Tales." Paper presented to Soil Mechs. and Fndn. Grp., Texas Section, ASCE, Lubbock, Texas.

Vijayvergiya, V. N. & Focht, J. A. Jr. 1972. "A New Way to Predict the Capacity of Piles in Clay." 4th Annual Offshore Tech. Conf., Houston, vol. 2: 865–874.

Walther, R. E. 1962. "Prestressed Rock Anchors." *Civil Eng., ASCE*, vol. 13, no. 1.

Wagner, A. A. 1953. "Lateral Load Tests on Piles for Design Information." Symp. on Lateral Load Tests on Piles. *ASTM, STP* 154: 59–72.

Walker, L. K. & Darvall, P. Le P. 1970. "Some Aspects of Dragdown on Piles." Proc. 2nd SE Asian Conf. on Soil Eng., Singapore: 121–137.

Walker, L. K. & Darvall, P. Le P. 1973. "Dragdown on Coated and Uncoated Piles." Proc. 8th Int. Conf. S.M. & F.E., Moscow, vol. 2.1: 257–262.

Warburton, G. 1964. *The Dynamic Behaviour of Structures*. Oxford: Pergamon.

Whitaker, T. 1957. "Experiments with Model Piles in Groups." *Geot.*, vol. 7: 147–167.

Whitaker, T. 1960. "Some Experiments on Model Piled Foundations in Clay." Proc. Symp. on Pile Fndns., 6th Conf. Int. Assoc. Bridge and Struct. Eng., Stockholm: 124–139.

Whitaker, T. & Cooke, R. W. 1961. "A New Approach to Pile Testing." Proc. 5th Int. Conf. S.M. & F.E. vol. 2: 171–176.

Whitaker, T. 1963. "The Constant Rate of Penetration Test for the Determination of the Ultimate Bearing Capacity of a Pile." Proc. Instn. Civ. Engrs, vol. 26: 119–123.

Whitaker, T. & Cooke, R. W. 1966. "An Investigation of the Shaft and Base Resistances of Large Bored Piles in London Clay." Proc. Symp. on Large Bored Piles: 7–49.

Whitaker, T. 1970. *The Design of Piled Foundations*. Oxford: Pergamon.

White, R. 1943. "Heavy Foundations Drilled into Rock." *Civ. Eng., ASCE*, vol. 13, no. 1.

Whitman, R. V. & Richart, F. E. 1967. "Design Procedure for Dynamically Loaded Foundations." *J.S.M.F.D., ASCE*, vol. 93, SM6: 169–193.

Wiesner, T. J. & Brown, P. T. 1975. "Behaviour of Piled Strip Footings Subjected to Concentrated Loads." Civ. Eng. Res. Rep. R275., Univ of Sydney, Aust.

Wilson, G. 1948. "A Relaxation Method for the Solution of Problems Concerning Axially Symmetrical Distributions of Load in an Elastic Medium." *Jnl. Inst. Civ. Engrs.*, London, No. 6, April: 149–166.

Wilson, G. 1950. "The Bearing Capacity of Screw Piles and Screwcrete Cylinders." *J. Inst. Civ. Engrs., London*, vol. 34: 4–93.

Wilson, S. D. & Hilts, D. E. 1967. "How to Determine Lateral Load Capacity of Piles." in *Pile-Foundation Know-How* (41–45). Washington: Amer. Wood Pres. Inst.

Wroth, C. P., Carter, J. P. & Randolph, M. F. 1979. "Stress Changes Around a Pile Driven into Cohesive Soil." Conf. on Recent Devel. in the Design and Constrn. of Piles. Inst. Civ. Engrs., London.

Woodward, R. & Boitano, J. (1961) - "Pile Loading Tests in Stiff Clays". Proc. 5th Int. Conf. S.M. & F.E., Vol. 2, 177.

Yamagata, K. 1963 - "The Yield-Bearing-Capacity of Bearing Piles". Proc. Int. Conf. S.M. & F.E. Budapest, 325–342.

Yegian, M. and Wright, S. G. (1973) - "Lateral Soil Resistance - Displacement Relationships for Pile Foundations in Soft Clays". 5th Annual Offshore Tech. Conf. Houston, Paper OTC1893, Vol. 2, 663–676.

Yoshimi, Y. (1964) - "Piles in Cohesionless Soils Subjected to Oblique Pull". J.S.M.F.D., ASCE, Vol. 90, SM6, 11.

Zeevaert, L. (1957) - "Foundation Design and Behaviour of Tower Latino Americana in Mexico City". Geotechnique, Vol. 7, No. 1, 115.

Zeevaert, L., (1959) - "Reduction of Point Bearing Capacity Because of Negative Friction". Proc. 1st Pan-Amer. Conf. S.M. & F.E., Vol. 3, 1145.

Zeevaert, L. (1973) - "Foundation Engineering for Difficult Subsoil Conditions." Van Nostrand Reinhold, New York.

Zienkiewicz, O. C. (1971) - "The Finite Element Method in Engineering Science." McGraw-Hill, London.

AUTHOR INDEX

SUBJECT INDEX